Imperial College of Science, Technology and Medicine
Department of Aeronautics

# Data-driven Modelling for Guided Wave Structural Health Monitoring and Prognostic Health Management on Aeronautical Structures

Hongmin Zhu

Submitted for the degree of Doctor of Philosophy and the Diploma of Imperial College,
May 2024

# Abstract

This thesis presents novel data-driven techniques and analyses for Guided Wave Structural Health Monitoring (GWSHM) and Prognostic Health Management (PHM) on aeronautical structures. Main attention is paid to damage detection and localisation on Carbon Fiber Reinforced Polymer (CFRP) panels together with the Remaining Useful Life (RUL) prediction of aircraft turbofans.

A baseline-dependent GWSHM approach on CFRP plates is proposed integrating the statistical autoregressive (AR) modelling and signal compression techniques. An adaptive block-wise down-sampling method is designed to compress guided wave signals and compared to other signal compression techniques, and the compressed measurements are processed by AR models to extract damage-sensitive features. Further validations are implemented on both quasi-isotropic and anisotropic CFRP coupons. Various variables, including the AR model parameters, number of tone burst cycles and signal compression ratios, are investigated regarding their effects on the damage detection and localisation.

Baseline-free GWSHM is investigated within the aeronautical composite cases. Existing baseline-free techniques are reviewed, with several of them experimentally compared considering material anisotropy, temperature variations, multiple damages, boundary reflections and structural complexities, e.g., stiffeners.

Furthermore, a novel data-driven baseline-free technique is presented based on unsupervised shapelets and shift-invariant dictionary learning. The proposed method can detect and localise potential damages in complex composite structures, e.g., stiffened panels, when integrated with the building block philosophy. The effectiveness and robustness of the proposed method is validated through experimental investigations and compared with several existing baseline-free techniques for damage detection and localisation under varying temperatures.

During the transition from GWSHM to PHM, the RUL prediction of aircraft engines is implemented by a proposed hybrid data-driven approach which is able to model degradation behaviour of turbofans under varying environmental and operational conditions (EOCs) while yielding satisfactory RUL estimates simultaneously.

## Copyright declaration

The copyright of this thesis rests with the author. Unless otherwise indicated, its contents are licensed under a Creative Commons Attribution-Non Commercial 4.0 International Licence (CC BY-NC).

Under this licence, you may copy and redistribute the material in any medium or format. You may also create and distribute modified versions of the work. This is on the condition that: you credit the author and do not use it, or any derivative works, for a commercial purpose.

When reusing or sharing this work, ensure you make the licence terms clear to others by naming the licence and linking to the licence text. Where a work has been adapted, you should indicate that the work has been changed and describe those changes. Please seek permission from the copyright holder for uses of this work that are not included in this licence or permitted under UK Copyright Law.

## Declaration of originality

I hereby declare that the thesis is composed by myself and the work presented in the thesis is the result of my original work. Information obtained from the work of others has been cited within the text and the reference list.

Hongmin Zhu

May 2024

## Acknowledgements

First, I would like to express my deepest gratitude to my main supervisor Professor Ferri Aliabadi for his sincere support on my transfer to the Department of Aeronautics and his supervision on my current PhD project. I am very grateful to Ferri for his deep insights into the academic research together with his trust and patience, which inspire me throughout my PhD research.

I am very grateful to my second supervisor Professor Zahra Sharif-Khodaei for her kind encouragement and inspiring supervision on my PhD research. I learned much from Zahra regarding not only the technical parts through discussions, but also her critical thinking and thorough analyses on research problems.

Meanwhile, I am thankful to my colleagues in the structural integrity and health monitoring (SI & HM) research group for their help and support. I would like to thank Professor Jennifer Whyte, Dr. Christian Onof and Dr. Panagiotis Angeloudis for their support when I was at the civil engineering department.

Finally, I would like to give special thanks and gratitude to my parents for their unconditional support within these years. I would be lost during the journey of PhD without their consistent support and help.

# Contents

**Abstract** **i**

**1 Introduction** **1**

1.1 Background . . . . . 1

1.2 Motivation . . . . . 6

1.3 Thesis outline . . . . . 8

1.4 Contributions . . . . . 9

**2 Fundamentals of SHM and PHM** **11**

2.1 Introduction . . . . . 11

2.2 Ultrasonic guided waves . . . . . 11

2.2.1 Guided waves in isotropic plates . . . . . 11

2.2.2 Guided waves in anisotropic media . . . . . 15

2.2.3 Guided waves in layered structures . . . . . 17

2.2.4 Phase velocity and Group velocity . . . . . 17

2.2.5 Dispersion curves . . . . . 18

2.3 Actuation, sensing and processing of guided waves . . . . . 19

2.3.1 Transducer type . . . . . 19

2.3.2 Transducer configurations . . . . . 20

2.3.3 Electromechanical (E/M) impedance analyses for transducers . . . . . 21

2.3.4 Signal processing in time and frequency domain . . . . . 23

2.4 Guided-wave damage detection and localisation . . . . . 28

2.4.1 Baseline-subtraction for damage detection . . . . . 28

2.4.2 Damage indices for damage detection . . . . . 29

2.4.3 Temperature compensation for baseline subtraction . . . . . 31

2.4.4 Damage localisation based on sparse array imaging . . . . . 32

2.4.5 Supportive C-Scan technique for damage imaging . . . . . 37

2.5 Failure prognostics for engineered structures . . . . . 37

2.5.1 Critical concepts in failure prognostics . . . . . 38

2.5.2 Failure prognostics approaches . . . . . 39

2.5.3 Metrics for the RUL prediction . . . . . 42

2.5.4 Summary . . . . . 43

**3 Baseline-based guided wave structural health monitoring of composite structures 45**

3.1 Introduction . . . . . 45

3.2 Theoretical background . . . . . 46

3.2.1 Time series and the AR models . . . . . 46

3.2.2 Signal compression techniques . . . . . 51

3.3 Proposed methodology . . . . . 52

3.4 Experimental setup . . . . . 59

3.5 Results of raw guided wave signals . . . . . 63

3.5.1 Autoregressive (AR) modelling results . . . . . 63

3.5.2 Results for damage detection and localisation . . . . . 68

3.5.3 GWSHM with varying tone burst cycles . . . . . 73

3.6 Results of compressed guided wave signals . . . . . 77

3.6.1 Autoregressive (AR) modelling results . . . . . 77

3.6.2 Damage detection and localisation on compressed signals . . . . . 83

3.6.3 Damage detection & localisation with varying toneburst cycles . . . . . 90

3.7 Computation time based on raw and compressed signals . . . . . 93

3.8 Summary . . . . . 94

**4 Baseline-free techniques for guided wave structural health monitoring 95**

4.1 Introduction . . . . . 95

4.2 Overview of common baseline-free techniques . . . . . 98

4.2.1 Time reversal (TR) imaging and its extensions . . . . . 98

4.2.2 Instantaneous baseline (IB) approach . . . . . 104

4.2.3 Reciprocity-based approach . . . . . 106

4.2.4 Modal based techniques . . . . . 108

4.2.5 Nonlinear frequency modulation (NFM) technique . . . . . 112

4.3 Critical factors for baseline-free techniques . . . . . 113

4.3.1 Varying environmental conditions . . . 113
4.3.2 Structural and geometrical complexities . . . 114
4.3.3 Multiple damages . . . 115
4.4 Experimental setup . . . 117
4.5 Experimental comparisons on baseline-free techniques . . . 119
4.5.1 Simulated damage cases . . . 119
4.5.2 Impact damage cases . . . 126
4.5.3 Experimental results under temperature variations . . . 130
4.5.4 Comparisons under geometric and structural complexities . . . 136
4.6 Summary . . . 148

**5 A data-driven baseline-free approach for SHM in composite structures 149**

5.1 Introduction . . . 149
5.2 Background . . . 151
5.2.1 Guided wave signals in composite structures . . . 151
5.2.2 Unsupervised shapelet learning . . . 152
5.3 Proposed methodology for baseline-free GWSHM . . . 156
5.3.1 Dictionary learning . . . 158
5.3.2 Damage detection and localisation . . . 161
5.4 Experimental setup . . . 162
5.5 Experimental results of the proposed technique . . . 163
5.5.1 Simulated damage cases . . . 163

5.5.2 Impact damage cases . . . 172

5.5.3 SHM results considering boundary reflections . . . 177

5.5.4 SHM results considering structural complexities . . . 182

5.6 Summary . . . 187

**6 A data-driven approach for failure prognostics of engineered structures 189**

6.1 Introduction . . . 189

6.2 Literature review . . . 190

6.2.1 Vector autoregressive model for failure prognostics . . . 190

6.2.2 Survival analysis combined with sensor signal forecasting . . . 191

6.3 Methodology . . . 192

6.3.1 Research framework . . . 192

6.3.2 Cox proportional hazards model with time-varying covariates . . . 193

6.3.3 Similarity matching of generated reliability indices . . . 195

6.3.4 Vector autoregressive models with exogenous variables (VARX) . . . 197

6.3.5 Conditional Granger causality (CGC) . . . 199

6.3.6 Grey model with Fourier series calibration (FGM) . . . 200

6.4 Case study: CMAPSS dataset . . . 202

6.4.1 Data sources . . . 202

6.4.2 Data pre-processing . . . 203

6.4.3 Implementation of the proposed method . . . 203

6.4.4 Fitting results of Cox proportional hazards model . . . 206

6.4.5 Results of similarity matching of reliability indices . . . . . 207

6.4.6 VARX fitting results . . . . . 207

6.4.7 Fitting and prediction of the FGM . . . . . 210

6.4.8 Results on the RUL prediction of turbofan units . . . . . 211

6.5 Summary . . . . . 213

**7 Conclusions and future directions** **214**

7.1 Conclusions . . . . . 214

7.2 Future work . . . . . 217

**Bibliography** **218**

**A Copyright permission** **253**

# List of Tables

1.1 Comparisons between the NDE and the SHM. . . . . 4

3.1 The CUSUM algorithm [138] for segmentation of guided wave signals. . . . . 57

3.2 Detailed information of the Coupon 1 and Coupon 2 . . . . . 60

3.3 Material properties for generating dispersion curves of Coupon 2. . . . . 62

3.4 ADF test result on a pristine signal of path 1-4, Coupon 1. . . . . 63

3.5 ADF test result on the entire measurements of Coupon 1. . . . . 64

3.6 ADF test result on the entire measurements of Coupon 2. . . . . 64

3.7 AR characteristic roots of path 1-4, Coupon 1 under pristine state . . . . . 67

3.8 ADF test result on compressed pristine signals of path 1-4, Coupon 1. . . . . 78

3.9 ADF test result on the entire compressed measurements of Coupon 1 with varying compression ratios. . . . . 78

3.10 ADF test result on the entire compressed measurements of Coupon 2 with varying compression ratios. . . . . 79

3.11 AR characteristic roots of compressed signals from path 1-4, Coupon 1 under pristine state. . . . . 81

3.12 $p$-values of J-B tests on AR residuals of compressed measurements from Coupon 1 and 2 . . . . . 83

3.13 Damage detection performance of Coupon 1 utilising AR residual integrated with different signal compression approaches. . . . . 86

3.14 Damage detection performance of Coupon 2 utilising AR residual integrated with different signal compression approaches. . . . . 86

3.15 Computation time of the AR-based approach for Coupon 1 and 2$*$. . . . . 93

4.1 Damage detection performance of the different baseline-free techniques for simulated damages under 20°C variations. . . . . 130

4.2 Damage detection performance of the different baseline-free techniques for impact damages under 10°C variations. . . . . 135

5.1 Localisation results for single simulated damages under temperature variations. . 166

5.2 Damage detection results for impact damages under temperature variations. . . 173

5.3 Localisation results for single impact damages under temperature variations. . . 176

5.4 Signal reconstruction performance and damage localisation accuracy of the proposed technique utilising the three dictionary generation strategies. . . . . 186

6.1 Fitting results of the Cox PHM with time-varying covariates based on the run-to-failure records of training set units. [36] . . . . . 207

6.2 Comparisons between the RMSE calculated by the proposed approach and other papers. [36] . . . . . 213

# List of Figures

1.1 Number of maintenance-related accidents and serious incidents within 2003-2017: (a) by year; (b) by country. [1] . . . . . 3

1.2 The entire PHM process. [21] . . . . . 6

2.1 An assumed homogeneous and isotropic plate with propagating guided waves, adapted from [39]. . . . . 12

2.2 Wave displacements of Lamb waves: (a) symmetric $S_0$ modes; (b) anti-symmetric $A_0$ modes. [15] . . . . . 14

2.3 Lamb wave dispersion curves of a traction-free aluminium plate: (a) phase velocity curves; (b) group velocity curves. The figure is adapted from [38]. . . . . 18

2.4 DuraAct piezoceramic transducers manufactured by the PI ceramics. . . . . 19

2.5 Transducer configurations particularly with piezoelectric wafers: (a) pitch-catch configuration; (b) pulse-echo configuration; (c) thickness mode; (d) passive sensing manner. Adapted from [40]. . . . . 21

2.6 E/M impedance for reproducibility check of mounted transducers on an impacted composite panel. [48] . . . . . 22

2.7 Sliding window techniques with (a) non-overlapping windows; (b) overlapping (rolling) windows. . . . . 26

2.8 The TOF triangulation approach for damage localisation.Adapted from [39]. . . 33

2.9 The TDOA approach for damage localisation. Adapted from [67]. . . . . 34

2.10 Elliptical distribution for imaging pixels. Adapted from [16]. . . . . 36

2.11 A basic illustration of the C-Scan transducer [73]. . . . . 37

3.1 50 kHz $A_0$ guided wave signal with the sampling frequency as 60 MS/s . . . . . 53

3.2 Proposed baseline-based method for damage detection and localisation. . . . . 58

3.3 CUSUM-based temporal segmentation on example Lamb wave tone bursts, including within the first wave packet. . . . . 59

3.4 Illustration of two CFRP coupons with mounted PZT transducers: (a) Coupon 1 with a diamond PZT array; (b) Coupon 2 with a rectangular PZT array. . . . 59

3.5 Group velocity estimation of 50kHz, $A_0$ Lamb wave mode for: (a) Coupon 1 under 25°C and (b) Coupon 2 under 20°C. . . . . 62

3.6 Dispersion curves of Coupon 2 in 0°: (left) group velocity curves; (right) phase velocity curves. . . . . 62

3.7 Lag order selection of AR models on a pristine signal of path 1-4, Coupon 1 utilising: (a) AIC; (b) BIC; (c) RMSE. . . . . 65

3.8 Lag order selection of AR models on pristine and damaged measurements of Coupon 1 utilising AIC, BIC, RMSE. . . . . 66

3.9 Lag order selection of AR models on pristine and damaged measurements of Coupon 2 utilising AIC, BIC, RMSE. . . . . 66

3.10 Diagnostics of the AR model on a pristine signal of path 1-4, Coupon 1: (a) *Q-Q* plot of the AR residual; (b) autocorrelation plot of the AR residual where the blue shaded area represents 95% confidence interval of the autocorrelation. . . . 67

3.11 Diagnostics of the AR model on a pristine signal of path 1-7, Coupon 2: (a) $Q$-$Q$ plot of the AR residual; (b) autocorrelation plot of the AR residual where the blue shaded area represents 95% confidence interval of the autocorrelation. . . . 68

3.12 Damage detection results of simulated damages on Coupon 1 under 25°C: (a) AR residual, $DI_1$; (c) AR residual, $DI_2$; (e) standard RAPID; (b, d, f) the corresponding zoomed view under pristine state. . . . . 69

3.13 Average imaging results of four simulated damages on Coupon 1. . . . . 70

3.14 Comparisons between the AR-based methods and the standard RAPID regarding the localisation errors for overall ten damages on Coupon 1 under 25°C. . . . . 71

3.15 Damage detection results of the 20 J impact damage on Coupon 2 under 20°C : (a) AR residual, $DI_1$; (c) AR residual, $DI_2$; (e) standard RAPID; (b, d, f) the corresponding zoomed view under pristine state. . . . . 72

3.16 Average imaging results of the 20 J impact damage on Coupon 2. . . . . 73

3.17 Lamb wave tone bursts of path 1-3, Coupon 2 under 20°C : (a) 3 cycle signal; (b) 5-cycle signal; (c) 8-cycle signal. The signal overlapping between first wave packets and boundary reflections are marked by red dashed areas. . . . . 74

3.18 Damage detection results of Coupon 1 under 25°C based on $DI_1$, AR residuals and: (a) 3-cycle signals; (c) 5-cycle signals; (e) 8-cycle signals; (b, d, f) the corresponding zoomed view under pristine state. . . . . 74

3.19 Comparisons between localisation errors of overall ten damages on Coupon 1 utilising the $DI_1$ on AR residuals with $3, 5, 8$ cycles. . . . . 75

3.20 Damage detection results of Coupon 2 under 20°C based on $DI_1$, AR residuals and: (a) 3-cycle signals; (c) 5-cycle signals; (e) 8-cycle signals; (b, d, f) the corresponding zoomed view under pristine state. . . . . 76

3.21 Average damage imaging results of Coupon 2 under 20°C based on $DI_1$, AR residuals and Lamb wave signals of $3, 5, 8$ cycles. . . . . 76

3.22 Adaptively compressed pristine signals (first wave packets) from path 1-4, Coupon 1 with colmpression ratios as: (a)1:50; (b)1: 100; (c) 1: 200; (d)1:500 . . . . . 79

3.23 Lag order selection of AR models on the entire compressed measurements of Coupon 1 utilising AIC, BIC, RMSE. . . . . 80

3.24 Lag order selection of AR models on the entire compressed measurements of Coupon 2 utilising AIC, BIC, RMSE. . . . . 81

3.25 Diagnostics of the AR model on a pristine signal of path 1-4, Coupon 1: (a, b) the residual Q-Q plot and residual autocorrelation of uncompressed signal respectively; (c, e, g, i) the residual Q-Q plots of compressed measurements with compression ratios as 1:50,1:100,1:200,1:500 respectively; (d, f, h, j) the corresponding residual autocorrelations of compressed measurements. The blue shaded area represents 95% confidence interval of the autocorrelation. . . . . 82

3.26 Damage detection results of simulated damages on Coupon 1 utilising the proposed AR residual and the adaptive signal compression with compression ratios as: (a) 1 : 50; (c) 1 : 100; (e) 1 : 200; (g) 1 : 500; (b, d, f, h) the corresponding zoomed view under pristine state. . . . . 84

3.27 Damage detection results of the impact damage on Coupon 2 utilising the proposed AR residual and the adaptive signal compression with compression ratios as: (a) 1: 50; (c) 1: 100; (e) 1: 200; (g) 1: 500; (b, d, f, h) the corresponding zoomed view under pristine state. . . . . 85

3.28 Average imaging results of a simulated damage on Coupon 1 based on the AR residual and varying signal compression techniques. . . . . 87

3.29 Localisation errors of overall ten simulated damages on Coupon 1 utilising the AR residual, varying signal compression techniques. . . . . 88

3.30 Average imaging results on the impact damage on Coupon 2 based on the AR residual and varying signal compression techniques. . . . . 89

3.31 Damage detection results of Coupon 1 based on AR residuals and 1 : 100 compressed measurements of: (a) 3 cycles; (c) 5 cycles; (e) 8 cycles; (b, d, f) the corresponding zoomed view under pristine state. . . . . 90

3.32 Localisation errors of overall ten damages on Coupon 1 based on AR residuals and 1 : 100 compressed measurements of 3,5,8 cycles. . . . . 91

3.33 Damage detection results of Coupon 2 based on AR residuals and 1 : 100 compressed measurements of: (a) 3 cycles; (c) 5 cycles; (e) 8 cycles; (b, d, f) the corresponding zoomed view under pristine state. . . . . 92

3.34 Average damage imaging results of Coupon 2 based on AR residuals and 1 : 100 compressed measurements of 3, 5, 8 cycles respectively. . . . . 92

4.1 Standard time-reversal (TR) procedures. [177] . . . . . 99

4.2 Different time-reversal schemes: (a) the standard time reversal process; (b) the modified time reversal (MTR) process proposed by [204]; (c) the virtual time reversal (VTR) process [203]. Adapted from [203]. . . . . 101

4.3 Frequency shift of response signals compared to 100kHz excitation signals due to the transducer tuning effects [205]. . . . . 103

4.4 Baseline-free damage localisation based on the reciprocity-based approach for (a) circular transducer array; (b) helical transducer array. [217] . . . . . 108

4.5 Effect of temperature variations on time reversibility of Lamb waves in a 3-mm aluminium plate: (a) experiment; (b) $2D$ FE simulation. [245] . . . . . 114

4.6 Damage localisation results of a 2 mm-thick aluminium plate. The two rows (from top to bottom) represent the standard VTR and the proposed method with transfer function compensation respectively. The three columns represent the damage imaging results based on $S_0$, $A_0$ and the modal fusion respectively. [205] 116

4.7 Damage imaging result of two damages in a 3 mm-thick aluminium plate. The result is obtained by the RTRM with the best reconstruction frequency of excitation signals. [206] . . . . . 117

4.8 400 mm × 400 mm CFRP coupon with simulated putty damages. [35] The 12 mounted PZT transducers are arranged in a circular configuration. . . . . 119

4.9 Real part impedance of the 12 mounted transducers. . . . . 120

4.10 Damage detection results of simulated damages at 20°C based on: (a) reciprocity-based approach; (c) IB technique; (e) VTR technique; (b, d, f) the corresponding zoomed views under intact state. . . . . 121

4.11 Images of simulated single damages on the 12-sensors coupon at 20°C. Red circles represent true damage areas and black crosses denote estimated damage locations. [35] . . . . . 123

4.12 Localisation error, $\varepsilon_d$, of the 10 simulated single damages utilising the IB, reciprocity-based and the VTR techniques. [35] . . . . . 124

4.13 Imaging results of simulated dual damages on the 12-sensors coupon at 20°C. Red circles represent true damage areas and black crosses denote estimated damage locations. [35] . . . . . 125

4.14 The CFRP composite plate with 9 mounted PZT sensors. The impact damages are located within the red areas. . . . . 127

4.15 Real part impedance of the 9 mounted transducers prior to (left) and after (right) the first impact. . . . . 127

4.16 Damage detection results of impact damages at 20°C based on: (a) reciprocity-based approach; (c) IB technique; (e) VTR technique; (b, d, f) the corresponding zoomed views under intact state. . . . . 128

4.17 Average imaging results of the single impact damage $D_1$ under 20°C, based on: (a) IB technique; (b) Reciprocity-based technique; (c) VTR technique. Red circles represent the true damage areas while the black crosses denote the estimated damage locations. . . . . 129

4.18 Average imaging results of dual impact damages under 20°C, based on: (a) IB technique; (b) Reciprocity-based technique; (c) VTR technique. . . . . 129

4.19 Damage detection results of simulated damages under 20°C variations based on: (a) reciprocity-based approach; (c) IB technique; (e) VTR technique; (b, d, f) the corresponding zoomed views under intact state.The horizontal dashed line represents the calibrated detection threshold. . . . . 131

4.20 Imaging results of single simulated damage on the 12-sensors coupon utilising VTR, reciprocity-based and the IB techniques. The imaging results are obtained under 20°C, 30°C and 40°C. [35] . . . . . 132

4.21 Comparisons between the IB, Reciprocity and VTR on localisation errors of single simulated damages under 20°C to 40°C with a 5°C gradient. Adapted from [35] since the error bars in this figure are calculated based on standard errors of localisation errors, which can reflect variations between damages at different locations, rather than the 95% confidence interval of localisation errors, which is used in [35]. . . . . 133

4.22 Damage detection results of impact damages under 10°C variations based on: (a) reciprocity-based approach; (c) IB technique; (e) VTR technique; (b, d, f) the corresponding zoomed views under intact state. . . . . 134

4.23 Imaging results of single impact damage on the 9-sensors coupon utilising VTR, reciprocity-based and the IB techniques. The imaging results are obtained under 20°C, 25°C and 30°C. . . . . 135

4.24 Comparisons between the IB, Reciprocity and VTR on localisation errors of single impact damages under 20°C, 25°C, 30°C. . . . . 136

4.25 Damage detection results of the impact damage on Coupon 2 at 20°C utilising: (a) reciprocity-based approach; (b) IB technique; (c) VTR technique. The horizontal dashed line represents the calibrated detection threshold. . . . . 137

4.26 Damage images of the Coupon 2 when utilising the virtual time reversal (VTR) technique together with: (a) damaged signals; (b) intact signals both in baseline-free manners. . . . . 138

4.27 50kHz tone burst responses from the Coupon 2: (a) path 1-2 with the overlapping part (red dashed area); (b) reconstruction of the input excitation signal for path 1-2; (c) path 1-4 with the overlapping part (red dashed area); (d) reconstruction of the input excitation signal for the path 1-4. . . . . 139

4.28 Damage imaging results of the Coupon 2 when following the reciprocity principle together with: (a) damaged signals; (b) intact signals both in baseline-free manners. 140

4.29 Damage imaging results of the Coupon 2 when utilising the instantaneous baseline (IB) approach together with: (a) damaged signals; (b) intact signals both in baseline-free manners. . . . . 140

4.30 Stiffened CFRP panel for investigations on baseline-free techniques: (a) the CFRP panel jointed by omega stiffeners and three impact damages within the red circles; (b) sensing network after removal of indirect transducer paths. . . . . 141

4.31 Damage detection results of impact damages on stiffened panel at 27°C based on: (a) reciprocity-based approach; (c) IB technique; (e) VTR technique; (b, d, f) the corresponding zoomed views under intact state. . . . . 142

4.32 Average imaging results on stiffened composite panel based on the IB technique: (a-c) full-scale, upper part and lower part imaging results utilising damaged measurements; (d-f) full-scale, upper part and lower part imaging results calibrated by intact measurements in baseline-free manners. . . . . 145

4.33 Average imaging results on stiffened composite panel based on the VTR technique: (a-c) full-scale, upper part and lower part imaging results utilising damaged measurements; (d-f) full-scale, upper part and lower part imaging results calibrated by intact measurements in baseline-free manners. . . . . 146

4.34 Figure 4.34. Imaging results of reciprocity principle on the stiffened composite panel based on the average of ten damaged measurements: (a-c) full-scale, upper part and lower part imaging results utilising damaged measurements; (d-f) the corresponding imaging results calibrated by intact measurements in baseline-free manners. . . . . 147

5.1 Extraction of a representative shapelet (Red) matched to its counterpart (Yellow) in a first wave packet (Blue). . . . . 153

5.2 Schematic sketch of the proposed methodology for unsupervised damage detection and localisation. . . . . 157

5.3 Illustration of dictionary learning approach. . . . . 159

5.4 Generation of shift-invariant dictionary with shapelet features. . . . . 160

5.5 Unsupervised shapelet features generated from the intact quasi-isotropic $M21-T800S$ coupon under 25°C. . . . . 162

5.6 Average reconstruction error $\varepsilon$ with different $k_c$ values. . . . . 164

5.7 $HI$ values under temperature variations: (a) for the entire monitoring history; (b) under intact state only. . . . . 165

5.8 Comparisons between the IB, reciprocity-based, VTR and the proposed shapelet-based approach when localising single simulated damages. . . . . 167

5.9 Single damage scenario $S\boldsymbol{C1}$ under 20°C: (a) damage imaging results;(b) $DI$ histograms with reciprocal paths ignored. . . . . 167

5.10 Damage scenario $\boldsymbol{SC1}$ under temperature variations: (a,c,e) damage imaging results under 20°C, 30°C, 40°C; (b,d,f) the corresponding distribution of $DI$ values. . . . . 168

5.11 Dual damage scenario $\boldsymbol{SC2}$ under temperature variations: (a,c,e) imaging results under 20°C, 30°C, 40°C;(b,d,f) the corresponding distribution of $DI$ values. . . . 170

5.12 Dual damage scenario $\boldsymbol{SC3}$ under temperature variations: (a,c,e) imaging results under 20°C, 30°C, 40°C;(b,d,f) the corresponding distribution of $DI$ values. . . . 171

5.13 Signal reconstruction for the single damage scenario $\boldsymbol{SC1}$: (a) damaged path $1-6$; (b) damaged path $2-10$; (c) undamaged path $2-4$; (d) undamaged path $3-7$. "$A$" and "$S$" represent the actuator and sensor respectively. . . . . 172

5.14 Investigation on impact damages: (a) a $M21-T800S$ coupon with two BVIDs; (b) the test coupon fixed to the drop tower. . . . . 173

5.15 $HI$ values for impact damages under temperature variations: (a) the entire monitoring history; (b) a zoomed view of the intact state. . . . . 174

5.16 Detection and localisation of the single damage $D_1$ under 20°C, 25°C, 30°C (from top to bottom): (a, d, g) damage imaging map; (b, e, h) $DI$ distribution and (c, f, i) $DI$ histograms with reciprocal paths and indirect paths ignored. . . . . 174

5.17 Comparisons between the IB, reciprocity-based, VTR and the proposed shapelet-based approach when localising single impact damages. . . . . 175

5.18 Dual damages $D_1$, $D_2$ under 20°C, 25°C, 30°C (from top to bottom): (a, d, g) damage imaging map; (b, e, h) $DI$ distribution and (c, f, i) $DI$ histograms with reciprocal paths and indirect paths ignored. . . . . 176

5.19 Dispersion removal on 50kHz guided wave tone bursts from the 300 mm×225 mm CFRP coupon at 20°C : (a) signal from transducer path 1-8 before and after the dispersion removal; (b) time-frequency presentation of raw signal from path 1-8; (c) time-frequency presentation of dispersion-removed signal from path 1-8; (d-f) the corresponding results for path 2-5. . . . . 179

5.20 Dispersion removal on 50kHz guided wave tone bursts from the 300 mm×225 mm CFRP coupon at 20°C : (a) signal from transducer path 1-2 before and after the dispersion removal; (b) time-frequency presentation of raw signal from path 1-2; (c) time-frequency presentation of dispersion-removed signal from path 1-2; (d-f) the corresponding results for path 5-7. . . . . 180

5.21 Damage detection results of the 20 J BVID at 20°C utilising the proposed baseline-free technique: (a) before dispersion removal; (c) after dispersion removal. The horizontal dashed line represents the calibrated detection threshold. 181

5.22 Damage localisation of the 20 J BVID at 20°C utilising the proposed baseline-free technique: (a, b) average damage images before and after dispersion removal respectively; (c, d) the corresponding damage index (DI) values with indirect reciprocal paths ignored. The horizontal dashed line represents the calibrated detection threshold. . . . . 182

5.23 Composite structures with increasing structural complexities. . . . . 183

5.24 Damage detection results of impact damages on stiffened panel based on the proposed method: (a) the entire monitoring history; (b) the corresponding zoomed view under intact state. . . . . 183

5.25 Damage detection and localisation of the stiffened panel based on the proposed technique: (a) the distribution of $DI$ values for the upper panel under intact and damaged conditions; (b) imaging of the first impact damage within the upper panel; (c) imaging of the first impact damage calibrated by intact measurements; (d-f) the corresponding results of the second impact damage within the lower panel. . . . . 184

6.1 Schematic sketch of the algorithm proposed in this research. [36] . . . . . 193

6.2 Illustration of the similarity matching process of reliability indices. [36] . . . . . 196

6.3 Inner structure of the turbofan employed in the C-MAPSS data sets. [36] . . . . 202

6.4 Statistical causal graphs of units in FD001 training set generated by the CGC test. [36] . . . . . 206

6.5 Similarity matching between the incomplete reliability index of the $37th$ unit in the test set and the complete reliability index of the (a) 45th (b) $28th$ (c) $98th$ (d) $93rd$ (e) $61st$ units as the five most similar reliability indices of units in the run-to-failure training set. The similarity decreases with the figure order. [36] . . 208

6.6 Box plot of the RMSE and the NRMSE of the in-sample fitting of the VARX models based on training set units. [36] . . . . . 209

6.7 In-sample fitting of (a) the first and (b) the second operational conditions of the unit 37 in FD001 test sets based on the FGM(1, 1) and ARIMA/ARMA calibration. [36] . . . . . 210

6.8 Out-of-sample prediction of (a) the first and (b) the second operational conditions of the unit 37 in FD001 test sets based on the FGM(1, 1) and ARIMA/ARMA calibration. [36] . . . . . 210

6.9 Predictions of the (a) incomplete reliability index and (b) reliability function of the test set unit 37th considering its five most similar reliability indices of the training set units. The online prediction of the reliability index for the unit $37th$ in the test set is updated by future values of the external operational conditions which are predicted by means of the FGM model. [36] . . . . . 212

6.10 Comparision between the actual RULs and their prediction values. [36] . . . . . 212

# Chapter 1

# Introduction

## 1.1 Background

Aircraft maintenance, as emphasized by regulatory bodies such as the European Aviation Safety Agency (EASA) since 2015 [1], stands as a cornerstone in ensuring the airworthiness of aircraft. This fundamental objective is pivotal for fostering safe, reliable, and functional aircraft operation under predefined working conditions [2]. The significance of adhering to proper maintenance procedures cannot be overstated, as lapses or inadequacies in maintenance schedules can precipitate serious incidents or accidents, with far-reaching societal, engineering, and economic ramifications, including [1] loss of life, grave injuries, and structural failures (e.g., latest failure of emergency exit of Boeing 737 Max [3]).

In light of recent investigations, exemplified in Fig. 1.1, spanning the period from 2003 to 2017, a staggering total of 112 maintenance-related accidents and serious incidents [1] were documented, attributing damages and structural failures to main aircraft components such as landing gears, power engines, fuselage, and wing structures [4]. Alarmingly, the majority of these incidents were traceable to insufficient or erroneous maintenance practices, exacerbated by the failure to promptly detect and rectify defects in aircraft structures [1]. This demonstrates the critical need for deploying advanced inspection and monitoring techniques to bolster the efficacy and integrity of maintenance protocols.

In tandem with international standards and directives, the Federal Aviation Administration (FAA) [5] of the United States issues guidelines and regulations that parallel the efforts of EASA in ensuring comprehensive aircraft maintenance practices. The FAA's directives, encapsulated in various advisory circulars, airworthiness directives, and regulatory requirements, [6] outline stringent protocols for aircraft maintenance, encompassing routine inspections, component replacements, and compliance checks with manufacturer specifications and service bulletins.

For instance, FAA Advisory Circular AC 43.13-1B [7] provides comprehensive guidance on acceptable methods, techniques, and practices for aircraft inspection, repair, and alteration. Moreover, FAA Advisory Circular AC 120-17B [8] delineates the framework for developing aircraft maintenance programs, emphasizing the importance of systematic approaches to maintenance planning, execution, and oversight to uphold operational safety and airworthiness.

Furthermore, in alignment with EASA's objectives, the FAA encourages the integration of advanced inspection and monitoring technologies into aircraft maintenance regimes [9]. By leveraging state-of-the-art tools and methodologies, such as structural health monitoring systems, non-destructive testing techniques, and condition-based maintenance strategies, aviation stakeholders can proactively identify potential structural anomalies and defects, thereby preempting safety hazards and optimizing maintenance resource allocation.

In essence, by harmonizing with both EASA guidelines and FAA directives, aviation authorities and industry practitioners can fortify aircraft maintenance frameworks, thereby fostering a culture of safety, reliability, and continuous improvement in the global aviation ecosystem. Through collaborative efforts and adherence to best practices, the aviation community aims to uphold the highest standards of airworthiness and operational excellence, ensuring the safe and sustainable advancement of air transportation worldwide.

During the past decades, non-destructive evaluation (NDE) has been widely adopted for the structural integrity inspection on engineering structures including the aircraft components. The NDE aims to process and analyse measurements from structures manually inspected with non-destructive testing (NDT) techniques, which include but are not limited to [10] ultrasonic testing, radiography, magnetic particle inspection, and liquid penetrant testing. In common practice, the non-destructive inspection is implemented on dismantled aircraft components with

removable instruments [11, 12] and usually requires accessible inspected structures during their downtime [12]. Such prerequisites restrict the NDE to an intermittent and preventive implementation [11] at fixed time intervals, rendering it time-consuming and expensive for grounded industrial applications.

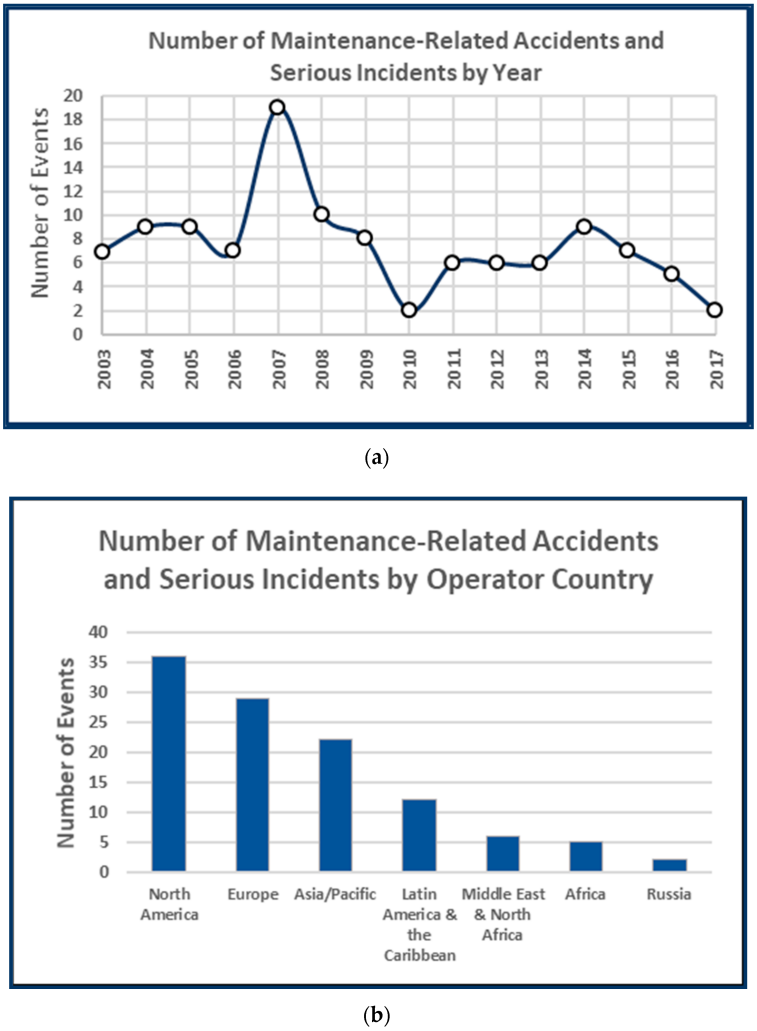


Figure 1.1: Number of maintenance-related accidents and serious incidents within 2003-2017: (a) by year; (b) by country. [1]

Recently, structural health monitoring (SHM) has been emerging as a technical landscape for structure integrity monitoring on aircraft structures. The SHM aims to interrogate the health condition of aircraft components based on transducer data while identifying, localising and characterising (if available) potential damages [13]. A promising application of the SHM in this domain is the diagnosis of Barely Visible Impact Damage (BVID) on composite fuselage manufactured of the Carbon Fibre Reinforced Polymer (CFRP) materials [14], where the impact damage could cause the delamination [12–14] and the reduction in compressive strength of the

composite laminates. Within such a scenario, the monitoring process can be implemented by surface-mounted piezoelectric transducers actuating ultrasonic guided waves and receiving the structural response of monitored components [15], whereas the detection and localisation of potential damages is established by subtraction between the collected response and pre-recorded intact measurements [16], i.e., baselines, of the same monitored structure.

Albeit employing several NDT techniques, e.g., ultrasonics [14,17], radiography [17], one main characteristic of the SHM, compared to the NDE, is the continuous monitoring on inspected structures with perpetually mounted or embedded transducers during the entire life cycle [11, 12]. Such a configuration not only reduces unnecessary preventive maintenance schedules, but also empowers a condition-based maintenance scheme by facilitating the maintenance staff with a comprehensive perspective of how the performance of aircraft structures evolve [11] in comparison with their past operational histories. The SHM also supports self-governing and remote monitoring of aircraft structures without the need for human intervention [12, 18]. A brief comparison between the NDE and the SHM is summarised in Table 1.1.

Table 1.1: Comparisons between the NDE and the SHM.

| | NDE | SHM |
|---|---|---|
| Frequency of operation | Intermittent | Continuous |
| Removable instruments for inspection/monitoring | Yes | No |
| Maintenance schemes | Preventive | Condition-based |
| Automatic operation | No | Yes |
| Human intervention for inspection/monitoring | Yes | No |

Typical SHM systems primarily focus on the in-situ detection and monitoring of the existing defects or faults, which are succeeded by condition-based maintenance schemes. However, insufficient attention has been paid to long-term degradation or deterioration in structural and mechanical performance of monitored structures due to factors including ageing, wearing, and the existence of damage. In order to minimise maintenance costs and prolong service

life of engineered systems, it is necessary to trace and prognose the degradation behaviour of system components based on real-time monitoring data so that any degraded components can be repaired or replaced timely prior to their end of service life and great losses of functionality. Such rationale has been recently pursued as a further goal for SHM [13]; that being said, the main attention currently remains at lower levels of SHM [19] including the damage detection, localisation and characterisation.

In comparison to SHM, prognostics and health management (PHM) provides a higher-level framework containing similar procedures but more emphasis on the prognostic assessment on engineering structures. The PHM prioritises the forecast on remnant life or the remaining useful life (RUL) [20] of aircraft components and exploits the estimated RUL information for flexible and efficient maintenance on aircraft structures. As shown in Fig. 1.2, the entire PHM process includes the data collection and pre-processing, the damage detection and isolation, the RUL prediction for failure prognostics, and the RUL-based maintenance decisions by the maintenance staff [21]. Regarding the prognostics stage, various approaches including the physics-based, statistical and machine learning (ML) based techniques [22] have been developed to enhance the accuracy of RUL estimates and consequently the efficiency of maintenance plans.

SHM and PHM are empowered with monitoring data but also encountered with several common challenges towards an effective and efficient health assessment on monitored structures. Firstly, measurements with unnecessarily high sampling frequencies are usually obtained during the data acquisition procedure, yielding heavy hardware burdens when storing, transmitting and processing the high volume of data. Such data deluge [23] also poses challenges when exploiting signal processing techniques to well distinguish and isolate the damage sensitive features from a plethora of irrelevant features. Moreover, the monitoring data is inevitably susceptible to uncertainties induced by environmental and operational variations (EOV) and measurement noises. A typical instance in the SHM domain is that the ultrasonic guided waves vary in both amplitude and phase under varying temperature and loading conditions [24]. Such variations can lead to signal distortions which mask the existence of damage-sensitive features, and consequently affect an accurate assessment and projection on the structural health.

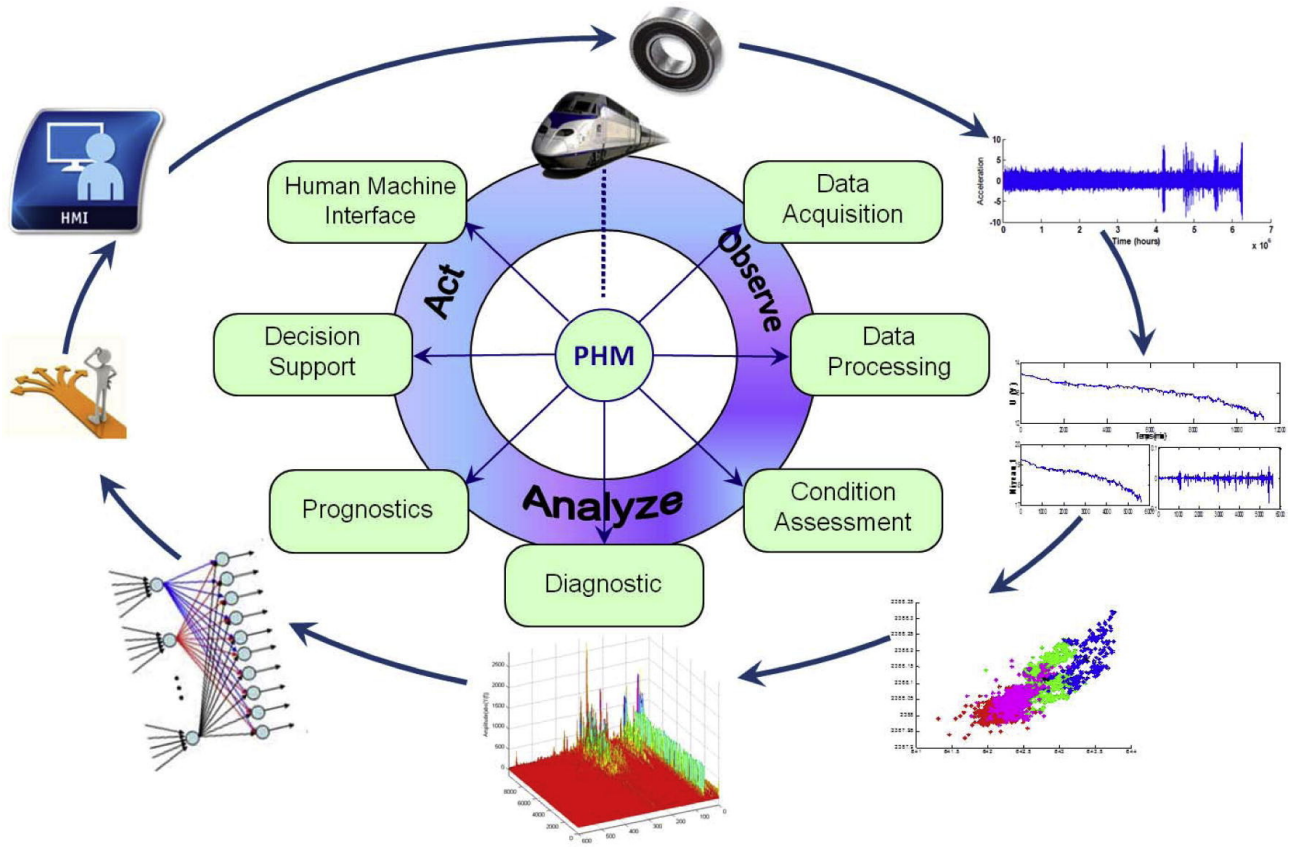


Figure 1.2: The entire PHM process. [21]

## 1.2 Motivation

This thesis aims to empower data driven perspectives into SHM and PHM on aircraft structures, which include damage detection, localisation on CFRP composite panels and failure prognostics, i.e., RUL prediction, on aircraft turbofan engines. The thesis is motivated by several existing challenges for SHM and PHM, and the motivations are listed as follows.

- **Processing of real-time monitoring data:** In practical engineering applications, the data acquisition of SHM and PHM can involve real-time transducer measurements with unnecessarily high sampling frequencies [25, 26]. The high-volume and oversampled monitoring data can incur indispensable computational time and biased estimates [27] when being directly inputted to developed statistical or ML-based models for the extraction of damage sensitive features. Such issues can be greatly alleviated if adopting proper signal processing techniques.

- **Baseline-dependent guided wave structural health monitoring (GWSHM) with effective damage sensitive features:** The baseline-dependent approach [16] for the GWSHM relies on the disparity between damaged measurements and intact baselines to unveil the existence of damages, e.g., BVID, within the monitored structures. One widely used technique in this branch is the reconstruction algorithm for probabilistic inspection of defects (RAPID) [16], where the simple Pearson correlation [28] between damaged and baseline measurements is employed as a sensitive feature to potential damages. Recently increasing attention has been paid to developing statistical or ML based damage sensitive features and their integration with the RAPID technique to improve performance for damage detection and localisation, whereas a representative example is the utilisation of autoregressive (AR) features for damage detection on metallic plates or quasi-isotropic composite structures [29–33]. However, few research in this realm has been extended to more complicated tasks including both damage detection and localisation on anisotropic composite structures. Moreover, the estimation of AR features based on oversampled guided wave measurements should be carefully investigated to circumvent high computational costs and model biases.
- **Reference-free GWSHM on anisotropic composite structures:** Baseline-free GWSHM techniques, which detect and localise damages without the need for baseline data, are essential considering the limited availability and quality of baselines under some circumstances [13]. Despite the recent developments in such field, there is a lack of comprehensive comparisons between baseline-free techniques considering various factors including material anisotropy, multiple damages, temperature variations, geometrical and structural complexities of the monitored structures. Moreover, it is worth developing novel baseline-free techniques which are competent to extract damage sensitive features while simultaneously overcoming limitations of the existing baseline-free techniques.
- **RUL prediction of aircraft components:** The remnant life prediction can provide useful information for an effective maintenance and health management on aircraft components [20], e.g., turbofan engine, but could be affected by incomplete monitoring records, varying environmental and operational conditions (EOC), and the lack of understanding

on cause-effect failure mechanisms of monitored components. Such factors need to be taken into consideration when developing effective RUL prediction techniques.

## 1.3 Thesis outline

This thesis focuses on the GWSHM and PHM techniques for damage diagnosis and prognosis of CFRP composite panels and turbofan engines, respectively, based on real-time monitoring data.

**Chapter 2** introduces fundamentals of the GWSHM including the propagation of guided waves, transducers for actuating and receiving guided waves, together with the guided wave based damage detection and localisation. The PHM is also introduced with particular emphasis on several critical concepts, e.g., RUL, and critical factors for the failure prognostics.

**Chapter 3** proposes a data-driven approach integrating the statistical autoregressive (AR) model and signal compression techniques to detect and localise damages in a baseline-dependent manner. The proposed method is statistically valid and computationally efficient while yielding competent performance to monitor damages within quasi-isotropic and anisotropic composite coupons.

**Chapter 4** provides a comprehensive review of baseline-free GWSHM techniques and carries out detailed experimental comparisons between several baseline-free techniques regarding their damage detection and localisation capabilities under material anisotropy, different damage types, temperature variations, geometric and structural complexities, e.g., stiffeners.

**Chapter 5** proposes a reference-free GWSHM technique for CFRP structures based on unsupervised shapelets and shift-invariant dictionary learning. The proposed technique is data-driven and requires little prior knowledge of guided wave propagation compared to several existing baseline-free techniques. Afterwards the performance of the proposed technique for detecting and localising synthetic or real impact damages is validated through experimental investigations on anisotropic CFRP coupons and stiffened panels.

In **Chapter 6**, a hybrid data-driven approach is proposed to estimate the RUL of aircraft turbofans based on a synthetic dataset of turbofan failures. The proposed method is able to

capture the degradation behaviour of turbofan engines under time varying EOCs and yields accurate RUL estimates when compared to several statistical or ML based techniques.

Final conclusions and future directions of the PhD research are drawn in **Chapter 7**.

## 1.4 Contributions

Main contributions of this thesis and the related publications are summarised as follows.

(1) Proposed a baseline-dependent technique for damage detection and localisation on CFRP structures utilising the damage-sensitive AR features of compressed guided wave measurements.

- Hongmin Zhu, Zahra Sharif Khodaei, and M.H. Aliabadi. (2023). Investigation into autoregressive model and signal compression for damage localisation. *AIP Conference Proceedings*, 2848(1). [34]

(2) Investigated and compared several baseline-free GWSHM techniques for damage detection and localisation on anisotropic CFRP structures.

- Hongmin Zhu, Zahra Sharif Khodaei, and M.H. Aliabadi. (2024). Investigation of baseline-free techniques for damage localisation on anisotropic composite structures. *Procedia Structural Integrity*, 52, 679-689. [35]
- Hongmin Zhu, Zahra Sharif Khodaei, and M.H. Aliabadi. Appraisal of baseline-free techniques for guided wave based structural health monitoring. *Ultrasonics*. (Under review)

(3) Proposed a data-driven baseline-free technique utilising unsupervised shapelets and shift-invariant dictionary learning for damage detection and localisation on anisotropic CFRP structures.

- Hongmin Zhu, Zahra Sharif Khodaei, and M.H. Aliabadi. Baseline-free damage detection and localisation on complex composite structures using unsupervised shapelets

and shift-invariant dictionary learning. *Mechanical Systems and Signal Processing.* (Under review)

(4) Proposed a hybrid data-driven approach to the RUL prediction of turbofan engines which operate under time-varying EOCs.

- Hongmin Zhu. (2021). Real-time prognostics of engineered systems under time varying external conditions based on the COX PHM and VARX hybrid approach. *Sensors*, 21(5), 1712. [36]
- Hongmin Zhu. (2021). Investigation into real-time influence of time varying operational conditions and sensor signals on reliability of engineered systems. *Proceedings of the 31st European Safety and Reliability Conference, ESREL 2021*, 71. [37]

# Chapter 2

# Fundamentals of SHM and PHM

## 2.1 Introduction

This chapter provides an overview of the fundamental principles within both Structural Health Monitoring (SHM) and Prognostics and Health Management (PHM) frameworks. The SHM section emphasizes ultrasonic guided waves, covering aspects such as wave propagation in diverse media (i.e. isotropic and anisotropic), actuation, sensing, and processing of guided waves, with applications in damage detection and localisation. In the PHM segment, essential concepts are introduced, followed by an examination of failure prognostic approaches and the presentation of various indicators. The chapter concludes by outlining challenges associated with current prognostic approaches.

## 2.2 Ultrasonic guided waves

### 2.2.1 Guided waves in isotropic plates

The guided wave propagation within homogeneous and isotropic plates is closely related to the governing equation of wave motion [15, 38, 39], which is shown as

$$\mu u_{i,jj} + (\lambda + \mu) u_{j,ij} + \rho f_i = \rho \ddot{u}_i (i, j = 1, 2, 3) \tag{2.1}$$

In some texts, the equation (2.1) is also called the Navier's displacement equation. The term $f_i$ is signified as body force while $\rho$ denotes the mass density [15, 38, 39]. In the equation, $u_i$ represents the wave displacement in direction $i$ while $u_{i,jj}$, $u_{j,ji}$ and $\ddot{u}_l$ are expressed as [38]

$$u_{i,jj} = \frac{\partial^2 u_i}{\partial x_1^2} + \frac{\partial^2 u_i}{\partial x_2^2} + \frac{\partial^2 u_i}{\partial x_3^2} \tag{2.2}$$

$$u_{j,ij} = \frac{\partial}{\partial x_i}\left(\frac{\partial u_1}{\partial x_1} + \frac{\partial u_2}{\partial x_2} + \frac{\partial u_3}{\partial x_3}\right) \tag{2.3}$$

$$\ddot{u}_l = \frac{\partial^2 u_i}{\partial t^2} \tag{2.4}$$

where $x_1$, $x_2$, $x_3$ correspond to the three dimensions of a plate with thickness $d$ [39], which is illustrated in Fig. 2.1, and $t$ is the propagation time of guided waves. Meanwhile, $\mu$ and $\lambda$ in (2.1) represent the shear modulus and Lame constant respectively [15, 38, 39]. The Lame constant $\lambda$ is further calculated as [15, 39]

$$\lambda = \frac{2\mu\nu}{1 - 2v} \tag{2.5}$$

where $\mu$ is the same with the equation (2.1) and $v$ is the Poisson's ratio.

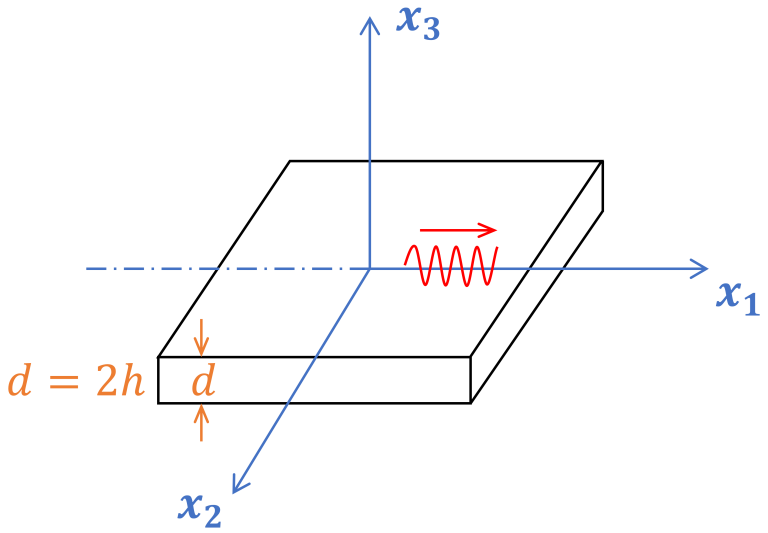


Figure 2.1: An assumed homogeneous and isotropic plate with propagating guided waves, adapted from [39].

Furthermore, it is hypothesised that the propagating guided waves are straight-crested along the $x_2$ direction [15], which indicates that the wave displacement equation is $x_2$-invariant. Plain

strain conditions [15] are also assumed so that no strains exist in the $x_2$ direction. With such assumptions, the equation (2.1) can be decomposed into the equations below based on the Helmholtz decomposition [15, 39].

$$\frac{\partial^2 \Psi}{\partial \mathrm{x}_1^2} + \frac{\partial^2 \Psi}{\partial \mathrm{x}_3^2} = \frac{1}{\mathrm{c}_\mathrm{L}^2} \frac{\partial^2 \Psi}{\partial \mathrm{t}^2} \tag{2.6}$$

$$\frac{\partial^2 \phi}{\partial \mathrm{x}_1^2} + \frac{\partial^2 \phi}{\partial \mathrm{x}_3^2} = \frac{1}{\mathrm{c}_\mathrm{T}^2} \frac{\partial^2 \phi}{\partial \mathrm{t}^2} \tag{2.7}$$

The equation (2.6) depicts propagating longitudinal waves whereas the equation (2.7) represents the governing equation of shear waves [15]. More specifically, $\psi$ and $\phi$ are wave displacement functions of the longitudinal and the shear waves respectively, while $c_L$ and $c_T$ represent velocities of the corresponding wave modes [15] and are calculated below.

$$c_L = \sqrt{\frac{\lambda + 2\mu}{\rho}}, c_T = \sqrt{\frac{\mu}{\rho}} \tag{2.8}$$

Following the equation (2.6) and (2.7), displacements and stresses of the isotropic plate are obtained as follows [38].

$$u_1 = \frac{\partial \psi}{\partial x_1} + \frac{\partial \phi}{\partial x_3} \tag{2.9a}$$

$$u_2 = 0 \tag{2.9b}$$

$$u_3 = \frac{\partial \psi}{\partial x_3} - \frac{\partial \phi}{\partial x_1} \tag{2.9c}$$

$$\sigma_{31} = \mu \left( \frac{\partial u_3}{\partial x_1} + \frac{\partial u_1}{\partial x_3} \right) = \mu \left( \frac{2\partial^2 \psi}{\partial x_1 \partial x_3} - \frac{\partial^2 \phi}{\partial x_1^2} + \frac{\partial^2 \phi}{\partial x_3^2} \right) \tag{2.9d}$$

$$\sigma_{33} = \lambda \left( \frac{\partial u_1}{\partial x_1} + \frac{\partial u_3}{\partial x_3} \right) + 2\mu \frac{\partial u_3}{\partial x_3} = \lambda \left( \frac{\partial^2 \psi}{\partial x_1^2} + \frac{\partial^2 \psi}{\partial x_3^2} \right) + 2\mu \left( \frac{\partial^2 \psi}{\partial x_3^2} - \frac{\partial^2 \phi}{\partial x_1 \partial x_3} \right) \tag{2.9e}$$

where $u_1$, $u_2$, $u_3$ denote the displacements in the $x_1$, $x_2$, $x_3$ direction and $\sigma_{31}, \sigma_{33}$ represent the corresponding stresses with the $x_2$ direction ignored. In the equation (2.9), $\sigma_{31}$ and $\sigma_{33}$ are restricted to zeros due to the top and bottom traction-free surfaces [15, 38] of the plate. Mathematically, the stresses satisfy the boundary condition below. [38]

$$\sigma_{33} = \sigma_{31} = 0 \text{ when } x_3 = \pm h \tag{2.10}$$

Simultaneously the potential solutions of equations (2.6) - (2.7) can be formulated as follows.

$$\psi = \Psi(x_3)\exp\left[i\left(kx_1 - \omega t\right)\right] \tag{2.11a}$$

$$\phi = \Phi(x_3)\exp\left[i\left(kx_1 - \omega t\right)\right] \tag{2.11b}$$

where $\exp(\cdot)$ represents the exponential function. [38]

The standing waves $\Psi(x_3)$ and $\Phi(x_3)$ then have the form as [15, 38]

$$\Psi(x_3) = A_1\sin(px_3) + A_2\cos(px_3) \tag{2.12a}$$

$$\Phi(x_3) = B_1\sin(qx_3) + B_2\cos(qx_3) \tag{2.12b}$$

where $p^2 = \frac{\omega^2}{c_L^2} - k^2, q^2 = \frac{\omega^2}{c_T^2} - k^2, k$ represents the wavenumber and $\omega$ denotes the angular frequency.

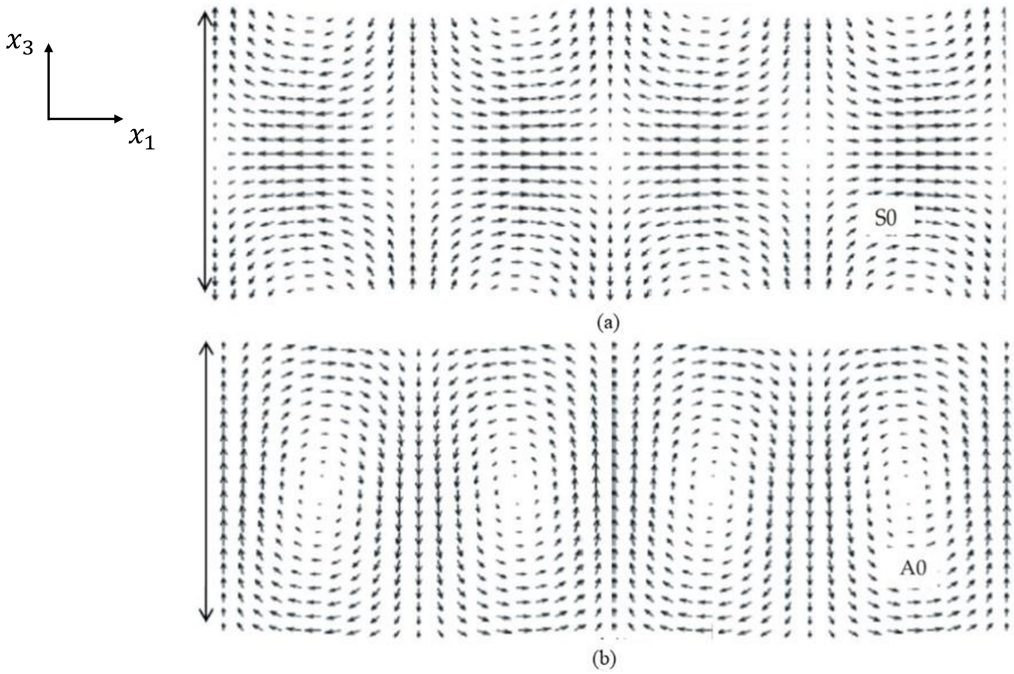


Figure 2.2: Wave displacements of Lamb waves: (a) symmetric $S_0$ modes; (b) anti-symmetric $A_0$ modes. [15]

According to the equation (2.12), symmetric (S) and anti-symmetric (A) modes of guided waves are defined by containing only sine or cosine terms in the equation. A visual representation comparing the wave displacements of the S and A modes for Lamb waves is displayed

in Fig. 2.2. Moreover, the symmetric modes indicate the cosine displacement functions in the $x_1$ direction and the sine displacement functions in the $x_3$ direction [38], and vice versa for the anti-symmetric modes. Consequently, the two wave modes differ in mathematical expressions of the displacements and stresses, thus being different when integrated with the boundary condition in equation (2.10). As an example, for the symmetric modes it is inferred from equation (2.12) that $\Psi(x_3) = A_2 \cos(px_3), \Phi(x_3) = B_1 \sin(qx_3)$. When plugging such equation and (2.9) into (2.10), it is obtained that [38]

$$\frac{\tan(qd)}{\tan(pd)} = \frac{4k^2qp\mu}{(\lambda k^2 + \lambda p^2 + 2\mu p^2)(k^2 - q^2)} \tag{2.13}$$

By integrating equation (2.8) into (2.9), the following equation is yielded [15, 38, 39].

$$\frac{\tan(qd)}{\tan(pd)} = -\frac{4k^2pq}{(k^2 - q^2)^2} \tag{2.14a}$$

Similarly, the equation (2.14b) is derived for the anti-symmetric wave modes.

$$\frac{\tan(qd)}{\tan(pd)} = -\frac{(k^2 - q^2)^2}{4k^2pq} \tag{2.14b}$$

The equation (2.14) is also presented as the Rayleigh-Lamb equation for isotropic and homogeneous plates [15].

### 2.2.2 Guided waves in anisotropic media

For homogeneous and anisotropic media, the Rayleigh-Lamb equation is no longer applicable [15]. In such cases, the Newton's Law and the Hooke's Law are shown in equation (2.15) and (2.16) respectively [38, 40]. Note that the same Cartesian coordinate system is adopted as in Fig. 2.1.

$$\frac{\partial \sigma_{ij}}{\partial x_j} = \rho \ddot{u}_i \quad (i, j = 1, 2, 3) \tag{2.15}$$

$$\sigma_{ij} = C_{ijkl}\varepsilon_{kl} \quad (i, j, k, l = 1, 2, 3) \tag{2.16}$$

In the equations above, $\sigma_{ij}$ represents the stress which acts on the surface of $x_i$ and in the direction of $x_j, C_{ijkl}$ is the stiffness tensor where $i, j$ remain the same as in $\sigma_{ij}$, $k, l$ symbolise each stress component of $\sigma_{ij}$, and $\varepsilon_{kl}$ signifies the corresponding strain component. [40]

Meanwhile, the $\varepsilon_{kl}$ is quantified by the strain displacement equation [38] shown in equation (2.17).

$$\varepsilon_{kl} = \frac{1}{2}\left(u_{l,k} + u_{k,l}\right) = \frac{1}{2}\left(\frac{\partial u_l}{\partial x_k} + \frac{\partial u_k}{\partial x_l}\right) \tag{2.17}$$

When integrating the equation (2.15) – (2.17), the wave displacement equation (2.18) [40] is yielded as follows.

$$\frac{1}{2}C_{ijkl}\left(\frac{\partial^2 u_k}{\partial x_j \partial x_l} + \frac{\partial^2 u_l}{\partial x_j \partial x_k}\right) = \rho\frac{\partial^2 u_i}{\partial t^2} \tag{2.18}$$

Similar to the equation 2.11, the $u_i (i = 1, 2, 3)$ has the following form [38].

$$u_i = U_i \exp\left(ik_1 x_1 + ik_3 x_3 - \omega t\right) \quad (i = 1, 2, 3) \tag{2.19}$$

where $U_i$ represents the standing wave solutions, while $k_1$, $k_3$ are wavenumbers in the $x_1$ and $x_3$ directions respectively. For convenience, it is assumed that $k_3 = Ck_1$ where $C$ is a variable reflecting the material anisotropy. Moreover, the displacement equation (2.18) can be turned into its matrix form when integrated with (2.19). The corresponding equation is shown in (2.20) [38].

$$\begin{bmatrix} M_{11} & M_{12} & M_{13} \\ M_{21} & M_{22} & M_{23} \\ M_{31} & M_{32} & M_{33} \end{bmatrix} \begin{bmatrix} U_1 \\ U_2 \\ U_3 \end{bmatrix} = 0 \tag{2.20}$$

where the matrix $\boldsymbol{M}$ contains elements which are related to stiffness tensor $C_{ijkl}$, the variable $C$, mass density $\rho$ and the wavenumber $k$. Note that equation (2.20) is confined to the traction-free boundary condition in (2.21) [38]. Finally, the guided wave propagation within the anisotropic media can be interpreted by solving (2.20) and (2.21).

$$\sigma_{3i} = 0 \text{ when } x_3 = \pm h \quad (i = 1, 2, 3) \tag{2.21}$$

### 2.2.3 Guided waves in layered structures

Considering that multi-layer structures are widely employed in engineering applications, its is worthy to investigate guided waves within such structures particularly for SHM purposes. In practice, it is hypothesised that each layer has a comparable thickness which is simultaneously compatible to the wavelength of guided waves [40]. Following such assumptions, a half-space model [40] would not be considered for further analyses.

When modelling guided wave propagation through multiple layers, there exist three common approaches, namely the global matrix method (GMM) [41, 42], the transfer matrix method (TMM) [43] and the stiffness matrix method (SMM) [44]. The GMM solves the modelling problem by constructing a global matrix for all the layers and adding boundary conditions on both top and bottom surfaces of layered structures [38]. The GMM is shown to be numerically robust [38] but susceptible to high computational burden when solving the large-size global matrix [40]. Comparatively, the TMM performs by recursively solving wave propagation equations through the transfer matrix of intermediate layers [38]. Such operations are implemented by matrix multiplications [38], and therefore greatly alleviate computation costs. However, when top surfaces differ much from bottom boundaries, which could be due to high-frequency guided waves or large thickness of structures, multiplying the transfer matrix could yield poor numerical stabilities [40], thus hindering the applicability of the TMM. To solve this problem, the SMM is developed by replacing the transfer matrices with stiffness matrices while exploiting displacement and stress conditions at structural boundaries [38, 40, 44].

### 2.2.4 Phase velocity and Group velocity

Phase velocity is defined as the speed of guided waves of individual phases [15] and is calculated by the following formula [15, 38].

$$c_p = \frac{\omega}{2\pi}\lambda = \frac{\omega}{k} \tag{2.22}$$

where $c_p$ represents the phase velocity, $\omega$ is the angular frequency of guided wave components, $\lambda$ is the wavelength while $k$ is the wavenumber of guided waves.

Compared to the phase velocity, group velocity is defined as the speed of a group of wave packets [15, 38]. The group velocity is calculated by the equation (2.23) [38].

$$c_g = \frac{d\omega}{dk} = c_p + k\frac{dc_p}{dk} \tag{2.23}$$

where $c_g$ denotes the group velocity and other variables remain the same as (2.22).

### 2.2.5 Dispersion curves

Guided waves are dispersive waves [15], i.e., the propagation velocities vary with wave frequencies, $f$, and structure thickness $d$. When interpreting the propagation of guided waves, it is essential to analyse wave velocities against $f$ and $d$, which is further reflected in dispersion curves.

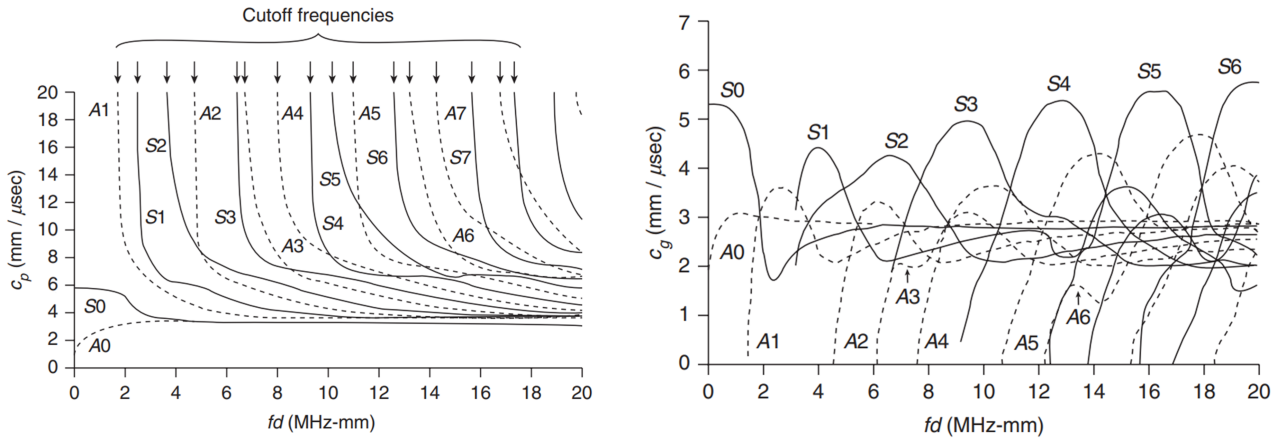


Figure 2.3: Lamb wave dispersion curves of a traction-free aluminium plate: (a) phase velocity curves; (b) group velocity curves. The figure is adapted from [38].

Fig. 2.3 shows an example of Lamb wave dispersion curves for an aluminium plate. Since the Lamb waves are guided plate waves, the corresponding dispersion curves for the isotropic plate can be obtained by solving the Rayleigh-Lamb equation. It is illustrated in Fig 2.3 that the propagation velocities vary with the frequency-thickness product $fd$ and there exist multiple curves corresponding to anti-symmetric (A) and symmetric (S) modes. Despite the multi-modality characteristics, a specific wave mode can be isolated by appropriately calibrating the excitation frequency of guided waves. This is due to that the specific mode can be filtered out

by its cut-off frequency [15, 38]. In practice, the $A_0$ and $S_0$ modes are commonly employed for damage detection and localisation purposes.

In terms of anisotropic structures, particularly the anisotropic composite plates with multiple layers, the Rayleigh-Lamb equation is not applied and other approaches, e.g., the GMM, TMM, SMM or the semi-analytical finite element (SAFE) technique [38], can be integrated to calculate the dispersion curves.

## 2.3 Actuation, sensing and processing of guided waves

### 2.3.1 Transducer type

In terms of the SHM on aerospace structures, the piezoelectric sensor utilised in this work is introduced as follows. Piezoelectric transducers are manufactured of asymmetric crystal materials which are dominated by the piezoelectric and its converse effects [45]. The piezoelectric effect indicates the ability to transfer stresses to electrical charges, while vice versa for the converse effect [40]. These two effects enable the piezoelectric transducers as actuators and sensors at the same time.

Figure 2.4: DuraAct piezoceramic transducers manufactured by the PI ceramics.

Lead zirconate titanate (PZT) transducers [15, 39, 40], as a piezoelectric ceramic type, have been extensively employed considering their high mechanical strengths, light weight, low manufacturing costs and convenience of use [40, 45]. Such transducers are usually manufactured as

thin wafers [15, 39], e.g., disks or squares, and can be mounted or embedded into interrogated structures [15,45]. However, the PZT transducers can be brittle in use [45], thus being hindered in further applications. To solve this problem, polymer coatings can be implemented on the PZTs to perform as both mechanical preload and electric insulation [45]. An example of the coated PZT transducers by the PI ceramics is shown in Fig. 2.4.

Furthermore, operational principles of the piezoelectric wafers are mathematically formulated as follows [40].

$$S_{ij} = s_{ij}^{E} T + d_{ij} E \tag{2.24}$$

$$D_j = d_j T + \varepsilon_j^{T} E \tag{2.25}$$

where $S_{ij}$ represents the mechanical strain in the $i$-$j$ plane, $T$ represents the mechanical stress, $E$ is the coupled electrical field, and $D$ is the electric displacement in the direction of $j$. $s^E$ is material's mechanical compliance when $E = 0$, $d$ is the piezoelectric constant and $\varepsilon^T$ is dielectric permittivity when $T = 0$. $i, j$ represent the directions of stress. [40]

### 2.3.2 Transducer configurations

Transducer configurations are crucial for the SHM, particularly when utilising the piezoelectric sensors, and need to be carefully considered prior to monitoring processes. In practice, the configurations can be categorised into sparse arrays and phased arrays [46], or the so-called compact arrays, in terms of distances between transducers. Transducers are far from each other in a sparse array while being adjacent in a phased array. It worth noting that the compact configurations are only valid when transducer spacings satisfy a near-field or a far-field assumption [46].

The transducer configurations can also be classified into an active sensing manner and a passive sensing manner, where in the former case transducers undertake signal emission and sensing tasks and in the latter transducers act as signal receivers only [40]. The active sensing manner is further comprised of the pitch-catch, pulse-echo, and thickness mode configurations [40]. As illustrated in Fig. 2.5, the pitch-catch configuration contains two transducers actuating and sensing acoustic signals separately while only one transducer is utilised for the same tasks

in the pulse-echo configuration. The thickness mode has a similar transducer setting to the pulse-echo manner but differs in a much higher excitation frequency and the performance as a thickness gauge [40]. Comparatively, transducers in the passive manner only perform as receivers responsive to elastic waves which are released by impacts or opening cracks [13, 40].

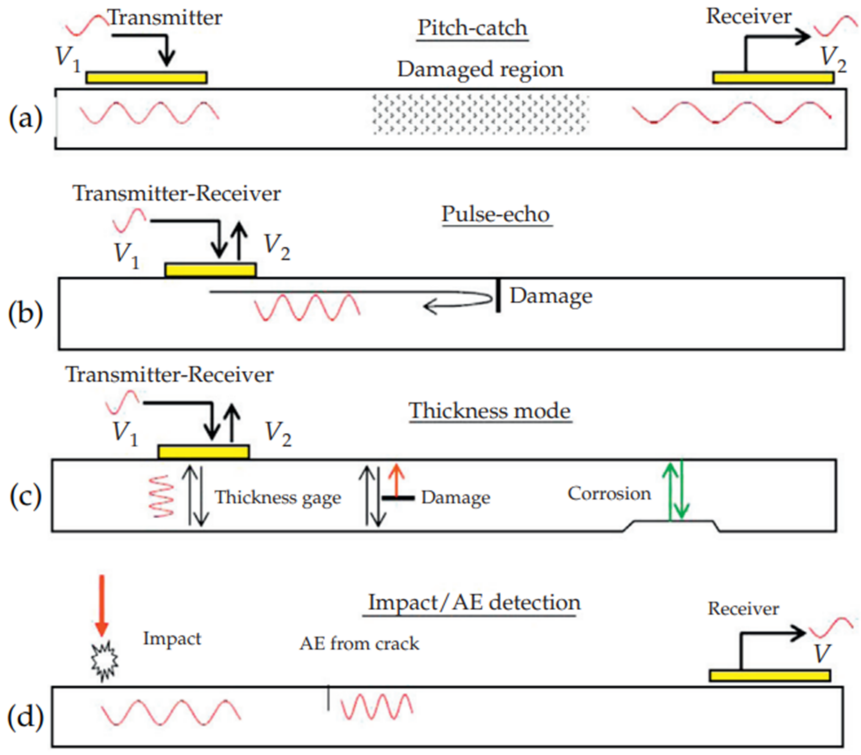


Figure 2.5: Transducer configurations particularly with piezoelectric wafers: (a) pitch-catch configuration; (b) pulse-echo configuration; (c) thickness mode; (d) passive sensing manner. Adapted from [40].

In this thesis, the PZT sensors are deployed for SHM purposes and full attention is paid to the active pitch-catch configuration together with sparse transducer arrays.

### 2.3.3 Electromechanical (E/M) impedance analyses for transducers

The electromechanical (E/M) impedance aims to characterise structural vibrations of inspected structures utilising high-frequency harmonics [40]. Such technique measures the electrical impedance of transducers with particular emphasis on the real part of the impedance, which reflects the mechanical properties of transducers [12]. When a transducer is mounted on a host structure, the real part reveals not only the transducer dynamics but also the structural

dynamics and resonance frequencies of the host structure [15].

When a PZT sensor is mounted on a host structure, the corresponding E/M impedance is formulated as follows when assuming the PZT patch as a thin bar structure [47].

$$Y = \frac{2\omega_s i w_s l_s}{h_s}\left[\frac{z_a}{z_s + z_a} d_{31}^2 Y^E \frac{2\tan\left(\frac{k_s l_s}{2}\right)}{k_s l_s} + \varepsilon_{33}^T - d_{31}^2 Y^E\right] \tag{2.26}$$

where $Y$ represents the admittance of the PZT patch when being mounted on the host structure while $Z_a$ and $Z_s$ are the mechanical impedances of the piezoceramic transducers and the host structure respectively [47]. $w_s$, $l_s$, and $h_s$ are individually denoted as the width, length and height of the PZT patch. $d_{31}$ is the piezoelectric strain coefficient in the $x_1 - x_3$ plane (see section 2.2) and $\varepsilon_{33}$ is a complex variable reflecting the PZT's electric permittivity [47]. $Y^E$ is the complex Young's modulus of the PZT transducers when $E = 0$ (see equation 2.24), while $\omega_s$ and $k_s$ are presented as the angular frequency and wavenumber of vibrating waves from the PZT patch [47]. Finally, the mechanical impedance of the mounted PZT patch, denoted as $Z$, is calculated as the reciprocal of $Y$.

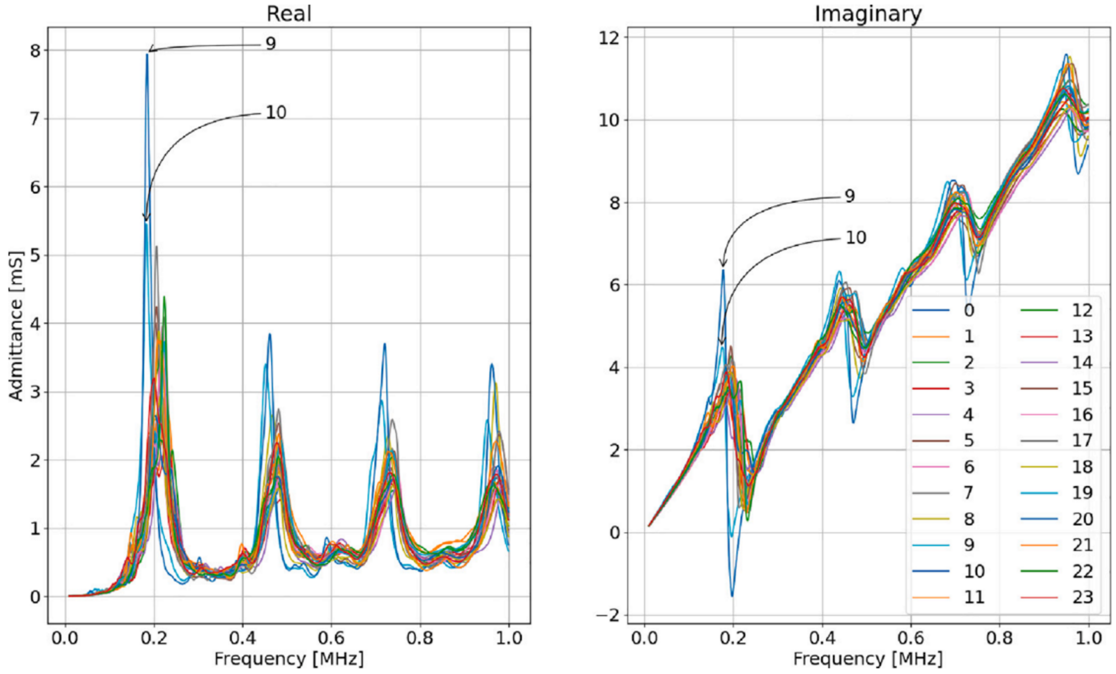


Figure 2.6: E/M impedance for reproducibility check of mounted transducers on an impacted composite panel. [48]

The E/M impedance technique is considered when checking repeatability of the mounted

PZT transducers [48]. Fig. 2.6 shows an example of utilising the E/M curves to inspect transducer bondings on a composite panel. Ideally all the transducers are supposed to have similar bonding conditions, which imply consistent amplitudes and resonance frequencies of different E/M spectra. Any shifts in the amplitude or resonance frequency could indicate potential abnormalities in the bonding conditions [48]. Accordingly, the sensors 9 and 10 in Fig. 2.6 are identified as abnormal and therefore their signals can be removed in further analyses.

### 2.3.4 Signal processing in time and frequency domain

During the SHM process Lamb wave signals are excited and received by the mounted PZT patches. Considering the multi-modal and dispersive characteristics of Lamb waves, narrowband signal excitations are usually preferred to preserve a single wave mode, and such excitations can be further implemented based on single-frequency tone bursts [49]. However, the narrowband excitations could suffer from limited data storage and high acquisition time when collecting Lamb wave responses with varying centre frequencies [50]. These problems can be solved by deploying broadband chirps for signal excitation and then applying deconvolution procedures [50] to isolate target frequency components. The mathematical formulation of the broadband chirp excitation is shown as follows [12].

$$s_1(t) = W(t) \sin\left[2\pi f_0 t + \frac{\pi\left(f_1 - f_0\right) t^2}{T}\right] \tag{2.27}$$

where $s_1(t)$ represents the actuated chirp signal, $T$ represents the duration of the excitation signal, $f_0$ and $f_1$ are the starting and the ending frequency for the signal excitation, and $W(t)$ is a rectangular time window with a duration of $T$. In this work, $f_0$ and $f_1$ are adopted as $10\text{kHz}, 600\text{kHz}$ respectively while the $T$ is set as $200\mu\text{s}$.

Furthermore, in terms of the chirp signals and the desired tone bursts, the following equations in the frequency domain are satisfied [50].

$$R_1(\omega) = G(\omega) S_1(\omega) \tag{2.28}$$

$$R_2(\omega) = G(\omega)S_2(\omega) \tag{2.29}$$

where $S_1(\omega), R_1(\omega)$ denote the actuated chirp and the chirp response, respectively, in the frequency domain, and $S_2(\omega), R_2(\omega)$ are similar but in tone burst forms. $G(\omega)$ is the transfer function between the actuated and the received signals. Note that $G(\omega)$ remains the same for both chirp and tone burst signals because such function is only related to the mounted transducers and the host structure.

Substituting (2.28) into (2.29), the tone burst response is expressed as [50]

$$R_2(\omega) = \frac{R_1(\omega)}{S_1(\omega)}S_2(\omega) \tag{2.30}$$

Since $S_1(\omega), R_1(\omega)$ are known for chirp signals, $R_2(\omega)$ is determined by $S_2(\omega)$. This enables the selection of a tone burst from the chirp signals with a desired centre frequency. When $R_2(\omega)$ is decided, its corresponding time domain signal is obtained and the following signal processing operations can then be implemented.

**Feature scaling:** The feature scaling aims to rearrange signals with varying ranges into the same scale so that a fast and stable data-driven model can be established [51]. Among various scaling operations, the Min-Max scaling [52] and the $z$-normalisation [52] are widely used in the community of machine learning and statistics. The Min-Max scaling is formulated below [52].

$$\boldsymbol{x}' = \frac{\boldsymbol{x} - \min(\boldsymbol{x})}{\max(\boldsymbol{x}) - \min(\boldsymbol{x})} \tag{2.31}$$

where $\boldsymbol{x}$ and $\boldsymbol{x}'$ represent a signal vector and its scaled form, max() and min() represent the maximum and the minimum operators. The Min-Max scaling transforms each processed signal into a fixed $0 - 1$ scale while preserving signal trends simultaneously. However, the Min-Max scaling is highly sensitive to data outliers [53].

The $z$-normalisation arranges signals in the same scale with the mean and the standard deviation as 0 and 1. Such operation is formulated in (2.32) [52].

$$\boldsymbol{x}' = \frac{\boldsymbol{x} - \mu}{\sigma} \tag{2.32}$$

In (2.32) $\boldsymbol{x}$ remains the same as (2.31), while $\mu$, $\sigma$ represent the mean and standard deviation value of $\boldsymbol{x}$ respectively and are both sensitive to data outliers [53].

**Signal windowing:** The signal windowing extracts a portion of signal by a weighted function on signal values [54]. For a discrete signal $\boldsymbol{x}(k)$, its windowed counterpart, $\boldsymbol{x}_w(k)$, is expressed as [55]

$$\boldsymbol{x}_w(k) = w(k)\boldsymbol{x}(k) \quad (k = 0, 1, \cdots, N_w - 1) \tag{2.33}$$

where $w(k)$ represents a signal window containing $N_w$ sampling points. Common window functions include the rectangular [55], Gaussian [56] and Hanning windows [55], whose formulae are shown as follows.

1) Rectangular window [55]:

$$w(k) = 1 \, (k = 0, 1, \cdots, N_w - 1) \tag{2.34}$$

The rectangular window is equivalent to simply truncating a signal with $N_w$ samples. However, such window could lead to severe spectral leakage of signal spectrum, namely the energy leak from main frequency component to side frequencies [57], and thus being limited in signal processing.

2) Gaussian window [56]:

$$w(k) = \exp\left(-\frac{k^2}{2\sigma_w^2}\right) (k = 0, 1, \cdots, N_w - 1) \tag{2.35}$$

where $\sigma_w$ correspond to the standard deviation of a Gaussian distribution and is related to the window length $N_w$.

3) Hanning (Hann) window [55]:

$$w(k) = \frac{1}{2}\left[1 - \cos\left(\frac{2\pi k}{n_c}\right)\right] (k = 0, 1, \cdots, N_w - 1) \tag{2.36}$$

where $n_c$ is the number of cycles within Hanning window. Compared to the rectangular window, the Hanning window is less affected by spectral leakage issues [39].

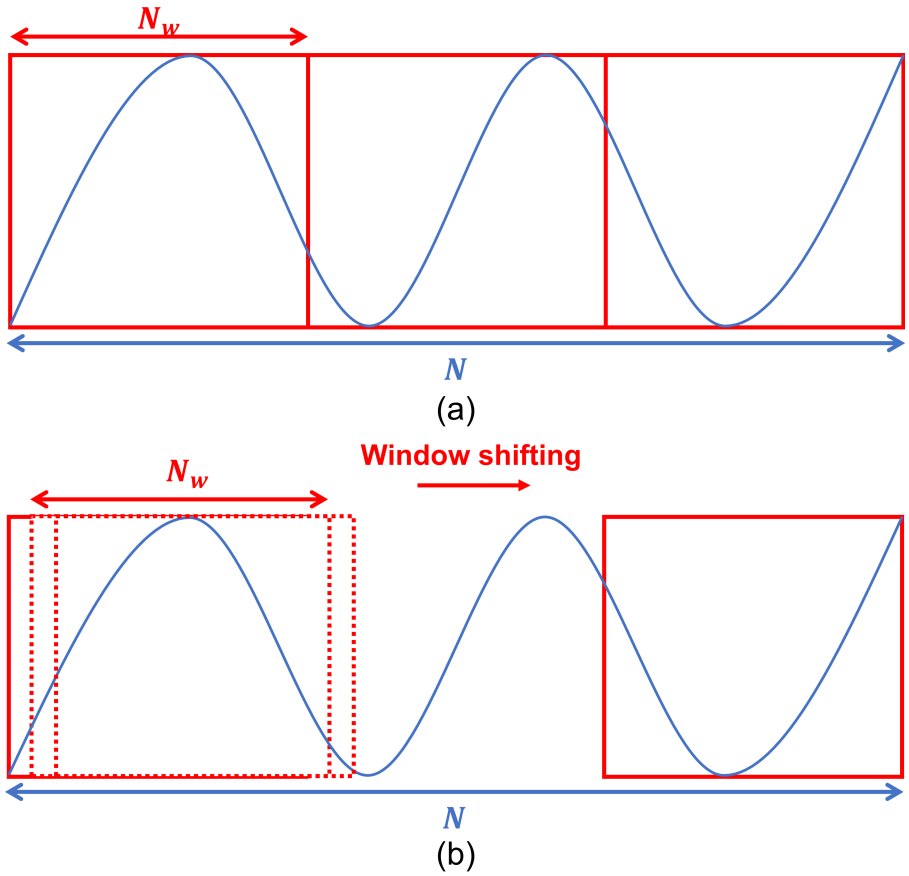


Figure 2.7: Sliding window techniques with (a) non-overlapping windows; (b) overlapping (rolling) windows.

In statistical and machine learning applications, a sliding window setting is also supported where consecutive signal windows are arranged with time shifts. Within such setting, two adjacent signal windows can be overlapped (rolling) or non-overlapped [58] in the time domain (see Fig. 2.7).

**Fourier transform (FT):** The FT [39, 55] is employed to transfer time domain signals into their frequency domain. For a continuous time-domain signal $f(t)$, the Fourier transform $\mathcal{F} : \mathbb{R} \to \mathbb{C}$ is shown below [39, 55].

$$\mathcal{F}(\omega) = \int_{-\infty}^{+\infty} f(t) e^{-2\pi i \omega t} dt \tag{2.37}$$

where $\mathcal{F}(\omega)$ is the Fourier spectrum of the signal and $\omega$ is the angular frequency.

Conversely, the inverse Fourier transform (IFT) is defined as follows to yield time-domain signals [39].

$$f(t) = \int_{-\infty}^{+\infty} \mathcal{F}(\omega) e^{2\pi i \omega t} d\omega \tag{2.38}$$

For the discrete signal $\boldsymbol{x}(n)$, the discrete Fourier transform (DFT) is considered instead in the equation (2.39), whereas the inverse DFT is shown in (2.40) [39].

$$\boldsymbol{X}(k) = \sum_{n=1}^{N} \boldsymbol{x}(n) e^{-\frac{2\pi i}{N} kn} (k = 1, 2, \ldots, N) \tag{2.39}$$

$$\boldsymbol{x}(\boldsymbol{n}) = \frac{1}{N} \sum_{k=1}^{N} \boldsymbol{X}(k) e^{\frac{2\pi i}{N} kn} (k = 1, 2, \ldots, N) \tag{2.40}$$

where $\boldsymbol{X}(k)$ is the DFT of $\boldsymbol{x}(n)$ and $N$ is the number of sampling points in $\boldsymbol{x}(n)$. The implementation of the standard DFT can be further improved by the fast Fourier transform (FFT) [39, 55], which has a lower computational complexity.

**Short-time Fourier transform (STFT):**

STFT is a 2-D time-frequency representation of continuous time signals [39] based on the FT. The STFT partitions complete signals into smaller segments with an equal duration [39], denoted as $\tau$, and subsequently implements the FT on each segment. The mathematical formulation of the STFT is shown in (2.41) [39].

$$S_{STFT}(\tau, \omega) = \int_{-\infty}^{+\infty} f(t) w(t - \tau) e^{-2\pi i \omega t} dt \tag{2.41}$$

where $S_{STFT}(\tau, \omega)$ is the time-frequency spectrum, $w$ is the window function which is usually a Gaussian or Hanning window, and other variables remain the same as (2.37).

Correspondingly, the discrete STFT is shown below [39].

$$\boldsymbol{X}(m, \omega) = \sum_{n=-\infty}^{+\infty} \boldsymbol{x}(n) w(n - m) e^{-2\pi i \omega n} \tag{2.42}$$

where $\boldsymbol{X}(m, \omega)$ is the spectrum of $\boldsymbol{x}(n), m$ is the window size when segmenting signals, and others are the same with (2.41).

Despite that the STFT could provide the local time-frequency information, such operation adopts a fixed window size when segmenting signals and therefore not suitable for signals with rapidly varying instantaneous frequencies [39].

**Hilbert transform (HT):** The HT aims to process analytical signals in the field of digital

signal processing and is mathematically expressed in (2.43) [39].

$$f_H(t) = \frac{1}{\pi} \int_{-\infty}^{+\infty} \frac{f(\tau)}{t-\tau} d\tau \tag{2.43}$$

where $f_H(t)$ is the HT of the signal $f(t)$. The complex analytical signal $f_C(t)$ is therefore defined as [39]

$$f_c(t) = f(t) + i f_H(t) \tag{2.44}$$

Finally, the signal envelope of $f(t)$, denoted as $\text{env}(t)$, is calculated as [39]

$$\text{env}(t) = |f_c(t)| \tag{2.45}$$

The HT can be implemented based on the FT and employed to generate signal envelopes of Lamb wave measurements. However, the standard HT could suffer from the Runge phenomenon [59], where the Hilbert envelope could oscillate near the boundary of a signal. An effective solution to such problem is to mirror the $f(t)$ prior to the HT.

## 2.4 Guided-wave damage detection and localisation

### 2.4.1 Baseline-subtraction for damage detection

In field of the GWSHM, the damage detection is usually accomplished in a baseline-subtraction manner where current and pristine signals are obtained and compared together to decide the health status of a monitored structure [16]. When a damage exists, the baseline comparison is mathematically expressed as follows [60].

$$\boldsymbol{b_i}(t) = \boldsymbol{g_i}(t) + \boldsymbol{\varepsilon_i}(t) \tag{2.46}$$

$$\boldsymbol{c_i}(t) = \boldsymbol{g_i}(t) + \boldsymbol{d_i}(t) + \boldsymbol{\varepsilon_i}(t) \tag{2.47}$$

$$\boldsymbol{r_i}(t) = \boldsymbol{c_i}(t) - \boldsymbol{b_i}(t) = \boldsymbol{d_i}(t) \tag{2.48}$$

where $\boldsymbol{c_i}(t)$ is the current (damaged) guided wave measurement from an arbitrary transducer path $i$; $\boldsymbol{b_i}(t)$ is the corresponding healthy baseline collected from the same monitored structure and the temperature condition; $\boldsymbol{g_i}(t)$ is representative of the structural complexities only, e.g., boundary reflections, the existence of stiffeners [60], thus remaining the same for both pristine and damaged signals; $\boldsymbol{\varepsilon_i}(t)$ is a mixture of manufacturing variations and measurement noises; $\boldsymbol{r_i}(t)$ in (2.48) denotes the residual between $\boldsymbol{c_i}(t)$ and $\boldsymbol{b_i}(t)$, and reflects only the damage information $\boldsymbol{d_i}(t)$ since the other factors are cancelled out.

However, the baseline subtraction could be degraded by signal distortions arising from temperature deviations [12] between the current and pristine measurements. Such issues can be alleviated by the temperature compensation on guided wave signals, which is introduced later in this chapter.

### 2.4.2 Damage indices for damage detection

The baseline-based damage detection is further implemented based on damage indices ($DI$s) [16], which aim to reflect the health condition of the monitored structure by quantifying discrepancies between the pristine and current signals. In terms of a transducer path $i$ with its pristine and current signals as $\boldsymbol{b_i}(n)$ and $\boldsymbol{c_i}(n)$ (in discrete time) respectively, the corresponding $DI$ can be formulated as follows.

1) Amplitude-based $DI$ [12]

$$DI = \max\left[\boldsymbol{c_i}(n) - \boldsymbol{b_i}(n)\right] = \max\left[\boldsymbol{r_i}(n)\right] \tag{2.49}$$

where $DI$ corresponds to the amplitude of the damage scattering signal $\boldsymbol{r}_i(t)$, which is calculated as the residual between $\boldsymbol{b_i}(t)$ and $\boldsymbol{c_i}(t)$.

2) Energy-based $DI$ [12, 61]

$$DI = \frac{\sum_{n=0}^{T_w} \left|\boldsymbol{c}_i(n) - \boldsymbol{b_i}(n)\right|^2}{\sum_{n=0}^{T_w} \left|\boldsymbol{b_i}(n)\right|^2} = \frac{\sum_{n=0}^{T_w} \left|\boldsymbol{r_i}(n)\right|^2}{\sum_{n=0}^{T_w} \left|\boldsymbol{b_i}(n)\right|^2} \tag{2.50}$$

where $DI$ is defined in a close form to the root mean squared deviation (RMSD) and calculated based on a signal window with the sampling duration $T_w$. The sign $|\cdot|$ corresponds to the absolute value function or the Hilbert envelope when the input signal is complex.

3) Correlation-based $DI$ [12, 16]

$$DI = 1 - |\text{corr}\left(\boldsymbol{c_i}(n), \boldsymbol{b_i}(n)\right)| = 1 - \left| \frac{\sum_{n=0}^{T_w} \left(\boldsymbol{c_i}(n) - \mu_c\right)\left(\boldsymbol{b_i}(n) - \mu_b\right)}{\sigma_c \sigma_b} \right| \tag{2.51}$$

where $DI$ is defined based on the Pearson correlation coefficient, which is denoted as $\text{corr}(\cdot), \sigma_b, \sigma_c$ denote the variance of $\boldsymbol{b_i}(n), \boldsymbol{c_i}(n)$ within a signal window of duration $T$, while other variables remain the same as (2.50).

Furthermore, a well-calibrated detection threshold on the $DI$ values is needed to distinguish the pristine and damaged states with high accuracy but low false alarms. The threshold is calibrated by the baseline data [14] which are collected from the same monitored structure and environmental condition, e.g., temperature, as the current measurements. Any transducer paths with $DI$ values greater than the threshold are identified as damaged, otherwise as defect-free. In practice, the $DI$s for individual transducer paths can be fused into the following statistical features [14].

$$\mu_{DI} = \frac{\sum_{i=1}^{N_s} DI_i}{N_s} \tag{2.52}$$

$$\sigma_{DI} = \sqrt{\frac{\sum_{i=1}^{N_S} \left(DI_i - \mu_{DI}\right)^2}{N_s - 1}} \tag{2.53}$$

$$\boldsymbol{\Theta} = \left[\mu_{DI}, \sigma_{DI}\right]^T \tag{2.54}$$

where $\mu_{DI}, \sigma_{DI}$ represent the mean and the standard deviation of the $DI$ values from $N_s$ different transducer paths, and $\boldsymbol{\Theta}$ is a $2 \times 1$-dimensional damage-sensitive vector reflecting the health status of the inspected structure. The damage detection can then be implemented by applying the Mahalanobis distance (MD) measure on $\boldsymbol{\Theta}$, which is shown as [14, 62]

$$MD\left(\boldsymbol{\Theta}_{\text{c}}, \boldsymbol{\Theta}_{\text{ref}}\right) = \sqrt{\left(\boldsymbol{\Theta}_{\text{c}} - \overline{\boldsymbol{\Theta}_{\text{ref}}}\right)^T \boldsymbol{S}_{\Theta}^{-1} \left(\boldsymbol{\Theta}_{\text{c}} - \overline{\boldsymbol{\Theta}_{\text{ref}}}\right)} \tag{2.55}$$

where $\mathbf{\Theta}_{\mathrm{c}}$, $\mathbf{\Theta}_{\mathrm{ref}}$ represent $\mathbf{\Theta}$ of the current and the reference (pristine) signals respectively, $\overline{\mathbf{\Theta}_{\mathrm{ref}}}$ denotes the average $\mathbf{\Theta}_{\mathrm{ref}}$, and $\boldsymbol{S}_{\Theta}^{-1}$ denotes the inverse of a $2 \times 2$- dimensional covariance matrix of $\mathbf{\Theta}_{\mathrm{ref}}$.The detection threshold is then calibrated by replacing the $\mathbf{\Theta}_{\mathrm{c}}$ with $\mathbf{\Theta}_{\mathrm{ref}}$ in (2.55), and any $\mathbf{\Theta}$ values with a greater MD than the threshold correspond to a damaged state. Note that the formulae (2.52)-(2.55) in [14, 62] are only applicable in a baseline-subtraction manner considering that the reference signals are required for calculating the MD.

### 2.4.3 Temperature compensation for baseline subtraction

It is well known that temperature variations introduce extra signal distortions of guided waves and could mask the existence of real damage signatures. More specifically, the distortions are manifested into the amplitude change and phase shift of the ultrasonic signals under varying temperatures. As an example, the phase or time shift can be expressed as follows [63].

$$\Delta t_i = \frac{d_i}{c_p}\left(\alpha \Delta T - \frac{\Delta c_p}{c_p}\right) \tag{2.56}$$

where $\Delta t_i$ denotes the time shift of a signal path $i$ under the temperature $T$ to $T + \Delta T$, $c_p$ denotes the phase velocity corresponding to the path $i$ at the current temperature $T$, $\Delta c_p$ denotes the phase velocity change under $T$ to $T + \Delta T$, $d_i$ represents the propagation distance of the path $i$, and $\alpha$ represents a thermal expansion coefficient which is much smaller than the relative change of $c_p$ [63].

More specifically, when temperature deviations exist between the current and the pristine measurements, namely the $\mathbf{\Theta}_{\mathrm{c}}$ and $\mathbf{\Theta}_{\mathrm{ref}}$ in (2.55), directly inputting these signals would much degrade the effectiveness of the baseline-subtraction and consequently yield high false alarms during the damage detection [12]. Nevertheless, such issues can be alleviated by compensating the temperature effects on guided wave signals. Common approaches for the temperature compensation include the optimal baseline selection (OBS) [64] and the stretch-based technique [24, 64–66]. The OBS collects historical baselines under varying temperatures and finds an optimal baseline yielding the highest similarity with the current signal [64]. The mathematical

formulation of the OBS is shown as follows [64].

$$m = \underset{m}{\operatorname{argmin}} \sum_{n=0}^{T_w} \left[\boldsymbol{c_i}(n, T) - \boldsymbol{b_i}\left(n, T_m\right)\right]^2 \tag{2.57}$$

where $T, T_m$ represent monitoring temperatures of the current signal and the optimal baseline respectively, $m$ represents the index of the optimal baseline, and others remain the same as (2.51).

Meanwhile, the stretch-based techniques, including but not limited to the baseline signal stretch (BSS) [24, 64], the scale transform (ST) [65], local peak coherence (LPC) [66], obtain a baseline at the current temperature $T$ by stretching or dilating another baseline at a different temperature $T_0$. Generally, the stretched-based methods can be formulated as [24]

$$\alpha, \beta = \underset{\alpha,\beta}{\operatorname{argmin}} \sum_{n=0}^{T_w} \left[\boldsymbol{c_i}(n, T) - \boldsymbol{b_i}\left(n, T_0, \alpha, \beta\right)\right]^2 \tag{2.58}$$

$$\boldsymbol{b_i}\left(n, T_0, \alpha, \beta\right) = \alpha \boldsymbol{b_i}\left(\beta n, T_0\right) \tag{2.59}$$

where $\boldsymbol{b_i}\left(n, T_0\right)$ represents the measured baseline of path $i$ at $T_0, \alpha, \beta$ denote the coefficients corresponding to the amplitude changes and phase shifts respectively under varying temperatures.

Although the OBS and the stretch-based techniques can reduce the temperature-induced signal distortions, the performance of these methods could suffer if the temperature difference between the current and the baseline signals exceeds a certain range, e.g., 15°C [48]. Moreover, an accurate and reliable calculation of the temperature compensation factors, namely $\alpha$ and $\beta$, is highly demanded especially for large complex structures [12, 24].

### 2.4.4 Damage localisation based on sparse array imaging

Following the damage identification scheme, a detected damage is then localised within the sensor coverage of a sparse transducer array. The damage localisation performs by generating grid pixels with their values reflecting damage signatures in the monitored area, and the pixels

with the highest value, or 99% quantile [62] at least, indicate the true damage location. Common techniques for the damage localisation are introduced as follows.

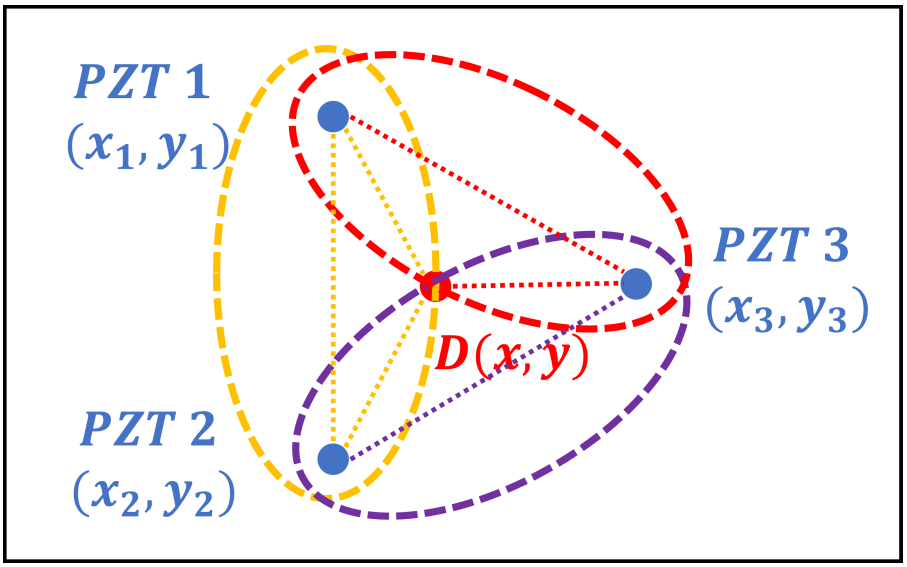


Figure 2.8: The TOF triangulation approach for damage localisation.Adapted from [39].

1) Time-of-flight (TOF) triangulation [39]. The damage localisation on a plate structure can be implemented by the triangular geometry between a potential damage and the adjacent transducer pairs, which is further illustrated in Fig. 2.8. In terms of an arbitrary transducer path, e.g., path 1-2 in Fig. 2.8, the damage triangulation is depicted below [39] considering the material anisotropy.

$$TOA_{1-D-2} = \frac{d_{1-D}}{c_{g,1-D}} + \frac{d_{D-2}}{c_{g,D-2}} \tag{2.60}$$

In (2.60), $TOA_{1-D-2}$ denotes the time of arrival (TOA) instant of the damage scattering signal $\boldsymbol{r_i}(t)$ for path 1-2, being consistent with the time span of guided waves propagating from the actuator 1 to the sensor 2 through the damage $D$, namely the TOF information; $d_{1-D}$, $d_{D-2}$ denote the forward and backward propagating distance, and $c_{g,1-D}$, $c_{g,D-2}$ represent the corresponding group velocities, which vary with different propagation angles of guided waves. Note that $d_{1-D}$, $d_{D-2}$ are confined to an ellipse when $TOA_{1-D-2}$ is determined and fixed as a constant. In this regard, only one imaging ellipse is insufficient for the damage localisation, and three transducers are required at least to generate

intersecting ellipses for damage location estimates [39]. In addition, the TOF triangulation usually demands a pitch-catch configuration [40] where each transducer acts as an actuator and sensor simultaneously.

2) Time-difference-of-arrival (TDOA) approach [39, 67]. The TDOA method relies on a specific transducer configuration where only one actuator is required while the others all operate as sensors [39]. As illustrated in Fig. 2.9, the TDOA is derived by (2.61) - (2.62) when assuming that the PZT 1 acts as the actuator [39].

$$TOA_{1-D-3} = \frac{d_{1-D}}{c_{g,1-D}} + \frac{d_{D-3}}{c_{g,D-3}} \tag{2.61}$$

where $TOA_{1-D-3}$, $d_{D-3}$, $c_{g,D-3}$ have the same physical meaning as (2.60) but are constrained to path 1-3. Moreover, the TDOA between the path 1-2 and 1-3, denoted as $\delta TOA_1$, is calculated as [39]

$$\delta TOA_1 = TOA_{1-D-2} - TOA_{1-D-3} = \frac{d_{D-2}}{c_{g,D-2}} - \frac{d_{D-3}}{c_{g,D-3}} \tag{2.62}$$

Once $TOA_{1-D-2}$, $TOA_{1-D-3}$ are obtained as constants, $d_{D-2}$ and $d_{D-3}$ follow a hyperbola form while the true damage location is then estimated by the intersecting hyperbola curves.

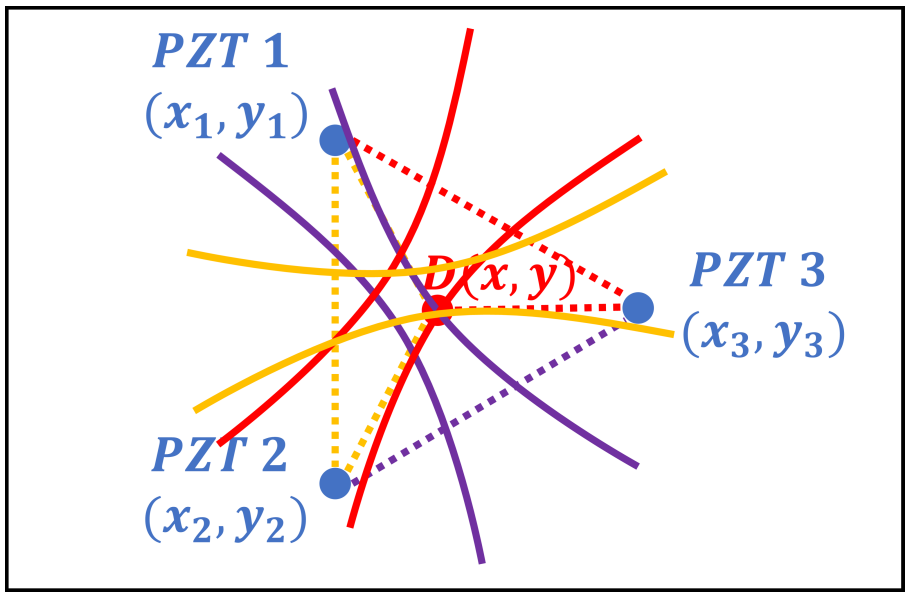


Figure 2.9: The TDOA approach for damage localisation. Adapted from [67].

3) Delay-and-sum (DAS) imaging [68]. The DAS beamforming is a time-shift averaging algorithm which fuses multi-channel signals to yield damage images [68]. In the DAS framework, the pristine and the current signals are firstly pre-processed as follows [68].

$$\widehat{c_i} = \frac{c_i}{A_{b_i}}\sqrt{\frac{1}{d_i}}, \widehat{b_i} = \frac{b_i}{A_{b_i}}\sqrt{\frac{1}{d_i}} \tag{2.63}$$

In (2.63), $A_{b_i}$ denotes the peak amplitude of $b_i$ (particularly the first wave packets) [69] and is consistently utilised for scaling $b_i$, $c_i$. $d_i$ denotes the propagation distance of path $i$, $\widehat{c_i}$, $\widehat{b_i}$ represent scaled current and pristine signals considering the geometrical spreading [68]. The envelope of damage scattering signals is then calculated as follows [68].

$$\text{env}\left(\widehat{r_i}\right) = \text{env}\left(\widehat{c_i} - \widehat{b_i}\right) \tag{2.64}$$

where env$(\cdot)$ denotes the Hilbert envelope and $\widehat{r_i}$ is the damage scattering signal of path $i$, namely the residual between $\widehat{c_i}$ and $\widehat{b_i}$. Furthermore, the damage value of an imaging pixel $P(x, y)$ is estimated as [68]

$$E(x,y) = \frac{1}{N_s}\sum_{i=1}^{n_s-1}\sum_{j=i+1}^{n_s}\text{env}\left(\widehat{r_{ij}}\right)\left(t_{ij}(x,y)\right) \tag{2.65}$$

$$t_{ij}(x,y) = \frac{\sqrt{(x-x_i)^2+(y-y_i)^2}}{c_{g,1}} + \frac{\sqrt{(x-x_j)^2+(y-y_j)^2}}{c_{g,2}} + t_{off} \tag{2.66}$$

where $n_s$ represents the number of transducers, $N_s = (n_s - 1)\, n_s$ represents the number of transducer paths (including reciprocal paths), $i, j$ denote the orders of actuator and receiver respectively, $c_{g,1}$, $c_{g,2}$ denote different group velocities of forward and backward propagating waves considering the material anisotropy, $t_{\text{off}}$ is a constant time offset due to the delay in signal acquisition [12, 68].

In real-life applications, the effectiveness of the standard DAS is susceptible to heavily overlapping guided wave modes due to boundary reflections [70]. Nevertheless, the related imaging artifacts can be alleviated by the minimum variance distortionless response (MVDR) [71] method.

4) Reconstruction Algorithm for Probabilistic Inspection of Damage (RAPID) [16] The RAPID tomography locates damages by the intersecting transducer paths where each path is an ellipse of imaging pixels [16]. Fig. 2.10 illustrates the imaging of a single transducer path, where the points $A$, $S$, $P$ individually represents the actuator, sensor and an imaging pixel. For a given pixel $P(x, y)$, its pixel value is yielded as [16]

$$\sum_{j=1}^{n_s-1}\sum_{k=1}^{n_s} SDC_{jk} \times \frac{\delta - R_{jk}(x,y)}{\delta - 1} \tag{2.67}$$

where $n_s$ is the number of transducers, $j$, $k$ correspond to the actuator and sensor of a transducer path $i$, while $SDC_{jk}$ represents the signal difference coefficient of path $j$ to $k$ and is equivalent to $DI_i$. $\delta$ is a scaling factor tuning the coverage of sensor paths and is adopted as 1.05 [16]. $R_{jk}(x, y)$ is formulated as [16]

$$R_{jk}(x,y) = \begin{cases} RD_{jk}(x,y) & RD_{jk}(x,y) < \delta \\ \delta & RD_{jk}(x,y) \geq \delta \end{cases} \tag{2.68}$$

where $RD_{jk}(x, y)$ follows [16]

$$RD_{jk}(x,y) = \frac{\sqrt{(x-x_j)^2 + (y-y_j)^2} + \sqrt{(x-x_k)^2 + (y-y_k)^2}}{\sqrt{(x_j-x_k)^2 + (y_j-y_k)^2}} \tag{2.69}$$

In (2.69), $(x_j, y_j)$ and $(x_k, y_k)$ represent coordinates of the actuator and the sensor respectively.

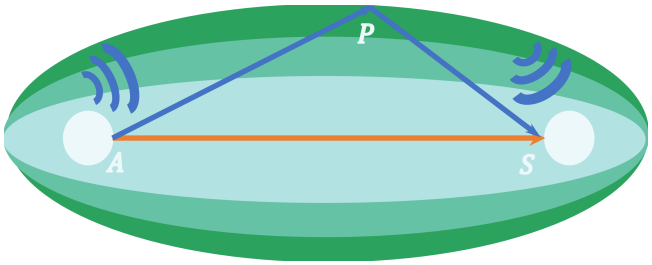


Figure 2.10: Elliptical distribution for imaging pixels. Adapted from [16].

### 2.4.5 Supportive C-Scan technique for damage imaging

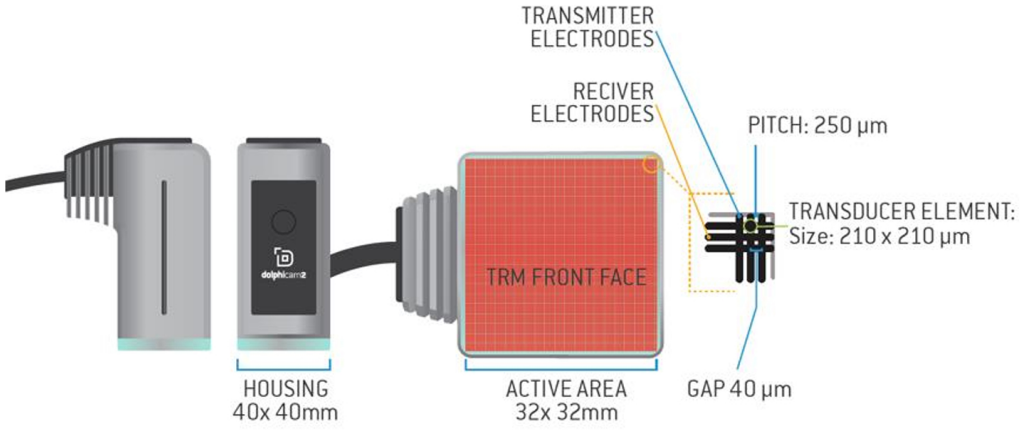


Figure 2.11: A basic illustration of the C-Scan transducer [73].

According to BS EN 1330-4 : 2010 [72], the C-Scan is defined as an ultrasonic technique to interrogate cross-section profiles of an inspected structure. In practice, the C-Scan images are shown based on the signal amplitude or the time-of-flight (TOF) features, and such images can be combined from multiple cross-sections to yield a through-thickness damage assessment of the structure [73].

In this thesis, the C-Scan process is implemented by the DolphiCam2 [73] to assist the damage detection and localisation by ultrasonic guided waves. A basic illustration of such device is shown in Fig. 2.11. More specifically, the DolphiCam2 possesses a 32 mm $\times$ 32 mm scanning aperture which can contain 128 $\times$ 128 imaging elements [73], thus ensuring a high resolution in the scanning images.

## 2.5 Failure prognostics for engineered structures

This section introduces several basic concepts and common approaches for failure prognostics. Part of this section with particular emphasis on the subsection 2.5.2 appears in Hongmin Zhu (2021) [36].

### 2.5.1 Critical concepts in failure prognostics

Reliability depicts the probability of a system, subsystem or component to perform required functions within a certain time period under real-life operational and environmental conditions [74, 75]. As a function of service time or service cycles, the reliability function or so-called survival function of an engineering system is depicted in the following formula [75].

$$S(t) = \Pr(T > t) \quad (t > 0) \tag{2.70}$$

In the formula above, $S(t)$ denotes reliability of the system at time (or time cycle) $t$ and Pr denotes the probability function, while $F(t)$ represents failure probability of the system, which can be described as [75]

$$F(t) = \Pr(T \leq t) = \int_0^t f(x)dx \quad (t > 0) \tag{2.71}$$

where $F(t)$ also represents the cumulative distribution function (CDF) of the failure while $f(t)$ represents the probability density function (PDF) of the failure.

Meanwhile, it is obvious that

$$S(t) + F(t) = 1 \quad (t > 0) \tag{2.72}$$

The failure rate function which depicts the frequency of system failures is then defined as [75]

$$h(t) = \frac{f(t)}{S(t)} \quad (t > 0) \tag{2.73}$$

The formula above can be transformed to (2.74) based on (2.72).

$$h(t) = \frac{dF(t)/dt}{1 - F(t)} = \frac{d(\ln(1 - F(t)))}{dt} \quad (t > 0) \tag{2.74}$$

The failure probability function can be calculated based on (2.74) as

$$F(t) = 1 - \exp\left(-\int_0^t h(x)dx\right) \quad (t > 0) \tag{2.75}$$

The reliability function is then calculated as follows [75].

$$S(t) = \exp\left(-\int_0^t h(x)dx\right) \quad (t > 0) \tag{2.76}$$

In real-life applications, the three-parameter (3-P) Weibull function is commonly employed to calculate the failure probability, and the CDF of such function is shown below [75].

$$F(t) = 1 - \exp\left(-\left(\frac{t-\gamma}{\theta}\right)^{\beta}\right) \quad (t > \gamma) \tag{2.77}$$

where $\gamma$, $\theta$, $\beta$ represent the location parameter which belongs to the interval $[0, +\infty)$, the scale parameter which reflects fluctuation of the 3-P Weibull distribution and the shape parameter determining the shape of the CDF respectively. $t$ and $F(t)$ are the same as (2.70) - (2.71).

The equation (2.77) can be transformed into the following form.

$$t = \theta \exp\left(\frac{1}{\beta}\ln\left(\ln\frac{1}{1-F(t)}\right)\right) + \gamma = \theta \exp\left(\frac{1}{\beta}\ln\left(\ln\frac{1}{S(t)}\right)\right) + \gamma \tag{2.78}$$

The three parameters of the 3-P Weibull distribution in (2.77) can be fitted in semilogarithmic coordinates of $t$ versus $\frac{1}{\beta}\ln\left(\ln\frac{1}{1-F(t)}\right)$, which is called graphical estimation [76].

Furthermore, according to the definition of reliability a system or subsystem with low reliability within a certain time period may fail to reach the required performance. For real-life engineered systems e.g. aerospace systems, civil infrastructure systems, unanticipated failures occurring in such systems will inevitably cause abrupt breakdown of the systems or their subsystems, which will further give rise to immense costs in maintenance. Thus, it is of vital significance to predict the reliability of the systems under real-life conditions and arrange for future maintenance schedules considering its advantages of being cost-saving and highly efficient for engineered systems.

### 2.5.2 Failure prognostics approaches

In the field of the reliability engineering, the term "*prognostics*" is proposed to summarise the process of the abovementioned reliability prediction [21]. The goal of the prognostics is to

predict the reliability of an engineered system and then to infer the failure time of the system based on degradation tests or statistical modelling with access to the failure data [77]. Furthermore, the concept called "*Remaining Useful Life (RUL)*", which is assumed as the subtraction between the End Of Life (EOL) and the current service time of the system [78], is proposed as the key parameter in prognostics. Within the past decades, there have existed a great amount of methods in prognostics with particular emphasis on prediction of the RUL. In terms of the methodology, such methods can generally be categorised into mainly three branches [79], namely the physics-based prognostics, the data-driven prognostics, and the fusion method, which is the combination of the previous two methods.

Among those methods, the physics-based prognostics or Physics of Failure (PoF) based prognostics aims to investigate the failure mechanism of a system and then to predict the RUL based on prior knowledge of the mechanism [80]. The main advantage of the PoF-based prognostics is its ability to reflect the failure mechanism in specific scenarios and to detect the failures in an engineered system [79, 81, 82]. However, there exist several limitations with this method. Firstly, the method requires parametric information of the properties of the materials or components employed in the system without considering the difficulties to gain complete access to the information [79] which may be due to both the real-life operating environment and sometimes the confidentiality [81] of data sources. Secondly, the situation to which the physics-based model is applied is highly restricted to a specific and single scenario [79] which will greatly affect the model's competence to forecast the system's failure time particularly when the system is encountered with several failures occurring or even interacting with others in various real-life scenarios simultaneously. Moreover, the method has rigorous requirement for the quality of the data acquired by degradation tests, thus causing immense costs when conducting the tests [79, 83, 84]. In addition, under some circumstances, the physics-based model, which is established and then further calibrated by means of the degradation tests, may have narrow applications in prognostics due to its complexity [81, 85].

Considering those limitations of the physics-based method, an alternative method, namely the data-driven prognostics, is then proposed. The essential idea of this method is to predict the reliability or the RUL of an engineered system solely based on the analysis of the failure data

without taking the failure mechanism of the system into consideration [86]. The ignorance of the failure mechanism avoids the weakness of the physics-based prognostics and broaden the applicability of the data-driven method. To predict the RUL, the data-driven prognostics can be further classified into the statistical learning prognostics and AI-based prognostics [87], where the former employs statistical approaches including conventional time series methods, e.g., Autoregressive Integrated Moving Average model [88,89], Markov models particularly Hidden Markov model [90,91], Wiener Process [92,93], proportional hazards model [94–97] and other statistical models [98–100], and the latter utilises the machine learning methods containing predominantly utilised Neural Networks(NNs) [101–105], Support Vector Machine (SVM) [97, 106, 107] and others [108, 109]. Compared with the physics-based prognostics, strengths of the data-driven prognostics are embodied within its ability to extract and analyse patterns of the data acquired in the complex engineered systems [106], its high accuracy for the RUL prediction [90] and its flexibility to analyse various kinds of engineered systems with different characteristics including multiple variates and nonlinearity [22]. Such strengths enable the data-driven prognostics to be a competitive and powerful tool for both condition-based maintenance and predictive maintenance [110].

In spite of its strengths the majority of the data-driven prognostics is often criticised for its requirement for the high-quality data acquired by degradation tests. In real-life operating conditions, data confidentiality, the lack of measuring instruments with high precision, extreme conditions and planned maintenance behaviour will lead to the acquisition of sparse and incomplete datasets with high uncertainties [22, 83, 111], thus posing difficulties for the data-driven method. Furthermore, some statistical prognostics approaches e.g. Markov models, Bayesian methods, proportional hazards model require the assumptions or the prior knowledge of the system [112] while the AI-based approaches struggle in uncertainty quantification of the predicted RUL or the reliability of the system [90]. For example, despite the ability of the proportional hazards model to analyse influence of environmental and operational conditions on the reliability of engineered systems, such model requires prior knowledge of the conditions [113] which is embodied within covariate functions in the proportional hazards model. Therefore, the efficiency and effectiveness of the proportional hazards model to predict the

system reliability under environmental and operational working conditions heavily depends on researchers' personal experience particularly in the process of choosing covariate variables [114], which more or less restricts the model's applicability. Moreover, even if the covariate functions were selected correctly, the effectiveness of the single proportional hazards model would still be limited mainly because that this model ignores dynamic selection and abandonment of covariate functions [114], which may lead to overfitting [113] and high computational costs of the model [22]. As explained above, those shortcomings restrict the efficiency and the applicability of the data-driven prognostics.

### 2.5.3 Metrics for the RUL prediction

In real-life applications, the RUL prediction is usually implemented with the health index ($HI$), which is an essential indicator revealing the real-time health condition of engineered systems. The $HI$ is assumed as generally decreasing [22] (despite local fluctuations) against the system operation time and reaching zero when the monitored system fails entirely. Following such run-to-failure rationale, the RUL can be formulated as

$$RUL = t_{HI=0} - t_c \tag{2.79}$$

where $t_{HI=0}$ represents the instant when the HI hits zero and is equivalent to the EOL for run-to-failure records [22], $t_c$ is the current operation time of the monitored system.

The performance of different RUL prediction algorithms can be further assessed with the following metrics [22].

1) Root mean square error (RMSE)

$$RMSE = \sqrt{\frac{1}{n_m}\sum_{i=1}^{n_m}\left(\widehat{RUL_l} - RUL_{i,\,\text{true}}\right)^2} \tag{2.80}$$

where $n_m$ is the number of machines for the RUL prediction while $\widehat{RUL}_i, RUL_{i,true}$ are the estimated RUL and the ground truth of the $i$-th ($1 \leq i \leq n_m$) unit respectively.

2) Mean absolute error (MAE)

$$\text{MAE} = \frac{1}{n_m}\sum_{i=1}^{n_m}\left|\widehat{RUL_i} - RUL_{i,true}\right| \tag{2.81}$$

where $n_m$, $\widehat{RUL_i}$, $RUL_{i,\text{ true}}$ remain the same as (2.81).

3) Confidence interval (CI) [22, 115]

$$\Pr\left(RUL_{i,\text{ true}} - \frac{CI_i}{2} \leq \widehat{RUL_i} \leq RUL_{i,\text{ true}} + \frac{CI_i}{2}\right) = 0.95 \tag{2.82}$$

where $CI_i$ represents the 95% confidence interval for the predicted RUL of the $i$-th $(1 \leq i \leq n_m)$ unit.

4) Exponential score metric [22, 116]

$$\text{Score} = \begin{cases} \exp\left(-\frac{\widehat{RUL_i} - RUL_{i,\text{ true}}}{13}\right) - 1 & \widehat{RUL_i} < RUL_{i,\text{ true}} \\ \exp\left(\frac{\widehat{RUL_i} - RUL_{i,\text{ true}}}{10}\right) - 1 & \widehat{RUL_i} \geq RUL_{i,\text{ true}} \end{cases} \tag{2.83}$$

Note that the above metrics require true RUL values for performance assessments on the RUL prediction algorithms. Readers are referred to [22] for more RUL-related metrics.

### 2.5.4 Summary

This chapter serves as an introductory overview of fundamental concepts in Structural Health Monitoring (SHM) and Prognostics and Health Management (PHM) in the context of the research outlined in the thesis. The SHM section primarily focuses on the applications of ultrasonic guided wave propagation in both isotropic and anisotropic media. Special attention is given to the acquisition and processing of guided wave signals for the purpose of damage detection and localisation. The chapter also addresses the impact of temperature variations on guided wave signals and introduces various temperature compensation techniques.

The PHM introduces key concepts such as reliability, failure prognostics, and Remaining

Useful Life (RUL). Furthermore RUL prediction through three branches: physics-based, data-driven, and fusion methods, along with the presentation of relevant metrics like RMSE and CI are described.

# Chapter 3

# Baseline-based guided wave structural health monitoring of composite structures

## 3.1 Introduction

In the field of guided wave based structural health monitoring (GWSHM), there is a growing interest in the application of autoregressive (AR) modelling. However, reported research primarily focuses on damage detection in metallic or quasi-isotropic structures [29–33], limiting the application of AR models to the more advanced composite structures. Furthermore, the conventional practice of directly inputting oversampled ultrasonic guided wave (UGW) signals into AR models, as observed in many previous studies [29–33], introduces the risk of model biases and increased computation time during structural health monitoring (SHM) applications. Hence, in this chapter a streamlined and proficient baseline-dependent approach for the GWSHM by integrating signal compression and autoregressive (AR) modelling on guided wave

[1]Part of this chapter, mainly involving the theoretical background and the experimental setup respectively in section 3.2 and section 3.4, appears in Hongmin Zhu, Zahra Sharif Khodaei, and M.H. Aliabadi. (2023) [34]. In this chapter, the parameter estimation of AR model, particularly the estimation of AR lag order, is totally different from the conference paper [34], leading to separate and different results on damage detection and localisation.

signals is introduced. The suggested adaptive signal compression is applied to the UGW signals, and subsequently, AR-based features are extracted from the compressed measurements. These AR-based features effectively capture the temporal structure of UGW signals, with deviations in temporal patterns between pristine and current measurements indicating the presence of damage. The proposed approach is subsequently employed for damage detection and localisation on both quasi-isotropic and anisotropic composite structures.

The rest of this chapter is structured as follows: Section 2 provides an introduction to the theoretical background of the proposed method and section 3 provides more details of the proposed methodology. Experimental results are presented in sections 4 to 7. The summary includes conclusive remarks for this chapter.

## 3.2 Theoretical background

### 3.2.1 Time series and the AR models

A time series is defined as an aggregate of observations within a certain time duration [117]. Therefore, ultrasonic guided wave signals are essentially time series but in a discrete-time manner where the data points are sampled within a fixed interval.

The autoregressive (AR) model has been widely applied in econometrics [118] to capture and interpret long-term temporal patterns [117] by correlating past and current values of time series. In this chapter, such model is utilised to extract temporal guided wave features which are sensitive to the presence of damage. The standard AR model can be formulated as follows [117].

$$X_t - \phi_1 X_{t-1} - \cdots - \phi_p X_{t-p} = Z_{p,t}(t = p+1, \ldots, N) \tag{3.1}$$

where $X_t$, $N$ are the current value and the sample size of time series respectively, $p(0 < p < t)$ is the order of time lags, $\phi_1, \ldots, \phi_p$ are AR coefficients of the $p$ lagged values $X_{t-1}, \ldots, X_{t-p}$, and $Z_{p,t} \sim N(0, \sigma^2)$ is a $p$-related independent and identically distributed (IID) error term where the variance $\sigma^2$ is assumed constant. By introducing a backshift operator $B$ such that

$BX_t = X_{t-1}$, the equation (3.1) is reformulated as [117]

$$\phi(B)X_t = Z_{p,t} \tag{3.2}$$

where $\phi(B) = 1 - \sum_{i=1}^{p} \phi_i B^i$ is the autoregressive polynomial of $AR(p)$ process.

The estimation of $p$ in (3.1) can be implemented based on criterion including the Akaike information criterion (AIC), the Bayesian information criterion (BIC), the partial autocorrelation function (PACF), the final prediction error (FPE) and the root mean squared error (RMSE) [32]. In this work, an optimal $p$ is obtained by integrating the results of AIC, BIC and RMSE. The AIC minimises the information loss when fitting data within a given model [119]. A general formulation of AIC is shown as [119]

$$AIC = -2\log(\boldsymbol{L}(\widehat{\boldsymbol{\theta}} \mid \boldsymbol{y})) + 2K \tag{3.3}$$

where $\boldsymbol{y}$ denotes the input data, $\boldsymbol{L}(\widehat{\boldsymbol{\theta}} \mid \boldsymbol{y})$ denotes the maximum-likelihood estimate of the model parameters $\boldsymbol{\theta}$ based on $\boldsymbol{y}, K$ is the number of model parameters. It is implied that the AIC compromises between the model bias and the penalty for model parsimony [120], which are reflected by the logarithmic term and $K$ respectively. When estimating $p$ in the AR model, the AIC is specified as [121, 122]

$$AIC = n\left(\log\left(\mathrm{Var}\left(\hat{Z}_{p,t}\right)\right) + 1\right) + 2(\hat{p} + 1) \tag{3.4}$$

where $n$ is the sample size, $\hat{p}$ is the estimated time lag, $\mathrm{Var}\,(\hat{z}_{p,t})$ is the residual variance dependent on $\hat{p}$. The $\hat{p}$ corresponding to the minimum AIC is determined as the AR order. Note that the AIC may lead to biased estimates when $n$ is relatively small [120, 122], i.e., $\frac{n}{\hat{p}+1} < 40$ [120], thus leading to a modified AIC measure, i.e., AICC [117,120,122]. Nevertheless, the AICC can yield extra computational difficulties since it introduces a second order estimate of $\hat{p}$ [120,122]. In this regard, the BIC [117,120] presented below is usually resorted to considering the small-sample issues.

$$BIC = -2\log(\boldsymbol{L}(\widehat{\boldsymbol{\theta}} \mid \boldsymbol{y})) + K\ln n \tag{3.5}$$

Compared to (3.3), BIC has a stronger penalty term $K \ln n$, and consequently gives a more parsimonious estimation of $p$ [123], i.e., smaller $\hat{p}$ values. When $n$ is large with respect to $\hat{p}$, the AIC usually leads to a better fitting of time series by exploiting a larger time lag [120].

Meanwhile, the RMSE for estimating the lag order $p$ [32] is defined as follows.

$$\mathrm{RMSE}(\hat{p}) = \sqrt{\frac{\mathrm{Var}\left(\hat{z}_{p,t}\right)}{n}} \tag{3.6}$$

where $\hat{p}, \mathrm{Var}\left(\hat{Z}_{p,t}\right), n$ are the same as (3.4). To circumvent overfitting of AR models, the optimal $p$ is found when the RMSE remain steady around $\hat{p}$.

The AR coefficients can be estimated based on the ordinary least squares (OLS) technique [124], the Yule-Walker equation [125] and the Burg's method [126]. For the sake of simplicity, the OLS is employed to estimate $\phi_i (i = 1, \ldots, p)$ and formulates (3.1) into [34, 124]

$$\boldsymbol{X_c} = \boldsymbol{X_p}\boldsymbol{\beta} + \boldsymbol{Z} \tag{3.7}$$

where $\boldsymbol{X}_c$ is a $(N-p) \times 1$ vector including the current values of time series from the $(p+1)$-th point to the $N$-th point, $\boldsymbol{X_p}$ is a $(N-p) \times (p+1)$ dimensional matrix containing the past values and a constant intercept term, $\boldsymbol{\beta}$ is the corresponding $(p+1) \times 1$ dimensional vector of the AR coefficients, while $\boldsymbol{Z}$ denotes the $(N-p) \times 1$ error term of the AR model [34]. The estimation of $\boldsymbol{\beta}$ is presented as [34, 124]

$$\widehat{\boldsymbol{\beta}} = \left(\boldsymbol{X_p}^T \boldsymbol{X_p}\right)^{-1} \boldsymbol{X_p}^T \boldsymbol{X_c} \tag{3.8}$$

where $\boldsymbol{T}$ and $()^{-1}$ represent the transpose and the inverse form of a matrix.

Furthermore, the implementation of AR model requires the stationarity of time series. A time series $\{\boldsymbol{X}_t\} (t \in \mathbb{N})$ is considered as (weak) stationary if its mean and covariance are time-invariant [117], which is formulated as [117]

$$\mu_{\boldsymbol{X}_t} = C_1 \tag{3.9}$$

$$\kappa_X(t, t+h) = E\left[\left(\boldsymbol{X}_t - \mu_{\boldsymbol{X}_t}\right)\left(\boldsymbol{X}_{t+h} - \mu_{\boldsymbol{X}_{t+h}}\right)\right] = C_2 \quad \forall h \in \mathbb{Z} \tag{3.10}$$

where $h$ is an arbitrary time lag, $\mu_{\boldsymbol{X}_t}, \mu_{\boldsymbol{X}_{t+h}}$ are mean values of $\{\boldsymbol{X}_t\}$ and the lagged series $\{\boldsymbol{X}_{t+h}\}$, $\kappa_X(t, t+h)$ denotes the covariance function between $\{\boldsymbol{X}_t\}$ and $\{\boldsymbol{X}_{t+h}\}$, and $C_1, C_2$ are constants. The (3.9) - (3.10) indicate the absence of any trend terms in a stationary time series. Such property circumvents spurious regression issues [27] when regressing $\boldsymbol{X_c}$ over $\boldsymbol{X_p}$ in (3.7) and ensures an unbiased estimate of $\boldsymbol{\beta}$.

The augmented Dickey-Fuller (ADF) test [117, 127] has been regularly adopted within the AR framework to interrogate the stationarity of time series. Recall that the $AR(p)$ process in (3.1) can be transformed into [117]

$$\Delta X_t = \phi_1' X_{t-1} + \phi_2' \Delta X_{t-1} + \cdots + \phi_p' \Delta X_{t-p+1} + Z_{p,t} \tag{3.11}$$

where $\Delta X_t = X_t - X_{t-1}, \phi_1' = \sum_{i=1}^{p} \phi_i - 1, \phi_k' = -\sum_{i=k}^{p} \phi_k (k = 2, \ldots, p)$, and $\phi_k$ represents the estimated AR coefficients. Since the $\Delta X_{t-k+1}$ terms are obtained through the first-order differencing, $\phi_1' X_{t-1}$ is the only trend term in (3.11). Hence, $\{\boldsymbol{X}_t\}$ is inferred as stationary if $\phi_1' < 0$ [117, 127]; otherwise, the $\phi_1' X_{t-1}$ would lead to deterministic or stochastic trends [127], e.g., random walk, in $\{\boldsymbol{X}_t\}$. Since the explosive behaviour of time series is not considered, the cases are precluded where $\phi_1' < -2$ or $\phi_1' > 0$ to ensure $|1 + \phi_1'| < 1$. Correspondingly, a single-sided hypothesis for the statistical ADF test is obtained as [117, 118, 127]

$$\mathcal{H}_0 : \phi_1' = 0; \quad \mathcal{H}_1 : \phi_1' < 0 \tag{3.12}$$

where $\mathcal{H}_0$ is the null hypothesis assuming that $\{\boldsymbol{X}_t\}$ is non-stationary, $\mathcal{H}_1$ is the alternative that rejects the $\mathcal{H}_0$ under specific conditions. The standard $t$-statistic is an intuitive option to test $\mathcal{H}_0$. However, such statistic is not applicable considering that $\phi_1'$ is not asymptotically normally distributed under the non-stationarity of $X_{t-1}$ [118]. A specific test statistic for $\mathcal{H}_0$ is therefore proposed as [117, 118, 127]

$$DF = \frac{\widehat{\phi_1'}}{\text{std}\left(\widehat{\phi_1'}\right)} \tag{3.13}$$

where $DF, \widehat{\phi}_1', \text{std}\left(\widehat{\phi}_1'\right)$ are the Dickey-Fuller statistic, the OLS estimate of $\phi_1'$ and the corresponding standard deviation, respectively. The distribution of DF is not normal nor asymptotically normal, and consequently sampled through numerical simulations [118], e.g., the Monte Carlo approach. A time series is then inferred as stationary if the calculated DF is smaller than a critical quantile, denoted as $\alpha$, of the DF distribution, thus rejecting the null hypothesis. The quantile $\alpha$ is called significance level and usually adopted as 0.05 in engineering applications [128]. For non-stationary time series, the differencing procedure [117], i.e., subtraction of the previous time series value from the current one, is recursively implemented until the differenced time series are fully detrended and stationary.

In addition, an appropriate selection of $p$ is essential to ensure an unbiased implementation of the ADF test since a large $p$ could yield power loss of the test [129]. A practical restriction on $p$ is proposed by [130] as

$$p_{\max} = \left[12 \cdot \left(\frac{N}{100}\right)^{0.25}\right] \tag{3.14}$$

where $p_{\max}$ denotes the maximum $p$ for the ADF test, $[\cdot]$ denotes the integer value function and $N$ remains the same as (3.1).

Moreover, common diagnostic checks can be performed as follows to validate the estimated AR model when applied to a stationary time series.

- **Residual autocorrelation.** The residual autocorrelation indicates the serial dependence between residual values at adjacent sampling points [27] and can be inspected by the autocorrelation function (ACF) plots of residuals [117].

- **Residual normality.** This property indicates the randomness of AR residuals and therefore an unbiased estimate of AR models. The residual normality can be interrogated by the quantile-quantile $(Q-Q)$ plot [131] which compares quantiles of the residual distribution and a normal distribution, combined with the Jarque-Bera (J-B) test statistic [132] as follows.

  $$JB = \frac{N}{6}\left(Skew^2 + \frac{(\text{ Kurt } - 3)^2}{4}\right) \tag{3.15}$$

  where $N$, $Skew$ and $Kurt$ represent the sample size, sample skewness and the sample

kurtosis respectively [132]. The J-B statistic follows the chi-squared distribution $\chi^2(2)$ and significance value $p < 0.05$ implies rejection of the null hypothesis that the sample is normally distributed [132].

- **Model stability.** According to (3.1) - (3.2), the AR model is considered as an inhomogeneous linear difference equation whose complementary solution satisfies the following characteristic equation [118, 133].

$$\lambda_k^p - \phi_1 \lambda_k^{p-1} - \cdots - \phi_p = 0 \tag{3.16}$$

where $\lambda_k (k = 1, \ldots, p)$ denotes all the characteristic roots and $\lambda_k \neq 0$. Hence, the equation is derived into (3.17) by multiplying $\lambda_k^{-p}$.

$$\phi_1 \lambda_k^{-1} + \cdots + \phi_p \lambda_k^{-p} = 1 \tag{3.17}$$

To ensure the convergence and stability of the AR model, the modulus of $\lambda_k$ must satisfy $|\lambda_k| > 1$, which implies that all the roots $\lambda_k$ fall outside a unit circle in a complex plane [117, 134]. The model stability is essential when utilizing the AR model for future predictions. Regarding an unstable AR model, its prediction performance would much degrade because $|\lambda_k| < 1$ could yield explosive predicted values. Nevertheless, the estimation of AR-based features is not much affected for the unstable AR process [135]. Therefore, the model stability is not essential when extracting the AR-based features for the SHM purposes.

### 3.2.2 Signal compression techniques

The signal compression aims to reduce the costs of signal transmission, storage, and processing stages by discarding redundant signal information. Common techniques for the signal compression include the uniform sampling and the Gaussian random sampling, which are shown as follows [34].

- **Uniform sampling.** The uniform sampling follows $\boldsymbol{x}_d[n] = \boldsymbol{x}[nT_d]$ [55], where $\boldsymbol{x}_d$ and $x$ represent the down-sampled and the raw signal respectively, $T_d$ represents a specific time interval for the down-sampling and $n$ is denoted as the $n$-th sampling point in the $\boldsymbol{x}_d$ [55].

- **Gaussian random sampling.** The Gaussian random sampling follows $x_{\boldsymbol{d}} = A\boldsymbol{x}$ [136], where $\boldsymbol{x_d}$ and $\boldsymbol{x}$ represent the down-sampled and the raw signal respectively, and $A$ represents the sampling matrix with elements obeying the Gaussian distribution. More specifically, elements of the sampling matrix follow $A_{i,j} \sim N\left(0, \frac{1}{M}\right)$ where $i$ and $j$ represent row and column of the elements, $N(\cdot)$ represents the Gaussian distribution and $M$ denotes the size of the down-sampled signal [136].

To circumvent signal aliasing issues [55], signals to be compressed should satisfy the Nyquist sampling theorem, namely $f_s > 2f_{\max}$, where $f_s, f_{\max}$ represent the signal sampling rate and the maximum frequency component of the signal [55].

## 3.3 Proposed methodology

In the domain of GWSHM, the signal acquisition particularly based on the chirp excitation is usually implemented following the oversampling procedure where the signal sampling rate highly exceeds the signal frequency to ensure high time resolution of collected guided wave signals. In this thesis, 50 kHz $A_0$ guided wave modes are extracted from chirp responses ranging from 10 kHz to 600 kHz whereas the sampling frequency is adopted as 60 MS/s, leading to highly oversampled guided wave signals in the time domain. As shown in Fig. 3.1, 30000 sampling points are collected from the targeted 50 kHz signal within the duration of 500 $\mu$s while 6600 points are obtained from the first wave packet of the $A_0$ mode. However, such configuration leads to high correlation between adjacent sampling points, which could bias the estimation of AR-based damage-sensitive features when directly implementing the standard AR model on oversampled signals. In this regard, integrating signal compression techniques into the standard AR model could largely alleviate the oversampling issue while enhancing the computational efficiency during the SHM tasks.

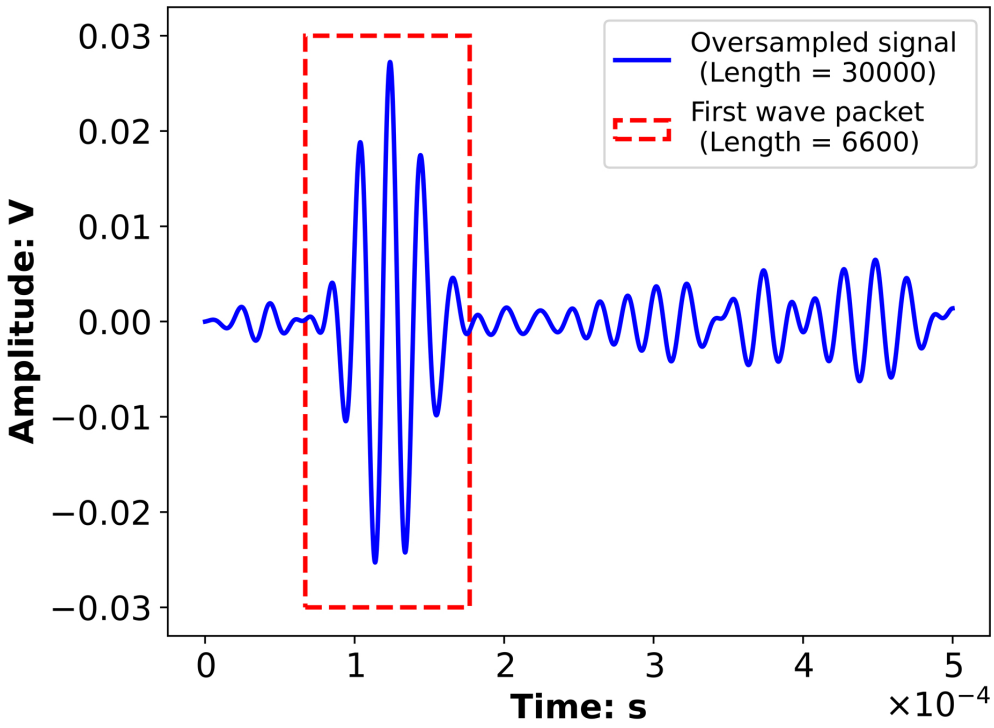


Figure 3.1: 50 kHz $A_0$ guided wave signal with the sampling frequency as 60 MS/s

In this chapter, the proposed baseline-based method for damage detection and localisation on composite structures is introduced integrating the AR features and signal compression techniques. As shown in the schematic sketch in Fig. 3.2, the proposed method is comprised of four main parts, which are explained as follows.

- **Signal acquisition and pre-processing.** Pristine and damaged signals are collected as guided wave chirps from the same inspected structure before and after the presence of damage. The chirp measurements are transformed into Lamb wave tone bursts following (2.28) - (2.30) while being denoised by a $4^{\text{th}}$ order Butterworth bandpass filter [137]. During the transform, the Hanning window in (2.36) is implemented to modulate the transformed tone bursts to alleviate spectrum leakage issues.

- **Signal compression** An adaptive signal compression technique based on the two-sided cumulative sum (CUSUM) [138] algorithm is proposed to compress the tone bursts while maintaining temporal structures of the signals. The proposed method is comprised of the following steps:

1) Temporal segmentation of guided wave signals. As illustrated in Fig. 3.3, a Lamb wave tone burst exhibits high temporal variations between several segments with different means and variances. Conventional signal compression approaches, e.g., the uniform sampling, may fail to well capture such signal variations, thus leading to signal distortions in the compressed measurements of raw tone bursts. In this regard, the two-sided CUSUM algorithm [138], originally proposed for quality control and change point detection, is employed to process the signal variations by partitioning the guided wave signals with detected changing points. The implementation of this algorithm is shown in Table 3.1.

   The main rationale of the two-sided CUSUM lies in a continuous detection on cumulative signal changes [138]. More specifically, a change point can be detected when the cumulative signal variations exceed a certain threshold, $Thr$. The threshold for change point detection is usually determined in an empirical manner and therefore adopted as 30% of the signal peak, which corresponds to the time of arrival (TOA), when processing a Lamb wave tone burst $\boldsymbol{X_t}$, as shown in Line 2, Table 3.1. Two real-time statistics, i.e., $g_i^+$and $g_i^-$, are then initialised for monitoring positive (increasing) and negative (decreasing) signal shifts respectively (Line 3), and constantly updated by the cumulative sum of signal changes between two adjacent points (Line 5-7) [138]. The accumulative shifts exceeding the detection threshold further indicate the presence of change points (Line 8-10). Finally, the $\Omega$ is returned which contains $K^*$ ($K^* \geq 1$) change points partitioning $\boldsymbol{X_t}$ into $K^*+1$ segments or blocks.

2) Block-wise down-sampling of guided wave signals. Uniform down-sampling procedures are implemented on each block after the temporal segmentation of guided wave signals. Regarding a specific block $\boldsymbol{X}_{i,t}^*$ ($i = 1, \ldots, K^*+1$) of $\boldsymbol{X_t}$, its compressed measurements $\boldsymbol{y_{i,t}^*}$ are yielded as

$$\boldsymbol{y_{i,t}^*} = A_i^* \boldsymbol{X_{i,t}^*} \tag{3.18}$$

   where $A_i^*$ denotes a $m_i^* \times n_i^*$ down-sampling matrix compressing $\boldsymbol{X}_{i,t}^*$ of $n_i^*$ sampling points into $\boldsymbol{y}_{i,t}^*$ of $m_i^*$ points. The $A_i^*$ for each block should satisfy the Nyquist

sampling theorem in section 3.2.2. Furthermore, the compressed measurement of the entire signal $\boldsymbol{X_t}$, denoted as $\boldsymbol{y_t^*}$, is expressed as

$$\boldsymbol{y_t^*} = \sum_{i=1}^{K^*+1} \boldsymbol{y}_{i,t}^* = \sum_{i=1}^{K^*+1} A_i^* \boldsymbol{X}_{i,t}^* = A^* \sum_{i=1}^{K^*+1} \boldsymbol{X}_{i,t}^* = A^* \boldsymbol{X_t} \tag{3.19}$$

where $A^*$ is a general matrix for compressing $\boldsymbol{X_t}$ while other variables remain the same as (3.18).

- **AR signal modelling on compressed measurements.** According to (3.8), the autoregressive coefficient $\boldsymbol{\beta}^*$ when establishing an AR model on the compressed measurement $\boldsymbol{y_t^*}$ is estimated as

$$\widehat{\boldsymbol{\beta^*}} = \left(\boldsymbol{y_p^{*T}} \boldsymbol{y_p^*}\right)^{-1} \boldsymbol{y_p^{*T}} \boldsymbol{y_c}^* \tag{3.20}$$

where $\widehat{\boldsymbol{\beta}^*}$ is the estimation of $\boldsymbol{\beta}^*$ whereas $\boldsymbol{y_p^*}, \boldsymbol{y}_c^*$ are the compressed version of $\boldsymbol{X_p}, \boldsymbol{X_c}$ respectively in (3.8). Note that 3.20 differs critically from [139] and [140] regarding the generated compressed measurements and the corresponding parameter estimation. Integrating (3.19) into (3.20), $\boldsymbol{\beta}^*$ is estimated as

$$\widehat{\boldsymbol{\beta^*}} = \left(\boldsymbol{X_p}^T A^{*T} A^* \boldsymbol{X_p}\right)^{-1} \boldsymbol{X_p}^T A^{*T} A^* \boldsymbol{X_c} = \left(\boldsymbol{X_p}^T G^* \boldsymbol{X_p}\right)^{-1} \boldsymbol{X_p}^T G^* \boldsymbol{X_c} \tag{3.21}$$

where $G^* = A^{*T} A^*$ and others remain the same as (3.8). It is implied that $\boldsymbol{\beta}^*$ has the similar form to (3.8) and only differs at $G^*$ due to the signal compression. Based on $\boldsymbol{\beta}^*$, the AR residual $\boldsymbol{Z}^*$ of $\boldsymbol{y_t^*}$ is calculated as $\boldsymbol{y_c^*} - \boldsymbol{y_p^*}\widehat{\boldsymbol{\beta}^*}$, similar to (3.7), and employed as a damage-sensitive feature for the GWSHM purposes.

- **Damage detection and localisation.** Two different damage indices ($DI$s) are generated based on AR features to reveal discrepancies between pristine and damaged measurements for the SHM purposes. The $DI_1$ is implemented as the Bhattacharyya distance measure [141] on the AR residual $\boldsymbol{Z}^*$, and is formulated below [141].

$$DI_{1,i} = \frac{1}{2} \ln \frac{{\sigma_{b,i}^*}^2 + {\sigma_{c,i}^*}^2}{2\sigma_{b,i}^* \sigma_{c,i}^*} \tag{3.22}$$

where $\sigma^*_{b,i}, \sigma^*_{c,i}$ represent the variances of $\boldsymbol{Z^*_{b,i}}, \boldsymbol{Z^*_{c,i}}$ at path $i$, and $\boldsymbol{Z^*_{b,i}}, \boldsymbol{Z^*_{c,i}}$ denote the AR residuals of compressed guided wave signals under baseline and current state respectively. For the sake of simplicity, the same lag order $p$ in (3.1) is adopted for AR models on pristine and damaged measurements. Consequently, the presence of damage is only implied by the discrepancies between $\boldsymbol{Z^*_{b,i}}$ and $\boldsymbol{Z^*_{c,i}}$. Another type of $DI$, i.e., $DI_2$, based on $\boldsymbol{Z}^*$ is proposed below, where corr$(\cdot)$ denotes the Pearson correlation.

$$DI_{2,i} = 1 - \left|\text{corr}\left(\boldsymbol{Z^*_{b,i}}, \boldsymbol{Z^*_{c,i}}\right)\right| \tag{3.23}$$

The damage detection is implemented following (2.53)-(2.56), where the Mahalanobis distance (MD) is employed to distinguish between the pristine and damaged states. The MD measure follows the chi-squared distribution $\chi^2(2)$ [14,62], where 2 denotes the degree of freedom, and therefore the detection threshold can be adopted as the distribution value with 99.9% confidence [14], i.e., $\chi^2_{0.999}(2)$. Consequently, any measurement with the corresponding MD value above the threshold is inferred as damaged, and vice versa. Furthermore, the detection performance is assessed by the following indicators adapted from [62].

$$TPR = TP/(TP + FN) \tag{3.24}$$

$$FAR = FP/(FP + TN) \tag{3.25}$$

$$ACC = (TP + TN)/(TP + TN + FP + FN) \tag{3.26}$$

where $TPR$, $FAR$, $ACC$ represent the true positive rate, the false alarm rate and the accuracy for the damage detection. $TP, TN, FP, FN$ denote the number of true positive, true negative, false positive and false negative outcomes respectively when regarding damage detection as a binary classification problem.

The standard RAPID algorithm in (2.67) - (2.69) is utilised for damage localisation because it allows a flexible use of the $DI$ features. $100 \times 100$ pixels are employed for damage imaging while the scaling factor $\delta$ in (2.67) - (2.68) is adopted as 1.05 [16]. The

performance metric for damage localisation is defined as [14, 62]

$$\varepsilon_d = \sqrt{(\hat{x} - x_d)^2 + (\hat{y} - y_d)^2} \tag{3.27}$$

where $\varepsilon_d$ is the trueness or localisation error between the average location estimates $(\hat{x}, \hat{y})$ and the true damage location $(x_d, y_d)$.

Table 3.1: The CUSUM algorithm [138] for segmentation of guided wave signals.

**Two-sided CUSUM ($\boldsymbol{X_t}$)**

**Input:** $X_t$ : guided wave signal of length $N$

**Output:** $\Omega$ : list of detected changing points

1. $\Omega \leftarrow [\,]$ // to store changing points of $X_t$
2. $Thr \leftarrow 0.3 * \max(X_t)$ // to determine an empirical detection threshold
3. $g_1^+ \leftarrow 0, g_1^- \leftarrow 0$ // to initialise the positive and negative shifts of $X_t$
4. **for** $i \leftarrow 2$ to $N$ **do**
5. $\quad s_i \leftarrow X_i - X_{i-1}$
6. $\quad g_i^+ \leftarrow \max\left(g_{i-1}^+ + s_i, 0\right)$ // to calculate accumulative positive shifts
7. $\quad g_i^- \leftarrow \max\left(g_{i-1}^- - s_i, 0\right)$ // to calculate accumulative negative shifts
8. $\quad$ **if** $g_i^+ > Thr$ **or** $g_i^- > Thr$ : **then**
9. $\quad\quad \Omega \leftarrow i$
10. $\quad\quad g_i^+ \leftarrow 0, g_i^- \leftarrow 0$ // reset the accumulative shifts
11. $\quad$ **end if**
12. **end for**
13. **return** $\Omega$

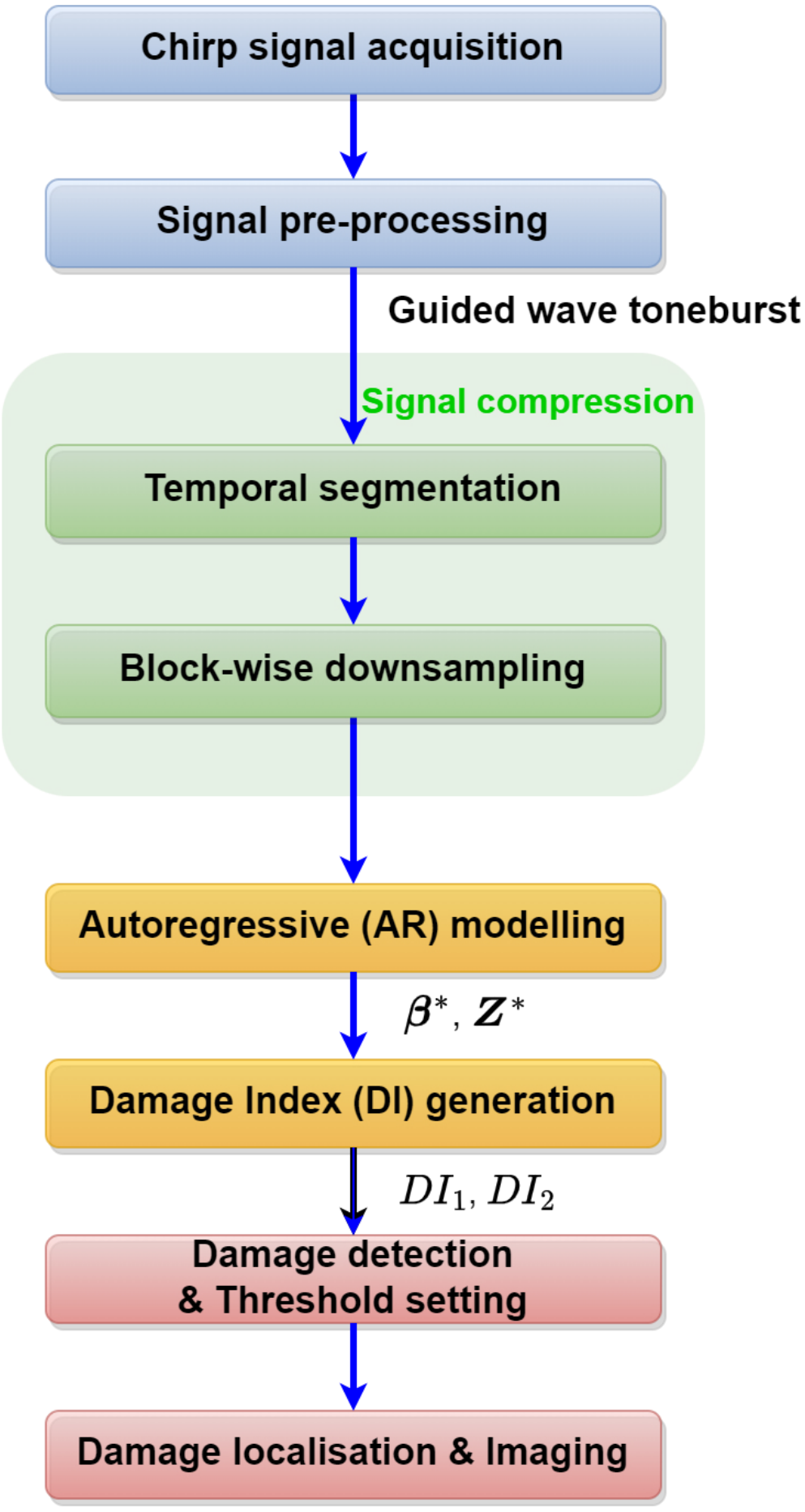


Figure 3.2: Proposed baseline-based method for damage detection and localisation.

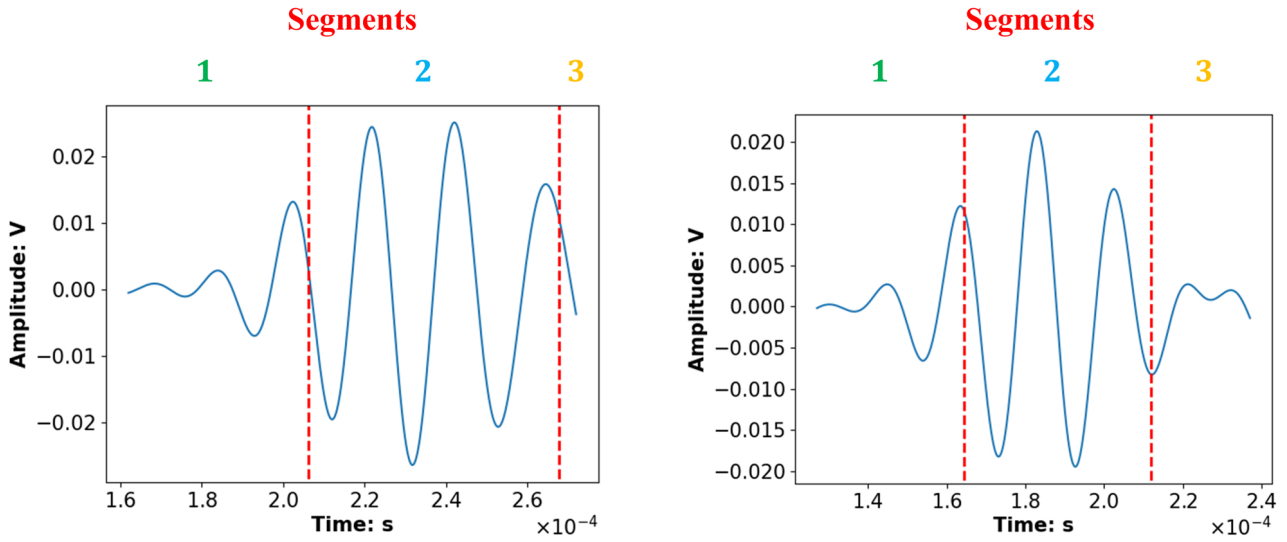


Figure 3.3: CUSUM-based temporal segmentation on example Lamb wave tone bursts, including within the first wave packet.

## 3.4 Experimental setup

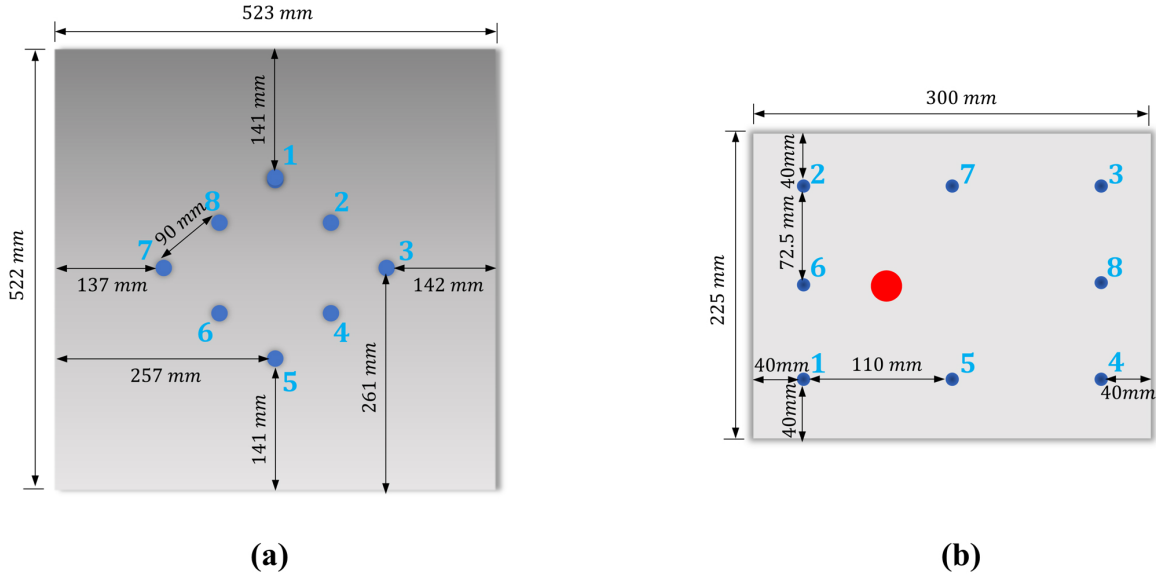


Figure 3.4: Illustration of two CFRP coupons with mounted PZT transducers: (a) Coupon 1 with a diamond PZT array; (b) Coupon 2 with a rectangular PZT array.

Experimental validations are implemented on two CFRP composite coupons, as illustrated in Fig. 3.4. More details of the specimens, including the material type, layer stacking sequence, specimen size, thickness, and the configuration of mounted transducers, are presented in Table 3.2. It is worth noting that the Coupon 1 is quasi-isotropic since the stacking sequence is well-balanced while the Coupon 2 [12] is regarded anisotropic due to the existence of extra

0° prepreg plies [12]. The Coupon 1 is implemented with 22 mm radius simulated damages situated at 10 different locations within the diamond network of 8 DuraAct PZT transducers and monitored under 25°C. According to Fig. 3.4(b), a 10 mm radius barely visible impact damage (BVID) with impact energy as 20 J is introduced to the Coupon 2 (within the red area) by the INSTRON CEAST 9350 impact tower [12]. The pristine and damaged measurements of Coupon 2 are collected under 20°C.

Table 3.2: Detailed information of the Coupon 1 and Coupon 2

| Specimen | Coupon 1 | Coupon 2 |
|---|---|---|
| Material type | M21/194/34%/T800S (M21 - T800S) | |
| Layer stacking sequence | $[0/\pm 45/90]_{2s}$ | $[\pm 45/0_2/90/0]_s$ |
| Specimen size | 523 mm × 522 mm | 300 mm × 225 mm |
| Thickness | 2.9 mm | 2.2 mm |
| Material anisotropy | Quasi-isotropic structure | Anisotropic |
| Transducer configuration | Diamond PZT array | Rectangular PZT array |
| Damage type | Simulated putty damage | Impact damage |

In terms of the data acquisition, 6V excitation signals are generated by a National Instrument (NI) signal generator. The chirp responses are collected by a PXI-5105 oscilloscope with sampling rate as 60MS/s. Signal pre-processing procedures are implemented where a 5-cycle Hanning window is adopted to generate tone burst signals, followed by the signal denoising with Butterworth bandpass filter of the fourth order. The centre frequency of the tone bursts is chosen as 50kHz, which corresponds to a predominant and damage-sensitive $A_0$ mode of Lamb waves [142].

In order to circumvent boundary reflections, only the first wave packets of Lamb wave tone bursts are considered as inputs for the signal compression and AR modelling procedures. When utilising the first arrival modes, the starting and ending time of the truncated packets are calculated as [14]

$$t_1 = \frac{d}{c_g}, t_2 = \frac{d}{c_g} + 1.1 \cdot \frac{n_c}{f_c} \tag{3.28}$$

where $t_1$ and $t_2$ denote the starting and ending time of the first wave packets, $d, n_c, f_c$ individually represent the transducer path distance, number of tone burst cycles (set as 5) and the centre frequency of signals (set as 50kHz ). $c_g$ denotes the group velocity of guided waves propagating along the transducer path and varies with propagation angles in anisotropic composite structures. A factor 1.1 is deployed to fully capture the first wave packet with an extra 10% length [14], yielding 6600 signal points for the first wave packet.

Moreover, $c_g$ is calculated by regressing the path distance on the time of arrival (TOA) of the entire-length pristine signals [68]. The arrival time is determined by the Rayleigh maximum likelihood estimation (RMLE) [143] on signal envelopes, which is formulated below [143].

$$\mathcal{L}(\zeta) = -\zeta \log \widehat{\sigma}_1^2(\zeta) - (N-\zeta) \log \hat{\sigma}_2^2(\zeta) + 2 \sum_{n=1}^{N} \log(h[n]) - N \tag{3.29}$$

where $\mathcal{L}(\zeta)$ denotes the maximum likelihood (ML) estimator of the arrival time candidate $\zeta, N$ is the signal length, $h[n]$ is the Hilbert signal envelope, while $\hat{\sigma}_1(\zeta)$, $\hat{\sigma}_2(\zeta)$ are two indicators presented as follows [143].

$$\hat{\sigma}_1(\zeta) = \sqrt{\frac{1}{2\zeta} \sum_{n=1}^{\zeta} h^2(n)} \tag{3.30}$$

$$\hat{\sigma}_2(\zeta) = \sqrt{\frac{1}{2(N-\zeta)} \sum_{n=\zeta+1}^{N} h^2(n)} \tag{3.31}$$

The estimated TOA $\zeta$ is then yielded as [143]

$$\hat{\zeta} := \operatorname{argmax} \mathcal{L}(\zeta) \tag{3.32}$$

Fig. 3.5 presents estimated group velocities of the Coupon 1 and Coupon 2 respectively utilising the $A_0$ wave mode under 50kHz. It is shown that the $c_g$ is estimated as 1343 m/s for the quasi-isotropic Coupon 1 under 25°C, accompanied by the $R$-squared value as 0.96 which indicates good fitting performance of the linear regression. Similarly, the experimental angular profile of $c_g$ is obtained for the Coupon 2 under 20°C considering material anisotropy and is consistent with the simulated result by the software [144] based on the SMM method in section 2.2.3. The numerical simulations yield dispersion curves in Fig. 3.6 utilising material properties

in Table 3.3.

Table 3.3: Material properties for generating dispersion curves of Coupon 2.

| $\rho\,[\mathrm{kg/m^3}]$ | $E_1[GPa]$ | $E_2[GPa]$ | $v_{12}$ | $v_{23}$ |
|---|---|---|---|---|
| 1600 | 141.2 | 8.675 | 0.312 | 0.45 |
| $G_{12}[GPa]$ | $G_{23}[GPa]$ | **Thickness [mm]** | **Stacking layer sequence** | |
| 4.29 | 3.1 | 2.2 | $[\pm 45/0_2/90/0]_s$ | |

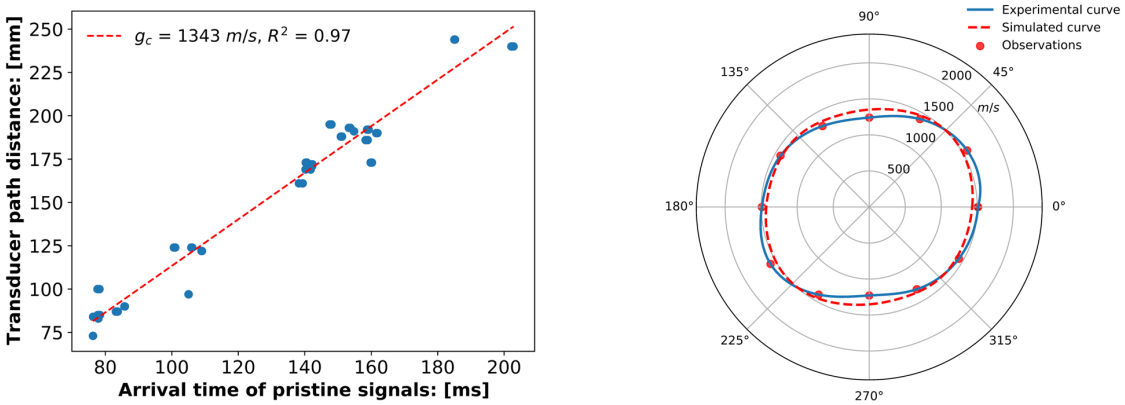


Figure 3.5: Group velocity estimation of 50kHz, $A_0$ Lamb wave mode for: (a) Coupon 1 under 25°C and (b) Coupon 2 under 20°C.

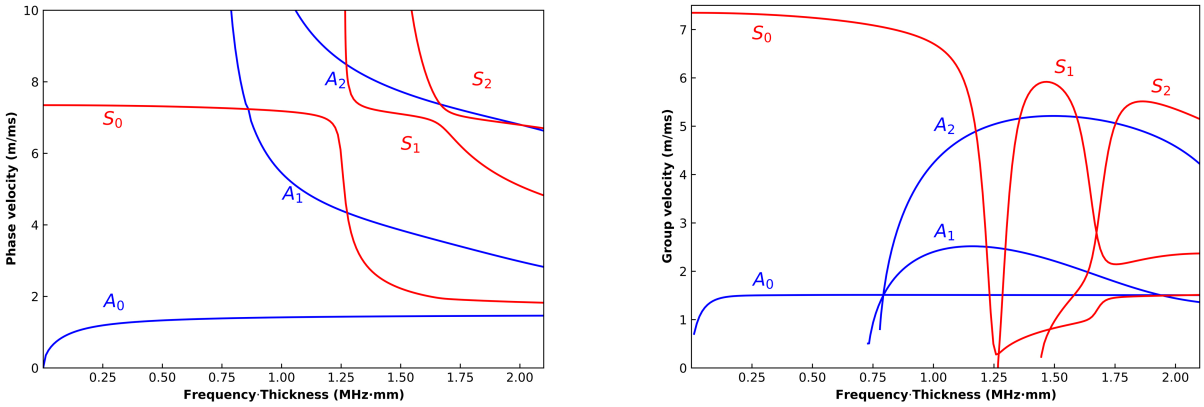


Figure 3.6: Dispersion curves of Coupon 2 in 0°: (left) group velocity curves; (right) phase velocity curves.

During the experiments, 90 measurements containing 60 pristine and 30 single damage records

are collected from Coupon 1 under 25°C, where half of the healthy measurements are utilised to calibrate the detection threshold. Meanwhile, 30 pristine and 15 single damage records are obtained from Coupon 2 under 20°C, where 15 pristine records are utilised for the threshold calibration.

## 3.5 Results of raw guided wave signals

The applicability of the AR-based features for baseline-dependent damage detection and localisation is firstly validated by directly extracting the damage-sensitive features from raw guided wave signals without employing signal compression approaches, and the corresponding results on composite coupons are presented in this section.

### 3.5.1 Autoregressive (AR) modelling results

As explained in section 3.2.1, stationary checks utilising the ADF test are firstly implemented on the uncompressed first wave packets of Lamb wave tone bursts prior to the AR modelling procedure. Table 3.4 shows an example result of the ADF test on a pristine signal from Coupon 1. Since the estimated DF value is smaller than $-1.94$ , the null hypothesis $\mathcal{H}_0$ in (3.12) is rejected under the 5% significance level. Therefore, the example signal is inferred as stationary and is directly inputted into the AR model.

Table 3.4: ADF test result on a pristine signal of path 1-4, Coupon 1.

| DF statistic | $p$-value | 1% level | 5% level | 10% level |
|---|---|---|---|---|
| -256.05 | 0.00 | -2.57 | -1.94 | -1.62 |

The ADF test result on the entire 90 measurements, i.e., $90 \times 56 = 5040$ path signals, of Coupon 1 is presented in Table 3.5. It is shown that 2882 signals of Coupon 1 are tested non-stationary under the significance level of 0.05. Among the nonstationary signals, 1912 signals are tested stationary when differenced once while the other 970 signals are differenced twice,

i.e., second differenced, prior to the stationarity. Similar results on Coupon 2 are presented in Table 3.6.

During the AR modelling, the lag order $p$ is estimated for individual signals based on the AIC, BIC and RMSE. The maximum range for estimating $p$ is adopted by (3.14) as 35 to circumvent overfitting of AR models. An illustration of the lag order selection is shown in Fig. 3.7 for a pristine signal in Coupon 1.

Table 3.5: ADF test result on the entire measurements of Coupon 1.

| Stationarity conditions | Stationary with no difference | Non-stationary with no difference | | Total |
|---|---|---|---|---|
| | | Stationary after $1^{st}$ difference | Stationary after $2^{nd}$ difference | |
| Number of signals | 2158 | 1912 | 970 | 5040 |

Table 3.6: ADF test result on the entire measurements of Coupon 2.

| Stationarity conditions | Stationary with no difference | Non-stationary with no difference | | Total |
|---|---|---|---|---|
| | | Stationary after $1^{st}$ difference | Stationary after $2^{nd}$ difference | |
| Number of signals | 1019 | 1256 | 245 | 2520 |

It is shown in Fig. 3.7 (a)-(b) that the lag order $p$ is adopted as 3 corresponding to the minimum AIC or BIC values. The AIC and BIC curves exhibit similar trends due to the same dominant term $-2\log(\boldsymbol{L}(\widehat{\boldsymbol{\theta}} \mid \boldsymbol{y}))$ in the formula (3.3) and (3.5). Meanwhile, $p = 2$ is determined following the RMSE curve in Fig. 3.7 (c), which corresponds to steady RMSE values against increasing time lags.

Fig. 3.8 presents the box plot of estimated lag orders for the guided wave signals of Coupon 1. The AIC and BIC yield consistent estimates of $p$ for both the pristine and damaged measurements, where the median value is estimated as 4. However, the median line in the cases of

AIC and BIC coincides with the lower 25% quartile, thus indicating a skewed distribution of $p$ values and further implying that the estimation by AIC or BIC is sensitive to varying transducer paths. Comparatively, the RMSE criterion leads to a parsimonious and robust estimate $p = 2$ for all the signals, which validates the assumption in section 3.3 that AR models on the pristine and damaged measurements possess the same lag order. Similar results for Coupon 2 are demonstrated in Fig. 3.9 where RMSE outperforms in the lag order selection. Therefore, $p = 2$ is finally adopted for Coupon 1 and 2 during the AR modelling.

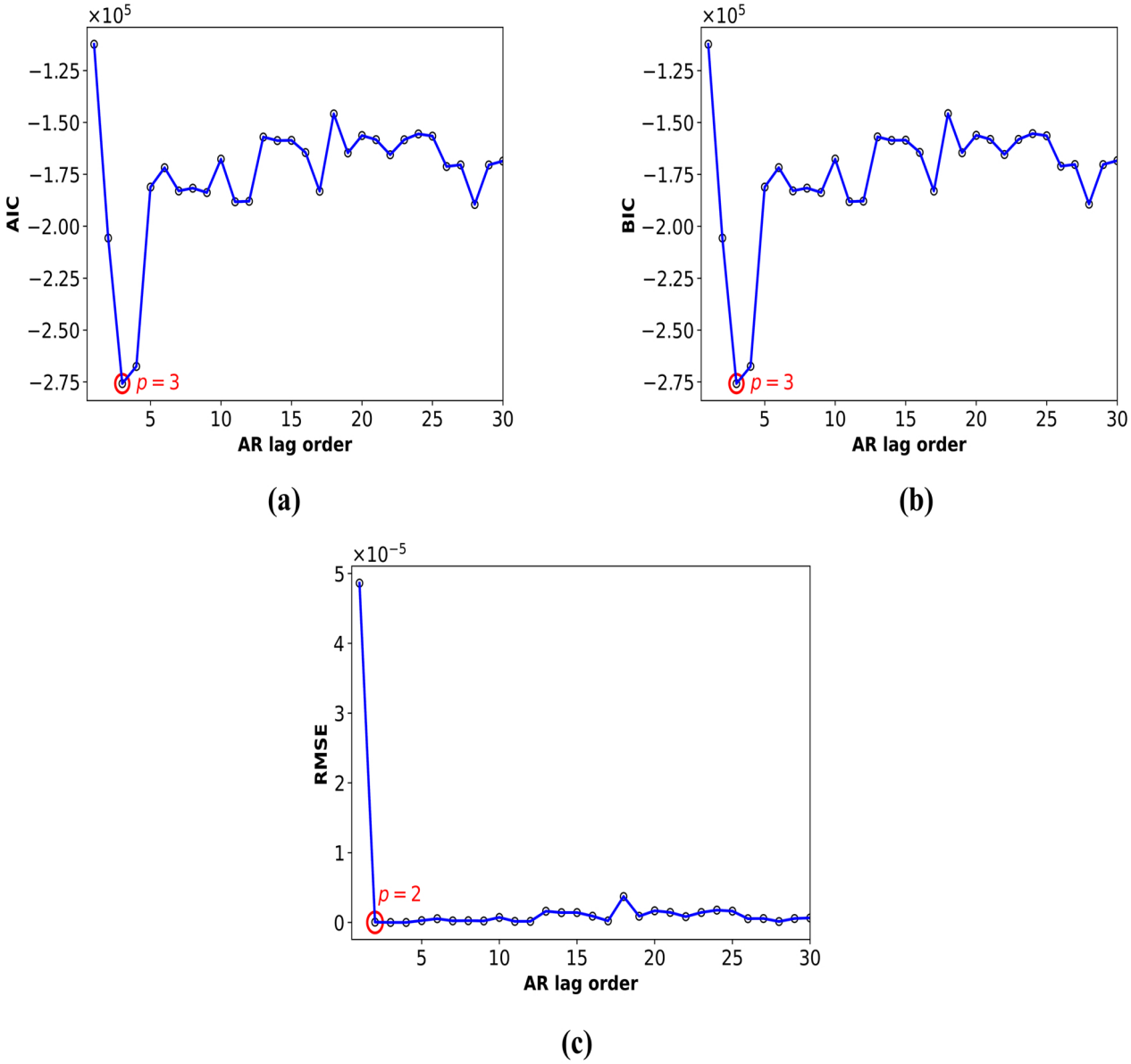


Figure 3.7: Lag order selection of AR models on a pristine signal of path 1-4, Coupon 1 utilising: (a) AIC; (b) BIC; (c) RMSE.

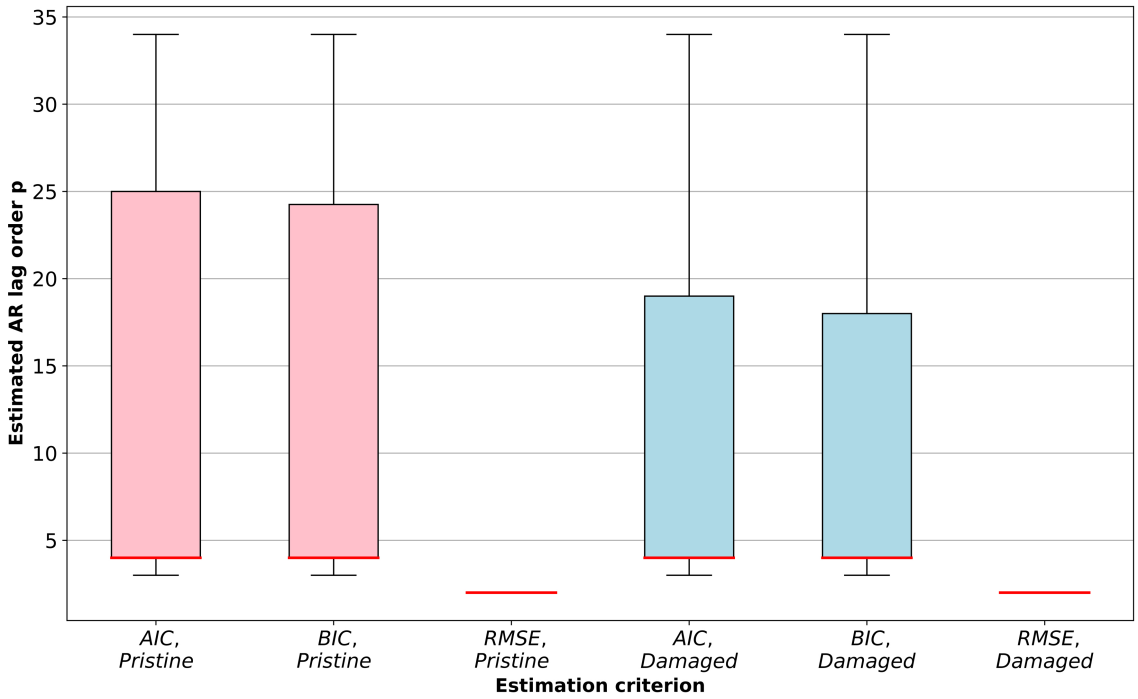


Figure 3.8: Lag order selection of AR models on pristine and damaged measurements of Coupon 1 utilising AIC, BIC, RMSE.

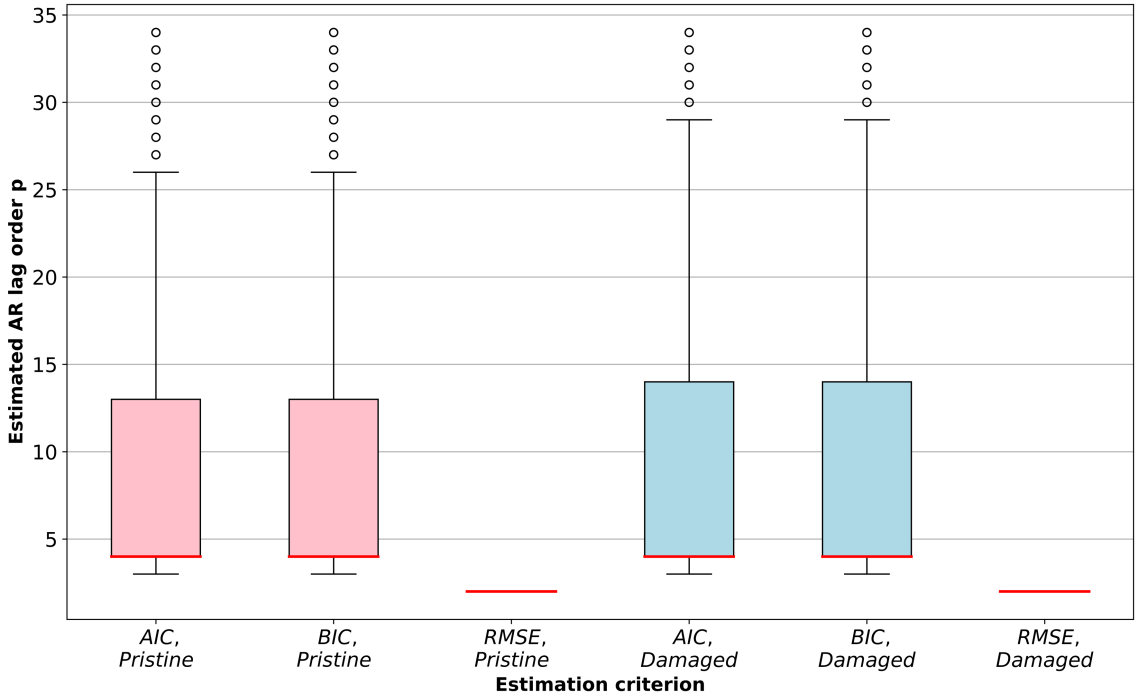


Figure 3.9: Lag order selection of AR models on pristine and damaged measurements of Coupon 2 utilising AIC, BIC, RMSE.

Further inspections on the stability of AR models are implemented based on whether the modulus of characteristic roots $\lambda_k$ in (3.16) is greater than 1. A typical example is shown in

Table 3.7 where the modulus values of $\lambda_k$ are no greater than 1, thus indicating instable AR models on the example guided wave signals. In a similar manner, nearly all the AR models are tested instable for Coupon 1, 2 under both pristine and damaged states. However, such results may not affect the estimation of damage sensitive AR parameters, which only depends on the fitting rather than the prediction performance of AR models, as discussed in the section 3.2.1.

Table 3.7: AR characteristic roots of path 1-4, Coupon 1 under pristine state

| Characteristic roots | Modulus | Model stability |
|---|---|---|
| $0.999 - 0.005j$ | 0.999 | Not stable |
| $0.999 + 0.005j$ | 0.999 | |

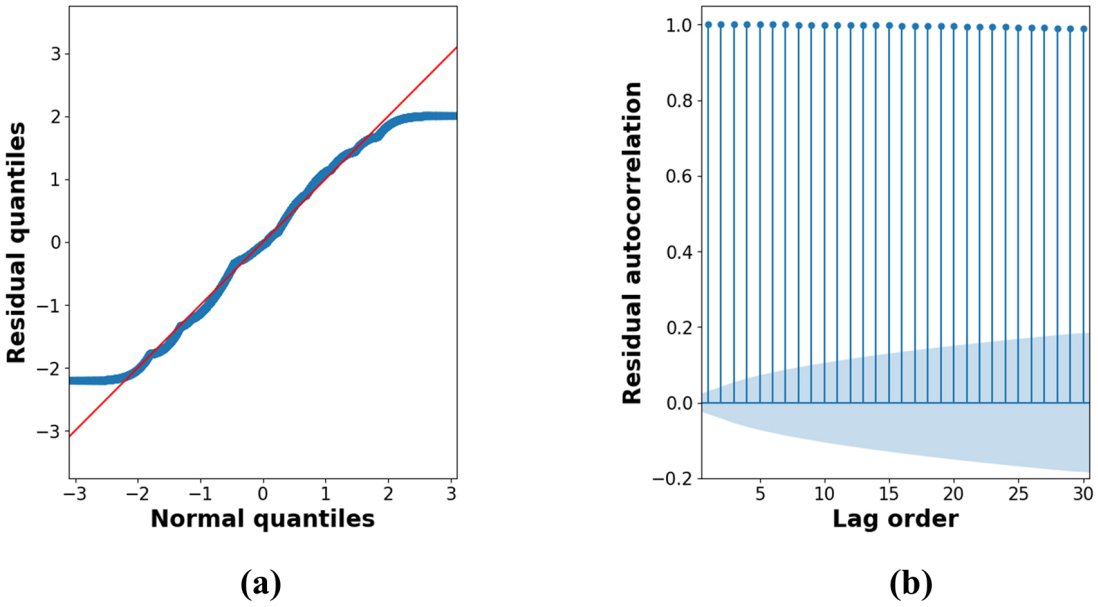


Figure 3.10: Diagnostics of the AR model on a pristine signal of path 1-4, Coupon 1: (a) $Q$-$Q$ plot of the AR residual; (b) autocorrelation plot of the AR residual where the blue shaded area represents 95% confidence interval of the autocorrelation.

The residual autocorrelation and residual normality are also interrogated for AR models on guided wave signals. Fig. 3.10 (a) and Fig. 3.11 (a) present $Q$-$Q$ plots on AR residuals of the example signals, where the 45° red reference line [145] indicates a well-match between the residual distribution and a normal distribution. It is demonstrated that the residual is inconsistent with the normal distribution at the upper and lower quantiles, and therefore not

normally distributed. Meanwhile, the residual autocorrelation targets to reveal whether the residual is dependent on its lagged values and violates the IID assumption in formula (3.1). As shown in Fig. 3.10 (b) and Fig. 3.11 (b), high correlation exists between adjacent residual values and decays slowly within the lag range as 30. The severe residual autocorrelation is mainly due to the highly oversampled signals under the 60MS/s sampling rate, which could mask the temporal structure of guided wave signals and lead to a biased estimate of AR parameters. Similar results of residual autocorrelation and non-normal residuals are obtained for nearly all the measurements from Coupon 1 and 2.

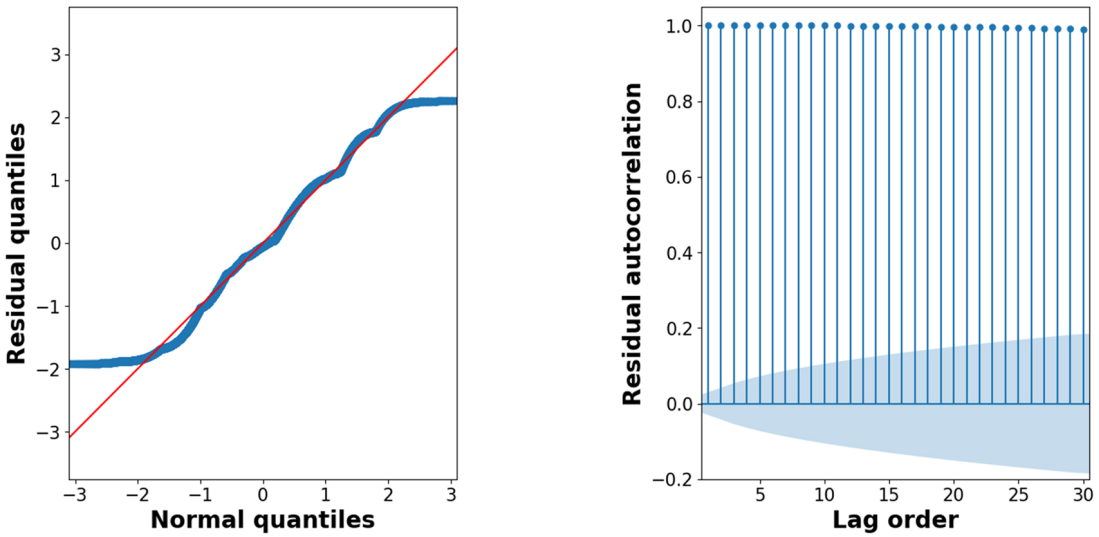


Figure 3.11: Diagnostics of the AR model on a pristine signal of path 1-7, Coupon 2: (a) $Q$-$Q$ plot of the AR residual; (b) autocorrelation plot of the AR residual where the blue shaded area represents 95% confidence interval of the autocorrelation.

### 3.5.2 Results for damage detection and localisation

The uncompressed first wave packets of Lamb wave signals are investigated for damage detection and localisation on Coupon 1 and 2. The damage detection is implemented on the damage-sensitive feature $\boldsymbol{\Theta} = [\mu, \sigma]^T$ in (2.54) where $\mu$ and $\sigma$ correspond to the mean and standard deviation of damage index ($DI$) values generated by the AR-based or the standard RAPID methods. The detection threshold is calibrated by the $\boldsymbol{\Theta}$ within pristine samples and any outliers falling on or outside the threshold are identified as damaged conditions.

Fig. 3.12 compares the damage detection results of Coupon 1 under 25°C utilising the AR residual and the standard RAPID. When employing the AR residual for damage detection, two different DIs, denoted as $DI_1, DI_2$, are generated in a similar manner to (3.22) - (3.23) but for uncompressed signals. It is shown in Fig. 3.12 (a, c, e) that the combination of the AR residual with $DI_1, DI_2$, and the standard RAPID, are capable to isolate and distinguish damaged and pristine measurements. The correlation-based $DI_2$ on the AR residual causes a false alarm in Fig. 3.12 (d), together with the accuracy and false alarm rate as 98% and 3% respectively. The declined performance on damage detection could be due to the sensitivity of Pearson correlation to local distortions embedded in the AR residuals.

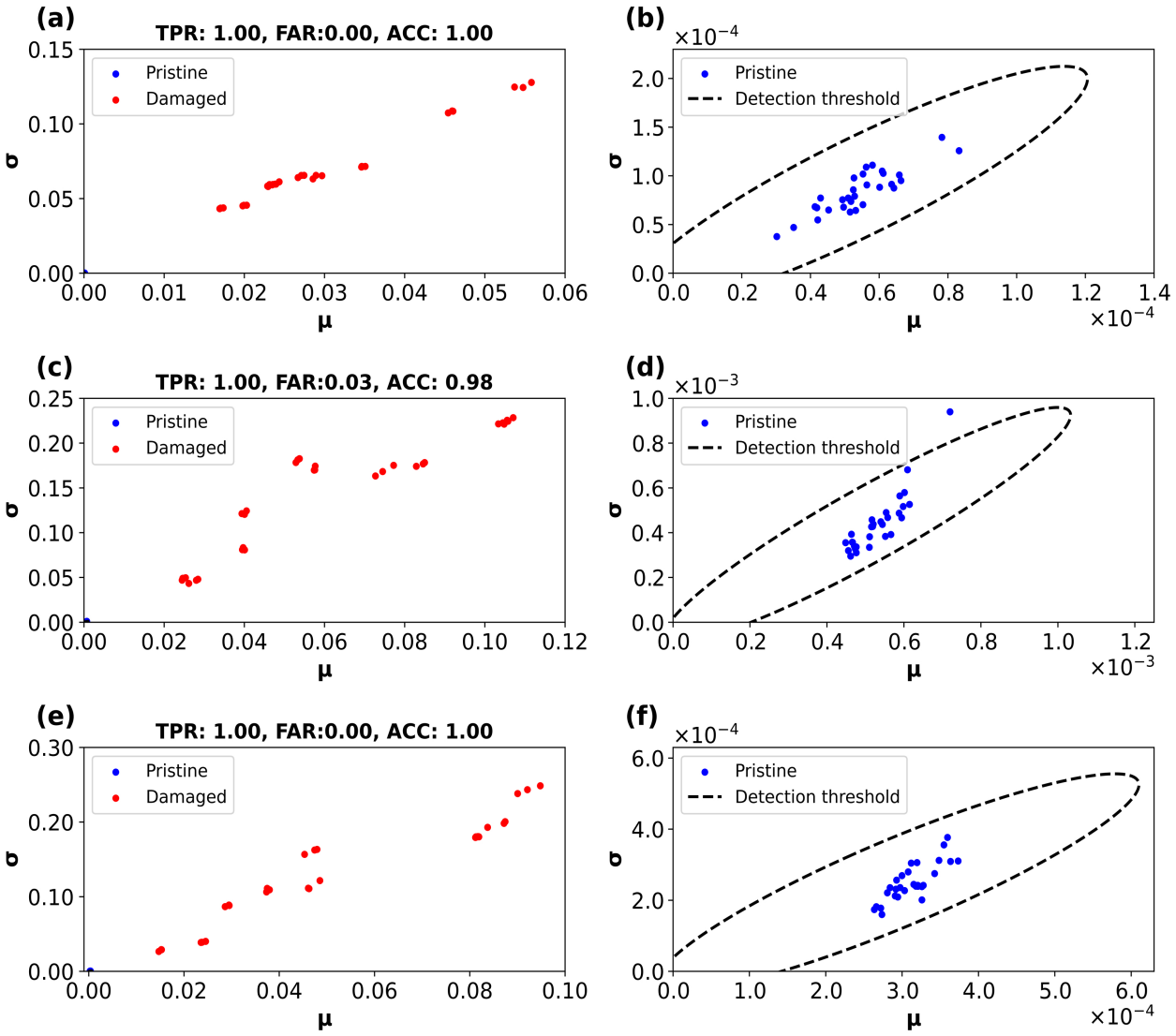


Figure 3.12: Damage detection results of simulated damages on Coupon 1 under 25°C: (a) AR residual, $DI_1$; (c) AR residual, $DI_2$; (e) standard RAPID; (b, d, f) the corresponding zoomed view under pristine state.

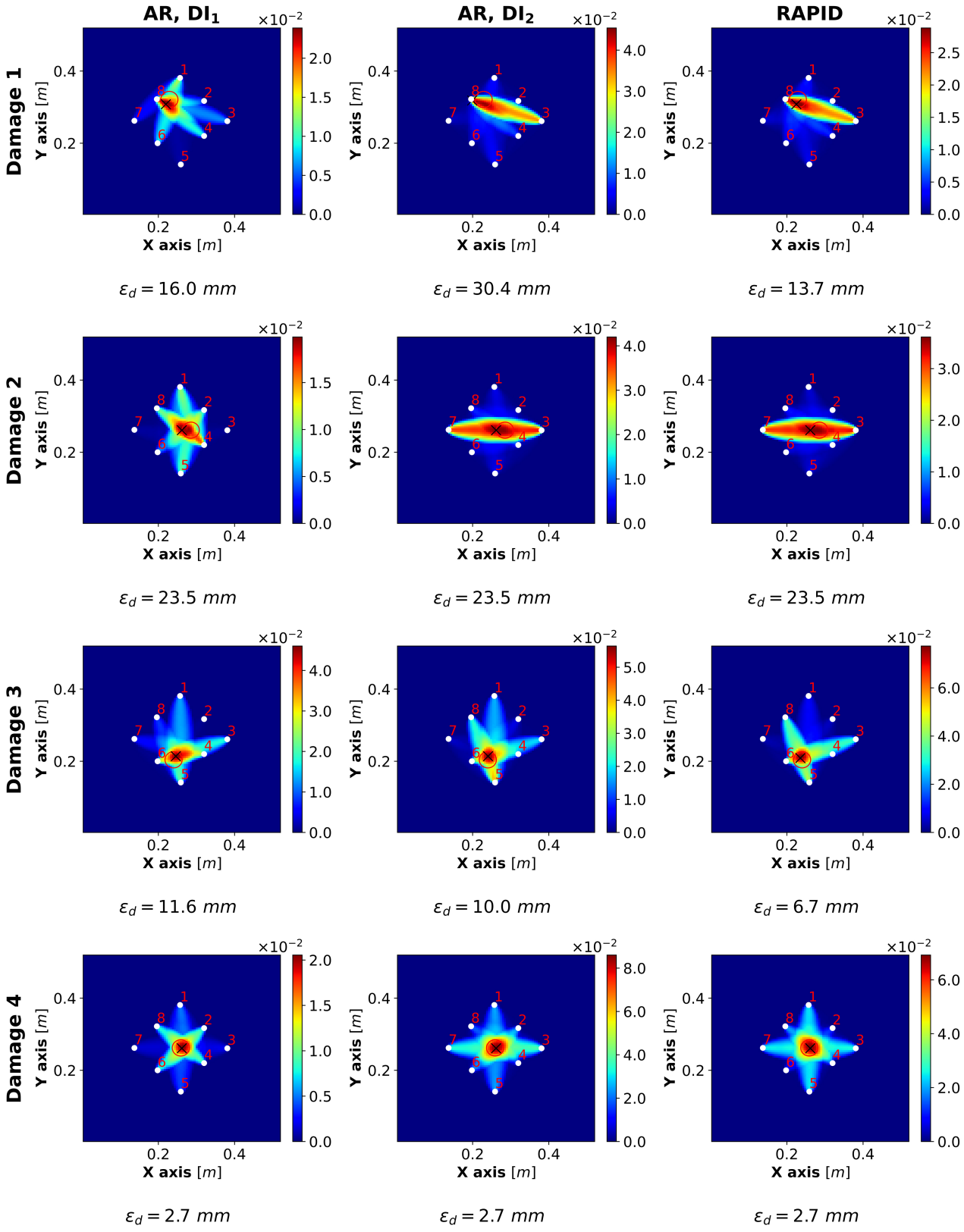


Figure 3.13: Average imaging results of four simulated damages on Coupon 1.

Fig. 3.13 demonstrates the imaging results of four (among ten) single damage scenarios on Coupon 1. It is shown that the AR-based methods are effective for damage localisation and

achieve comparable damage imaging results to the standard RAPID algorithm. However, the correlation-based $DI_2$ on AR residuals and the standard RAPID could suffer from severe imaging artifacts when localising the simulated damage 1 and 2. Comparatively, the $DI_1$ on AR residuals greatly alleviates such imaging artifacts and yields a robust estimate of true damage locations.

Furthermore, the localisation errors of overall ten simulated damages are compared in Fig. 3.14 based on the AR-based and the standard RAPID methods. The average localisation errors when utilising the $DI_1, DI_2$ on AR residuals and the standard RAPID are 21.5 mm, 20.9 mm and 22.0 mm, together with the standard errors as 4.7 mm, 4.4 mm and 5.4 mm respectively, thus validating equivalent performances of the AR-based methods to the standard RAPID in terms of the damage localisation. Nevertheless, there is still room to improve the damage localisation performance of the AR-based techniques.

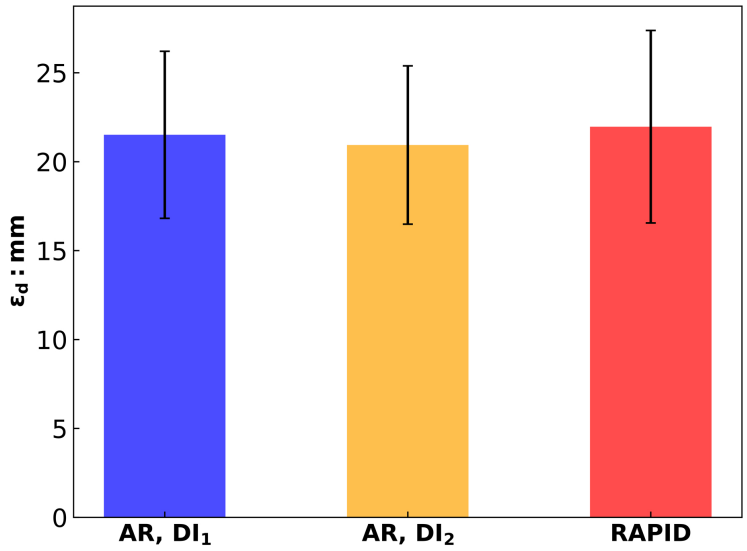


Figure 3.14: Comparisons between the AR-based methods and the standard RAPID regarding the localisation errors for overall ten damages on Coupon 1 under 25°C.

Fig. 3.15 presents damage detection results of the 20 J impact damage on Coupon 2 under 20°C. It is indicated that the $DI_1$ on AR residual is competent to identify and isolate the impact damage while yielding no false alarms during the damage detection, whereas the $DI_2$ on AR residual and the standard RAPID yield 7% false alarms and the reduced 97% detection accuracies. Similar to Fig. 3.12, the results on Coupon 2 validate the effectiveness and robustness of the Bhattacharyya distance based $DI_1$ when combined with the AR residual for the

damage detection of BVID on anisotropic composite structures. Compared to $DI_2$, the $DI_1$ in (3.22) yields improved damage detection performance utilising the variance of AR residuals, which is robust against local signal distortions in time domain. Meanwhile, the ability of the AR-based methods for damage localisation is demonstrated in Fig. 3.16, where the $DI_1, DI_2$ on AR residuals lead to localisation errors as 34.8 mm and 26.4 mm respectively. The damage localisation performance of $DI_1$ requires improvements compared to the standard RAPID, which corresponds to the 32.3 mm error when localising the 20 J BVID damage under 20°C.

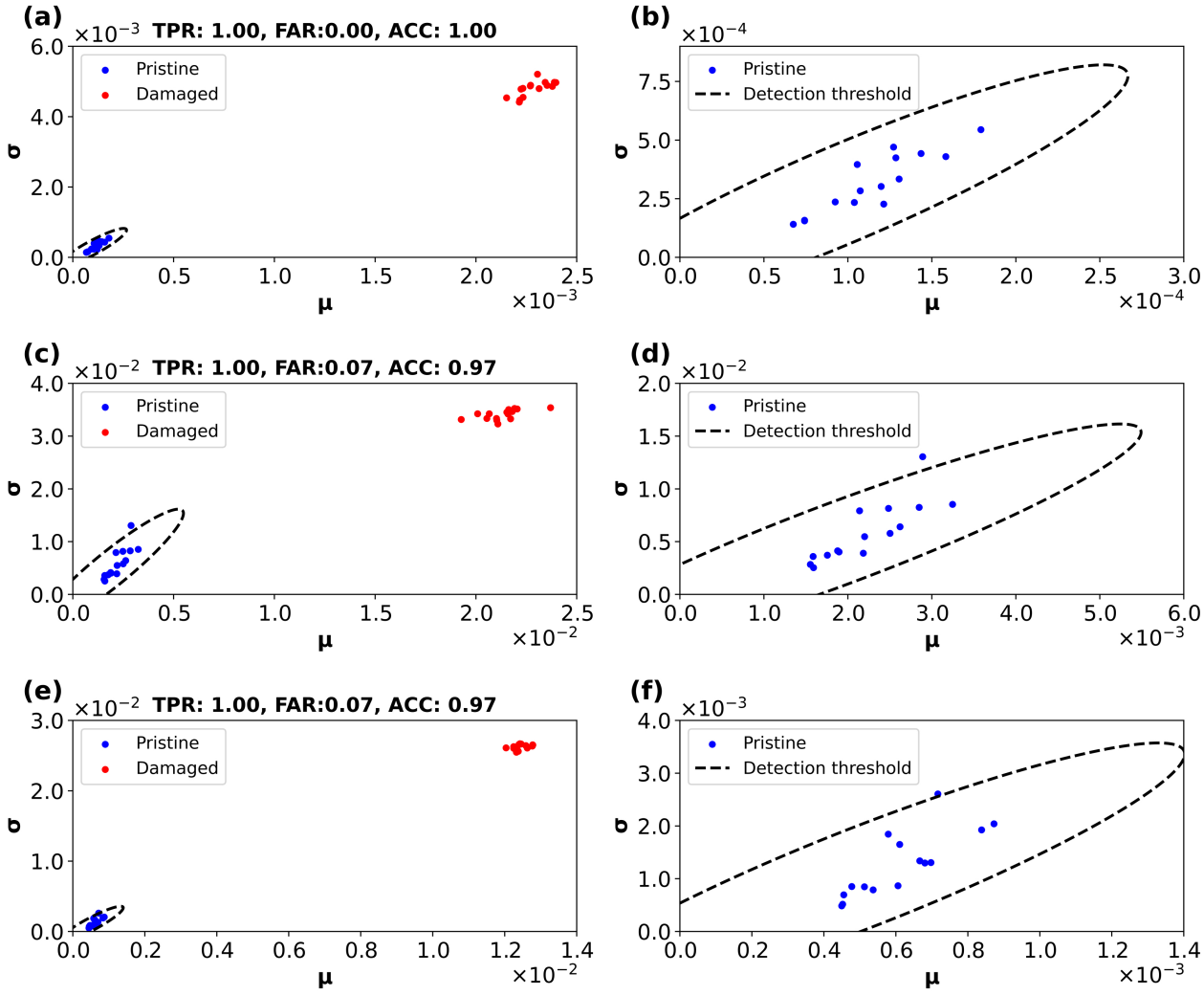


Figure 3.15: Damage detection results of the 20 J impact damage on Coupon 2 under 20°C : (a) AR residual, $DI_1$; (c) AR residual, $DI_2$; (e) standard RAPID; (b, d, f) the corresponding zoomed view under pristine state.

In spite of the effectiveness on damage detection and localisation on composite structures, the direct implementation of the AR model on uncompressed guided wave tone bursts is likely to be theoretically invalid and unjustified considering nearly all the AR residuals violate the IID

assumption in formula (3.1) as discussed in section 3.5.1, which could lead to biased estimates of the AR-based features. Such issues may be masked when comparing mis-estimated AR features of pristine and damaged signals during the SHM tasks but remain essential during applications of the AR model. In this regard, the proposed approach integrating signal compression, as investigated in section 3.6, can justify the use of AR models while being effective to detect and localise potential damages.

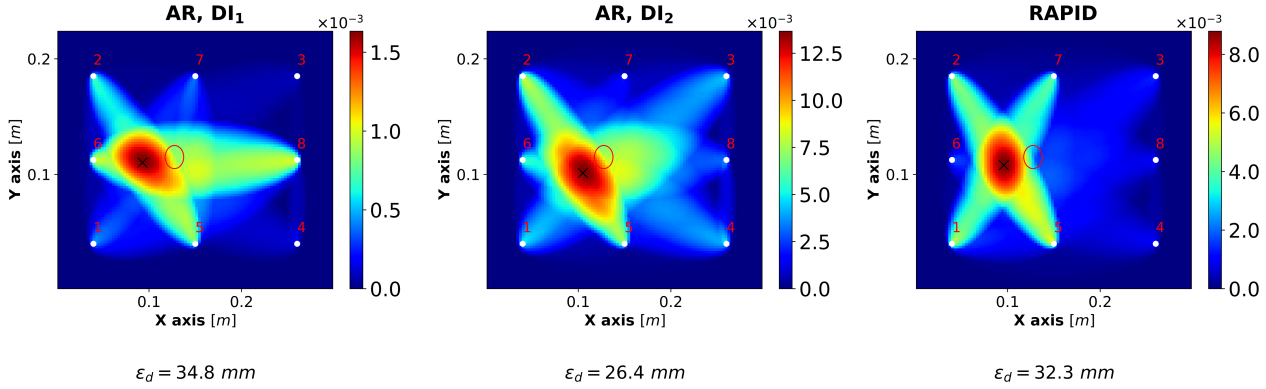


Figure 3.16: Average imaging results of the 20 J impact damage on Coupon 2.

### 3.5.3 GWSHM with varying tone burst cycles

An appropriate selection of the number of cycles, i.e., $n_c$ in (3.28), is essential when processing Lamb wave tone bursts for the SHM purposes. Lower $n_c$ implies decreased signal durations and reduced computational costs of signal processing [146], while larger $n_c$ values, accompanied with narrower signal bandwidths and reduced dispersion terms [147], could yield enhanced signal-to-noise ratios (SNRs) but potential difficulties when handling overlapping echoes from structural boundaries. A visual example illustrating the effect of number of cycles is presented in Fig. 3.17, where signals are collected from the same transducer path 1-3 of Coupon 2 but with 3, 5 and 8 cycles respectively. It is shown that Lamb wave signals containing 5 or 8 cycles have more compact waveforms and finer time resolutions than the 3-cycle signal. However, there exist the signal overlapping to varying extents between first wave packets and boundary-reflected modes of Lamb wave signals containing 3, 5 or 8 cycles. More specifically, the first wave packet is severely overlapped with boundary reflections in the 8-cycle case, rendering it challenging to distinguish and isolate the two modes simultaneously.

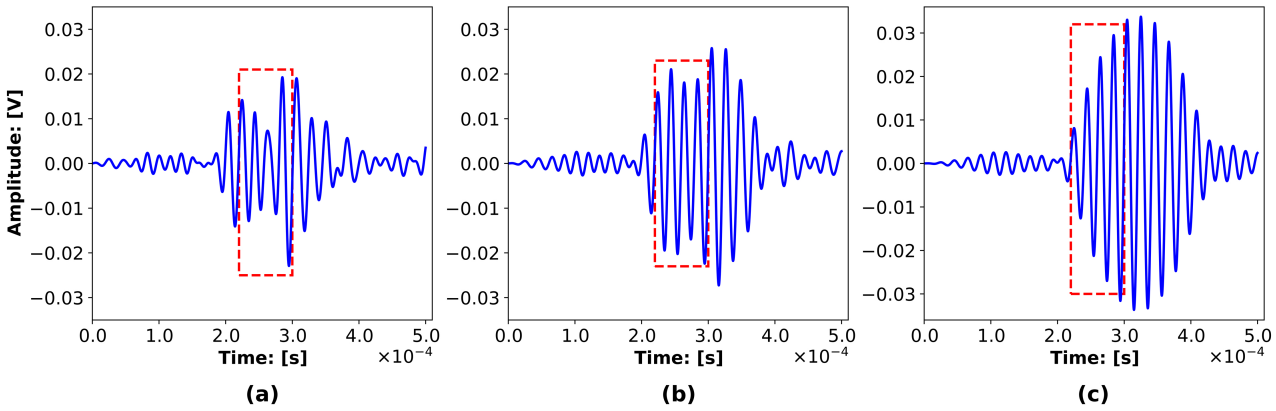


Figure 3.17: Lamb wave tone bursts of path 1-3, Coupon 2 under 20°C : (a) 3 cycle signal; (b) 5-cycle signal; (c) 8-cycle signal. The signal overlapping between first wave packets and boundary reflections are marked by red dashed areas.

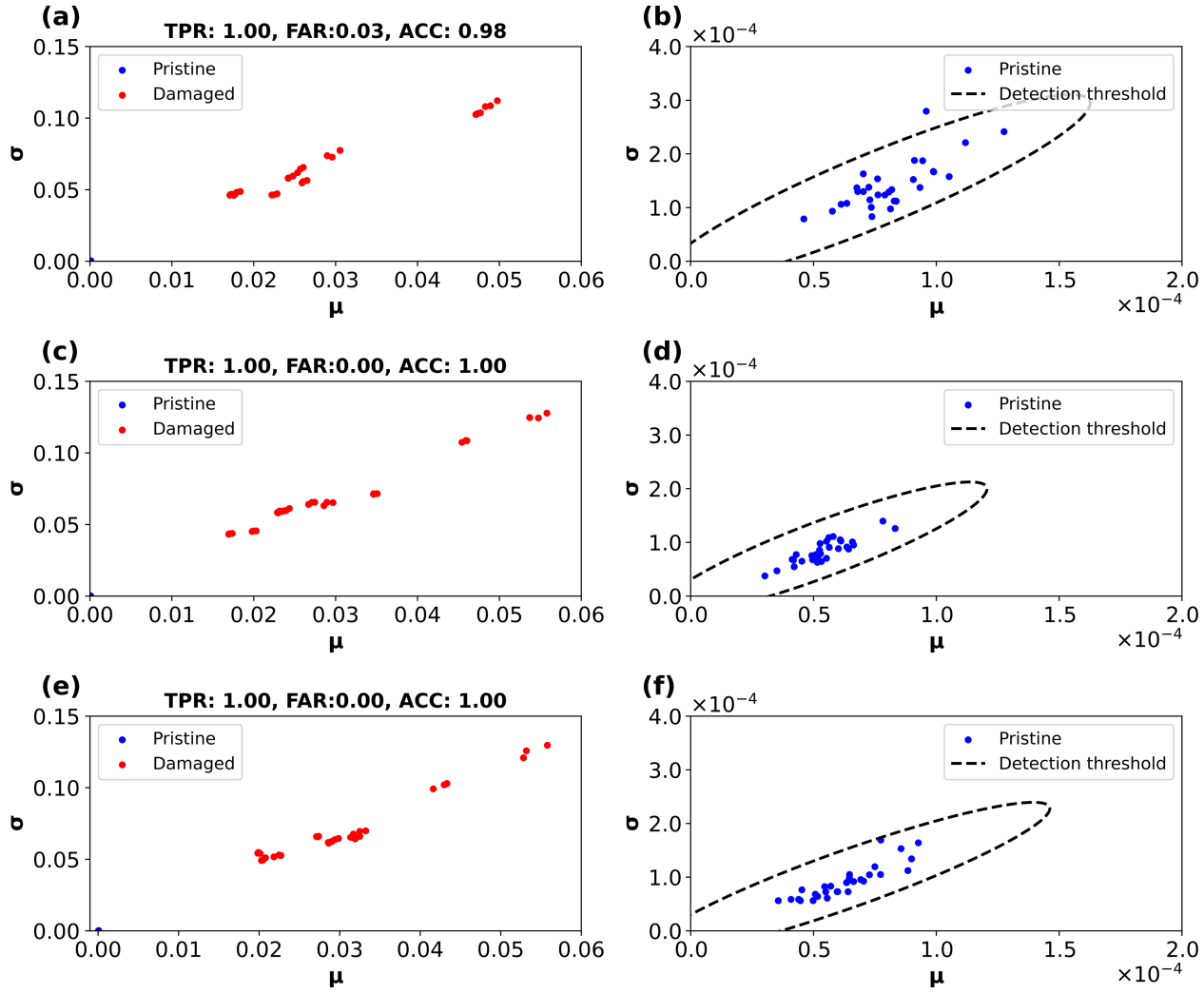


Figure 3.18: Damage detection results of Coupon 1 under 25°C based on $DI_1$, AR residuals and: (a) 3-cycle signals; (c) 5-cycle signals; (e) 8-cycle signals; (b, d, f) the corresponding zoomed view under pristine state.

Moreover, Fig. 3.18 presents damage detection results of Coupon 1 based on Lamb wave signals of varying cycles. As discussed in section 3.5.2, the $DI_1$ on AR residuals is adopted considering its effectiveness and robustness for the damage detection. It is shown that the application of 3-cycle signals yields 3% false alarms, which could be caused by limited resolution in the signal time domain. Meanwhile, the other two cases reach zero false alarms despite a data point close to but within the detection threshold in the 8-cycle case. Fig. 3.19 compares localisation errors of ten simulated damages on Coupon 1 considering varying tone burst cycles. The average localisation errors based on 3, 5, 8 -cycle signals are 22.7 mm, 21.5 mm and 20.8 mm, with the corresponding standard errors as 4.9 mm, 4.7 mm and 4.8 mm respectively, indicating modest localisation performance of the 3-cycle case.

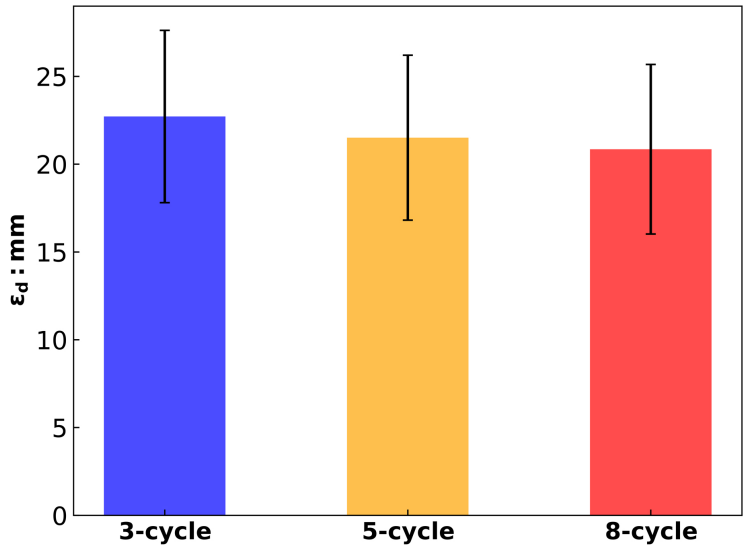


Figure 3.19: Comparisons between localisation errors of overall ten damages on Coupon 1 utilising the $DI_1$ on AR residuals with $3, 5, 8$ cycles.

Damage detection on Coupon 2, as illustrated in Fig. 3.20, exhibits consistent results to Coupon 1 when considering varying cycles of guided wave signals. The application of 3-cycle signals leads to 7% false alarms while the other two cases reach no false alarms during the detection. Nevertheless, there exist decreased capability of the 8-cycle case to distinguish between damaged and pristine states, which is likely attributed to the severe overlapping between first wave packets and boundary-reflected modes, interfering with an effective extraction of damage-sensitive features.

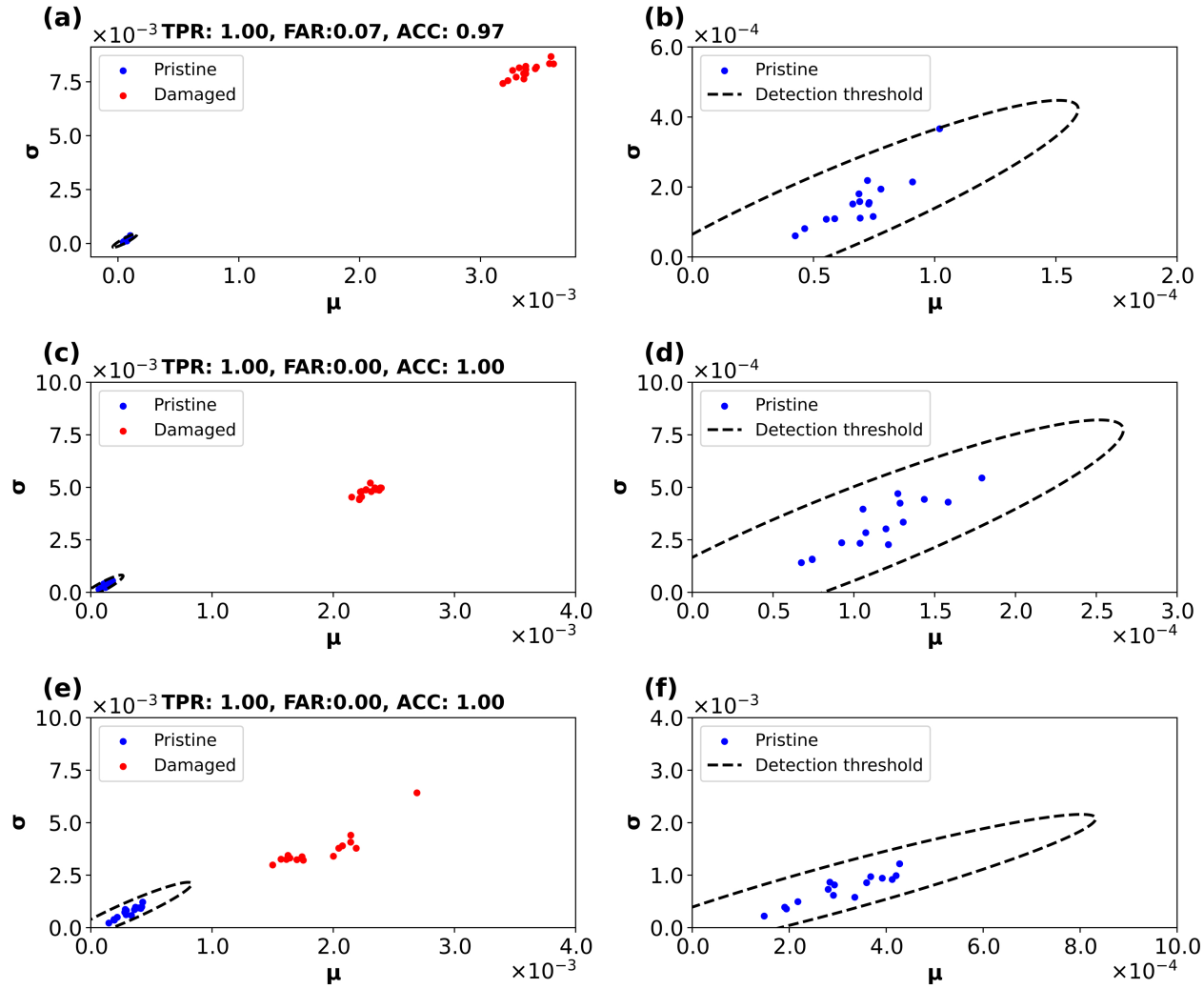


Figure 3.20: Damage detection results of Coupon 2 under 20°C based on $DI_1$, AR residuals and: (a) 3-cycle signals; (c) 5-cycle signals; (e) 8-cycle signals; (b, d, f) the corresponding zoomed view under pristine state.

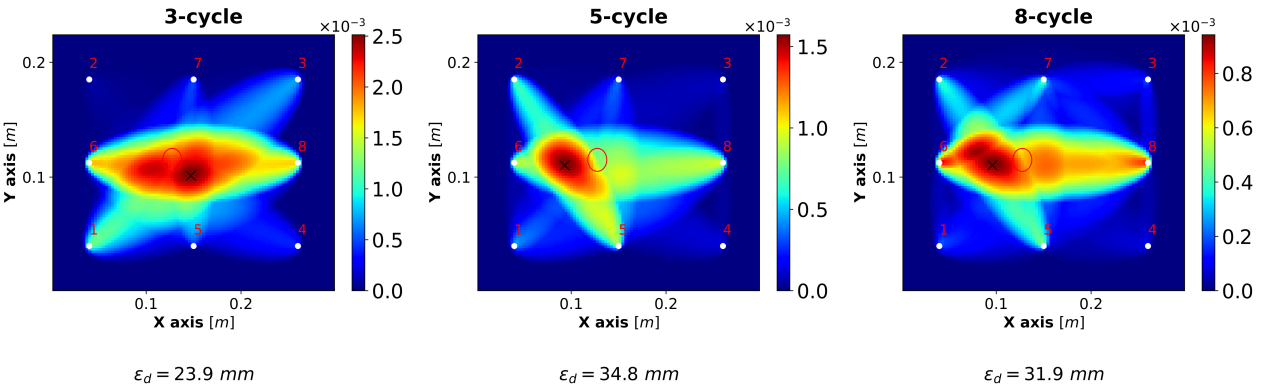


Figure 3.21: Average damage imaging results of Coupon 2 under 20°C based on $DI_1$, AR residuals and Lamb wave signals of $3, 5, 8$ cycles.

Fig. 3.21 presents the damage imaging results of Coupon 2 under 20°C utilising tone bursts

of varying cycles. Despite that 3-cycle signals achieve the localisation error as 23.9 mm, such cases suffer from severe imaging artifacts which is likely to mask the true damage location. Meanwhile, the 5-cycle and 8-cycle cases suggest damage location estimates with 34.8 mm and 31.9 mm errors respectively, while the latter case is interfered with imaging artifacts in the vicinity of the true damage. Integrating the results in Fig. 3.20 and Fig. 3.21, the 5-cycle tone bursts are primarily adopted for damage detection and localisation on composite structures.

## 3.6 Results of compressed guided wave signals

In this section, the proposed approach integrating the adaptive signal compression technique and the AR modelling process is validated through damage detection and localisation on composite coupons, and related results are demonstrated and analysed. Comparisons are implemented between the adaptive compression and common compression techniques regarding their effects on damage detection and localisation when combined with the AR-based damage sensitive features. Results for damage identification and imaging are also presented when utilising compressed guided wave signals with varying number of tone burst cycles.

### 3.6.1 Autoregressive (AR) modelling results

Prior to the AR modelling, raw guided wave signals are compressed in the proposed adaptive manner with varying compression ratios, i.e., $1:50, 1:100, 1:200, 1:500$, and the stationarity of the compressed signals is interrogated by the ADF test. Table 3.8 shows the test result of compressed pristine signals of an example path 1-4, Coupon 1 and exhibits stationarity of the compressed signal despite varying compression ratios considering all the $p$-values below 0.05 . Furthermore, the stationarity conditions of the compressed measurements of Coupon 1 and Coupon 2 against varying compression ratios are presented in Table 3.9 and Table 3.10 respectively. It is indicated that compression ratios as $1:50$ and $1:100$ yield stationary conditions of the entire compressed measurements from Coupon 1 and 2, which is due to the removal of redundant sampling points and therefore a denoised and smoothed version

of processed signals. However, the stationary condition of compressed measurements could degrade when compression ratios reach 1 : 200 and 1 : 500. This declined performance could be attributed to increased signal distortions when compression ratio approaches towards the lower limit 1 : 600 (see Fig. 3.22) which is restricted by the Nyquist sampling theorem in section 3.2.2.

Table 3.8: ADF test result on compressed pristine signals of path 1-4, Coupon 1.

| Compression ratios | DF statistic | *p*-value | 1% level | 5% level | 10% level |
|---|---|---|---|---|---|
| 1 : 50 | -6.20 | 0.00 | -2.58 | -1.94 | -1.61 |
| 1 : 100 | -2.56 | 0.01 | -2.61 | -1.95 | -1.61 |
| 1 : 200 | -4.73 | 0.00 | -2.67 | -1.96 | -1.61 |
| 1 : 500 | -3.06 | 0.00 | -2.90 | -1.97 | -1.58 |

Table 3.9: ADF test result on the entire compressed measurements of Coupon 1 with varying compression ratios.

| Stationarity conditions | Compression ratios | Stationary with no difference | Non-stationary with no difference | | | Total |
|---|---|---|---|---|---|---|
| | | | Stationary after 1st difference | Stationary after 2nd difference | Non-stationary after 2nd difference | |
| Number of signals | 1 : 50 | 5040 | 0 | 0 | 0 | 5040 |
| | 1 : 100 | 5040 | 0 | 0 | 0 | 5040 |
| | 1 : 200 | 3749 | 1176 | 113 | 2 | 5040 |
| | 1 : 500 | 3554 | 603 | 520 | 363 | 5040 |

Table 3.10: ADF test result on the entire compressed measurements of Coupon 2 with varying compression ratios.

| Stationarity conditions | Compression ratios | Stationary with no difference | Non-stationary with no difference | | | Total |
|---|---|---|---|---|---|---|
| | | | Stationary after 1st difference | Stationary after 2nd difference | Non-stationary after 2nd difference | |
| Number of signals | 1 : 50 | 2520 | 0 | 0 | 0 | 2520 |
| | 1 : 100 | 2520 | 0 | 0 | 0 | 2520 |
| | 1 : 200 | 1676 | 593 | 251 | 0 | 2520 |
| | 1 : 500 | 1743 | 481 | 201 | 95 | 2520 |

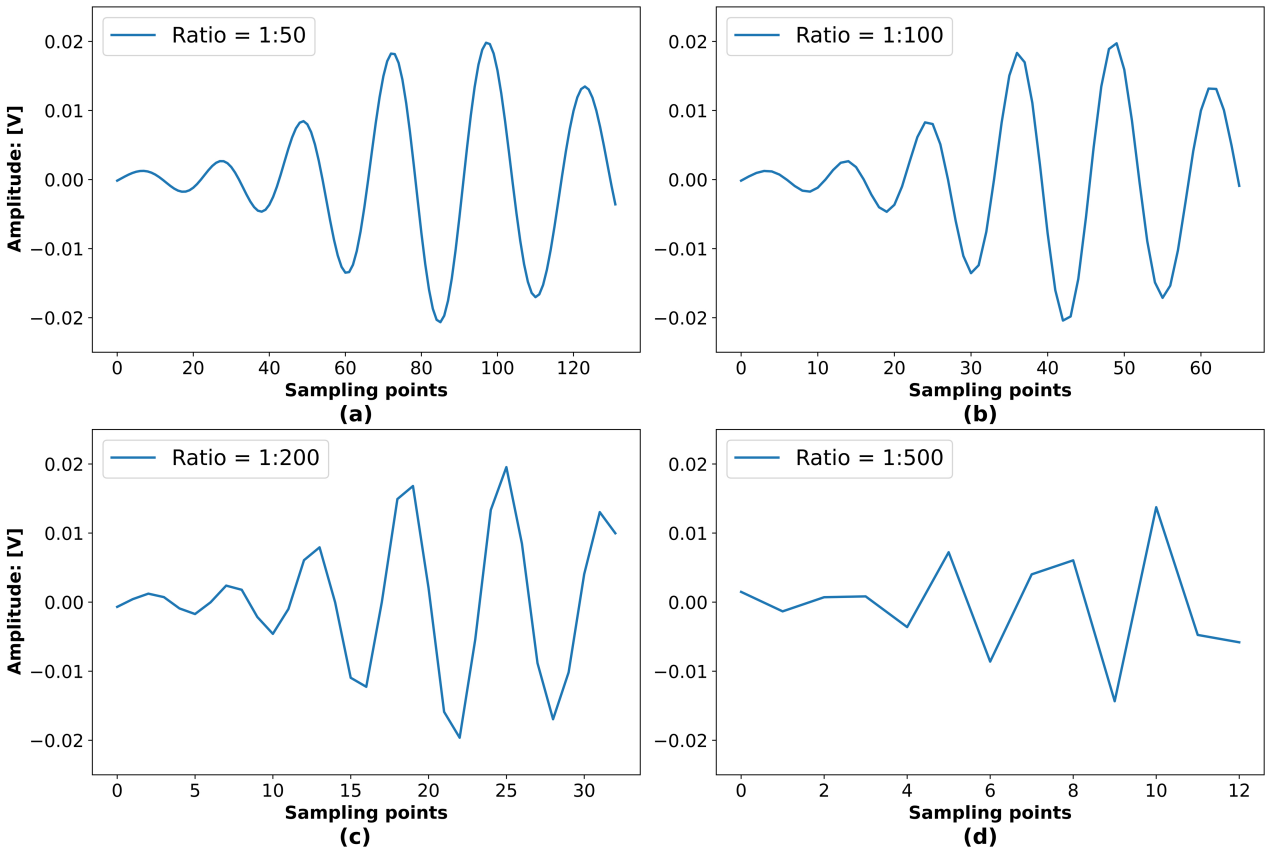


Figure 3.22: Adaptively compressed pristine signals (first wave packets) from path 1-4, Coupon 1 with colmpression ratios as: (a)1:50; (b)1: 100; (c) 1: 200; (d)1:500

Fig. 3.23 and Fig. 3.24 exhibits the selected AR lag orders for the entire compressed measure-

ments of Coupon 1 and 2, respectively. The maximum range for estimating the lag order $p$ is determined through (3.14), and therefore decreases with increasing compression ratios and decreasing signal lengths. It is shown that the AIC and BIC criteria are prone to yield $p$ estimates which are larger than the RMSE approach and sensitive to outliers and varying compression ratios, while the RMSE criterion leads to parsimonious and robust lag order estimates against the signal compression.

The stability of AR models on compressed measurements of Coupon 1 and 2 are inspected and an example is presented in Table 3.11 which contains the characteristic roots of AR models on compressed signals of pristine path 1-4, Coupon 1. Despite the signal compression with varying ratios, the AR models on compressed measurements are tested unstable considering that the modulus values are smaller than 1. Such result is consistent with Table 3.7 which investigates an uncompressed pristine signal from the same transducer path, suggesting that the signal compression does not ensure the stability of AR models.

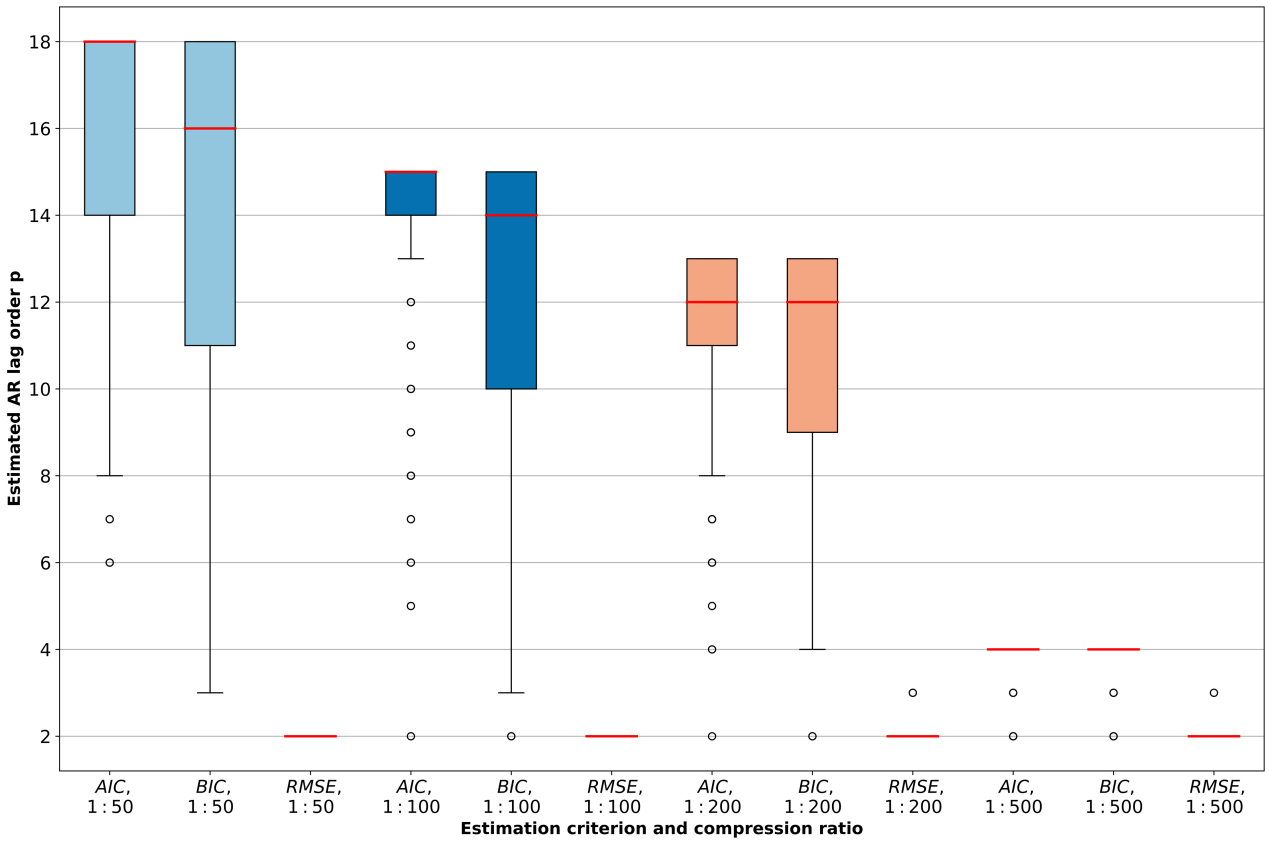


Figure 3.23: Lag order selection of AR models on the entire compressed measurements of Coupon 1 utilising AIC, BIC, RMSE.

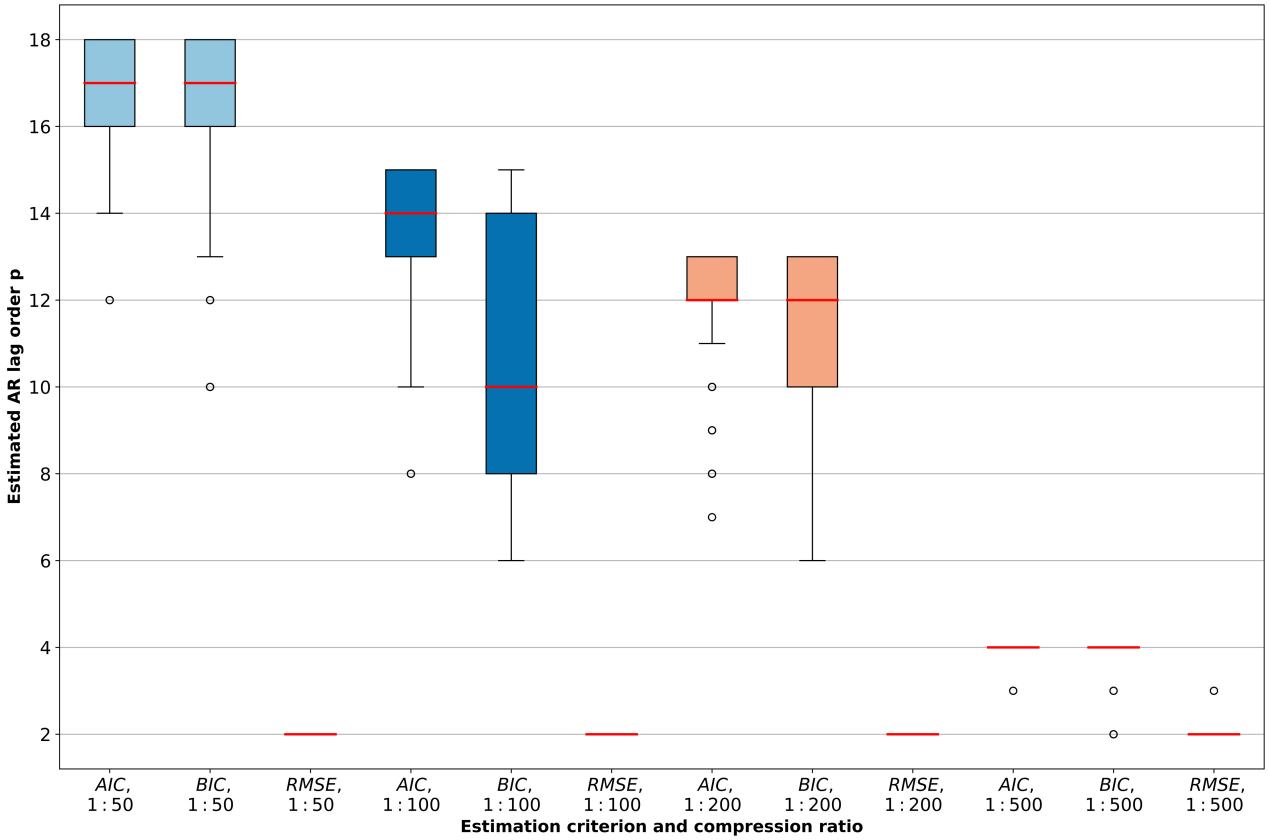


Figure 3.24: Lag order selection of AR models on the entire compressed measurements of Coupon 2 utilising AIC, BIC, RMSE.

Table 3.11: AR characteristic roots of compressed signals from path 1-4, Coupon 1 under pristine state.

| Compression ratios | Characteristic roots | Modulus | Model stability |
|---|---|---|---|
| 1 : 50 | $0.967 \pm 0.248j$ | 0.998 | Not stable |
| 1 : 100 | $0.873 \pm 0.479j$ | 0.996 | Not stable |
| 1 : 200 | $0.531 \pm 0.836j$ | 0.991 | Not stable |
| 1 : 500 | $-0.678 \pm 0.656j$ | 0.943 | Not stable |

Fig. 3.25 presents the residual Q-Q plot and the residual autocorrelation of example compressed signals from Coupon 1. As illustrated in Fig. 3.25 (a), the AR residual of the uncompressed signal is tested non-normal considering the inconsistency with normal distribution at the upper and lower quantiles, together with the J-B $p$ value below 0.05 which accepts the non-normal hypothesis of residuals.

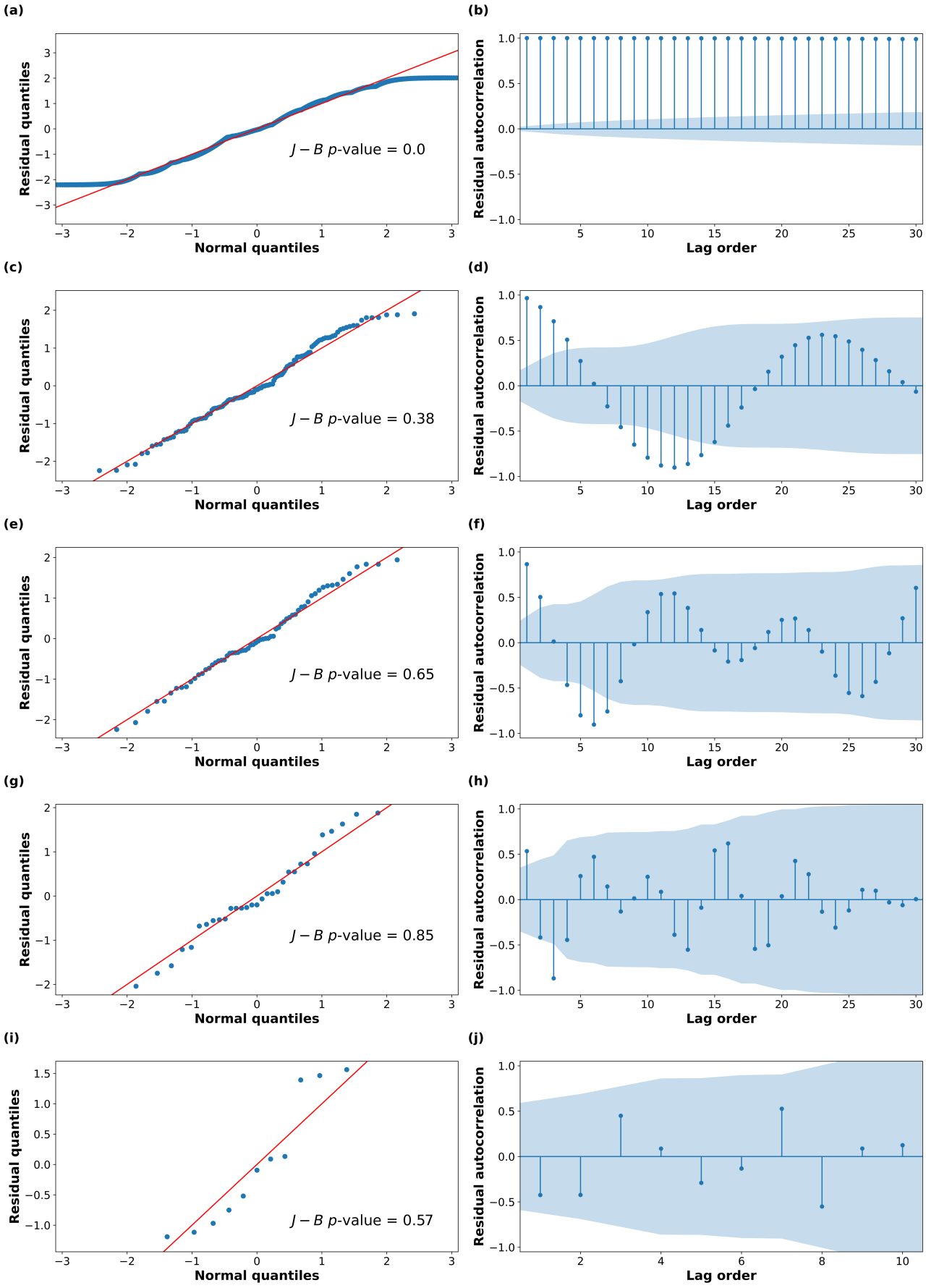


Figure 3.25: Diagnostics of the AR model on a pristine signal of path 1-4, Coupon 1: (a, b) the residual Q-Q plot and residual autocorrelation of uncompressed signal respectively; (c, e, g, i) the residual Q-Q plots of compressed measurements with compression ratios as 1:50,1:100,1:200,1:500 respectively; (d, f, h, j) the corresponding residual autocorrelations of compressed measurements. The blue shaded area represents 95% confidence interval of the autocorrelation.

Meanwhile, Fig. 3.25 (c, e, g, i) indicate that the residual distribution of compressed measurements is better matched with normal distribution in the 45° reference line. Meanwhile, the residuals of compressed signals are tested as normally distributed considering the J-B $p$ values above 0.05. Detailed results are shown in Table 3.12 where the number of non-normal residuals (with $p < 0.05$) is greatly reduced as the compression ratio decreases towards 1:500. It is suggested that the residual normality of the entire compressed measurements from Coupon 1 and 2 is improved compared to uncompressed counterparts.

Moreover, Fig. 3.25 (b) implies the high correlation between adjacent residual values in the uncompressed signal, which violates the assumption of independent AR residuals in (3.1). As shown in Fig. 3.25 (d, f, h, j), such issue is greatly alleviated in the compressed measurements considering the residual autocorrelation decays rapidly with increasing time lags. Similar results are found among the entire compressed measurements from Coupon 1 and 2, ensuring normally distributed and independent AR residuals of the compressed measurements which satisfy the basic IID assumption of AR model in formula (3.1).

Table 3.12: $p$-values of J-B tests on AR residuals of compressed measurements from Coupon 1 and 2

| Compression ratios | Coupon 1 | | Coupon 2 | |
|---|---|---|---|---|
| | Number of measurements | | | |
| | $p < 0.05$ | Total | $p < 0.05$ | Total |
| No compression | 5040 | | 2429 | |
| 1 : 50 | 34 | | 25 | |
| 1 : 100 | 15 | 5040 | 15 | 2520 |
| 1 : 200 | 0 | | 15 | |
| 1 : 500 | 0 | | 0 | |

### 3.6.2 Damage detection and localisation on compressed signals

The damage detection performance of the proposed approach integrating the AR-based features and the adaptive signal compression technique is firstly validated on Coupon 1 and the

results are presented in Fig. 3.26. The damage detection is implemented on the damage-sensitive features $\mu$ and $\sigma$ in (2.54) and the threshold setting for damage detection remains consistent with section 3.5.2 for uncompressed measurements.

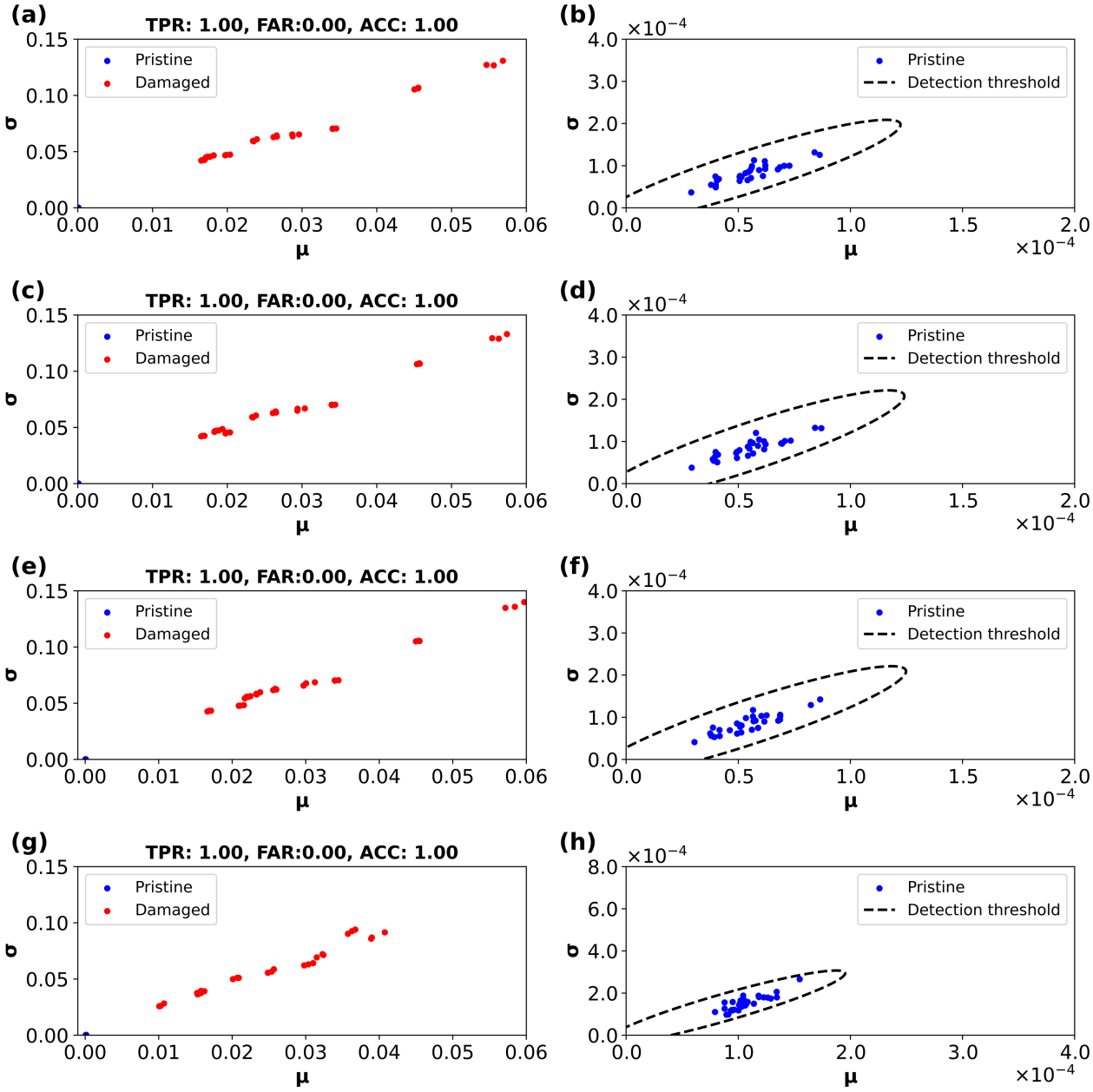


Figure 3.26: Damage detection results of simulated damages on Coupon 1 utilising the proposed AR residual and the adaptive signal compression with compression ratios as: (a) 1 : 50; (c) 1 : 100; (e) 1 : 200; (g) 1 : 500; (b, d, f, h) the corresponding zoomed view under pristine state.

It is shown in Fig. 3.26 (a, c, e, g) that the proposed approach on compressed guided wave measurements is capable to distinguish and identify simulated damages on Coupon 1 while remaining robust detection performance as $TPR = 1.00, FAR = 0.00, ACC = 1.00$ against

varying compression ratios. Fig. 3.26 (b, d, f, h) reveal that the detection threshold based on the Mahalanobis distance remain stable scales against decreasing compression ratios despite the increase of threshold and therefore the decreased detection capability when compression ratio reaches 1 : 500, which could be attributed to increased signal distortions (see Fig. 3.22).

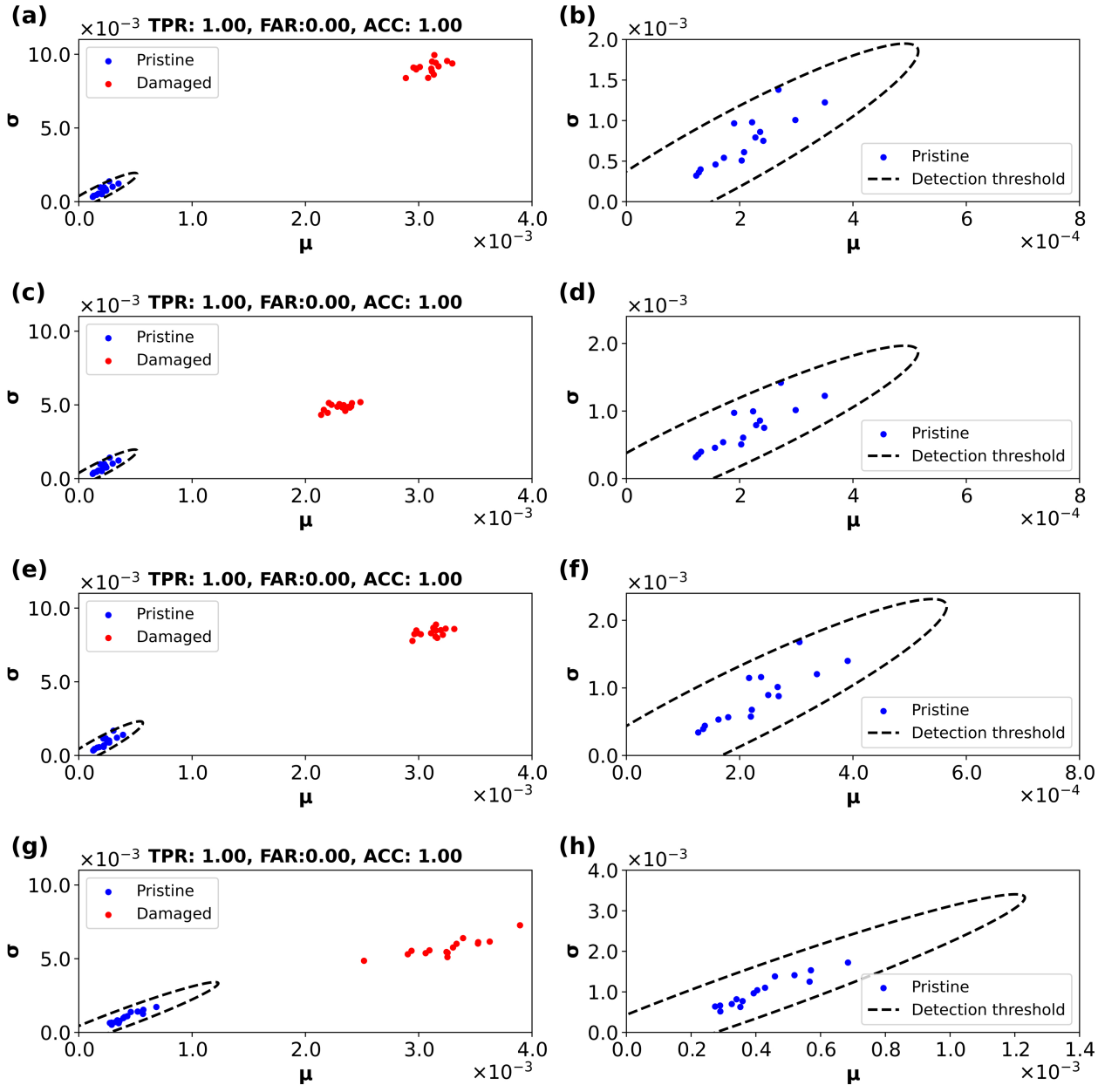


Figure 3.27: Damage detection results of the impact damage on Coupon 2 utilising the proposed AR residual and the adaptive signal compression with compression ratios as: (a) 1: 50; (c) 1: 100; (e) 1: 200; (g) 1: 500; (b, d, f, h) the corresponding zoomed view under pristine state.

When integrating AR models with different down-sampling techniques, i.e., uniform sampling and Gaussian random sampling, the corresponding detection results are compared with the

proposed adaptive signal compression in Table 3.13. The Gaussian sampling yields slightly increased false alarms when the compression ratio reaches 1 : 500. Nevertheless, the three signal compression techniques yield comparable performance when detecting simulated damages on Coupon 1.

Table 3.13: Damage detection performance of Coupon 1 utilising AR residual integrated with different signal compression approaches.

| Compression | Proposed | | | Uniform sampling | | | Gaussian sampling | | |
|---|---|---|---|---|---|---|---|---|---|
| ratios | TPR | FAR | ACC | TPR | FAR | ACC | TPR | FAR | ACC |
| 1 : 50 | 1.00 | 0.00 | 1.00 | 1.00 | 0.00 | 1.00 | 1.00 | 0.00 | 1.00 |
| 1 : 100 | 1.00 | 0.00 | 1.00 | 1.00 | 0.00 | 1.00 | 1.00 | 0.00 | 1.00 |
| 1 : 200 | 1.00 | 0.00 | 1.00 | 1.00 | 0.00 | 1.00 | 1.00 | 0.00 | 1.00 |
| 1 : 500 | 1.00 | 0.00 | 1.00 | 1.00 | 0.00 | 1.00 | 1.00 | 0.03 | 0.98 |

Fig. 3.27 indicates effectiveness and robustness of the proposed approach when detecting the 20 J impact damage on Coupon 2 based on compressed signals with varying compression ratios, and 100% accuracy are yielded for the damage detection. As shown in Table 3.14, the uniform sampling or Gaussian sampling on guided wave measurements may cause false detection alarms while the proposed adaptive approach leads to robust detection performance in the presence of signal compression together with boundary reflections of Coupon 2.

Table 3.14: Damage detection performance of Coupon 2 utilising AR residual integrated with different signal compression approaches.

| Compression | Proposed | | | Uniform sampling | | | Gaussian sampling | | |
|---|---|---|---|---|---|---|---|---|---|
| ratios | TPR | FAR | ACC | TPR | FAR | ACC | TPR | FAR | ACC |
| 1 : 50 | 1.00 | 0.00 | 1.00 | 1.00 | 0.00 | 1.00 | 1.00 | 0.00 | 1.00 |
| 1 : 100 | 1.00 | 0.00 | 1.00 | 1.00 | 0.07 | 0.97 | 1.00 | 0.07 | 0.97 |
| 1 : 200 | 1.00 | 0.00 | 1.00 | 1.00 | 0.07 | 0.97 | 1.00 | 0.07 | 0.97 |
| 1 : 500 | 1.00 | 0.00 | 1.00 | 1.00 | 0.00 | 1.00 | 1.00 | 0.07 | 0.97 |

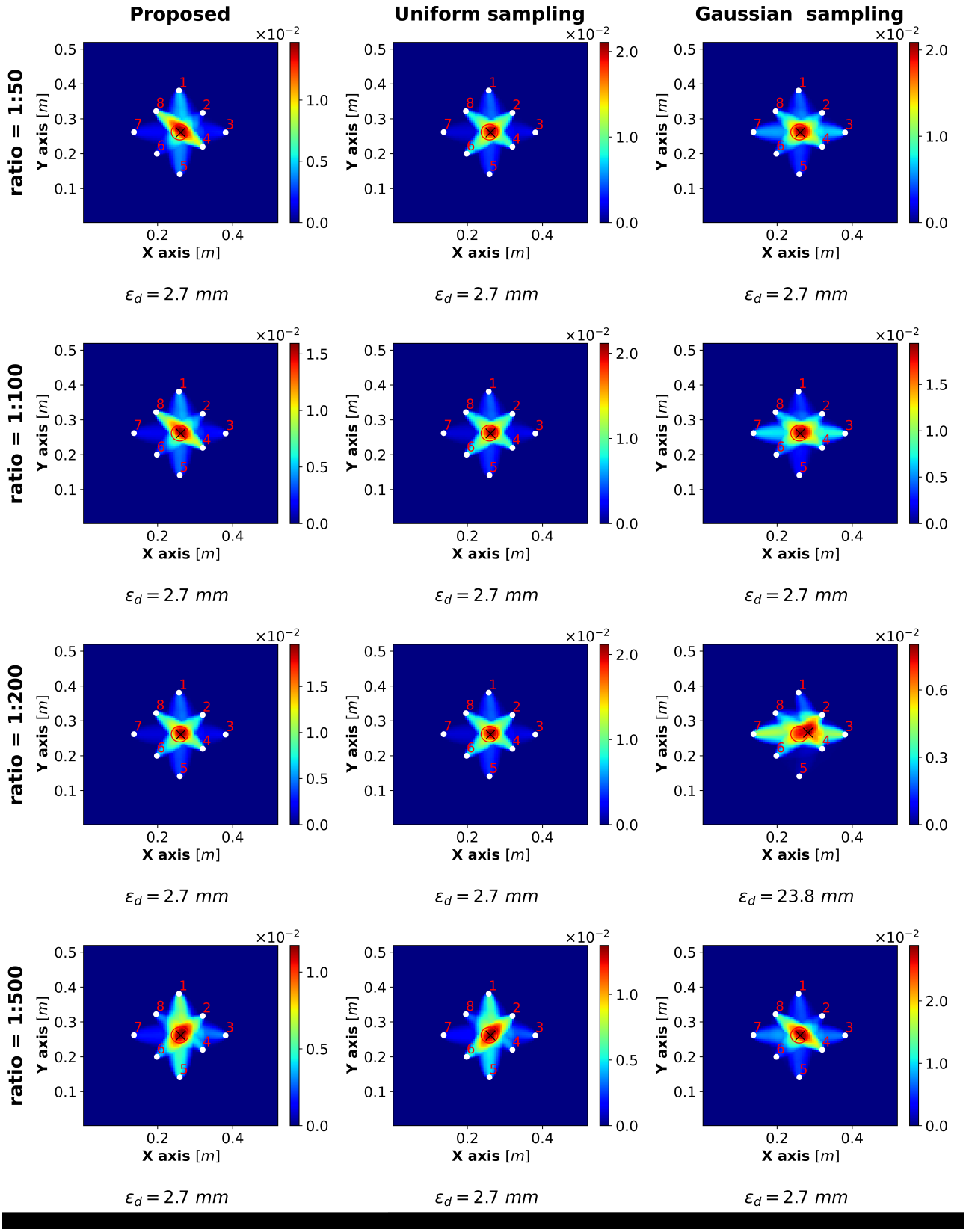


Figure 3.28: Average imaging results of a simulated damage on Coupon 1 based on the AR residual and varying signal compression techniques.

Fig. 3.28 presents a simulated damage on Coupon 1 localised utilising the AR-based features and various signal compression techniques. The compared signal compression techniques contribute to comparable imaging results and localisation errors of the centre damage. It is illustrated that the proposed adaptive sampling and the uniform sampling yield robust damage localisation performance against varying compression ratios while the Gaussian random sampling may lead to deviating damage location estimates towards decreasing compression ratios, e.g., $1:200$, which could be associated with corrupted compressed measurements by random noises. The findings in Fig. 3.28 are supported by Fig. 3.29 which compares the average localisation errors of ten simulated damages on Coupon 1 utilising measurements compressed by different techniques. The compared techniques achieve equivalent localisation errors with compression ratios above $1:200$ whereas the Gaussian sampling could lead to increased errors as compression ratio decreases.

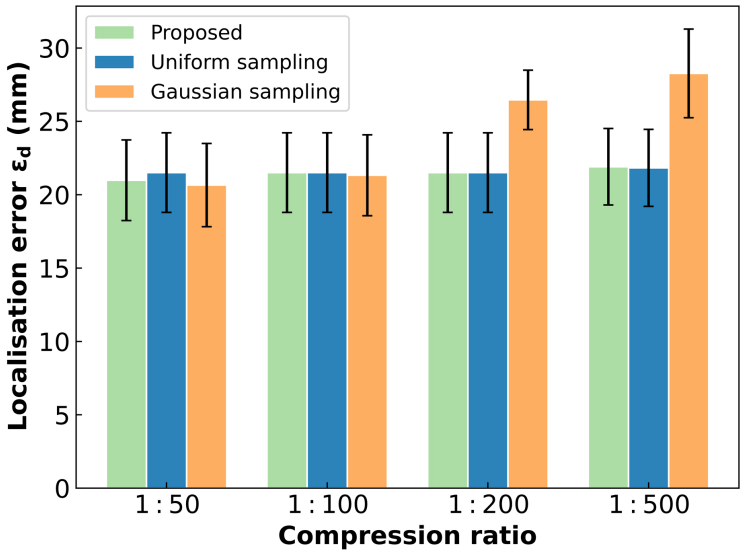


Figure 3.29: Localisation errors of overall ten simulated damages on Coupon 1 utilising the AR residual, varying signal compression techniques.

Fig. 3.30 demonstrates average imaging results of the 20 J impact damage on Coupon 2 integrating different signal compression techniques with the AR model. Increasing localisation errors of the impact damage are obtained by the Gaussian sampling against decreasing compression ratios while the other two techniques maintain relatively stable localisation errors. Despite that the Gaussian sampling can achieve more accurate damage location estimates, e.g., when compression ratios are $1:50$ and $1:100$, the corresponding imaging results may suffer

from severe imaging artifacts interfering with the true damage location.

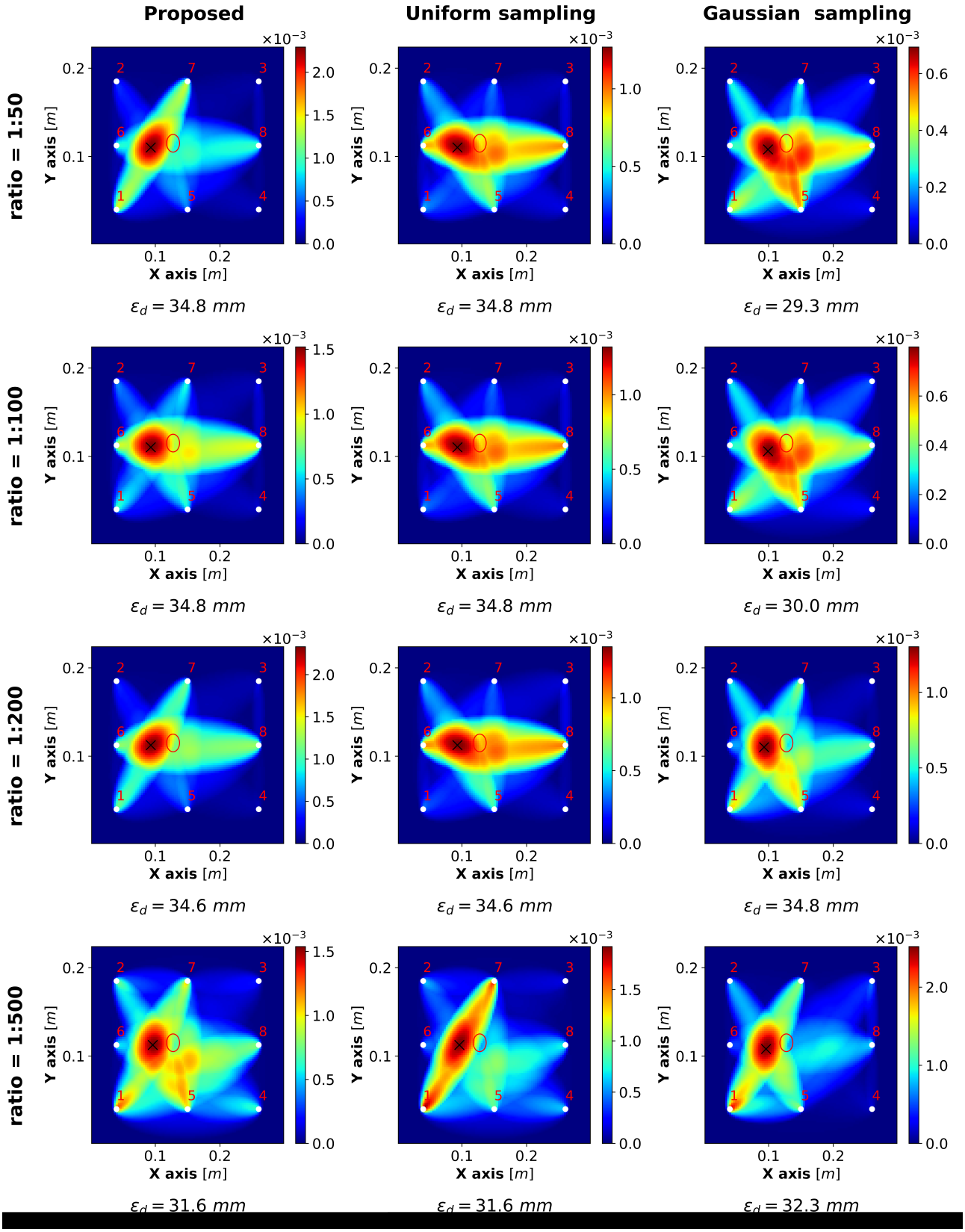


Figure 3.30: Average imaging results on the impact damage on Coupon 2 based on the AR residual and varying signal compression techniques.

Fig. 3.30 shows that compressed signals based on the proposed approach leads to robust damage images against varying compression ratios while exhibiting fewer artifacts than the uniform sampling, which is due to the adaptive capture on temporal variations of guided wave measurements. Moreover, the three sampling techniques cause degraded damage images with artifacts in the vicinity of transducers due to distorted compressed signals when the compression ratio reaches 1:500. Nevertheless, the AR residuals of compressed measurements are capable to identify the impact damage in such case.

### 3.6.3 Damage detection & localisation with varying toneburst cycles

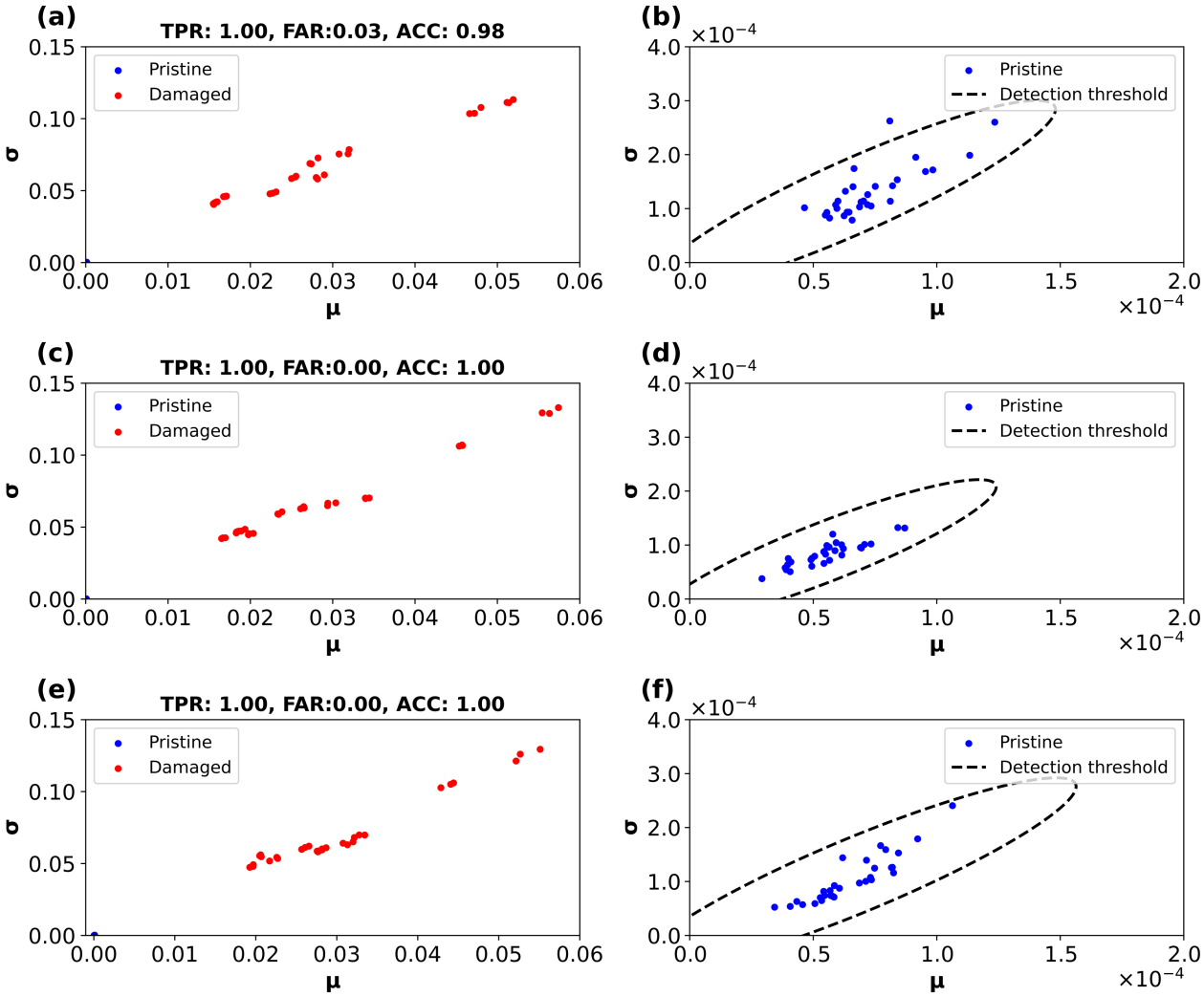


Figure 3.31: Damage detection results of Coupon 1 based on AR residuals and 1 : 100 compressed measurements of: (a) 3 cycles; (c) 5 cycles; (e) 8 cycles; (b, d, f) the corresponding zoomed view under pristine state.

The proposed approach for damage detection and localisation is investigated on Coupon 1 and 2 employing compressed guided wave tone bursts with varying number of cycles. The compression ratio is determined as 1 : 100 for illustration considering the results in section 3.6.2.

Regarding damage detection on Coupon 1, Fig. 3.31 provides similar results to Fig. 3.18 but on compressed measurements. The proposed method is proved effective to detect the simulated damages against varying number of cycles in spite of slightly increased false alarms caused by the 3-cycle compressed signals. Fig. 3.32 shows that the 3-, 5- and 8-cycle signals lead to comparable average localisation errors, i.e., 21.8 mm, 21.5 mm, 20.7 mm, of ten simulated damages on Coupon 1, along with standard errors as 5.0 mm, 4.7 mm and 4.9 mm, respectively.

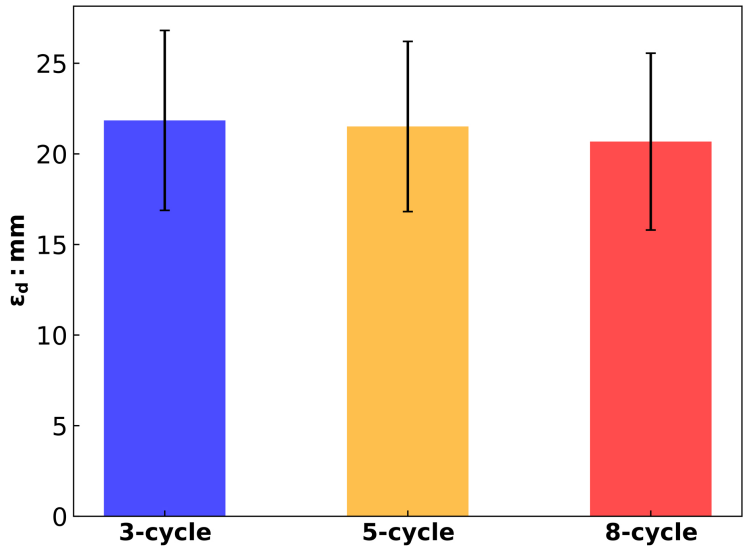


Figure 3.32: Localisation errors of overall ten damages on Coupon 1 based on AR residuals and 1 : 100 compressed measurements of 3,5,8 cycles.

In the case of Coupon 2, Fig. 3.33 exhibits that 3-cycle and 5-cycle compressed signals are competent to distinguish and identify damaged states with 100% accuracy and zero false alarms, while 8-cycle signals induce misidentification of damaged states and therefore the degraded detection accuracy as 77%. The declined performance is likely due to signal compression entangled with the severe signal overlapping with boundary-reflected modes in 8-cycle signals (see Fig. 3.17), which much complicates the effective extraction of AR-based damage sensitive features. Similar findings are obtained when utilising compression ratios from 1 : 50 to 1 : 500.

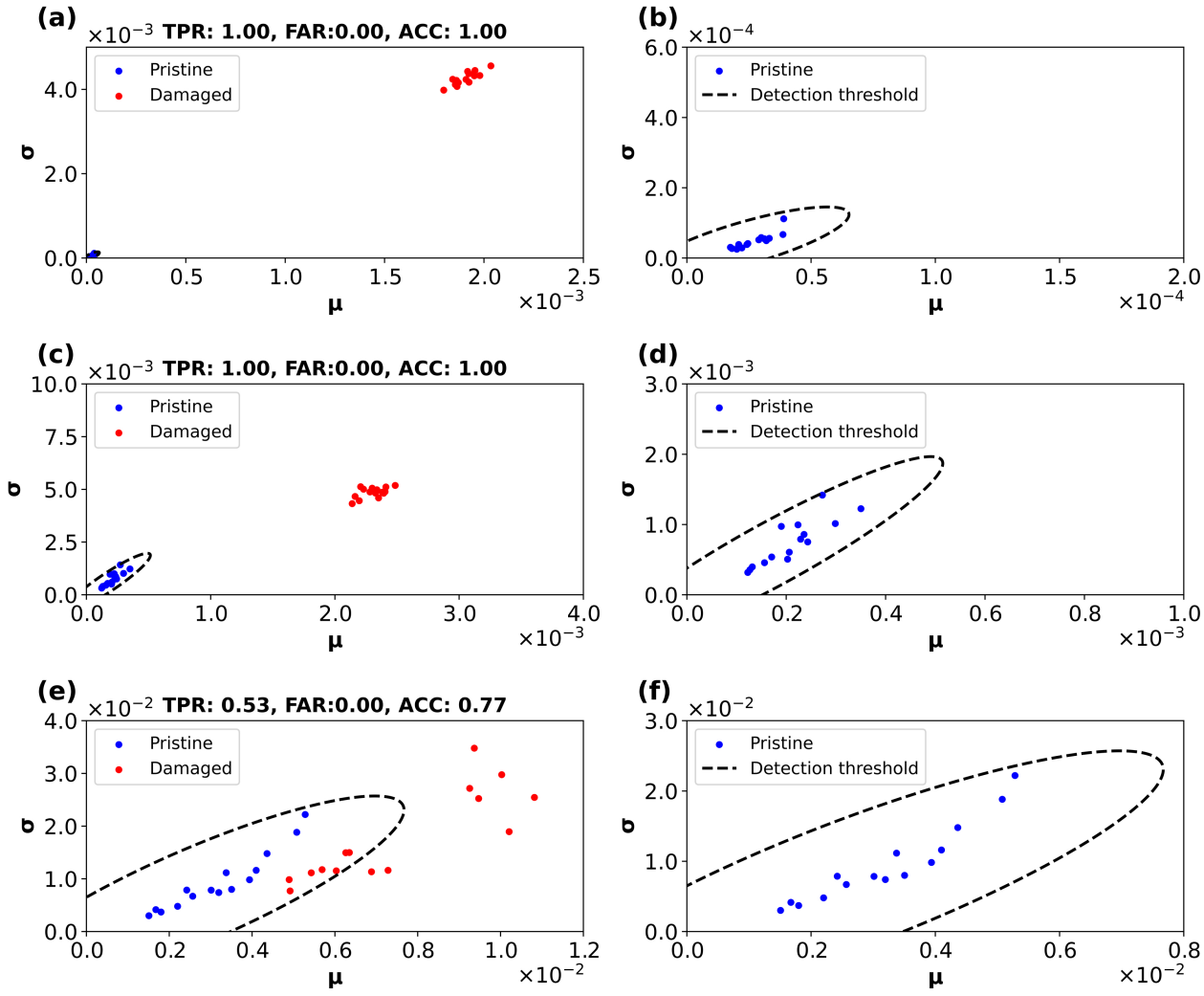


Figure 3.33: Damage detection results of Coupon 2 based on AR residuals and 1 : 100 compressed measurements of: (a) 3 cycles; (c) 5 cycles; (e) 8 cycles; (b, d, f) the corresponding zoomed view under pristine state.

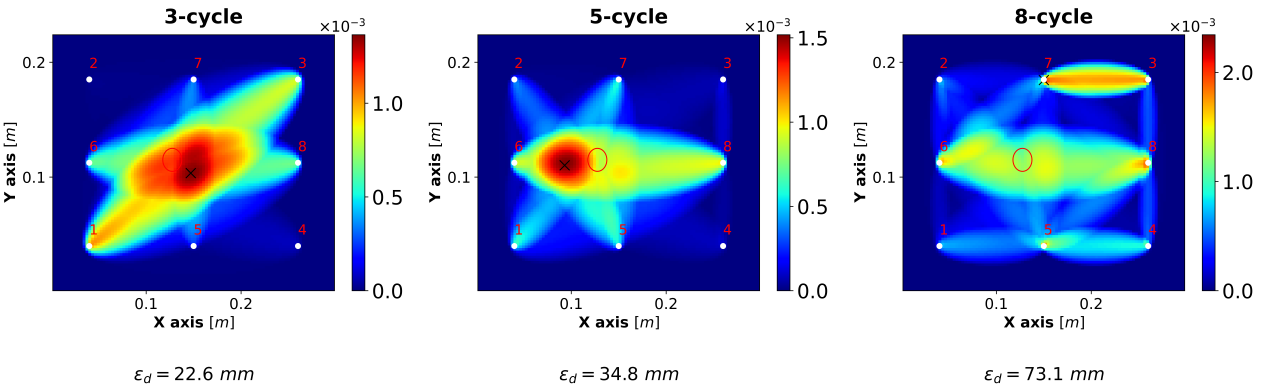


Figure 3.34: Average damage imaging results of Coupon 2 based on AR residuals and 1 : 100 compressed measurements of 3, 5, 8 cycles respectively.

Fig. 3.34 displays the average damage images based on compressed measurements of vary-

ing cycles. The 3-cycle signals lead to the average localisation error as 22.6 mm but imaging artifacts adjacent to the impact damage, while in the 8-cycle case the damage becomes unidentifiable. Comparatively, the 5-cycle case yields fewer imaging artifacts and consistent damage images with the standard RAPID in Fig. 3.16.

## 3.7 Computation time based on raw and compressed signals

Table 3.15 presents the computation time of the AR-based approach employing the entire raw and compressed measurements from Coupon 1 and 2, where the compressed signals are obtained by the proposed adaptive sampling. The total computation time is reduced 30-41 times and 43-55 times in the case of Coupon 1 and 2 respectively based on compressed measurements. Meanwhile, the proposed approach greatly reduces the signal processing time with AR models while consuming stable signal compression time against varying compression ratios. Such findings validate that the proposed approach is computationally efficient while maintaining robust performance for damage detection and localisation.

Table 3.15: Computation time of the AR-based approach for Coupon 1 and 2∗.

| Compression ratios | Measurements from Coupon 1 | | | Measurements from Coupon 2 | | |
|---|---|---|---|---|---|---|
| | Computation time: $s$ | | | | | |
| | Signal compression | AR processing | Total | Signal compression | AR processing | Total |
| No compression | – | 3308.9 | 3308.9 | – | 2472.2 | 2472.2 |
| 1 : 50 | 45.0 | 63.1 | 108.1 | 23.1 | 33.3 | 56.4 |
| 1 : 100 | 44.6 | 53.8 | 98.4 | 24.1 | 25.9 | 50.0 |
| 1 : 200 | 45.2 | 48.0 | 93.2 | 24.2 | 25.7 | 49.9 |
| 1 : 500 | 44.7 | 33.5 | 78.2 | 24.2 | 20.0 | 44.2 |

* The computation is implemented utilising the Intel(R) Core(TM) i7 −10750H CPU.

## 3.8 Summary

In this chapter, a data-driven approach is proposed, combining the statistical autoregressive (AR) model with adaptive signal compression for damage detection and localisation on both quasi-isotropic and anisotropic composite coupons. Initially, damage-sensitive features based on AR are extracted from uncompressed guided wave measurements, proving their effectiveness in identifying and localizing potential damages on composite structures. However, the direct input of uncompressed signals can result in highly autocorrelated, non-normal residuals, and prolonged computation time, limiting the practical application of the AR model for the structural health monitoring (SHM) purposes. To address this, the proposed adaptive sampling is introduced to compress guided wave measurements before the AR modelling process. This compression significantly alleviates residual autocorrelation and non-normality on compressed measurements, justifying the utilization of AR models. Furthermore, the effects of different signal compression techniques on damage detection and localisation are investigated when integrated with the AR-based features. Compressed measurements by the proposed adaptive sampling lead to robust damage detection performance and fewer imaging artifacts against varying compression ratios when compared to the uniform sampling and the Gaussian random sampling.

Comparable performances are also obtained for damage detection and localisation when employing both raw and compressed guided wave tone bursts of 3, 5 and 8 cycles respectively. However, the 8-cycle case can lead to degraded performance in the presence of signal compression and severe boundary reflections.

As shown, the developed adaptive compression results in a compression time reduction of at least 30 times compared to uncompressed cases, demonstrating the substantial computational efficiency achieved by the proposed approach in the SHM tasks.

# Chapter 4

# Baseline-free techniques for guided wave structural health monitoring

## 4.1 Introduction

As introduced in Chapter 3, the baseline-dependent approach has been widely employed for the guided wave structural health monitoring (GWSHM) on composite structures. However, the robustness and effectiveness of such methodology are susceptible to varying environmental and operational conditions (EOCs) together with degradation of bonding conditions between transducers and the tested structures [13, 148], where in both cases the true damage signatures are masked by signal distortions due to changes in the external conditions. Furthermore, the availability and quality of the baseline measurements [13] may not be sufficient for the baseline comparisons in real-life scenarios, thus further limiting a wider applicability of the baseline subtraction approach.

In this regard, the baseline-free approach has been emerging in recent years considering its capability to detect and localise potential damages without the need to have a baseline measurement referring to the structure's pristine state. The basic principle of baseline-free

[1]Part of this chapter is published in Hongmin Zhu, Zahra Sharif Khodaei, and M.H. Aliabadi. (2024) [35]

[2]Portions of this chapter have been submitted for publication as *Hongmin Zhu, Zahra Sharif Khodaei, and M.H. Aliabadi. Appraisal of baseline-free techniques for guided wave based structural health monitoring.*

GWSHM involves monitoring the changes in guided wave signals as they interact with the inspected structure. Any alteration in the wave propagation characteristics, including time-of-flight, dispersion, or amplitude [149–151], can be indicative of damage or defects. Research and development in this field are ongoing, with continuous improvements in signal processing techniques, machine learning algorithms, and sensor technologies, targeting to enhance the accuracy and reliability of baseline-free guided wave SHM systems. Related methodologies developed up-to-date include:

- Statistical and data-driven approaches: Baseline-free techniques rely on statistical and data-driven approaches to establish models of the structure's normal behaviour. These models can capture the variability and changes in the structure's response due to damage or aging. Statistical and machine learning algorithms, including Bayesian learning [152–154], clustering algorithms, e.g., K-means [155], density-based spatial clustering of applications with noise (DBSCAN) [156], artificial neural networks [157], have been employed to develop these models. These techniques allow for continuous monitoring and real-time anomaly detection.

- Feature extraction and selection: Effective feature extraction and selection play a crucial role in baseline-free techniques. Various signal processing techniques including wavelet transforms, e.g., continuous wavelet transform (CWT) [158, 159] and Hough transform [160], Fourier analysis and time-frequency analysis [46, 160], are used to extract relevant features from the guided wave signals. Feature selection methods, including principal component analysis (PCA) [161] and information gain [153], are utilised to reduce dimensionality and enhance the detection performance.

- Damage localisation and quantification: Baseline-free guided wave techniques aim to not only detect anomalies but also provide information on the location and severity of the damage. Localisation algorithms [162, 163] utilize wave propagation characteristics, such as time-of-flight and signal arrival times, to estimate the location of the damage. Quantification techniques, such as changes in signal amplitude, wave velocity, or energy distribution, are employed to assess the severity of the damage [156, 164].

- Advanced signal processing: Advancements in signal processing have contributed significantly to the effectiveness of baseline-free techniques. Time-reversal techniques [165], phased array systems [46], and mode separation [166] techniques have been employed to enhance signal-to-noise ratios, improve wave focusing, and mitigate the effects of dispersion and attenuation. These advancements enable accurate detection and localisation of damage in engineering structures.

- Integration with structural surrogates: Baseline-free techniques can be integrated with structural models or surrogates which generate intact signals of monitored structures so that no experimental baselines are required for damage detection and estimation. Finite element models [154, 167], analytical models [153], and data-driven models, e.g., digital twins [168], can be integrated with guided wave monitoring data to improve the accuracy of damage assessment and provide insights into the structural behaviour.

- Field applications and validation: Baseline-free guided wave techniques have been successfully applied in various field applications, including aerospace, civil infrastructure, and mechanical systems. Researchers and practitioners have conducted extensive validation studies on real-world structures [169, 170] to demonstrate the reliability and effectiveness of these techniques. Field deployments have shown the potential for early detection, continuous monitoring, and condition-based maintenance.

However, baseline-free techniques present challenges in establishing reliable statistical models, designing effective signal processing algorithms, and training accurate machine learning models to differentiate between benign changes and actual damage. Furthermore, the existing reference-free techniques more or less rely on several hypotheses or the so-called "implicit baselines" [171] which may be applicable only for a specific material type or sensor configuration, and therefore it is necessary to distinguish between different baseline-free techniques prior to implementing them for engineering applications. Bearing these challenges in mind, this chapter aims to provide a detailed review and a multi-dimensional comparison across several existing reference-free techniques.

This chapter is organised as follows. Section 4.2 introduces the recent research into the

baseline-free techniques. Section 4.3 further investigates several factors which affect the validity and performance of the reference-free approach while section 4.4 and 4.5 provide experimental comparisons between different baseline-free techniques. Conclusive remarks for this chapter are drawn in section 4.6.

## 4.2 Overview of common baseline-free techniques

Baseline-free techniques for damage detection, localisation, and characterisation if available, with particular emphasis on their applications in ultrasonic guided wave-based methods, are reviewed as follows in the context of composite aeronautical structures.

### 4.2.1 Time reversal (TR) imaging and its extensions

The concept of time reversibility has been extensively investigated in various fields including acoustics and earth science [172–174] prior to its applications to guided waves for the SHM purposes. As an inherent characteristic of acoustic waves propagating in linear medium, the time reversal of the propagating waves is defined as the process to reconstruct input signals excited from a transmitter by time-reversing the corresponding response signals at the receiver and further re-emitting the time-reversed responses to the transmitter [165, 175]. From a theoretical perspective, the feasibility and effectiveness of the time reversal approach is based on time symmetry of the linear propagation of acoustic waves [173, 176], namely the hypothesis that the time-reversed version of the acoustic displacement function remains the solution of the wave propagation equation. However, such time reversibility will be affected by potential non-linearities, i.e., damages existing in the inspected medium which break the time symmetry of the original wave propagation equation [165, 175, 176]. It follows that the time reversal technique is a promising method for structural health monitoring, particularly in the context of damage detection and localisation.

The schematic of the time reversal implementation is shown in Fig. 4.1. As illustrated, the first step of the time reversal process is to transmit an excitation guided wave signal from

transducer $A$ and the corresponding response is received by transducer $B$. Subsequently the response signal is time-reversed and re-emitted to transducer $A$ for the reconstruction of the original excitation signal, formulated as follows [165, 177].

First, assuming the excitation signal in the frequency domain is denoted as $f_A(\omega)$, where the symbol $\omega$ represents the angular frequency of a signal, the corresponding response signal at transducer B, $f_B(\omega)$, is then formulated as

$$f_B(\omega) = f_A(\omega)G(\omega, r) \tag{4.1}$$

where $G(\omega, r)$ represents the structural transfer function or the so-called frequency response function of the transducer path between $A$ and $B$, and such function is dependent on the angular frequency $\omega$ and $r$, the propagation distance of guided waves along the transducer path $A$-$B$. Note that the transfer function is assumed to be the same for a single transducer path and its reciprocal path.

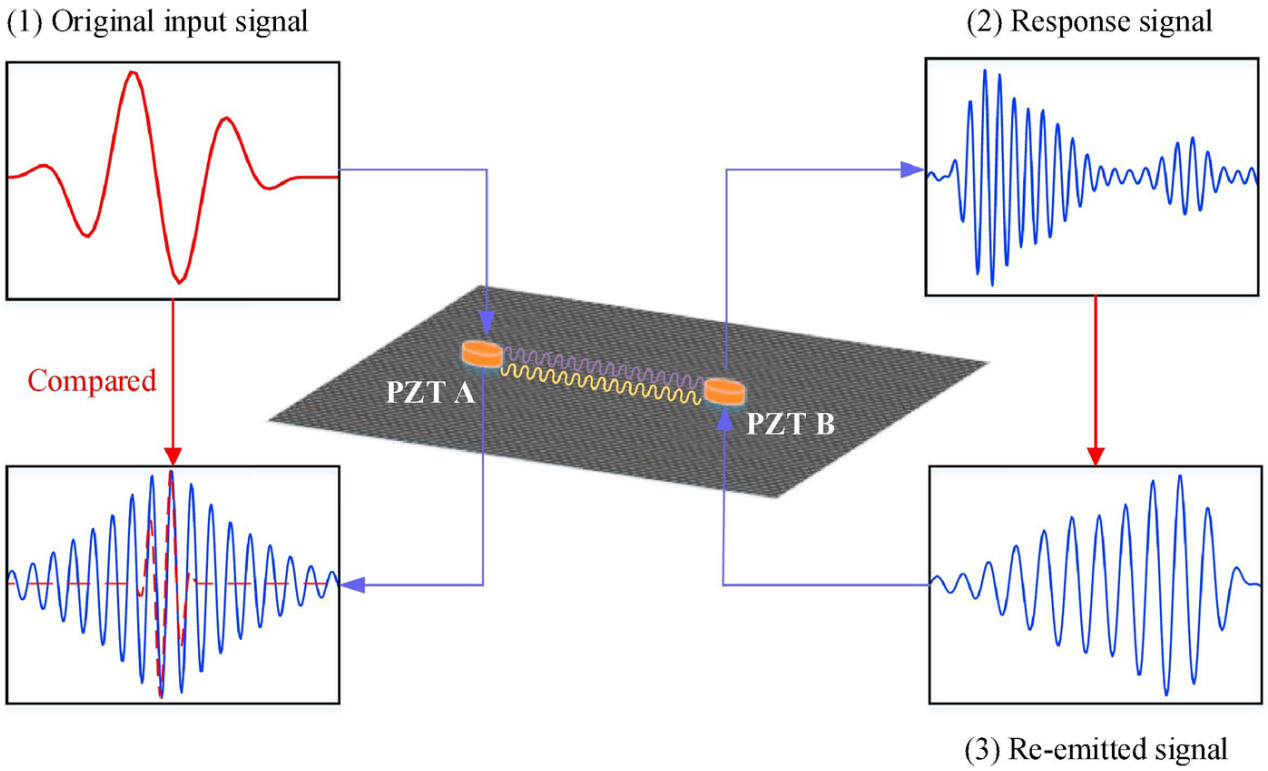


Figure 4.1: Standard time-reversal (TR) procedures. [177]

Afterwards the response signal is further reversed in the time domain, which corresponds to

the complex conjugate operation (denoted as $*$) in the frequency domain. In this regard, the time-reversed response $f_{TB}(\omega)$ can be calculated as [165]

$$f_{TB}(\omega) = f_B^*(\omega) \tag{4.2}$$

Meanwhile, considering that the time-reversed signal is further emitted to transducer $A$, the reconstructed actuation signal at A, $f_{TR}(\omega)$, is finally estimated as [165, 177]

$$f_{TR}(\omega) = f_{TB}(\omega)G(\omega, r) = f_B^*(\omega)G(\omega, r) \tag{4.3}$$

Furthermore, considering that the time reversal can be applied to current signals, such technique has been widely adopted in a baseline-free manner for damage detection and localisation. Early work in this area mainly focused on thorough investigations and analyses on the potential critical factors affecting the performance of the time reversal approach and the applicability of such approach to different types of materials. Woo et al. [165] investigated the frequency dependency of the time reversal operators and further pointed out that the multi-frequency content within the excitation signals will cause varying scales of the time reversal operators at different excitation frequencies, thus hindering perfect reconstructions of the input excitation signals. Accordingly, they proposed a practical technical framework integrating the narrow-band excitation and wavelet signal processing techniques to ensure that only a single frequency component is contained in the excitation signals.

Based on the same technical framework, further investigations were delved into boundary reflections and signal window selections [175, 178, 179], which could affect the time reversibility of the Lamb wave excitation signals. In addition, the time reversal techniques were also applied to engineering structures with different materials, including metallic structures [180], quasi-isotropic composite structures [165, 181, 182] and anisotropic composite structures [183, 184].

Recently the time reversal approach has been persistently evolving in terms of its wide applicability to various damage scenarios. More specifically, applications of such approach to impact localisation in a passive sensing manner were investigated by Qiu et al. [185] and De Simone et al. [186]. Meanwhile, the time reversal technique was also applied to multiple dam-

age types including corrosion [187–190], cracks [191], bolt loosening [192–194] and to various engineering structures such as concrete structures [189, 190, 195], pipelines [196–198] and helicopter blades [199]. The time reversal techniques were also integrated with vibration-based measurement techniques, e.g., Laser Doppler vibrometer [200–202], to yield multi-source data fusion for an accurate and robust damage detection and localisation.

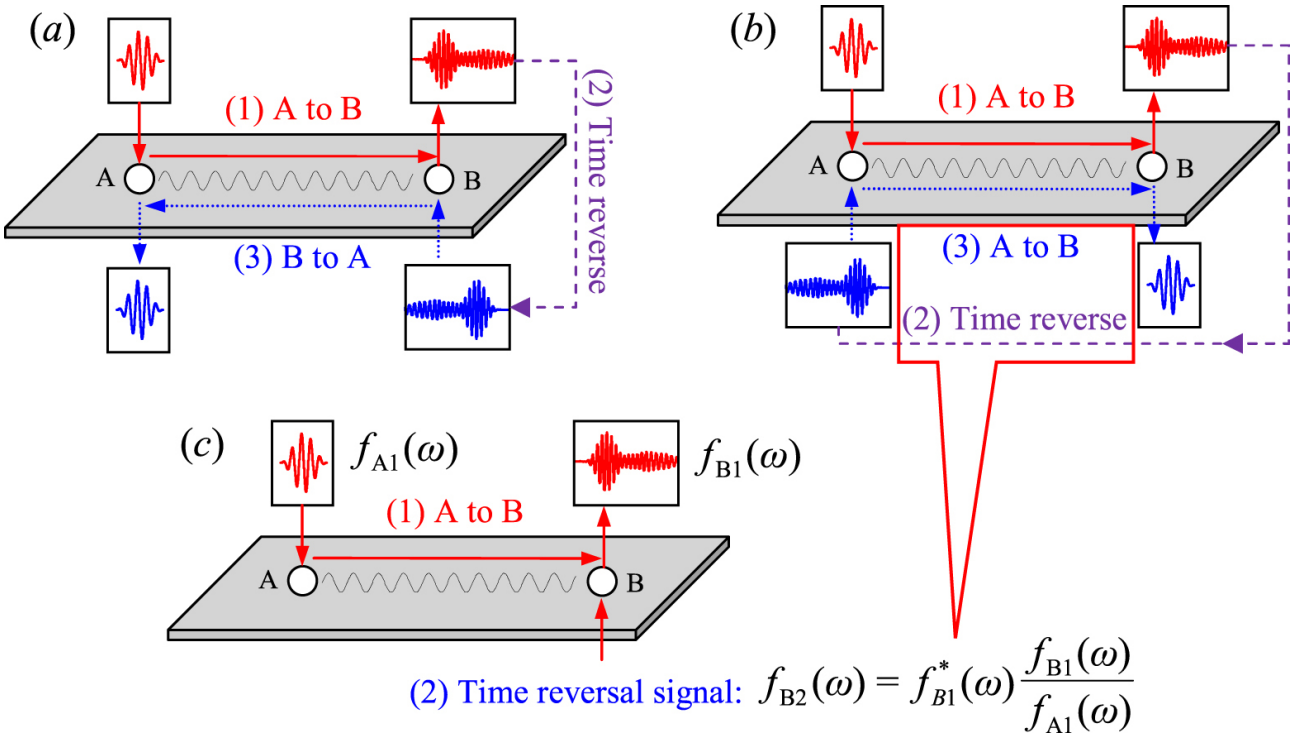


Figure 4.2: Different time-reversal schemes: (a) the standard time reversal process; (b) the modified time reversal (MTR) process proposed by [204]; (c) the virtual time reversal (VTR) process [203]. Adapted from [203].

In spite of the recent developments, there exist several limitations of the standard time-reversal approach and one of them is the rigid hardware requirement for transducers. During the standard time reversal process the receivers are not only expected to receive the response signals, but also are required to re-emit the time-reversed response signals [203,204], which could lead to high hardware costs and may be impractical for real-life applications. A first attempt to relax the hardware requirements was introduced where only one transducer is responsible to transmit the excitation signals and the time-reversed response signals simultaneously while the other transducers remain receivers in the sensor configuration [204]. Furthermore, the hardware constraints were further relaxed by Liu et al. [203] where the re-emitting process is no longer

required and a simple pitch-catch configuration is proposed for implementing the entire time reversal process (see Fig. 4.2). More specifically, in this work the structural transfer function $G(\omega, r)$ can be calculated by the excitation signals and the response signals in the frequency domain (see the equation (4.4)) for further reconstruction of the input excitation signals, where the transfer functions from actuation signals to the corresponding responses remain the same along both the forward-propagating and the backward-propagating wave paths, and therefore the physical time reversal excitation process can be fully replaced by the following mathematical operations [203].

$$G(\omega, r) = \frac{f_B(\omega)}{f_A(\omega)} \tag{4.4}$$

$$f_{TR}(\omega) = f_A^*(\omega) G^*(\omega, r) G(\omega, r) \tag{4.5}$$

Following the reconstruction of input excitation signals, the damage index in the VTR method is defined as [205]

$$DI = 1 - \frac{\left| \int_{t_0}^{t_1} I(t) V(t) dt \right|}{\sqrt{\int_{t_0}^{t_1} I^2(t) dt \int_{t_0}^{t_1} V^2(t) dt}} \tag{4.6}$$

where $I(t), V(t)$ respectively represent input excitation signal and the reconstructed signal utilising the formula (4.4) to (4.5) and the inverse fast Fourier transform (IFFT); $t_0$ and $t_1$ define the time interval for comparing $I(t)$ and $V(t)$.

The implementation of the VTR technique has helped reduce hardware costs for SHM applications using the time reversal family of methods. However, there are still several challenges that need to be addressed for real-life applications:

- Transducer tuning effects: Transducers used for wave generation and sensing may exhibit tuning effects, causing shifted central frequencies in the response signals (see Fig. 4.3). These frequency shifts can lead to inaccuracies in the estimated transfer functions during the time reversal process, resulting in distorted reconstructed actuation signals. Such inaccuracies can be mitigated by compensating the transfer functions by their amplitudes, as suggested by previous studies [177, 205].

- Numerical instabilities: Reconstructing input excitations in the time domain can sometimes lead to numerical instabilities. These issues can be addressed by adopting frequency

domain techniques, such as transfer function estimation and the inverse fast Fourier transform (IFFT), as suggested in some studies [206]. Alternatively, avoiding time-domain reconstruction altogether, as proposed by Castro et al. [207], can also help mitigate such numerical instabilities.

- Sensitivity to environmental and operational variations: Baseline-free techniques could exhibit different SHM capabilities under varying environmental and operational conditions. Changes in temperature, humidity, loading conditions, etc., can influence wave propagation behaviour, affecting the damage detection and localisation performance of baseline-free techniques. Robust algorithms and adaptive techniques are needed to account for these varying conditions and maintain the accuracy of the SHM system. This issue will be discussed later in section 4.3.

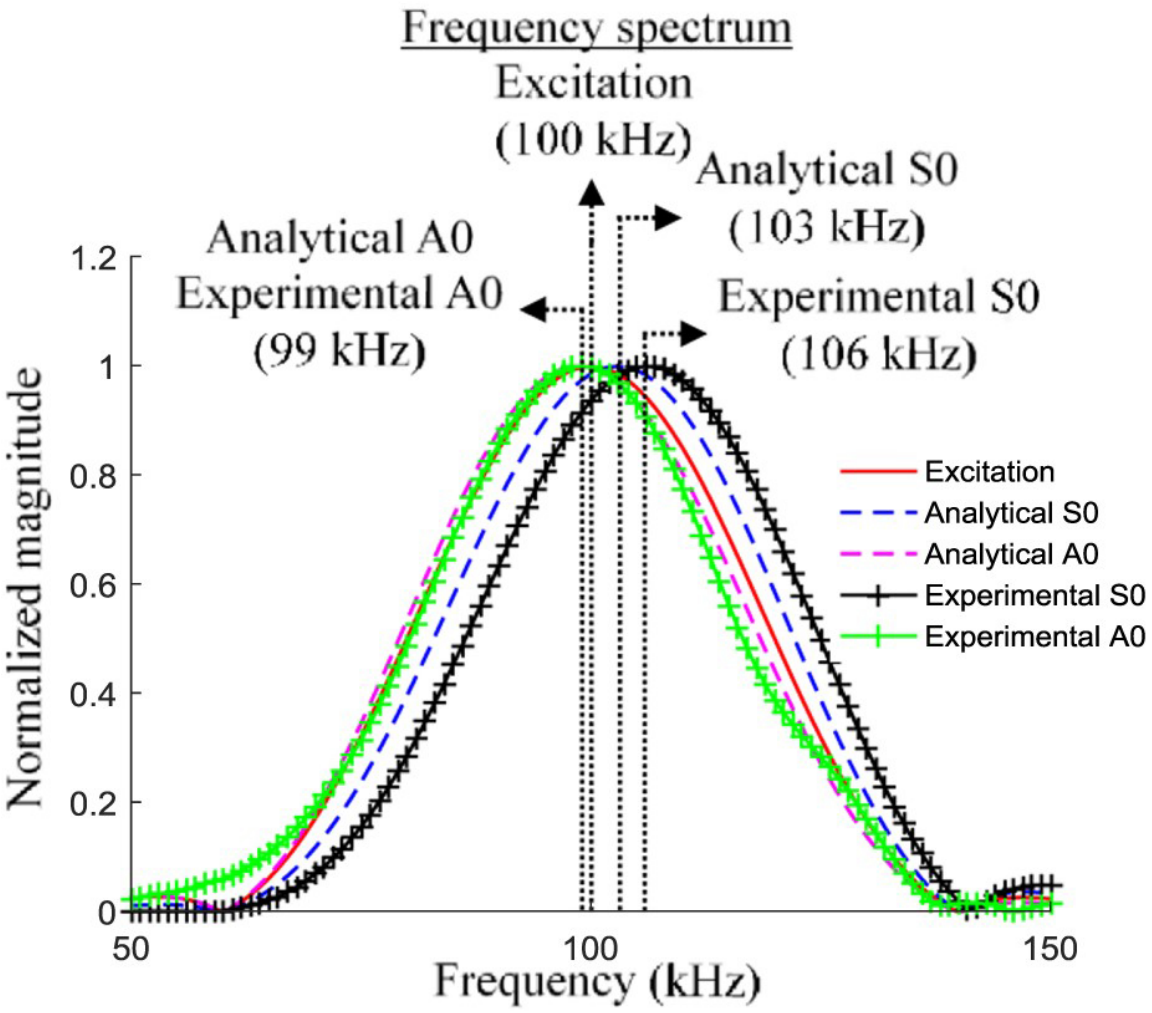


Figure 4.3: Frequency shift of response signals compared to 100kHz excitation signals due to the transducer tuning effects [205].

### 4.2.2 Instantaneous baseline (IB) approach

The central hypothesis behind the IB approach is that damage is typically localised to only a few transducer paths, while the majority of transducer pair responses remain unaffected and can be considered as undamaged [208]. Namely, the damage affects only specific areas or regions of the structure, while the majority of the structure remains undamaged. The IB approach exploits the undamaged transducer pair responses as an "in-situ baseline" [208]. The baseline represents the reference response that would be obtained from the structure in its original, undamaged state. By using this baseline, the IB approach aims to identify and isolate the potential damages in the structure.

Furthermore, it is assumed that a transducer path passing through potential damages will contain reduced energy compared to its undamaged equivalent paths which have similar path distances and propagation angles. In this regard, the damage index for a transducer path can be formulated as follows [209].

$$DI_{i,j} = 1 - \frac{E_{i,j}}{E_i} \tag{4.7}$$

where $i$ and $j$ represent the $i$-th group of equivalent transducer paths and the $j$-th path in the $i$-th group of paths. $E_{i,j}$ and $E_i$ denote the energy of the $j$-th signal from the $i$-th group, and the maximum energy of signals from the $i$-th group respectively [209].

The energy of a signal $R(t)$ transmitted from transducer $A$ to $B$ is then defined as [209]

$$E = \int_{t_0}^{t_1} R_{AB}^2(t)dt \tag{4.8}$$

where $t_0$ and $t_1$ represent the start and the end of the first wave packet respectively.

The instantaneous baseline (IB) method offers high flexibility for structural health monitoring (SHM) tasks by eliminating the need for historical baselines or prior knowledge of the structure being inspected. The IB technique has garnered increasing research interest due to its applicability and effectiveness in damage detection and localisation. Anton et al. [208] proposed creating instantaneous baselines by categorizing transducer paths into groups with equal path distances. They identified potential damage-sensitive paths showing abnormal statistical features and successfully detected and localised simulated damages in metallic plates.

Park et al. [210] utilised the IB technique to detect and localise artificial damages within an aluminium plate. They investigated the performance of the method in both pitch-catch and pulse-echo configurations, achieving satisfactory results in both cases. Salmanpour et al. [60] partitioned inspected structures into cells, with some cells containing local damages and others serving as the baseline area, and generated instantaneous baselines by projecting the baseline area onto the inspected area using equivalent transducer paths. They successfully detected and localised potential damages, including complex structures like stiffened composite panels and under varying temperature conditions. It is worth noting that this method is suitable for structures with repeated geometrically similar cells and may not be applicable to non-symmetric and non-periodic structures. Wang et al. [211] and Wu et al. [212] integrated the IB methodology with nonlinear ultrasonic guided waves for detecting and localising early-stage cracks. Mesnil et al. [48] demonstrated the effectiveness of the IB approach in identifying damage in curved composite panels. The approach has been successful in identifying different types of damage in curved composite panels under varying temperatures and varying frequencies of guided waves [48]. These studies illustrate the versatility and effectiveness of the IB method in various SHM applications, particularly in damage detection and localisation. However, it is essential to note that the IB method's applicability may be limited to certain structural geometries or conditions, as highlighted in Salmanpour et al.'s study [60]. For structures with repetitive and symmetric cells, the IB technique is well-suited, but it may not be suitable for more complex and asymmetric structures.

Despite the recent developments, a wider application of the IB technique is limited due to the following aspects. Firstly, the instantaneous baselines are generated by aggregating and comparing a set of transducer paths with the same path distances [208, 210] and propagation angles, where the latter condition is required particularly for anisotropic materials. This is to ensure that the path signals for comparisons will have nearly identical waveforms so that further identification and localisation of potential damages can then be easily implemented within the equivalent transducer paths. However, such requirements for the nearly identical transducer paths can be rather rigid under real-life scenarios especially when there exist only a few transducers for the real-time monitoring and consequently insufficient transducer paths for

the instantaneous baseline generation. To solve such problem, Qiu et al. [213, 214] attempted to compensate the different path distances so that in such case different sensor paths can be compared. Nevertheless, their methodology neglected potential differences in the propagation angles and therefore cannot be implemented on anisotropic structures, which greatly restricts the applicability of their proposed approach. Another challenge lies in requirement of the IB technique for identical transducer conditions [48] which further include positioning, wiring and bonding of the mounted transducers. Fortunately, such challenge can be alleviated by adopting the diagnostic film [215] or the SMART layer technology [216].

Furthermore, as discussed earlier one basic hypothesis of the instantaneous baseline approach lies in that most of the transducer paths remains undamaged even when a potential damage is introduced. Practically such hypothesis becomes delicate when there exist multiple damages simultaneously within the inspected structures. Very few research has generated instantaneous baselines for the case of multiple damages. Moreover, a more generic solution is needed to detect and localise multiple damages not only within metallic plates [209], but also within anisotropic composite structures.

### 4.2.3 Reciprocity-based approach

Reciprocity-based techniques in SHM leverage the principle of reciprocity in wave propagation to detect and localise potential damages in engineering structures. Reciprocity refers to the symmetry between the responses obtained when a wave is transmitted from one transducer to another and when the same wave is transmitted in the reverse direction [217]. For approximately linear media [217], the guided wave signals measured between pairs of transducers traveling in opposite directions (reciprocal paths) should be similar when the structure is undamaged. This is due to the reversal symmetry of the linear wave propagation [217]. However, when nonlinear scattering damages are present in the inspected structure, the reversal symmetry between reciprocal paths will be broken. The presence of damage will cause asymmetry or discrepancies between the responses measured along reciprocal paths. By comparing the responses from reciprocal paths and identifying the asymmetry or discrepancies, it is possible

to detect and localise the existence of potential damages in the structure. The analysis of these discrepancies can provide valuable information about the location and severity of the damage. The corresponding damage index is proposed as [217]

$$DI = 1 - \frac{\left| \int_{t_0}^{t_1} R_{AB}(t) R_{BA}(t) dt \right|}{\sqrt{\int_{t_0}^{t_1} R_{AB}^2(t) dt \int_{t_0}^{t_1} R_{BA}^2(t) dt}} \tag{4.9}$$

where $R_{AB}(t)$ and $R_{BA}(t)$ denote a signal transmitted from transducer $A$ to $B$ and its reciprocal signal; $t_0$ and $t_1$ define the time interval for comparing $R_{AB}(t)$ and $R_{BA}(t)$.

The application of the reciprocity principle for baseline-free damage detection and localisation has been an area of growing research interest in recent years. Several studies have demonstrated the effectiveness of this approach in various structural configurations and materials. Scalerandi et al. [218] investigated the acoustic signals from reciprocal transducer paths when there exist local cracks in a concrete beam. They found that local cracks lead to differences between the reciprocal paths and such discrepancies are to a large extent strengthened when the locations of the monitoring transducers are highly asymmetrical towards the potential damages. Meanwhile, Huang et al. [217, 219] extended the reciprocity-based approach to the quasi-isotropic composite plates. They successfully detected and localised damages with calibrated excitation signals and highly asymmetrical transducer arrays with particular emphasis on the helical arrays in the former research, while in the latter they successfully captured damage locations by utilising edge-reflected guided waves. Recently Du et al. [220] further developed the work of [217] with enhanced sensitivities by extracting and adopting secondary scattering waves.

Furthermore, the reciprocity principle can be integrated with other baseline-free techniques, including the mode conversion [221, 222] and statistical algorithms [155], for accurate results in damage detection and localisation. Such combinations enable the reciprocity principles to be more applicable and flexible when being employed for damage detection and localisation purposes.

Indeed, the reciprocity-based approach has shown promising results for damage detection and localisation, but it also has limitations that need to be addressed for further applications and practical use. The effectiveness of the reciprocity-based approach is reported as highly sensitive

to the relative locations between potential damages and the mounted transducers [217, 218]. The breaking of reciprocity due to localised damage is dependent on the distances between the nonlinear damage scatterer and the corresponding monitoring sensors [217]. If the potential damage is asymmetrical within a transducer path, the forward-propagating guided waves and their reciprocal counterparts will attenuate with different scales when passing through the damage. This leads to amplified discrepancies between signals from reciprocal paths when there is an asymmetrical damage between transducers. Such analyses have been further validated by [217] where asymmetrical transducer arrays, e.g., a helical sensor configuration, can yield better damage localisation results than the symmetric circular arrays (see Fig. 4.4). Simultaneously, when applying the reciprocal principles, a prior knowledge of the potential damaged areas is actually required for further calibration of transducer arrangements [217], which may be impractical for real-life applications. Such problems need to be resolved prior to more applications of the reciprocity-based approach.

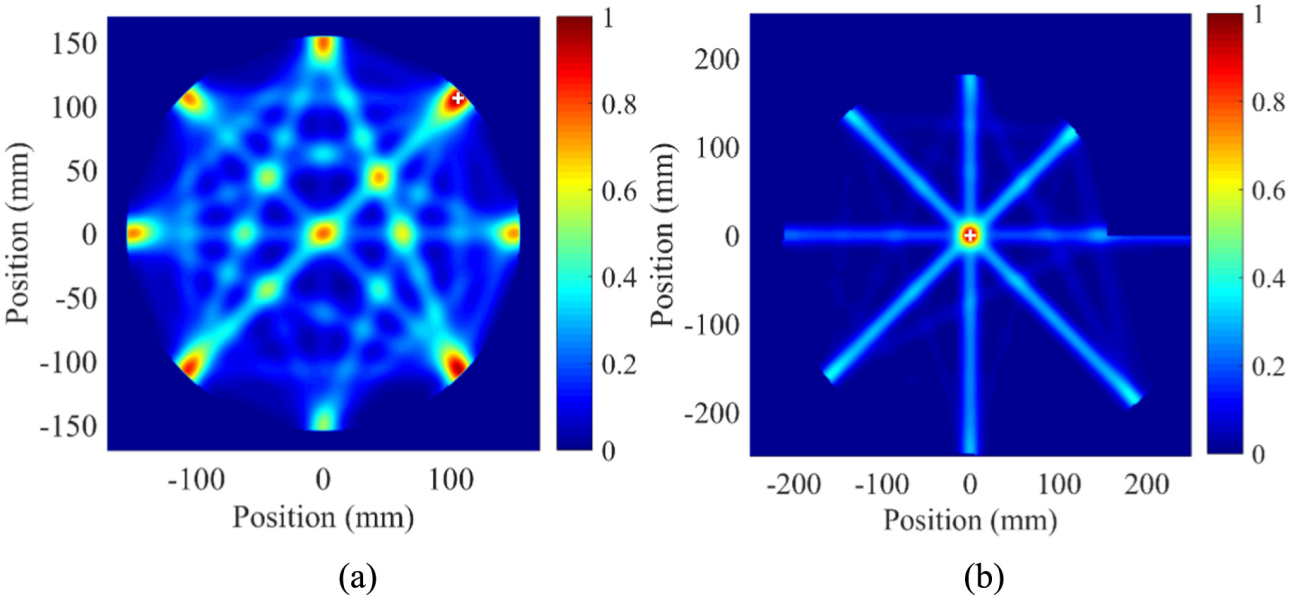


Figure 4.4: Baseline-free damage localisation based on the reciprocity-based approach for (a) circular transducer array; (b) helical transducer array. [217]

### 4.2.4 Modal based techniques

In the previous sections, mainly three different techniques, namely the time reversal (TR), instantaneous baseline (IB) and the reciprocity principle, are introduced for the damage detec-

tion and localisation. Among these baseline-free techniques, one shared characteristic is that a pairwise comparison is needed between the current measurements and the generated reference signals. More specifically, in terms of the TR approach a pairwise comparison is implemented between the original excitation signals and the reconstructed signals, whereas in the latter two cases the current measurements are further compared to the virtual instantaneous baseline signals and reciprocal path signals respectively. However, as discussed earlier, the virtual referenced data may not be generated properly due to various reasons including inappropriate sensor arrangements, anisotropic structures for inspection and multiple damages within the interrogated structures. In this regard, it is necessary to directly extract damage-sensitive features from the current measurements rather than creating the virtual references for the SHM purposes.

Following such rationale, it becomes essential to thoroughly understand and then interpret the propagation process of guided waves, particularly the interactions between the propagating waves and potential damages. However, the interpretations could be rather difficult considering not only multimodal dispersion behaviour [223–225] of guided waves but also high structural complexities [226, 227] of the inspected structures. To overcome these difficulties, two main techniques, namely the mode separation and mode conversion, have been persistently investigated in recent years.

Considering the multimodal properties of guided waves, mode separation or the so-called mode decomposition aims to remove unnecessary wave modes and to only extract and isolate the damage-sensitive features, including the damage scattering modes [159, 228], from guided wave signals. When utilising such modal techniques for damage detection and localisation, an exemplar case is illustrated in the work by [228]. In their work, when a damage exists within or near an actuator-receiver path, two stages of the guided wave propagation are presented simultaneously: the forward propagation and the backward propagation. Furthermore, considering that the forward-propagation process contains no damage-scattering modes of the propagating guided waves, Lee et al. [228] further extracted the damage-sensitive information by subtracting the forward-propagating signals from the back-propagating counterparts. By such procedures, only the damage scattering modes of guided wave signals were conserved while the other irrel-

evant modes were removed.

With a similar goal, the mode separation can also be implemented adequately by removing velocity dispersions between potential overlapping modes within guided wave signals. More specifically, since different wave modes have different group velocities, several critical modal components, including the dominant modes, the damage scattering modes and the boundary reflections, could be overlapped together [229]. Such mixing of different wave modes will inevitably hinder an accurate extraction of the damage-sensitive features which are essential to damage detection and localisation. To address this problem, Zhou et al. [166] utilised the so-called dispersion removal technique to alleviate the multimode dispersions. They further found that the various modes are clearly separated and the damage-scattering modes can subsequently be isolated and extracted. Meanwhile, the time frequency analyses on current guided wave measurements have also been proved useful for the mode separation purposes. According to Gao et al. [230], current measurements of Lamb wave signals were analysed in their time-frequency representations and a frequency-wavenumber domain filter was further implemented to improve the performance of the mode extraction and the reconstruction of the corresponding modal components. In addition, the mode separation can also be accomplished by optimising the sensor arrangements [231, 232] so that different wave modes can be naturally separated without utilising analytical or numerical techniques to interpret the guided wave propagations.

Similar to the mode separation, in the realm of the mode conversion an equal attention is paid to the modal domain information of guided wave signals. Nevertheless, the main rationale of the mode conversion technique is different. More specifically, the mode conversion is equivalent to the mode-shifting of guided waves when propagating through a potential damage in the interrogated engineering structures. Practically, in terms of Lamb waves such regime shift is usually manifested into the conversion [221] from $S_0$ to $A_0$ modes after the damage scattering, or vice versa, at a certain central frequency of the Lamb wave signals. Since the original modal components and the converted modes have different group velocities, this discrepancy can be further utilised for damage localisation if combined with the time of arrival (TOA) information of different modes and the triangular localisation [221]. When being deployed for the SHM purposes, the mode conversion method has exhibited its high accuracy and wide applicability

to various material types and damage scenarios. In terms of the material types, Jia et al. [221] developed an analytical solution of the measured Lamb wave signals with the converted $A_0$ modes and estimated the TOA and the group velocity of both the $A_0$ and $S_0$ components. Based on the estimated modal information and the triangular localisation method, accurate damage localisation results were yielded for a single transducer path on metallic plates. Similar investigations were also implemented on metallic plates by Sohn and his collaborators [233,234] and further extended to composite plates together with real-life structures including both concrete [235] and composite beams [236]. Furthermore, the mode conversion technique has also been widely employed to different damage scenarios including notches [221], cracks [237, 238] and delamination [159, 239].

However, there exist several limitations of the modal analyses, which further include both the mode separation and mode conversion, despite the recent contributions of these techniques to the community of the baseline-free SHM. First, a successful implementation of the modal techniques requires that all the critical modes within guided wave signals, mainly the dominant modes and the damage scattering modes, are clearly separated and isolated [240]; otherwise, estimations of the TOA and the group velocity for different modal components will be largely affected and therefore lead to erroneous results for damage detection and localisation. Theoretically such problem can be simply solved by either pre-determining the group velocities or adjusting the sensor arrangements [231, 232] so that different wave modes can be spatially separated. Nevertheless, the former solution could be impractical for real-life applications whereas the latter could be affected by varying temperature conditions (see section 4.3).

Furthermore, the modal analyses, which involve calculations of the TOA and the group velocities, could lead to inaccurate results [221] when being applied to anisotropic structures. This is because the modal information may vary with the propagation angles of guided waves. Though previous research indicated the effectiveness of the modal-based method for anisotropic cases, it still remains a challenge to propose a generic solution for the anisotropy problems.

### 4.2.5 Nonlinear frequency modulation (NFM) technique

The Nonlinear Frequency Modulation (NFM) technique is an emerging approach for baseline-free damage detection and localisation. The main principle of NFM involves simultaneous application of high-frequency (HF) and low-frequency (LF) input signals to interrogate and detect damages in structures [241–244], e.g., the opening and closing cracks. More specifically, if a nonlinear damage is introduced into the inspected structures, such structural nonlinearities will be amplified by the modulation between the HF and the LF components and there will exist the corresponding frequency sidebands in the modulated signals [243]. The NFM technique can be further formulated as [243].

$$\boldsymbol{u}_S = \boldsymbol{u}_{b\pm a} e^{-i(\omega_{b\pm}\omega_a)t} + \text{ c.c.} \tag{4.10}$$

where $\boldsymbol{u}_S$ represents modulation of the propagating LF and HF components, denoted as $a$ and $b$, and centre frequencies of the two waves are denoted as $\omega_a$ and $\omega_b$; $\boldsymbol{u}_{b\pm a}$ represents the amplitude at the sideband frequency $\omega_b \pm \omega_a$, whereas c.c. represents the complex conjugate [243]. Furthermore, the nonlinear index (NI) is defined as the standard deviation of $\boldsymbol{u}_S$ [243] to quantify nonlinear effects due to the damages.

$$NI = \text{std}\left(\boldsymbol{u}_S\right) \tag{4.11}$$

In recent years, the NFM technique has been gaining its popularity for the baseline-free damage detection due to its high sensitivity to the early-stage nonlinear damages. In this realm, Lim et al. [243] employed the modulation technique with a fixed high frequency range and a sweeping lower frequency range. More specifically, during the modulation process they extracted damage-sensitive features by constantly adjusting the central frequency of the LF inputs, and further defined a nonlinear damage index based on the modulated outputs [243]. Afterwards they implemented their approach to detect potential cracks in an aluminium plate [243] and achieved robust results against varying temperature and loading conditions. Meanwhile, for engineering applications the modulation technique was also implemented to detect damage cracks in alloys by Mevissen and Meo [244]. However, when utilising the frequency modulation

technique, frequency ranges of the input signal need to be tuned to yield the optimal performances of such technique for the damage detection tasks. In addition, it is worthy to note that the previous work primarily focuses on metallic structures and cases for composite structures deserve further investigations.

## 4.3 Critical factors for baseline-free techniques

### 4.3.1 Varying environmental conditions

Baseline-free GWSHM techniques, including the proposed data-driven approach in Chapter 5, are expected to yield robust SHM capabilities under varying temperatures. However, temperature variation can indeed pose challenges to the performance of several baseline-free techniques, including the TR method [245] and modal analysis [221] of guided wave signals. Changes in temperature can affect the properties of materials, alter wave propagation behaviour, and introduce additional complexities in the signal analysis process. In terms of the TR family, Sharma and Kapuria [245] investigated the time reversibility of Lamb waves based on a pitch-catch configuration and their results indicated that the time reversibility is affected by the temperature variations and the excitation frequency, namely the central frequency of excitation signals (see Fig. 4.5). Alternatively, for a given excitation frequency the time reversibility may fluctuate greatly with the temperature variations, and such fluctuations can be attributed to the instability of adhesive layers between the inspected structures and the mounted transducers [245]. However, the authors found that the effects of temperature variations become minimal over the time reversibility when a specific value, or the so-called best reconstruction frequency [245], is selected for the excitation frequency. Such frequency value is determined when the corresponding excitation signal and its reconstructed counterparts have the highest similarities [245, 246]. Integrating the best reconstruction frequency, Sharma et al. [247] further validated their proposed refined time reversal method (RTRM) when detecting cracks on metallic panels under temperature variations. It was found that the integrated RTRM remains nearly invariable under varying temperature levels [247]. Apart from the TR based

methods, Mesnil et al. [48] validated effectiveness of the IB technique for damage detection on curved woven composites under varying temperatures. Despite the research above, further investigations are expected for composite structures, not only for the damage detection, but also for the localisation tasks.

Apart from the time-reversal based method, the modal analyses of guided wave signals can also be affected by the temperature variations. This is because the critical parameters, e.g., group velocities, utilised in the modal methods are proved to be highly sensitive to temperature variations [148, 248–250]. In addition, it is commonly assumed by previous research that the temperature variations are uniformly distributed within the interrogated structures. However, such assumptions may not hold true for structures with large sizes, high structural complexities or local temperature increase [251]. In such cases, other baseline-free techniques, including the instantaneous baseline approach, may not be reliable anymore in terms of damage detection and localisation.

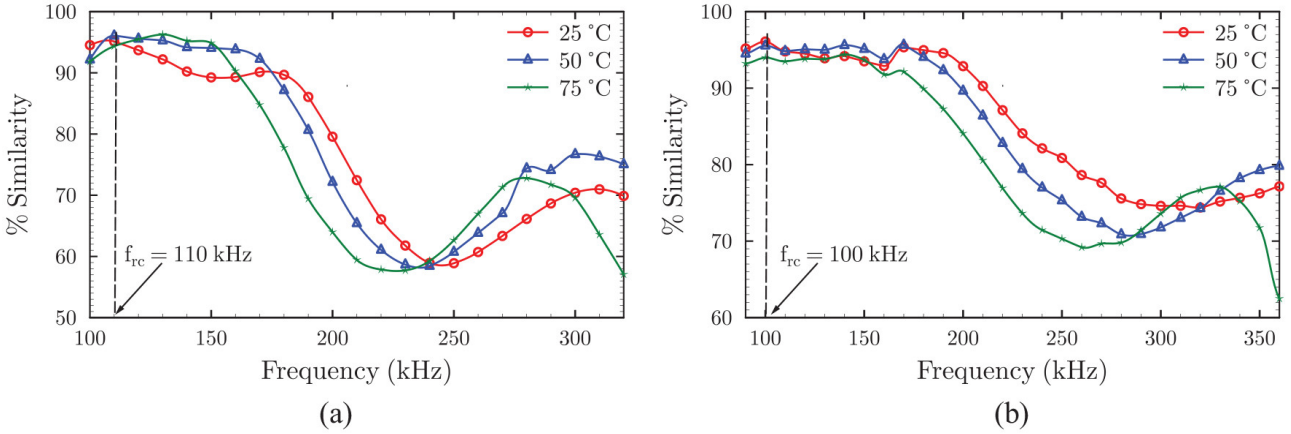


Figure 4.5: Effect of temperature variations on time reversibility of Lamb waves in a 3-mm aluminium plate: (a) experiment; (b) $2D$ FE simulation. [245]

### 4.3.2 Structural and geometrical complexities

Material properties play a critical role in the implementation and effectiveness of baseline-free techniques for damage detection and localisation, particularly in the realm of guided wave-based structural health monitoring (SHM). One crucial material property that significantly affects the performance of guided wave based SHM is whether the inspected structure is isotropic or anisotropic. For isotropic or quasi-isotropic structures, the group velocities of guided waves

are considered uniform for different transducer paths. This uniformity simplifies the analysis and interpretation of wave signals, making it relatively straightforward to implement certain baseline-free techniques, such as time reversal or instantaneous baseline, for accurate damage localisation results. However, in the case of anisotropic structures, the group velocities of guided waves can vary with propagation angle. This variation makes the mode conversion and wave propagation analysis more complicated. As a result, implementing certain guided wave-based techniques, especially those relying on accurate knowledge of wave velocities and mode conversion behaviours, can be challenging in anisotropic laminates. Material damping [252] is another property which may affect the performance of baseline-free approaches, particularly in the case of time-reversal methods [176,177]. According to Xiao et al. [176], the damping scenarios including both the physical damping can harm the perfect reconstruction of the excitation signals even under healthy states of the inspected structures. Meanwhile, the damage-sensitive features can also be masked by the damping features, thus leading to the erroneous damage localisation. In this regard, it is necessary to exclude the effects of material damping when utilising the time reversal techniques.

For baseline free methods such as the IB method, structural symmetry is vital. This means that the method will be applicable to grid-based structures, where each sensor grid is reproducible and is represented by a neighbouring grid of the same property. This may not be the case for complex geometrical structures, e.g., large-size stiffened panels, with manholes and openings. In addition, boundary reflection [209, 249] from stiffener edges, frames or openings can challenge the signal interpretation, thus degrading the performance of baseline-free techniques. However, few research has considered the cases with heavy boundary reflections in terms of baseline-free techniques.

### 4.3.3 Multiple damages

The ability of baseline-free techniques to detect and localise multiple damages, including dual damages, is a critical aspect of their practical applicability in real-world SHM scenarios. Both the TR and IB techniques have been explored for this purpose. The standard TR approach was employed by [191] to localise two notches in an aluminium plate and the results further validated

the ability of the time-reversal approach for multi-damage localisation despite the estimation errors of real damage locations and several artifacts existing in the damage imaging results. Meanwhile, the standard TR approach can also be implemented in the wavefield domain for an accurate localisation of multiple damages. Furthermore, considering high physical burden of the stand approach Wang and Shen [205] implemented the VTR to detect two damages in an aluminium plate (see Fig. 4.6) and they found that the transfer function compensation can to a large extent improve the localisation performance of the VTR technique in the case of multiple damages. Kannusamy et al. [206] further proposed the RTRM to localise damages in metallic plates and their proposed methodology was validated for the dual-damage cases (see Fig. 4.7). The capability of the multi-damage detection and localisation was also validated for the IB method by Sun et al. [209], where two damages are able to be accurately localised in an aluminium plate. However, despite these contributions few research has been implemented to detect and localise multiple damages in anisotropic structures, e.g., anisotropic composite plates. In this regard, thorough investigations need to be implemented on various structures.

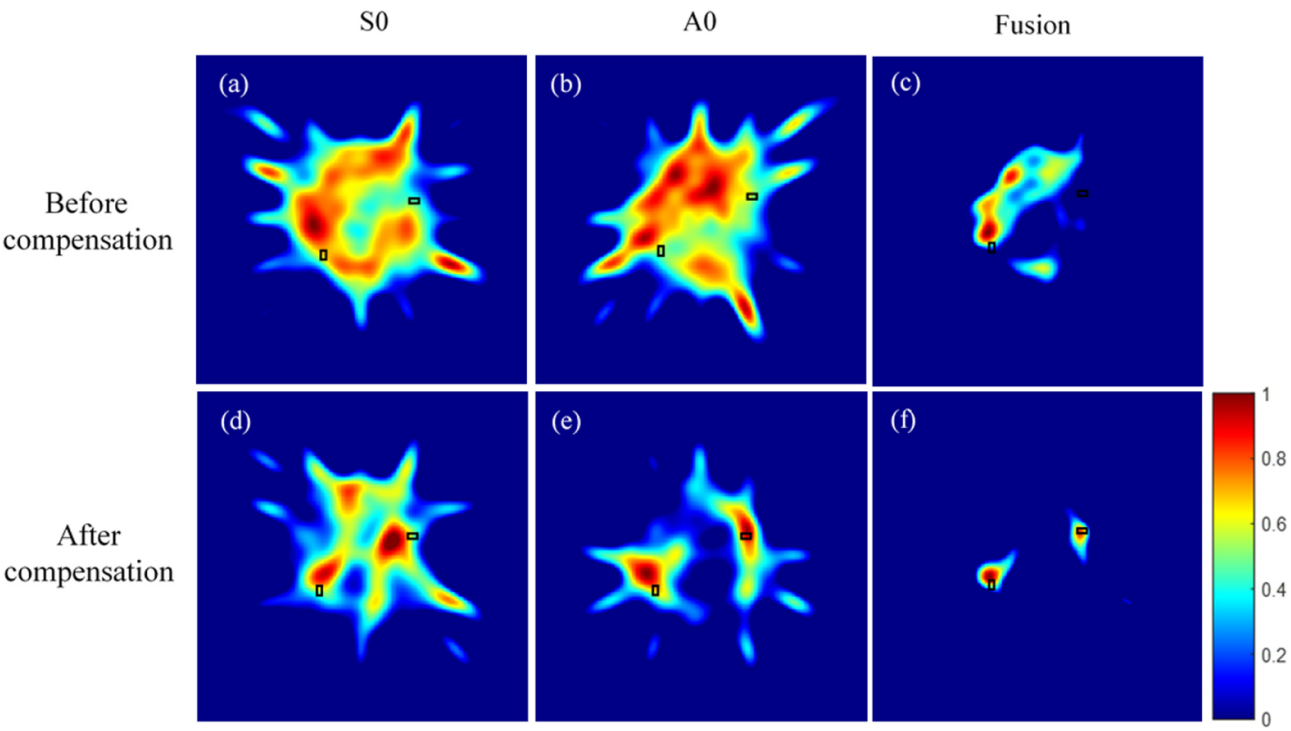


Figure 4.6: Damage localisation results of a 2 mm-thick aluminium plate. The two rows (from top to bottom) represent the standard VTR and the proposed method with transfer function compensation respectively. The three columns represent the damage imaging results based on $S_0, A_0$ and the modal fusion respectively. [205]

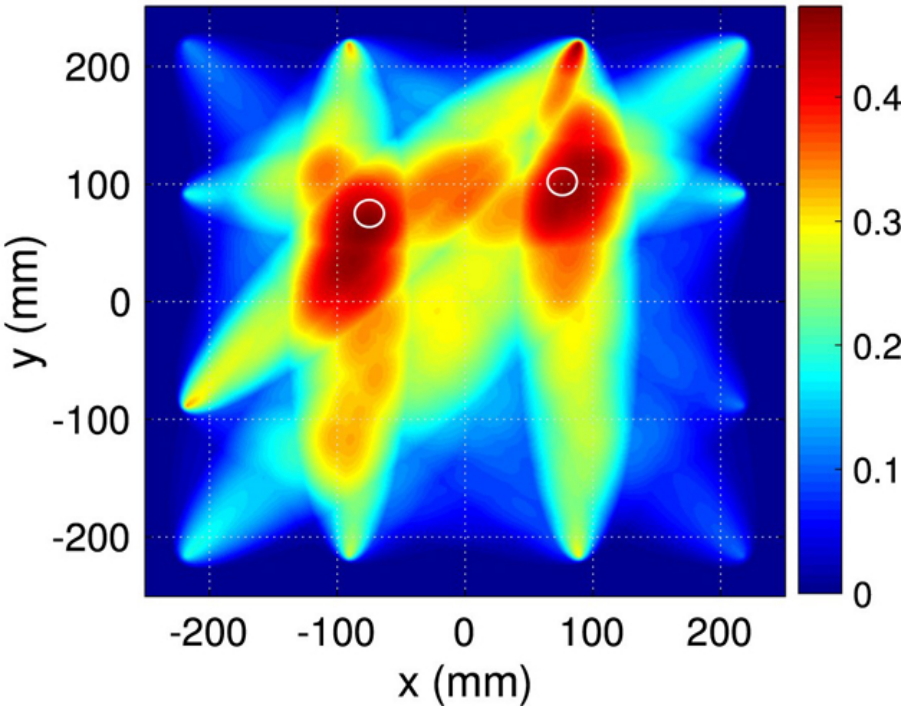


Figure 4.7: Damage imaging result of two damages in a 3 mm-thick aluminium plate. The result is obtained by the RTRM with the best reconstruction frequency of excitation signals. [206]

## 4.4 Experimental setup

To further compare and analyse the baseline-free techniques, related experiments are implemented on anisotropic Carbon Fibre Reinforced Polymer (CFRP) composite structures including coupon plates and stiffened panels, which are all manufactured of $M21/194/34\%/T800S$ ($M21$ -$T800S$) laminates with the stacking sequence as $[\pm 45/0_2/90/0]_s$. The transducer bonding is inspected based on the Electro-mechanical Impendence (EMI) analyses. During the experiments, the DuraAct (PI ceramic) transducers are operated in a pitch-catch configuration where the transducers can act as actuators and sensors simultaneously. Following such configuration, the signal excitation and sensing are carried out respectively by a National Instrument (NI) signal generator and a $PXI$-5105 oscilloscope, where the amplitude of excitation and the sampling rate are adopted as 6 V and 60MS/s respectively.

Furthermore, the 5-cycle Hanning-windowed 50kHz tone bursts are obtained in the same manner as section 3.4. The first wave packets of guided wave signals, corresponding to the predominant $A_0$ mode, are extracted following formula (3.28). During the signal denoising, the

signal crosstalks or the so-called electromagnetic interference noises are also removed based on the duration of excitation signals.

After the signal processing procedures, the damage index ($DI$) values for different transducer paths are yielded by formula (4.6), (4.7), (4.9) when implementing the VTR, IB and the reciprocity-based technique respectively, and integrated as the Signal Difference Coefficient (SDC) into the RAPID tomography [16]. The RAPID tomography [16], as introduced in section 2.4.4, is employed for damage imaging and the imaging parameter $\beta$ is adopted as 1.05 as suggested by Zhao et al. [16]. Meanwhile, $100 \times 100$ (length $\times$ width) imaging pixels are employed for composite coupons while $150 \times 150$ pixels are utilised for large-size stiffened panels.

In order to indicate the health condition of a monitored structure, a health index ($HI$) is established by fusing the $DI$s. The $HI$ is proposed as

$$HI = DI_{95\%} \tag{4.12}$$

where $DI_{95\%}$ represents the 95% quantile of the $DI$ values. Note that the Mahalanobis distance (MD) in Chapter 3 is not utilised for baseline-free damage detection considering the unavailability of reference signals.

In the context of damage detection, a detection threshold for the HI is essential to well distinguish between healthy and damaged conditions of a structure. When utilising baseline-free techniques, the threshold value needs to be calibrated by intact signals in advance prior to the monitoring process. The calibration is done by feeding intact signals into the baseline-free methods and calculating the corresponding HI values. The threshold is then obtained as follows [14].

$$Thr = HI_{p,99.9\%} \tag{4.13}$$

where $HI_{p,99.9\%}$ is denoted as the 99.9% precent of HI values under intact states. Accordingly, a damaged state is expected if $HI > Thr$ is satisfied, and vice versa. The performance for damage detection is then evaluated by the binary classification framework in formula (3.24) - (3.26).

Regarding the damage localisation, the localisation accuracy of baseline-free techniques is

investigated by the localisation error $\varepsilon_d$ in formula (3.27). In the thesis, the $\varepsilon_d$ is utilised only for single-damage scenarios considering difficulties to identify and isolate all the dual damages.

Since all the experiments are carried out based on sparse sensor arrays together with a pitch-catch manner, several techniques based on phased array configurations, e.g., multiple signal classification (MUSIC) technique [46], or the nonlinear ultrasonic techniques, e.g., the NFM technique, will not be considered in the experimental validations. More specifically, the VTR, IB and the reciprocity-based techniques, which have been widely utilised in the baseline-free manner, are investigated in terms of their performances under various circumstances, including anisotropic CFRP structures, multi-site damages, varying environmental conditions and structural complexities.

## 4.5 Experimental comparisons on baseline-free techniques

### 4.5.1 Simulated damage cases

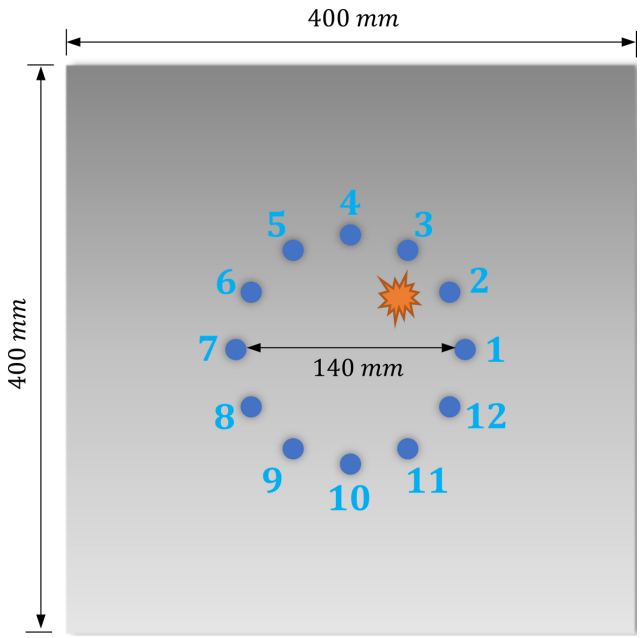


Figure 4.8: 400 mm × 400 mm CFRP coupon with simulated putty damages. [35] The 12 mounted PZT transducers are arranged in a circular configuration.

The compared baseline-free techniques are evaluated on a 400 mm × 400 mm× 2.2 mm (Length × Width × Thickness) $M21$-$T800S$ CFRP coupon (see Fig. 4.8) mounted with 12

PZT transducers. Bonding conditions of the transducers are inspected by the electro-mechanical impedance (EMI) curves. Fig. 4.9 displays the real part impedance of the mounted transducers. It is shown that the impedance curves yield similar peak frequencies, i.e., resonance frequencies, and peak amplitudes within 200-400kHz, thus indicating consistent bonding conditions of the 12 transducers.

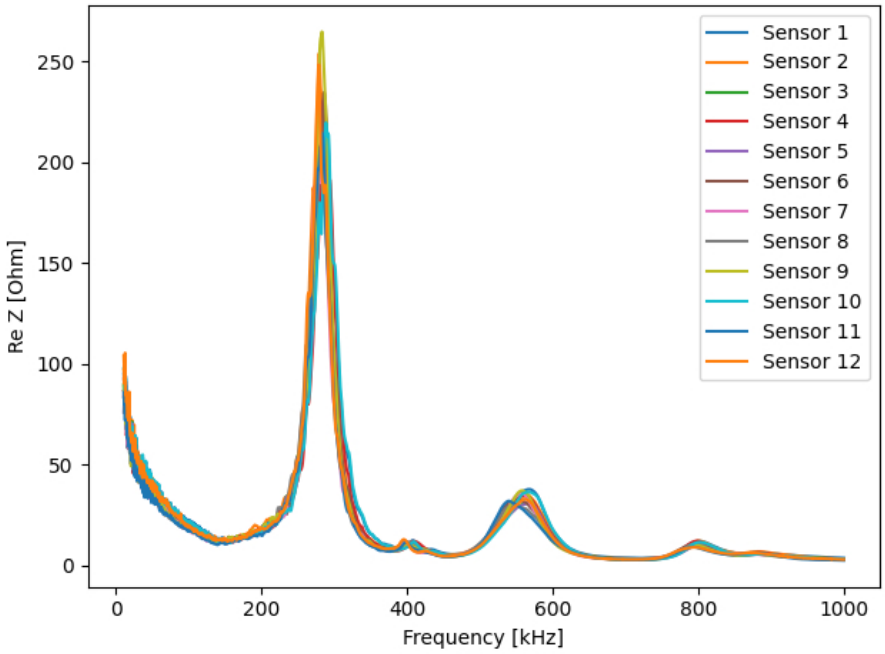


Figure 4.9: Real part impedance of the 12 mounted transducers.

The simulated damage is manufactured of synthetic rubbers with radius as 15 mm. The 12-sensors coupon is implemented by single and dual simulated damages at different locations while being monitored under 20°C - 40°C in a Lab Companion EF-21E oven. The oven heating is operated with a 5°C gradient and the temperatures are measured within ±1°C error. During the monitoring process, $200, 100, 100$ measurements are collected under the intact state, single and dual damage scenarios respectively, whereas 100 intact records at each temperature level are integrated for the detection threshold calibration.

Fig. 4.10 displays the damage detection results of simulated damages at 20°C utilising different baseline-free techniques. The detection thresholds for the reciprocitybased, IB and VTR techniques are determined as $2.13 \times 10^{-3}$, 0.325 and $1.53 \times 10^{-2}$ respectively. The IB and VTR yield the 99% and 100% detection accuracy respectively while the reciprocity-based technique leads to only 93% accuracy due to the decreased capability to identify damaged measurements.

Note that the $HI$ values may vary with damage scenarios where the single and dual damages are situated at different locations.

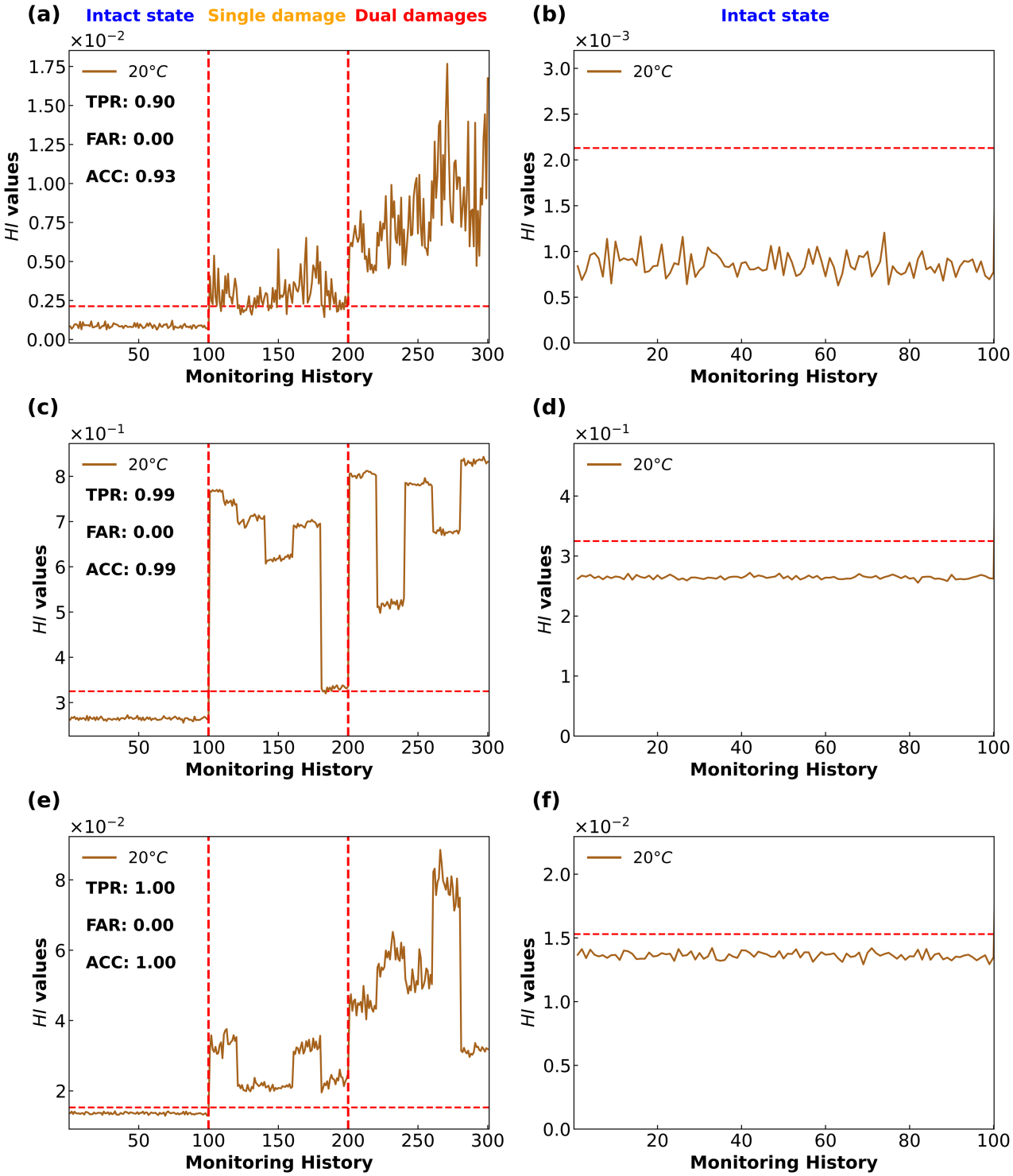


Figure 4.10: Damage detection results of simulated damages at 20°C based on: (a) reciprocity-based approach; (c) IB technique; (e) VTR technique; (b, d, f) the corresponding zoomed views under intact state.

Regarding the damage localisation, imaging results of four simulated single damages are illustrated in Fig. 4.11. It is shown that the compared baseline-free techniques are able to localise single damages at different locations within the circular transducer array. Among the three methods, the VTR and the reciprocity-based techniques yield similar overall accuracies and variances, which are superior to the IB method, when localising the four damages. Furthermore, the simulated damages from different locations within the circular transducer network can also be well localised by the VTR technique and the reciprocity principle due to high sensor coverage at the locations. Comparatively, the IB technique yields modest localisation performances and may even fail for accurate damage localisation under specific damage scenarios. For example, when the potential damage is located at the centre of the 12 transducers, in the case of the damage 4, such damage cannot be accurately localised by the IB technique considering that no equivalent through-centre transducer paths can be utilised for the anisotropic CFRP plate. Regarding the same damage case, the reciprocity-based approach can identify and localise the simulated damage 4 in Fig. 4.11, which is situated symmetrically between transducer pairs. This finding differs from the results in [217] and validates the effectiveness of reciprocity technique under symmetric transducer positionings.

The localisation accuracy of all the ten single damages utilising the compared baseline-free techniques are compared in Fig. 4.12. The VTR technique is shown to yield the lowest localisation errors as 8.6 mm and error variations as 1.1 mm, indicating high effectiveness of such technique to localise the single damages. Meanwhile, the reciprocity-based technique has a moderate performance with the localisation error and the error variation as 11.1 mm and 1.7 mm respectively. The IB technique, however, causes the poorest performance when localising the 10 single damages mainly because such technique is highly dependent on sensor positionings and can be held back by specific damage scenarios, e.g., the damage case 4 where a putty damage is simulated at centre of the circular transducer arrays and no equivalent paths can be utilised considering the anisotropy of composite structure.

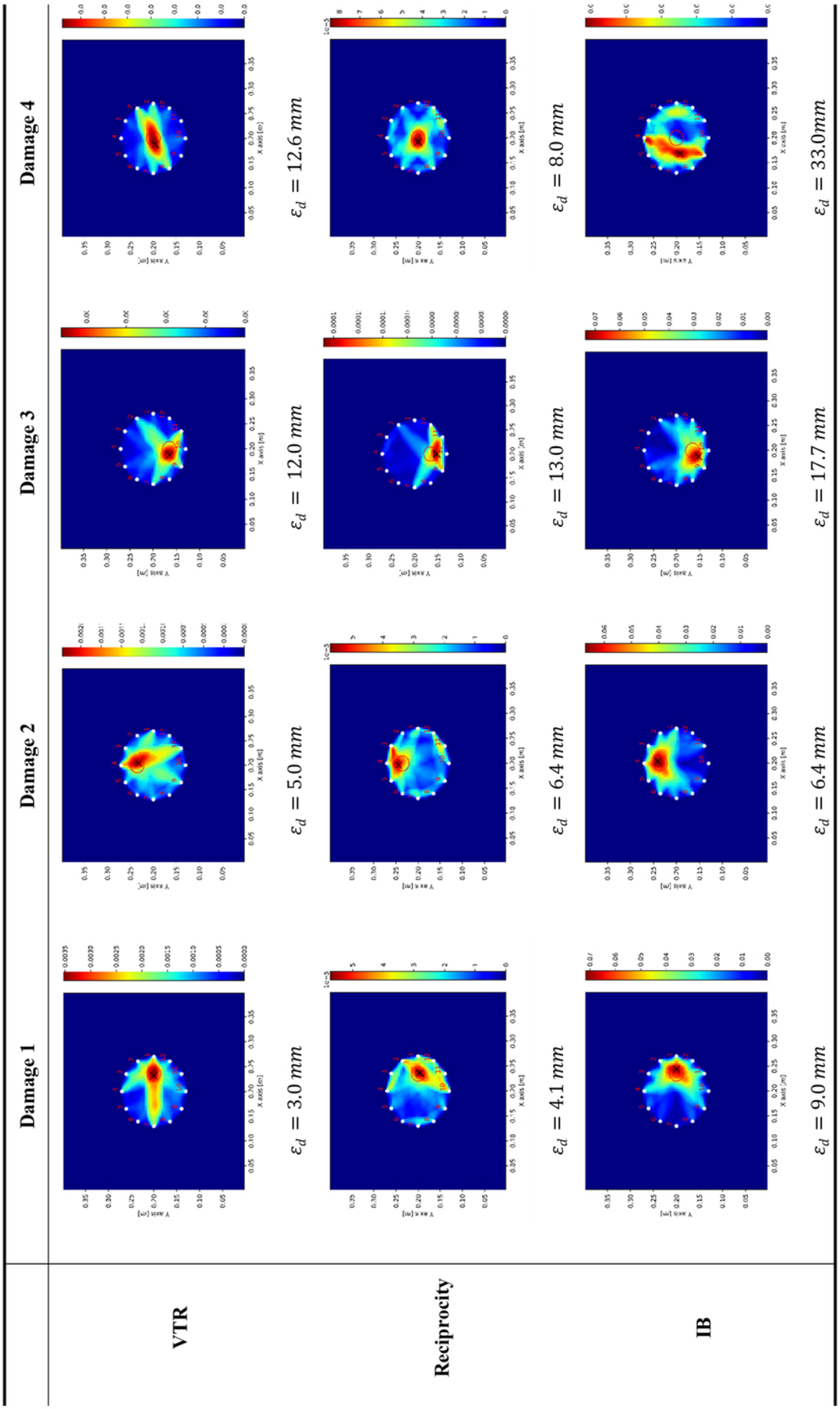


Figure 4.11: Images of simulated single damages on the 12-sensors coupon at 20°C. Red circles represent true damage areas and black crosses denote estimated damage locations. [35]

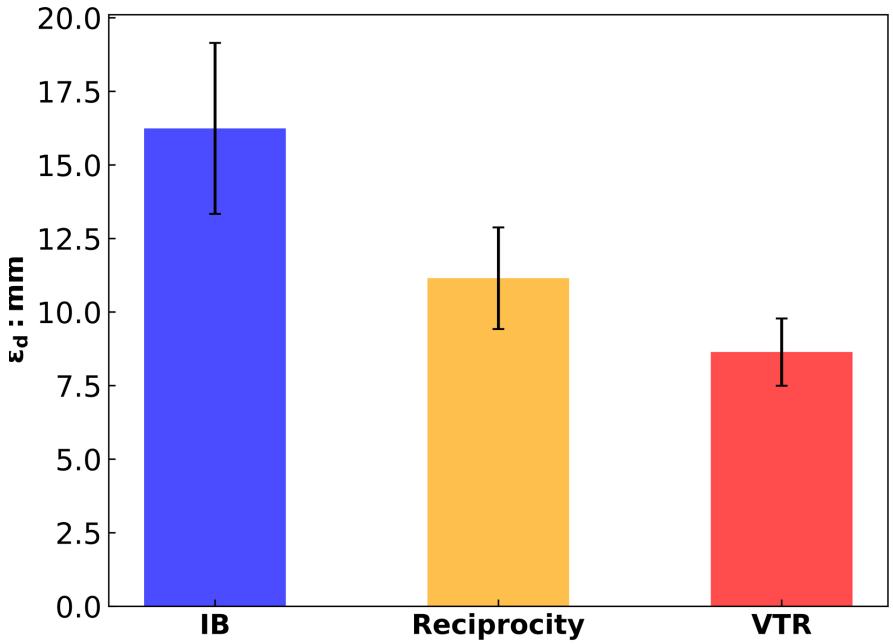


Figure 4.12: Localisation error, $\varepsilon_d$, of the 10 simulated single damages utilising the IB, reciprocity-based and the VTR techniques. [35]

The IB, reciprocity principle and the VTR techniques are further validated on the 12-sensors plate with simulated dual damages. 10 dual-damage scenarios are investigated where damages with the same radius as 15 mm are located at various locations, and the results of four typical scenarios are illustrated in Fig. 4.13. More specifically, it is shown that under scenarios 1,3 and 4, where two adjacent damages are situated at off-centre locations, the reciprocity-based method is competent to identify and localise the dual damages at the same time despite that under scenario 4 estimated damage areas may overlap with each other, and such overlapping consequently complicates well separation of the damages. In contrast, the IB and the VTR techniques are able to detect increasing pixel values around the true damage locations but may fail to concurrently localise the dual damages under scenario 1 and 3 where one putty damage is masked or overlapped by another in the imaging results. Meanwhile, when adjacent damages are located near the centre of circular transducer array, i.e., scenario 2, such dual damages can be detected by the VTR and the reciprocity-based approach but coming with the risk of overlapping pixel values in the middle of two damages. Under the same scenario the IB technique can only localise single damage while ignoring another left near-centre damage, which could be due to the lack of sufficient equivalent through-centre paths for comparisons.

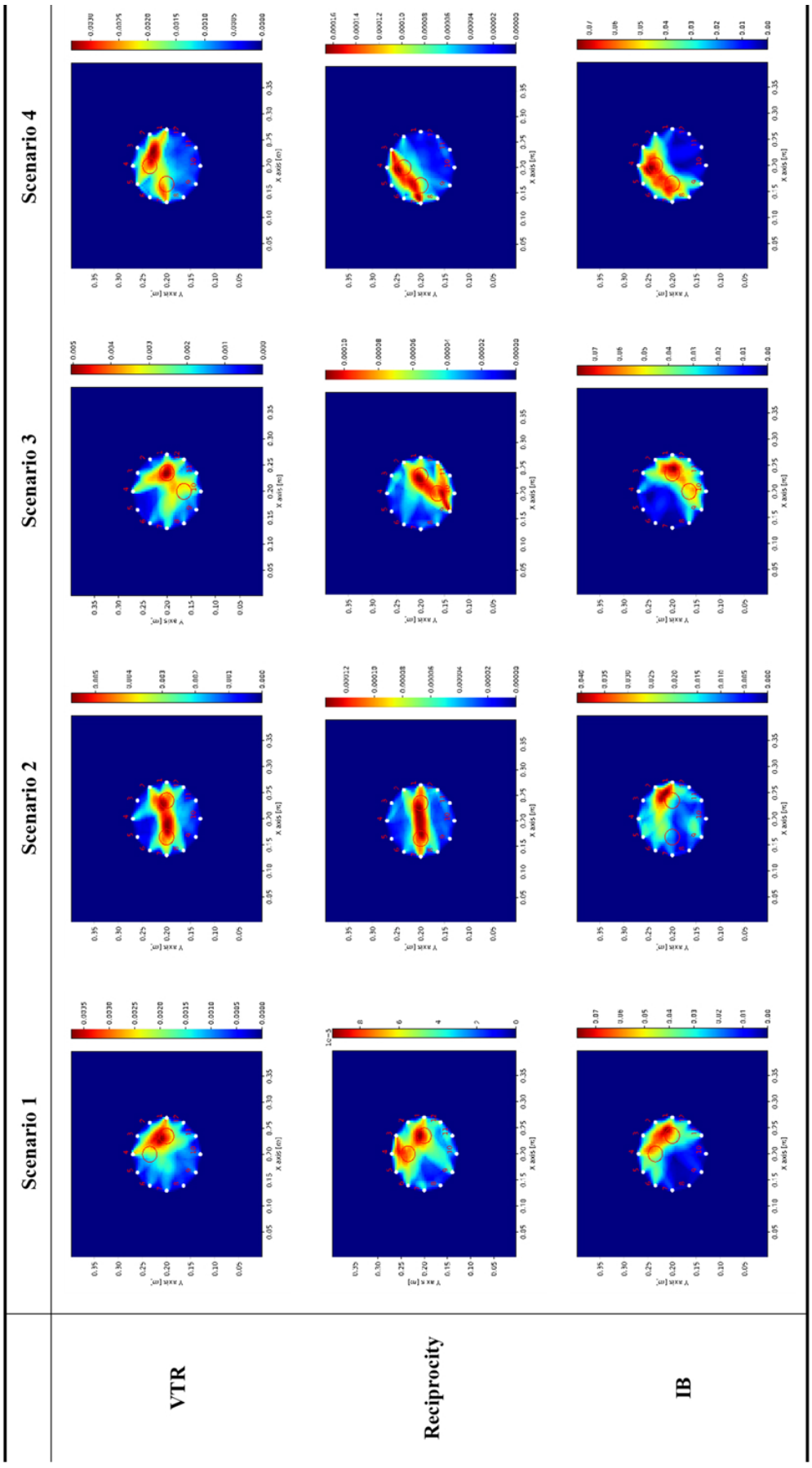


Figure 4.13: Imaging results of simulated dual damages on the 12-sensors coupon at 20°C. Red circles represent true damage areas and black crosses denote estimated damage locations. [35]

### 4.5.2 Impact damage cases

Impact damage cases are also investigated where a 350 mm × 350 mm × 2.2 mm (Length × Width × Thickness) $M21-$ T800S CFRP coupon is impacted by the Instron CEAST 9350 drop tower, leading to two 25 J impact damages of 15 mm radius chronologically. Fig. 4.14 shows the composite coupon with mounted transducers in a square configuration, together with two impact damages (within the red areas) and their C-Scan images. Fig. 4.15 demonstrates the EMI curves of 9 mounted PZT transducers prior to and after the first impact. Fig. 4.15 (a) shows that all the transducers maintain consistent bonding conditions under the intact state, while Fig. 4.15 (b) exhibits obvious shift of transducer 7 in both resonance frequency and peak amplitude, thus implying the abnormal bonding condition of the transducer after the first impact. However, results for damage detection and localisation will later show the robustness of the compared baseline-free techniques against the abnormal bonding.

The impacted coupon is monitored under $20°C, 25°C, 30°C$, while 60,30,30 measurements are obtained at each temperature level, corresponding to the intact state, single and dual damage cases respectively. The detection threshold is calibrated integrating 30 intact measurements at single temperatures.

Fig. 4.16 demonstrates detection results of different baseline-free techniques on impact damages at 20°C. The IB and VTR techniques are competent to distinguish damaged states while the reciprocity-based technique suffers from the false negatives in Fig. 4.16 (a), leading to limited detection capability with the only 71% accuracy.

Fig. 4.17 shows average imaging results of the first impact damage $D_1$ at 20°C based on different baseline-free techniques. It is illustrated that the three baseline-free techniques are capable to localise the single damage despite that the imaging pixel values arranged in different scales. More specifically, the localisation error $\varepsilon_d$ equals to 3.5 mm for the VTR, IB and reciprocity-based methods, implying the equivalence of the three techniques in this case of single impact damage.

In the case of dual impact damages, it is shown in Fig. 4.18 that the compared baseline-free techniques have different capacities to localise the dual damages simultaneously. As indicated in Fig. 4.18 (a, b), the IB and the reciprocity-based techniques are able to localise dual damages

simultaneously. However, only the first impact damage is well localised by the VTR technique, while the second damage is masked by imaging artifacts at the transducer path 1-4 and 4-5 despite the increase of HI values compared to single damage cases in Fig. 4.16 (e).

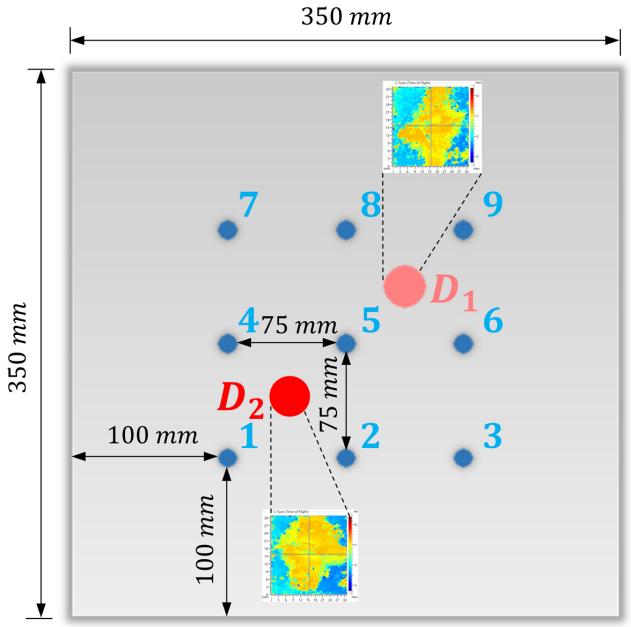


Figure 4.14: The CFRP composite plate with 9 mounted PZT sensors. The impact damages are located within the red areas.

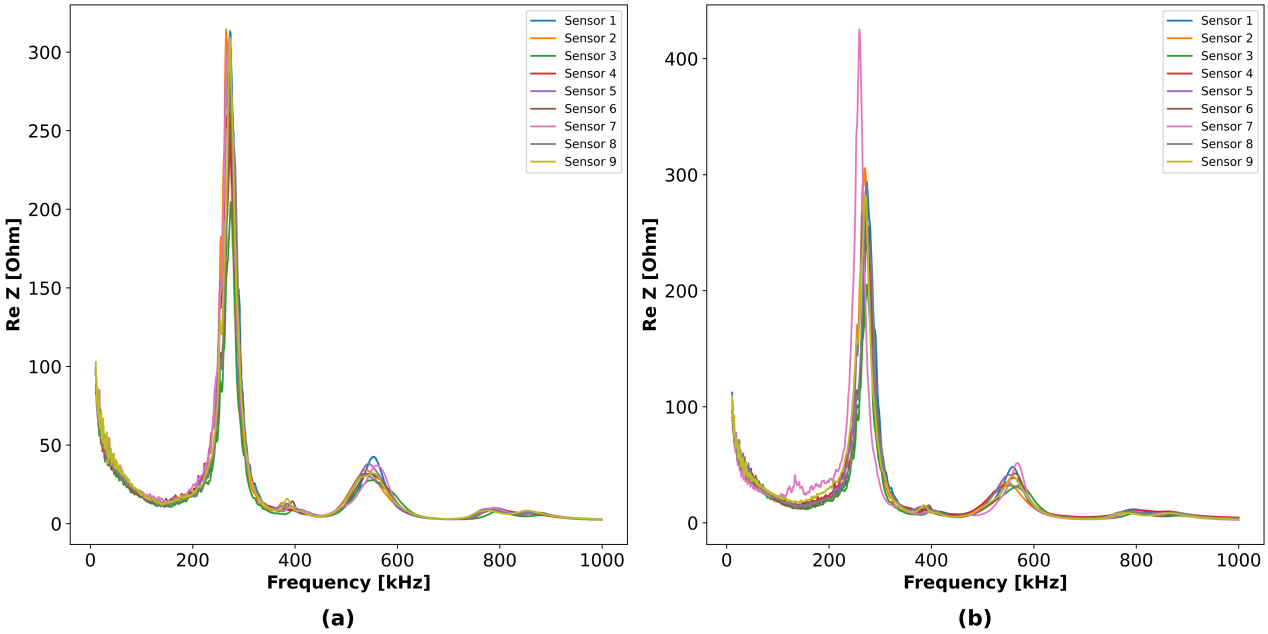


Figure 4.15: Real part impedance of the 9 mounted transducers prior to (left) and after (right) the first impact.

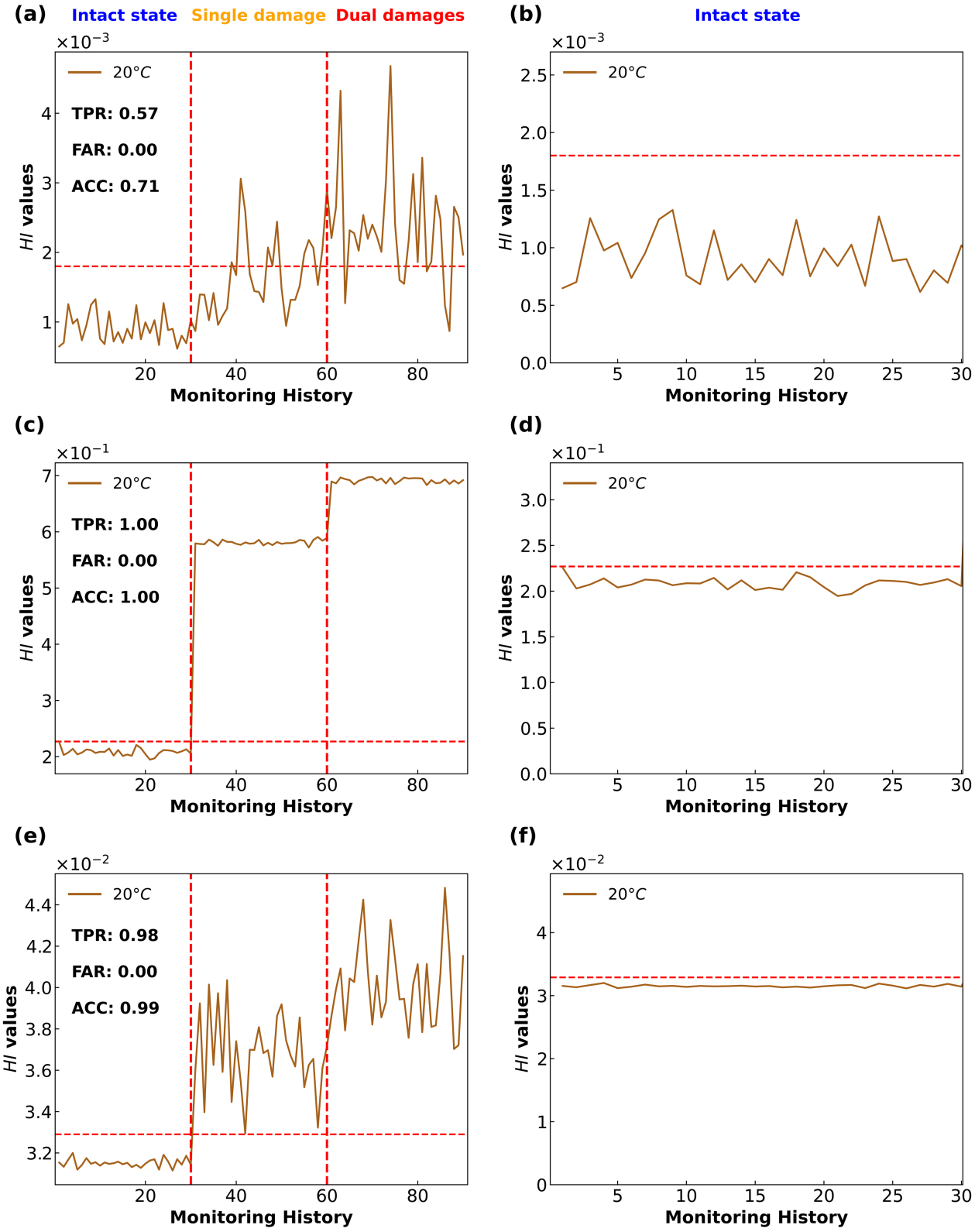


Figure 4.16: Damage detection results of impact damages at 20°C based on: (a) reciprocity-based approach; (c) IB technique; (e) VTR technique; (b, d, f) the corresponding zoomed views under intact state.

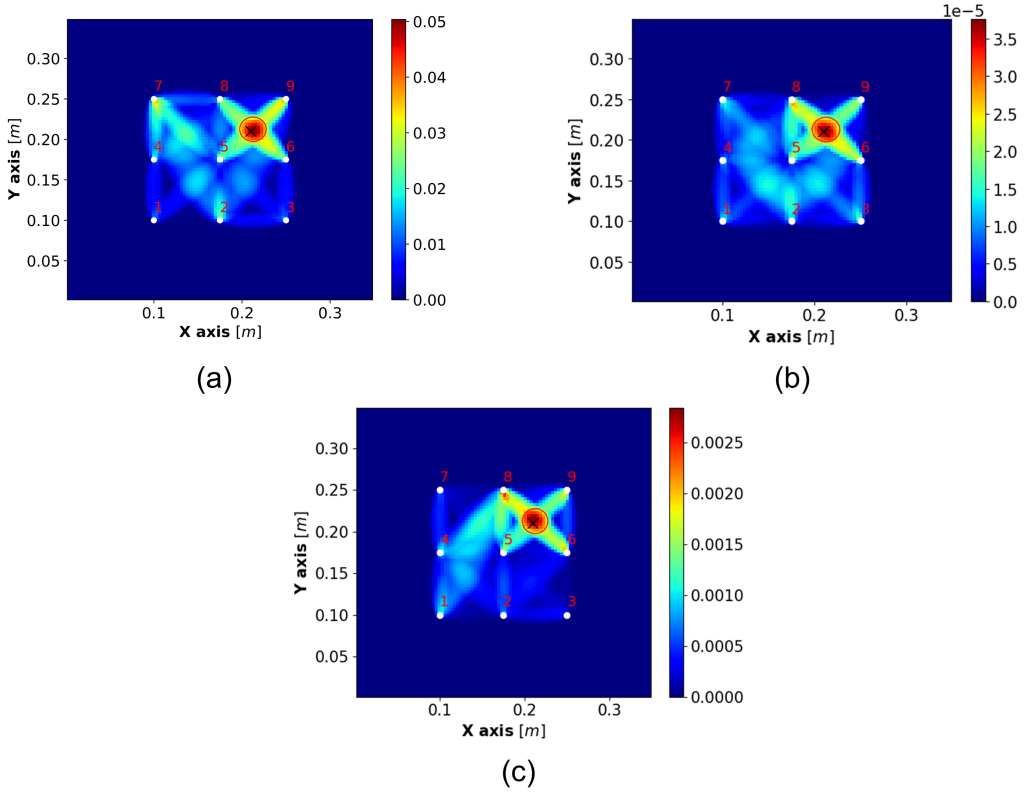


Figure 4.17: Average imaging results of the single impact damage $D_1$ under 20°C, based on: (a) IB technique; (b) Reciprocity-based technique; (c) VTR technique. Red circles represent the true damage areas while the black crosses denote the estimated damage locations.

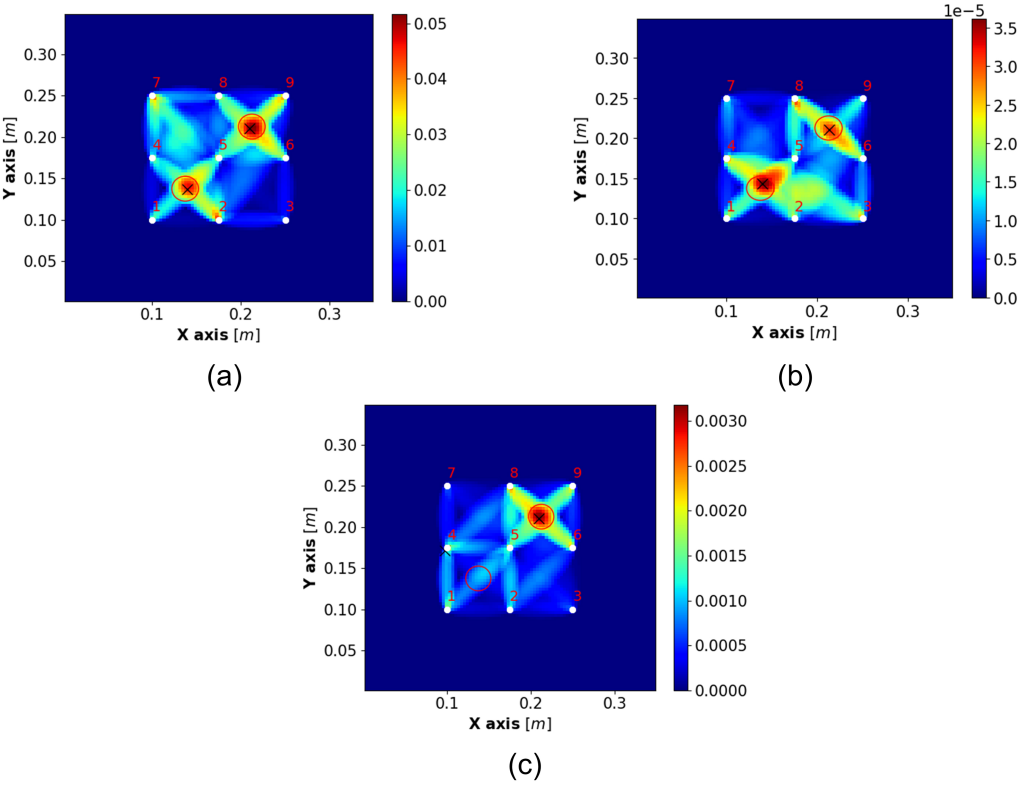


Figure 4.18: Average imaging results of dual impact damages under 20°C, based on: (a) IB technique; (b) Reciprocity-based technique; (c) VTR technique.

### 4.5.3 Experimental results under temperature variations

In contrast to the standard baseline subtraction approach, the baseline-free techniques are expected to be robust against varying environmental and operational conditions (EOCs). To validate such rationale, the baseline-free techniques are implemented on simulated damage cases under 20°C to 40°C, and the corresponding results for damage detection are shown in Table 4.1 and Fig. 4.19.

Table 4.1: Damage detection performance of the different baseline-free techniques for simulated damages under 20°C variations.

| Temperature | Reciprocity-based | | | IB | | | VTR | | |
|---|---|---|---|---|---|---|---|---|---|
| | TPR | FAR | ACC | TPR | FAR | ACC | TPR | FAR | ACC |
| 20°C | 0.90 | 0.00 | 0.93 | 0.99 | 0.00 | 0.99 | 1.00 | 0.00 | 1.00 |
| 25°C | 0.94 | 0.04 | 0.95 | 1.00 | 0.00 | 1.00 | 1.00 | 0.00 | 1.00 |
| 30°C | 0.99 | 0.02 | 0.99 | 1.00 | 0.00 | 1.00 | 1.00 | 0.00 | 1.00 |
| 35°C | 0.97 | 0.00 | 0.98 | 1.00 | 0.00 | 1.00 | 1.00 | 0.00 | 1.00 |
| 40°C | 0.99 | 0.00 | 1.00 | 1.00 | 0.00 | 1.00 | 1.00 | 0.00 | 1.00 |

Table 4.1 indicates that the IB and VTR techniques are competent to detect damaged states and remain robust damage detection performance against 20°C variations, as validated in Fig. 4.19 (c-f) where the intact and damaged states are separated at varying temperatures. Comparatively, the reciprocity-based method is capable to detect the simulated damages but yields the detection accuracy slightly varying with increasing temperatures, accompanied with 4% and 2% false alarms at 25°C and 30°C respectively. As illustrated in Fig. 4.19 (a), the HI curve of such approach at 40°C slightly increases compared to lower temperatures, e.g., 20°C. Since the detection threshold is calibrated considering temperature variations, the damage cases at lower temperature levels are susceptible to misidentification as intact states, thus leading to lower true positive rates at 20°C. For the reciprocity-based method, which simply compares signals from reciprocal transducer paths, the increase of $HI$ curves could be due to additional signal noises as temperature rises.

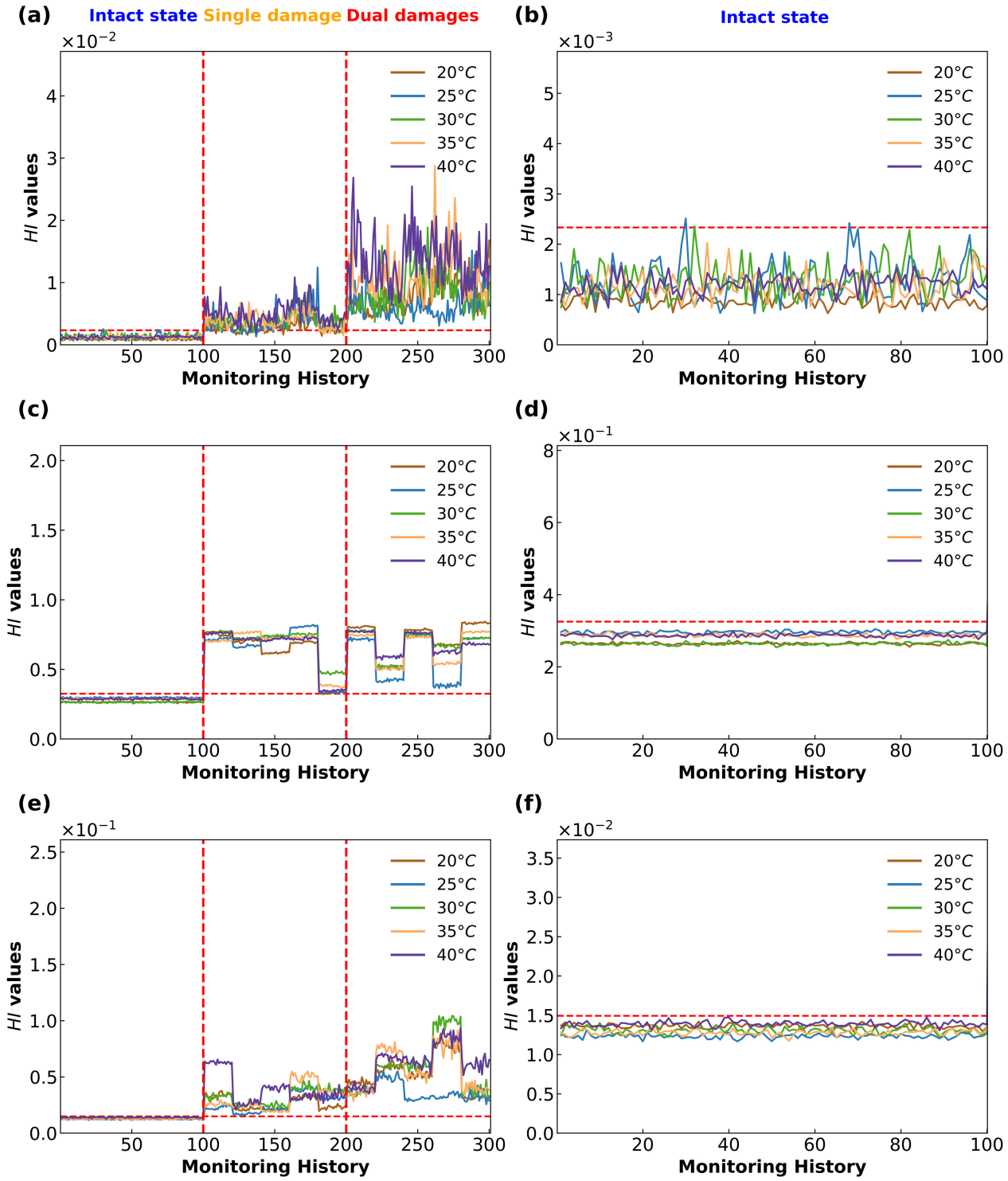


Figure 4.19: Damage detection results of simulated damages under 20°C variations based on: (a) reciprocity-based approach; (c) IB technique; (e) VTR technique; (b, d, f) the corresponding zoomed views under intact state.The horizontal dashed line represents the calibrated detection threshold.

In terms of damage localisation, Fig. 4.20 illustrates imaging results of single damages on the 12-sensors coupon under 20°C, 30°C and 40°C. It is shown that the investigated baseline-free techniques are capable of identifying and localising damages under temperature variations of 20°C.

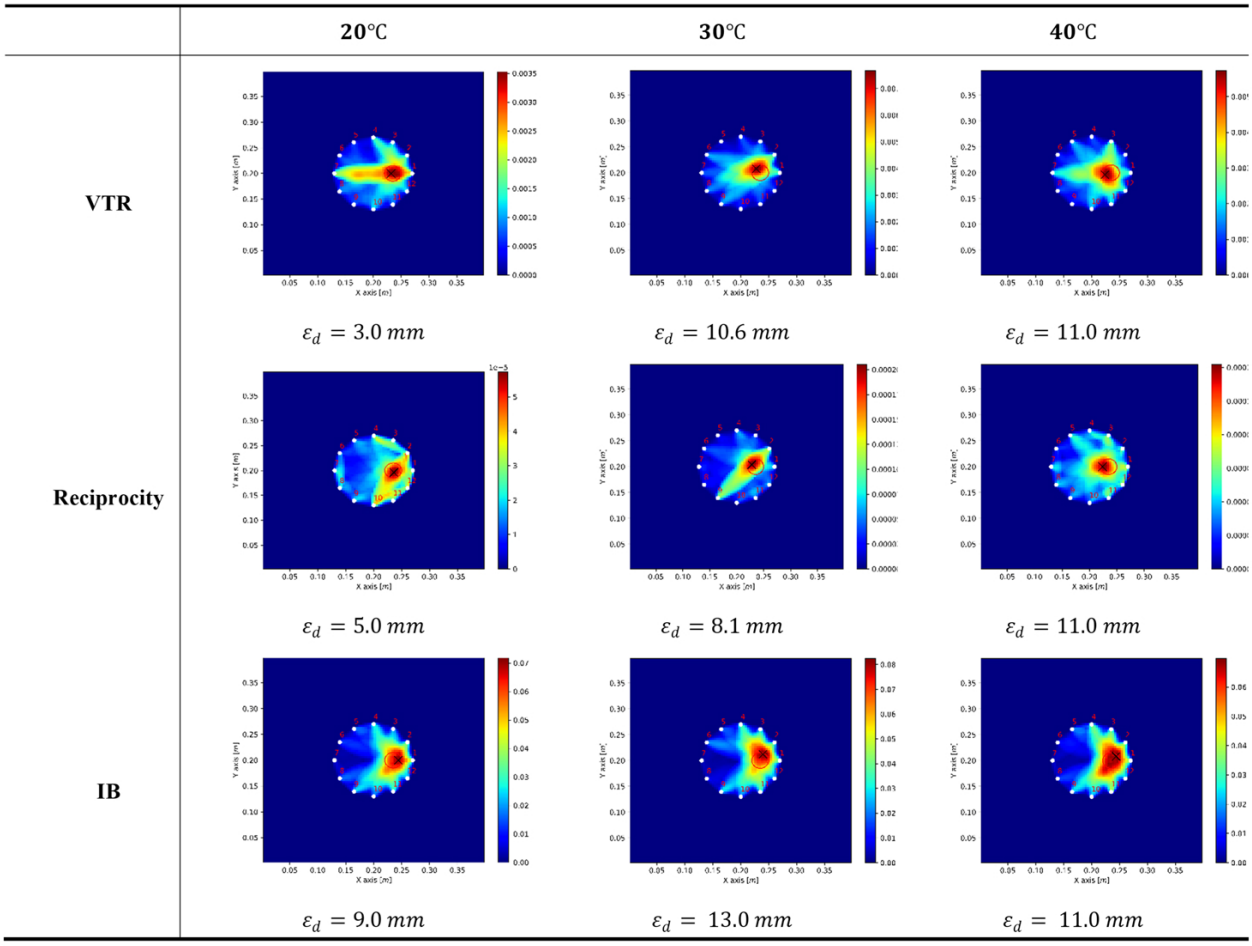


Figure 4.20: Imaging results of single simulated damage on the 12-sensors coupon utilising VTR, reciprocity-based and the IB techniques. The imaging results are obtained under 20°C, 30°C and 40°C. [35]

Results of the simulated damages under temperature variations are shown in Fig. 4.21. It is shown that the VTR technique mostly yields the highest localisation accuracy among the three techniques. It is further implied that the effectiveness and localisation accuracy of the IB technique highly depend on the sensor positionings. As discussed earlier, the IB technique could fail to well localise damages due to the lack of sufficient equivalent paths, and such failure leads to much larger localisation errors compared to the other techniques. Furthermore, when temperature increases from 20°C to 40°C the localisation errors of the reciprocity-based method vary within approximately 2 mm while the VTR technique seems slightly sensitive

to temperature variations. Meanwhile, the VTR and the reciprocity-based techniques exhibit similar standard errors (within 2 mm ) of $\varepsilon_d$ at different temperatures, which validates the robustness of such baseline-free techniques for damage localisation.

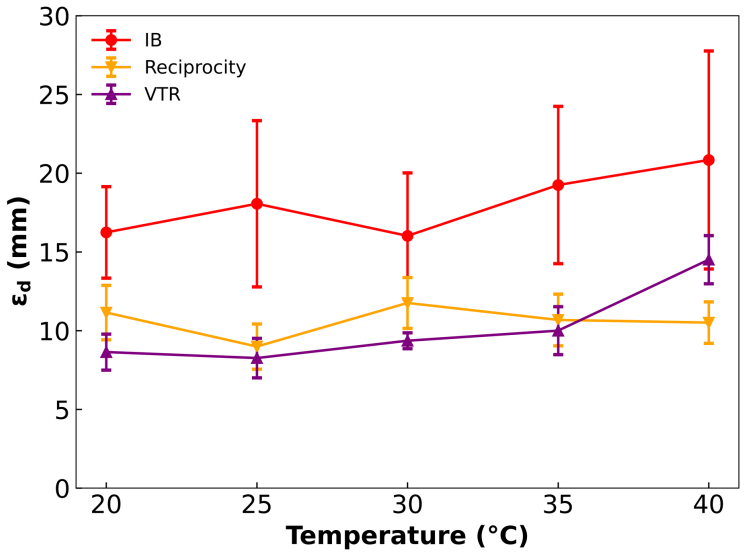


Figure 4.21: Comparisons between the IB, Reciprocity and VTR on localisation errors of single simulated damages under 20°C to 40°C with a 5°C gradient. Adapted from [35] since the error bars in this figure are calculated based on standard errors of localisation errors, which can reflect variations between damages at different locations, rather than the 95% confidence interval of localisation errors, which is used in [35].

Regarding real-life impact damages, detection results under 10°C variations are shown in Table 4.2 and Fig. 4.22. Table 4.2 indicates that the IB technique is competent to identify the impact damages under varying temperatures while achieving high detection accuracies simultaneously, as validated in Fig. 4.22 (c-d) where the intact and damage cases are well separated. This is because that such method operates by comparing equivalent transducer paths of the same distance and propagation angles, and therefore greatly alleviates the effect of temperature variations on damage detection. Meanwhile, the VTR technique can lead to high detection performance but the slightly lowered detection accuracy at 30°C, where 5 of the 60 damage cases are misidentified as intact. Comparatively, the detection performance of reciprocity method yields the worst among the baseline-free techniques and is susceptible to temperature variations, as similar to simulated damage cases. It is further illustrated in Fig. 4.22 (a - b) that the $HI$ curves of reciprocity-based technique are inclined to higher values as temperature increases. Since the detection threshold is calibrated by intact signals under

varying temperatures, the risk exists of misidentifying damage cases at lower temperatures, leading to only 71% and 78% detection accuracies at 20°C and 25°C respectively.

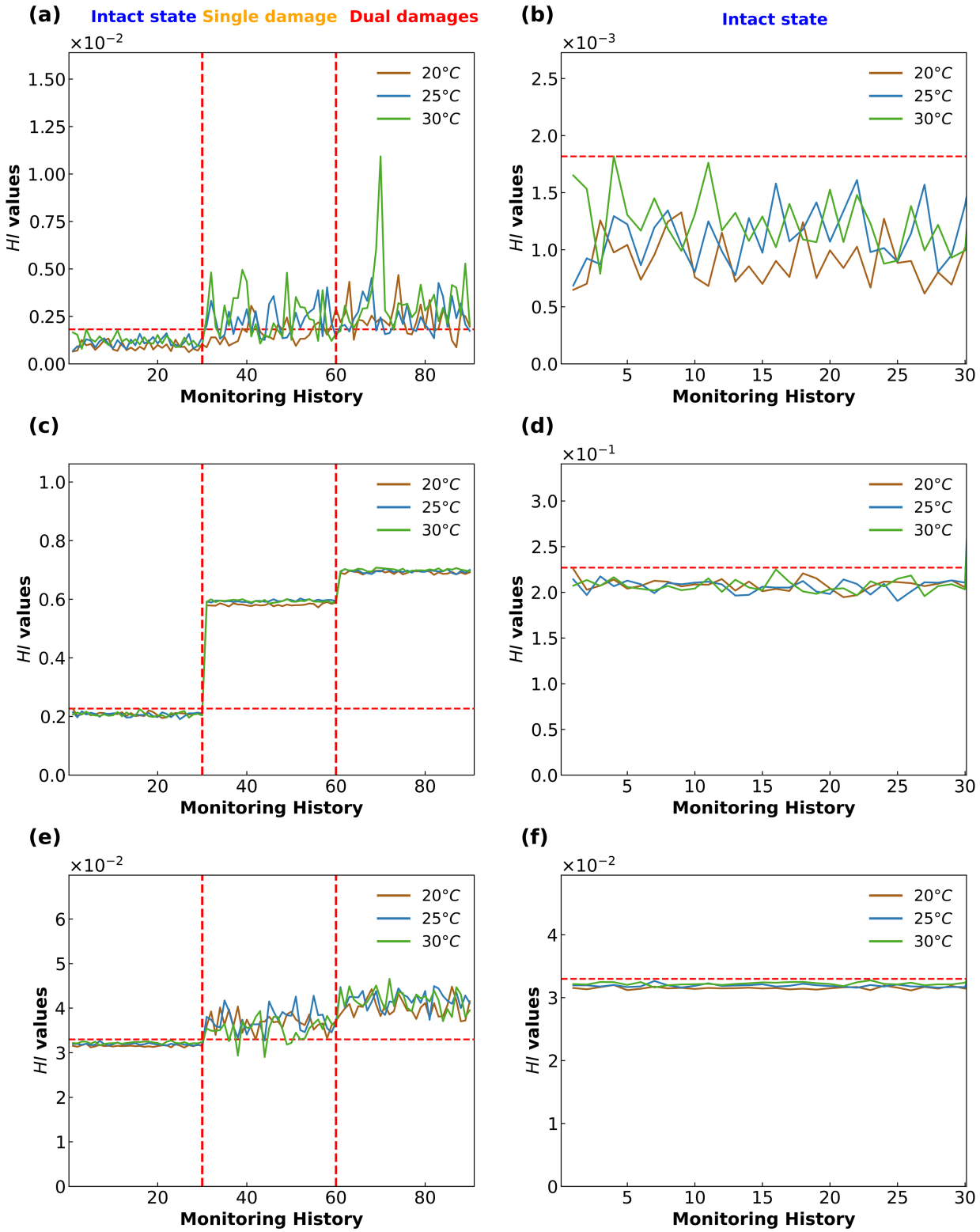


Figure 4.22: Damage detection results of impact damages under 10°C variations based on: (a) reciprocity-based approach; (c) IB technique; (e) VTR technique; (b, d, f) the corresponding zoomed views under intact state.

Table 4.2: Damage detection performance of the different baseline-free techniques for impact damages under 10°C variations.

| Temperature | Reciprocity-based | | | IB | | | VTR | | |
|---|---|---|---|---|---|---|---|---|---|
| | TPR | FAR | ACC | TPR | FAR | ACC | TPR | FAR | ACC |
| 20°C | 0.57 | 0.00 | 0.71 | 1.00 | 0.00 | 1.00 | 0.98 | 0.00 | 0.99 |
| 25°C | 0.67 | 0.00 | 0.78 | 1.00 | 0.00 | 1.00 | 0.98 | 0.00 | 0.99 |
| 30°C | 0.77 | 0.03 | 0.83 | 1.00 | 0.00 | 1.00 | 0.92 | 0.00 | 0.94 |

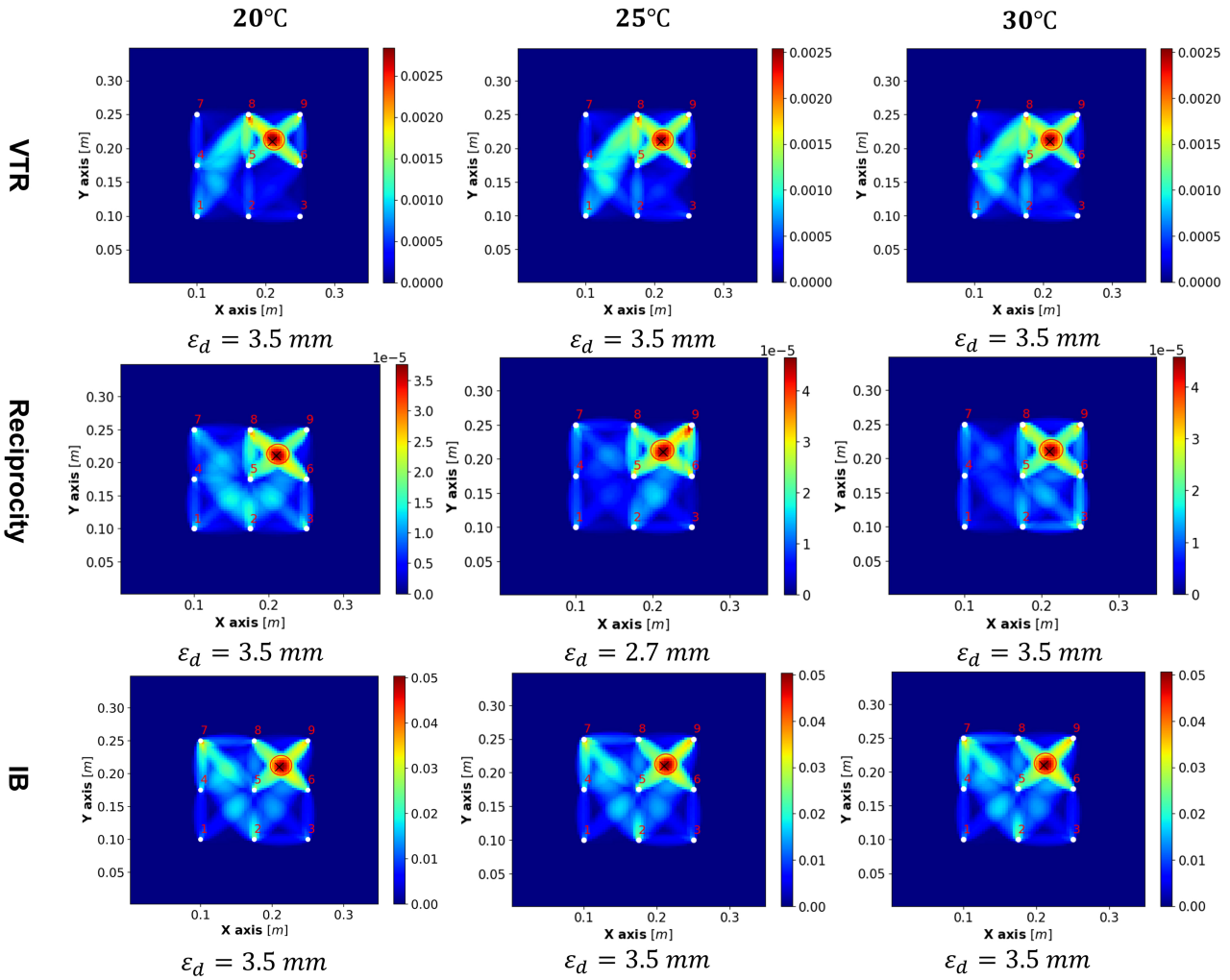


Figure 4.23: Imaging results of single impact damage on the 9-sensors coupon utilising VTR, reciprocity-based and the IB techniques. The imaging results are obtained under 20°C, 25°C and 30°C.

Fig. 4.23 presents imaging results of the single impact damage $D_1$ under temperature variations from 20°C to 30°C. It is shown that the three investigated techniques yield robust

damage imaging results under 10°C variations. It is worth noting that the damage localisation by the VTR technique is not affected by the abnormal bonding condition of transducer 7 (see Fig. 4.15) while the single impact damage is clearly identified from the damage images. The applications of the reciprocity-based and IB techniques also ensure a clear identification of the impact damage despite the wild increase of pixel values in the vicinity of transducer 7.

Fig. 4.24 compares the localisation errors, i.e., $\varepsilon_d$, of different baseline-free techniques in the case of identified single impact damage $D_1$ at varying temperatures. It is shown that the individual baseline-free techniques yield robust average localisation errors close to 3.5 mm when localising identified single damages under 10°C variations. Meanwhile, comparable localisation errors are achieved by the reciprocity-based, IB and VTR techniques, implying consistency of the baseline-free techniques when localising the single impact damage. It is indicated that the reciprocity-based technique is capable to identify and localise the impact damage $D_1$ located in the middle of transducer path 5-9 and 6-8. Such finding is different from the results in [217] and validates the effectiveness of reciprocity technique under symmetric transducer positionings.

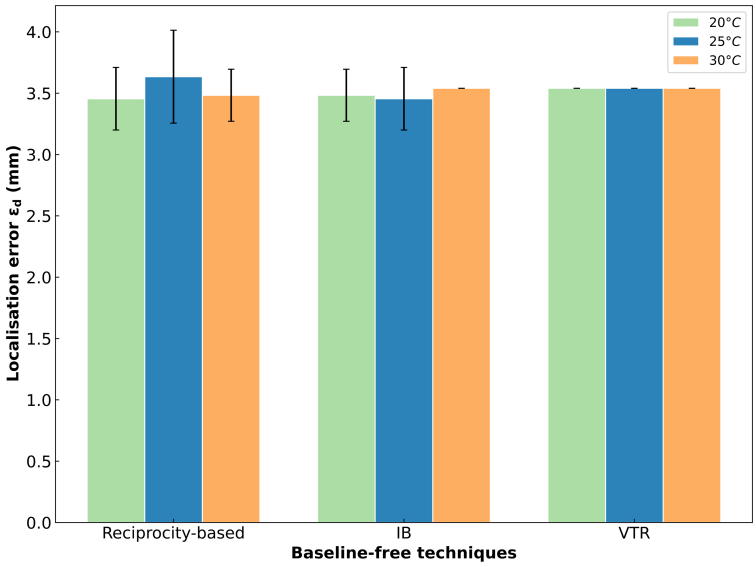


Figure 4.24: Comparisons between the IB, Reciprocity and VTR on localisation errors of single impact damages under 20°C, 25°C, 30°C.

### 4.5.4 Comparisons under geometric and structural complexities

The performance of baseline-free techniques when identifying and localising damages can also be affected by geometric and structural complexities which include geometric boundaries

and the potential stiffeners jointed on composite structures. The effect of geometric boundaries is firstly investigated based on the 300 mm × 225 mm Coupon 2 under 20°C (see Chapter 3), where the transducers are much closer to the specimen boundaries. Considering that all the sensors are only 40 mm away from the specimen boundaries horizontally or vertically or both, the collected guided wave signals, even under intact state of the specimen, are prone to boundary reflections. In this regard, the three baseline-free techniques are attempted to detect and localise the single impact damage on the 8-sensors plate.

As introduced in Chapter 3, 30 intact and 15 damaged measurements are collected at 20°C during the monitoring process, while the detection threshold is determined based on the first 15 intact measurements. Fig. 4.25 shows the damage detection results of Coupon 2 at 20°C utilising different baseline-free techniques. It is indicated that the three techniques are not able to detect damaged states considering that the corresponding $HI$ values below the detection threshold cannot be well distinguished from the intact states.

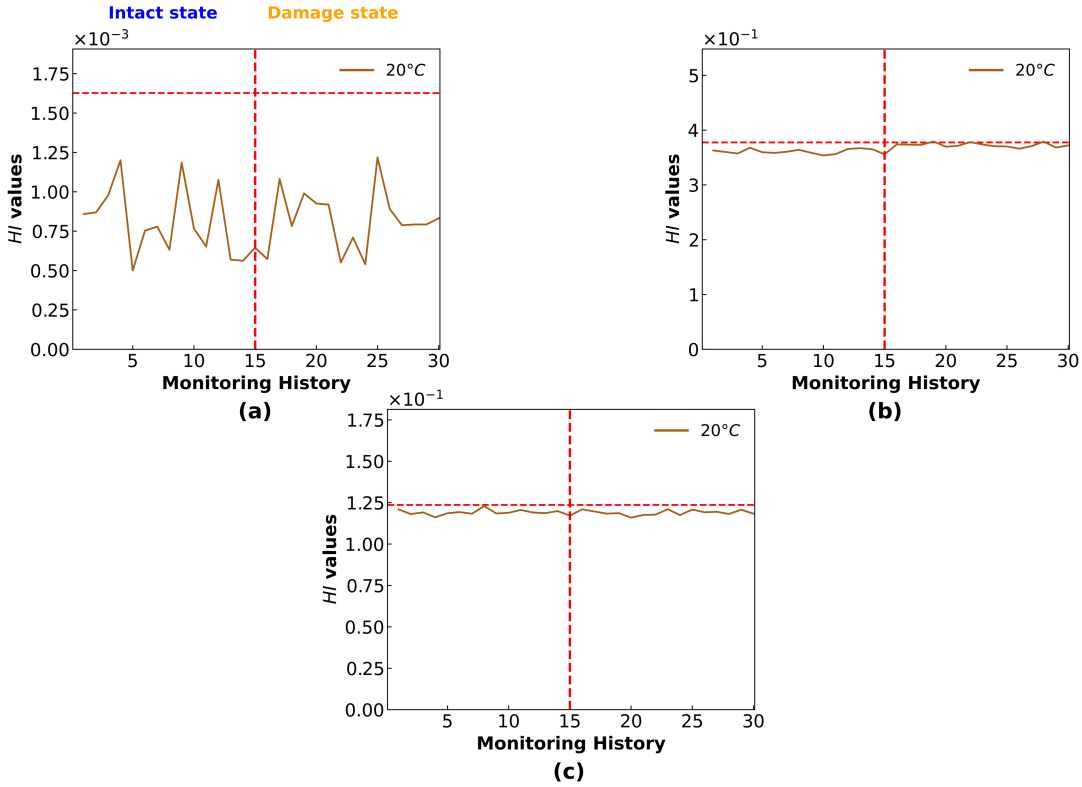


Figure 4.25: Damage detection results of the impact damage on Coupon 2 at 20°C utilising: (a) reciprocity-based approach; (b) IB technique; (c) VTR technique. The horizontal dashed line represents the calibrated detection threshold.

As shown in Fig. 4.26 (a), when utilising the VTR technique, the real damage near the centre of the specimen is severely masked by the adjacent imaging artifacts (within yellow dashed area) and other artifacts near the boundaries (within red dashed area), which synchronously exist when utilising the intact signals only in a baseline-free manner. Furthermore, considering that the transducers are located close to the boundaries of the coupon, the boundary reflections of guided wave signals become considerable in terms of the damage localisation. More specifically, in such cases the boundary reflections are likely to be overlapped with the first arrival packet, which further yields the large deviations between the input excitation signals and the reconstructed input signals and finally lead to the high imaging artifacts in the Fig. 4.26.

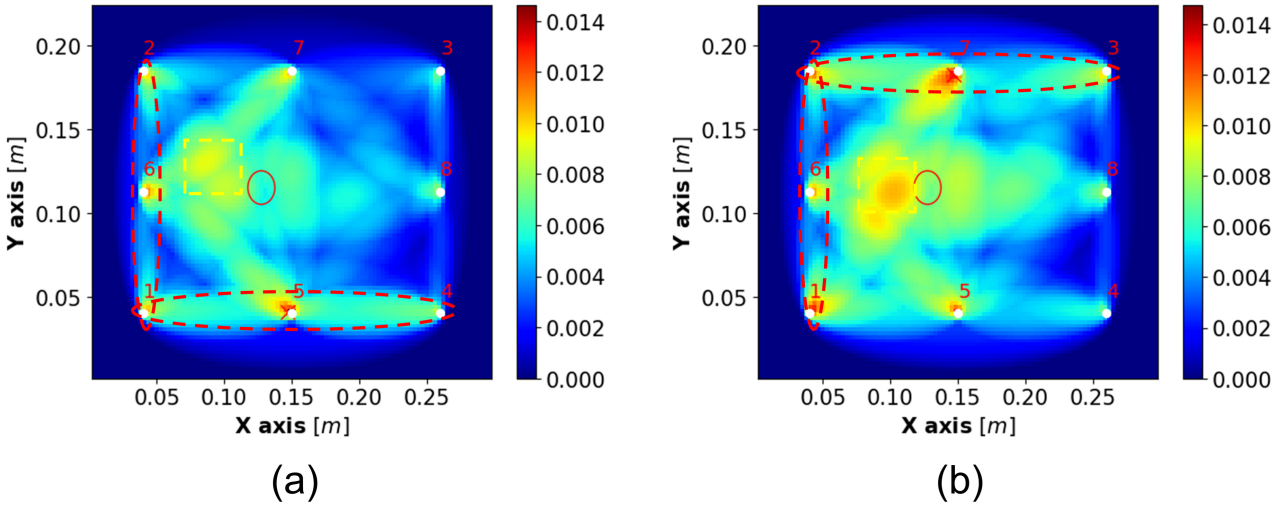


Figure 4.26: Damage images of the Coupon 2 when utilising the virtual time reversal (VTR) technique together with: (a) damaged signals; (b) intact signals both in baseline-free manners.

To illustrate the overlap between the first arrival mode and the boundary reflections, together with its influence on the signal reconstruction, the 50kHz tone burst signals of the transducer path 1-2 and path 1-4 are analysed as an example and the corresponding results are shown in Fig. 4.27. It is presented that within both transducer paths there exist overlapping between the first wave packet in the $A_0$ mode and the boundary reflections, which is due to the close distance between the transducers and the specimen boundaries. Furthermore, such overlapping further gives rise to large signal distortions of the reconstructed signal and consequently yields the high imaging artifacts near the boundaries.

The damage imaging results following the reciprocity principle are shown in Fig. 4.28. Similar

to the VTR technique, the reciprocity-based damage localisation is similarly affected by the imaging artifacts near the bottom boundaries (red dashed area) and the true damage location (near the blue dashed area) is obscured. Meanwhile, as shown in the Fig. 4.29 the damage imaging result based on the IB approach also suffers from the boundary reflections. To alleviate the imaging artifacts, further actions need to be taken to separate the potential overlapping between first arrival packets and modes related to boundary reflections.

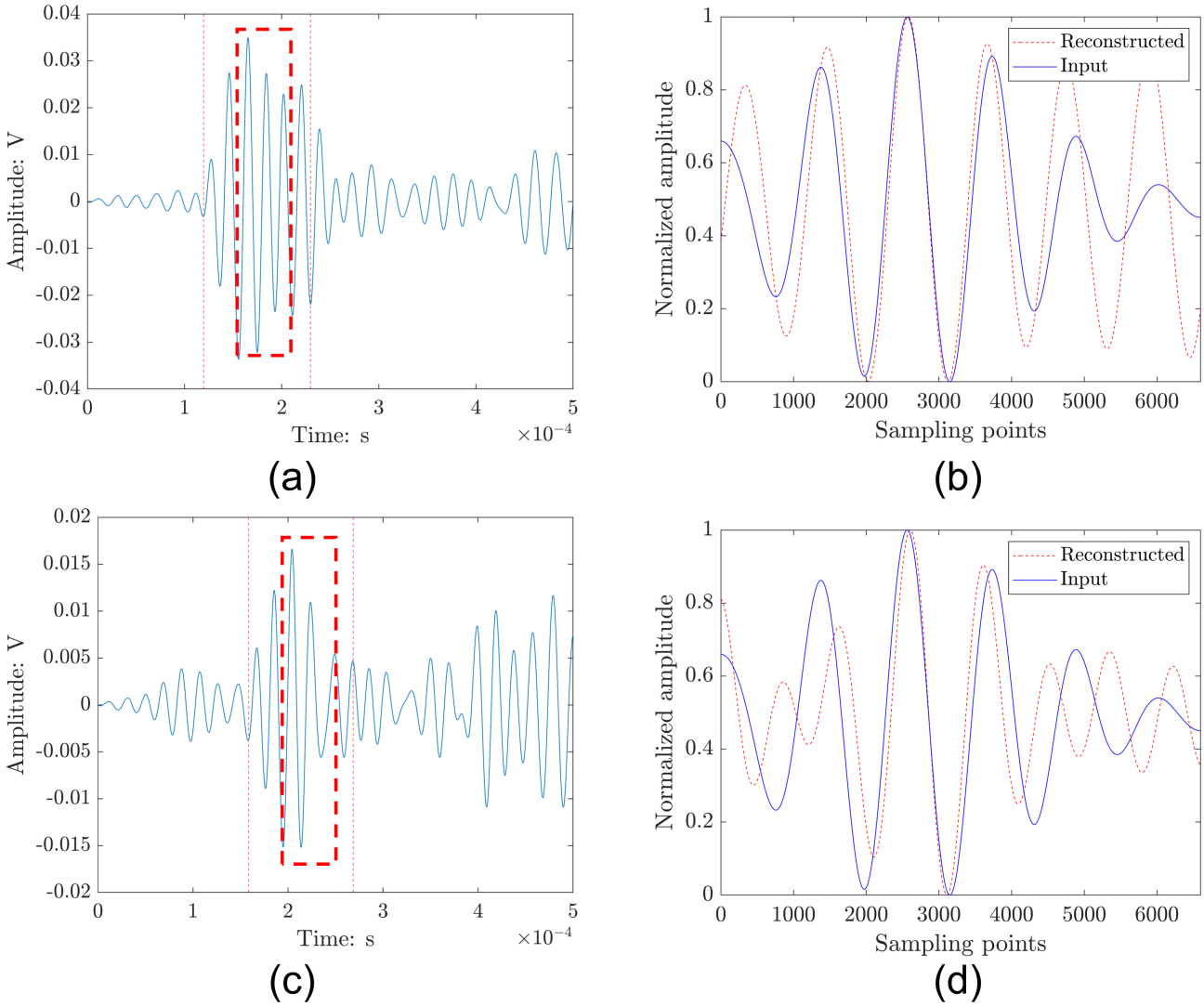


Figure 4.27: 50kHz tone burst responses from the Coupon 2: (a) path 1-2 with the overlapping part (red dashed area); (b) reconstruction of the input excitation signal for path 1-2; (c) path 1-4 with the overlapping part (red dashed area); (d) reconstruction of the input excitation signal for the path 1-4.

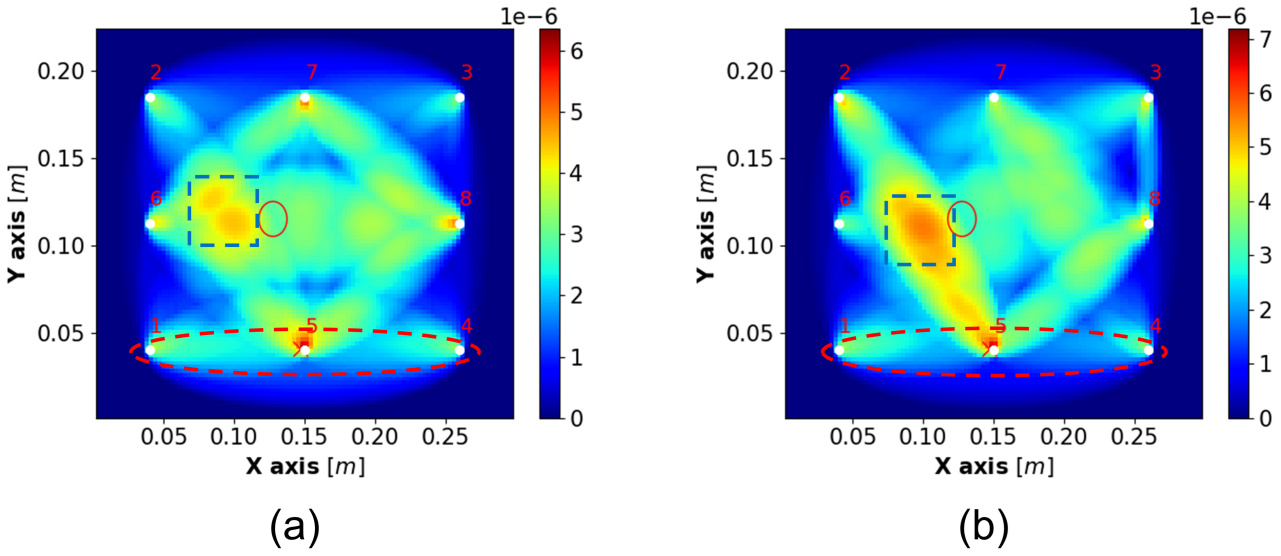


Figure 4.28: Damage imaging results of the Coupon 2 when following the reciprocity principle together with: (a) damaged signals; (b) intact signals both in baseline-free manners.

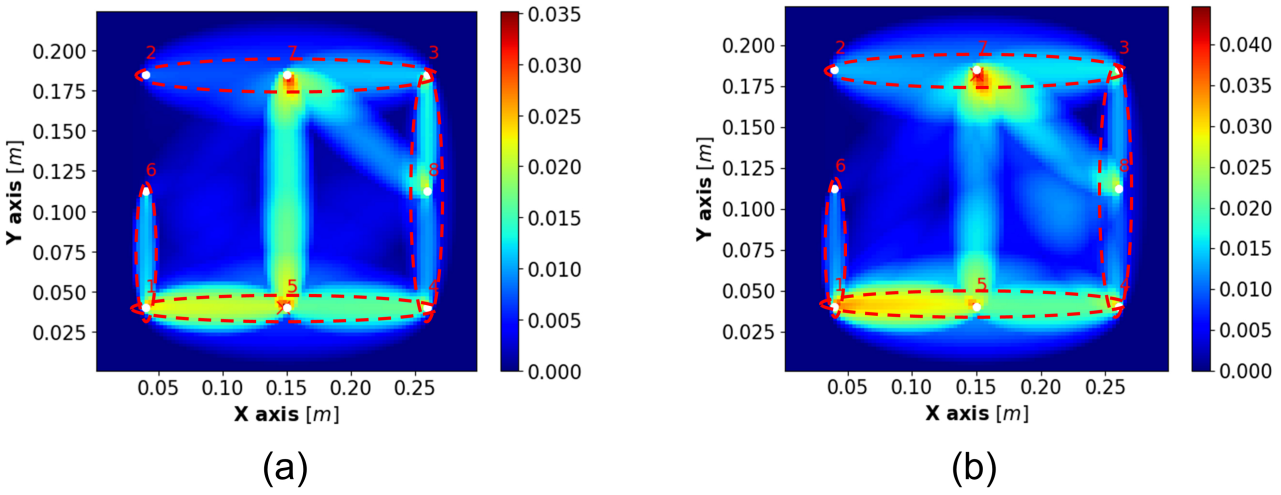


Figure 4.29: Damage imaging results of the Coupon 2 when utilising the instantaneous baseline (IB) approach together with: (a) damaged signals; (b) intact signals both in baseline-free manners.

Apart from the boundary reflections, the potential effects of stiffeners are also investigated by upscaling the IB, reciprocity principle and the VTR techniques for large-size stiffened panels. A 1624 mm × 940 mm stiffened CFRP panel manufactured with $M21 - T800S$ laminates and stacking layers as $[\pm 45/0_2/90/0]_s$ is employed for the investigation. As shown in Fig. 4.30 (a), four parallel 30 mm high omega stiffeners are jointed on the CFRP panel and 12 PZT transducers are arranged in three rows and in the middle between every two stiffeners [14]. As a part of the SHERLOC CleanSky2 programme [14], two 15 mm radius impact damages on

the stiffened panel (as shown in red circles), corresponding to the impact energy as 20 J and 35 J chronologically, are investigated in this work, while the first impact damage is located on the stiffener hat and the other at the stiffener foot. During the damage localisation a sensing network with optimal transducer paths [14], as shown in Fig. 4.30 (b), is employed for the stiffened panel. Within such network, long-distance transducer paths which cross the stiffeners twice, e.g., path 1-12, are ignored to circumvent severe signal distortions. For the same reason, diagonal paths within every 8 sensors, i.e., path 1-8, 4-5, 5-12, 8-9 and their reciprocal paths, are not selected.

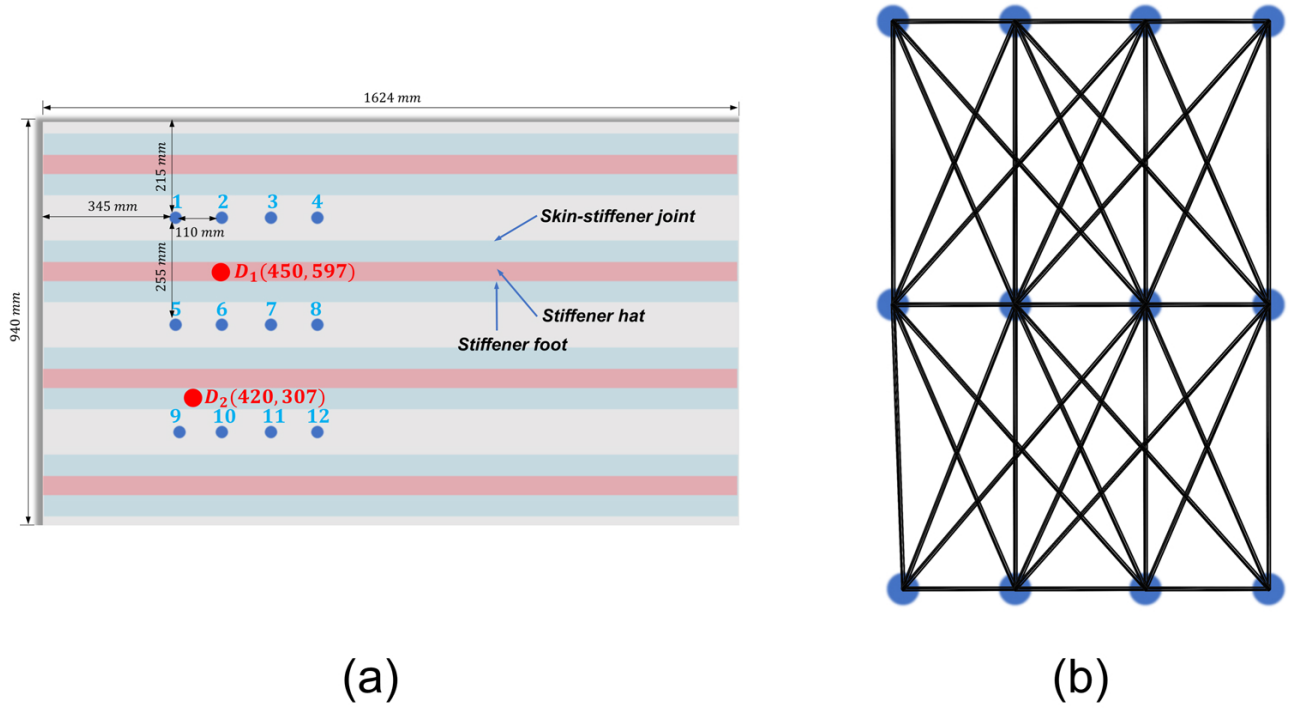


Figure 4.30: Stiffened CFRP panel for investigations on baseline-free techniques: (a) the CFRP panel jointed by omega stiffeners and three impact damages within the red circles; (b) sensing network after removal of indirect transducer paths.

Furthermore, 30 intact and 30 damaged measurements are collected from the stiffened composite panel at 24°C and 27°C respectively. Among the damaged records, 15 measurements correspond to the existence of the single impact damage within the upper part of the panel while the remaining damaged records include two damages at the same time. The detection threshold for the stiffened CFRP panel is calibrated by the first 15 intact measurements, which are subsequently excluded when evaluating the damage detection performance of baseline-free techniques.

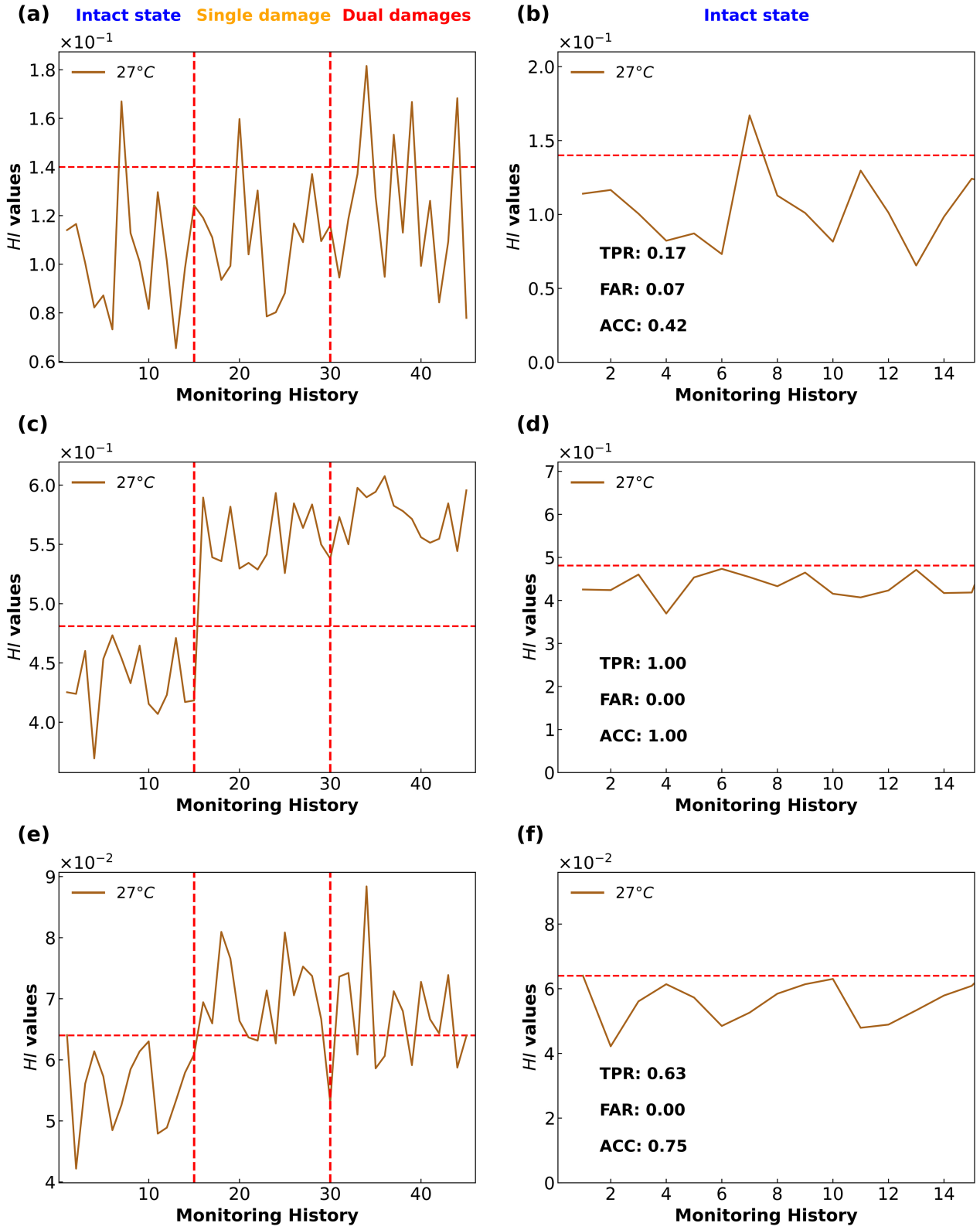


Figure 4.31: Damage detection results of impact damages on stiffened panel at 27°C based on: (a) reciprocity-based approach; (c) IB technique; (e) VTR technique; (b, d, f) the corresponding zoomed views under intact state.

Fig. 4.31 presents the damage detection performance of several baseline-free techniques im-

plemented on the stiffened panel. As seen from the Fig. 4.31 (c-d), the IB technique based on the proposed HI is competent to distinguish between damaged and intact states with 100% detection accuracy and no false alarms while being able to detect the slight increase of $HI$ values within the dual damage state, compared to the single damage cases. The competence of the IB technique for damage detection on the stiffened panel could be partly due to the comparisons between equivalent transducer paths of similar path distance and propagation angles, which can alleviate the adverse effect of signal distortions induced by structural complexities. Meanwhile, the proposed $HI$, i.e., the 95% quantile of $DI$ values, also ensures an effective representation of damage sensitive DIs when integrated with the IB technique.

Moreover, Fig. 4.31 (e-f) show that the VTR technique is capable of damage detection but yields only 75% detection accuracy caused by the misidentification of damaged measurements. The weakened detection capability of the VTR technique is likely due to the mode conversion of guided waves in the vicinity of stiffeners [253], leading to distorted $A_0$ wave packets and consequently reduced reconstruction performance of input excitation signals, which masks true damage sensitive features and yields noises in the $DI$ values particularly under the intact state. Comparatively, Fig. 4.31 (a-b) show that the reciprocity-based technique yields the worst performance among the three baseline-free techniques when detecting impact damages on the stiffened panel. It is indicated that such technique cannot detect most damaged measurements and is susceptible to signal noises particularly under the intact state.

Regarding the damage localisation, Fig. 4.32 presents the average imaging results of the IB technique based on all the 30 damaged measurements from the stiffened panel. As shown in Fig. 4.32 (a), the two impact damages yield increasing pixel values around the damage locations (within black circles), which preliminarily validates the ability of the IB approach to identify damages on the stiffened panel. It is further indicated that the second impact damage within the lower part of the panel has the highest severity and masks the first damage to a certain extent, which is consistent with the impact energy of the two damages. Despite this, the different damages can be unveiled when utilising the upper or lower part of sensor networks, which are shown in Fig. 4.32 (b-c) respectively. It is illustrated in Fig. 4.32 (b) that the IB technique is able to identify the first 20 J impact damage (at black cross) but suffers from imaging artifacts

in the middle of transducer path 3-7. Nevertheless, such artifacts are not reflected in the $HI$, i.e., 95% quantile of $DI$ values, thus not affecting the detection performance of the IB technique shown in Fig. 4.31 (c). Meanwhile, the second 35 J impact damage can be clearly identified by the IB approach with localisation error as 22.8 mm. Moreover, the effectiveness of the IB is further validated by calibrating with intact signals from the panel but in a baseline-free manner. The main rationale of the calibration is to alleviate potential artifacts from the stiffened panel by inputting the damaged and intact signals separately into the baseline-free techniques and generate two sets of $DI$ values. The $DI$ values representing the intact conditions are subtracted from the $DI$s of the damaged conditions, and their residuals are employed for the damage imaging. Based on the calibration, consistent but improved damage imaging results are displayed in Fig. 4.32 (d-f) where imaging artifacts are greatly alleviated and the two impact damages are well isolated. Note that the localisation error of the second impact damage may increase but remain satisfactory after the calibration and the removal of imaging artifacts.

Fig. 4.33 presents imaging results of the VTR technique based on all the damaged measurements from the stiffened panel. Fig. 4.33 (b-c) exhibit that the damage images are susceptible to imaging artifacts occurring in adjacent transducer paths, which could lead to an erroneous estimate of the true damage locations. The imaging artifacts can be alleviated by the calibration with intact measurements, yielding reduced localisation errors for the two impact damages.

As discussed earlier, the reciprocity-based technique yields much limited capability to detect impact damages on the stiffened panel. Nevertheless, it is shown in Fig. 4.34 that such technique can achieve satisfactory damage imaging results and localisation accuracies based on the average of only ten damaged measurements. This indicates that the reciprocity principle may not be suitable for practical applications since experimental conditions including transducer installations need to be carefully controlled during the implementation of such method.

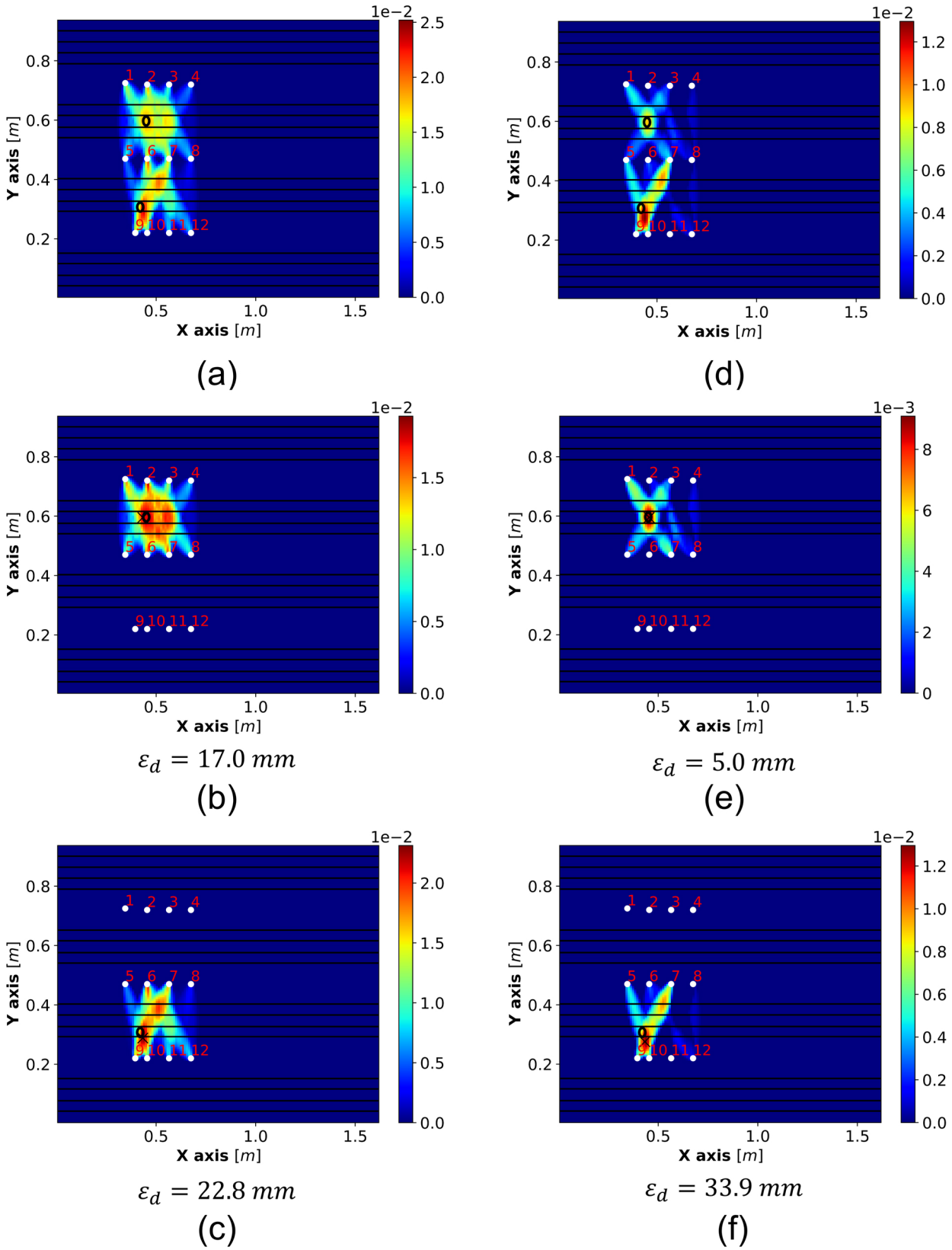


Figure 4.32: Average imaging results on stiffened composite panel based on the IB technique: (a-c) full-scale, upper part and lower part imaging results utilising damaged measurements; (d-f) full-scale, upper part and lower part imaging results calibrated by intact measurements in baseline-free manners.

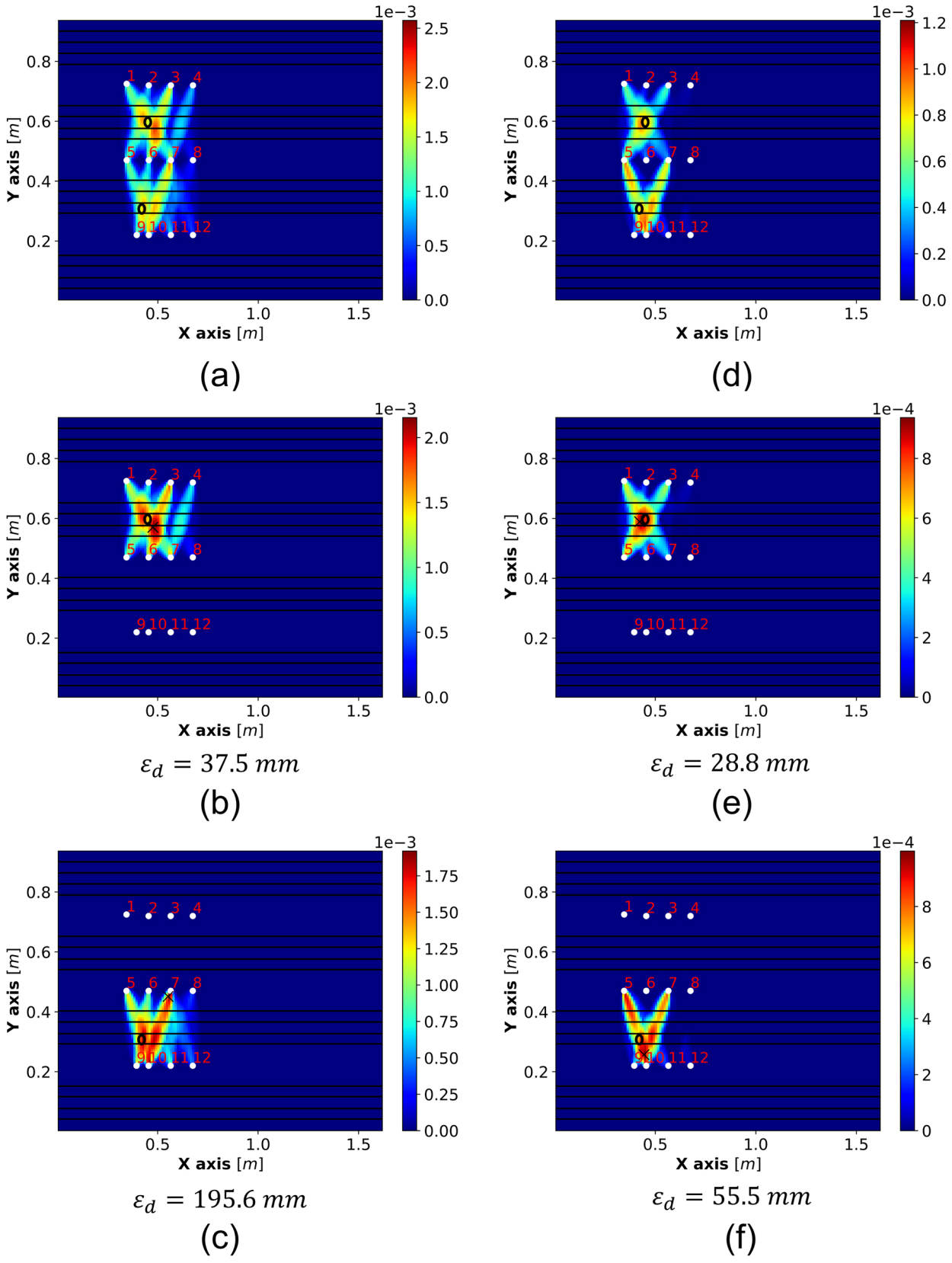


Figure 4.33: Average imaging results on stiffened composite panel based on the VTR technique: (a-c) full-scale, upper part and lower part imaging results utilising damaged measurements; (d-f) full-scale, upper part and lower part imaging results calibrated by intact measurements in baseline-free manners.

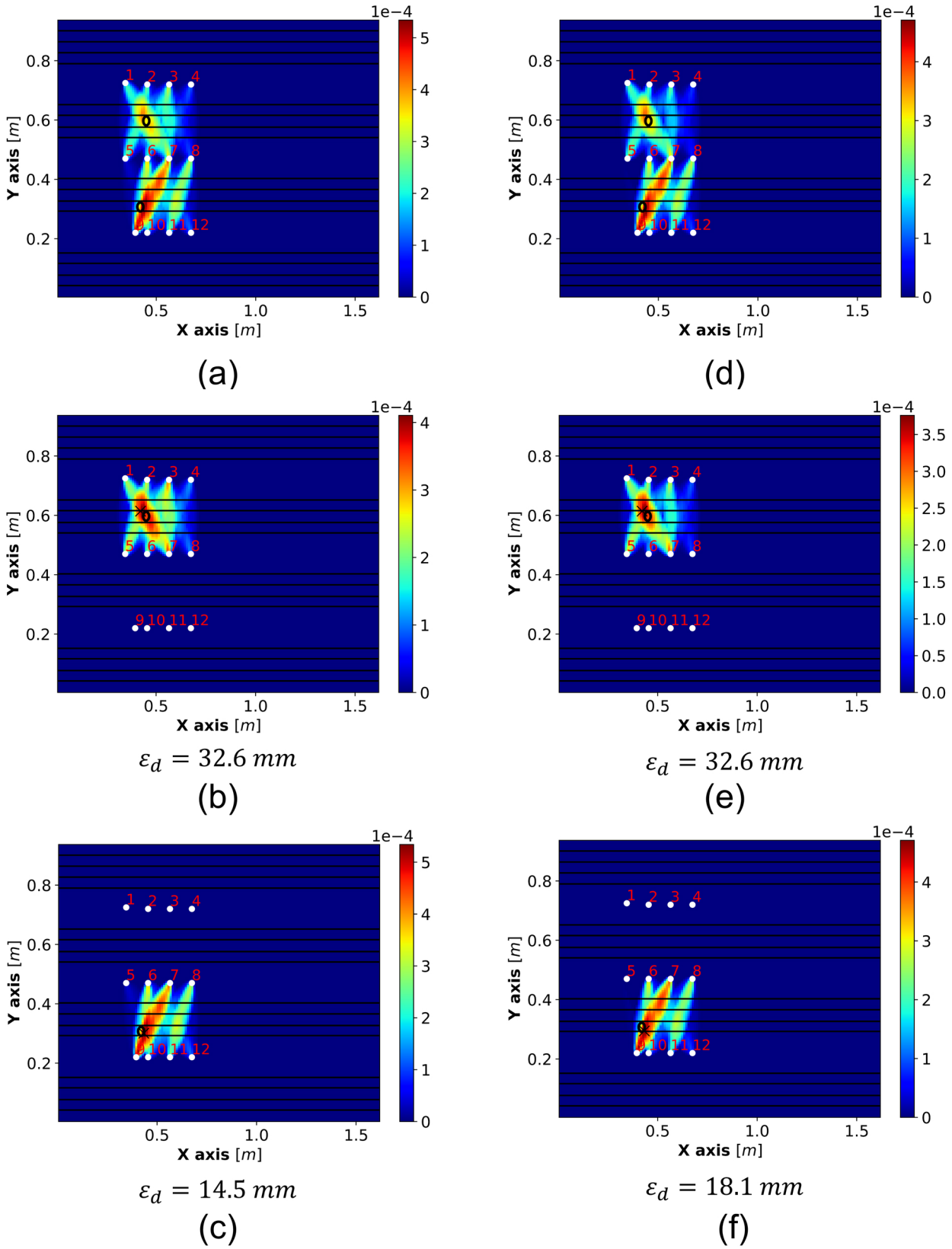


Figure 4.34: Figure 4.34. Imaging results of reciprocity principle on the stiffened composite panel based on the average of ten damaged measurements: (a-c) full-scale, upper part and lower part imaging results utilising damaged measurements; (d-f) the corresponding imaging results calibrated by intact measurements in baseline-free manners.

## 4.6 Summary

In this section, several reference-free techniques for guided wave-based structural health monitoring (GWSHM) are thoroughly reviewed, including the Time Reversal (TR), Virtual Time Reversal (VTR), Instantaneous Baseline (IB), reciprocity-based methods, modal analysis, and Nonlinear Frequency Modulation (NFM). Each technique's principles, strengths, and limitations are discussed in detail, providing a comprehensive understanding of their capabilities and challenges.

Meanwhile, this section identifies and reviews critical factors that can significantly affect the performance of baseline-free techniques in damage detection and localisation. These factors include varying environmental conditions, e.g., temperature variations, geometric and structural complexities, and different damage scenarios. Understanding these factors is crucial for ensuring the reliability and accuracy of the baseline-free techniques in real-world applications.

Furthermore, this section conducts experimental comparisons between the VTR, IB, and reciprocity-based techniques. The experimental investigations are implemented on both simulated and real-life impact damages, considering the presence of multiple damages, the temperature variations, boundary reflections and structural complexities, e.g., stiffeners.

# Chapter 5

# A data-driven baseline-free approach for SHM in composite structures

## 5.1 Introduction

The applications of baseline-free techniques introduced in Chapter 4 are constrained by several limitations. Most baseline-free techniques necessitate hypothetical interpretation of guided wave propagation. The interpretations usually involve physical processes which encompass the time reversal symmetry, reciprocity and multi-modal dispersion behaviour of guided waves. However, the physics-based hypotheses could be only approximately valid due to various factors including but not confined to nonlinear media [217, 218], interactions between transducers and guided waves [205], excitation frequencies of guided waves [175] and positioning of transducers [208, 217]. Such limitation could further lead to false alarms in the process of damage detection and localisation, thus hindering effectiveness and efficiency of the baseline-free techniques.

In this chapter a data-driven framework based on dictionary learning for baseline-free damage detection and localisation in guided wave structural health monitoring (GWSHM) is developed.

[1]Portions of this chapter have been submitted for publication as *Hongmin Zhu, Zahra Sharif Khodaei, and M.H. Aliabadi. Baseline-free damage detection and localisation on complex composite structures using unsupervised shapelets and shift-invariant dictionary learning.*

This approach minimizes the need for extensive physical knowledge of guided wave propagation. Dictionary learning is highlighted as a flexible method for isolating damage-sensitive features and has shown promise in vibration-based structural damage detection [254] and fault diagnosis on rotating machinery [255]. While dictionary learning has gained attraction in various fields, including vibration-based damage detection, its application in the realm of GWSHM, particularly in a baseline-free manner, has received relatively less attention. Recent work by Nokhbatolfoghahai et al. [256] utilised an analytical dictionary of Lamb waves to identify and localise simulated damages in a stiffened composite plate. However, it constructed the dictionary using baseline-subtracted signals, making it less suited for a true baseline-free approach. K. Supreet Alguri et al. [257] employed surrogate modelling for baseline-free damage detection on metallic plates. It developed a learned dictionary based on pristine signals from surrogate structures and used it to generate synthetic baselines for tested specimens [257]. However, acquiring experimental surrogates might pose challenges. K. Supreet Alguri et al. [258] building on their previous work, introduced digital surrogates as a counterpart to the inspected structures. Nevertheless, both experimental and digital surrogates were required to have identical geometry to the inspected structures, thus being limited in practical applications. Finally, Li and Chattopadhyay [259] incorporated a dictionary learning technique called matching pursuit decomposition (MPD) as part of their proposed reference-free algorithm. However, the use of structured Gaussian atoms for the matching pursuit algorithm might not fully capture the dispersion behaviour of guided waves.

Given the above limitations, it is essential to consider a reference-free technique which can be simply implemented in time domain and highly flexible so that no specific constraints, e.g., on specimen geometry or transducer positioning, are needed for inspected structures. In this chapter, a baseline-free technique based on dictionary learning, unsupervised shapelets [260] and building block (BB) philosophy [261] is proposed for damage detection and localisation on composite structures. The proposed method is capable of generating representative shapelet features of guided wave signals from an intact structure which has different sizes, material properties, or sensor positioning with the tested structure. The generated shapelets are then formulated into a shift-invariant dictionary for further reconstruction of current measurements

in the presence of damage. Compared to the existing work on unsupervised shapelets [262–264], it is shown that the proposed method supports a transfer learning setting, namely to support the knowledge transfer of guided wave information across different structures while yielding good detection and localisation performance for damages. When monitoring complex structures, e.g., a stiffened composite panel, the BB philosophy is integrated so that the guided wave signals can be captured by shapelet features learnt from structures of increasing complexities, i.e., coupons and monostringer elements.

The remainder of the chapter is organised as follows. Section 5.2 introduces the background knowledge while section 5.3 proposes the shapelet-based reference-free methodology for the GWSHM purposes. Section 5.4 and 5.5 present results for damage detection and localisation on composite structures considering temperature variations, boundary reflections and structural complexities. Conclusive remarks of the chapter are drawn in section 5.6.

## 5.2 Background

### 5.2.1 Guided wave signals in composite structures

To illustrate the Lamb wave propagation in composite structures, e.g., carbon-fiber plates, a single-frequency component of Lamb waves propagating in circular fronts can be formulated as follows [265].

$$s(r,t) = \frac{A}{\sqrt{r}} e^{-\gamma r} e^{i(\omega t - kr)} \tag{5.1}$$

where $s(t,r)$ represents the Lamb wave response at the propagation distance $r$ and the propagating time $t$, $A$ represents the signal amplitude of excitation signals, $\omega$ is the angular frequency of the single wave component, while $\gamma$ and $k$ are denoted as the wave damping coefficient and wavenumber respectively. Two terms $\frac{1}{\sqrt{r}}$ and $e^{-i\gamma t}$ indicate the wave attenuation induced by the geometric spreading and the material damping individually [265]. Meanwhile, since $\gamma$ and $k$ are direction dependent, the introduced formulation is able to depict the anisotropic propagation of Lamb waves within composite laminates.

It is worth noting that practically the single-frequency assumption may not be valid anymore

considering frequency sidebands in response signals. In such case, $\omega$ can represent the center frequency corresponding to the dominant frequency components [229]. It is also implied from (5.1) that when $A$ and $\omega$ is determined along with a specific lamb wave mode, the response signal $s$ is determined by only $r$, $\gamma$ and $k$. That is to say, the three elements perform as scaling and stretching factors. A basic signal shape of Lamb waves could exist so that after the scaling and stretching transform such basic shape can yield any target signals in the Lamb wave measurements. This perspective paves a way to interpreting and modelling the Lamb wave responses in a data mining perspective.

### 5.2.2 Unsupervised shapelet learning

Time series shapelets are a type of data structure used in time series data mining and analysis. They are designed to capture distinctive local patterns, or "shapes" within a time series [266]. These patterns can be critical for tasks such as classification, clustering, and anomaly detection in time series data [266]. In recent years, time series shapelets have been widely employed in various fields considering high effectiveness and flexibility of such extracted features when classifying and clustering time-domain signals. An example of the extracted shapelets is illustrated in Fig. 5.1, where local patterns of guided wave signals are captured in red curves. The identified patterns correspond to similar signal shapes and can be transferred from one time series to another through time-domain shifting, scaling and stretching transforms.

The implementation of the shapelet learning is originally proposed by [266], where shapelets are extracted in a supervised manner and class labels are mandatory during the model training process. Nevertheless, the labelled data are not always accessible while the data labelling itself could be time-consuming and error prone. These limitations further give rise to the learning of unsupervised shapelets which require no prior information of class labels. In practice the extraction of unsupervised shapelets can be carried out by either the gradient descent optimization [267] or the brute-force approach [260]. The shapelet optimization approach, however, employs a hyperparameter controlling the smoothness of generated shapelets. Such parameter needs to be tuned carefully; otherwise, the generated shapelets could be too smoothed to capture the oscillating behaviour of guided wave signals. In this regard, this chapter imple-

ments the brute-force manner to generate shapelets and the standard brute-force algorithm is introduced later in this section.

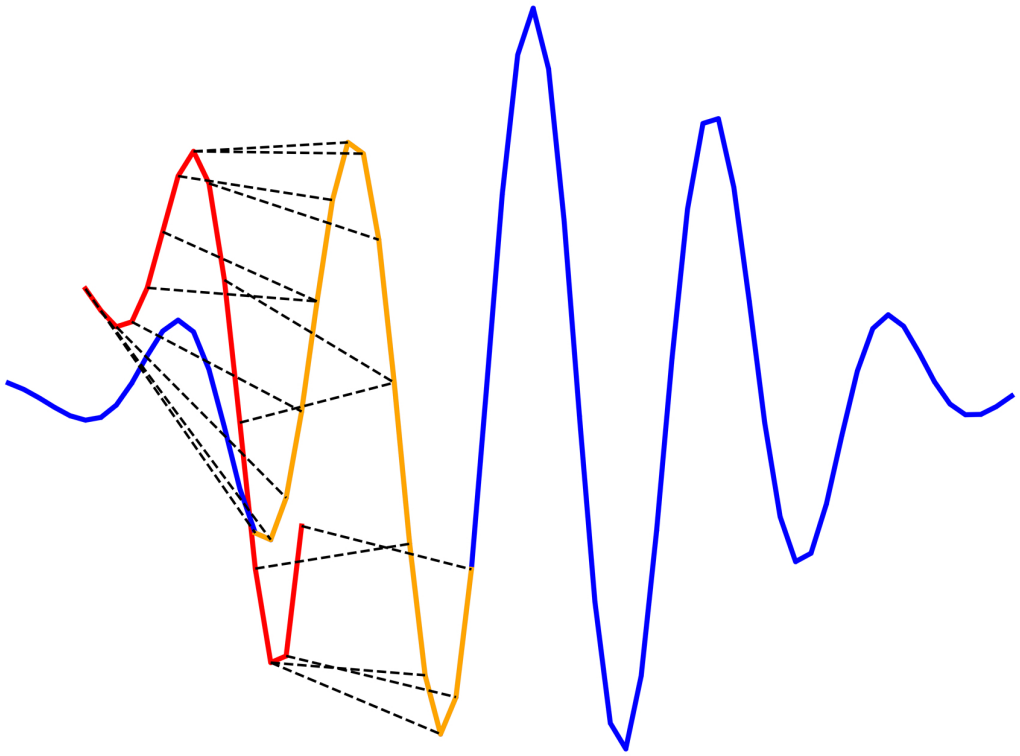

Figure 5.1: Extraction of a representative shapelet (Red) matched to its counterpart (Yellow) in a first wave packet (Blue).

According to [260], a shapelet candidate, denoted as $\boldsymbol{S}$, is formulated as a representative subsequence of a time series data set $\{\boldsymbol{D}_{N\times K}\}$ where $N$ and $K$ represent the signal length and number of the multivariate time series respectively. $N$ represents the length of guided wave signals while $K$ represents the number of signals. The shapelet is supposed to have a length of $l$ and the distance between the shapelet and a single signal $\boldsymbol{T}$ in $\{\boldsymbol{D}_{N\times K}\}$ is defined as [260]

$$\text{sdist}(\boldsymbol{S},\boldsymbol{T}) = \min_{1\le i\le N-l} \text{dist}\left(\boldsymbol{S},\boldsymbol{T}_{i:i+l}\right)(1\le l\le N) \tag{5.2}$$

where $\boldsymbol{T}_{i:i+l}$ represents a sliding-windowed segment of $\boldsymbol{T}$ with the same length, $l$, as the shapelet; $\text{dist}(\cdot)$ represents a distance or similarity measure set in a Euclidean or the dynamic time warping (DTW) [268] manner. A $K\times 1$ dimensional distance vector between $\boldsymbol{S}$ and all the

signals in $\{\boldsymbol{D}_{N\times K}\}$ is then calculated by [260]

$$\text{sdist}(\boldsymbol{S},\boldsymbol{D}) = \min_{1\le i\le N-l} \text{sdist}\left(\boldsymbol{S},\boldsymbol{D}_{i:i+l,j}\right)(1\le l\le N, 1\le j\le K) \tag{5.3}$$

where $D_{i:i+l,j}$ is a $l$-length segment of $j$ th signal in the data set $\boldsymbol{D}$.

It can be inferred from (5.3) that if $\{\boldsymbol{D}_{N\times K}\}$ is well distinguished by $\text{sdist}(\boldsymbol{S},\boldsymbol{D})$ into a set of time series in $\boldsymbol{D}$, denoted as $\boldsymbol{D}_1$, and the rest of $\boldsymbol{D}$, denoted as $\boldsymbol{D}_2$, then $\boldsymbol{S}$ is considered to reflect local patterns of $\boldsymbol{D}_1$. Furthermore, a specific threshold for $\text{sdist}(\boldsymbol{S},\boldsymbol{D})$ is needed so that the maximum distance between $\boldsymbol{D}_1$ and $\boldsymbol{S}$ is below the threshold, and vice versa for $\boldsymbol{D}_2$. Such threshold is determined by maximizing the discrepancies between $\boldsymbol{D}_1$ and $\boldsymbol{D}_2$ through the gap score below [260].

$$\text{gap} \leftarrow (m_2 - s_2) - (m_1 - s_1) \tag{5.4}$$

where $m_1$, $m_2$ refer to mean values of the distances between $\boldsymbol{S}$ and $\boldsymbol{D}_1$, $\boldsymbol{D}_2$ respectively, while $s_1$, $s_2$ represent the corresponding stand deviations. Further restrictions should also be implemented on the sizes of $\boldsymbol{D}_1$, $\boldsymbol{D}_2$, denoted as $|\boldsymbol{D}_1|$, $|\boldsymbol{D}_2|$, to circumvent single anomalies when calculating the gap score. For this purpose, $r$ is defined as the ratio between $|\boldsymbol{D}_1|$ and $|\boldsymbol{D}_2|$ and is illustrated as [260].

$$\frac{1}{k_c} < r = \frac{|\boldsymbol{D}_1|}{|\boldsymbol{D}_2|} < \left(1 - \frac{1}{k_c}\right) \tag{5.5}$$

where $k_c$ is a positive integer indicating the number of clusters in $\boldsymbol{D}$ and is determined by grid search. The calculation of gap score only continues when $r$ falls within the range by (5.5).

Finally, by extending the above process to the case of multiple shapelets, all potential shapelets can be extracted by the following steps. Readers are referred to [260] for more details related to the unsupervised shapelet learning.

- Step 1: Define the input dataset $\boldsymbol{D}$ and the shapelet length $Len$.
- Step 2: Implement a sliding window to extract all the shapelet candidates $\boldsymbol{s}$ from $\boldsymbol{T}(i : i + Len - 1)(i = 1, \cdots, N - Len + 1)$, where $\boldsymbol{T}$ is originally adopted as the first column of $D$.

- Step 3: Compute gap score between $\boldsymbol{s}$ and $\boldsymbol{D}$ based on (5.2)-(5.5). The gap score reflects the discriminating performance of $\boldsymbol{s}$ on $\boldsymbol{D}$.

- Step 4: Find the shapelet candidate with the maximum gap score and store it as an extracted shapelet $\hat{\boldsymbol{s}}$.

- Step 5: Compute the distances between $\hat{\boldsymbol{s}}$ and $\boldsymbol{D}$, utilizes the distances to cluster $\boldsymbol{D}$ into $\boldsymbol{D}_1, \boldsymbol{D}_2$ where $\boldsymbol{D}_1$ is the cluster of time series containing $\hat{\boldsymbol{s}}, \boldsymbol{D}_2$ is the remaining set for clustering. The clustering process is implemented based on a distance threshold $\theta$ for $\boldsymbol{D}_1$, which is expressed as [260]

$$\theta \leftarrow \text{mean}\left(\text{dis}\left(\boldsymbol{D_1}\right)\right) + \text{std}\left(\text{dis}\left(\boldsymbol{D_1}\right)\right) \tag{5.6}$$

  where $dis\left(\boldsymbol{D_1}\right)$ contains distances between $\hat{\boldsymbol{s}}$ and all the time series in $\boldsymbol{D_1}$.

- Step 6: Find the time series in $\boldsymbol{D}$ which has the largest distance to $\hat{\boldsymbol{s}}$, denoted as $\boldsymbol{T}_1$, update $\boldsymbol{T}$ with $\boldsymbol{T}_1$.

- Step 7: Remove $\boldsymbol{D}_1$ from $\boldsymbol{D}$, update $\boldsymbol{D}$ as $\boldsymbol{D} - \overline{\boldsymbol{D}}$. This step ensures that signals close enough to the current shapelet $\hat{s}$ are all removed prior to the next iterative step to find new shapelets, and therefore avoids the high similarity between each extracted shapelets.

- Step 8: Repeat the step 2-7 until all the time series in $\boldsymbol{D}$ are clustered. If $|\boldsymbol{D_1}| == 1$, stop the algorithm and store all the extracted shapelets.

The steps above describe an iterative process [260] to extract representative shapelets which can best distinguish or cluster time series in the dataset $\boldsymbol{D}$. More specifically, step 2 starts to isolate shapelets from a single signal $\boldsymbol{T}$, which is usually chosen as the first signal in $\boldsymbol{D}$. Different segments of $\boldsymbol{T}$ are stored temporarily as shapelet candidates and their gap scores are calculated in step 3. Since the gap score reflects performance of the shapelet candidate to distinguish and cluster time series in $\boldsymbol{D}$, the candidate corresponding to the maximum gap score is then determined as a shapelet of $\boldsymbol{D}$, as shown in step 4. In step 5, time series in $\boldsymbol{D}$ are clustered into different subgroups based on their distances to the extracted shapelet (see (5.2)). In order to find other representative shapelets of $\boldsymbol{D}$, step 6 starts from a signal in

another subgroup which is the least similar (or has the largest distance) to the current shapelet. Meanwhile, signals close enough to the existing shapelet are removed in step 7 to circumvent high similarity between each shapelets. The steps 2-7 are iteratively implemented until all the time series in $\boldsymbol{D}$ are clustered.

## 5.3 Proposed methodology for baseline-free GWSHM

This section presents a baseline-free methodology based on unsupervised shapelets and dictionary learning to detect and localise potential damages on composite structures. The main rationale of the proposed method is to construct a virtual baseline for inspected structures by extracting and transferring guided wave information from a healthy structure, which has different mechanical properties, specimen size, or sensor configurations. As shown in Fig. 5.2, the proposed method can be first implemented at the coupon level. Within this level, shapelets are first generated based on pristine signals collected from an intact coupon 1 under a single temperature level. More specifically, the unsupervised shapelet learning is involved when generating representative shapelet features of the guided wave measurements $\boldsymbol{D}$. Since signals are usually obtained with high sampling rates, it would be highly time-consuming to extract shapelets directly from $\boldsymbol{D}$. A possible solution could be the symbolic aggregate approximation (SAX) [269], which approximates the entire length signals into a list of letters. However, such operation could lead to false alarms when identifying shapelets and a simple signal compression is considered instead as

$$\boldsymbol{T_d}[n] = \boldsymbol{T}\left[n\varphi_d\right] \tag{5.7}$$

where $\boldsymbol{T_d}$ is a down-sampled version of $\boldsymbol{T}, n$ is the $n$-th sampling point in $\boldsymbol{T_d}$; $\varphi_d\,(\varphi_d \in \mathbb{N}^*)$ is denoted as a fixed interval for down-sampling, or the reciprocal of the compression ratio, and is set as 100. Afterwards a time window is applied to extract the first wave packet of $\boldsymbol{T}$, the start, namely the time of arrival (TOA), and the end of first arrival mode are marked as $t_1, t_2$. For $\boldsymbol{T_d}$, the corresponding points are defined as $t_1', t_2'$, where

$$t_1' = t_1/\varphi_d \tag{5.8}$$

$$t_2' = t_2/\varphi_d \tag{5.9}$$

The shapelet features are extracted based on $\boldsymbol{T_d}(t_1' : t_2')$ and an example of this is shown in Fig. 5.1, where a shapelet is identified from a compressed first wave packet of guided wave signals.

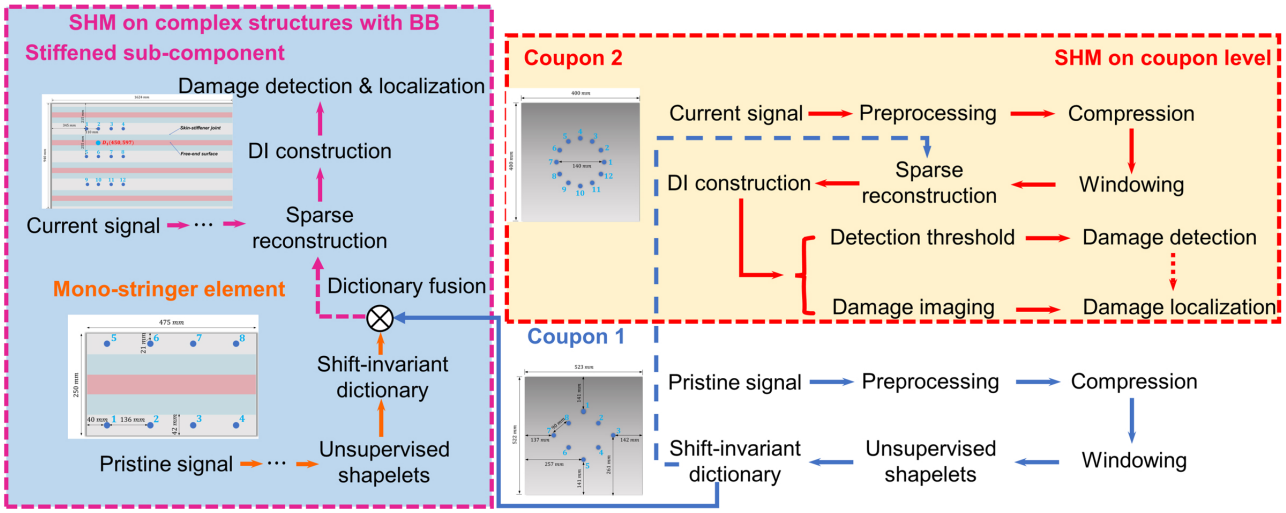


Figure 5.2: Schematic sketch of the proposed methodology for unsupervised damage detection and localisation.

During the shapelet generation, the DTW measure, rather than the standard Euclidean distance in [260], is adopted in (5.2)-(5.3) considering its competence to yield optimal alignments between time series [270]. Furthermore, the shapelets are utilized for dictionary construction. Since the built dictionary contains the intact information only, when employing such dictionary to reconstruct current measurements of another coupon 2, damage signatures are naturally embedded in the discrepancies between the current signals and the reconstructed counterpart, namely the virtual baseline for coupon 2 in Fig. 5.2. Following this rationale, damages on the tested structures can be identified and localised without any experimental baselines from the same structure. Meanwhile, the current guide wave measurements for damage detection and localisation further go through the signal scaling procedure as follows [53, 271].

$$\tilde{T} = \frac{\boldsymbol{T} - \text{median}(\boldsymbol{T})}{\text{IQR}(\boldsymbol{T})} \tag{5.10}$$

where $\boldsymbol{T}$ is a raw guided wave signal, median $(\cdot)$ is the median value of $\boldsymbol{T}$, and $IQR(\cdot)$ is denoted as the interquartile range between the first (25%) and the third (75%) quartiles of $\boldsymbol{T}$. Such

scaling is implemented to ensure that the reconstruction of current guided wave measurements is not affected by outliers in signal amplitudes under temperature variations.

Another main novelty of the proposed approach is manifested into the integration of the BB philosophy [261] to reconstruct the UGW responses of complex composite structures, which remain challenging for most existing baseline-free techniques. When modelling a stiffened composite panel, shapelets of a flat composite coupon may not capture the signal distortions induced by reflection, transmission, reflection and mode conversion of guided waves around stiffeners [253]. Meanwhile, the BB approach turns to test and analyse a series of specimens with increasing levels of scales and complexities [261]. As illustrated in Fig. 5.2, shapelets can be generated upon a defect-free mono-stringer element to imitate the influence of stiffeners and subsequently aggregated with another set of shapelets from flat coupons. The fused dictionary is utilised to reconstruct current measurements from a stiffened composite panel. The damage detection and localisation can be further implemented based on the deviations between the current signals and the reconstructed pristine counterpart. In the following sub-sections, 5.3.1 illustrates details of the dictionary learning process while 5.3.2 explains procedures for damage detection and localisation.

### 5.3.1 Dictionary learning

The dictionary learning is defined as a process decomposing target signals into a linear combination of learnt dictionary atoms [272]. For current guided wave measurements $\{\boldsymbol{R}_{N\times K}\}$ (see Fig. 5.3), where $N$, $K$ are the same as in section 5.2.2, its reconstruction $\widehat{\boldsymbol{R}}$ can be obtained by a $N \times M$ dictionary $\boldsymbol{\Phi}$ and a $M \times K$ sparse coefficient matrix $\boldsymbol{X}$, where $M$ stands for the number of atoms in $\boldsymbol{\Phi}$ and $M > K$ is assumed for an overcomplete dictionary. Furthermore, the dictionary learning process can be formulated as below [272].

$$\min_{\boldsymbol{X}} \left( \|\boldsymbol{R} - \boldsymbol{\Phi}\mathbf{X}\|^2 + \lambda \|\boldsymbol{X}\|_1 \right) \tag{5.11}$$

where $\|\cdot\|_1$ and $\|\cdot\|$ are the $\ell 1$ and $\ell 2$ form; $\lambda$ is a regularization parameter to avoid overfitting of $\boldsymbol{R}$. The formula (5.11) can be solved through method of optimal directions (MOD) [273], k-SVD (Singular Value Decomposition) [274] or basis pursuit denoising (BPDN) [275]. In this

chapter, an iterative greedy dictionary learning algorithm named orthogonal matching pursuit (OMP) [276] is utilized considering its fast implementation. See further implementation of the OMP in [276]. Note that a stopping criterion for OMP is needed to stop unnecessary computations when

$$\varepsilon_i = \left\| \boldsymbol{R}_i - \widehat{\boldsymbol{R}_i} \right\|^2 (i = 1, 2, \cdots, K) < \text{ tol} \tag{5.12}$$

where $\varepsilon_i$ is the residual norm, namely the reconstruction error, when fitting the $i$ th signal in $\{\boldsymbol{R}_{N\times K}\}$; tol is the tolerance for $\varepsilon_i$ and adopted as 1. If the stopping criterion has never been met during iterations, the OMP would be early stopped after 100 iterations.

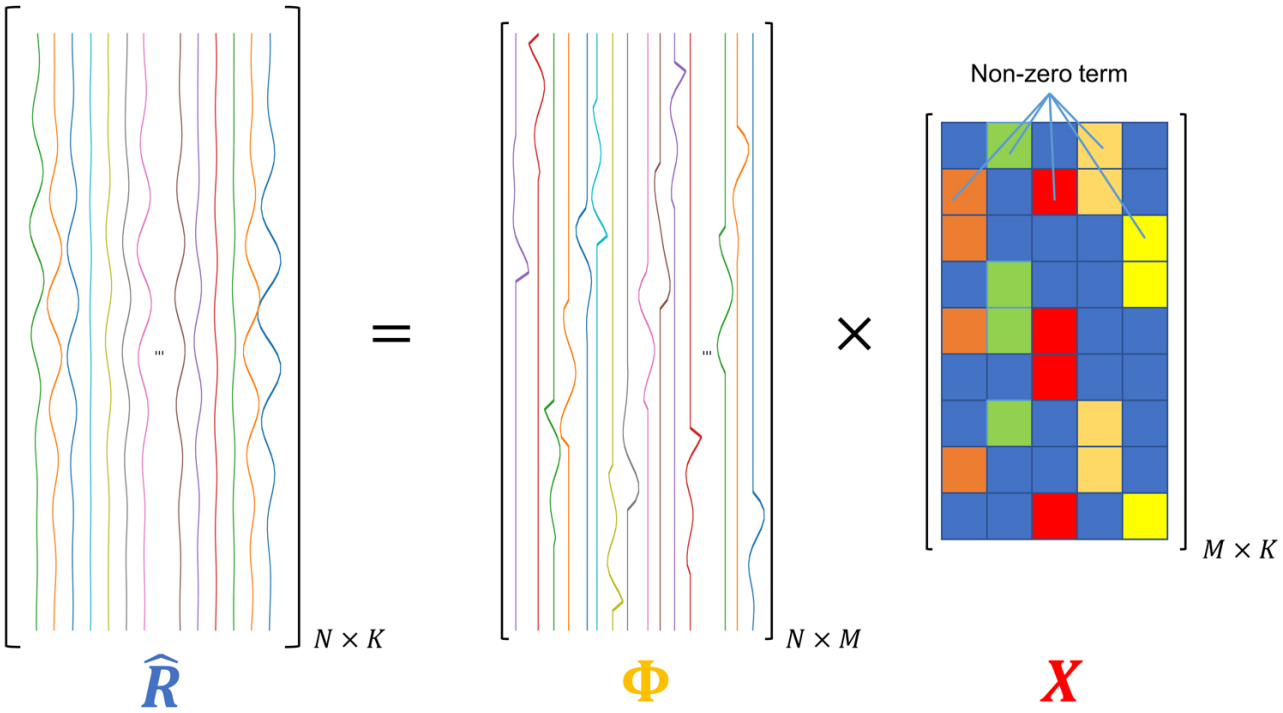


Figure 5.3: Illustration of dictionary learning approach.

During the signal reconstruction, a well-defined dictionary is also essential whose atoms are competent to capture guided wave characteristics. The generation of dictionary atoms can be assisted with shapelet features since such features encompass shared patterns of guided wave signals. However, shapelets have shorter lengths than the fitted signals and cannot be directly employed as a dictionary. An intuitive alternative to generating dictionary atoms is to arrange shapelet features in a shift-invariant form [262, 263]. As shown in Fig. 5.4, a given shapelet $\hat{s}$ is shifted from the first position up to the $(\boldsymbol{N} - |\hat{\boldsymbol{s}}| + 1)$-th position, where $\boldsymbol{N}$ and $|\hat{\boldsymbol{s}}|$ separately represent the length of $\boldsymbol{R}_i (i = 1, 2, \cdots, K)$ and $\hat{\boldsymbol{s}}$. Such operation yields a set of dictionary

atoms with the same shapelet content but different time phase delays, thus being suitable when fitting multi-channel guided wave signals. When the shift-invariant dictionary is formed, it is considered as $\boldsymbol{\Phi}$ to reconstruct the current measurements $\{\boldsymbol{R}_{N\times K}\}$ in (5.11).

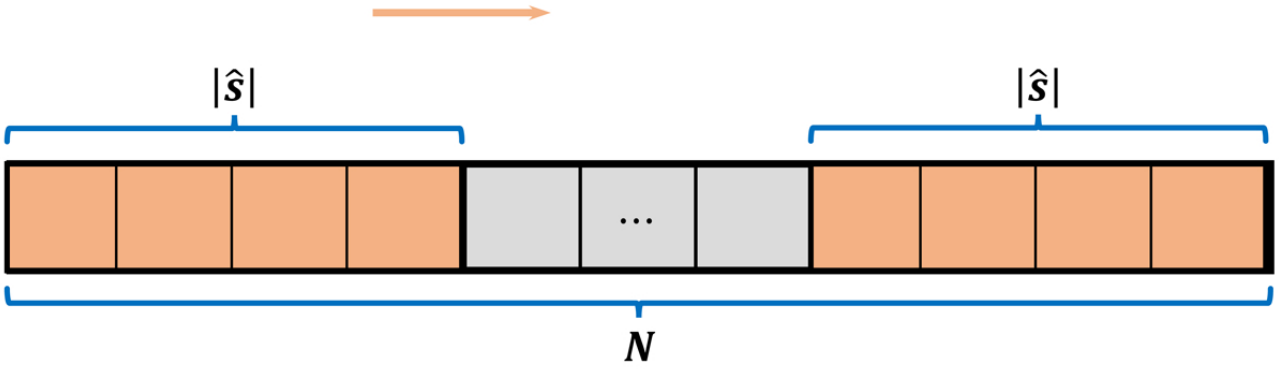


Figure 5.4: Generation of shift-invariant dictionary with shapelet features.

When a damage exists, damage signatures are embedded in $\{\boldsymbol{R}_{N\times K}\}$ and virtual baselines will be reconstructed by $\{\boldsymbol{R}_{N\times K}\}$ and $\boldsymbol{\Phi}$ together. However, due to the damage scattering, guided waves, particularly the first wave packets, will experience energy losses when propagating through damages. Such losses can be further interpreted as information losses of guided wave signals, and consequently are manifested in reduced amplitudes of the damaged measurements. Hence, reconstructing the virtual baselines by damaged measurements becomes an ill-posed inverse problem and prior knowledge is then needed for a reasonable reconstruction.

More specifically, amplitudes of the virtual baseline signals need to be pre-estimated as a constraint on the signal reconstruction. Given that in (5.1) the signal amplitude is expressed in the form $\frac{A}{\sqrt{r}}e^{-\gamma r}$, for two arbitrary paths $i$, $j$, namely the $i$-th and $j$-th column in $\{\boldsymbol{R}_{N\times K}\}$ $(1 \leq i, j \leq K)$, their signal amplitudes when undamaged are denoted as $\widehat{A}_l, \widehat{A}_j$ and expressed as follows.

$$\widehat{A}_l e^{\gamma_i r_i}\sqrt{r_i} = \widehat{A_j} e^{\gamma_j r_j}\sqrt{r_j} \equiv C \tag{5.13}$$

where $r_i$, $r_j$ are the propagation distance of path $i$,$j$, $\gamma_i$, $\gamma_j$ are the corresponding damping coefficients, while $C$ is a constant representing the amplitude of excitation signals. When estimating $\widehat{A}_i$ in (5.13) using current measurements $\{\boldsymbol{R}_{N\times K}\}$, which could contain damaged signals, the priority is to determine $C$ by calculating and comparing the $\widehat{A}_i e^{\gamma_i r_i}\sqrt{r_i}$ terms for each signal. Noting that such product terms could be lowered by the reduced amplitudes of

damaged signals, $C$ is adopted as the median of all the product values.

A ratio $w_i$ is then defined between $\widehat{A}_l$ and the amplitudes in current signals, assigned as $A_i$. Such ratio satisfies $0 < w_i \leq 1$ and can modify (5.11) into

$$\min_{\boldsymbol{X}_i} \left( \|\boldsymbol{R}_i - w_i \boldsymbol{\Phi} \mathbf{X}_i\|^2 + \lambda \|\boldsymbol{X}_i\|_1 \right), \text{ where } w_i = A_i / \widehat{A_i}, (i = 1, 2, \cdots, K) \tag{5.14}$$

The formula (5.14) aims to reconstruct a virtual baseline signal $\widehat{\boldsymbol{R}_i}$ corresponding to the current signal $\boldsymbol{R}_i$. By implementing an amplitude constraint $w_i$ on the dictionary learning process, $\widehat{\boldsymbol{R}_i}$ satisfies

$$\widehat{\boldsymbol{R}_l} = w_i \boldsymbol{\Phi} \mathbf{X}_{\mathrm{i}} \tag{5.15}$$

### 5.3.2 Damage detection and localisation

After the signal reconstruction, the discrepancies between current measurements, $\boldsymbol{R}_i$, and the reconstructed baselines, $\widehat{\boldsymbol{R}_i}$, can be quantified as a damage index ($DI$) to reflect health conditions of an engineered structure. Assuming that a structure is monitored by $N_s$ transducers in a pitch-catch manner, then the total number of transducer paths $K$ follows $K = N_s (N_s - 1)$ when reciprocal paths are included. Meanwhile, the $DI$ for the sensor path $i (i = 1, 2, \cdots, K)$ is formulated as [14]

$$DI_i = 1 - \left| \mathrm{corr} \left( \boldsymbol{R}_i, \widehat{\boldsymbol{R}_i} \right) \right| \tag{5.16}$$

where $|\cdot|$ is the absolute value operator and $\mathrm{corr}(\cdot)$ is the Pearson correlation coefficient. The $DI$ can also be defined by the Fourier transform in frequency domain. Nevertheless, only the time-domain based DI in (5.16) is considered in this work.

In the context of damage detection, the proposed $HI$ in the formula (4.12), i.e., the 95% quantile of DI values, is employed to indicate the health condition of a monitored structure. The detection threshold is calibrated by the 99.9% quantile of $HI$ values under the healthy state, as shown in formula (4.13). The performance for damage detection is then evaluated by the binary classification framework where the true positive rate (TPR), the false alarm rate (FAR) and the accuracy (ACC) are obtained following formula (3.24) - (3.26).

Meanwhile, the trueness, i.e., the localisation error $\varepsilon_d$ in formula (3.27), and precision [277] are

deployed as performance indicators for the damage localisation. Assuming that $q \quad (q \in N^*)$ repeated measurements yield the damage location estimates as $(\widehat{x}_u, \widehat{y}_l)\,(i = 1, 2 \cdots, q)$, the precision is defined as follows [62, 278].

$$\text{Precision} = \pi\alpha\beta \tag{5.17}$$

where $\alpha, \beta$ satisfy $\alpha = \sqrt{\lambda_1 \chi^2_{0.95}(2)}, \beta = \sqrt{\lambda_2 \chi^2_{0.95}(2)}$. $\lambda_1$, $\lambda_2$ represent the eigenvalues of the vector estimates $(\widehat{x}_l, \widehat{y}_l)\,(i = 1, 2 \cdots, q)$. $\chi^2_{0.95}(2)$ is the 95% confidence of $\chi^2(2)$ distribution.

## 5.4 Experimental setup

The proposed baseline-free technique is interrogated by detecting and localising both the simulated and real-life impact damages on the anisotropic $M21 - T800S$ composite structures which have been investigated in Chapter 4. The signal acquisition and pre-processing procedures are implemented in the same manner as previously in Chapter 4, where the first $A_0$ packets of 50kHz 5-cycle Hanning-windowed guided wave tone bursts with the excitation amplitude as $6V$ are prepared for further analyses.

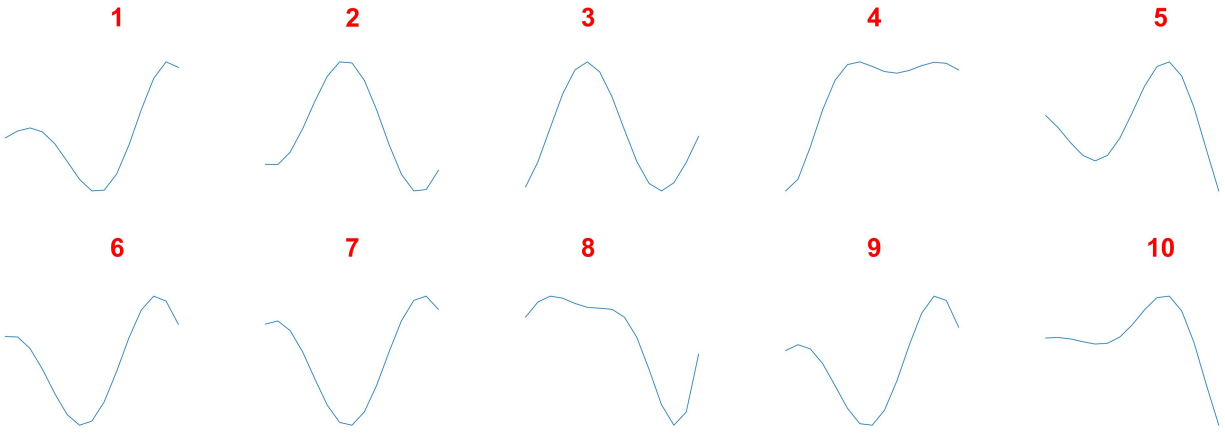


Figure 5.5: Unsupervised shapelet features generated from the intact quasi-isotropic $M21 - T800S$ coupon under 25°C.

Meanwhile, unsupervised shapelets are extracted from an intact quasi-isotropic $M21 - T800S$ coupon at 25°C as introduced in Chapter 3 (see Fig. 3.4(a)), whereas the coupon for shapelet extraction is manufactured of different geometry (including thickness), transducer configuration

and the stacking layer sequence from the inspected anisotropic composite structures. The extracted shapelets, as demonstrated in Fig. 5.5, are subsequently formed into a shift-invariant dictionary for further investigations.

During the implementation of shapelet-based dictionary learning, the damage index ($DI$) values are obtained through (5.16) and further integrated into the RAPID tomography. The settings of imaging parameter $\beta$ and the number of imaging pixels are identical to section 4.4 when applied to various monitored structures.

Furthermore, the shapelet-based technique is intensively validated in terms of its capability and effectiveness for damage detection and localisation. More concretely, the investigations focus on both simulated and real impact damages, single and dual damage scenarios, the structural complexities, together with the robustness of the proposed baseline-free method against temperature variations. Meanwhile, comparisons are also made to widely adopted baseline-free techniques, mainly the VTR [205], IB [209] and the reciprocity principle [217], regarding the damage localisation performance.

## 5.5 Experimental results of the proposed technique

### 5.5.1 Simulated damage cases

The SHM performance of the proposed baseline-free technique is firstly investigated by simulated damage scenarios under 20°C temperature variations, as introduced in section 4.5.1. According to the section, the threshold for damage detection is calibrated by half of intact measurements prior to online monitoring process.

The shapelet length $\widehat{|s|}$ and the number of clusters $k_c$ need to be determined during the shapelet extraction (see section 5.2.2). For the sake of simplicity, it is assumed that all the shapelets are extracted with the same length rather than varying lengths. In order to keep shapelets short and representative, an appropriate shapelet length is set close to but no more than 0.3 times the length of training signals [279]. In this work, first wave packets of the compressed guided wave signals are utilised to generate shapelets. The length of each first wave packet is calculated as $5/\left(50\times10^3\right)\times60\times10^6\times1.1/100=66$, where $5, 50\times10^3, 60\times10^6, 1/100$

are values for the number of toneburst cycles, center frequency of signals, sampling rate, and compression ratio respectively. Meanwhile, 1.1 is a redundancy factor to capture the entire wave packets. For a given signal with 66 datapoints, its shapelet length is set as 15, approximately 0.25 times the signal length.

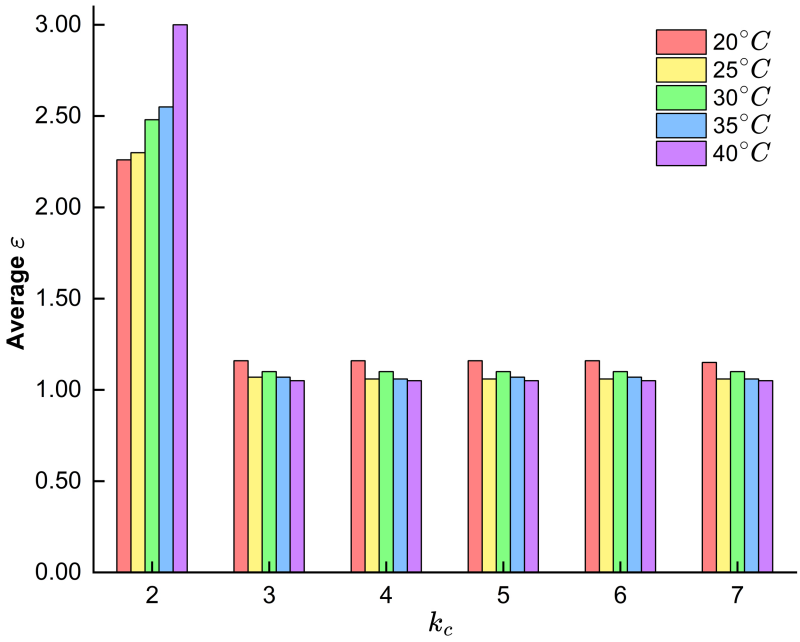


Figure 5.6: Average reconstruction error $\varepsilon$ with different $k_c$ values.

When the shapelet length is fixed, the $k_c$ value is determined by average reconstruction errors $\varepsilon$ (see (5.12)) of current guided wave measurements from 20°C to 40°C. Fig. 5.6 shows the average $\varepsilon$ against varying temperatures and $k_c$ values. It is illustrated that when $k_c$ equals to 2 the reconstruction errors not only reach their highest, but also significantly exceed 1 corresponding to the stopping criterion of the OMP algorithm. In such case, the generated shapelets are not well representative of guided wave signals. When $k_c$ starts from 3, the average errors are greatly reduced and remain steady under 20°C to 40°C. Hence, $k_c = 3$ is adopted for the shapelet extraction.

Fig. 5.7 shows the evolution of $HI$ values when simulated damages are monitored under temperature variations. The horizontal dashed line represents the detection threshold, which is calibrated by pristine signals under 20°C to 40°C and then calculated as $3.40 \times 10^{-3}$ by formula

(4.12) - (4.13). It is further illustrated in Fig. 5.7 (a) that the $HI$ values of damaged cases are well above the detection threshold while for intact cases the $HI$ values remain lower than the threshold under 20°C variations. In this case, $TPR = 1, FAR = 0, ACC = 1$ are yielded for all temperature levels. A zoomed view of the intact cases is then shown in Fig. 5.7 (b), where the corresponding $HI$ values are below the threshold consistently under temperature variations.

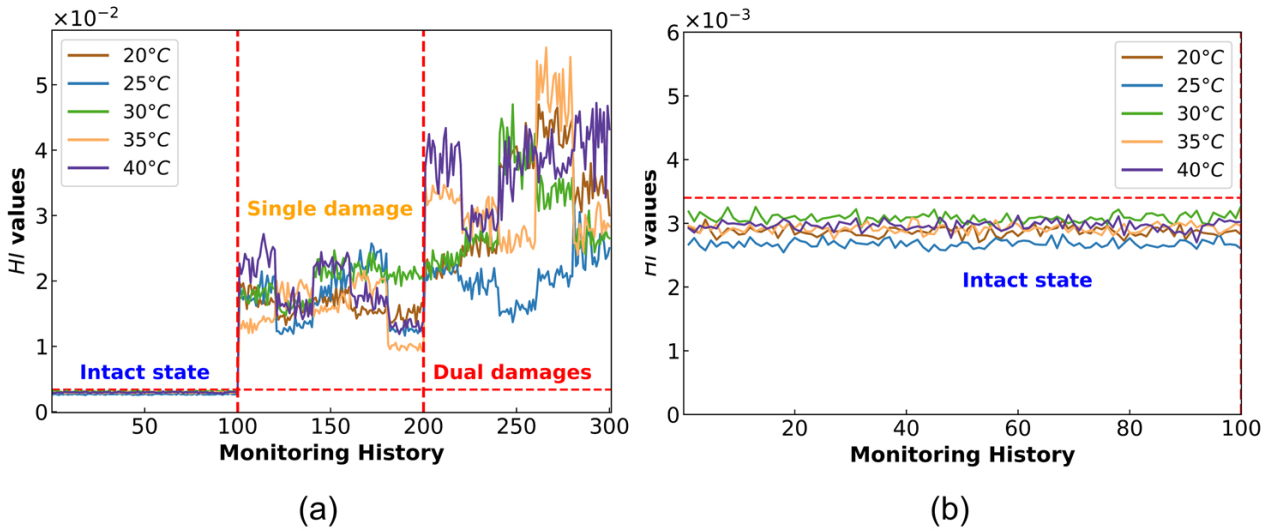


Figure 5.7: $HI$ values under temperature variations: (a) for the entire monitoring history; (b) under intact state only.

Furthermore, in terms of the single damage cases similar trends of HIs are yielded under 20°C variations. There also exist fluctuations in the $HI$ curves for single temperature levels. Such variations are likely due to the different damage locations which further lead to varying distribution of $DI$s and thus the involved HI values. Despite that, the $HI$ values within the single damage scenarios are overlapped and stable under varying temperatures so that no false alarms are reached during the damage detection.

Compared to the single damage cases, however, the $HI$ curves within the dual damage scenarios exhibit relative high fluctuations. This is because the dual damages may not always be simultaneously identified particularly in the cases where the two damages are closely located, e.g. with only 19 mm distance. In such cases, one damage could be masked by another, thus leading to fluctuating HI values within the dual-damage cases.

In terms of damage localisation, the single damage cases are primarily investigated considering the potential difficulties to well localise dual damages. Table 5.1 presents the trueness and

the precision as two indicators for assessing the damage localisation performance. It is shown that the mean trueness values, namely the average localisation errors, for damages at different locations are no greater than 10 mm while the corresponding standard errors (S. E.) remain stable and lower than 1.6 mm under 20°C variations, thus confirming the damage localisation capability of the proposed baseline-free technique. Another factor affecting the trueness values is embodied within uncertainties of damage positioning. Such uncertainties could lead to relative high S.E. trueness values for individual temperatures, e.g., 35°C. During the monitoring process simulated damages are implemented at different locations under one temperature and then removed for the next temperature level. Therefore, it would become inevitable to introduce the positioning uncertainties when repeatedly adding the artificial damages. Simultaneously, the precision depicts deviations of the estimated damage locations [278]. As shown in Table 5.1, the mean precision values remain lower than 26.52 $mm^2$ under the temperature variations while the S.E. values could be slightly higher due to individual large values of precision. Such values are comparable to [278] and therefore suggest robustness of the damage localisation performance with repeated measurements.

Table 5.1: Localisation results for single simulated damages under temperature variations.

| Temperature /°C | Trueness /mm | | Precision /$mm^2$ | |
|---|---|---|---|---|
| | Mean | S.E. | Mean | S.E. |
| 20 | 7.8 | 1.0 | 0.00 | 0.00 |
| 25 | 6.7 | 0.7 | 4.35 | 4.12 |
| 30 | 8.4 | 1.1 | 4.86 | 4.61 |
| 35 | 7.6 | 1.6 | 26.52 | 25.16 |
| 40 | 9.8 | 0.9 | 0.00 | 0.00 |

Further comparisons are made in Fig. 5.8 between the IB, reciprocity-based, VTR and the proposed shapelet-based technique when localising the single simulated damages at different locations. The proposed method achieves the overall best localisation accuracies among the baseline-free techniques and robust localisation errors against temperature variations. Comparatively, the IB technique yields the worst performance when localising simulated damages, which is due to the lack of equivalent through-centre transducer paths for comparisons, as illustrated in section 4.5.1.

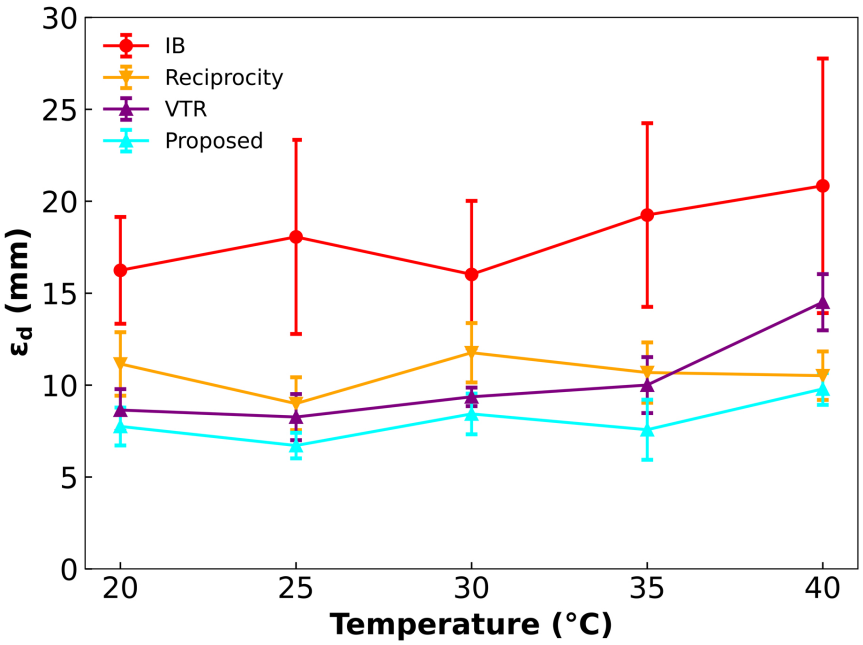


Figure 5.8: Comparisons between the IB, reciprocity-based, VTR and the proposed shapelet-based approach when localising single simulated damages.

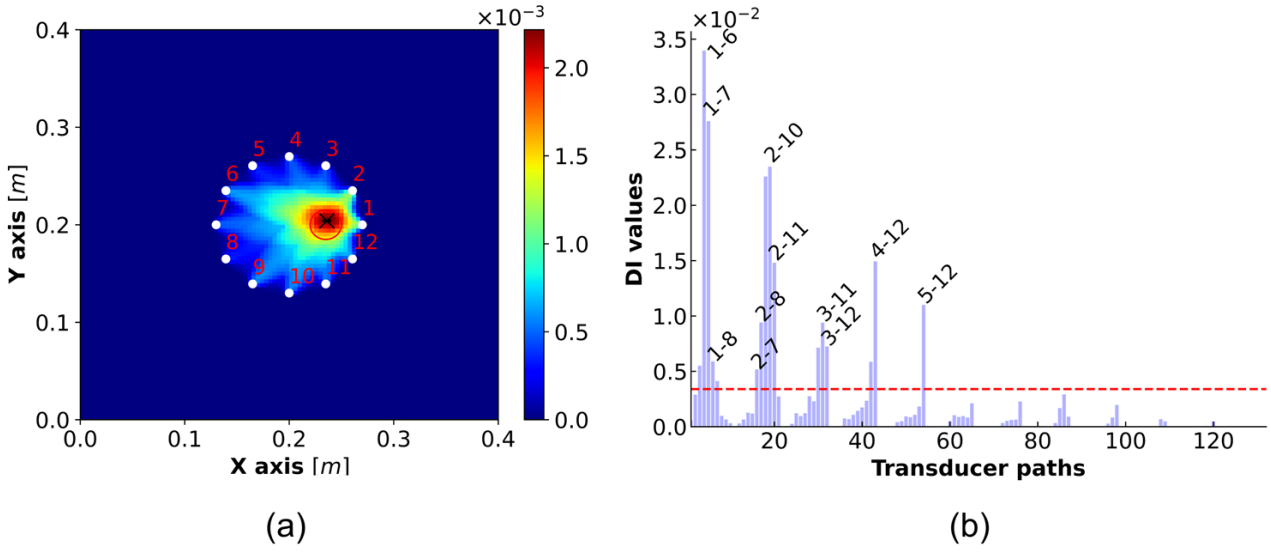


Figure 5.9: Single damage scenario $SC1$ under 20°C: (a) damage imaging results;(b) $DI$ histograms with reciprocal paths ignored.

As an example, a single damage case (named $\boldsymbol{SC1}$ ) and its imaging result are given in Fig. 5.9. The simulated damage is slituated on the right side within the circular transducer array and then monitored under 20°C. As shown in Fig. 5.9 (a), the estimated damage location marked as black cross is consistent with the true damage area within the red circle, thus further validating the effectiveness of the proposed method for damage localisation. Meanwhile, Fig. 5.9

(b) exhibits that several critical transducer paths, e.g., path $1-6$, $1-7$, $2-10$ and $4-12$, are detected as damaged with the $DI$ values greater than the calibrated threshold. Such result is consistent with the damage imaging result, which implies the damage is successfully identified and localised with the proposed method.

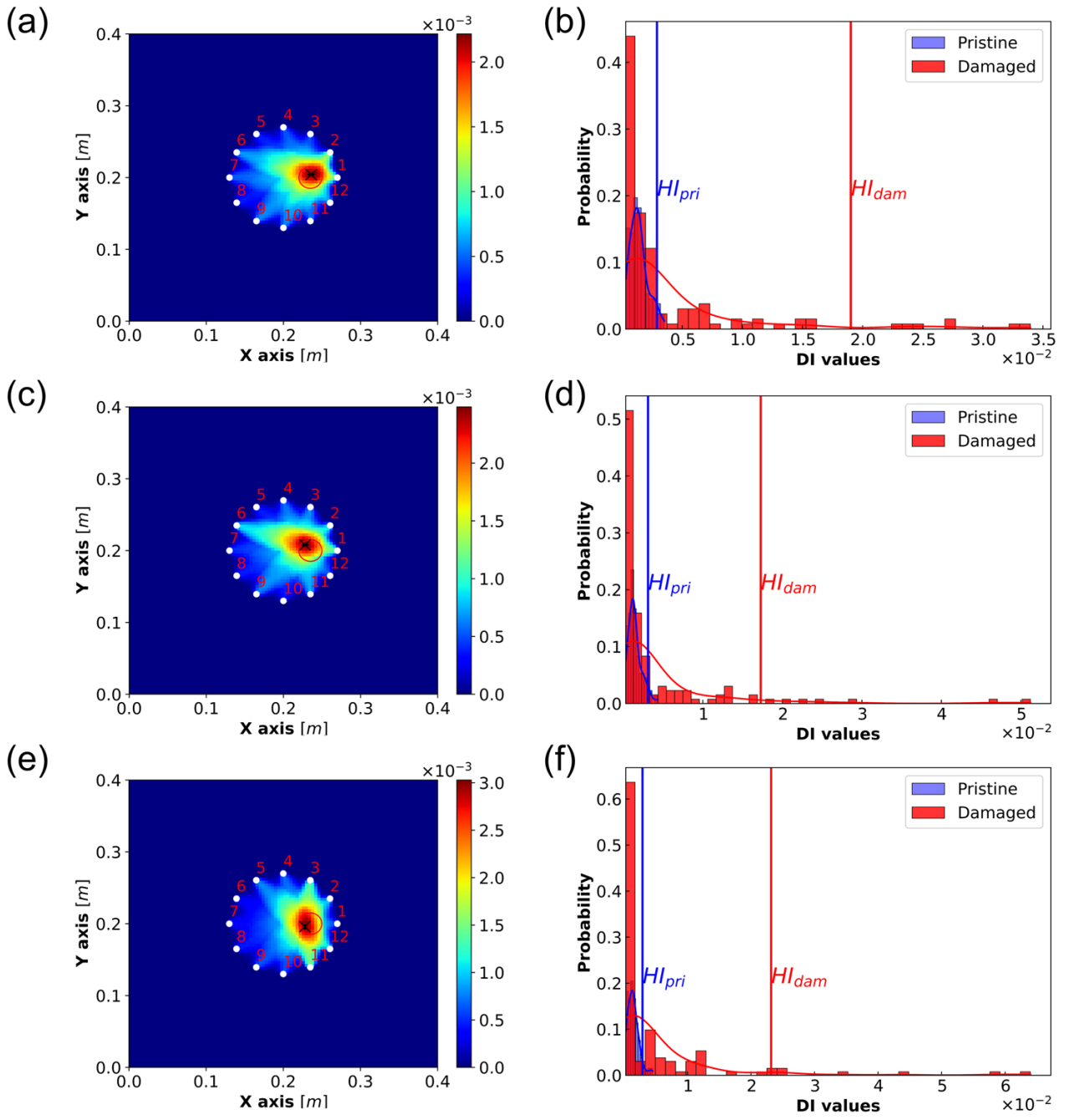


Figure 5.10: Damage scenario ***SC1*** under temperature variations: (a,c,e) damage imaging results under 20°C, 30°C, 40°C; (b,d,f) the corresponding distribution of $DI$ values.

Fig. 5.10 demonstrates the imaging results and the distribution of $DI$ values for the ***SC1***

under temperature variations. The figures in the right columns present histograms of $DI$ values and the probability density function (PDF) curves calculated by the kernel density estimation (KDE). As an example, Fig. 5.10 (b) compares the $DI$ distribution of damaged and intact states under 20°C. $DI$ values of the two conditions are obtained by separately inputting the damaged or pristine signals. It is further shown in Fig. 5.10 (b) that the $DI$s under intact state follow an approximately Gaussian distribution, which is clearly not the case for the damaged conditions. Moreover, the PDF curves for the two conditions have similar peak locations but the main differences are manifested into several extreme values in the damaged $DI$s, which correspondingly lead to a right skewed distribution. Such finding further validates that the damage information is confined to few transducer paths while most paths are regarded as undamaged.

Meanwhile, it is evident that the $HI$ in formula (4.12) is competent to distinguish between the intact and damaged states. In Fig. 5.10 (b) the $HI$s for intact and damaged states, denoted as $HI_{pri}$, $HI_{dam}$, are determined as $2.89 \times 10^{-3}$ and $1.90 \times 10^{-2}$ respectively. Since the proposed HI adopts the 95% quantile of $DI$s, such index can capture the extreme $DI$ values in the presence of damage, thus being competent for damage detection purposes. Similar results under 30°C and 40°C are obtained in Fig. 5.10, suggesting the effectiveness of the proposed method when detecting the single damage against 20°C variations of temperature.

The imaging results of dual damage scenarios are also obtained and two example cases named $\boldsymbol{SC2}$, $\boldsymbol{SC3}$ are presented in Fig. 5.11 and Fig. 5.12. Fig. 5.11 shows that two damages can be identified under 20°C and 30°C when they are sparsely distributed with distance as 40 mm. Nevertheless, the imaging artifacts at 40°C could make it difficult to well isolate the two damages. Another example is demonstrated in Fig. 5.12 where two damages are only 19 mm far from each other. In such case it would become challenging to localise the two damages simultaneously since one damage is likely to be masked by the other in the imaging results.

According to section 5.3.1, the reconstruction of virtual baseline signals is performed by the dictionary learning process with shapelet-based atoms. Fig. 5.13 shows an example of signal reconstruction for the single damage scenario $\boldsymbol{SC1}$ under 20°C. According to the figure, the transducer paths $1-6$, $2-10$ are identified as damaged paths while paths $2-4$ and $3-7$

are regarded as defect-free. In terms of the paths $2-4$ and $3-7$ in Fig. 5.13 (c, d), the reconstructed pristine signals are well fitted to the experimental baseline and consistent with the current signals, which implies the defect-free state of the transducer paths.

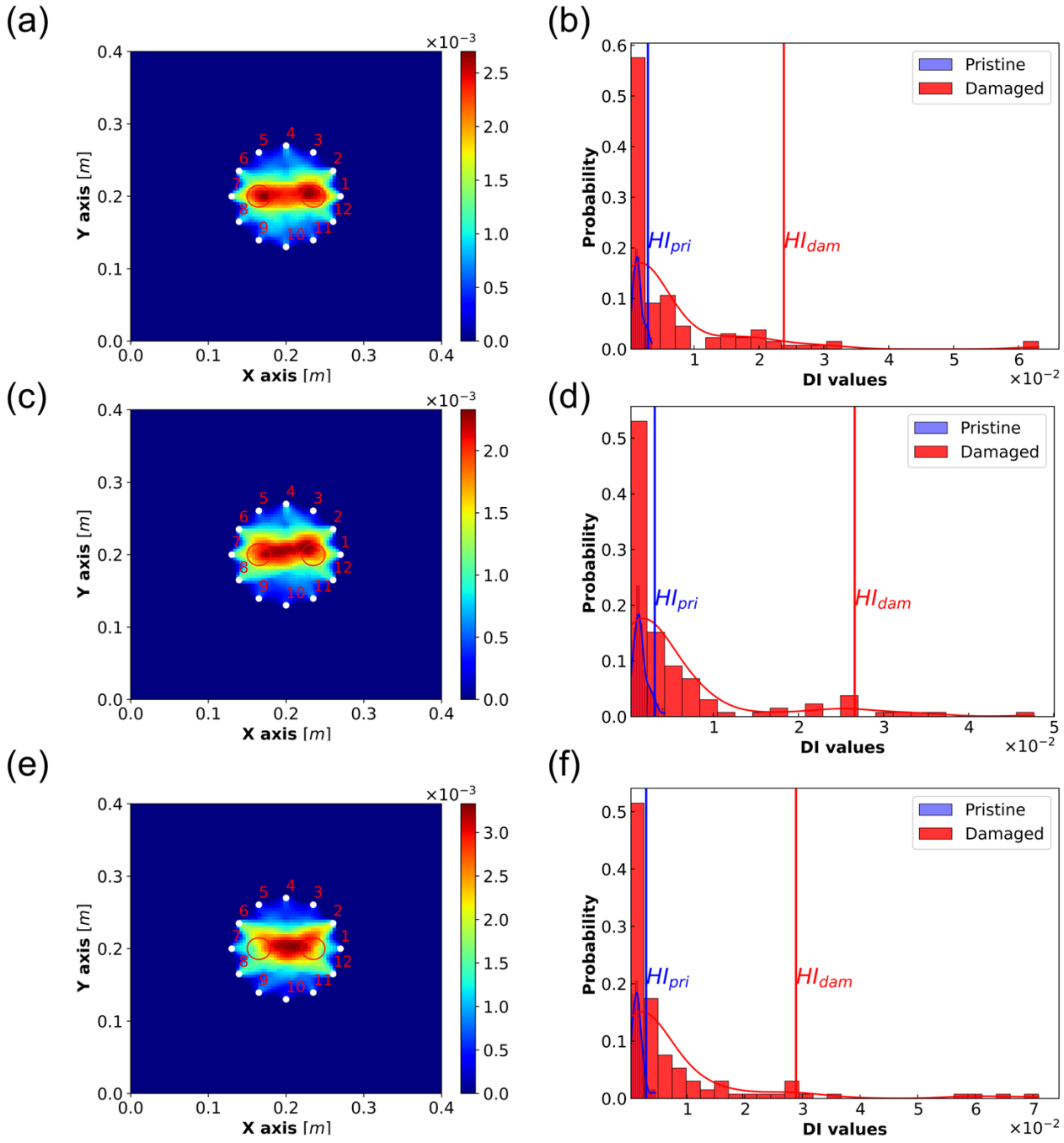


Figure 5.11: Dual damage scenario ***SC2*** under temperature variations: (a,c,e) imaging results under 20°C, 30°C, 40°C;(b,d,f) the corresponding distribution of $DI$ values.

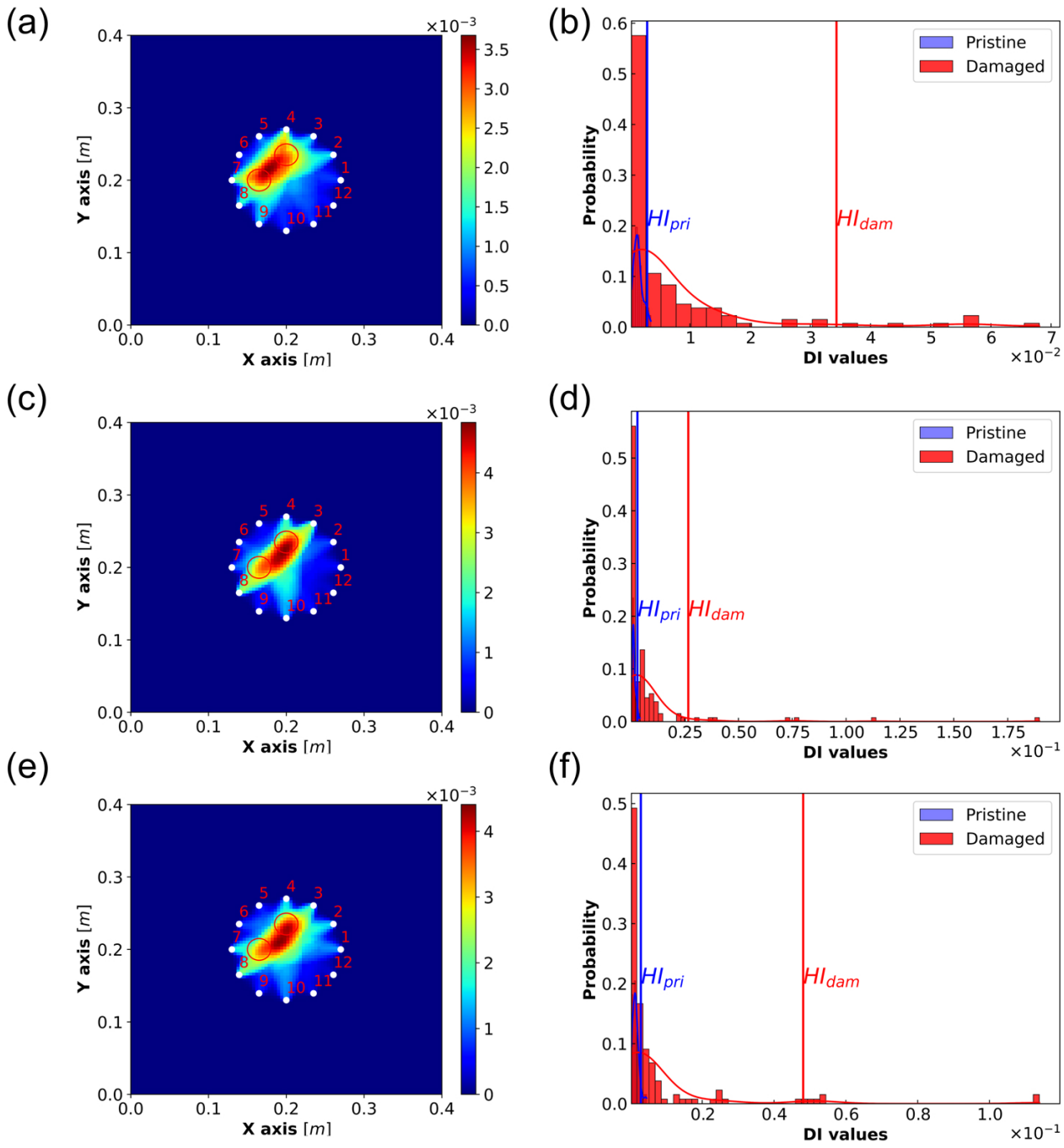


Figure 5.12: Dual damage scenario ***SC3*** under temperature variations: (a,c,e) imaging results under 20°C, 30°C, 40°C;(b,d,f) the corresponding distribution of $DI$ values.

Reasonable results are also yielded in Fig. 5.13 (a, b) for the damaged paths $1-6$, $2-10$. More specifically, the reconstructed pristine signal is consistent with the experimental counterpart for the path $2-10$ despite slight phase delays. In practice, the phase recovery for the reconstructed pristine signals is challenging particularly considering that the damage information is an unknown prior for the signal reconstruction. With. regard to the path $1-6$,

there exist deviations between the experimental and the reconstructed baseline, particularly within the second half of the first wave packet. This is because the dictionary learning process in formula (5.14) adopts a fixed ratio $w$ for amplitude recovery of pristine signals, and such ratio may not always capture the scaling variations in signal amplitudes. However, it is shown in Fig. 5.9 that such problem will not affect the identification of damaged paths, nor the damage localisation results considering that the correlation-coefficient based $DI$ in formula (5.16) is robust to the varying amplitude scalings.

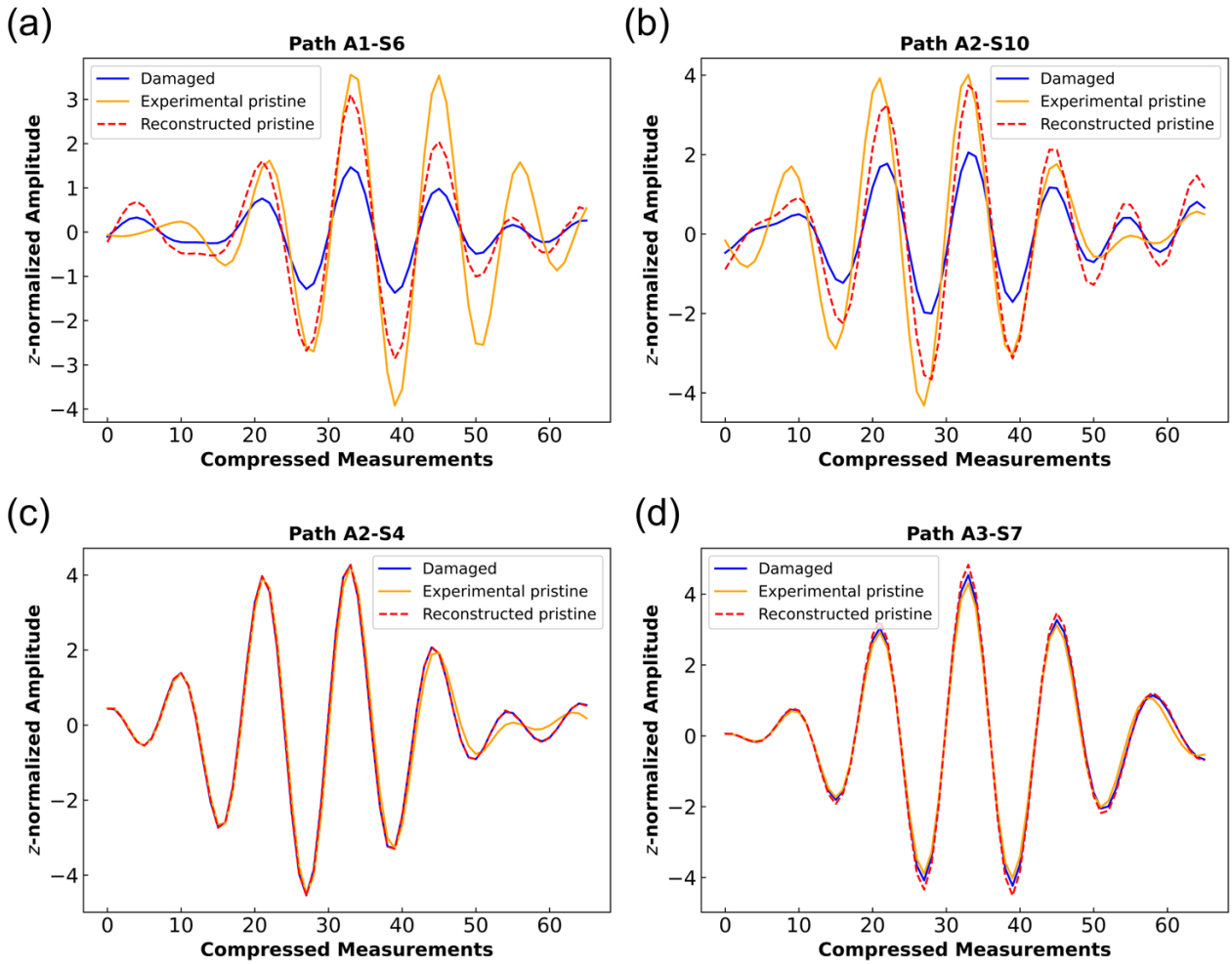


Figure 5.13: Signal reconstruction for the single damage scenario ***SC*1**: (a) damaged path $1-6$; (b) damaged path $2-10$; (c) undamaged path $2-4$; (d) undamaged path $3-7$. "$A$" and "$S$" represent the actuator and sensor respectively.

### 5.5.2 Impact damage cases

Apart from simulated damages, the baseline-free method is applied to impact damage cases, as introduced in section 4.5.2, for further validation. Fig. 5.14 (a) displays the 350 mm ×

350 mm × 2 mm test coupon with C-Scan images of the impact damages while the test rig for the impact tests is shown in Fig. 5.14 (b). During the monitoring process, intact and damaged measurements are collected under 20°C to 30°C, while half of the intact signals are utilised for the threshold calibration of damage detection.

Fig. 5.15 shows the monitoring history of $HI$s for the impacted coupon. Since $HI$s of the intact state remain stable against 10°C variations, the detection threshold is calibrated by the pristine HI values from 20°C to 30°C and therefore calculated as $2.98 \times 10^{-3}$. It turns out in Fig. 5.15 (a) and (b) that the baseline-free technique is effective for damage detection with zero false alarm rates and overall high accuracies under 10°C variations, as further presented in Table 5.2.

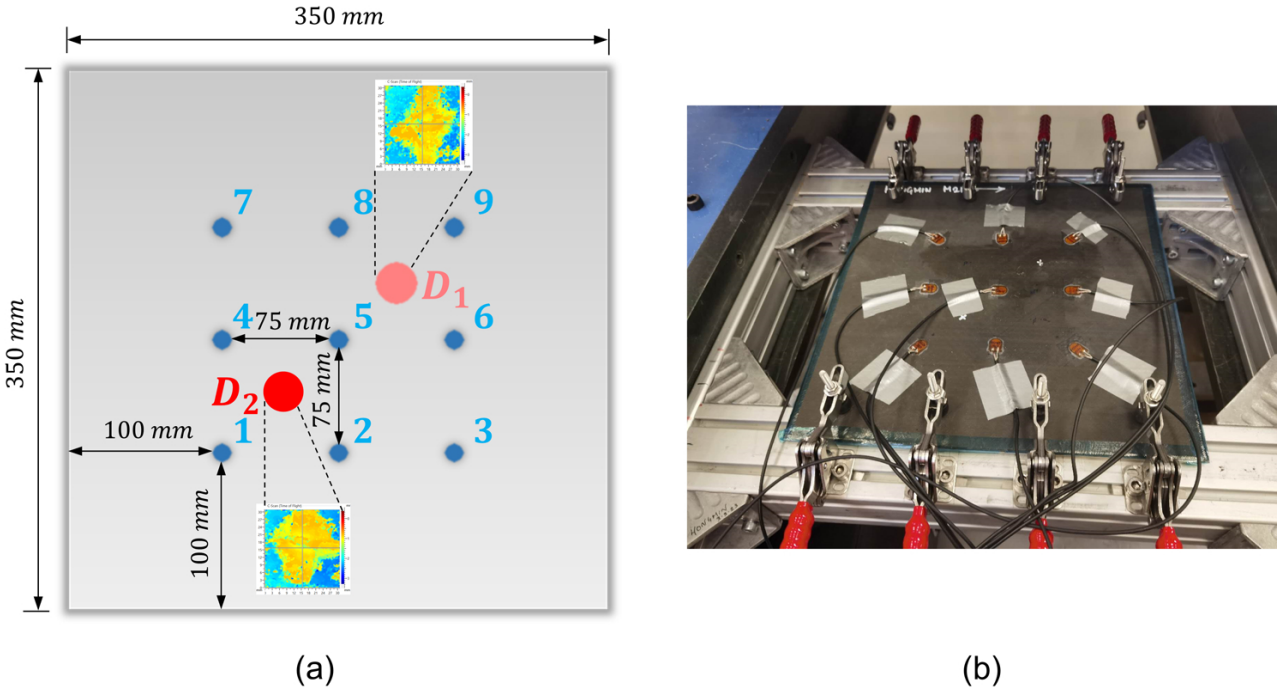


Figure 5.14: Investigation on impact damages: (a) a $M21 - T800S$ coupon with two BVIDs; (b) the test coupon fixed to the drop tower.

Table 5.2: Damage detection results for impact damages under temperature variations.

| Temperature /°C | $TPR$ | $FAR$ | $ACC$ |
|---|---|---|---|
| 20 | 1.00 | 0.00 | 1.00 |
| 25 | 1.00 | 0.00 | 1.00 |
| 30 | 1.00 | 0.00 | 1.00 |

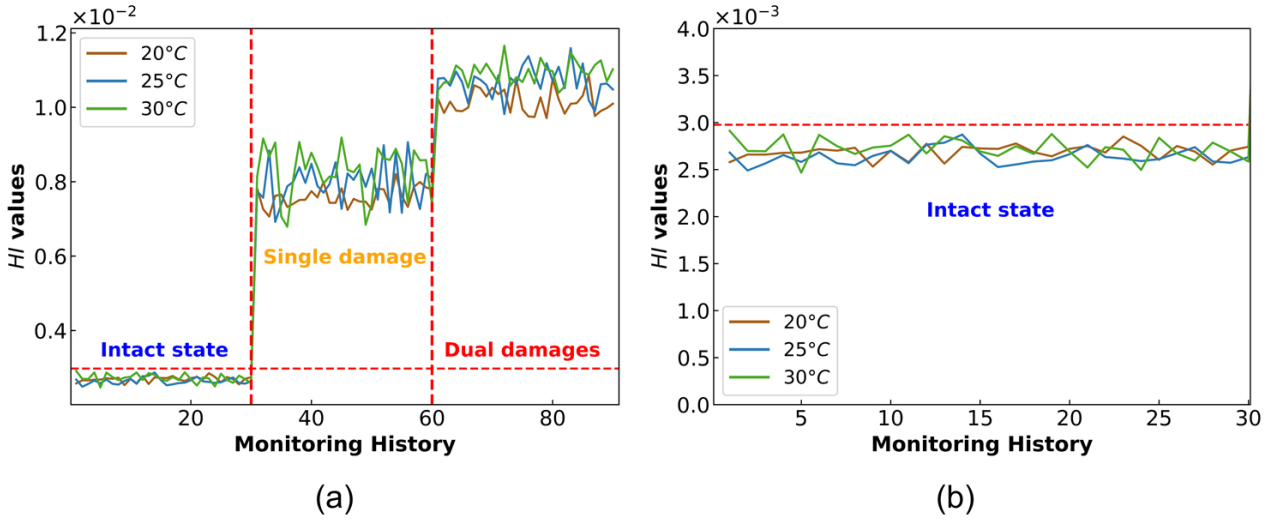


Figure 5.15: $HI$ values for impact damages under temperature variations: (a) the entire monitoring history; (b) a zoomed view of the intact state.

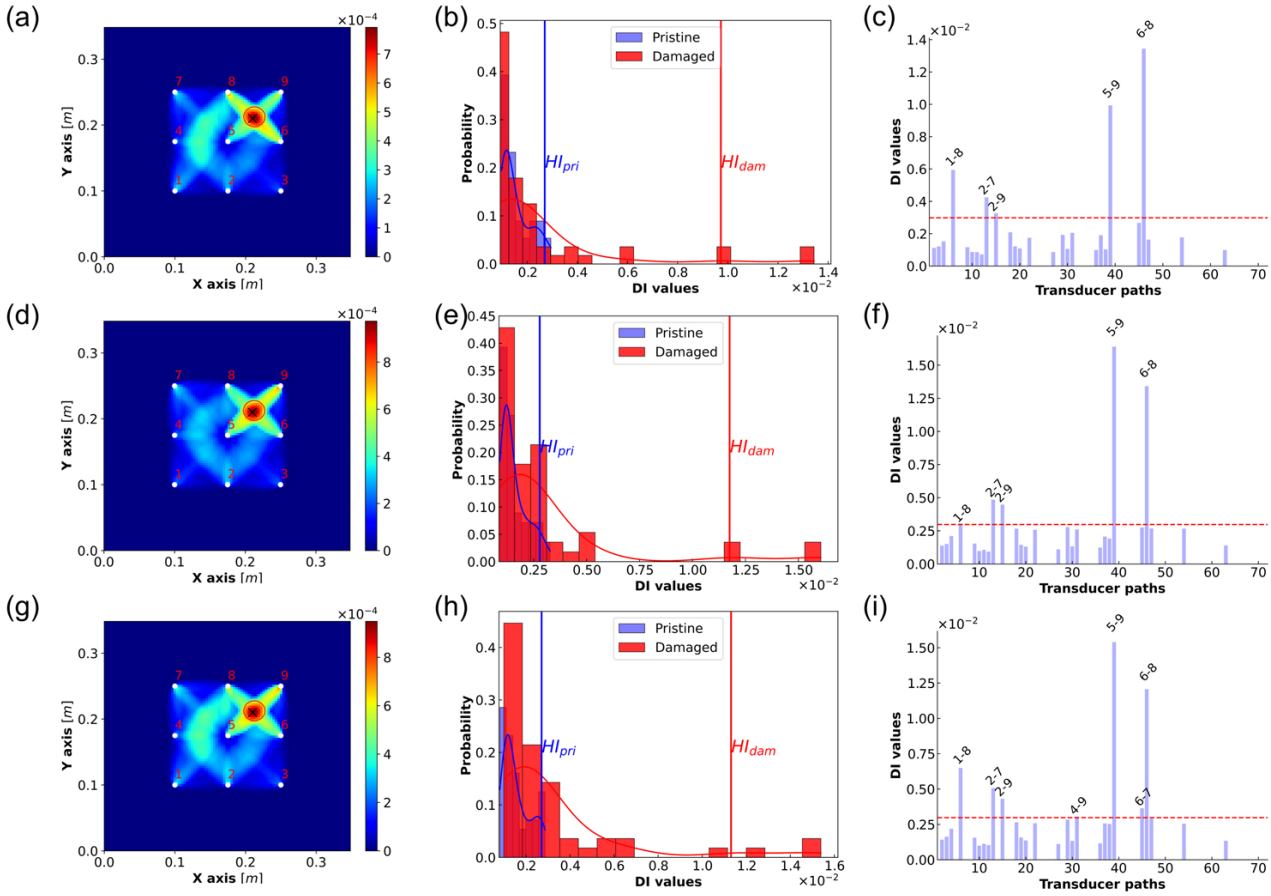


Figure 5.16: Detection and localisation of the single damage $D_1$ under 20°C, 25°C, 30°C (from top to bottom): (a, d, g) damage imaging map; (b, e, h) $DI$ distribution and (c, f, i) $DI$ histograms with reciprocal paths and indirect paths ignored.

Fig. 5.16 (a) shows the imaging result and the DI values when only the damage $D_1$ is im-

plemented. It is evident that the true damage area is identified and estimated against 10°C variations. Similar to the simulated damages, the $HI_dam$ is greater than the $HI_pri$ for different temperature levels and is able to capture the extreme DI values in the presence of damage. The DI histograms for all the transducer paths indicates that the damaged paths $2-9$, $5-9$, $6-8$ are identified under 10°C variations in spite of false alarms existing in specific paths $1-8$ and $2-7$.

Meanwhile, the localisation performance of the proposed method for the single impact damage is analysed in Table 5.3. It is reported that under 20°C to 30°C the damage is accurately estimated with the average trueness as 3.5 mm. Since the damage location is fixed during the monitoring process, positioning uncertainties of the damage are greatly alleviated and the zero S.E. values are yielded, suggesting high robustness of the damage location estimates with repeated measurements. Such result is further validated by the zero precision values under 10°C variations. In addition, when compared to reciprocity-based, IB and VTR techniques the proposed method yields comparable localisation accuracies under 10°C variations, as illustrated in Fig. 5.17.

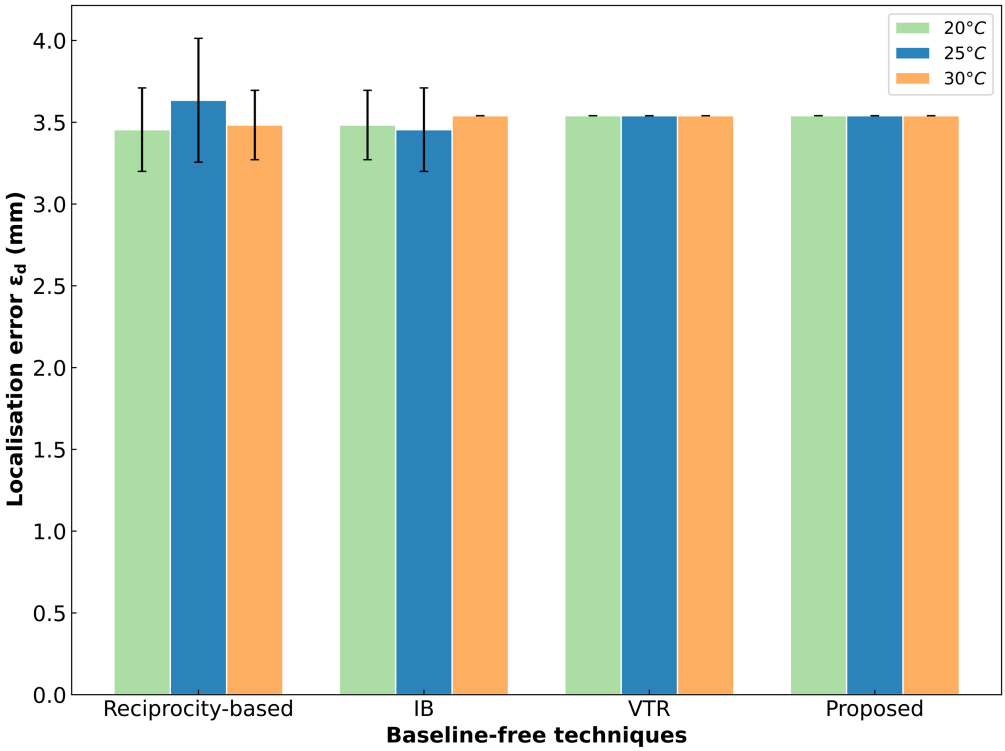


Figure 5.17: Comparisons between the IB, reciprocity-based, VTR and the proposed shapelet-based approach when localising single impact damages.

Table 5.3: Localisation results for single impact damages under temperature variations.

| Temperature °C | Trueness/mm | | Precision/mm$^2$ | |
|---|---|---|---|---|
| | Mean | S.E. | Mean | S.E. |
| 20 | 3.5 | 0.0 | 0.00 | 0.00 |
| 25 | 3.5 | 0.0 | 0.00 | 0.00 |
| 30 | 3.5 | 0.0 | 0.00 | 0.00 |

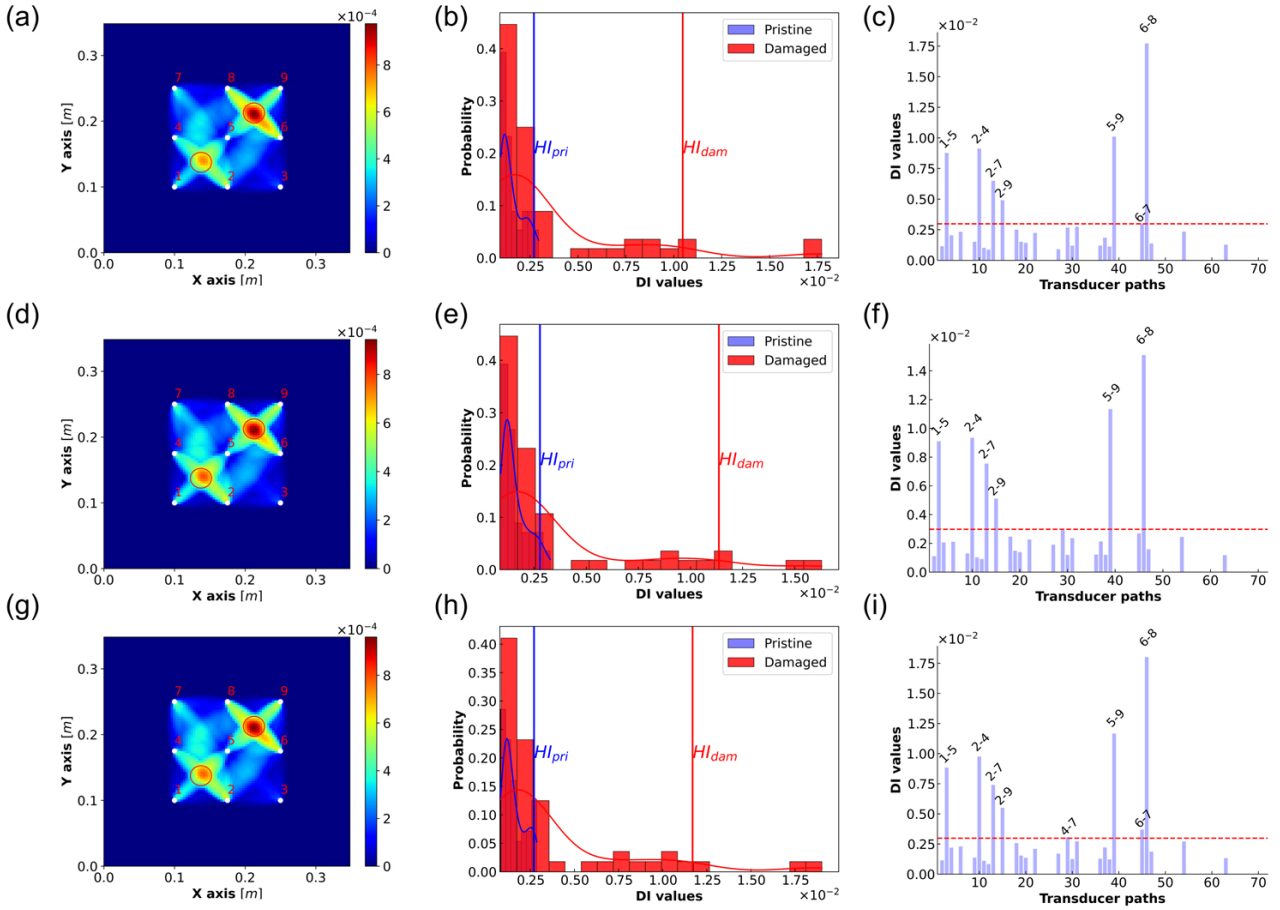


Figure 5.18: Dual damages $D_1$, $D_2$ under 20°C, 25°C, 30°C (from top to bottom): (a, d, g) damage imaging map; (b, e, h) $DI$ distribution and (c, f, i) $DI$ histograms with reciprocal paths and indirect paths ignored.

In terms of the dual impact damages $D_1$, $D_2$, Fig. 5.18 presents that such scenarios can be detected based on the $HI$s. The $D_1$ is identified by paths $5-9$, $6-8$ while $D_2$ is detected by paths $1-5$, $2-4$. Other critical paths are also unveiled including paths $2-7$ and $2-9$. Moreover, the $DI$ values for transducer paths remain stable under 10°C temperature variations.

### 5.5.3 SHM results considering boundary reflections

The proposed baseline-free technique is further utilised to detect and localise the 20 J BVID on the 300 mm × 225 mm CFRP coupon (see section 4.5.4), where the boundary reflected guided wave modes could interfere with an effective damage detection and localisation. In this section, the dispersion removal technique, as proposed in [229], is implemented to alleviate the adverse effect of boundary reflections while being integrated with the proposed reference-free method for the SHM purposes.

The dispersion removal aims to remove the dispersion and to enhance the interpretability and time domain resolution of ultrasonic guided wave signals. In this section the dispersion removal is utilised to pre-process guided wave measurements and is implemented based on the work by [229]. Consider an ultrasonic wave excited and propagating from an actuator to the corresponding sensor, and the starting point of wave propagation defined as $x = 0$, the ultrasonic wave excited at the actuator is formulated as [229]

$$f(t) = E_m(t)e^{i\omega_0 t} \tag{5.18}$$

where $f(t)$ represents the excited signal, $E_m(t)$ represents the modulated signal envelope and $\omega_0$ is the centre frequency of the excited signal. Afterwards, the Fourier transform of the incident wave is presented as

$$\mathcal{F}(\omega) = \int_{-\infty}^{\infty} f(t)e^{-i\omega t}dt \tag{5.19}$$

Integrating formula (5.1) and (5.19), a frequency component of the propagating wave at the distance $r$ can be formulated as [229]

$$f(t, r) = \frac{1}{2\pi}\int_{-\infty}^{\infty} \mathcal{F}(\omega)e^{i(\omega t - kr)}d\omega \tag{5.20}$$

where $k$ represents the wavenumber of the component at the frequency $\omega$. Furthermore, by combining (5.18) and (5.19), (5.20) can be formulated as follows [229].

$$f(t) = \frac{1}{2\pi}\int_{-\infty}^{+\infty} M\left(\omega - \omega_0\right) e^{i(\omega t - kr)}d\omega \tag{5.21}$$

where $M$ represents the Fourier transform of the $E_m$ in (5.18).

Meanwhile, regarding the dispersion relations between $\omega$ and $k$, the corresponding mathematical formulation is described as [229]

$$k = k_0 + k_1 (\omega - \omega_0) + o\left((\omega - \omega_0)^2\right) \tag{5.22}$$

where $k_0$ and $k_1$ represent coefficients in the first-order Taylor expansion. By inserting (5.22) into (5.21) and implementing the inverse Fourier transform, the higher order dispersion can be removed and finally the guided wave propagation after the dispersion removal is presented as follows [229].

$$\tilde{f}(t, r) = E_m (t - k_1 r) e^{i(\omega_0 t - k_0 r)} \tag{5.23}$$

Fig. 5.19 shows the effect of dispersion removal on 50kHz guided wave tone bursts which are collected from the 300 mm $\times$ 225 mm CFRP coupon at 20°C. Fig. 5.19 (a) demonstrates that the dispersion removal procedure can well isolate the first wave packet of $A_0$ mode and alleviate its overlapping with boundary reflections, as shown between the vertical dashed lines. Fig. 5.19 (b-c) validate that the implementation of dispersion removal can yield a finer time domain resolution of the first $A_0$ packet while suppressing the weak frequency component between dashed lines which corresponds to the signal overlapping with boundary reflections. Similar results of another example path $2-5$ are presented in Fig. 5.19 (d-f) where a more selective first wave packet with finer time resolution is distinguished from the subsequent boundary reflections after the dispersion removal.

However, for specific transducer paths the implementation of dispersion removal technique could suffer from the severe overlapping between first wave packets and boundary reflections. Regarding the path 1-2, Fig. 5.20 (a) indicates that the overlapped section between dashed lines fails to be separated and remains after the dispersion removal, which leads to a poor time-domain resolution of the dispersion-removed first wave packet in Fig. 5.20 (c). Similar results for path 5-7 are presented in Fig. 5.20 (d-f) where the dispersion removal procedure exhibits limited capability to decompose the overlapped section (between dashed lines) into separate wave packets.

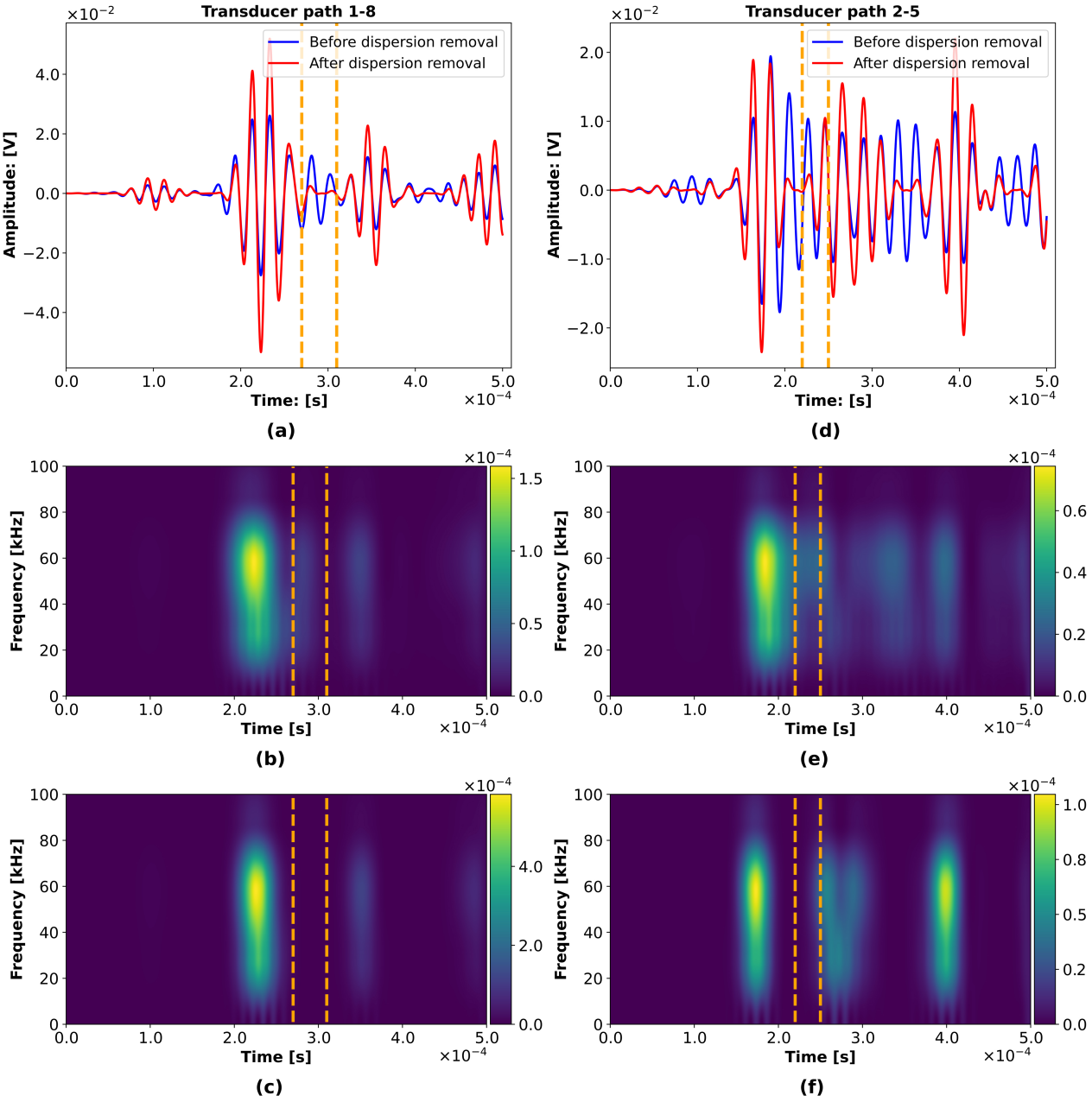


Figure 5.19: Dispersion removal on 50kHz guided wave tone bursts from the 300 mm × 225 mm CFRP coupon at 20°C : (a) signal from transducer path 1-8 before and after the dispersion removal; (b) time-frequency presentation of raw signal from path 1-8; (c) time-frequency presentation of dispersion-removed signal from path 1-8; (d-f) the corresponding results for path 2-5.

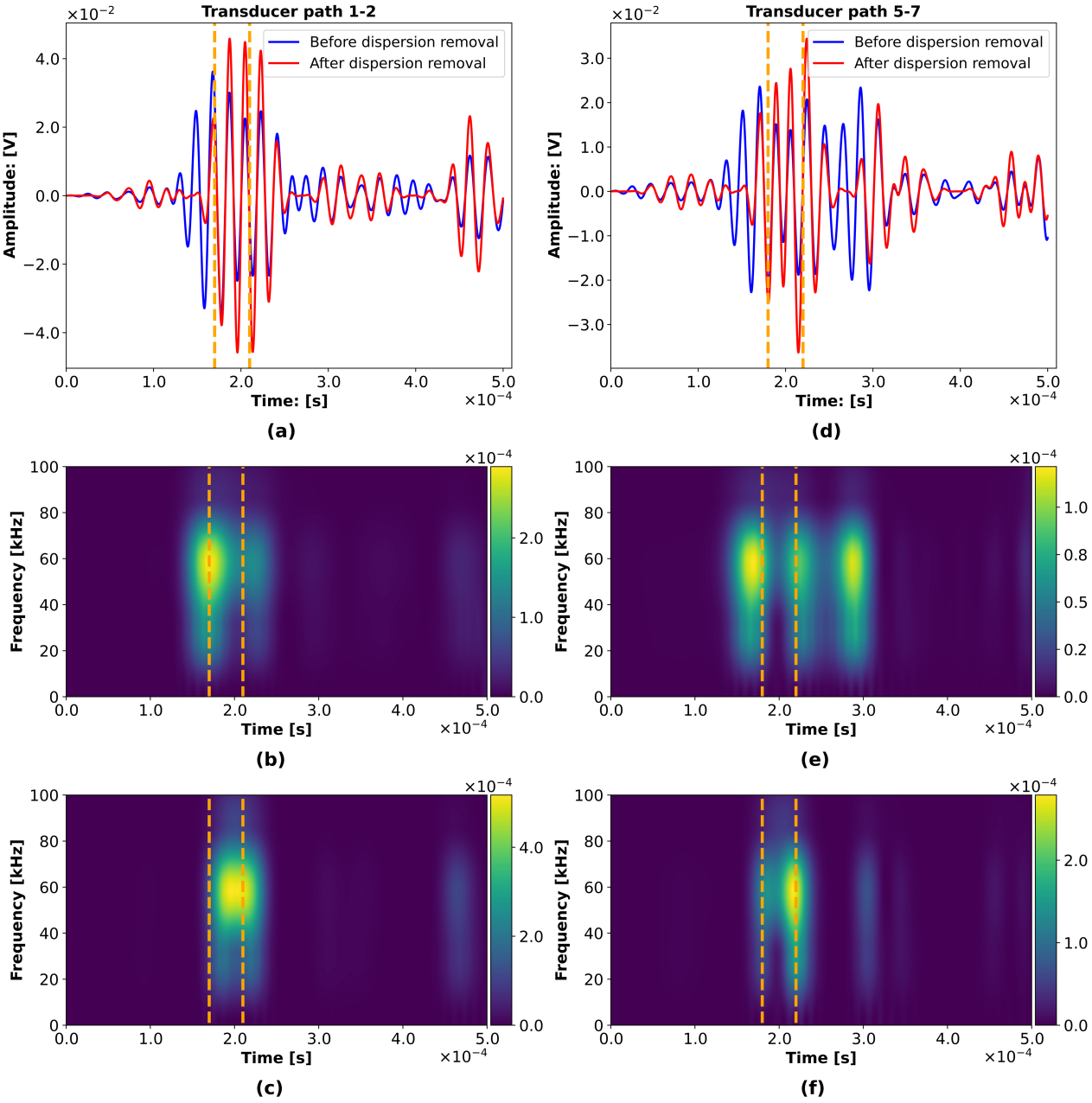


Figure 5.20: Dispersion removal on 50kHz guided wave tone bursts from the 300 mm × 225 mm CFRP coupon at 20°C : (a) signal from transducer path 1-2 before and after the dispersion removal; (b) time-frequency presentation of raw signal from path 1-2; (c) time-frequency presentation of dispersion-removed signal from path 1-2; (d-f) the corresponding results for path 5-7.

Fig. 5.21 demonstrates the performance of the proposed baseline-free technique for damage detection on the 20 J BVID at 20°C. As shown in Fig. 5.21 (a), the proposed technique fails to distinguish intact and damaged states with the only 50% accuracy and 0 true positive rate. This is likely due to the signal overlapping between first wave packets and boundary reflections, which could lead to a mismatch of dictionary atoms. Meanwhile, Fig. 5.21 (b) presents that the proposed reference-free method achieves improved damage detection performance when integrated with the dispersion removal procedure, yielding the detection accuracy and the false alarm rate as 97% and 7% respectively.

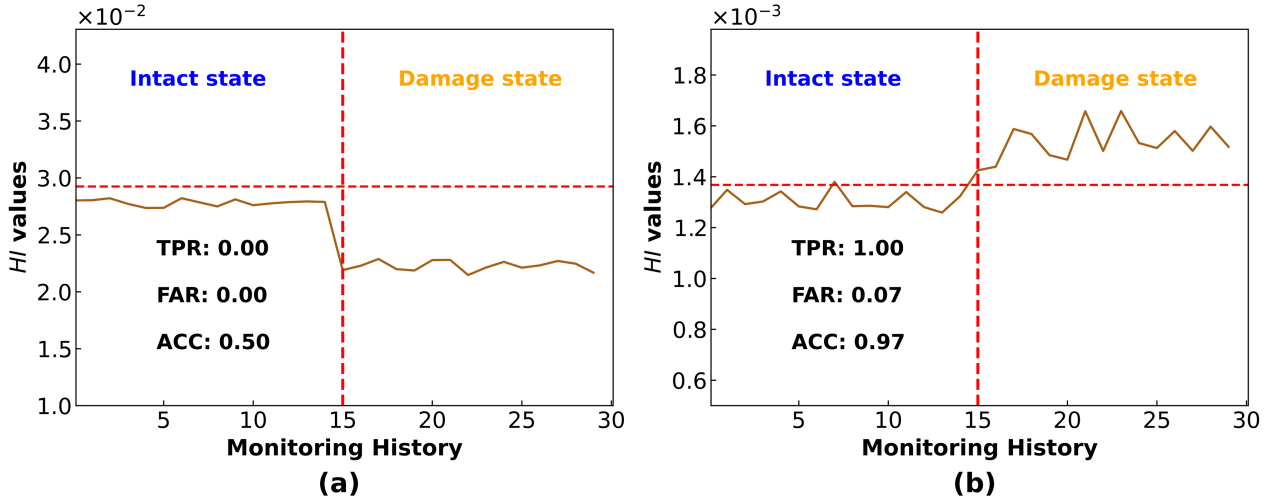


Figure 5.21: Damage detection results of the 20 J BVID at 20°C utilising the proposed baseline-free technique: (a) before dispersion removal; (c) after dispersion removal. The horizontal dashed line represents the calibrated detection threshold.

Fig. 5.22 presents damage imaging results of the 20 J BVID prior to and after the dispersion removal on guided wave measurements. When solely implementing the proposed reference-free method, the impact damage is unidentifiable with the DI values below the detection threshold, as illustrated in Fig. 5.22 (a, c). In contrast, Fig. 5.22 (b, d) shows that the implementation on the dispersion-removed signals lead to improved damage images where the BVID is localised within the identified damaged paths 1-7, 2-5, 4-6 with the localisation error as 35.7 mm, thus indicating the effectiveness of the dispersion removal as a signal pre-processing procedure to enhance capability of the proposed baseline-free technique for damage detection and localisation tasks. Nevertheless, there remains room to further improve the damage imaging result by alleviating imaging artifacts in the vicinity of transducer 4 and 7 .

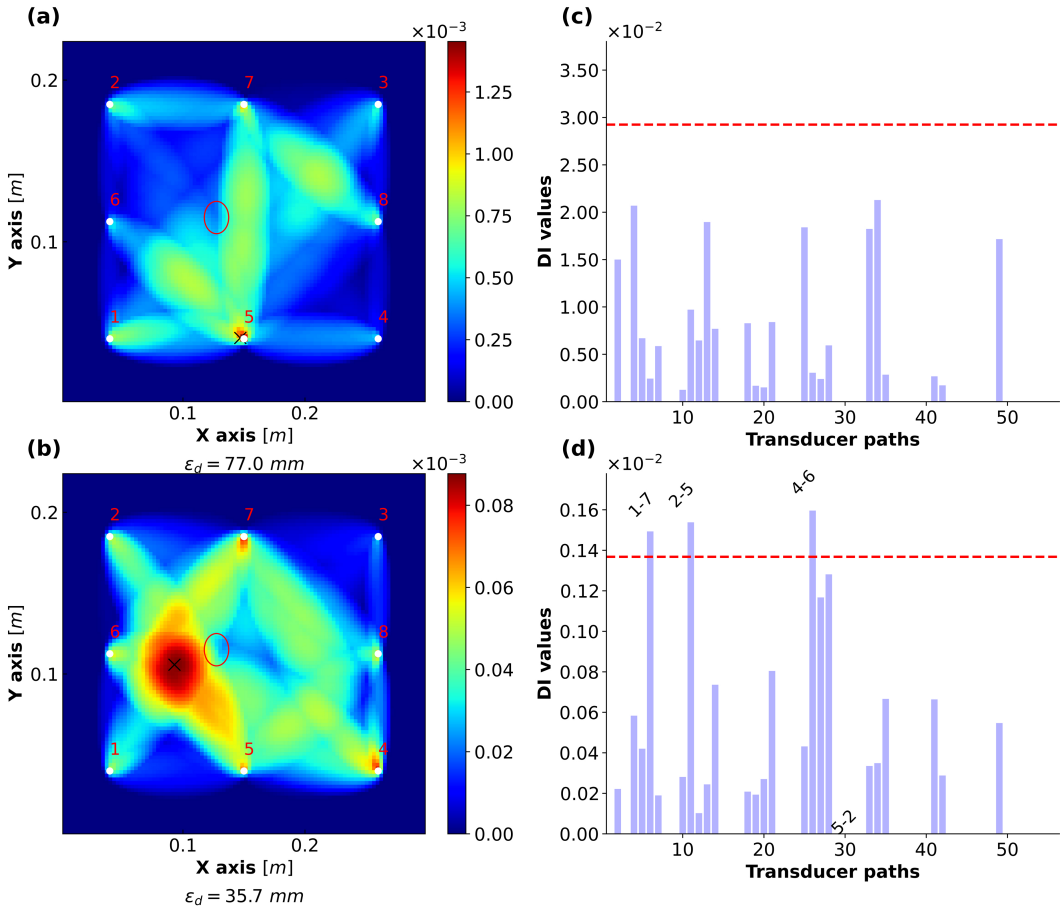


Figure 5.22: Damage localisation of the 20 J BVID at 20°C utilising the proposed baseline-free technique: (a, b) average damage images before and after dispersion removal respectively; (c, d) the corresponding damage index (DI) values with indirect reciprocal paths ignored. The horizontal dashed line represents the calibrated detection threshold.

### 5.5.4 SHM results considering structural complexities

The proposed baseline-free technique is validated on the stiffened CFRP panel case in section 4.5.4, where 30 intact and 30 damaged measurements are obtained and half of the intact measurements are utilised for calibrating the detection threshold. When detecting and localising the two impact damages on the stiffened panel, unsupervised shapelets are not only generated from the flat composite coupon (see Fig. 5.5), but also from an intact 475 mm × 250 mm $M21 - T800S$ mono-stringer element at 25°C, which is manufactured with a 30 mm high omega stiffener and the stacking layer sequence as $[\pm 45/0_2/90/0]_s$. More specifically, 10 and

11 shapelets are generated based on guided wave measurements from the flat coupon and the mono-stringer element, leading to the two shapelet-based dictionaries containing 510 and 561 atoms respectively. Following the BB approach, the dictionaries from coupon and element levels are fused to reconstruct signals from the sub-component level structure, i.e., the large-size stiffened panel. The composite structures with increasing levels of structural complexities are shown in Fig. 5.23.

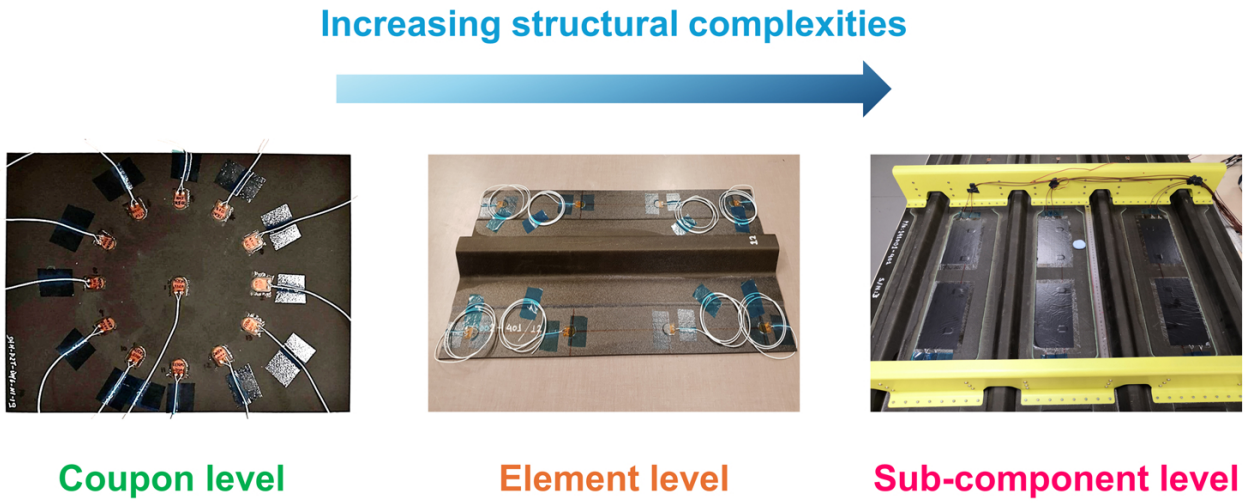


Figure 5.23: Composite structures with increasing structural complexities.

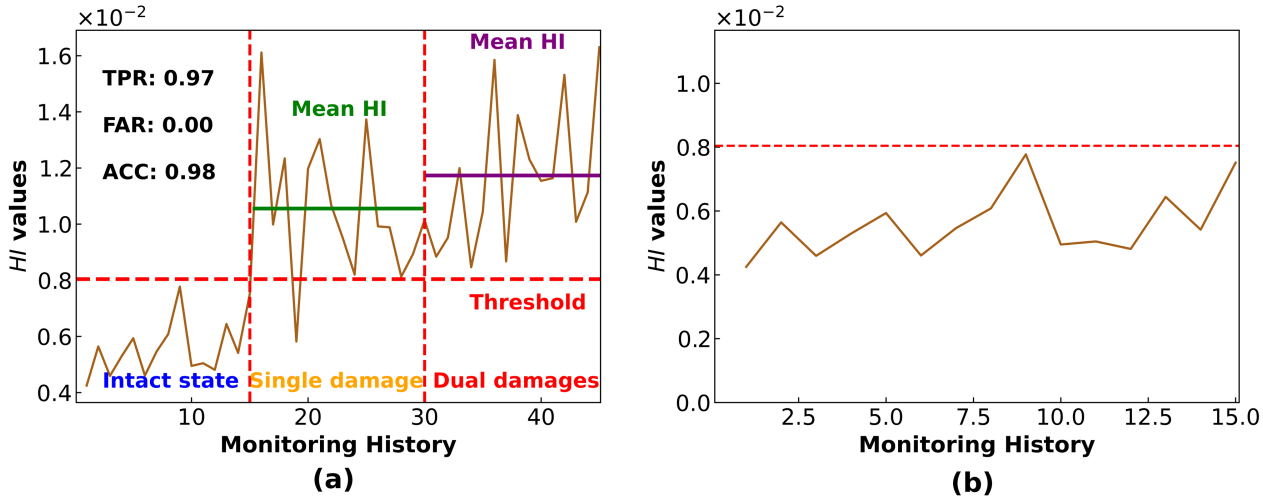


Figure 5.24: Damage detection results of impact damages on stiffened panel based on the proposed method: (a) the entire monitoring history; (b) the corresponding zoomed view under intact state.

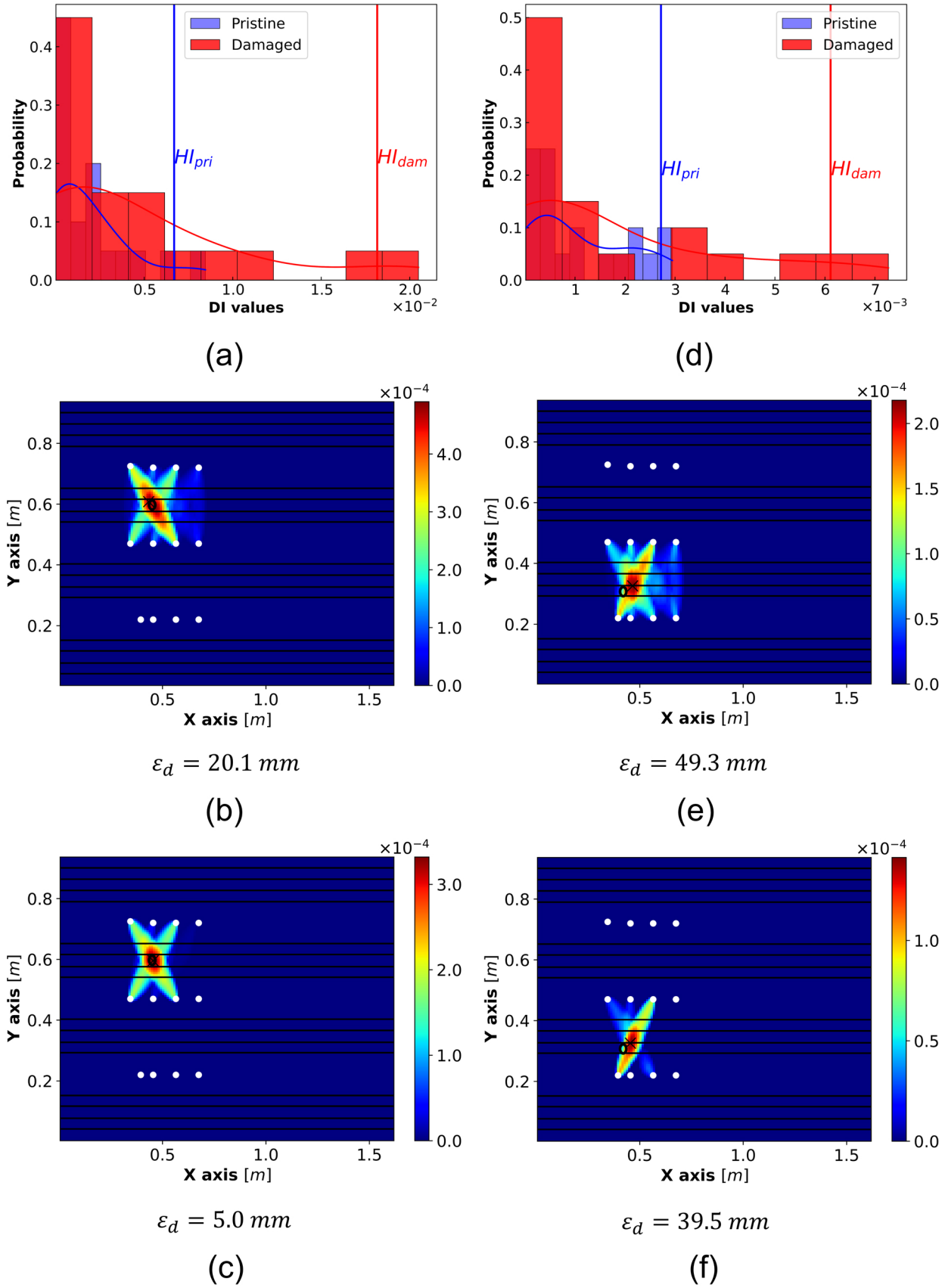


Figure 5.25: Damage detection and localisation of the stiffened panel based on the proposed technique: (a) the distribution of $DI$ values for the upper panel under intact and damaged conditions; (b) imaging of the first impact damage within the upper panel; (c) imaging of the first impact damage calibrated by intact measurements; (d-f) the corresponding results of the second impact damage within the lower panel.

Fig. 5.24 demonstrates the damage detection results of the stiffened panel utilising the fused shapelet-based dictionary. As shown from the figure, the proposed baseline-free technique is capable to distinguish between intact and damaged measurements, leading to the zero false alarm rate and 98% detection accuracy. It is also presented that the average HI value (in coloured horizontal lines) slightly increases after the second impact damage is implemented at the stiffener foot of the panel. The limited capability of the proposed approach to detect the second impact damage could be due to the mixing of damage scattering, mode conversion and reflection of guided waves at the stiffener foot [253], which leads to irregular signal distortions and consequently the mismatch of shapelet-based dictionary atoms. Further investigations are required to alleviate such issue and enhance the detection capability of the proposed method.

Fig. 5.25 demonstrates the results of damage detection and localisation on the two impact damages which are located within the upper and lower part of the stiffened panel respectively. The detection of the local impact damages is implemented separately on the upper and lower panel. Fig. 5.25 (a) indicates that the first 20 J impact damage is clearly identified within the upper panel and leads to an increased $HI$ compared to the intact state. Fig. 5.25 (b) shows that the proposed baseline-free technique is capable to localise the first damage with 20.1 mm error. After the calibration with intact measurements, the first damage is localised with 5.0 mm error and alleviated imaging artifacts, as illustrated in Fig. 5.25 (c). Meanwhile, Fig. 5.25 (d-f) shows that the second 35 J impact damage is identified and localised with the errors as 49.3 mm and 39.5 mm prior to and after the calibration with intact signals. Nevertheless, the severity of the second damage, as presented in Fig. 5.25 (e-f), is inconsistent with the impact energy, and therefore warrants further investigations in damage quantification.

In this work, the generation of shapelet-based dictionary is essential for reconstructing guided wave measurements. As shown below, three different strategies for the dictionary generation are investigated based on shapelets from the flat coupon (Strategy A), mono-stringer element (Strategy B), and the fusion of both (BB approach) respectively.

- Strategy **A**: dictionary generation based on shapelets of coupon level;
- Strategy **B**: dictionary generation based on shapelets of element level;
- **BB** approach: dictionary generation fusing shapelets of coupon and element levels.

During the investigation, the standard root mean square error (RMSE) between the guided wave measurement and its reconstructed counterpart is utilised to assess the signal reconstruction performance of the proposed method when adopting different shapelet-based dictionaries. The RMSE metric is formulated as follows.

$$RMSE_i = \sqrt{\frac{1}{N}\sum_{k=1}^{N}\left(\boldsymbol{R}_{i,k} - \widehat{\boldsymbol{R}_{i,k}}\right)^2} \tag{5.24}$$

where $\boldsymbol{R}_{i,k}$ and $\widehat{\boldsymbol{R}_{l,k}}$ represent the $k$-th sampling point of the guided wave signal and the reconstructed counterpart, respectively, from the $i$-th transducer path, and $N$ represents the length of $\boldsymbol{R}_{i,k}$ and $\widehat{\boldsymbol{R}_{l,k}}$.

Table 5.4: Signal reconstruction performance and damage localisation accuracy of the proposed technique utilising the three dictionary generation strategies.

| Number of atoms | Average RMSE | | | Average localisation errors /mm | | | | | |
|---|---|---|---|---|---|---|---|---|---|
| | | | | Damage 1 | | | Damage 2 | | |
| | Strategy **A** | Strategy **B** | **BB** | Strategy **A** | Strategy **B** | **BB** | Strategy **A** | Strategy **B** | **BB** |
| 5 | 0.97 | 0.97 | 0.97 | 28.1 | 28.1 | 28.1 | 68.4 | 61.7 | 61.7 |
| 10 | 0.54 | 0.50 | 0.50 | 28.1 | 27.5 | 27.5 | 61.7 | 56.7 | 56.7 |
| 20 | 0.30 | 0.27 | 0.27 | 21.0 | 21.0 | 21.0 | 59.5 | 49.3 | 49.3 |
| 40 | 0.17 | 0.16 | 0.16 | 20.1 | 20.1 | 20.1 | 49.3 | 49.3 | 49.3 |
| 60 | 0.15 | 0.15 | 0.15 | 20.1 | 20.1 | 20.1 | 49.3 | 49.3 | 49.3 |

Table 5.4 compares the signal reconstruction performance and the damage localisation accuracy of the proposed baseline-free technique based on different shapelet-based dictionaries. During the comparison, varying number of dictionary atoms are employed to reconstruct guided wave measurements and the corresponding results are listed in the table. It is shown that the average RMSE value of all the transducer paths reaches 0.97 when utilising only 5 atoms from different dictionaries, together with localisation errors of the two impact damages as 28.1 mm and 61.7 mm based on the BB approach. The average RMSE value greatly decreases with the

increasing number of atoms devoted to the signal reconstruction until the number of atoms reaches 40, where the average RMSE remains steadily within 0.16-0.17 and the localisation errors are 20.1 mm and 49.3 mm respectively for the two impact damages.

Furthermore, Table 5.4 indicates that the dictionary based on shapelets from monostringer elements (Strategy **B**), compared to the flat coupon case (Strategy **A**), can lead to up to 10% reduction in the average RMSE and the improvement of damage localisation accuracy as up to 10.2 mm when utilising varying number of atoms for the signal reconstruction and damage localisation purposes. This result implies that the dictionary based on the mono-stringer element can better capture and reconstruct guided wave signals from the stiffened panel when given limited number of dictionary atoms for signal reconstruction, considering the element-level structure and the stiffened panel share similar structural complexities. Meanwhile, it is presented that the fusion of dictionaries (BB approach) maintains the performance of the element-based dictionary and achieves lower RMSE and localisation errors than singly utilising the coupon-based dictionary, which represents lower structural complexities. The discrepancies in the RMSE and localisation errors utilising the different dictionaries are alleviated when the number of atoms exceed 40, which could be attributed to a finer combination of sufficient shapelet-based dictionary atoms to interpret the structural complexities.

## 5.6 Summary

A novel baseline-free technique for guided wave based damage detection and localisation on composite structures is presented in this chapter. The method employs unsupervised shapelets and shift-invariant dictionary learning to reconstruct a virtual baseline for monitored structures. This is achieved by extracting and transferring shapelets from an intact coupon which can differ with the monitored structure with regard to specimen size, stacking layers, sensor configuration, and monitoring temperature. Damage detection and localisation are then implemented based on deviations between the current and the reconstructed signals.

Following the rationale of the BB philosophy, the proposed baseline-free technique is also capable to reconstruct current measurements of a stiffened composite panel utilising an over-

complete dictionary which is generated by shapelets from a flat composite coupon and a mono-stringer element.

The results demonstrate that the proposed method exhibits high detection capability for the coupons, even in the presence of temperature variations of 20°C. It also demonstrates accurate and temperature-robust performance in localising single damages. Moreover, the proposed method yields comparable localisation accuracies to other baseline-free techniques, particularly the IB, reciprocity principle, and VTR under varying temperatures. Nevertheless, perfect isolation of damage might be challenging for dual damage cases, especially when the damages are adjacent.

This chapter further applied the proposed baseline-free method to the detection and localisation of the BVIDs on a large-size stiffened panel, which includes higher structural complexities than the flat coupon. The findings indicate that the proposed method can still detect and localise impact damage, albeit with increased localisation errors. Moreover, the performance of the shapelet-based technique may degrade when potential damage is located near the stiffener foots, which is likely due to signal distortions caused by guided wave reflection, transmission, and mode conversion.

Meanwhile, it is validated in the case of stiffened panel that the BB approach, i.e., the fusion of dictionaries representing different structural complexities, can lead to better signal reconstruction performance and damage localisation accuracy than simply employing the coupon-based dictionary with lower structural complexities. Nevertheless, such disparity can be alleviated when sufficient number of dictionary atoms are employed to reconstruct guided wave measurements, which could lead to a better interpretation of the structural complexities.

# Chapter 6

# A data-driven approach for failure prognostics of engineered structures

## 6.1 Introduction

Following the damage detection and localisation in previous chapters, this chapter focuses on the higher-level failure prognosis, i.e., remaining useful life (RUL) prediction, of aircraft components with particular emphasis on the aircraft turbofan engine. In spite of recent contributions there remain several unsolved challenges towards an accurate RUL prediction of engineered structures. Firstly, the modelling of real-time environmental and operational condition (EOC) and its effect on the RUL of engineered systems, including their individual subsystems and components, have not been conclusively addressed. Furthermore, there may exist interdependencies particularly mutual causal relationships from a statistical perspective, between monitoring signals that were measured by sensors arranged in different sub-systems or components. These may, to some extent, reflect how failures of the engineered systems propagate inside these systems. It follows that such information related to the potential failure mechanism can be valuable for an efficient and effective model to be established with high accuracy in so far as it identifies the critical factors having an impact upon the reliability prediction. Nevertheless,

[1]A large portion of this chapter appears in Hongmin Zhu. (2021) [36]

there has been little research investigating the interdependencies between different parts of the engineered systems under real-life conditions based on monitoring sensor signals which can define information regarding the potential failure mechanism that would usefully be integrated into the reliability modelling of the engineered systems. Recently the standard graph neural network (GNN) [280] and the graph convolutional network (GCN) [281] have been employed for the failure prognostics to model monitoring signals into undirected graphs [280, 281]. However, such deep learning model could suffer from high computational costs and limited capability to interpret cause-effect mechanisms between multiple sensor signals [282].

In this regard, this chapter proposes a hybrid data-driven technique integrating the Cox proportional hazards model (Cox PHM) [283] and the vector autoregressive model with exogenous variables (VARX) [284] for the prediction of degradation behaviour and the RUL of engineered systems under time-varying EOCs. The Cox PHM model generates reliability indices of turbofan units while the VARX model is employed to associate the reliability indices with real-time sensor signals and time-varying EOCs for degradation modelling of turbofans. During the VARX modelling, the pairwise conditional Granger causality (CGC) [285] test is implemented to reveal statistical causal relationships between multiple sensor signals and identify critical sensors for feature selection. The proposed method is validated on the Commercial Modular Aero-Propulsion System Simulation (C-MAPSS) [286] dataset and outperforms several benchmarks regarding prediction accuracy of the RUL.

The remainder of the chapter is organised as follows. Section 6.2 reviews data-driven techniques for failure prognostics with particular emphasis on the related Cox PHM and the vector autoregressive (VAR) models. Section 6.3 introduces the proposed hybrid data-driven technique for RUL prediction while section 6.4 presents results and discussions on the C-MAPSS dataset. Conclusive remarks are drawn in section 6.5.

## 6.2 Literature review

### 6.2.1 Vector autoregressive model for failure prognostics

Recently the vector autoregressive (VAR) model has been applied to failure prognostics considering its competence to model and forecast multiple sensor signals as multivariate time series.

In this realm, Li et al. [287], Zhao and Gao [288], and Han et al. [289] employed principal component analysis (PCA) and the VAR for feature extraction and prognostics of faults, respectively. Hochstein et al. [290] proposed a generic framework based on a regime switching Bayesian VAR model for prognostics, while Zheng et al. [291] combined the VAR and Granger causality (GC) tests together, a technique that had previously been commonly utilised in econometrics. With this combination, they developed a method to detect and predict computer failures. Moreover, Zheng et al. [291] constructed a topological causal network to make a preliminary investigation of the failure mechanism of computer software. Meanwhile, those papers, except Zheng et al. [291], only employed the VAR model as a multivariate tool for diagnostics or prognostics in an engineered system, without further investigating the relationships between different subsystems or components and potential cause–effect failure mechanisms of the system, which can, to some extent, be reflected in the statistical causal relationships (e.g., by means of the GC test) between sensors arranged in different subsystems or components.

In spite of the potential that the VAR has to integrate external EOCs (e.g., ambient temperature, humidity, and operational conditions) into reliability modelling to predict the reliability function and the RUL of the engineered systems, such conditions are not considered in most published publications that are related to the VAR applied to reliability engineering. Although environmental conditions were considered in [287], they were only considered to be endogenous variables rather than exogenous variables, thus potentially causing a misspecification of the statistical model that was built in the research. Actually, the environmental or operational conditions considered to be exogenous factors usually have considerable influence on the engineered systems, including aircraft structures [292], civil infrastructure systems [293], and manufacturing systems [81]. In this regard, the VARX model is worth further investigations which extends the standard VAR model by integrating the EOCs as exogenous variables for failure prognostics.

### 6.2.2 Survival analysis combined with sensor signal forecasting

Recently the survival analysis technique has been combined with sensor signal forecasting techniques, which, to a large extent, reflect the real-time performance of the engineered systems

to yield a real-time estimate of the reliability functions of the engineered systems. Refs. [104,107] employed the Kaplan–Meier estimation and support vector machine (SVM) for prediction of the RUL and the reliability function of engineered systems while Tran et al. [97] employed the Cox PHM with time dependent covariates and the SVM for the same purpose. In addition, Du et al. [294] employed the VAR model to predict covariates and then utilised the Cox PHM model to predict the conditional reliability function and the RUL that is based on prediction of covariates. Wen et al. [295] integrated the neural networks (NN) and the Cox PHM model for the RUL prediction of gas turbine engines, which considers nonlinear interactions between sensor signals and system reliability. However, during the online prediction of the RUL and system reliability, the covariates, namely both the sensor signals and the EOCs, may have time-lagging effects on the system reliability and RUL prediction, and such time-lagging effects have rarely been considered in the previous research. In this work, the time-lagging effects of covariates on system reliability are modelled by the proposed method combining the Cox PHM and VARX models, where the reliability function is considered dependent on time-lagged covariates.

## 6.3 Methodology

### 6.3.1 Research framework

In this chapter, the RUL prediction is implemented for a test set of turbofan engines based on a training set of turbofans with complete failure records. A schematic sketch of the proposed algorithm for the RUL prediction is shown in Fig. 6.1. As shown in this figure, in offline training stage the Cox PHM model considering time-varying covariates is employed to generate reliability indices for different individual failure records after data pre-processing. Regarding the training set units, the generated reliability indices are modelled by means of the VARX together with the critical sensor signals with reduced dimension selected by the pairwise conditional Granger causality (CGC) test which takes the influence of environmental or operation conditions into consideration. The built VARX model is competent to model the dynamic time-lagging influence of the sensor signals as endogenous variables and other exogenous variables, namely the

time-varying operational conditions, on the reliability index. In terms of online prediction stage, reliability indices of the incomplete online records in the test set are generated by means of the Cox PHM with time varying covariates for further similarity matching with reliability indices generated from the training set at the offline stage. Afterwards the trained VARX models based on offline failure records in the training set which are most similar to the incomplete records in the test set will be employed to predict future values of reliability indices of the incomplete online records and the corresponding RUL with a pre-defined threshold. During the online prediction stage, the Fourier grey model (FGM) [296] is utilised for predictions of external operational conditions in the incomplete data records, which may have small sample size, to update the online prediction. The detailed information is described as follows.

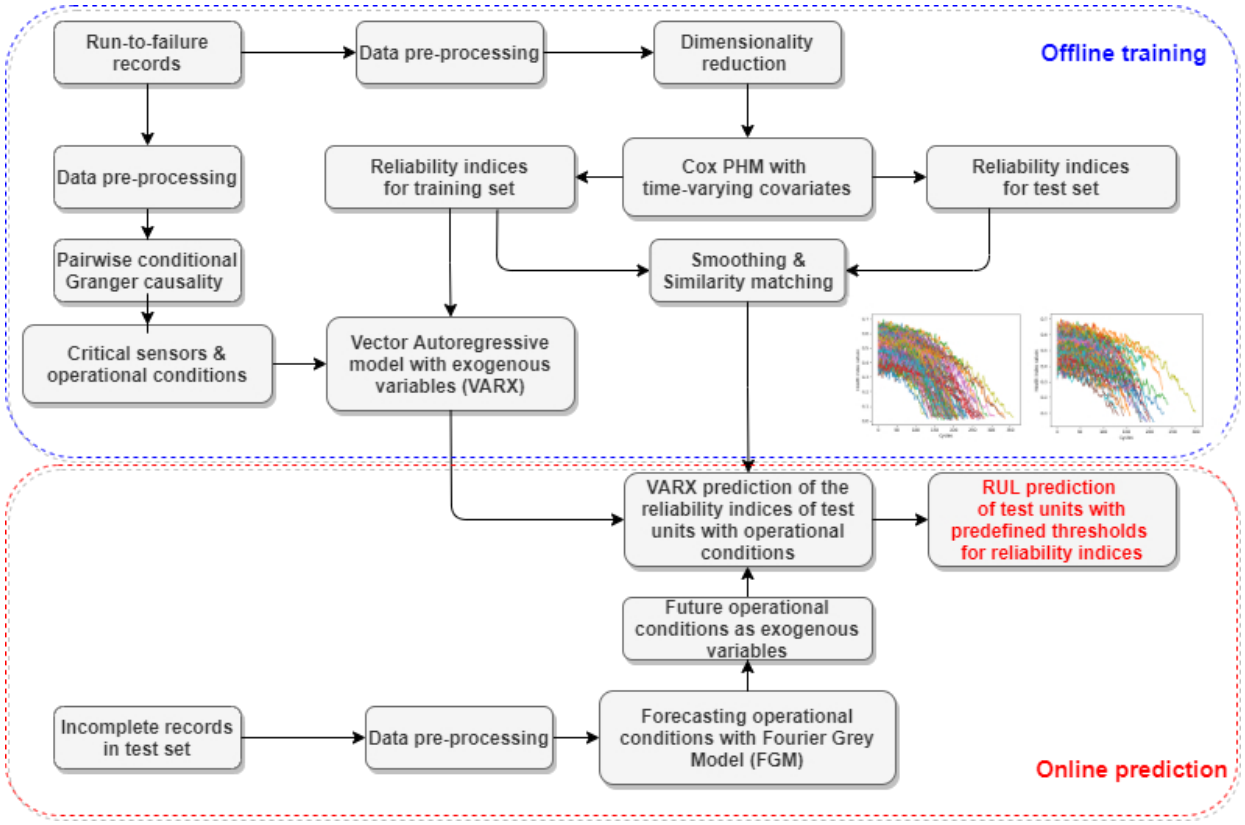


Figure 6.1: Schematic sketch of the algorithm proposed in this research. [36]

### 6.3.2 Cox proportional hazards model with time-varying covariates

In this chapter the Cox proportional hazards model (Cox PHM) is employed to generate reliability indices of turbofan units based on sensor signals and time-varying EOCs. Since

being proposed in 1972 by Cox [283], the Cox PHM has been regarded as a powerful tool in the field of survival analysis and has been widely employed in other fields, e.g. medical research [297], economics [298] and reliability engineering due to its competence to model the impact of covariates on the survival probability or the reliability of a specific system. In the framework of the standard Cox PHM, the hazard function considering a certain set of time-invariant covariates can be expressed in the following formulae [283].

$$h(t|x) = h_0(t) \exp(w^T x) \tag{6.1}$$

where $h(t|x)$ represents the hazard function considering the influence of time-invariant covariates, $h_0(t)$ represents the baseline hazard function which can be estimated by Kaplan-Meier estimation, $x$ and $w$ represent the covariates and the coefficients of the covariates respectively. Correspondingly, the survival function or the so-called reliability function considering time-invariant covariates can be further calculated as shown in (6.2).

$$R(t|x) = \exp(-H(t|x)) = \exp(-\int_0^t h(u|x)du) = \exp(-\int_0^t h_0(u)du) \exp(w^T x) \tag{6.2}$$

where $R(t|x)$ represents the reliability function considering the influence of covariates, $H(t|x)$ represents the cumulative hazard function, and $t$ represents the time during the failure process of an engineered system.

However, in the field of the reliability engineering with particular emphasis on the failure prognostics, the conventional Cox PHM model assuming its covariates are time-invariant are not intuitively perceivable in the practical sense. The main reason for this lies in that the covariates namely the sensor signals and the external environmental and operational conditions are time-dependent in this case. Accordingly, the reliability function considering time-dependent covariates is shown in (6.3).

$$R(t|x) = \exp(-\int_0^t h(u|x)du) = \exp(-\int_0^t h_0(u) \exp(w^T x(t))du) \tag{6.3}$$

where $x(t)$ represents the covariates dependent on the time $t$ and other items remain the same with those in (6.2). Furthermore, the time-dependent covariates can be further classified into the time varying covariates and covariates with time varying coefficients [299] where in the latter case the covariates themselves are assumed to be fixed but their influence on the system reliability is time-varying. In this chapter, the Cox proportional hazards model (Cox PHM) with time-varying covariates is established to generate the reliability indices of both the run-to-failure records in the training set and the incomplete right-censored failure records in the test set. Please note that it is theoretically difficult to directly generate reliability functions as the reliability indices of both the training set and the test set for comparison considering the right-censoring of the test set [299]. In this regard, an exponential relative hazards function $I(t|x)$ in the form of $\exp(w^T x(t))$ as shown in (6.4) is proposed as reliability index for both the training set and the test set. The proposed reliability index are able to reflect the dynamic influence of the time-varying covariates on the system degradation behaviour prior to failure.

$$I(t|x) = \exp(-\exp(w^T x(t))) \tag{6.4}$$

### 6.3.3 Similarity matching of generated reliability indices

The essential idea of the similarity matching is to match the reliability indices of the test turbofan units with their corresponding training set units which have similar degradation trends based on the Euclidean distance [300]. Such procedure enables a fast and efficient RUL prediction based on historical failure records in the training set. In this work, the similarity-based matching is implemented between reliability indices of the training set units and the test set units, which are generated by the Cox PHM with time-varying covariates. A diagram employed to illustrate the similarity matching process is shown in Fig. 6.2.

According to Wang et al. [300], the distance between two curves of reliability indices is calculated utilising an Euclidean measure, which is shown in (6.5).

$$d(I^i, I'^j) = \left(\frac{1}{T_j}\sum_{m=1}^{T_j}({I_m}^i - {I'_{m+\tau}}^j)^2\right)^{\frac{1}{2}} \tag{6.5}$$

where $I^i$ and $I'^j$ represent the reliability indices of the training set $i$ and the test set $j$ respectively, $T_j$ is the length of the real-time reliability indices of the test set $j$, $\tau$ represents the time-lag between the reliability indices of the test units and the indices of the training units. Similar to [301], the maximum time lag is set as 30 to prevent mismatching between the reliability indices and to save the high computational cost.

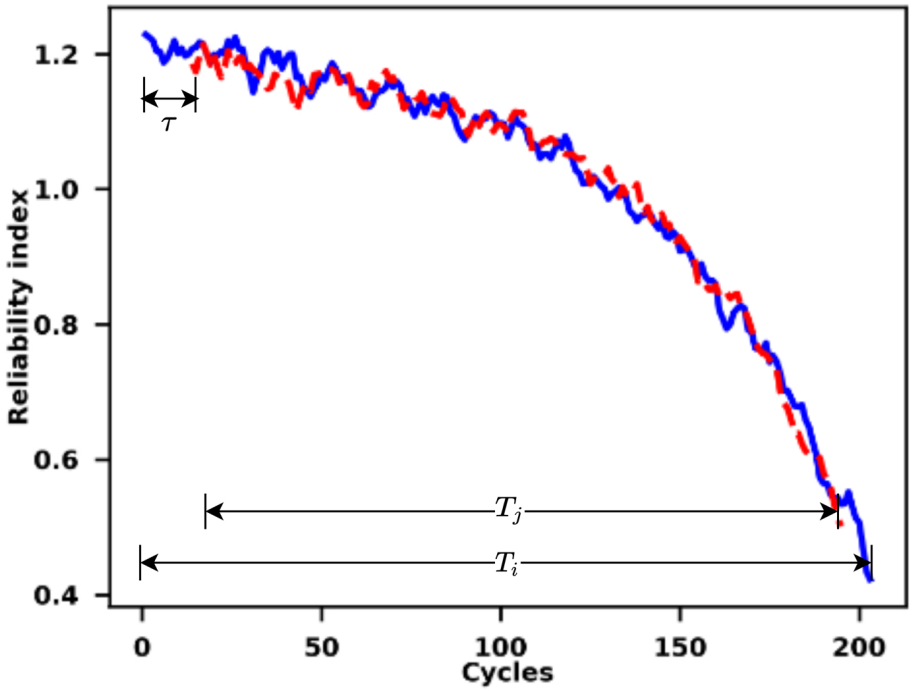


Figure 6.2: Illustration of the similarity matching process of reliability indices. [36]

Furthermore, the similarity between the reliability indices can be calculated by (6.6) [302].

$$Similarity(I^i, I'^j) = \exp\left(-\frac{d^2(I^i, I'^j)}{\lambda}\right) \tag{6.6}$$

where $\lambda$ is relaxing parameter which is set as 0.002 [302].

For a specific matching between the unit $i$ in the training set and the unit $j$ in the test set, the RUL of the test unit $j$ based on the training set $i$ considering the time lag $\tau$ is calculated by (6.7).

$$RUL_j{}^i = T_i - T_j - \tau \tag{6.7}$$

where the $T_i$ is the length of the reliability indices of the run-to-failure training set $i$.Afterwards the overall RUL of the test unit $j$ is calculated by the average of the RULs based on a set of

training units which have the largest similarities with the test unit $j$ in terms of their reliability indices, which is shown as (6.8).

$$RUL_j = \frac{1}{N} \sum_{i \in G} {RUL_j}^i \tag{6.8}$$

where $RUL_j$ is the overall RUL of the test unit $j$ and $G$ represents the group containing the training units whose reliability indices have the largest similarities with the reliability index of the test unit $j$. $N$ is the size of the group $G$ and is set as 5 in this chapter to avoid the high computational cost. Meanwhile, considering the uncertainties when matching similarities between a test unit with short and right-censored records and a training unit with run-to-failure records, the restriction of the maximum RUL for all the test units is set as 150 [303, 304].

In this chapter, the results obtained by the similarity matching will not be directly used for the RUL prediction. The reason for this is that the typical similarity matching algorithm assumes that the future degradation trajectory of the incomplete records including the future variations of the external operational conditions can be calculated by the degradation trajectories of several offline run-to-failure records which are most similar to the incomplete data records to be predicted with the RUL. In other words, the variations and uncertainties of the future operational conditions for the incomplete data records are ignored in the typical similarity matching algorithm. To address this problem, the similarity matching algorithm is employed here only to generate the reliability indices of both the offline run-to-failure records and the incomplete records for online prediction of the RUL. The results obtained by the similarity matching in this chapter mainly the matched failure records and some critical parameters including $T_i$,$T_j$ and $\tau$ will be utilised by the VARX model described as follows for further online prediction of the RUL for the incomplete data records.

### 6.3.4 Vector autoregressive models with exogenous variables (VARX)

The VARX model is utilised to associate the generated reliability index with real-time sensor signals and EOCs for the online RUL prediction of turbofan engines. As a natural extension of the vector autoregressive (VAR) model that enables the integration of the information provided

by exogenous variables into such models, the VARX model [284, 305] is of the following form.

$$\boldsymbol{Y}_t = \alpha + \sum_{i=1}^{p} \phi_i \boldsymbol{Y}_{t-i} + \sum_{j=1}^{q} \beta_i \boldsymbol{X}_{t-j} + \epsilon_t \tag{6.9}$$

As shown in (6.9), $\boldsymbol{Y}$ represents a $k$-dimensional vector of time series as endogenous variables, $\boldsymbol{X}$ represents an $n$-dimensional vector of time series as exogenous variables. $\alpha$ denotes the constant term of the VARX model. $\epsilon_t$ represents the independent identically distributed (IID) residuals of the VARX model. $p$ and $q$ are denoted as the order of time lags for modelling endogenous variables and exogenous variables respectively, which can be determined by means of the AIC, BIC and the RMSE criteria in section 3.2. In this chapter, the AIC is deployed to determine the order of the VARX model [306]. $\phi_i$ represents the coefficient matrices in front of the endogenous variables with dimension $k \times k$ and is estimated by means of the ordinary least squares (OLS) technique. Similarly, $\beta_i$ represents the coefficient matrices in front of the exogenous variables with dimension $k \times n$.

In this work, the vector autoregressive model with exogenous variables, namely the VARX model, is employed to associate the reliability indices of heterogeneous individual units which are previously generated by means of the Cox proportional hazards model (Cox PHM) considering time-varying covariates with the real-time monitoring signals of these units to model and analyse the real-time influence of the time-varying sensor signals and external conditions namely the operational conditions in the case of the C-MAPSS data set on the variations of the generated time-varying reliability indices of individual units. More specifically, according to (6.1) and (6.9),if the time-lagging effects of covariates including the operational conditions in this case are considered, then the hazard function at a time point $t$ can be obtained as follows.

$$h(t|x) = \alpha' + \sum_{i=1}^{p} \gamma_i h(t-i|x) + \sum_{i=1}^{p} \phi_i{}' \boldsymbol{Y'}_{t-i} + \sum_{j=1}^{q} \beta_i{}' \boldsymbol{X}_{t-j} + \epsilon_t{}' \tag{6.10}$$

where $h(t|x)$ represents the hazard function at time $t$ in (6.1) which is also an endogenous variable in the VARX model, $p$ and $q$ represent the order of time lags for modelling endogenous variables and exogenous variables respectively, $\boldsymbol{Y'}$ represents the endogenous variables excluding the $h(t|x)$, namely the sensor signals,$\boldsymbol{X}$ represents the exogenous variables namely

the operational conditions in this work. In (6.10), $\gamma_i$,$\phi_i{}'$ and $\beta_i{}'$ represent the coefficients to be estimated, and $\epsilon_t{}'$ is the error term to be estimated.

Accordingly, if applying (6.10) to (6.4), therefore the VARX model is built in (6.11).

$$I(t|x) = \alpha' + \sum_{i=1}^{p} \gamma_i I(t-i|x) + \sum_{i=1}^{p} \phi_i{}' \boldsymbol{Y}'_{t-i} + \sum_{j=1}^{q} \beta_i{}' \boldsymbol{X}_{t-j} + \epsilon_t{}' \tag{6.11}$$

where $I(t|x)$ is the reliability index estimated by the Cox PHM with time-varying covariates in (6.4),and other symbols have the same meaning with (6.10).

### 6.3.5 Conditional Granger causality (CGC)

The Granger Causality test, as a representative technique of statistical causal inference, has been commonly employed in various fields including economics and neuroscience. In this work, such test is employed to select critical sensor signals and EOCs for the VARX modelling. The idea of the Granger Causality test lies in that if lagged values of one time series denoted as $\boldsymbol{X}$ are valuable to predict current values of another time series $\boldsymbol{Y}$, the $\boldsymbol{X}$ is then defined as the "Granger cause" [307] of the $\boldsymbol{Y}$.

As an extension of the typical GC test, the idea of the Conditional Granger Causality (CGC) test [285, 308, 309] is similar to that of the typical GC test but it considers the influence of third-party mediating variables namely $\boldsymbol{Z}$ when judging statistical causal relationships between pairwise variables. The calculation of the CGC based on the VAR model is described as follows [285].

$$\boldsymbol{\Psi}_{\boldsymbol{X}\rightarrow\boldsymbol{Y}|\boldsymbol{Z}} \equiv \ln \frac{\Sigma_{yy,r}}{\Sigma_{yy}} \tag{6.12}$$

where $\Sigma_{yy} = cov(\boldsymbol{\epsilon}_{y,t})$ represents the covariance matrix of residuals $\boldsymbol{\epsilon}_{y,t}$ of the VAR model including the variable $\boldsymbol{X}$ as the potential cause of $\boldsymbol{Y}$ conditional on $\boldsymbol{Z}$, $\Sigma_{yy,r} = cov(\boldsymbol{\epsilon}_{y,t,r})$ represents the covariance matrix of residuals $\boldsymbol{\epsilon}_{y,t,r}$ of the VAR model excluding the variable $\boldsymbol{X}$.

The CGC test is employed in this research to investigate the interdependencies with particular emphasis on causal relationships between pairwise sensor signals considering remaining sensor signals and external conditions as mediating variables which may have effects on the statistical

causal relationships. In this regard, the CGC test can assist with identifying the most critical sensor signals to thoroughly reveal the potential failure mechanism of the engineered systems and further reduce the dimensions of the input variables for the VARX model mentioned above. According to (6.12), the results obtained by the CGC test depend on the lag order of the VAR model. However, high order conditional Granger causality requires a corresponding high order VAR/VARX model to be established and may lead to instability of the estimated VAR/VARX models for the high-dimensional case. Considering that, the causal relationships between sensor signals and external conditions and selection of critical sensor signals as inputs for the VARX model are determined mainly based on a first order CGC test for the sake of simplicity [310].

### 6.3.6 Grey model with Fourier series calibration (FGM)

Grey systems theory (GST) was proposed by [311] to analyse complex systems existing in various kinds of fields including engineering [91, 312, 313] and economics [314, 315]. The proposed GST is composed of mainly two subparts which are grey relational analysis (GRA) and the grey model (GM) respectively [316]. The former is commonly used to infer the unknown relationships between two or more series while the latter has been widely utilised to predict the behaviour of uncertain and complex systems with limited data sets available. In this regard, the GM family can be utilised to predict incomplete EOCs as inputs of the VARX model.

More specifically, the original differential equation to generate the GM is called grey differential equation (GDE) [311]. For instance, a commonly employed differential equation is described as follows in discretised form [316].

Among the GM family, the GM(1, 1) model [316] whose formulae are shown as follows, is the most widely employed GM model.

$$s_k^0 + az_k^1 = b \qquad (k = 1, 2, \cdots, n) \tag{6.13}$$

$$s_k^1 = \sum_{i=1}^{k} s_i^0 \tag{6.14}$$

$$z_k^1 = \frac{s_{k-1}^1 + s_k^1}{2} \tag{6.15}$$

where $s_k^0$ represents the original series with $k = 1, 2, \cdots, n$ ($n$ is the length of the whole series), $a$, $b$ are grey parameters to be estimated, and $z_k^1$ is defined by formula (6.15).

According to the current literature, the original GM has several disadvantages. The main disadvantage of the GM is its overshooting problems with exceptional data points [312, 317] and its instability when processing the series which are mainly dominated by fluctuation or cyclical terms [318]. Considering the disadvantages mentioned above, the grey model with the error calibration by the Fourier series (FGM) [296], as a natural extension of the typical GM, is employed to forecast future values of the external conditions namely the EOCs, because of its ability to process sequences with nonnegligible fluctuation terms without losing its robustness when forecasting future values of the predicted sequences. Meanwhile, the residuals between the sample values and in-sample predictions by the GM are modified by means of the high-order Fourier series [319]. More specifically, the error calibration by means of the Fourier series is illustrated as follows [296].

$$\epsilon^{(0)}(k) = \frac{1}{2}a_0 + \sum_{i=1}^{k}\left[a_i \cos ik\omega + b_i \sin ik\omega\right] \qquad k = 2, 3, 4, \cdots, n \tag{6.16}$$

$$\boldsymbol{P} = \begin{bmatrix} 1/2 & \cos 2\omega & \sin 2\omega & \cdots & \cos 2k\omega & \sin 2k\omega \\ 1/2 & \cos 3\omega & \sin 3\omega & \cdots & \cos 3k\omega & \sin 3k\omega \\ 1/2 & \cos 4\omega & \sin 4\omega & \cdots & \cos 4k\omega & \sin 4k\omega \\ \vdots & \vdots & \vdots & \vdots & \vdots & \\ 1/2 & \cos n\omega & \sin n\omega & \cdots & \cos nk\omega & \sin nk\omega \end{bmatrix} \tag{6.17}$$

$$C = (\boldsymbol{P}^T\boldsymbol{P})^{-1}\boldsymbol{P}^T\epsilon_0 \tag{6.18}$$

$$\epsilon_0 = \{\epsilon^{(0)}(2), \epsilon^{(0)}(3), \cdots, \epsilon^{(0)}(n)\} \tag{6.19}$$

where $k_0 = \frac{n-3}{2}$ represents the order of the Fourier series, $\omega = \frac{2}{\pi}$ is a parameter related to the frequency of the Fourier series, $\boldsymbol{P}$ is the matrix of the Fourier series terms, $C$ represents fitted values of the residuals by means of the Fourier series, and $\epsilon_0$ is denoted as the sequence of the residuals at different time points namely $\epsilon^{(0)}(k)(k = 2, 3, \cdots, n)$. Considering the limitation of the Fourier series to model random fluctuations of the residuals sequence, the subtraction be-

tween the residuals and its fitted sequence by means of the Fourier series is further modelled by means of the autoregressive integrated moving average (ARIMA) or the autoregressive moving average (ARMA) model to calibrate the random variations.

## 6.4 Case study: CMAPSS dataset

### 6.4.1 Data sources

The turbofan failure data sets obtained by the so-called "Commercial Modular Aero-Propulsion System Simulation (C-MAPSS)" [286] software were employed for case studies in this chapter to preliminarily validate the feasibility and effectiveness of the proposed approach. In such data sets, the degradation behavior of the turbofan (shown in Fig. 6.3) working under three kinds of operational conditions was measured with 21 sensors [286]. The data sets also contain the order of units consisting of the turbofan and the time order for data records of each unit [286].

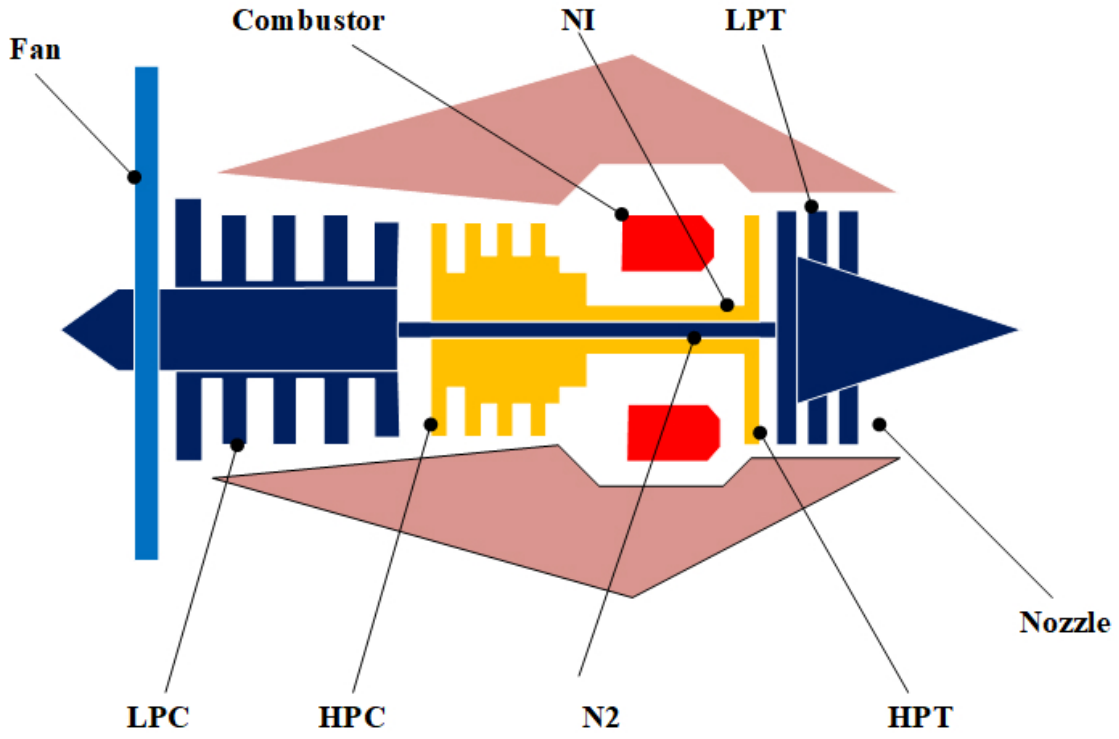


Figure 6.3: Inner structure of the turbofan employed in the C-MAPSS data sets. [36]

Apart from that, the whole data sets can be separated into four subsets simulated under different operational conditions and each can be further categorised into the run-to-failure

training data sets namely the training sets and the incomplete test sets both with 100 units. In this chapter, the proposed approach will be first implemented on the training set of the first subset called the "FD001" data set. After being implemented on the training sets, the model will be implemented on the test sets for prediction of the individual reliability indices and corresponding RULs.

### 6.4.2 Data pre-processing

For both the training sets and the test sets, several unchanging columns in them are removed. The remaining data set only contains 2 different operational conditions and 15 different sensor signals. Afterwards the Min-Max scaling is implemented on both the data sets to transfer different scales in all the time series into a $[0, 1]$ scale. A simple moving average filter with a window size of 5 is then utilised to smooth the sensor signals. Since the VARX model and the CGC test assume their input time series to be stationary, the monitoring signals including the sensor signals and signals of the operational conditions as well as the generated time series of the individual reliability indices are again tested for stationarity by means of the augmented Dickey-Fuller (ADF) tests with the significance level to be 0.05, and all the non-stationary time series are differenced until they pass the stationary test. The order for the difference is set to 1 according to the ADF test.

### 6.4.3 Implementation of the proposed method

- **Implementation of the Cox PHM with time-varying covariates:** As mentioned earlier, the monitoring signals of turbofan units in the training set with complete run-to-failure records, including the external conditions, will be utilised by the Cox proportional hazards model (Cox PHM) with time-varying covariates [320] to generate individual reliability indices for the RUL prediction of test units. Prior to the reliability modelling based on the Cox PHM model, the principal component analysis (PCA) is implemented on the smoothed monitoring signals to reduce the high-dimensionality of the data. The threshold for the cumulative variance ratio is set as 0.90 and three principal components are selected with their variance ratios to be 0.76, 0.09 and 0.06 respectively. After its

training stage based on the training set, the trained PHM model is further implemented on the incomplete test sets to generate incomplete reliability indices of the test set units for further similarity matching.

- **Implementation of the pairwise conditional Granger causality (CGC) tests:** In terms of the time series modelling of the monitoring signals and the individual reliability functions generated by the Cox PHM approach, the pairwise CGC test [285, 321] is then implemented preliminarily to identify several critical monitoring signals which may greatly influence the reliability indices and thus the RULs of the individual units, considering different external conditions where the units perform their functions. By means of the CGC tests with significance level set as 0.05 in this chapter, the statistical causal relationships between multivariate sensor signals of the failure data of training set units can be illustrated. For example, the first-order statistical causal relationships between different sensor signals in the run-to-failure records of units in the FD001 training sets are shown in Fig. 6.4. As shown in Fig. 6.4, the nodes with net outflow greater than 0, namely the $8th$, $9th$, $14th$, $15th$, $21st$ sensor signals, are defined as critical sensor signals for modelling the degradation behaviour of units in the FD001 training set, which is to some extent consistent with the results of the sensor selection mentioned in [322]. For example, as shown from the Fig. 6.4, the inflow of the sensor signal $9th$ is 5 while the outflow of this sensor is 10, so the $9th$ sensor signal whose net outflow is 5 is chosen as one of the critical sensor signals. The results obtained by the CGC tests provide a simplified structure with reduced dimensions of variables for the subsequent VARX model to be implemented.

- **Implementation of the VARX model:** The VARX model with the time series of the external conditions as exogenous variables is then established based upon the previous CGC tests which identify the several critical monitoring signals for further time series modelling of the individual reliability functions and reveal the topological structure of a cluster of sensor signals measured from different parts of the units namely the turbofans. As mentioned in section 6.3.4, input variables for the VARX model include the reliability indices generated by the Cox PHM model of individual units and critical sensor signals for

degradation modelling of the units as endogenous variables, and the external conditions namely the operational conditions where the individual units perform their functions as exogenous variables.

After estimation of the lag parameters namely $p$ and $q$, a VARX($p$, $q$) model is employed in this chapter to model the relationships between the sensor signals and the time series of the generated reliability indices. Considering that the VARX models for different units in the training set may have different lag orders, different $p$ and $q$ values are estimated by means of the AIC for different VARX models of individual units in training set. In spite of that, the maximum lag order is set as 10 and 2 for $p$ and $q$ respectively to prevent overfitting and instability of the VARX($p$, $q$) model. The maximum time step for the VARX forecasting is determined preliminarily to be no more than 150 in a similar way to [303, 304]. The forecasting process for different units in both the FD001 training sets and test sets will cease once the predicted reliability functions reach the failure thresholds previously established by the implementation of the Cox PHM model which generates individual reliability indices of training set units.

- **Forecast of the external conditions using the FGM:** The time series of the external conditions namely the environmental and operational conditions (EOCs), as shown in the C-MAPSS data sets, are required to be updated so as to trigger VARX predictions of the individual reliability indices of test set units. Considering the large uncertainties and small sample size of the EOCs, the grey model with error calibration by the Fourier series (FGM) is then implemented to forecast the future values of such external conditions based on the incomplete test sets. The incomplete time series of the EOCs were also scaled into $[0, 1]$ using the Min-Max scaling and then smoothed in the same way with the failure data of training set units to avoid potential instability issues of the GM.

- **Prediction of RULs for the test set utilising the models based on the train set:** After reliability indices of the individual units in the training set are generated by means of the Cox PHM model and the generated reliability functions are modelled by the VARX model with the real-time sensor signals of the training set units and the prediction horizon to be 150, the trained model based on the training set will be implemented on the

test set with the aid of results obtained by the similarity matching to forecast the RULs of the individual units in the test set. For individual test set units, if their predicted relability indices reach the failure threshold which is defined as the last reliability index value of their similar training set units, then the VARX prediction is stopped and the corresponding RUL of the test set unit is calculated.

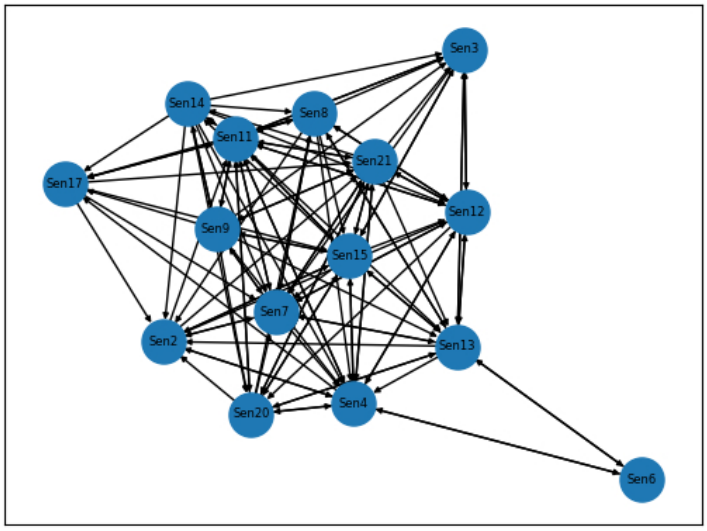


Figure 6.4: Statistical causal graphs of units in FD001 training set generated by the CGC test. [36]

### 6.4.4 Fitting results of Cox proportional hazards model

The run-to-failure records of the training set units are fitted by the Cox PHM model with time-varying covariates to generate the reliability indices. The estimated hazard ratios of input variables and their confidence intervals, $z-$scores and $p-$values of the input variables of the Cox PHM are shown in Table 6.1. The fitting results show that the first principal component namely the $PC1$ in the Table 6.1 has the largest hazard ratio 3.59 with its $p-$value to be smaller than 0.005 which indicates that the $PC1$ is a statistically significant factor which has the strongest influence on the degradation behaviour of turbofan units in the training set. Compared to the $PC1$, the second and the third principal component namely the $PC2$ and $PC3$ in this case have weaker influence on the turbofans' degradation behaviour and are statistically insignificant. Such results are in consistent with the variance ratios of the three

principal components which are mentioned in the section 6.4.3. According to the variance ratios of the $PC1$, $PC2$ and $PC3$, it can be interpreted that the influence of the $PC1$ on the turbofan degradation behaviour is much stronger than that of the $PC2$ and $PC3$. However, the $PC2$ and $PC3$ are stiil contained in the Cox PHM model to hold as much information as possible related to the turbofan degradation behaviour based on the complete failure records in the training set.

Table 6.1: Fitting results of the Cox PHM with time-varying covariates based on the run-to-failure records of training set units. [36]

| Variable | Hazard ratio | Lower 95% | Upper 95% | z | p value | Partial Log-likelihood | Penaliser |
|---|---|---|---|---|---|---|---|
| PC 1 | 3.59 | 2.67 | 4.83 | 8.43 | $< 0.005$ | | |
| PC 2 | 1.61 | 0.87 | 2.98 | 1.50 | 0.13 | -328.05 | 0.01 |
| PC 3 | 0.71 | 0.26 | 1.94 | -0.66 | 0.51 | | |

### 6.4.5 Results of similarity matching of reliability indices

As an example, the similarity matching results for the incomplete reliability index of the $37th$ unit in the test set are shown in Fig. 6.5. According to Fig. 6.5,the relability index of the $37th$ unit in the test set matches with the $45th$, $28th$, $98th$, $93rd$ and $61st$ unit in the training set from the $7th$, $20th$,$1st$, $2nd$, $30th$ cycles respectively. Such information is further employed by the VARX model to predict the future reliability index of a certain unit in the test set based on reliability indices of a set of units in the training set whose reliability indices are most similar to the reliability index of the specific unit in the test set.

### 6.4.6 VARX fitting results

As mentioned in section 6.4.3, VARX models with different lag parameters for both the endogenous and exogenous variables are established for training set units. The overall performance of VARX models when applied to fitting the in-sample reliability indices based on the failure records of training set units is plotted in Fig. 6.6. In Fig. 6.6, both the root mean square error (RMSE) and the normalised root mean square error (NRMSE) of fitting the generated relaibility indices of training set unit in a single VARX model are defined in (6.20) and (6.21).

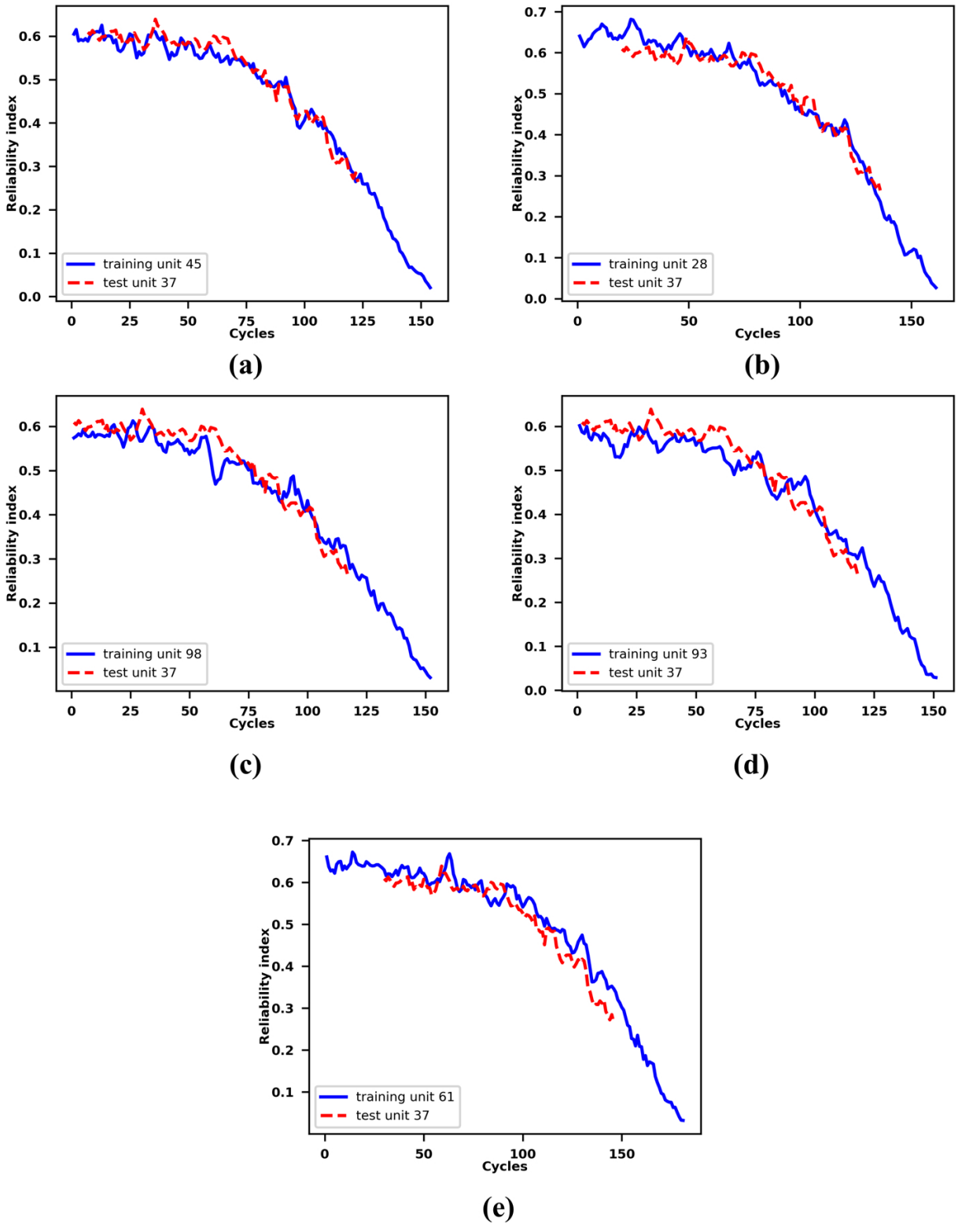


Figure 6.5: Similarity matching between the incomplete reliability index of the $37th$ unit in the test set and the complete reliability index of the (a) 45th (b) $28th$ (c) $98th$ (d) $93rd$ (e) $61st$ units as the five most similar reliability indices of units in the run-to-failure training set. The similarity decreases with the figure order. [36]

$$RMSE_{VARX} = \left(\frac{\sum_{i=1}^{N_I} \left(I_i - \hat{I}_i\right)^2}{N_I}\right)^{\frac{1}{2}} \tag{6.20}$$

$$NRMSE_{VARX} = \frac{\left(\frac{\sum_{i=1}^{N_I} \left(I_i - \hat{I}_i\right)^2}{N_I}\right)^{\frac{1}{2}}}{I^{max} - I^{min}} \tag{6.21}$$

where $RMSE_{VARX}$ and $NRMSE_{VARX}$ are the $RMSE$ and the $NRMSE$ of fitting the generated reliability indices by means of a single VARX model, $N_I$ represents the length of the generated reliability indices, $I_i$ and $\hat{I}_i$ represent actual value and fitted value of the generated reliability indices at the point $i$, $I^{max}$ and $I^{min}$ represent the maximum and the minimum value of the actual generated reliability indices.

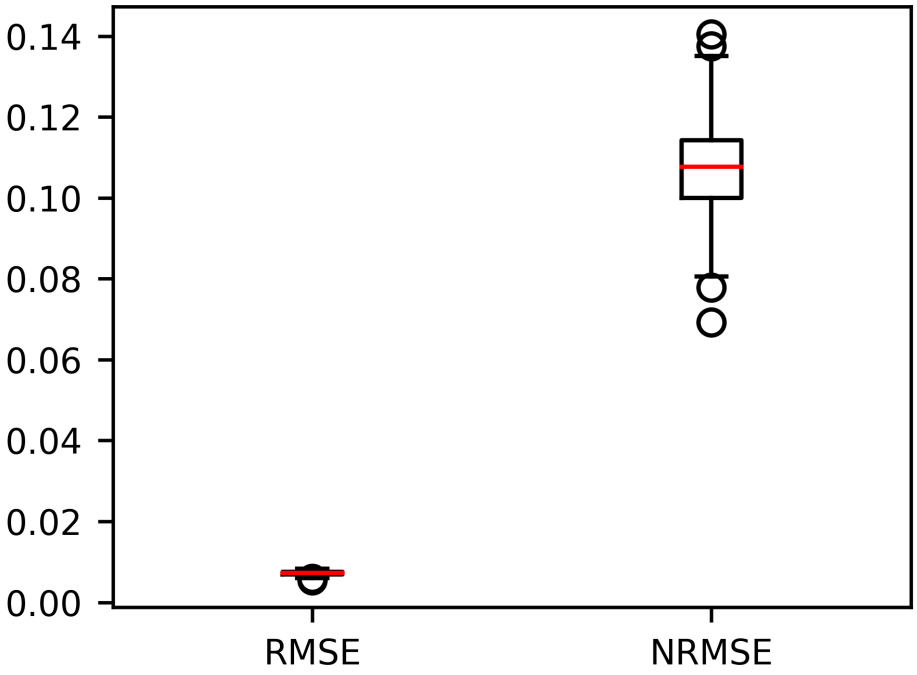


Figure 6.6: Box plot of the RMSE and the NRMSE of the in-sample fitting of the VARX models based on training set units. [36]

As shown in Fig. 6.6, the median value of the $RMSE$s is 0.0072 with its 25% and 75% percentile to be 0.0069 and 0.0075 respectively. The median value of the $NRMSE$s is 0.1077 with its 25% and 75% percentile to be 0.0999 and 0.1142 respectively. The results show that the VARX model has high accuracy when fitting the generated reliability indices of units in the training set.

### 6.4.7 Fitting and prediction of the FGM

As an example, the results of the in-sample fitting and the out-of-sample prediction by means of the fourier grey model (FGM) for the different operational conditions of an example unit in the test set are shown in Fig. 6.7 and Fig. 6.8 respectively.

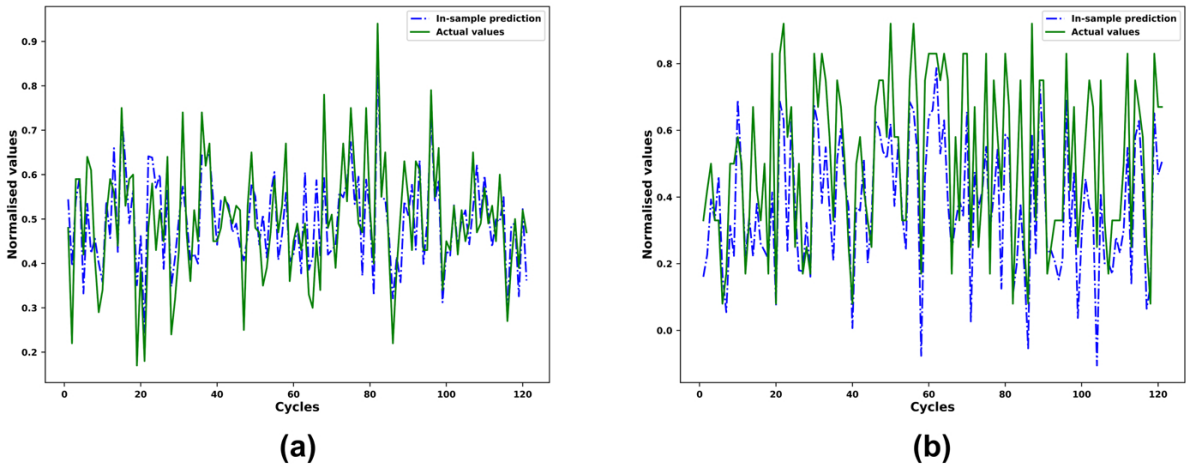


Figure 6.7: In-sample fitting of (a) the first and (b) the second operational conditions of the unit 37 in FD001 test sets based on the FGM(1, 1) and ARIMA/ARMA calibration. [36]

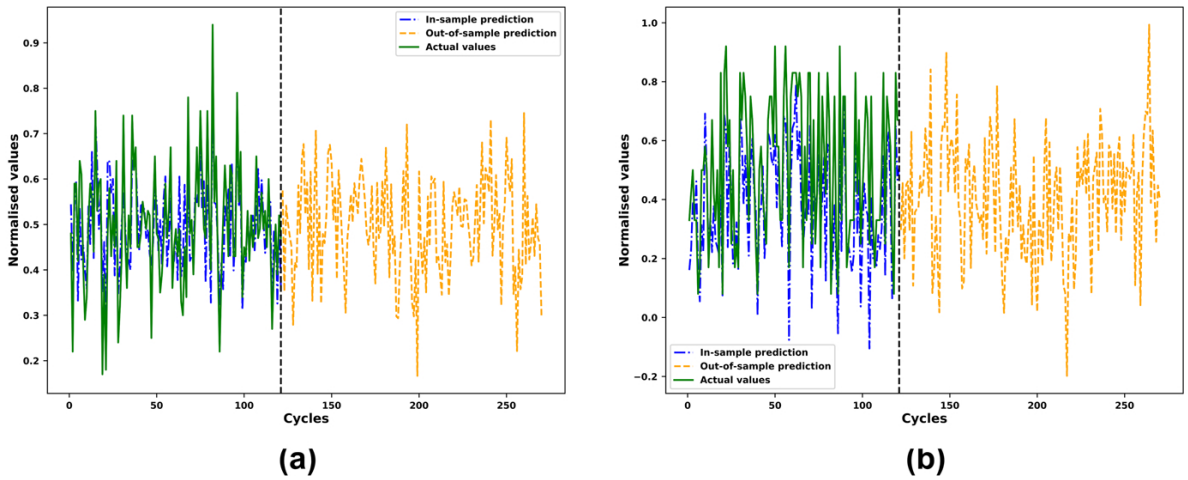


Figure 6.8: Out-of-sample prediction of (a) the first and (b) the second operational conditions of the unit 37 in FD001 test sets based on the FGM(1, 1) and ARIMA/ARMA calibration. [36]

Fig. 6.7 illustrates the in-sample fitting results of the first and the second operational conditions for the $37th$ unit in the test set. The RMSE and the NRMSE of fitting the first operational conditions for the $37th$ test set unit are 0.08 and 0.11 while the RMSE and the NRMSE of fitting the second operational conditions for the same unit are calculated as 0.19 and 0.10,

which shows competence of the FGM for in-sample fitting of the actual signals of operational conditions. For all the units in the test set, the mean RMSE and the mean NRMSE of fitting the first operational conditions are calculated as 0.15 and 0.23 respectively while both the values of fitting the second operational conditions are calculated as 0.23 and 0.18. Regarding the out-of-sample prediction in Fig. 6.8, the prediction horizon is set as 150 which is consistent with the prediction step set in the section 6.4.3 for the VARX model. The performance of the FGM for out-of-sample prediction will be reflected in the final results of the RUL prediction.

### 6.4.8 Results on the RUL prediction of turbofan units

The results of the RUL prediction of all the units in the test set are obtained by means of the approach proposed in this chapter. As an example, the process of the RUL prediction of the $37th$ unit in the test set is illustrated. The future values of operational conditions predicted by means of the FGM model are employed to update VARX predictions of the generated reliability indices of the $37th$ test set unit based on the VARX models of the training set units which have the most similar reliability indices to the incomplete reliability index of the $37th$ test set unit. For example, according to the Fig. 6.5, the VARX models trained based on the $45th$, $28th$, $98th$, $93rd$ and $61st$ unit in the training set are employed to predict the future reliability index values of the $37th$ unit in the test set with future values of the exogenous variables namely the operational conditions updated by the FGM. The prediction process will be stopped if the future reliability index values of the test set unit $37th$ reach the pre-defined threshold which is shown in the horizontal dashed lines in the Fig. 6.9 (a). More specifically, based on the failure records of the $45th$, $28th$, $98th$, $93rd$ and $61st$ unit in the training set, the corresponding RULs of the $37th$ test set unit are predicted as 54, 46, 31, 62 and 31 repsectively. Afterwards the final RUL of the $37th$ test unit is calculated by the average of the five RUL values obtained earlier and is determined as 44 while the truth RUL is 21 for the $37th$ test unit.

After the reliability index is estimated, the predicted reliability functions of the $37th$ test unit based on the $45th$, $28th$, $98th$, $93rd$ and $61st$ training units are shown in Fig. 6.9 (b). Finally the comparison between actual values and the predicted values of the RULs is shown in Fig. 6.10, which indicates the competence of the proposed approach to predict RULs for

turbofan units in the test set.

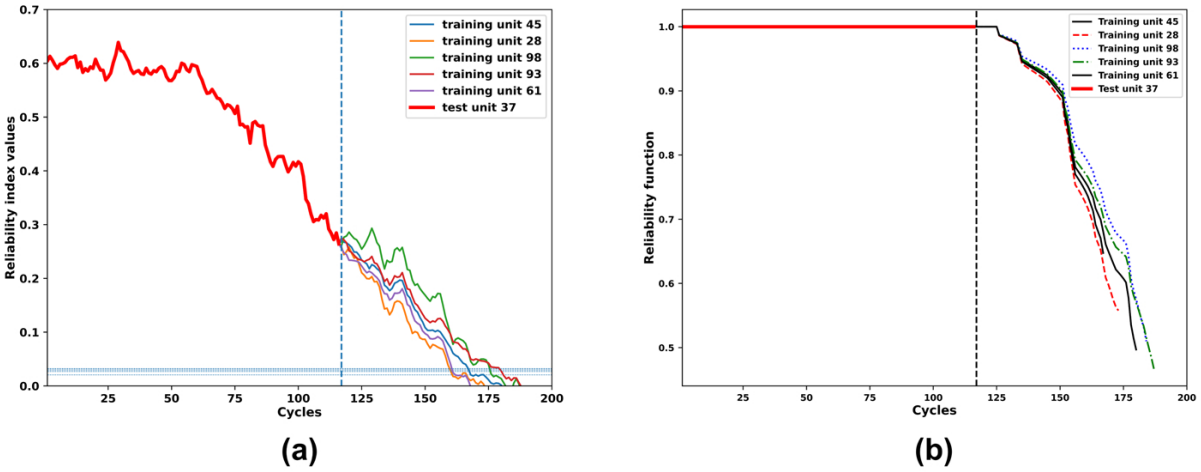


Figure 6.9: Predictions of the (a) incomplete reliability index and (b) reliability function of the test set unit 37th considering its five most similar reliability indices of the training set units. The online prediction of the reliability index for the unit $37th$ in the test set is updated by future values of the external operational conditions which are predicted by means of the FGM model. [36]

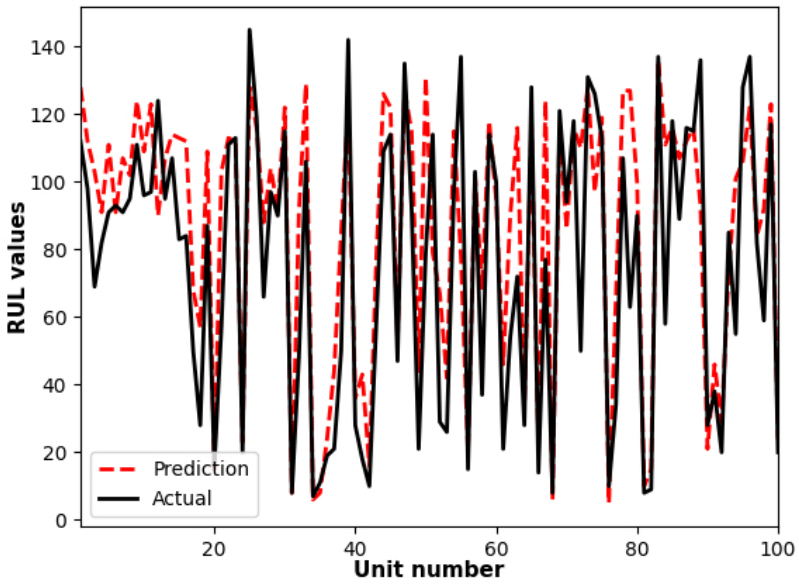


Figure 6.10: Comparision between the actual RULs and their prediction values. [36]

The proposed method is implemented on all the 100 test units in the FD001 data set to predict the RULs of all the test units for comparison with results which are obtained by other papers. More specifically the Root Mean Square Error (RMSE) is employed in this chapter for reasonable comparisons between the prediction accuracy of the RUL by means of different

methods. The results for the comparison are shown in Table 6.2. As shown in the table, the prediction accuracy of the proposed method is higher than that obtained by some benchmarking approaches, but there is still room for the prediction accuracy of the proposed approach to be improved.

Table 6.2: Comparisons between the RMSE calculated by the proposed approach and other papers. [36]

| **Methods** | VAR(42) [323] | SVM&ARIMA [323] | FPCA [324] | **Proposed method** | CNN [325] |
|---|---|---|---|---|---|
| **RMSE** | 47.63* | 39.68* | 28.06 | 23.35 | 18.45 |

(∗ corresponds to the best model proposed in the paper.)

## 6.5 Summary

This chapter proposes a hybrid approach based on the Cox PHM with time-varying covariates and the VARX model to predict the real-time reliability function and the RUL of individual aircraft turbofans performing their functions under time-varying EOCs. The CGC test is implemented to unveil statistical causal relationships between different sensor signals and identify critical sensors for the VARX modelling. Meanwhile, the proposed method is competent to reflect the influence of EOCs on the degradation behaviour and, therefore, the RUL of turbofan engines. Afterwards the proposed method is validated on the FD001 test set of the C-MAPSS dataset and exhibits high accuracy for RUL prediction compared to several benchmark models.

# Chapter 7

# Conclusions and future directions

## 7.1 Conclusions

This thesis focuses on data-driven approaches for the structural health monitoring (SHM) on aeronautical composites together with the prognostics and health management (PHM) on turbofan engines, which aim to enhance the capability of real-time monitoring and predictive maintenance on aircraft structures. The contributions and findings of this thesis are summarised as follows.

Firstly, a data-driven baseline-dependent approach integrating the autoregressive (AR) model and the adaptive signal compression is proposed for damage detection and localisation on both quasi-isotropic and anisotropic carbon fibre reinforced polymer (CFRP) coupons. The parameter estimation and diagnostics of the AR model, including inspections on the residual autocorrelation, residual normality and model stability, are implemented on guided wave measurements before and after the signal compression. It is shown that the highly autocorrelated and non-normal residuals can be greatly alleviated after signal compression procedures, which satisfies model assumptions and ensures valid applications of the AR model. Meanwhile, the applicability and effectiveness of the AR models are validated when detecting and localising both simulated damages and real-life barely visible impact damages (BVIDs) based on both raw and compressed guided wave measurements. When establishing AR models on compressed

guided wave signals, the proposed adaptive signal compression based on the two-sided cumulative sum (CUSUM) algorithm is compared to the common uniform sampling and the random Gaussian sampling regarding their effects on damage detection and localisation. Among the three compression techniques, the proposed adaptive sampling leads to robust damage detection performance and damage images with fewer imaging artifacts against varying compression ratios. The proposed method on compressed measurements achieves equivalent damage detection and localisation capability to the uncompressed cases but leads to a compression time reduction of at least 30 times, thus being effective and computationally efficient for the SHM tasks. Comparable results on the SHM are also obtained when employing both raw and compressed guided wave tone bursts of 3, 5 and 8 cycles respectively. It is demonstrated that the 8-cycle tone bursts can lead to degraded performance in the presence of signal compression and severe boundary reflections.

Furthermore, baseline-free guided wave approaches are investigated for the SHM purposes considering potential limitations of the baseline-dependent approach. In this realm, experimental comparisons between the virtual time reversal (VTR), the instantaneous baseline (IB) and the reciprocity-based techniques are carried out for anisotropic composite coupons and large-size stiffened panels, considering the effects of temperature variations, damage types (simulated or impact damages), multiple damages, boundary reflections and structural complexities. Results show that the three baseline-free techniques are able to detect and localise single damages while the IB could cause high localisation errors due to the sensitivity to transducer configurations. In the case of dual damages, the VTR could fail to identify different damages simultaneously due to the mask of imaging artifacts. Meanwhile, the compared reference-free techniques are able to detect and localise both simulated and impact damages under temperature variations, whereas the detection threshold and the detection accuracy of reciprocity-based technique could vary with increasing temperatures. The IB and VTR can also detect impact damages on the stiffened composite panel with 100% and 75% accuracy, while the reciprocity based method exhibits much lower capability as 42% to detect such damages. In addition, boundary reflections of guided waves could largely affect detection and localisation capabilities of the investigated baseline-free techniques.

Afterwards a data-driven baseline-free technique based on ultrasonic guided waves is proposed for the SHM on aeronautical composite structures. Such technique is established based on the unsupervised shapelets and the shift-invariant dictionary learning and can be integrated with the building block (BB) philosophy for damage detection and localisation on complex structures, e.g., stiffened composite panel. Compared to the IB, VTR and the reciprocity-based techniques, the proposed method requires little prior knowledge of guided wave propagation and is insensitive to different transducer configurations. Experimental investigations are carried out on flat coupons and stiffened panels manufactured of the identical composite material and anisotropic layup sequence. Results indicate that the proposed technique is competent to detect and localise both simulated damages and BVIDs within flat coupons under temperature variations. In the case of stiffened panel, the shapelet-based method integrated with the BB philosophy yields the 98% detection accuracy and localisation errors as 20.1 mm, 49.3 mm respectively for two BVIDs. In addition, it is demonstrated that the damage detection and localisation capabilities of the proposed approach are affected by the overlapping between boundary reflections and first wave packets in guided wave tone bursts. Nevertheless, such signal overlapping can be alleviated by dispersion removal techniques to yield better performance for damage detection and localisation.

Finally, this thesis proposes a hybrid data-driven approach for the remaining useful life (RUL) prediction of aircraft engines performing under varying environmental and operational conditions (EOCs). Main rationale of the proposed methodology lies in the combination of the Cox proportional hazard model (Cox PHM) with time-varying covariates and the vector autoregressive model with exogenous variables (VARX). Meanwhile, the conditional granger causality (CGC) test is implemented to reveal statistical causal relationships between sensor signals collected from different parts of engines and identify critical sensors for the VARX modelling. Numerical validations are carried out based on turbofan failure datasets, which include sensor records of turbofans and the related EOCs. Results demonstrate that the proposed method achieves the prediction error, i.e., the root mean square error (RMSE), as 23.35 and is competent for the RUL prediction as compared with several baseline approaches.

## 7.2 Future work

Future work of the thesis is summarised as follows for the structural health monitoring and failure prognostics on aeronautical structures.

Chapter 3 proposes a baseline-dependent approach which integrates the statistical autoregressive model and signal compression techniques for damage detection and localisation on flat composite coupons. Future work in this realm includes:

- Applications to complex composite structures. The applicability of the proposed baseline-dependent technique requires further investigations considering structural complexities within composite panels, e.g., stiffeners, holes, rivets.

- Damage characterisation. The proposed technique might provide detailed damage information by characterising the size and shape of potential damages within composite structures.

- Integration with temperature compensation techniques. Temperature compensation techniques can be integrated to enhance the SHM capability of the proposed baseline-dependent technique when baseline and current measurements are obtained under different temperatures.

Chapter 4 experimentally analyses and compares the SHM performance of several baseline-free techniques considering temperature variations, material anisotropy, structural complexities and boundary reflections. Further work on this topic includes:

- Experimental investigations into baseline-free GWSHM techniques which are based on phased transducer arrays or nonlinear guided wave modes.

- Extension of damage scenarios. Baseline-free GWSHM techniques can be experimentally investigated under extended damage scenarios including different damage types and severities together with varying loading conditions on composite structures.

Chapter 5 proposes a data-driven baseline-free GWSHM technique based on unsupervised shapelets and shift-invariant dictionary learning. The proposed technique can be further investigated through following directions.

- Further applications to complex composite structures. Experimental investigations into the proposed technique can be further implemented on composite panels with different structural characteristics, e.g., holes, openings, rivets.
- Accurate phase reconstruction of pristine signals. As shown in Chapter 5, the proposed baseline-free technique may not well capture phase information of experimental pristine signals. Therefore, accurate phase retrieval of reconstructed pristine signals is needed to enhance damage detection and localisation performance of the proposed technique.
- Applications to aircraft composite panels under real-life scenarios which include but are not limited to large temperature variations (more than 20 $^{\circ}C$), varying loading conditions, and sensor failures.

Chapter 6 proposes a hybrid data-driven approach to predict the RUL of aircraft engines under varying EOCs while investigating statistical causal relationships between sensor signals collected from turbofan units. Further explorations in this field include:

- Improvement on RUL prediction performance. It is worth developing more accurate and efficient RUL prediction techniques based on advanced machine learning and signal processing algorithms in the realm of machine learning, signal processing and statistics.
- Integration with physical models of aircraft engines. The integration of prior physical knowledge can lead to a better understanding of degradation behaviour of turbofan engines and enhance the explainability of data-driven RUL prediction techniques.

# Bibliography


[1] Insley, J., & Turkoglu, C. (2020). A contemporary analysis of aircraft maintenance-related accidents and serious incidents. *Aerospace*, 7(6), 81.

[2] European Commission.(n.d.). Mobility and Transport - Airworthiness. Available at: https://transport.ec.europa.eu/transport-modes/air/aviation-safety/aviation-safety-rules/airworthiness_en (Accessed: 31 March 2024).

[3] David Shepardson. (2024).'Boeing 737 MAX 9 door plug bolts appeared to be missing on Alaska jet, NTSB says', *Reuters*, 07 February. Available at: https://www.reuters.com/business/aerospace-defense/us-safety-regulator-release-initial-report-boeing-737-max-cabin-blowout-agency-2024-02-06/ (Accessed: 31 March 2024).

[4] Airbus. (2013). FAST (Flight Airworthiness Support Technology). *Airbus Technical Magazine: special edition* $A350XWB$.

[5] Federal Aviation Administration.(n.d.). Available at: https://www.faa.gov/ (Accessed: 31 March 2024).

[6] Federal Aviation Administration.(2023). Regulations & Policies. Available at: https://www.faa.gov/regulations_policies (Accessed: 31 March 2024).

[7] Federal Aviation Administration.(1998). AC 43.13-1B - Acceptable Methods, Techniques, and Practices - Aircraft Inspection and Repair [Large AC. This includes Change 1.].

[8] Federal Aviation Administration.(2018). AC 120-17B - Reliability Program Methods—Standards for Determining Time Limitations.

[9] Federal Aviation Administration.(2022). AC 43-218 - Operational Authorization of Integrated Aircraft Health Management System.

[10] Karbhari, V. M. (2013). Introduction: the future of non-destructive evaluation (NDE) and structural health monitoring (SHM). In *Non-Destructive Evaluation (NDE) of Polymer Matrix Composites*, Woodhead Publishing, pp.3-11.

[11] Cawley, P. (2018). Structural health monitoring: Closing the gap between research and industrial deployment. *Structural health monitoring*, 17(5), 1225-1244.

[12] Yue, N. (2020). Stochastic analysis of guided wave structural health monitoring for aeronautical composites (Doctoral dissertation, Imperial College London).

[13] Mitra, M., & Gopalakrishnan, S. (2016). Guided wave based structural health monitoring: A review. *Smart Materials and Structures*, 25(5), 053001.

[14] Yue, N., Khodaei, Z. S., & Aliabadi, M. H. (2021). Damage detection in large composite stiffened panels based on a novel SHM building block philosophy. *Smart Materials and Structures*, 30(4), 045004.

[15] Giurgiutiu, V. (2007). Structural health monitoring: with piezoelectric wafer active sensors. Elsevier.

[16] Zhao, X., Gao, H., Zhang, G., Ayhan, B., Yan, F., Kwan, C., & Rose, J. L. (2007). Active health monitoring of an aircraft wing with embedded piezoelectric sensor/actuator network: I. Defect detection, localization and growth monitoring. *Smart materials and structures*, 16(4), 1208.

[17] Civera, M., & Surace, C. (2022). Non-destructive techniques for the condition and structural health monitoring of wind turbines: A literature review of the last 20 years. *Sensors*, 22(4), 1627.

[18] Meyendorf, N., Ida, N., Singh, R., & Vrana, J. (2023). NDE 4.0: Progress, promise, and its role to industry 4.0. *NDT & E International*, 102957.

[19] Tibaduiza Burgos, D. A., Gomez Vargas, R. C., Pedraza, C., Agis, D., & Pozo, F. (2020). Damage identification in structural health monitoring: A brief review from its implementation to the use of data-driven applications. *Sensors*, 20(3), 733.

[20] Xiongzi, C., Jinsong, Y., Diyin, T., & Yingxun, W. (2011, August). Remaining useful life prognostic estimation for aircraft subsystems or components: A review. In *IEEE 2011 10th international conference on electronic measurement & instruments* (Vol. 2, pp. 94-98). IEEE.

[21] Javed, K., Gouriveau, R., & Zerhouni, N. (2017). State of the art and taxonomy of prognostics approaches, trends of prognostics applications and open issues towards maturity at different technology readiness levels. *Mechanical Systems and Signal Processing*, 94, 214-236.

[22] Lei, Y., Li, N., Guo, L., Li, N., Yan, T., & Lin, J. (2018). Machinery health prognostics: A systematic review from data acquisition to RUL prediction. *Mechanical systems and signal processing*, 104, 799-834.

[23] Cremona, C., & Santos, J. (2018). Structural health monitoring as a big-data problem. *Structural Engineering International*, 28(3), 243-254.

[24] Yue, N., & Aliabadi, M. H. (2020). A scalable data-driven approach to temperature baseline reconstruction for guided wave structural health monitoring of anisotropic carbon-fibre-reinforced polymer structures. *Structural Health Monitoring*, 19(5), 1487-1506.

[25] Liang, D., Han, Q., Cai, Y., Yu, K., & Zhang, Y. (2022). Compressive sampling system based on random demodulation for active and passive structural health monitoring. *Smart Materials and Structures*, 31(6), 065005.

[26] Wang, P., & Gao, R. X. (2015). Adaptive resampling-based particle filtering for tool life prediction. *Journal of Manufacturing Systems*, 37, 528-534.

[27] Hyndman, R. J., & Athanasopoulos, G. (2018). Forecasting: principles and practice. OTexts.

[28] Lee Rodgers, J., & Nicewander, W. A. (1988). Thirteen ways to look at the correlation coefficient. *The American Statistician*, 42(1), 59-66.

[29] Park, G., Figueiredo, E., Farinholt, K. M., & Farrar, C. R. (2010, April). Time series predictive models of piezoelectric active-sensing for SHM applications. In *Health Monitoring of Structural and Biological Systems 2010* (Vol. 7650, pp. 32-43). SPIE.

[30] Wei, Z., Yam, L. H., & Cheng, L. (2005). NARMAX model representation and its application to damage detection for multi-layer composites. *Composite Structures*, 68(1), 109-117.

[31] Amer, A., Ahmed, S., & Kopsaftopoulos, F. (2024). Probabilistic State Estimation Under Varying Loading States via the Integration of Time-Varying Autoregressive and Gaussian Process Models. *Structural Health Monitoring*, 14759217231220548.

[32] Nardi, D., Lampani, L., Pasquali, M., & Gaudenzi, P. (2016). Detection of low-velocity impact-induced delaminations in composite laminates using Auto-Regressive models. *Composite Structures*, 151, 108-113.

[33] Wang, K., Zhang, J., Shen, Y., Karkera, B., Croxford, A. J., & Wilcox, P. D. (2022). Defect detection in guided wave signals using nonlinear autoregressive exogenous method. *Structural Health Monitoring*, 21(3), 1012-1030.

[34] Hongmin Zhu, Zahra Sharif Khodaei, and M.H. Aliabadi. (2023). Investigation into autoregressive model and signal compression for damage localisation. *AIP Conference Proceedings*, 2848(1).

[35] Hongmin Zhu, Zahra Sharif Khodaei, and M.H. Aliabadi. (2024). Investigation of baseline-free techniques for damage localisation on anisotropic composite structures. *Procedia Structural Integrity*, 52, 679-689.

[36] Hongmin Zhu. (2021). Real-time prognostics of engineered systems under time varying external conditions based on the COX PHM and VARX hybrid approach. *Sensors*, 21(5), 1712.

[37] Hongmin Zhu. (2021). Investigation into real-time influence of time varying operational conditions and sensor signals on reliability of engineered systems. *Proceedings of the 31st European Safety and Reliability Conference, ESREL 2021*, 71.

[38] Rose, J. L. (2014). Ultrasonic guided waves in solid media. Cambridge university press.

[39] Su, Z., & Ye, L. (2009). Identification of damage using Lamb waves: from fundamentals to applications (Vol. 48). Springer Science & Business Media.

[40] Giurgiutiu, V. (2015). Structural health monitoring of aerospace composites. Elsevier.

[41] Lowe, M. J. (1995). Matrix techniques for modeling ultrasonic waves in multilayered media. *IEEE transactions on ultrasonics, ferroelectrics, and frequency control*, 42(4), 525-542.

[42] Knopoff, L. (1964). A matrix method for elastic wave problems. *Bulletin of the Seismological Society of America*, 54(1), 431-438.

[43] Thomson, W. T. (1950). Transmission of elastic waves through a stratified solid medium. *Journal of applied Physics*, 21(2), 89.

[44] Rokhlin, S. I., & Wang, L. (2002). Stable recursive algorithm for elastic wave propagation in layered anisotropic media: Stiffness matrix method. *The Journal of the Acoustical Society of America*, 112(3), 822-834.

[45] PI Ceramic.(n.d.). Piezoelektrische Aktoren Piezoelectric Actuators. Available at: https://www.physikinstrumente.com/fileadmin/user_upload/pi_ceramic/files/catalog_CAT/PI_CAT128E_R3_Piezoelectric_Actuators.pdf (Accessed: 31 March 2024).

[46] Xu, C., Wang, J., Yin, S., & Deng, M. (2022). A focusing MUSIC algorithm for baseline-free Lamb wave damage localization. *Mechanical Systems and Signal Processing*, 164, 108242.

[47] Bhalla, S., & Soh, C. K. (2004). Structural health monitoring by piezo-impedance transducers. I: Modeling. *Journal of Aerospace Engineering*, 17(4), 154-165.

[48] Mesnil, O., Recoquillay, A., Fisher, C., Serey, V., Sharma, S., & d'Almeida, O. (2023). Self-referenced robust guided wave based defect detection: Application to woven composite parts of complex shape. *Mechanical Systems and Signal Processing*, 188, 109948.

[49] Alleyne, D. N., & Cawley, P. (1992). The interaction of Lamb waves with defects. *IEEE transactions on ultrasonics, ferroelectrics, and frequency control*, 39(3), 381-397.

[50] Michaels, J. E., Lee, S. J., Croxford, A. J., & Wilcox, P. D. (2013). Chirp excitation of ultrasonic guided waves. *Ultrasonics*, 53(1), 265-270.

[51] Nkikabahizi, C., Cheruiyot, W., & Kibe, A. (2022). Chaining Zscore and feature scaling methods to improve neural networks for classification. *Applied Soft Computing*, 123, 108908.

[52] Chakrabarti, S., et.al.. (2008). Data mining: know it all. Morgan Kaufmann.

[53] Zhu, J., Ge, Z., Song, Z., & Gao, F. (2018). Review and big data perspectives on robust data mining approaches for industrial process modeling with outliers and missing data. *Annual Reviews in Control*, 46, 107-133.

[54] Prabhu, K. M. (2014). Window functions and their applications in signal processing. Taylor & Francis.

[55] Oppenheim, A. V. (2010). Discrete-time signal processing (3rd edition). Pearson Education.

[56] Theodoridis, S., Kopsinis, Y., & Slavakis, K. (2014). Sparsity-aware learning and compressed sensing: An overview. *Academic Press Library in Signal Processing*, 1, 1271-1377.

[57] Roberts, G. (1998). A computationally efficient power-of-two window for spectral analysis. In *1998 IEEE Aerospace Conference Proceedings* (Vol. 4, pp. 221-230). IEEE.

[58] Dehghani, A., Sarbishei, O., Glatard, T., & Shihab, E. (2019). A quantitative comparison of overlapping and non-overlapping sliding windows for human activity recognition using inertial sensors. *Sensors*, 19(22), 5026.

[59] Diethelm, K. (1999). A method for the practical evaluation of the Hilbert transform on the real line. *Journal of computational and applied mathematics*, 112(1-2), 45-53.

[60] Salmanpour, M. S., Khodaei, Z. S., & Aliabadi, M. H. (2016). Instantaneous baseline damage localization using sensor mapping. *IEEE Sensors Journal*, 17(2), 295-301.

[61] Jin, H., Yan, J., Liu, X., Li, W., & Qing, X. (2021). Quantitative defect inspection in the curved composite structure using the modified probabilistic tomography algorithm and fusion of damage index. *Ultrasonics*, 113, 106358.

[62] Giannakeas, I. N., Sharif Khodaei, Z., & Aliabadi, M. H. (2023). An up-scaling temperature compensation framework for guided wave–based structural health monitoring in large composite structures. *Structural Health Monitoring*, 22(2), 777-798.

[63] Croxford, A. J., Wilcox, P. D., Drinkwater, B. W., & Konstantinidis, G. (2007). Strategies for guided-wave structural health monitoring. *Proceedings of the Royal Society A: Mathematical, Physical and Engineering Sciences*, 463(2087), 2961-2981.

[64] Croxford, A. J., Moll, J., Wilcox, P. D., & Michaels, J. E. (2010). Efficient temperature compensation strategies for guided wave structural health monitoring. *Ultrasonics*, 50(4-5), 517-528.

[65] Harley, J. B., & Moura, J. M. (2012). Scale transform signal processing for optimal ultrasonic temperature compensation. *IEEE transactions on ultrasonics, ferroelectrics, and frequency control*, 59(10), 2226-2236.

[66] Lu, Y., & Michaels, J. E. (2005). A methodology for structural health monitoring with diffuse ultrasonic waves in the presence of temperature variations. *Ultrasonics*, 43(9), 717-731.

[67] Xu, J., Zhu, W., Qiu, X., & Xiang, Y. (2023). A Novel Baseline-Free Method for Damage Localization Using Guided Waves Based on Hyperbola Imaging Algorithm. *Sensors*, 23(4), 2050.

[68] Michaels, J. E. (2008). Detection, localization and characterization of damage in plates with an in situ array of spatially distributed ultrasonic sensors. *Smart Materials and Structures*, 17(3), 035035.

[69] Michaels, J. E., & Michaels, T. E. (2007). Guided wave signal processing and image fusion for in situ damage localization in plates. *Wave motion*, 44(6), 482-492.

[70] Muller, A., Robertson-Welsh, B., Gaydecki, P., Gresil, M., & Soutis, C. (2017). Structural health monitoring using lamb wave reflections and total focusing method for image reconstruction. *Applied Composite Materials*, 24, 553-573.

[71] Hall, J. S., & Michaels, J. E. (2010). Minimum variance ultrasonic imaging applied to an in situ sparse guided wave array. *IEEE transactions on ultrasonics, ferroelectrics, and frequency control*, 57(10), 2311-2323.

[72] The British Standards Institution. (2010). Non-destructive testing - Terminology (BS EN 1330-4:2010).

[73] Dolphitech. (n.d.). DolphiCam2 Transducer Module (TRM) Technology Note.

[74] Frankel, E. G. (1984). Systems reliability and risk analysis. Springer Science & Business Media.

[75] Høyland, A. and Rausand, M.. (1994). System reliability theory, models and statistical methods. John Wiley & Sons.

[76] Stone, G. C. and van Heeswijk, R. G. (1977). Parameter Estimation For The Weibull Distribution. *IEEE Transactions on Electrical Insulation*, EI-12(4), 253–261.

[77] ISO. (2015). Condition monitoring and diagnostics of machines - Prognostics (BS ISO 13381-1:2015).

[78] Sankararaman, S., Daigle, M. J. and Goebel, K.. (2014). Uncertainty quantification in remaining useful life prediction using first-order reliability methods. *IEEE Transactions on Reliability*, 63(2), 603-619.

[79] Sun, B. et al. (2012). Benefits and challenges of system prognostics. *IEEE Transactions on Reliability*, 61(2), 323-335.

[80] Liao, L. and Köttig, F. (2014). Review of hybrid prognostics approaches for remaining useful life prediction of engineered systems, and an application to battery life prediction. *IEEE Transactions on Reliability*, 63(1), 191-207.

[81] Denson, W. (1998). The History of Reliability Prediction. *IEEE Transactions on Reliability*, 47(3), 321-328.

[82] Pecht, M. (2009). Prognostics and Health Management of Electronics in *Encyclopedia of Structural Health Monitoring*. John Wiley & Sons, Ltd.

[83] Heng, A., Zhang, S., et al. (2009). Rotating machinery prognostics:State of the art, challenges and opportunities. *Mechanical Systems and Signal Processing*, 23(3), 724-739.

[84] Sutharssan, T. et al. (2012). Prognostics and health monitoring of high power LED. *Micromachines*, 3(1), 78-100.

[85] Wileman, A. J. (2016). An Investigation into the Prognosis of Electromagnetic Relays (Doctoral dissertation, Cranfield university).

[86] Pecht, M. (2010). A Prognostics and Health Management Roadmap for Information and Electronics-Rich Systems. *IEICE Fundamentals Review*, 3(4), 25-32.

[87] Eker, O. F., Camci, F., & Jennions, I. K. (2012). Major challenges in prognostics: Study on benchmarking prognostics datasets. In *PHM Society European Conference*.

[88] Abbasnejad, S. and Mirabadi, A. (2018). Predicting the failure of railway point machines by using Autoregressive Integrated Moving Average and Autoregressive-Kalman methods. *Proceedings of the Institution of Mechanical Engineers, Part F:Journal of Rail and Rapid Transit*, 232(6), 1790-1799.

[89] Guclu, A. et al. (2010). Prognostics with autoregressive moving average for railway turnouts. *Annual Conference of the Prognostics and Health Management Society, PHM 2010*, 1-6.

[90] Al-Dahidi, S. et al. (2016). Remaining useful life estimation in heterogeneous fleets working under variable operating conditions. *Reliability Engineering and System Safety*, 156, 109-124.

[91] Peng, Y. and Dong, M. (2011). A hybrid approach of HMM and grey model for age-dependent health prediction of engineering assets. *Expert Systems with Applications*, 38(10), 12946-12953.

[92] Le Son, K. et al. (2013). Remaining useful life estimation based on stochastic deterioration models:A comparative study. *Reliability Engineering and System Safety*, 112, 165-175.

[93] Xu, X., et al. (2019). State-of-health estimation for lithium-ion batteries based on Wiener process with modeling the relaxation effect. *IEEE Access*, 7, 105186-105201.

[94] Kuang, F. et al. (2014). Manufacturing process reliability evaluation based on Granger causality test and Cox model. *ICRMS 2014 - Proceedings of 2014 10th International Conference on Reliability, Maintainability and Safety*. IEEE, 132-136.

[95] Liu, J., Li, X. and Peng, C. (2016). Reliability analysis for multi-component degraded system subject to multiple dependent competing failure process. *Proceedings of 2015 Prognostics and System Health Management Conference, PHM 2015*. IEEE, 1-5.

[96] Safaei, F., Ahmadi, J. and Balakrishnan, N. (2019). A repair and replacement policy for repairable systems based on probability and mean of profits. *Reliability Engineering and System Safety*, 183, 143-152.

[97] Tran, V. T. et al. (2012). Machine performance degradation assessment and remaining useful life prediction using proportional hazard model and support vector machine. *Mechanical Systems and Signal Processing*, 32, 320-330.

[98] Anoop, M. B., Raghuprasad, B. K. and Balaji Rao, K. (2012). A Refined Methodology for Durability-Based Service Life Estimation of Reinforced Concrete Structural Elements Considering Fuzzy and Random Uncertainties. *Computer-Aided Civil and Infrastructure Engineering*, 27(3), 170-186.

[99] Peng, Y., Wang, Y. and Zi, Y. (2019). Switching State-Space Degradation Model with Recursive Filter/Smoother for Prognostics of Remaining Useful Life. *IEEE Transactions on Industrial Informatics*, 15(2), 822-832.

[100] Yousefi, N., Coit, D. W., Song, S., & Feng, Q. (2019). Optimization of on-condition thresholds for a system of degrading components with competing dependent failure processes. *Reliability engineering & system safety*, 192, 106547.

[101] Ben Ali, J. et al. (2015). Accurate bearing remaining useful life prediction based on Weibull distribution and artificial neural network. *Mechanical Systems and Signal Processing*, 56, 150-172.

[102] Li, X., Ding, Q. and Sun, J. Q. (2018). Remaining useful life estimation in prognostics using deep convolution neural networks. *Reliability Engineering and System Safety*, 172, 1-11.

[103] Zhao, Z., Liang, B., Wang, X., & Lu, W. (2017). Remaining useful life prediction of aircraft engine based on degradation pattern learning. *Reliability Engineering and System Safety*, 164, 74-83.

[104] Heng, A., Tan, A. C., Mathew, J., Montgomery, N., Banjevic, D., & Jardine, A. K. (2009). Intelligent condition-based prediction of machinery reliability. *Mechanical systems and signal processing*, 23(5), 1600-1614.

[105] Santhosh, T. V., Gopika, V., Ghosh, A. K., & Fernandes, B. G. (2018). An approach for reliability prediction of instrumentation & control cables by artificial neural networks and Weibull theory for probabilistic safety assessment of NPPs. *Reliability Engineering and System Safety*, 170, 31-44.

[106] Atamuradov, V., Medjaher, K., Camci, F., Zerhouni, N., Dersin, P., & Lamoureux, B. (2019). Feature selection and fault-severity classification-based machine health assessment methodology for point machine sliding-chair degradation. *Quality and Reliability Engineering International*, 35(4), 1081-1099.

[107] Widodo, A., & Yang, B. S. (2011). Machine health prognostics using survival probability and support vector machine. *Expert Systems with Applications*, 38(7), 8430-8437.

[108] Xu, D., et al. (2018). RUL prediction of electronic controller based on multiscale characteristic analysis. *Mechanical Systems and Signal Processing*, 113, 253-270.

[109] Yu, J. (2018). State of health prediction of lithium-ion batteries: Multiscale logic regression and Gaussian process regression ensemble. *Reliability Engineering and System Safety*, 174, 82-95.

[110] Matt, G. et al. (2018). Digitally enabled reliability: Beyond predictive maintenance. McKinsey & Company.

[111] Zio, E. (2009). Reliability engineering:Old problems and new challenges. *Reliability Engineering and System Safety*, 94(2), 125-141.

[112] Si, X. S. et al. (2011). Remaining useful life estimation - A review on the statistical data driven approaches. *European Journal of Operational Research*, 213(1), 1-14.

[113] Kattan, M. W., Hess, K. R., & Beck, J. R. (1998). Experiments to determine whether recursive partitioning (CART) or an artificial neural network overcomes theoretical limitations of Cox proportional hazards regression. *Computers and Biomedical Research*, 31(5), 363-373.

[114] Sikorska, J. Z., Hodkiewicz, M., & Ma, L. (2011). Prognostic modelling options for remaining useful life estimation by industry. *Mechanical systems and signal processing*, 25(5), 1803-1836.

[115] Yang, F., et al. (2016). Health index-based prognostics for remaining useful life predictions in electrical machines. *IEEE Transactions on Industrial Electronics*, 63(4), 2633-2644.

[116] Saxena, A., Goebel, K., Simon, D., & Eklund, N. (2008). Damage propagation modeling for aircraft engine run-to-failure simulation. In *2008 international conference on prognostics and health management*, IEEE, 1-9.

[117] Brockwell, P. J., & Davis, R. A. (2002). Introduction to time series and forecasting (3rd edition). Springer New York.

[118] Hamilton, J. D. (1994). Time series analysis. Princeton university press.

[119] Akaike, H. (1974). A new look at the statistical model identification. *IEEE transactions on automatic control*, 19(6), 716-723.

[120] Anderson, D., & Burnham, K. (1998). Model selection and multi-model inference (2nd edition). NY: Springer-Verlag.

[121] Shibata, R. (1976). Selection of the order of an autoregressive model by Akaike's information criterion. *Biometrika*, 63(1), 117-126.

[122] Hurvich, C. M., & Tsai, C. L. (1989). Regression and time series model selection in small samples. *Biometrika*, 76(2), 297-307.

[123] Brewer, M. J., Butler, A., & Cooksley, S. L. (2016). The relative performance of AIC, AICC and BIC in the presence of unobserved heterogeneity. *Methods in Ecology and Evolution*, 7(6), 679-692.

[124] Durbin, J. (1960). The fitting of time-series models. *Revue de l'Institut International de Statistique*, 233-244.

[125] Chattopadhyay, S., Jhajharia, D., & Chattopadhyay, G. (2011). Univariate modelling of monthly maximum temperature time series over northeast India: neural network versus Yule–Walker equation based approach. *Meteorological Applications*, 18(1), 70-82.

[126] Marple, L. (1980). A new autoregressive spectrum analysis algorithm. *IEEE Transactions on Acoustics, Speech, and Signal Processing*, 28(4), 441-454.

[127] Dickey, D. A., & Fuller, W. A. (1979). Distribution of the estimators for autoregressive time series with a unit root. *Journal of the American Statistical Association*, 74(366a), 427-431.

[128] Dao, P. B., Staszewski, W. J., & Klepka, A. (2017). Stationarity-based approach for the selection of lag length in cointegration analysis used for structural damage detection. *Computer-Aided Civil and Infrastructure Engineering*, 32(2), 138-153.

[129] Ng, S., & Perron, P. (2001). Lag length selection and the construction of unit root tests with good size and power. *Econometrica*, 69(6), 1519-1554.

[130] Schwert, G. W. (2002). Tests for unit roots: A Monte Carlo investigation. *Journal of business & economic statistics*, 20(1), 5-17.

[131] Thode, H. C. (2002). Testing for normality. CRC press.

[132] Jarque, C. M.,& Bera, A. K. (1980). Efficient tests for normality, homoscedasticity and serial independence of regression residuals. *Economics letters*, 6(3), 255-259.

[133] Pollock, D. S. G., Green, R. C., & Nguyen, T. (1999). Handbook of time series analysis, signal processing, and dynamics. Academic Press Inc..

[134] Cross, E. (2012). On structural health monitoring in changing environmental and operational conditions (Doctoral dissertation, University of Sheffield).

[135] Chuang, C. S., & Chan, N. H. (2002). Empirical likelihood for autoregressive models, with applications to unstable time series. *Statistica Sinica*, 387-407.

[136] Baraniuk, R. G. (2007). Compressive sensing [lecture notes]. *IEEE signal processing magazine*, 24(4), 118-121.

[137] Sharif-Khodaei, Z., & Aliabadi, M. H. (2014). Assessment of delay-and-sum algorithms for damage detection in aluminium and composite plates. *Smart materials and structures*, 23(7), 075007.

[138] Basseville, M., & Nikiforov, I. V. (1993). Detection of abrupt changes: theory and application (Vol. 104). Englewood Cliffs: Prentice hall.

[139] Testa, M., & Magli, E. (2016). Compressive estimation and imaging based on autoregressive models. *IEEE Transactions on Image Processing*, 25(11), 5077-5087.

[140] Bian, X., Xu, W., Wang, Y., Lu, L., & Wang, S. (2021). Direct feature extraction and diagnosis of ECG signal in the compressed domain. *IEEE Sensors Journal*, 21(15), 17096-17106.

[141] Houghton, J. R., & Shen, P. (1990). Ultrasonic reflector classification with autoregressive models. *Journal of Research in Nondestructive Evaluation*, 1(4), 235-246.

[142] de Sa Rodrigues, F., Giannakeas, I. N., Khodaei, Z. S., & Aliabadi, F. M. (2023). Probability based damage detection on a composite fuselage panel based on large data set of guided wave signals. *NDT & E International*, 139, 102924.

[143] Flynn, E. B., Todd, M. D., Wilcox, P. D., Drinkwater, B. W., & Croxford, A. J. (2011). Maximum-likelihood estimation of damage location in guided-wave structural health monitoring. *Proceedings of the Royal Society A: Mathematical, Physical and Engineering Sciences*, 467(2133), 2575-2596.

[144] Huber, A. (2018). Dispersion Calculator.

[145] Heckert, N., et al. (2002). Handbook 151:NIST/SEMATECH e-Handbook of Statistical Methods, NIST Interagency/Internal Report (NISTIR), National Institute of Standards and Technology, Gaithersburg, MD (Accessed April 4, 2024).

[146] Poddar, B., Kumar, A., Mitra, M., & Mujumdar, P. M. (2011). Time reversibility of a Lamb wave for damage detection in a metallic plate. *Smart Materials and Structures*, 20(2), 025001.

[147] Wilcox, P. D. (1998). Lamb wave inspection of large structures using permanently attached transducers (Doctoral dissertation, Imperial College London).

[148] Gorgin, R., Luo, Y., & Wu, Z. (2020). Environmental and operational conditions effects on Lamb wave based structural health monitoring systems: A review. *Ultrasonics*, 105, 106114.

[149] Li, D., Jing, Z., & Jin, M. (2017). Plate-like structure damage location identification based on Lamb wave baseline-free probability imaging method. *Advances in Mechanical Engineering*, 9(1), 1687814016685702.

[150] Tabatabaeipour, M., Hettler, J., Delrue, S., & Van Den Abeele, K. (2017). Visualization of delaminations in composite structures using a baseline-free, sparse array imaging technique based on nonlinear Lamb wave propagation. *Acta Acustica united with Acustica*, 103(6), 987-997.

[151] Fan, H., Gao, F., Li, W., & Zhang, K. (2023). A Two-Step Model-Based Reconstruction and Imaging Method for Baseline-Free Lamb Wave Inspection. *Symmetry*, 15(6), 1171.

[152] Cantero-Chinchilla, S., Malik, M. K., Chronopoulos, D., & Chiachio, J. (2021). Bayesian damage localization and identification based on a transient wave propagation model for composite beam structures. *Composite Structures*, 267, 113849.

[153] He, S., & Ng, C. T. (2016). A probabilistic approach for quantitative identification of multiple delaminations in laminated composite beams using guided waves. *Engineering Structures*, 127, 602-614.

[154] Yan, W. J., Chronopoulos, D., Papadimitriou, C., Cantero-Chinchilla, S., & Zhu, G. S. (2020). Bayesian inference for damage identification based on analytical probabilistic model of scattering coefficient estimators and ultrafast wave scattering simulation scheme. *Journal of Sound and Vibration*, 468, 115083.

[155] He, T., Xing, G., Li, Y., Li, Q., & Zhou, S. (2020). A novel baseline-free defect detection and localization method of welded steel plate based on reciprocity loss. *Measurement Science and Technology*, 32(2), 025602.

[156] Jagadeeshwar, T. L., Kalyani, S., Rajagopal, P., & Srinivasan, B. (2022). Statistics-based baseline-free approach for rapid inspection of delamination in composite structures using ultrasonic guided waves. *Structural Health Monitoring*, 21(6), 2719-2731.

[157] de Castro Ribeiro, M. G., Kubrusly, A. C., Ayala, H. V. H., & Dixon, S. (2021). Machine learning-based corrosion-like defect estimation with shear-horizontal guided waves improved by mode separation. *IEEE Access*, 9, 40836-40849.

[158] Bagheri, A., Li, K., & Rizzo, P. (2013). Reference-free damage detection by means of wavelet transform and empirical mode decomposition applied to Lamb waves. *Journal of Intelligent Material Systems and Structures*, 24(2), 194-208.

[159] Soleimanpour, R., & Ng, C. T. (2017). Locating delaminations in laminated composite beams using nonlinear guided waves. *Engineering Structures*, 131, 207-219.

[160] Testoni, N., De Marchi, L., & Marzani, A. (2016). Detection and characterization of delaminations in composite plates via air-coupled probes and warped-domain filtering. *Composite Structures*, 153, 773-781.

[161] Reitz, T., & Fritzen, C. P. (2021). A novel baseline-free approach for acousto-ultrasonic crack monitoring of rotating axles. *Structural Health Monitoring*, 20(3), 990-1003.

[162] Huthwaite, P., & Simonetti, F. (2013). High-resolution guided wave tomography. *Wave Motion*, 50(5), 979-993.

[163] Hanfei, Z., et al. (2020). Multi-sensor network for industrial metal plate structure monitoring via time reversal ultrasonic guided wave. *Measurement*, 152, 107345.

[164] Wang, J., Shen, Y., Rao, D., & Xu, W. (2021). Physical-virtual time reversing of nonlinear Lamb waves for fatigue crack detection and quantification. *Mechanical Systems and Signal Processing*, 160(107921).

[165] Woo, H., Sohn, H., Law, K. H., & Farrar, C. R. (2007). Time reversal active sensing for health monitoring of a composite plate. *Journal of Sound and Vibration*, 302, 50–66.

[166] Zhou, K., Zheng, Y., Zhang, J., Xu, X., Ma, S., & Wu, Z. (2019). A reconstruction-based mode separation method of Lamb wave for damage detection in plate structures. *Smart Materials and Structures*, 28(3).

[167] Zhang, J., et al. (2021). Baseline-free damage diagnostic imaging approach relying on the extraction of converted modes of ultrasonic guided waves. *Journal of Aerospace Engineering*, 34(6), 04021071.

[168] Alguri, K. S., Chia, C. C., & Harley, J. B. (2021). Sim-to-Real: Employing ultrasonic guided wave digital surrogates and transfer learning for damage visualization. *Ultrasonics*, 111, 106338.

[169] Kwon, O., Sohn, H., Jang, J., Choi, J., Ma, Z., & Lim, H. J. (2023). Baseline-free absolute strain estimation for cylindrical structures. *Engineering Structures*, 291, 116439.

[170] Lim, H. J., Kim, Y., Koo, G., Yang, S., Sohn, H., Bae, I. H., & Jang, J. H. (2016). Development and field application of a nonlinear ultrasonic modulation technique for fatigue crack detection without reference data from an intact condition. *Smart Materials and Structures*, 25(9), 095055.

[171] Worden, K., Farrar, C. R., Manson, G., & Park, G. (2007). The fundamental axioms of structural health monitoring. *Proceedings of the Royal Society A: Mathematical, Physical and Engineering Sciences*, 463(2082), 1639–1664.

[172] Fink, M. (1996). Time reversal in acoustics. *Contemporary Physics*, 37(2), 95–109.

[173] Fink, M. (2006). Time-reversal acoustics in complex environments. *Geophysics*, 71(4).

[174] Wapenaar, K., & Thorbecke, J. (2017). Virtual sources and their responses, Part I: time-reversal acoustics and seismic interferometry. *Geophysical Prospecting*, 65(6), 1411-1429.

[175] Woo, H., Bum, S., & Sohn, H. (2009). Understanding a time reversal process in Lamb wave propagation. *Wave Motion*, 46(7), 451–467.

[176] Xiao, H., Shen, Y., Xiao, L., Qu, W., & Lu, Y. (2018). Damage detection in composite structures with high-damping materials using time reversal method. *Nondestructive Testing and Evaluation*, 33(3), 329-345.

[177] Huang, L., Zeng, L., Lin, J., & Luo, Z. (2018). An improved time reversal method for diagnostics of composite plates using Lamb waves. *Composite Structures*, 190, 10-19.

[178] Anderson, B. E., Ulrich, T. J., & Le Bas, P.-Y. (2013). Comparison and visualization of focusing wave fields from various time reversal techniques in elastic media. *The Journal of the Acoustical Society of America*, 134(6), EL527–EL533.

[179] Zumpano, G., & Meo, M. (2007). A new nonlinear elastic time reversal acoustic method for the identification and localization of stress corrosion cracking in welded plate-like structures - A simulation study. *International Journal of Solids and Structures*, 44(11–12), 3666–3684.

[180] Gangadharan, R., Murthy, C. R. L., Gopalakrishnan, S., & Bhat, M. R. (2009). Time reversal technique for health monitoring of metallic structure using Lamb waves. *Ultrasonics*, 49(8), 696–705.

[181] Gangadharan, R., Murthy, C. R. L., Gopalakrishnan, S., & Bhat, M. R. (2009). Time reversal health monitoring of a composite structure using Lamb waves. *Collection of Technical Papers - AIAA/ASME/ASCE/AHS/ASC Structures, Structural Dynamics and Materials Conference*, 3(3).

[182] Qiang, W., & Shenfang, Y. (2009). Baseline-free imaging method based on new pzt sensor arrangements. *Journal of Intelligent Material Systems and Structures*, 20(14), 1663–1673.

[183] Ciampa, F., & Meo, M. (2012). Impact detection in anisotropic materials using a time reversal approach. *Structural Health Monitoring*, 11(1), 43-49.

[184] Eremin, A., Glushkov, E., Glushkova, N., & Lammering, R. (2019). Guided wave time-reversal imaging of macroscopic localized inhomogeneities in anisotropic composites. *Structural Health Monitoring*, 18(5–6), 1803–1819.

[185] Qiu, L., Yuan, S., Zhang, X., & Wang, Y. (2011). A time reversal focusing based impact imaging method and its evaluation on complex composite structures. *Smart Materials and Structures*, 20(10), 105014.

[186] Simone, M. E. De, Ciampa, F., & Meo, M. (2019). A hierarchical method for the impact force reconstruction in composite structures. *Smart Materials and Structures*, 28, 085022.

[187] Du, G., Kong, Q., Wu, F., Ruan, J., & Song, G. (2016). An experimental feasibility study of pipeline corrosion pit detection using a piezoceramic time reversal mirror. *Smart Materials and Structures*, 25(3), 037002.

[188] Huo, L., Li, C., Jiang, T., & Li, H. N. (2018). Feasibility study of steel bar corrosion monitoring using a piezoceramic transducer enabled time reversal method. *Applied Sciences*, 8(11), 2304.

[189] Mustapha, S., Lu, Y., Li, J., & Ye, L. (2014). Damage detection in rebar-reinforced concrete beams based on time reversal of guided waves. *Structural Health Monitoring*, 13(4), 347–358.

[190] Zhao, G., Zhang, D., Zhang, L., & Wang, B. (2018). Detection of defects in reinforced concrete structures using ultrasonic nondestructive evaluation with piezoceramic transducers and the time reversal method. *Sensors*, 18(12), 4176.

[191] Miao, X., Wang, D., Ye, L., Lu, Y., Li, F., & Meng, G. (2011). Identification of dual notches based on time-reversal lamb waves and a damage diagnostic imaging algorithm. *Journal of Intelligent Material Systems and Structures*, 22(17), 1983–1992.

[192] Liang, Y., Li, D., Kong, Q., & Song, G. (2016). Load monitoring of the pin-connected structure using time reversal technique and piezoceramic transducers - A feasibility study. *IEEE Sensors Journal*, 16(22), 7958–7966.

[193] Parvasi, S. M., Ho, S. C. M., Kong, Q., Mousavi, R., & Song, G. (2016). Real time bolt preload monitoring using piezoceramic transducers and time reversal technique—A numerical study with experimental verification. *Smart Materials and Structures*, 25(8), 085015.

[194] Tao, W., Shaopeng, L., Junhua, S., & Yourong, L. (2016). Health monitoring of bolted joints using the time reversal method and piezoelectric transducers. *Smart Materials and Structures*, 25(2), 025010.

[195] Kocur, G. K., Saenger, E. H., Grosse, C. U., & Vogel, T. (2016). Time reverse modeling of acoustic emissions in a reinforced concrete beam. *Ultrasonics*, 65, 96–104.

[196] Nguyen, L. T., Kocur, G. K., & Saenger, E. H. (2018). Defect mapping in pipes by ultrasonic wavefield cross-correlation: A synthetic verification. *Ultrasonics*, 90, 153-165.

[197] Xu, Y., Luo, M., Liu, Q., Du, G., & Song, G. (2019). PZT transducer array enabled pipeline defect locating based on time-reversal method and matching pursuit de-noising. *Smart Materials and Structures*, 28(7), 075019.

[198] Zhang, G., Zhu, J., Song, Y., Peng, C., & Song, G. (2018). A Time Reversal Based Pipeline Leakage Localization Method with the Adjustable Resolution. *IEEE Access*, 6, 26993–27000.

[199] Ciampa, Francesco, & Meo, M. (2014). Impact localization on a composite tail rotor blade using an inverse filtering approach. *Journal of Intelligent Material Systems and Structures*, 25(15), 1950–1958.

[200] He, J., Rocha, D. C., & Sava, P. (2020). Guided wave tomography based on least-squares reverse-time migration. *Structural Health Monitoring*, 19(4), 1237–1249.

[201] He, J., & Yuan, F. G. (2015). Damage identification for composite structures using a cross-correlation reverse-time migration technique. *Structural Health Monitoring*, 14(6), 558–570.

[202] He, J., & Yuan, F. G. (2017). Lamb-wave-based two-dimensional areal scan damage imaging using reverse-time migration with a normalized zero-lag cross-correlation imaging condition. *Structural Health Monitoring*, 16(4), 444–457.

[203] Liu, Z., Yu, H., Fan, J., Hu, Y., He, C., & Wu, B. (2015). Baseline-free delamination inspection in composite plates by synthesizing non-contact air-coupled Lamb wave scan method and virtual time reversal algorithm. *Smart Materials and Structures*, 24(4), 045014.

[204] Watkins, R., & Jha, R. (2012). A modified time reversal method for Lamb wave based diagnostics of composite structures. *Mechanical Systems and Signal Processing*, 31, 345–354.

[205] Wang, J., & Shen, Y. (2019). An enhanced Lamb wave virtual time reversal technique for damage detection with transducer transfer function compensation. *Smart Materials and Structures*, 28(085017), 1–16.

[206] Kannusamy, M., Kapuria, S., & Sasmal, S. (2022). An efficient Lamb wave-based virtual refined time-reversal method for damage localization in plates using broadband measurements. *Ultrasonics*, 124, 106767.

[207] Castro, B. A. De, Member, S., Baptista, F. G., Member, S., Ardila-rey, J. A., & Ciampa, F. (2022). Baseline-Free Damage Imaging Algorithm Using Spatial Frequency Domain Virtual Time Reversal. *IEEE Transactions on Industrial Informatics*, 18(8), 5043–5054.

[208] Anton, S. R., Inman, D. J., & Park, G. (2009). Reference-free damage detection using instantaneous baseline measurements. *AIAA journal*, 47(8), 1952-1964.

[209] Sun, H., Zhang, A., Wang, Y., & Qing, X. (2019). Baseline-free damage imaging for metal and composite plate-type structures based on similar paths. *International Journal of Distributed Sensor Networks*, 15(4), 1550147719843054.

[210] Park, S., Anton, S. R., Kim, J. K., Inman, D. J., & Ha, D. S. (2010). Instantaneous baseline structural damage detection using a miniaturized piezoelectric guided waves system. *KSCE Journal of Civil engineering*, 14, 889-895.

[211] Wang, J., Shen, Y., Rao, D., & Xu, W. (2021). An instantaneous-baseline multi-indicial nonlinear ultrasonic resonance spectral correlation technique for fatigue crack detection and quantification. *Nonlinear Dynamics*, 103, 677–698.

[212] Wu, W., Qu, W., Xiao, L., & Inman, D. J. (2016). Detection and localization of fatigue crack with nonlinear instantaneous baseline. *Journal Of Intelligent Material Systems and Structures*, 27(12), 1577–1583.

[213] Qiu, J., Li, F., & Zhu, Y. (2018). An improved instantaneous baseline method for pipe structures based on distance compensation using guided waves. *Measurement Science and Technology*, 29(10), 105106.

[214] Qiu, J., Li, F., & Abbas, S. (2019). A baseline-free damage detection approach based on distance compensation of guided waves. *Journal of Low Frequency, Noise, Vibration and Active Control*, 38(3-4), 1132–1148.

[215] Bekas, D. G., Sharif-Khodaei, Z., & Aliabadi, M. F. (2018). An innovative diagnostic film for structural health monitoring of metallic and composite structures. *Sensors*, 18(7), 2084.

[216] Lin, M., & Chang, F. K. (2002). The manufacture of composite structures with a built-in network of piezoceramics. *Composites Science and Technology*, 62(7–8), 919–939.

[217] Huang, L., Zeng, L., & Lin, J. (2017). Baseline-free damage detection in composite plates based on the reciprocity principle. *Smart materials and Structures*, 27(1), 015026.

[218] Scalerandi, M., Bruno, C. L. E., Gliozzi, A. S., & Bocca, P. G. (2012). Break of reciprocity principle due to localized nonlinearities in concrete. *Ultrasonics*, 52(6), 712–719.

[219] Huang, L., Zeng, L., Lin, J., & Zhang, N. (2020). Baseline-free damage detection in composite plates using edge-reflected Lamb waves. *Composite Structures*, 247, 112423.

[220] Du, F., Zeng, L., Huang, L., & Rao, J. (2023). A refined lamb wave reciprocity-based method with enhanced sensitivity for damage detection in composite laminates. *Ultrasonics*, 132, 106980.

[221] Jia, H., Liu, H., Zhang, Z., Dai, F., Liu, Y., & Leng, J. (2020). A baseline-free approach of locating defect based on mode conversion and the reciprocity principle of Lamb waves. *Ultrasonics*, 102, 106063.

[222] Zuo, P., & Huthwaite, P. (2022). Quantitative mapping of thickness variations along a ray path using geometrical full waveform inversion and guided wave mode conversion. *Proceedings of the Royal Society A*, 478(2257), 20210602.

[223] Marchi, L. De, Ruzzene, M., & Xu, B. (2010). Warped Basis Pursuit for Damage Detection Using Lamb Waves. *IEEE Transactions on Ultrasonics, Ferroelectrics, and Frequency Control*, 57(12), 2734–2741.

[224] Ratassepp, M., Fan, Z., & Lasn, K. (2016). Wave mode extraction from multimodal wave signals in an orthotropic composite plate. *Ultrasonics*, 71, 223–230.

[225] Xu, K., Ta, D., & Wang, W. (2010). Multiridge-based analysis for separating individual modes from multimodal guided wave signals in long bones. *IEEE Transactions on Ultrasonics, Ferroelectrics, and Frequency Control*, 57(11), 2480–2490.

[226] Bertoncini, F., Cappelli, M., Cordella, F., & Raugi, M. (2016). Non-invasive on-line monitoring for nuclear power plants using guided waves propagating in steel pipes with different types of structural complexity. *International Conference on Nuclear Engineering, Proceedings, ICONE*, 1, 1–7.

[227] Li, G., Neerukatti, R. K., & Chattopadhyay, A. (2018). Ultrasonic guided wave propagation in composites including damage using high-fidelity local interaction simulation. *Journal of Intelligent Material Systems and Structures*, 29(5), 969–985.

[228] Lee, S. J., et al. (2012). Baseline-free guided wave imaging via adaptive source removal. *Structural Health Monitoring*, 11(4), 472–481.

[229] Liu, L., & Yuan, F. G. (2010). A linear mapping technique for dispersion removal of Lamb waves. *Structural Health Monitoring*, 9(1), 75–86.

[230] Gao, F., Zeng, L., Lin, J., & Luo, Z. (2017). Mode separation in frequency–wavenumber domain through compressed sensing of far-field Lamb waves. *Measurement Science and Technology*, 28(7), 075004.

[231] Hall, J. S., & Michaels, J. E. (2009). On a model-based calibration approach to dynamic baseline estimation for structural health monitoring. *AIP Conference Proceedings*, 1096, 896–903.

[232] Lizé, E., Rébillat, M., & Mechbal, N. (2018). Optimal dual-PZT sizing and network design for baseline-free SHM of complex anisotropic composite structures. *Smart Materials and Structures*, 27(115018).

[233] Kim, S. B., & Sohn, H. (2008). Instantaneous crack detection using dual PZT transducers. *Proc. SPIE 6935, Health Monitoring of Structural and Biological Systems*, 693509.

[234] Sohn, H., & Kim, S. B. (2010). Development of Dual PZT Transducers for Reference-Free Crack Detection in Thin Plate Structures. *IEEE Transactions on Ultrasonics, Ferroelectrics, and Frequency Control*, 57(1), 229–240.

[235] Zima, B., & Ke, R. (2019). Reference-free determination of debonding length in reinforced concrete beams using guided wave propagation. *Construction and Building Materials*, 207, 291–303.

[236] Aryan, P., Kotousov, A., Ng, C. T., & Cazzolato, B. S. (2017). A baseline-free and non-contact method for detection and imaging of structural damage using 3D laser vibrometry. *Structural Control and Health Monitoring*, 24(4), e1894.

[237] Bhuiyan, M. Y., Shen, Y., & Giurgiutiu, V. (2016). Guidedwave based crack detection in the rivet hole using global analytical with local FEM approach. *Materials*, 9(7).

[238] Yeung, C., & Ng, C. T. (2019). Time-domain spectral finite element method for analysis of torsional guided waves scattering and mode conversion by cracks in pipes. *Mechanical Systems and Signal Processing*, 128, 305–317.

[239] Gao, T., Liu, X., Zhu, J., Zhao, B., & Qing, X. (2021). Multi-frequency localized wave energy for delamination identification using laser ultrasonic guided wave. *Ultrasonics*, 116, 106486.

[240] Aliabadi, M. H. F., & Khodaei, Z. S. (2017). Structural Health Monitoring for Advanced Composite Structures. World Scientific Publishing Europe Ltd.

[241] Duffour, P., Morbidini, M., & Cawley, P. (2006). A study of the vibro-acoustic modulation technique for the detection of cracks in metals. *The Journal of the Acoustical Society of America*, 119(3), 1463-1475.

[242] Klepka, A., Pieczonka, L., Staszewski, W. J., & Aymerich, F. (2014). Impact damage detection in laminated composites by non-linear vibro-acoustic wave modulations. *Composites Part B: Engineering*, 65, 99–108.

[243] Lim, H. J., Sohn, H., Desimio, M. P., & Brown, K. (2014). Reference-free fatigue crack detection using nonlinear ultrasonic modulation under various temperature and loading conditions. *Mechanical Systems and Signal Processing*, 45(2), 468–478.

[244] Mevissen, F., & Meo, M. (2022). Creep detection of Hastelloy X material for gas turbine components with nonlinear ultrasonic frequency modulation. *Materials Characterization*, 191, 112099.

[245] Sharma, B. N., & Kapuria, S. (2020). Time reversibility of Lamb waves in thin plates with surface-bonded piezoelectric transducers is temperature invariant at the best reconstruction frequency. *Structural Health Monitoring*, 00(0), 1–15.

[246] Agrahari, J. K., & Kapuria, S. (2016). Effects of adhesive , host plate , transducer and excitation parameters on time reversibility of ultrasonic Lamb waves. *Ultrasonics*, 70, 147–157.

[247] Sharma, B. N., Kapuria, S., Arockiarajan, A., & Kannusamy, M. (2023). Baseline-free damage detection and sizing under varying temperatures using Lamb waves without temperature compensation. *Structural Health Monitoring*, 14759217231153435.

[248] Perfetto, D., Sharif Khodaei, Z., De Luca, A., Aliabadi, M. H., & Caputo, F. (2022). Experiments and modelling of ultrasonic waves in composite plates under varying temperature. *Ultrasonics*, 126, 106820.

[249] Raghavan, A., & Cesnik, C. E. S. (2008). Effects of elevated temperature on guided-wave structural health monitoring. *Journal of Intelligent Material Systems and Structures*, 19(12), 1383–1398.

[250] Salama, K., & Ling, C. K. (1980). The effect of stress on the temperature dependence of ultrasonic velocity. *Journal of Applied Physics*, 51(3), 1505–1509.

[251] Moll, J., Eremin, A. A., & Golub, M. V. (2018). The influence of global and local temperature variation on elastic guided wave excitation, propagation and scattering. *9th European Workshop on Structural Health Monitoring, EWSHM 2018*, 1–12.

[252] Schubert, K. J., & Herrmann, A. S. (2012). On the influence of moisture absorption on Lamb wave propagation and measurements in viscoelastic CFRP using surface applied piezoelectric sensors. *Composite Structures*, 94(12), 3635–3643.

[253] Han, C., Yang, G., Wang, J., & Guo, X. (2020). The research on propagation characteristics of acoustic emission signals in stiffened plates based on the multipath propagation model. *Ultrasonics*, 108, 106177.

[254] Chen, Z., Pan, C., & Yu, L. (2018). Structural damage detection via adaptive dictionary learning and sparse representation of measured acceleration responses. *Measurement*, 128, 377-387.

[255] Han, T., Jiang, D., Sun, Y., Wang, N., & Yang, Y. (2018). Intelligent fault diagnosis method for rotating machinery via dictionary learning and sparse representation-based classification. *Measurement*, 118, 181-193.

[256] Nokhbatolfoghahai, A., Navazi, H. M., & Groves, R. M. (2022). Use of dictionary learning for damage localization in complex structures. *Mechanical Systems and Signal Processing*, 180, 109394.

[257] Alguri, K. S., Melville, J., & Harley, J. B. (2018). Baseline-free guided wave damage detection with surrogate data and dictionary learning. *The Journal of the Acoustical Society of America*, 143(6), 3807-3818.

[258] Alguri, K. S., Chia, C. C., & Harley, J. B. (2021). Sim-to-Real: Employing ultrasonic guided wave digital surrogates and transfer learning for damage visualization. *Ultrasonics*, 111, 106338.

[259] Li, G., & Chattopadhyay, A. (2018). Multi-dimensional signal processing and mode tracking approach for guided wave based damage localization in X-COR sandwich composite. *Mechanical Systems and Signal Processing*, 109, 134-149.

[260] Zakaria, J., Mueen, A., & Keogh, E. (2012). Clustering time series using unsupervised-shapelets. In *2012 IEEE 12th International Conference on Data Mining, IEEE*, 785-794.

[261] MIL-HDBK-17-3F. Department of Defense handbook, composite materials handbook - polymer matrix composites materials usage, design, and analysis, Vol.3, 2002.

[262] Zhang, J., Zeng, B., Shen, W., & Gao, L. (2022). A one-class Shapelet dictionary learning method for wind turbine bearing anomaly detection. *Measurement*, 197, 111318.

[263] Zheng, G., Yang, Y., & Carbonell, J. (2016). Efficient shift-invariant dictionary learning. In *Proceedings of the 22nd ACM SIGKDD International Conference on Knowledge Discovery and Data Mining*, 2095-2104.

[264] Iranmehr, E., Böhnert, T., Paz, E., Martins, M., & Ferreira, R. (2023). Unsupervised Extraction of Shape-based Signal Patterns for Incoming Signal Recognition. *IEEE Sensors Journal*.

[265] Gresil, M., & Giurgiutiu, V. (2015). Prediction of attenuated guided waves propagation in carbon fiber composites using Rayleigh damping model. *Journal of Intelligent Material Systems and Structures*, 26(16), 2151-2169.

[266] Ye, L., & Keogh, E. (2009). Time series shapelets: a new primitive for data mining. In *Proceedings of the 15th ACM SIGKDD international conference on Knowledge discovery and data mining*, 947-956.

[267] Grabocka, J., Schilling, N., Wistuba, M., & Schmidt-Thieme, L. (2014). Learning time-series shapelets. In *Proceedings of the 20th ACM SIGKDD international conference on Knowledge discovery and data mining*, 392-401.

[268] Müller, M. (2007). Dynamic time warping. Information retrieval for music and motion, 69-84. Springer.

[269] Lin, J., Keogh, E., Lonardi, S., & Chiu, B. (2003). A symbolic representation of time series, with implications for streaming algorithms. In *Proceedings of the 8th ACM SIGMOD workshop on Research issues in data mining and knowledge discovery*, 2-11.

[270] Pilario, K. E., Tielemans, A., & Mojica, E. R. E. (2022). Geographical discrimination of propolis using dynamic time warping kernel principal components analysis. *Expert Systems with Applications*, 187, 115938.

[271] Ahsan, M. M., Mahmud, M. P., Saha, P. K., Gupta, K. D., & Siddique, Z. (2021). Effect of data scaling methods on machine learning algorithms and model performance. *Technologies*, 9(3), 52.

[272] Mairal, J., Bach, F., Ponce, J., & Sapiro, G. (2009). Online dictionary learning for sparse coding. In *Proceedings of the 26th annual international conference on machine learning*, 689-696.

[273] Engan, K., Aase, S. O., & Husoy, J. H. (1999). Method of optimal directions for frame design. In *1999 IEEE International Conference on Acoustics, Speech, and Signal Processing. Proceedings. ICASSP99*, Vol.5, 2443-2446.

[274] Aharon, M., Elad, M., & Bruckstein, A. (2006). K-SVD: An algorithm for designing overcomplete dictionaries for sparse representation. *IEEE Transactions on signal processing*, 54(11), 4311-4322.

[275] Chen, S. S., Donoho, D. L., & Saunders, M. A. (2001). Atomic decomposition by basis pursuit. *SIAM review*, 43(1), 129-159.

[276] Cai, T. T., & Wang, L. (2011). Orthogonal matching pursuit for sparse signal recovery with noise. *IEEE Transactions on Information theory*, 57(7), 4680-4688.

[277] BS ISO 5725-1:1994. Accuracy (trueness and precision) of measurement methods and results: general principles and definitions.

[278] Yue, N., & Aliabadi, M. H. (2021). Hierarchical approach for uncertainty quantification and reliability assessment of guided wave-based structural health monitoring. *Structural Health Monitoring*, 20(5), 2274-2299.

[279] Beggel, L., Kausler, B. X., Schiegg, M., Pfeiffer, M., & Bischl, B. (2019). Time series anomaly detection based on shapelet learning. *Computational Statistics*, 34, 945-976.

[280] Li, T., Zhou, Z., Li, S., Sun, C., Yan, R., & Chen, X. (2022). The emerging graph neural networks for intelligent fault diagnostics and prognostics: A guideline and a benchmark study. *Mechanical Systems and Signal Processing*, 168, 108653.

[281] Wang, L., Cao, H., Xu, H., & Liu, H. (2022). A gated graph convolutional network with multi-sensor signals for remaining useful life prediction. *Knowledge-Based Systems*, 252, 109340.

[282] Zhou, Y., Zheng, H., Huang, X., Hao, S., Li, D., & Zhao, J. (2022). Graph neural networks: Taxonomy, advances, and trends. *ACM Transactions on Intelligent Systems and Technology*, 13(1), 1-54.

[283] Cox, D. R. (1972). Regression models and life-tables. *Journal of the Royal Statistical Society: Series B (Methodological)*, 34(2), 187-202.

[284] Tsay, R. S. (2013). Multivariate time series analysis: with R and financial applications. John Wiley & Sons.

[285] Geweke, J. F. (1984). Measures of conditional linear dependence and feedback between time series. *Journal of the American Statistical Association*, 79(388), 907-915.

[286] A. Saxena and K. Goebel (2008). Turbofan Engine Degradation Simulation Data Set, NASA Prognostics Data Repository, NASA Ames Research Center, Moffett Field, CA.

[287] Li, G., Qin, S. J., Ji, Y., & Zhou, D. (2010). Reconstruction based fault prognosis for continuous processes. *Control Engineering Practice*, 18(10), 1211-1219.

[288] Zhao, C., & Gao, F. (2015). Online fault prognosis with relative deviation analysis and vector autoregressive modeling. *Chemical Engineering Science*, 138, 531-543.

[289] Han, M., Li, J., Han, B., & Zhong, K. (2019). Fault subspace decomposition and reconstruction theory based online fault prognosis. *Control Engineering Practice*, 85, 121-131.

[290] Hochstein, A., Ahn, H. I., Leung, Y. T., & Denesuk, M. (2014). Switching vector autoregressive models with higher-order regime dynamics application to prognostics and health

management. In *2014 International conference on prognostics and health Management*, 1-10.

[291] Zheng, P., Zhou, Y., Lyu, M. R., & Qi, Y. (2014). Granger causality-aware prediction and diagnosis of software degradation. In *2014 IEEE International Conference on Services Computing*, 528-535.

[292] Farrar, C. R., & Lieven, N. A. (2007). Damage prognosis: the future of structural health monitoring. *Philosophical Transactions of the Royal Society A: Mathematical, Physical and Engineering Sciences*, 365(1851), 623-632.

[293] Aktan, A. E., Helmicki, A. J., & Hunt, V. J. (1998). Issues in health monitoring for intelligent infrastructure. *Smart Materials and Structures*, 7(5), 674.

[294] Du, Y., Wu, T., Zhou, S., & Makis, V. (2020). Remaining useful life prediction of lubricating oil with dynamic principal component analysis and proportional hazards model. *Proceedings of the Institution of Mechanical Engineers, Part J: Journal of Engineering Tribology*, 234(6), 964-971.

[295] Wen, Y., Guo, X., Son, J., & Wu, J. (2023). A neural-network-based proportional hazard model for IoT signal fusion and failure prediction. *IISE Transactions*, 55(4), 377-391.

[296] Zhou, D., Al-Durra, A., Zhang, K., Ravey, A., & Gao, F. (2019). A robust prognostic indicator for renewable energy technologies: A novel error correction grey prediction model. *IEEE Transactions on Industrial Electronics*, 66(12), 9312-9325.

[297] Bender, R., Augustin, T., & Blettner, M. (2005). Generating survival times to simulate Cox proportional hazards models. *Statistics in medicine*, 24(11), 1713-1723.

[298] Lane, W. R., Looney, S. W., & Wansley, J. W. (1986). An application of the Cox proportional hazards model to bank failure. *Journal of Banking & Finance*, 10(4), 511-531.

[299] Fisher, L. D., & Lin, D. Y. (1999). Time-dependent covariates in the Cox proportional-hazards regression model. *Annual review of public health*, 20(1), 145-157.

[300] Wang, T., Yu, J., Siegel, D., & Lee, J. (2008). A similarity-based prognostics approach for remaining useful life estimation of engineered systems. In *2008 international conference on prognostics and health management*, 1-6.

[301] Anis, M. D., Taghipour, S., & Lee, C. G. (2020, January). Optimal RUL estimation: A state-of-art digital twin application. In *2020 annual reliability and maintainability symposium (RAMS)*, 1-7.

[302] Yu, W., Kim, I. Y., & Mechefske, C. (2020). An improved similarity-based prognostic algorithm for RUL estimation using an RNN autoencoder scheme. *Reliability Engineering & System Safety*, 199, 106926.

[303] Heimes, F. O. (2008). Recurrent neural networks for remaining useful life estimation. In *2008 international conference on prognostics and health management*, 1-6.

[304] Zheng, S., Ristovski, K., Farahat, A., & Gupta, C. (2017). Long short-term memory network for remaining useful life estimation. In *2017 IEEE international conference on prognostics and health management (ICPHM)*, 88-95.

[305] Tsay, R.S. (2018). All-Purpose Toolkit for Analyzing Multivariate Time Series (MTS) and Estimating Multivariate Volatility Models. Available at: https://github.com/d-/MTS (Accessed: 09 April 2024)

[306] Chakrabarti, A., & Ghosh, J. K. (2011). AIC, BIC and recent advances in model selection. Philosophy of statistics, 583-605.

[307] Sargent, T. J. (1977). The demand for money during hyperinflations under rational expectations: I. *International Economic Review*, 59-82.

[308] Charakopoulos, A. K., Katsouli, G. A., & Karakasidis, T. E. (2018). Dynamics and causalities of atmospheric and oceanic data identified by complex networks and Granger causality analysis. *Physica A: Statistical Mechanics and its Applications*, 495, 436-453.

[309] Chen, Y., Bressler, S. L., & Ding, M. (2006). Frequency decomposition of conditional Granger causality and application to multivariate neural field potential data. *Journal of neuroscience methods*, 150(2), 228-237.

[310] Przymus, P., Hmamouche, Y., Casali, A., & Lakhal, L. (2017, November). Improving multivariate time series forecasting with random walks with restarts on causality graphs. In *2017 IEEE International Conference on Data Mining Workshops (ICDMW)*, 924-931.

[311] Ju-Long, D. (1982). Control problems of grey systems. *Systems & control letters*, 1(5), 288-294.

[312] Atwa, Y. M., & El-Saadany, E. F. (2009). Reliability evaluation for distribution system with renewable distributed generation during islanded mode of operation. *IEEE Transactions on Power Systems*, 24(2), 572-581.

[313] Tabaszewski, M., & Cempel, C. (2015). Using a set of GM (1, 1) models to predict values of diagnostic symptoms. *Mechanical Systems and Signal Processing*, 52, 416-425.

[314] Kayacan, E., Ulutas, B., & Kaynak, O. (2010). Grey system theory-based models in time series prediction. *Expert systems with applications*, 37(2), 1784-1789.

[315] Kung, L. M., & Yu, S. W. (2008). Prediction of index futures returns and the analysis of financial spillovers—A comparison between GARCH and the grey theorem. *European Journal of Operational Research*, 186(3), 1184-1200.

[316] Julong, D. (1989). Introduction to grey system theory. *The Journal of grey system*, 1(1), 1-24.

[317] Ho, P. H. (2010). Forecasting construction manpower demand by gray model. *Journal of Construction Engineering and Management*, 136(12), 1299-1305.

[318] Lin, Y. H., & Lee, P. C. (2007). Novel high-precision grey forecasting model. *Automation in construction*, 16(6), 771-777.

[319] Bezuglov, A., & Comert, G. (2016). Short-term freeway traffic parameter prediction: Application of grey system theory models. *Expert Systems with Applications*, 62, 284-292.

[320] Davidson-Pilon, C. (2019). lifelines: survival analysis in Python. *Journal of Open Source Software*, 4(40), 1317.

[321] Roelstraete, B., & Rosseel, Y. (2011). FIAR: an R package for analyzing functional integration in the brain. *Journal of Statistical Software*, 44, 1-32.

[322] Ramasso, E. (2014). Investigating computational geometry for failure prognostics in presence of imprecise health indicator: Results and comparisons on c-mapss datasets. In *PHM society european conference*, Vol.2, No.1.

[323] Ordóñez, C., Lasheras, F. S., Roca-Pardinas, J., & de Cos Juez, F. J. (2019). A hybrid ARIMA–SVM model for the study of the remaining useful life of aircraft engines. *Journal of Computational and Applied Mathematics*, 346, 184-191.

[324] Zhang, B., Zheng, K., Huang, Q., Feng, S., Zhou, S., & Zhang, Y. (2020). Aircraft engine prognostics based on informative sensor selection and adaptive degradation modeling with functional principal component analysis. *Sensors*, 20(3), 920.

[325] Sateesh Babu, G., Zhao, P., & Li, X. L. (2016). Deep convolutional neural network based regression approach for estimation of remaining useful life. In *Database Systems for Advanced Applications:21st International Conference, DASFAA 2016*, Part I 21, 214-228.

# Appendix A

# Copyright permission

| Page No. | Type of work: | Name of work | Source of work | Copyright holder and contact | permission requested on | I have permission yes /no | Permission note |
|---|---|---|---|---|---|---|---|
| 3 | figure | Figure 1.1: Number of maintenance-related accidents and serious incidents within 2003-2017: (a) by year; (b) by country. | A contemporary analysis of aircraft maintenance-related accidents and serious incidents. Aerospace, 7(6), 81 (2020) | © MDPI | 11.04.24 | yes | Licensed under an open access Creative Commons CC BY 4.0 license |
| 6 | figure | Figure 1.2: The entire PHM process. | State of the art and taxonomy of prognostics approaches, trends of prognostics applications and open issues towards maturity at different technology readiness levels. Mechanical Systems and Signal Processing, 94, 214-236 (2017) | © Elsevier | 11.04.24 | yes | Written permission |
| 12 | figure | Figure 2.1: An assumed homogeneous and isotropic plate with propagating guided waves, adapted from [38]. | Identification of damage using Lamb waves: from fundamentals to applications (Vol. 48) (2009) | © Springer Science & Business Media | 11.04.24 | yes | Written permission |
| 14 | figure | Figure 2.2: Wave displacements of Lamb waves: (a) symmetric S0 modes; (b) anti-symmetric A0 modes. | Structural health monitoring: with piezoelectric wafer active sensors (2007) | © Elsevier | 11.04.24 | yes | Written permission |
| 18 | figure | Figure 2.3: Lamb wave dispersion curves of a traction-free aluminium plate: (a) phase velocity curves; (b) group velocity curves. The figure is adapted from [37]. | Ultrasonic guided waves in solid media (2007) | Cambridge University Press | 11.04.24 | yes | Written permission |

| Page No. | Type of work: | Name of work | Source of work | Copyright holder and contact | permission requested on | I have permission yes /no | Permission note |
|---|---|---|---|---|---|---|---|
| 21 | figure | Figure 2.5: Transducer configurations particularly with piezoelectric wafers: (a) pitch-catch configuration; (b) pulse-echo configuration; (c) thickness mode; (d) passive sensing manner. Adapted from [39]. | Structural health monitoring of aerospace composites (2015) | © Elsevier | 11.04.24 | yes | Written permission |
| 22 | figure | Figure 2.6: E/M impedance for reproducibility check of mounted transducers on an impacted composite panel. | Self-referenced robust guided wave based defect detection: Application to woven composite parts of complex shape. Mechanical Systems and Signal Processing, 188, 109948 (2023) | © Elsevier | 11.04.24 | yes | Written permission |
| 34 | figure | Figure 2.8: The TOF triangulation approach for damage localisation. Adapted from [38]. | Identification of damage using Lamb waves: from fundamentals to applications (Vol. 48) (2009) | © Springer Science & Business Media | 11.04.24 | yes | Written permission |
| 35 | figure | Figure 2.9: The TDOA approach for damage localisation. Adapted from [66]. | A Novel Baseline-Free Method for Damage Localization Using Guided Waves Based on Hyperbola Imaging Algorithm. Sensors, 23(4), 2050 (2023) | © MDPI | 11.04.24 | yes | Licensed under an open access Creative Commons CC BY 4.0 license |
| 37 | figure | Figure 2.10: Elliptical distribution for imaging pixels. Adapted from [16]. | Active health monitoring of an aircraft wing with embedded piezoelectric sensor/actuator network: I. … Smart materials and structures, 16(4), 1208 (2007) | © IOP Publishing | 11.04.24 | yes | Written permission |

| Page No. | Type of work: | Name of work | Source of work | Copyright holder and contact | permission requested on | I have permission yes /no | Permission note |
|---|---|---|---|---|---|---|---|
| 37 | figure | Figure 2.11: A basic illustration of the C-Scan transducer [72]. | DolphiCam2 Transducer Module (TRM) Technology Note | Dolphitech | 12.04.24 | yes | Written permission |
| 98 | figure | Figure 4.1: Standard time-reversal (TR) procedures. [176]. | An improved time reversal method for diagnostics of composite plates using Lamb waves. Composite Structures, 190, 10-19 (2018) | © Elsevier | 11.04.24 | yes | Written permission |
| 100 | figure | Figure 4.2: Different time-reversal schemes …. Adapted from [202]. | Baseline-free delamination inspection in composite plates by synthesizing non-contact air-coupled Lamb wave scan method and virtual time reversal algorithm. Smart Materials and Structures, 24(4), 045014 (2015) | © IOP Publishing | 11.04.24 | yes | Licensed under an open access Creative Commons Attribution 3.0 licence |
| 102 | figure | Figure 4.3: Frequency shift of response signals compared to 100kHz excitation signals due to the transducer tuning effects [204]. | An enhanced Lamb wave virtual time reversal technique for damage detection with transducer transfer function compensation. Smart Materials and Structures, 28(085017), 1–16 (2019) | © IOP Publishing | 11.04.24 | yes | Written permission |
| 107 | figure | Figure 4.4: Baseline-free damage localisation based on the reciprocity-based approach … | Baseline-free damage detection in composite plates based on the reciprocity principle. Smart materials and Structures, 27(1), 015026 (2017) | © IOP Publishing | 11.04.24 | yes | Written permission |

| Page No. | Type of work: | Name of work | Source of work | Copyright holder and contact | permission requested on | I have permission yes /no | Permission note |
|---|---|---|---|---|---|---|---|
| 113 | figure | Figure 4.5: Effect of temperature variations on time reversibility of Lamb waves in a 3-mm aluminium plate: (a) experiment; (b) 2D FE simulation. [244] | Time reversibility of Lamb waves in thin plates with surface-bonded piezoelectric transducers is temperature invariant at the best reconstruction frequency. Structural Health Monitoring, 00(0), 1–15 (2020) | © Sage Publishing | 24.04.24 | yes | Written permission |
| 115 | figure | Figure 4.6: Damage localisation results of a 2 mm-thick aluminium plate. … | An enhanced Lamb wave virtual time reversal technique for damage detection with transducer transfer function compensation. Smart Materials and Structures, 28(085017), 1–16 (2019) | © IOP Publishing | 11.04.24 | yes | Written permission |
| 116 | figure | Figure 4.7: Damage imaging result of two damages in a 3 mm-thick aluminium plate. The result is obtained by the RTRM with the best reconstruction frequency of excitation signals. [205] | An efficient Lamb wave-based virtual refined time-reversal method for damage localization in plates using broadband measurements. Ultrasonics, 124, 106767 (2022) | © Elsevier | 11.04.24 | yes | Written permission |

# ELSEVIER LICENSE TERMS AND CONDITIONS

Apr 15, 2024

This Agreement between Mr. HONGMIN ZHU ("You") and Elsevier ("Elsevier") consists of your license details and the terms and conditions provided by Elsevier and Copyright Clearance Center.

| | |
|---|---|
| License Number | 5766130489188 |
| License date | Apr 11, 2024 |
| Licensed Content Publisher | Elsevier |
| Licensed Content Publication | Mechanical Systems and Signal Processing |
| Licensed Content Title | State of the art and taxonomy of prognostics approaches, trends of prognostics applications and open issues towards maturity at different technology readiness levels |
| Licensed Content Author | Kamran Javed,Rafael Gouriveau,Noureddine Zerhouni |
| Licensed Content Date | Sep 15, 2017 |
| Licensed Content Volume | 94 |
| Licensed Content Issue | n/a |
| Licensed Content Pages | 23 |
| Start Page | 214 |
| End Page | 236 |
| Type of Use | reuse in a thesis/dissertation |
| Portion | figures/tables/illustrations |
| Number of figures/tables/illustrations | 1 |
| Format | both print and electronic |
| Are you the author of this Elsevier article? | No |
| Will you be translating? | No |
| Title of new work | Data-driven Modelling for Guided Wave Structural Health Monitoring and Prognostic Health Management on Aeronautical Structures |
| Institution name | Imperial College London |
| Expected presentation date | Jul 2024 |
| Order reference number | abcd |
| Portions | Fig. 2. PHM cycle |
| Requestor Location | Mr. HONGMIN ZHU<br>Exhibition Road<br><br>London, other<br>United Kingdom<br>Attn: Mr. HONGMIN ZHU |
| Publisher Tax ID | GB 494 6272 12 |
| Billing Type | Invoice |
| Billing Address | Mr. HONGMIN ZHU<br>Exhibition Road<br><br>London, United Kingdom<br>Attn: Mr. HONGMIN ZHU |
| Total | **0.00 GBP** |
| Terms and Conditions | |

## INTRODUCTION

1. The publisher for this copyrighted material is Elsevier. By clicking "accept" in connection with completing this licensing transaction, you agree that the following terms and conditions apply to this transaction (along with the Billing and Payment terms and conditions established by Copyright Clearance Center, Inc. ("CCC"), at the time that you opened your RightsLink account and that are available at any time at https://myaccount.copyright.com).

## GENERAL TERMS

2. Elsevier hereby grants you permission to reproduce the aforementioned material subject to the terms and conditions indicated.

3. Acknowledgement: If any part of the material to be used (for example, figures) has appeared in our publication with credit or acknowledgement to another source, permission must also be sought from that source. If such permission is not obtained then that material may not be included in your publication/copies. Suitable acknowledgement to the source must be made, either as a footnote or in a reference list at the end of your publication, as follows:
"Reprinted from Publication title, Vol /edition number, Author(s), Title of article / title of chapter, Pages No., Copyright (Year), with permission from Elsevier [OR APPLICABLE SOCIETY COPYRIGHT OWNER]." Also Lancet special credit - "Reprinted from The Lancet, Vol. number, Author(s), Title of article, Pages No., Copyright (Year), with permission from Elsevier."

4. Reproduction of this material is confined to the purpose and/or media for which permission is hereby given. The material may not be reproduced or used in any other way, including use in combination with an artificial intelligence tool (including to train an algorithm, test, process, analyse, generate output and/or develop any form of artificial intelligence tool), or to create any derivative work and/or service (including resulting from the use of artificial intelligence tools).

5. Altering/Modifying Material: Not Permitted. However figures and illustrations may be altered/adapted minimally to serve your work. Any other abbreviations, additions, deletions and/or any other alterations shall be made only with prior written authorization of Elsevier Ltd. (Please contact Elsevier's permissions helpdesk here). No modifications can be made to any Lancet figures/tables and they must be reproduced in full.

6. If the permission fee for the requested use of our material is waived in this instance, please be advised that your future requests for Elsevier materials may attract a fee.

7. Reservation of Rights: Publisher reserves all rights not specifically granted in the combination of (i) the license details provided by you and accepted in the course of this licensing transaction, (ii) these terms and conditions and (iii) CCC's Billing and Payment terms and conditions.

8. License Contingent Upon Payment: While you may exercise the rights licensed immediately upon issuance of the license at the end of the licensing process for the transaction, provided that you have disclosed complete and accurate details of your proposed use, no license is finally effective unless and until full payment is received from you (either by publisher or by CCC) as provided in CCC's Billing and Payment terms and conditions. If full payment is not received on a timely basis, then any license preliminarily granted shall be deemed automatically revoked and shall be void as if never granted. Further, in the event that you breach any of these terms and conditions or any of CCC's Billing and Payment terms and conditions, the license is automatically revoked and shall be void as if never granted. Use of materials as described in a revoked license, as well as any use of the materials beyond the scope of an unrevoked license, may constitute copyright infringement and publisher reserves the right to take any and all action to protect its copyright in the materials.

9. Warranties: Publisher makes no representations or warranties with respect to the licensed material.

10. Indemnity: You hereby indemnify and agree to hold harmless publisher and CCC, and their respective officers, directors, employees and agents, from and against any and all claims arising out of your use of the licensed material other than as specifically authorized pursuant to this license.

11. No Transfer of License: This license is personal to you and may not be sublicensed, assigned, or transferred by you to any other person without publisher's written permission.

12. No Amendment Except in Writing: This license may not be amended except in a writing signed by both parties (or, in the case of publisher, by CCC on publisher's behalf).

13. Objection to Contrary Terms: Publisher hereby objects to any terms contained in any purchase order, acknowledgment, check endorsement or other writing prepared by you, which terms are inconsistent with these terms and conditions or CCC's Billing and Payment terms and conditions. These terms and conditions, together with CCC's Billing and Payment terms and conditions (which are incorporated herein), comprise the entire agreement between you and publisher (and CCC) concerning this licensing transaction. In the event of any conflict between your obligations established by these terms and conditions and those established by CCC's Billing and Payment terms and conditions, these terms and conditions shall control.

14. Revocation: Elsevier or Copyright Clearance Center may deny the permissions described in this License at their sole discretion, for any reason or no reason, with a full refund payable to you. Notice of such denial will be made using the contact information provided by you. Failure to receive such notice will not alter or invalidate the denial. In no event will Elsevier or Copyright Clearance Center be responsible or liable for any costs, expenses or damage incurred by you as a result of a denial of your permission request, other than a refund of the amount(s) paid by you to Elsevier and/or Copyright Clearance Center for denied permissions.

## LIMITED LICENSE

The following terms and conditions apply only to specific license types:

15. **Translation**: This permission is granted for non-exclusive world **English** rights only unless your license was granted for translation rights. If you licensed translation rights you may only translate this content into the languages you requested. A professional translator must perform all translations and reproduce the content word for word preserving the integrity of the article.

16. **Posting licensed content on any Website**: The following terms and conditions apply as follows: Licensing material from an Elsevier journal: All content posted to the web site must maintain the copyright information line on the bottom of each image;

A hyper-text must be included to the Homepage of the journal from which you are licensing at http://www.sciencedirect.com/science/journal/xxxxx or the Elsevier homepage for books at http://www.elsevier.com; Central Storage: This license does not include permission for a scanned version of the material to be stored in a central repository such as that provided by Heron/XanEdu.
Licensing material from an Elsevier book: A hyper-text link must be included to the Elsevier homepage at http://www.elsevier.com . All content posted to the web site must maintain the copyright information line on the bottom of each image.

**Posting licensed content on Electronic reserve**: In addition to the above the following clauses are applicable: The web site must be password-protected and made available only to bona fide students registered on a relevant course. This permission is granted for 1 year only. You may obtain a new license for future website posting.
17. **For journal authors:** the following clauses are applicable in addition to the above:
**Preprints:**
A preprint is an author's own write-up of research results and analysis, it has not been peer-reviewed, nor has it had any other value added to it by a publisher (such as formatting, copyright, technical enhancement etc.).
Authors can share their preprints anywhere at any time. Preprints should not be added to or enhanced in any way in order to appear more like, or to substitute for, the final versions of articles however authors can update their preprints on arXiv or RePEc with their Accepted Author Manuscript (see below).
If accepted for publication, we encourage authors to link from the preprint to their formal publication via its DOI. Millions of researchers have access to the formal publications on ScienceDirect, and so links will help users to find, access, cite and use the best available version. Please note that Cell Press, The Lancet and some society-owned have different preprint policies. Information on these policies is available on the journal homepage.
**Accepted Author Manuscripts:** An accepted author manuscript is the manuscript of an article that has been accepted for publication and which typically includes author-incorporated changes suggested during submission, peer review and editor-author communications.
Authors can share their accepted author manuscript:

- immediately
    - via their non-commercial person homepage or blog
    - by updating a preprint in arXiv or RePEc with the accepted manuscript
    - via their research institute or institutional repository for internal institutional uses or as part of an invitation-only research collaboration work-group
    - directly by providing copies to their students or to research collaborators for their personal use
    - for private scholarly sharing as part of an invitation-only work group on commercial sites with which Elsevier has an agreement
- After the embargo period
    - via non-commercial hosting platforms such as their institutional repository
    - via commercial sites with which Elsevier has an agreement

In all cases accepted manuscripts should:

- link to the formal publication via its DOI
- bear a CC-BY-NC-ND license - this is easy to do
- if aggregated with other manuscripts, for example in a repository or other site, be shared in alignment with our hosting policy not be added to or enhanced in any way to appear more like, or to substitute for, the published journal article.

**Published journal article (JPA):** A published journal article (PJA) is the definitive final record of published research that appears or will appear in the journal and embodies all value-adding publishing activities including peer review co-ordination, copy-editing, formatting, (if relevant) pagination and online enrichment.
Policies for sharing publishing journal articles differ for subscription and gold open access articles:
**Subscription Articles:** If you are an author, please share a link to your article rather than the full-text. Millions of researchers have access to the formal publications on ScienceDirect, and so links will help your users to find, access, cite, and use the best available version.
Theses and dissertations which contain embedded PJAs as part of the formal submission can be posted publicly by the awarding institution with DOI links back to the formal publications on ScienceDirect.
If you are affiliated with a library that subscribes to ScienceDirect you have additional private sharing rights for others' research accessed under that agreement. This includes use for classroom teaching and internal training at the institution (including use in course packs and courseware programs), and inclusion of the article for grant funding purposes.
**Gold Open Access Articles:** May be shared according to the author-selected end-user license and should contain a CrossMark logo, the end user license, and a DOI link to the formal publication on ScienceDirect.
Please refer to Elsevier's posting policy for further information.
18. **For book authors** the following clauses are applicable in addition to the above: Authors are permitted to place a brief summary of their work online only. You are not allowed to download and post the published electronic version of your chapter, nor may you scan the printed edition to create an electronic version. **Posting to a repository:** Authors are permitted to post a summary of their chapter only in their institution's repository.

19. **Thesis/Dissertation**: If your license is for use in a thesis/dissertation your thesis may be submitted to your institution in either print or electronic form. Should your thesis be published commercially, please reapply for permission. These requirements include permission for the Library and Archives of Canada to supply single copies, on demand, of the complete thesis and include permission for Proquest/UMI to supply single copies, on demand, of the complete thesis. Should your thesis be published commercially, please reapply for permission. Theses and dissertations which contain embedded PJAs as part of the formal submission can be posted publicly by the awarding institution with DOI links back to the formal publications on ScienceDirect.

**Elsevier Open Access Terms and Conditions**

You can publish open access with Elsevier in hundreds of open access journals or in nearly 2000 established subscription journals that support open access publishing. Permitted third party re-use of these open access articles is defined by the author's choice of Creative Commons user license. See our open access license policy for more information.

**Terms & Conditions applicable to all Open Access articles published with Elsevier:**

Any reuse of the article must not represent the author as endorsing the adaptation of the article nor should the article be modified in such a way as to damage the author's honour or reputation. If any changes have been made, such changes must be clearly indicated.

The author(s) must be appropriately credited and we ask that you include the end user license and a DOI link to the formal publication on ScienceDirect.

If any part of the material to be used (for example, figures) has appeared in our publication with credit or acknowledgement to another source it is the responsibility of the user to ensure their reuse complies with the terms and conditions determined by the rights holder.

**Additional Terms & Conditions applicable to each Creative Commons user license:**

**CC BY:** The CC-BY license allows users to copy, to create extracts, abstracts and new works from the Article, to alter and revise the Article and to make commercial use of the Article (including reuse and/or resale of the Article by commercial entities), provided the user gives appropriate credit (with a link to the formal publication through the relevant DOI), provides a link to the license, indicates if changes were made and the licensor is not represented as endorsing the use made of the work. The full details of the license are available at http://creativecommons.org/licenses/by/4.0.

**CC BY NC SA:** The CC BY-NC-SA license allows users to copy, to create extracts, abstracts and new works from the Article, to alter and revise the Article, provided this is not done for commercial purposes, and that the user gives appropriate credit (with a link to the formal publication through the relevant DOI), provides a link to the license, indicates if changes were made and the licensor is not represented as endorsing the use made of the work. Further, any new works must be made available on the same conditions. The full details of the license are available at http://creativecommons.org/licenses/by-nc-sa/4.0.

**CC BY NC ND:** The CC BY-NC-ND license allows users to copy and distribute the Article, provided this is not done for commercial purposes and further does not permit distribution of the Article if it is changed or edited in any way, and provided the user gives appropriate credit (with a link to the formal publication through the relevant DOI), provides a link to the license, and that the licensor is not represented as endorsing the use made of the work. The full details of the license are available at http://creativecommons.org/licenses/by-nc-nd/4.0. Any commercial reuse of Open Access articles published with a CC BY NC SA or CC BY NC ND license requires permission from Elsevier and will be subject to a fee.

Commercial reuse includes:

- Associating advertising with the full text of the Article
- Charging fees for document delivery or access
- Article aggregation
- Systematic distribution via e-mail lists or share buttons

Posting or linking by commercial companies for use by customers of those companies.

20. **Other Conditions**:

v1.10

**Questions? E-mail us at customercare@copyright.com.**

# Marketplace

This is a License Agreement between Hongmin Zhu ("User") and Copyright Clearance Center, Inc. ("CCC") on behalf of the Rightsholder identified in the order details below. The license consists of the order details, the Marketplace Permissions General Terms and Conditions below, and any Rightsholder Terms and Conditions which are included below.

All payments must be made in full to CCC in accordance with the Marketplace Permissions General Terms and Conditions below.

| | | | |
|---|---|---|---|
| **Order Date** | 12-Apr-2024 | **Type of Use** | Republish in a thesis/dissertation |
| **Order License ID** | 1472869-1 | | |
| **ISBN-13** | 9781447126744 | **Publisher** | Springer-Verlag |
| | | **Portion** | Image/photo/illustration |

## LICENSED CONTENT

| | | | |
|---|---|---|---|
| **Publication Title** | Identification of damage using Lamb waves : from fundamentals to applications | **Country** | Germany |
| | | **Rightsholder** | Springer Nature BV |
| | | **Publication Type** | Book |
| **Author/Editor** | Su, Z., Ye, L. | | |
| **Date** | 01/01/2009 | | |
| **Language** | English | | |

## REQUEST DETAILS

| | | | |
|---|---|---|---|
| **Portion Type** | Image/photo/illustration | **Distribution** | U.K. and Commonwealth (excluding Canada) |
| **Number of Images / Photos / Illustrations** | 2 | **Translation** | Original language of publication |
| **Format (select all that apply)** | Print, Electronic | **Copies for the Disabled?** | No |
| **Who Will Republish the Content?** | Academic institution | **Minor Editing Privileges?** | No |
| **Duration of Use** | Life of current edition | **Incidental Promotional Use?** | No |
| **Lifetime Unit Quantity** | Up to 4,999 | **Currency** | GBP |
| **Rights Requested** | Main product | | |

## NEW WORK DETAILS

| | | | |
|---|---|---|---|
| **Title** | Data-driven Modelling for Guided Wave Structural Health Monitoring and Prognostic Health Management on Aeronautical Structures | **Institution Name** | Imperial College London |
| | | **Expected Presentation Date** | 2024-07-01 |
| **Instructor Name** | Ferri Aliabadi | | |

## ADDITIONAL DETAILS

| | |
|---|---|
| **The Requesting Person / Organization to Appear on the License** | Hongmin Zhu |

## REQUESTED CONTENT DETAILS

| | | | |
|---|---|---|---|
| **Title, Description or Numeric Reference of the Portion(s)** | Figure 2.1, Figure 6.5 | **Title of the Article / Chapter the Portion Is From** | Fundamentals and Analysis of Lamb Waves; Algorithms for Damage Identification – Fusion of Signal Features. |
| **Editor of Portion(s)** | N/A | **Author of Portion(s)** | Su, Z.; Ye, L. |
| **Volume / Edition** | 2009 | **Publication Date of Portion** | 2009-01-01 |
| **Page or Page Range of Portion** | 16,203 | | |

## Marketplace Permissions General Terms and Conditions

The following terms and conditions ("General Terms"), together with any applicable Publisher Terms and Conditions, govern User's use of Works pursuant to the Licenses granted by Copyright Clearance Center, Inc. ("CCC") on behalf of the applicable Rightsholders of such Works through CCC's applicable Marketplace transactional licensing services (each, a "Service").

1) **Definitions.** For purposes of these General Terms, the following definitions apply:

"License" is the licensed use the User obtains via the Marketplace platform in a particular licensing transaction, as set forth in the Order Confirmation.

"Order Confirmation" is the confirmation CCC provides to the User at the conclusion of each Marketplace transaction. "Order Confirmation Terms" are additional terms set forth on specific Order Confirmations not set forth in the General Terms that can include terms applicable to a particular CCC transactional licensing service and/or any Rightsholder-specific terms.

"Rightsholder(s)" are the holders of copyright rights in the Works for which a User obtains licenses via the Marketplace platform, which are displayed on specific Order Confirmations.

"Terms" means the terms and conditions set forth in these General Terms and any additional Order Confirmation Terms collectively.

"User" or "you" is the person or entity making the use granted under the relevant License. Where the person accepting the Terms on behalf of a User is a freelancer or other third party who the User authorized to accept the General Terms on the User's behalf, such person shall be deemed jointly a User for purposes of such Terms.

"Work(s)" are the copyright protected works described in relevant Order Confirmations.

2) **Description of Service.** CCC's Marketplace enables Users to obtain Licenses to use one or more Works in accordance with all relevant Terms. CCC grants Licenses as an agent on behalf of the copyright rightsholder identified in the relevant Order Confirmation.

3) **Applicability of Terms.** The Terms govern User's use of Works in connection with the relevant License. In the event of any conflict between General Terms and Order Confirmation Terms, the latter shall govern. User acknowledges that Rightsholders have complete discretion whether to grant any permission, and whether to place any limitations on any grant, and that CCC has no right to supersede or to modify any such discretionary act by a Rightsholder.

4) **Representations; Acceptance.** By using the Service, User represents and warrants that User has been duly authorized by the User to accept, and hereby does accept, all Terms.

5) **Scope of License; Limitations and Obligations.** All Works and all rights therein, including copyright rights, remain the sole and exclusive property of the Rightsholder. The License provides only those rights expressly set forth in the terms and conveys no other rights in any Works

6) **General Payment Terms.** User may pay at time of checkout by credit card or choose to be invoiced. If the User chooses to be invoiced, the User shall: (i) remit payments in the manner identified on specific invoices, (ii) unless otherwise specifically stated in an Order Confirmation or separate written agreement, Users shall remit payments upon receipt of the relevant invoice from CCC, either by delivery or notification of availability of the invoice via the Marketplace platform, and (iii) if the User does not pay the invoice within 30 days of receipt, the User may incur a service charge of 1.5% per month or the maximum rate allowed by applicable law, whichever is less. While User may exercise the rights in the License immediately upon receiving the Order Confirmation, the License is automatically revoked and is null and void, as if it had never been issued, if CCC does not receive complete payment on a timely basis.

7) **General Limits on Use.** Unless otherwise provided in the Order Confirmation, any grant of rights to User (i) involves only the rights set forth in the Terms and does not include subsequent or additional uses, (ii) is non-exclusive and non-transferable, and (iii) is subject to any and all limitations and restrictions (such as, but not limited to, limitations on

duration of use or circulation) included in the Terms. Upon completion of the licensed use as set forth in the Order Confirmation, User shall either secure a new permission for further use of the Work(s) or immediately cease any new use of the Work(s) and shall render inaccessible (such as by deleting or by removing or severing links or other locators) any further copies of the Work. User may only make alterations to the Work if and as expressly set forth in the Order Confirmation. No Work may be used in any way that is unlawful, including without limitation if such use would violate applicable sanctions laws or regulations, would be defamatory, violate the rights of third parties (including such third parties' rights of copyright, privacy, publicity, or other tangible or intangible property), or is otherwise illegal, sexually explicit, or obscene. In addition, User may not conjoin a Work with any other material that may result in damage to the reputation of the Rightsholder. Any unlawful use will render any licenses hereunder null and void. User agrees to inform CCC if it becomes aware of any infringement of any rights in a Work and to cooperate with any reasonable request of CCC or the Rightsholder in connection therewith.

8) **Third Party Materials.** In the event that the material for which a License is sought includes third party materials (such as photographs, illustrations, graphs, inserts and similar materials) that are identified in such material as having been used by permission (or a similar indicator), User is responsible for identifying, and seeking separate licenses (under this Service, if available, or otherwise) for any of such third party materials; without a separate license, User may not use such third party materials via the License.

9) **Copyright Notice.** Use of proper copyright notice for a Work is required as a condition of any License granted under the Service. Unless otherwise provided in the Order Confirmation, a proper copyright notice will read substantially as follows: "Used with permission of [Rightsholder's name], from [Work's title, author, volume, edition number and year of copyright]; permission conveyed through Copyright Clearance Center, Inc." Such notice must be provided in a reasonably legible font size and must be placed either on a cover page or in another location that any person, upon gaining access to the material which is the subject of a permission, shall see, or in the case of republication Licenses, immediately adjacent to the Work as used (for example, as part of a by-line or footnote) or in the place where substantially all other credits or notices for the new work containing the republished Work are located. Failure to include the required notice results in loss to the Rightsholder and CCC, and the User shall be liable to pay liquidated damages for each such failure equal to twice the use fee specified in the Order Confirmation, in addition to the use fee itself and any other fees and charges specified.

10) **Indemnity.** User hereby indemnifies and agrees to defend the Rightsholder and CCC, and their respective employees and directors, against all claims, liability, damages, costs, and expenses, including legal fees and expenses, arising out of any use of a Work beyond the scope of the rights granted herein and in the Order Confirmation, or any use of a Work which has been altered in any unauthorized way by User, including claims of defamation or infringement of rights of copyright, publicity, privacy, or other tangible or intangible property.

11) **Limitation of Liability.** UNDER NO CIRCUMSTANCES WILL CCC OR THE RIGHTSHOLDER BE LIABLE FOR ANY DIRECT, INDIRECT, CONSEQUENTIAL, OR INCIDENTAL DAMAGES (INCLUDING WITHOUT LIMITATION DAMAGES FOR LOSS OF BUSINESS PROFITS OR INFORMATION, OR FOR BUSINESS INTERRUPTION) ARISING OUT OF THE USE OR INABILITY TO USE A WORK, EVEN IF ONE OR BOTH OF THEM HAS BEEN ADVISED OF THE POSSIBILITY OF SUCH DAMAGES. In any event, the total liability of the Rightsholder and CCC (including their respective employees and directors) shall not exceed the total amount actually paid by User for the relevant License. User assumes full liability for the actions and omissions of its principals, employees, agents, affiliates, successors, and assigns.

12) **Limited Warranties.** THE WORK(S) AND RIGHT(S) ARE PROVIDED "AS IS." CCC HAS THE RIGHT TO GRANT TO USER THE RIGHTS GRANTED IN THE ORDER CONFIRMATION DOCUMENT. CCC AND THE RIGHTSHOLDER DISCLAIM ALL OTHER WARRANTIES RELATING TO THE WORK(S) AND RIGHT(S), EITHER EXPRESS OR IMPLIED, INCLUDING WITHOUT LIMITATION IMPLIED WARRANTIES OF MERCHANTABILITY OR FITNESS FOR A PARTICULAR PURPOSE. ADDITIONAL RIGHTS MAY BE REQUIRED TO USE ILLUSTRATIONS, GRAPHS, PHOTOGRAPHS, ABSTRACTS, INSERTS, OR OTHER PORTIONS OF THE WORK (AS OPPOSED TO THE ENTIRE WORK) IN A MANNER CONTEMPLATED BY USER; USER UNDERSTANDS AND AGREES THAT NEITHER CCC NOR THE RIGHTSHOLDER MAY HAVE SUCH ADDITIONAL RIGHTS TO GRANT.

13) **Effect of Breach.** Any failure by User to pay any amount when due, or any use by User of a Work beyond the scope of the License set forth in the Order Confirmation and/or the Terms, shall be a material breach of such License. Any breach not cured within 10 days of written notice thereof shall result in immediate termination of such License without further notice. Any unauthorized (but licensable) use of a Work that is terminated immediately upon notice thereof may be liquidated by payment of the Rightsholder's ordinary license price therefor; any unauthorized (and unlicensable) use that is not terminated immediately for any reason (including, for example, because materials containing the Work cannot reasonably be recalled) will be subject to all remedies available at law or in equity, but in no event to a payment of less than three times the Rightsholder's ordinary license price for the most closely analogous licensable use plus Rightsholder's and/or CCC's costs and expenses incurred in collecting such payment.

14) **Additional Terms for Specific Products and Services.** If a User is making one of the uses described in this Section 14, the additional terms and conditions apply:

a) ***Print Uses of Academic Course Content and Materials (photocopies for academic coursepacks or classroom handouts).*** For photocopies for academic coursepacks or classroom handouts the following additional terms apply:

i) The copies and anthologies created under this License may be made and assembled by faculty members individually or at their request by on-campus bookstores or copy centers, or by off-campus copy shops and other similar entities.

ii) No License granted shall in any way: (i) include any right by User to create a substantively non-identical copy of the Work or to edit or in any other way modify the Work (except by means of deleting material immediately preceding or following the entire portion of the Work copied) (ii) permit "publishing ventures" where any particular anthology would be systematically marketed at multiple institutions.

iii) Subject to any Publisher Terms (and notwithstanding any apparent contradiction in the Order Confirmation arising from data provided by User), any use authorized under the academic pay-per-use service is limited as follows:

A) any License granted shall apply to only one class (bearing a unique identifier as assigned by the institution, and thereby including all sections or other subparts of the class) at one institution;

B) use is limited to not more than 25% of the text of a book or of the items in a published collection of essays, poems or articles;

C) use is limited to no more than the greater of (a) 25% of the text of an issue of a journal or other periodical or (b) two articles from such an issue;

D) no User may sell or distribute any particular anthology, whether photocopied or electronic, at more than one institution of learning;

E) in the case of a photocopy permission, no materials may be entered into electronic memory by User except in order to produce an identical copy of a Work before or during the academic term (or analogous period) as to which any particular permission is granted. In the event that User shall choose to retain materials that are the subject of a photocopy permission in electronic memory for purposes of producing identical copies more than one day after such retention (but still within the scope of any permission granted), User must notify CCC of such fact in the applicable permission request and such retention shall constitute one copy actually sold for purposes of calculating permission fees due; and

F) any permission granted shall expire at the end of the class. No permission granted shall in any way include any right by User to create a substantively non-identical copy of the Work or to edit or in any other way modify the Work (except by means of deleting material immediately preceding or following the entire portion of the Work copied).

iv) Books and Records; Right to Audit. As to each permission granted under the academic pay-per-use Service, User shall maintain for at least four full calendar years books and records sufficient for CCC to determine the numbers of copies made by User under such permission. CCC and any representatives it may designate shall have the right to audit such books and records at any time during User's ordinary business hours, upon two days' prior notice. If any such audit shall determine that User shall have underpaid for, or underreported, any photocopies sold or by three percent (3%) or more, then User shall bear all the costs of any such audit; otherwise, CCC shall bear the costs of any such audit. Any amount determined by such audit to have been underpaid by User shall immediately be paid to CCC by User, together with interest thereon at the rate of 10% per annum from the date such amount was originally due. The provisions of this paragraph shall survive the termination of this License for any reason.

b) ***Digital Pay-Per-Uses of Academic Course Content and Materials (e-coursepacks, electronic reserves, learning management systems, academic institution intranets).*** For uses in e-coursepacks, posts in electronic reserves, posts in learning management systems, or posts on academic institution intranets, the following additional terms apply:

i) The pay-per-uses subject to this Section 14(b) include:

A) **Posting e-reserves, course management systems, e-coursepacks for text-based content,** which grants authorizations to import requested material in electronic format, and allows electronic access to this material to members of a designated college or university class, under the direction of an instructor designated by the college or university, accessible only under appropriate electronic controls (e.g., password);

B) **Posting e-reserves, course management systems, e-coursepacks for material consisting of photographs or other still images not embedded in text,** which grants not only the authorizations described in Section 14(b)(i)(A) above, but also the following authorization: to include the requested material in course materials for use consistent with Section 14(b)(i)(A) above, including any necessary resizing, reformatting or modification of the resolution of such requested material (provided that such modification does not alter the underlying

editorial content or meaning of the requested material, and provided that the resulting modified content is used solely within the scope of, and in a manner consistent with, the particular authorization described in the Order Confirmation and the Terms), but not including any other form of manipulation, alteration or editing of the requested material;

C) **Posting e-reserves, course management systems, e-coursepacks or other academic distribution for audiovisual content,** which grants not only the authorizations described in Section 14(b)(i)(A) above, but also the following authorizations: (i) to include the requested material in course materials for use consistent with Section 14(b)(i)(A) above; (ii) to display and perform the requested material to such members of such class in the physical classroom or remotely by means of streaming media or other video formats; and (iii) to "clip" or reformat the requested material for purposes of time or content management or ease of delivery, provided that such "clipping" or reformatting does not alter the underlying editorial content or meaning of the requested material and that the resulting material is used solely within the scope of, and in a manner consistent with, the particular authorization described in the Order Confirmation and the Terms. Unless expressly set forth in the relevant Order Conformation, the License does not authorize any other form of manipulation, alteration or editing of the requested material.

ii) Unless expressly set forth in the relevant Order Confirmation, no License granted shall in any way: (i) include any right by User to create a substantively non-identical copy of the Work or to edit or in any other way modify the Work (except by means of deleting material immediately preceding or following the entire portion of the Work copied or, in the case of Works subject to Sections 14(b)(1)(B) or (C) above, as described in such Sections) (ii) permit "publishing ventures" where any particular course materials would be systematically marketed at multiple institutions.

iii) Subject to any further limitations determined in the Rightsholder Terms (and notwithstanding any apparent contradiction in the Order Confirmation arising from data provided by User), any use authorized under the electronic course content pay-per-use service is limited as follows:

A) any License granted shall apply to only one class (bearing a unique identifier as assigned by the institution, and thereby including all sections or other subparts of the class) at one institution;

B) use is limited to not more than 25% of the text of a book or of the items in a published collection of essays, poems or articles;

C) use is limited to not more than the greater of (a) 25% of the text of an issue of a journal or other periodical or (b) two articles from such an issue;

D) no User may sell or distribute any particular materials, whether photocopied or electronic, at more than one institution of learning;

E) electronic access to material which is the subject of an electronic-use permission must be limited by means of electronic password, student identification or other control permitting access solely to students and instructors in the class;

F) User must ensure (through use of an electronic cover page or other appropriate means) that any person, upon gaining electronic access to the material, which is the subject of a permission, shall see:

- a proper copyright notice, identifying the Rightsholder in whose name CCC has granted permission,
- a statement to the effect that such copy was made pursuant to permission,
- a statement identifying the class to which the material applies and notifying the reader that the material has been made available electronically solely for use in the class, and
- a statement to the effect that the material may not be further distributed to any person outside the class, whether by copying or by transmission and whether electronically or in paper form, and User must also ensure that such cover page or other means will print out in the event that the person accessing the material chooses to print out the material or any part thereof.

G) any permission granted shall expire at the end of the class and, absent some other form of authorization, User is thereupon required to delete the applicable material from any electronic storage or to block electronic access to the applicable material.

iv) Uses of separate portions of a Work, even if they are to be included in the same course material or the same university or college class, require separate permissions under the electronic course content pay-per-use Service. Unless otherwise provided in the Order Confirmation, any grant of rights to User is limited to use completed no later than the end of the academic term (or analogous period) as to which any particular permission is granted.

v) Books and Records; Right to Audit. As to each permission granted under the electronic course content Service, User shall maintain for at least four full calendar years books and records sufficient for CCC to determine the numbers of copies made by User under such permission. CCC and any representatives it may designate shall have the right to audit such books and records at any time during User's ordinary business hours, upon two days' prior notice. If any such audit shall determine that User shall have underpaid for, or underreported, any electronic copies used by three percent (3%) or more, then User shall bear all the costs of any such audit; otherwise, CCC shall bear the costs of any such audit. Any amount determined by such audit to have been underpaid by User shall immediately be paid to CCC by User, together with interest thereon at the rate of 10% per annum from the date such amount was originally due. The provisions of this paragraph shall survive the termination of this license for any reason.

c) ***Pay-Per-Use Permissions for Certain Reproductions (Academic photocopies for library reserves and interlibrary loan reporting) (Non-academic internal/external business uses and commercial document delivery).*** The License expressly excludes the uses listed in Section (c)(i)-(v) below (which must be subject to separate license from the applicable Rightsholder) for: academic photocopies for library reserves and interlibrary loan reporting; and non-academic internal/external business uses and commercial document delivery.

i) electronic storage of any reproduction (whether in plain-text, PDF, or any other format) other than on a transitory basis;

ii) the input of Works or reproductions thereof into any computerized database;

iii) reproduction of an entire Work (cover-to-cover copying) except where the Work is a single article;

iv) reproduction for resale to anyone other than a specific customer of User;

v) republication in any different form. Please obtain authorizations for these uses through other CCC services or directly from the rightsholder.

Any license granted is further limited as set forth in any restrictions included in the Order Confirmation and/or in these Terms.

d) ***Electronic Reproductions in Online Environments (Non-Academic-email, intranet, internet and extranet).*** For "electronic reproductions", which generally includes e-mail use (including instant messaging or other electronic transmission to a defined group of recipients) or posting on an intranet, extranet or Intranet site (including any display or performance incidental thereto), the following additional terms apply:

i) Unless otherwise set forth in the Order Confirmation, the License is limited to use completed within 30 days for any use on the Internet, 60 days for any use on an intranet or extranet and one year for any other use, all as measured from the "republication date" as identified in the Order Confirmation, if any, and otherwise from the date of the Order Confirmation.

ii) User may not make or permit any alterations to the Work, unless expressly set forth in the Order Confirmation (after request by User and approval by Rightsholder); provided, however, that a Work consisting of photographs or other still images not embedded in text may, if necessary, be resized, reformatted or have its resolution modified without additional express permission, and a Work consisting of audiovisual content may, if necessary, be "clipped" or reformatted for purposes of time or content management or ease of delivery (provided that any such resizing, reformatting, resolution modification or "clipping" does not alter the underlying editorial content or meaning of the Work used, and that the resulting material is used solely within the scope of, and in a manner consistent with, the particular License described in the Order Confirmation and the Terms.

15) **Miscellaneous.**

a) User acknowledges that CCC may, from time to time, make changes or additions to the Service or to the Terms, and that Rightsholder may make changes or additions to the Rightsholder Terms. Such updated Terms will replace the prior terms and conditions in the order workflow and shall be effective as to any subsequent Licenses but shall not apply to Licenses already granted and paid for under a prior set of terms.

b) Use of User-related information collected through the Service is governed by CCC's privacy policy, available online at www.copyright.com/about/privacy-policy/.

c) The License is personal to User. Therefore, User may not assign or transfer to any other person (whether a natural person or an organization of any kind) the License or any rights granted thereunder; provided, however, that, where applicable, User may assign such License in its entirety on written notice to CCC in the event of a transfer of all or substantially all of User's rights in any new material which includes the Work(s) licensed under this Service.

d) No amendment or waiver of any Terms is binding unless set forth in writing and signed by the appropriate parties, including, where applicable, the Rightsholder. The Rightsholder and CCC hereby object to any terms contained in any

writing prepared by or on behalf of the User or its principals, employees, agents or affiliates and purporting to govern or otherwise relate to the License described in the Order Confirmation, which terms are in any way inconsistent with any Terms set forth in the Order Confirmation, and/or in CCC's standard operating procedures, whether such writing is prepared prior to, simultaneously with or subsequent to the Order Confirmation, and whether such writing appears on a copy of the Order Confirmation or in a separate instrument.

e) The License described in the Order Confirmation shall be governed by and construed under the law of the State of New York, USA, without regard to the principles thereof of conflicts of law. Any case, controversy, suit, action, or proceeding arising out of, in connection with, or related to such License shall be brought, at CCC's sole discretion, in any federal or state court located in the County of New York, State of New York, USA, or in any federal or state court whose geographical jurisdiction covers the location of the Rightsholder set forth in the Order Confirmation. The parties expressly submit to the personal jurisdiction and venue of each such federal or state court.

*Last updated October 2022*

Dear Hongmin Zhu

We hereby grant you permission to reprint the material below at no charge in your thesis subject to the following conditions:

**RE: RE: Structural Health Monitoring, ISBN: 9780120887606, 2008, Victor Giurgiutiu, Figure 6.7 and text excerpt with 84 words**

1. If any part of the material to be used (for example, figures) has appeared in our publication with credit or acknowledgment to another source, permission must also be sought from that source. If such permission is not obtained then that material may not be included in your publication/copies.

2. Suitable acknowledgment to the source must be made, either as a footnote or in a reference list at the end of your publication, as follows:

"This article was published in Publication title, Vol number, Author(s), Title of article, Page Nos, Copyright Elsevier (or appropriate Society name) (Year)."

3. Your thesis may be submitted to your institution in either print or electronic form.

4. Reproduction of this material is confined to the purpose and/or media for which permission is hereby given. The material may not be reproduced or used in any other way, including use in combination with an artificial intelligence tool (including to train an algorithm, test, process, analyse, generate output and/or develop any form of artificial intelligence tool), or to create any derivative work and/or service (including resulting from the use of artificial intelligence tools).

5. This permission is granted for non-exclusive world English rights only. For other languages please reapply separately for each one required. Permission excludes use in an electronic form other than submission. Should you have a specific electronic project in mind please reapply for permission.

6. As long as the article is embedded in your thesis, you can post/share your thesis in the University repository.

7. Should your thesis be published commercially, please reapply for permission.

8. Posting of the full article/ chapter online is not permitted. You may post an abstract with a link to the Elsevier website www.elsevier.com, or to the article on ScienceDirect if it is available on that platform.

**Thanks & Regards,**
**Roopa Lingayath**
Sr. Copyrights Specialist, Copyrights Team
**ELSEVIER** | Health Content Management
+91 44 3378 4167 office
r.lingayath@elsevier.com

## PARTIES:

1. **Cambridge University Press** (Licensor); and
2. **Hongmin Zhu** (Licensee).

Thank you for your recent permission request. Some permission requests for use of material published by the Licensor, such as this one, are now being facilitated by PLSclear.

Set out in this licence cover sheet (the **Licence Cover Sheet**) are the principal terms under which Licensor has agreed to license certain Licensed Material (as defined below) to Licensee. The terms in this Licence Cover Sheet are subject to the attached General Terms and Conditions, which together with this Licence Cover Sheet constitute the licence agreement (the **Licence**) between Licensor and Licensee as regards the Licensed Material. The terms set out in this Licence Cover Sheet take precedence over any conflicting provision in the General Terms and Conditions.

## Free Of Charge Licence Terms

| | |
|---|---|
| Licence Date: | 12/04/2024 |
| PLSclear Ref No: | 92842 |

## The Licensor

| | |
|---|---|
| Company name: | Cambridge University Press |
| Address: | University Printing House<br>Shaftesbury Road<br>Cambridge<br>CB2 8BS<br>GB |

## The Licensee

| | |
|---|---|
| Licensee Contact Name: | Hongmin Zhu |
| Licensee Address: | Exhibition Road, South Kensington<br>London<br>SW7 2AZ<br>United Kingdom |

## Licensed Material

| | |
|---|---|
| title: | Ultrasonic Guided Waves in Solid Media |
| ISBN: | 9781107048959 |
| publisher: | Cambridge University Press |

| | |
|---|---|
| Are you requesting permission to reuse the cover of the publication? | No |
| Figure number & title | Figure 6.8. Dispersion curves for a traction-free aluminum plate. |
| Page numbers | 89 |
| Are you the author of the content that you are requesting to reuse? | No |
| Will you be changing or editing the image? | Yes |
| Will it be cropped? | Yes |
| Full details of how it will be altered | The figure will be arranged horizontally to save space instead of being arranged vertically in the original figure. |

## For Use In Licensee's Publication(s)

| | |
|---|---|
| usage type | Book, Journal, Magazine or Academic Paper-Thesis or Dissertation |
| Will your dissertation be placed in an online repository? | Yes |
| Author | Hongmin Zhu |
| Language | English |
| Title of dissertation/thesis | Data-driven Modelling for Guided Wave Structural Health Monitoring and Prognostic Health Management on Aeronautical Structures |
| University or institution | Imperial College London |
| Unlimited circulation? | No |

## Rights Granted

| | |
|---|---|
| Exclusivity: | Non-Exclusive |
| Format: | Thesis or Dissertation |
| Language: | English |
| Territory: | UK & Commonwealth |
| Duration: | Lifetime of Licensee's Edition |
| Maximum Circulation: | 4 |

## GENERAL TERMS AND CONDITIONS

**1. Definitions and Interpretation**

1.1 Capitalised words and expressions in these General Terms and Conditions have the meanings given to them in the Licence Cover Sheet.

1.2 In this Licence any references (express or implied) to statutes or provisions are references to those statutes or provisions as amended or re-enacted from time to time. The term including will be construed as illustrative, without limiting the sense or scope of the words preceding it. A reference to in writing or written includes faxes and email. The singular includes the plural and vice versa.

**2. Grant of Rights**

2.1 The Licensor grants to Licensee the non-exclusive right to use the Licensed Material as specified in the Licence Cover Sheet.

2.2 The rights licensed to Licensee under this Licence do not include the right to use any third party copyright material incorporated in the Licensed Material. Licensee should check the Licensed Material carefully and seek permission for the use of any such third party copyright material from the relevant copyright owner(s).

2.3 Unless otherwise stated in the Licence Cover Sheet, the Licensed Material may be:

2.3.1 subjected to minor editing, including for the purposes of creating alternative formats to provide access for a beneficiary person (provided that any such editing does not amount to derogatory treatment); and/or

2.3.2 used for incidental promotional use (such as online retail providers' search facilities).

2.4 Save as expressly permitted in this Licence or as otherwise permitted by law, no use or modification of the Licensed Material may be made by Licensee without Licensor's prior written permission.

**3. Copyright Notice and Acknowledgement**

3.1 Licensee must ensure that the following notices and acknowledgements are reproduced prominently alongside each reproduction by Licensee of the Licensed Material:

3.1.1 the title and author of the Licensed Material;

3.1.2 the copyright notice included in the Licensed Material; and

3.1.3 the statement "Reproduced with permission of The Licensor through PLSclear."

**4. Reversion of Rights**

4.1 The rights licensed to Licensee under this Licence will terminate immediately and automatically upon the earliest of the following events to occur:

4.1.1 the Licensed Material not being used by Licensee within 18 months of the Licence Date;

4.1.2 expiry of the Licence Duration; or

4.1.3 the Maximum Circulation being reached.

**5. Miscellaneous**

5.1 By using the Licensed Material, Licensee will be deemed to have accepted all the terms and conditions contained in this Licence.

5.2 This Licence contains the entire understanding and agreement of the parties relating to its subject matter and supersedes in all respects any previous or other existing arrangements, agreements or understandings between the parties whether oral or written in relation to its subject matter.

5.3 Licensee may not assign this Licence or any of its rights or obligations hereunder to any third party without Licensor's prior written consent.

5.4 This Licence is governed by and shall be construed in accordance with the laws of England and Wales and the parties hereby irrevocably submit to the non-exclusive jurisdiction of the Courts of England and Wales as regards any claim, dispute or matter arising under or in relation to this Licence.

Dear Hongmin Zhu,

We hereby grant you permission to reprint the material below at no charge in your thesis subject to the following conditions:

**RE: Victor Giurgiutiu, Structural Health Monitoring of Aerospace Composites, 2015, ISBN: 9780124096059, Figure 7, Chapter 6. Use of PWAS transducers for damage detection with propagating and standing guided waves in thin-wall structures.**

**Proposed use: Thesis/Dissertation.**

1. If any part of the material to be used (for example, figures) has appeared in our publication with credit or acknowledgement to another source, permission must also be sought from that source. If such permission is not obtained then that material may not be included in your publication/copies.

2. Suitable acknowledgment to the source must be made, either as a footnote or in a reference list at the end of your publication, as follows:
"This article was published in Publication title, Vol number, Author(s), Title of article, Page Nos, Copyright Elsevier (or appropriate Society name) (Year)."

3. Your thesis may be submitted to your institution in either print or electronic form.

4. Reproduction of this material is confined to the purpose for which permission is hereby given

5. This permission is granted for non-exclusive world English rights only. For other languages please reapply separately for each one required. Permission excludes use in an electronic form other than submission. Should you have a

specific electronic project in mind please reapply for permission.

6. Should your thesis be published commercially, please reapply for permission.

This includes permission for the Library and Archives of Canada to supply single copies, on demand, of the complete thesis. Should your thesis be published commercially, please reapply for permission- Canada
This includes permission for UMI to supply single copies, on demand, of the complete thesis. Should your thesis be published commercially, please reapply for permission-ROW

7. Posting of the full article online is not permitted. You may post an abstract with a link to the Elsevier website www.elsevier.com, or to the article on ScienceDirect if it is available on that platform.

8. Article can used be in the University library if it is embedded in the thesis and not used commercially.

Kind regards,

**Thomas Rexson Yesudoss**
Copyrights Specialist
**ELSEVIER** | HCM - Health Content Management

Visit Elsevier Permissions

# ELSEVIER LICENSE
# TERMS AND CONDITIONS

Apr 15, 2024

This Agreement between Mr. HONGMIN ZHU ("You") and Elsevier ("Elsevier") consists of your license details and the terms and conditions provided by Elsevier and Copyright Clearance Center.

| | |
|---|---|
| License Number | 5766131133396 |
| License date | Apr 11, 2024 |
| Licensed Content Publisher | Elsevier |
| Licensed Content Publication | Mechanical Systems and Signal Processing |
| Licensed Content Title | Self-referenced robust guided wave based defect detection: Application to woven composite parts of complex shape |
| Licensed Content Author | Olivier Mesnil,Arnaud Recoquillay,Clément Fisher,Valentin Serey,Sanjay Sharma,Oscar d'Almeida |
| Licensed Content Date | Apr 1, 2023 |
| Licensed Content Volume | 188 |
| Licensed Content Issue | n/a |
| Licensed Content Pages | 1 |
| Start Page | 109948 |
| End Page | 0 |
| Type of Use | reuse in a thesis/dissertation |
| Portion | figures/tables/illustrations |
| Number of figures/tables/illustrations | 1 |
| Format | both print and electronic |
| Are you the author of this Elsevier article? | No |
| Will you be translating? | No |
| Title of new work | Data-driven Modelling for Guided Wave Structural Health Monitoring and Prognostic Health Management on Aeronautical Structures |
| Institution name | Imperial College London |
| Expected presentation date | Jul 2024 |
| Order reference number | abcd |
| Portions | Fig. 17. Impedance measurement from the 24 sensors instrumented on the woven composite samples. |
| Requestor Location | Mr. HONGMIN ZHU<br>Exhibition Road<br><br>London, other<br>United Kingdom<br>Attn: Mr. HONGMIN ZHU |
| Publisher Tax ID | GB 494 6272 12 |
| Total | **0.00 GBP** |
| Terms and Conditions | |

## INTRODUCTION

1. The publisher for this copyrighted material is Elsevier. By clicking "accept" in connection with completing this licensing transaction, you agree that the following terms and conditions apply to this transaction (along with the Billing and Payment terms and conditions established by Copyright Clearance Center, Inc. ("CCC"), at the time that you opened your RightsLink account and that are available at any time at https://myaccount.copyright.com).

## GENERAL TERMS

2. Elsevier hereby grants you permission to reproduce the aforementioned material subject to the terms and conditions indicated.
3. Acknowledgement: If any part of the material to be used (for example, figures) has appeared in our publication with credit or acknowledgement to another source, permission must also be sought from that source. If such permission is not obtained then that material may not be included in your publication/copies. Suitable acknowledgement to the source must be made, either as a footnote or in a reference list at the end of your publication, as follows:
"Reprinted from Publication title, Vol /edition number, Author(s), Title of article / title of chapter, Pages No., Copyright (Year), with permission from Elsevier [OR APPLICABLE SOCIETY COPYRIGHT OWNER]." Also Lancet special credit - "Reprinted from The Lancet, Vol. number, Author(s), Title of article, Pages No., Copyright (Year), with permission from Elsevier."
4. Reproduction of this material is confined to the purpose and/or media for which permission is hereby given. The material may not be reproduced or used in any other way, including use in combination with an artificial intelligence tool (including to train an algorithm, test, process, analyse, generate output and/or develop any form of artificial intelligence tool), or to create any derivative work and/or service (including resulting from the use of artificial intelligence tools).
5. Altering/Modifying Material: Not Permitted. However figures and illustrations may be altered/adapted minimally to serve your work. Any other abbreviations, additions, deletions and/or any other alterations shall be made only with prior written authorization of Elsevier Ltd. (Please contact Elsevier's permissions helpdesk here). No modifications can be made to any Lancet figures/tables and they must be reproduced in full.
6. If the permission fee for the requested use of our material is waived in this instance, please be advised that your future requests for Elsevier materials may attract a fee.
7. Reservation of Rights: Publisher reserves all rights not specifically granted in the combination of (i) the license details provided by you and accepted in the course of this licensing transaction, (ii) these terms and conditions and (iii) CCC's Billing and Payment terms and conditions.
8. License Contingent Upon Payment: While you may exercise the rights licensed immediately upon issuance of the license at the end of the licensing process for the transaction, provided that you have disclosed complete and accurate details of your proposed use, no license is finally effective unless and until full payment is received from you (either by publisher or by CCC) as provided in CCC's Billing and Payment terms and conditions. If full payment is not received on a timely basis, then any license preliminarily granted shall be deemed automatically revoked and shall be void as if never granted. Further, in the event that you breach any of these terms and conditions or any of CCC's Billing and Payment terms and conditions, the license is automatically revoked and shall be void as if never granted. Use of materials as described in a revoked license, as well as any use of the materials beyond the scope of an unrevoked license, may constitute copyright infringement and publisher reserves the right to take any and all action to protect its copyright in the materials.
9. Warranties: Publisher makes no representations or warranties with respect to the licensed material.
10. Indemnity: You hereby indemnify and agree to hold harmless publisher and CCC, and their respective officers, directors, employees and agents, from and against any and all claims arising out of your use of the licensed material other than as specifically authorized pursuant to this license.
11. No Transfer of License: This license is personal to you and may not be sublicensed, assigned, or transferred by you to any other person without publisher's written permission.
12. No Amendment Except in Writing: This license may not be amended except in a writing signed by both parties (or, in the case of publisher, by CCC on publisher's behalf).
13. Objection to Contrary Terms: Publisher hereby objects to any terms contained in any purchase order, acknowledgment, check endorsement or other writing prepared by you, which terms are inconsistent with these terms and conditions or CCC's Billing and Payment terms and conditions. These terms and conditions, together with CCC's Billing and Payment terms and conditions (which are incorporated herein), comprise the entire agreement between you and publisher (and CCC) concerning this licensing transaction. In the event of any conflict between your obligations established by these terms and conditions and those established by CCC's Billing and Payment terms and conditions, these terms and conditions shall control.
14. Revocation: Elsevier or Copyright Clearance Center may deny the permissions described in this License at their sole discretion, for any reason or no reason, with a full refund payable to you. Notice of such denial will be made using the contact information provided by you. Failure to receive such notice will not alter or invalidate the denial. In no event will Elsevier or Copyright Clearance Center be responsible or liable for any costs, expenses or damage incurred by you as a result of a denial of your permission request, other than a refund of the amount(s) paid by you to Elsevier and/or Copyright Clearance Center for denied permissions.

## LIMITED LICENSE

The following terms and conditions apply only to specific license types:
15. **Translation**: This permission is granted for non-exclusive world **English** rights only unless your license was granted for translation rights. If you licensed translation rights you may only translate this content into the languages you requested. A professional translator must perform all translations and reproduce the content word for word preserving the integrity of the article.
16. **Posting licensed content on any Website**: The following terms and conditions apply as follows: Licensing material from an Elsevier journal: All content posted to the web site must maintain the copyright information line on the bottom of each image; A hyper-text must be included to the Homepage of the journal from which you are licensing at http://www.sciencedirect.com/science/journal/xxxxx or the Elsevier homepage for books at http://www.elsevier.com; Central Storage: This license does not include permission for a scanned version of the material to be stored in a central repository such as that provided by Heron/XanEdu.

Licensing material from an Elsevier book: A hyper-text link must be included to the Elsevier homepage at http://www.elsevier.com . All content posted to the web site must maintain the copyright information line on the bottom of each image.

**Posting licensed content on Electronic reserve**: In addition to the above the following clauses are applicable: The web site must be password-protected and made available only to bona fide students registered on a relevant course. This permission is granted for 1 year only. You may obtain a new license for future website posting.
17. **For journal authors:** the following clauses are applicable in addition to the above:
**Preprints:**
A preprint is an author's own write-up of research results and analysis, it has not been peer-reviewed, nor has it had any other value added to it by a publisher (such as formatting, copyright, technical enhancement etc.).
Authors can share their preprints anywhere at any time. Preprints should not be added to or enhanced in any way in order to appear more like, or to substitute for, the final versions of articles however authors can update their preprints on arXiv or RePEc with their Accepted Author Manuscript (see below).
If accepted for publication, we encourage authors to link from the preprint to their formal publication via its DOI. Millions of researchers have access to the formal publications on ScienceDirect, and so links will help users to find, access, cite and use the best available version. Please note that Cell Press, The Lancet and some society-owned have different preprint policies. Information on these policies is available on the journal homepage.
**Accepted Author Manuscripts:** An accepted author manuscript is the manuscript of an article that has been accepted for publication and which typically includes author-incorporated changes suggested during submission, peer review and editor-author communications.
Authors can share their accepted author manuscript:

- immediately
    - via their non-commercial person homepage or blog
    - by updating a preprint in arXiv or RePEc with the accepted manuscript
    - via their research institute or institutional repository for internal institutional uses or as part of an invitation-only research collaboration work-group
    - directly by providing copies to their students or to research collaborators for their personal use
    - for private scholarly sharing as part of an invitation-only work group on commercial sites with which Elsevier has an agreement
- After the embargo period
    - via non-commercial hosting platforms such as their institutional repository
    - via commercial sites with which Elsevier has an agreement

In all cases accepted manuscripts should:

- link to the formal publication via its DOI
- bear a CC-BY-NC-ND license - this is easy to do
- if aggregated with other manuscripts, for example in a repository or other site, be shared in alignment with our hosting policy not be added to or enhanced in any way to appear more like, or to substitute for, the published journal article.

**Published journal article (JPA):** A published journal article (PJA) is the definitive final record of published research that appears or will appear in the journal and embodies all value-adding publishing activities including peer review co-ordination, copy-editing, formatting, (if relevant) pagination and online enrichment.
Policies for sharing publishing journal articles differ for subscription and gold open access articles:
**Subscription Articles:** If you are an author, please share a link to your article rather than the full-text. Millions of researchers have access to the formal publications on ScienceDirect, and so links will help your users to find, access, cite, and use the best available version.
Theses and dissertations which contain embedded PJAs as part of the formal submission can be posted publicly by the awarding institution with DOI links back to the formal publications on ScienceDirect.
If you are affiliated with a library that subscribes to ScienceDirect you have additional private sharing rights for others' research accessed under that agreement. This includes use for classroom teaching and internal training at the institution (including use in course packs and courseware programs), and inclusion of the article for grant funding purposes.
**Gold Open Access Articles:** May be shared according to the author-selected end-user license and should contain a CrossMark logo, the end user license, and a DOI link to the formal publication on ScienceDirect.
Please refer to Elsevier's posting policy for further information.
18. **For book authors** the following clauses are applicable in addition to the above: Authors are permitted to place a brief summary of their work online only. You are not allowed to download and post the published electronic version of your chapter, nor may you scan the printed edition to create an electronic version. **Posting to a repository:** Authors are permitted to post a summary of their chapter only in their institution's repository.
19. **Thesis/Dissertation**: If your license is for use in a thesis/dissertation your thesis may be submitted to your institution in either print or electronic form. Should your thesis be published commercially, please reapply for permission. These requirements include permission for the Library and Archives of Canada to supply single copies, on demand, of the complete thesis and include permission for Proquest/UMI to supply single copies, on demand, of the complete thesis. Should your thesis be published commercially, please reapply for permission. Theses and dissertations which contain embedded PJAs as part of

the formal submission can be posted publicly by the awarding institution with DOI links back to the formal publications on ScienceDirect.

**Elsevier Open Access Terms and Conditions**

You can publish open access with Elsevier in hundreds of open access journals or in nearly 2000 established subscription journals that support open access publishing. Permitted third party re-use of these open access articles is defined by the author's choice of Creative Commons user license. See our open access license policy for more information.

**Terms & Conditions applicable to all Open Access articles published with Elsevier:**

Any reuse of the article must not represent the author as endorsing the adaptation of the article nor should the article be modified in such a way as to damage the author's honour or reputation. If any changes have been made, such changes must be clearly indicated.

The author(s) must be appropriately credited and we ask that you include the end user license and a DOI link to the formal publication on ScienceDirect.

If any part of the material to be used (for example, figures) has appeared in our publication with credit or acknowledgement to another source it is the responsibility of the user to ensure their reuse complies with the terms and conditions determined by the rights holder.

**Additional Terms & Conditions applicable to each Creative Commons user license:**

**CC BY:** The CC-BY license allows users to copy, to create extracts, abstracts and new works from the Article, to alter and revise the Article and to make commercial use of the Article (including reuse and/or resale of the Article by commercial entities), provided the user gives appropriate credit (with a link to the formal publication through the relevant DOI), provides a link to the license, indicates if changes were made and the licensor is not represented as endorsing the use made of the work. The full details of the license are available at http://creativecommons.org/licenses/by/4.0.

**CC BY NC SA:** The CC BY-NC-SA license allows users to copy, to create extracts, abstracts and new works from the Article, to alter and revise the Article, provided this is not done for commercial purposes, and that the user gives appropriate credit (with a link to the formal publication through the relevant DOI), provides a link to the license, indicates if changes were made and the licensor is not represented as endorsing the use made of the work. Further, any new works must be made available on the same conditions. The full details of the license are available at http://creativecommons.org/licenses/by-nc-sa/4.0.

**CC BY NC ND:** The CC BY-NC-ND license allows users to copy and distribute the Article, provided this is not done for commercial purposes and further does not permit distribution of the Article if it is changed or edited in any way, and provided the user gives appropriate credit (with a link to the formal publication through the relevant DOI), provides a link to the license, and that the licensor is not represented as endorsing the use made of the work. The full details of the license are available at http://creativecommons.org/licenses/by-nc-nd/4.0. Any commercial reuse of Open Access articles published with a CC BY NC SA or CC BY NC ND license requires permission from Elsevier and will be subject to a fee.

Commercial reuse includes:

- Associating advertising with the full text of the Article
- Charging fees for document delivery or access
- Article aggregation
- Systematic distribution via e-mail lists or share buttons

Posting or linking by commercial companies for use by customers of those companies.

20. **Other Conditions**:

v1.10

**Questions? E-mail us at customercare@copyright.com.**

# Marketplace

This is a License Agreement between Hongmin Zhu (“User”) and Copyright Clearance Center, Inc. (“CCC”) on behalf of the Rightsholder identified in the order details below. The license consists of the order details, the Marketplace Permissions General Terms and Conditions below, and any Rightsholder Terms and Conditions which are included below.

All payments must be made in full to CCC in accordance with the Marketplace Permissions General Terms and Conditions below.

| | | | |
|---|---|---|---|
| **Order Date** | 11-Apr-2024 | **Type of Use** | Republish in a thesis/dissertation |
| **Order License ID** | 1472498-1 | | |
| **ISSN** | 0964-1726 | **Publisher** | IOP Publishing |
| | | **Portion** | Image/photo/illustration |

## LICENSED CONTENT

| | | | |
|---|---|---|---|
| **Publication Title** | Smart Materials and Structures | **Country** | United Kingdom of Great Britain and Northern Ireland |
| **Author/Editor** | Institute of Physics (Great Britain), Society of Photo-optical Instrumentation Engineers. | **Rightsholder** | IOP Publishing, Ltd |
| | | **Publication Type** | Journal |
| **Date** | 01/01/1992 | | |
| **Language** | English | | |

## REQUEST DETAILS

| | | | |
|---|---|---|---|
| **Portion Type** | Image/photo/illustration | **Distribution** | U.K. and Commonwealth (excluding Canada) |
| **Number of Images / Photos / Illustrations** | 1 | **Translation** | Original language of publication |
| **Format (select all that apply)** | Print, Electronic | **Copies for the Disabled?** | No |
| **Who Will Republish the Content?** | Academic institution | **Minor Editing Privileges?** | No |
| **Duration of Use** | Life of current edition | **Incidental Promotional Use?** | No |
| **Lifetime Unit Quantity** | Up to 4,999 | **Currency** | GBP |
| **Rights Requested** | Main product | | |

## NEW WORK DETAILS

| | | | |
|---|---|---|---|
| **Title** | Data-driven Modelling for Guided Wave Structural Health Monitoring and Prognostic Health Management on Aeronautical Structures | **Institution Name** | Imperial College London |
| | | **Expected Presentation Date** | 2024-07-01 |
| **Instructor Name** | Ferri Aliabadi | | |

## ADDITIONAL DETAILS

| | | | |
|---|---|---|---|
| **Order Reference Number** | N/A | **The Requesting Person / Organization to Appear on the License** | Hongmin Zhu |

## REQUESTED CONTENT DETAILS

| | | | |
|---|---|---|---|
| **Title, Description or Numeric Reference of the Portion(s)** | Figure 8. Illustration of the elliptical distribution function of the RAPID algorithm | **Title of the Article / Chapter the Portion Is From** | Active health monitoring of an aircraft wing with embedded piezoelectric sensor/actuator network: I. Defect detection, localization and growth monitoring |
| **Editor of Portion(s)** | N/A | | |
| **Volume / Edition** | 16 | | |
| **Page or Page Range of Portion** | 1212 | **Author of Portion(s)** | Institute of Physics (Great Britain); Society of Photo-optical Instrumentation Engineers. |
| | | **Issue, if Republishing an Article From a Serial** | N/A |
| | | **Publication Date of Portion** | 2007-06-29 |

## RIGHTSHOLDER TERMS AND CONDITIONS

These special terms and conditions are in addition to the standard terms and conditions for CCC's Republication Service and, together with those standard terms and conditions, govern the use of the Works. As the User you will make all reasonable efforts to contact the author(s) of the article which the Work is to be reused from, to seek consent for your intended use. Contacting one author who is acting expressly as authorised agent for their co-author(s) is acceptable. User will reproduce the following wording prominently alongside the Work: the source of the Work, including author, article title, title of journal, volume number, issue number (if relevant), page range (or first page if this is the only information available) and date of first publication; and a link back to the article (via DOI); and if practicable, and IN ALL CASES for new works published under any of the Creative Commons licences, the words "© IOP Publishing. Reproduced with permission. All rights reserved" Without the express permission of the author(s) and the Rightsholder of the article from which the Work is to be reused, User shall not use it in any way which, in the opinion of the Rightsholder, could: (i) distort or alter the author(s)' original intention(s) and meaning; (ii) be prejudicial to the honour or reputation of the author(s); and/or (iii) imply endorsement by the author(s) and/or the Rightsholder. This licence does not apply to any article which is credited to another source and which does not have the copyright line '© IOP Publishing Ltd'. User must check the copyright line of the article from which the Work is to be reused to check that IOP Publishing Ltd has all the necessary rights to be able to grant permission. User is solely responsible for identifying and obtaining separate licences and permissions from the copyright owner for reuse of any such third party material/figures which the Rightsholder is not the copyright owner of. The Rightsholder shall not reimburse any fees which User pays for a republication license for such third party content. This licence does not apply to any material/figure which is credited to another source in the Rightsholder's publication or has been obtained from a third party. User must check the Version of Record of the article from which the Work is to be reused, to check whether any of the material in the Work is third party material. Third party citations and/or copyright notices and/or permissions statements may not be included in any other version of the article from which the Work is to be reused and so cannot be relied upon by the User. User is solely responsible for identifying and obtaining separate licences and permissions from the copyright owner for reuse of any such third party material/figures where the Rightsholder is not the copyright owner. The Rightsholder shall not reimburse any fees which User pays for a republication license for such third party content. User and CCC acknowledge that the Rightsholder may, from time to time, make changes or additions to these special terms and conditions without express notification, provided that these shall not apply to permissions already secured and paid for by User prior to such change or addition. User acknowledges that the Rightsholder (which includes companies within its group and third parties for whom it publishes its titles) may make use of personal data collected through the service in the course of their business. If User is the author of the Work, User may automatically have the right to reuse it under the rights granted back when User transferred the copyright in the article to the Rightsholder. User should check the copyright form and the relevant author rights policy to check whether permission is required. If User is the author of the Work and does require permission for proposed reuse of the Work, User should select 'Author of requested content' as the Requestor Type. The Rightsholder shall not reimburse any fees which User pays for a republication license. If User is the author of the article which User wishes to reuse in User's thesis or dissertation, the republication licence covers the right to include the Version of Record of the article, provided it is not then shared or deposited online. User must include citation details. Where User wishes to share their thesis or dissertation online, they should remove the Version of Record before uploading it. User may include a Preprint or the Accepted Manuscript (after the embargo period) in the online version of the thesis or dissertation, provided they do so in accordance with the Rightsholder's policies on sharing Preprints or Accepted Manuscripts. User may need to obtain separate permission for any third party content included within the article. User must check this with the copyright owner of such third party content. Any online or commercial use of User's thesis or dissertation containing the article, including publication via ProQuest, would need to be expressly notified in writing to the Rightsholder at the time of request and would require separate written permission from the Rightsholder. As well as CCC, the Rightsholder shall have the right to bring any legal action that it deems necessary to enforce its rights should it consider that the Work infringes those rights in any way. For content reuse requests that qualify for permission under the STM Permissions Guidelines, which may be

updated from time to time, the STM Permissions Guidelines supplement the terms and conditions contained in this license.
If you are producing a new book or article to be published by another STM Signatory publisher, please choose "Reuse in a book under STM Guidelines" or "Reuse in a journal under STM Guidelines." You can consult the STM Guidelines website to see whether your new publisher is a signatory to the STM Permissions Guidelines.

## Marketplace Permissions General Terms and Conditions

The following terms and conditions ("General Terms"), together with any applicable Publisher Terms and Conditions, govern User's use of Works pursuant to the Licenses granted by Copyright Clearance Center, Inc. ("CCC") on behalf of the applicable Rightsholders of such Works through CCC's applicable Marketplace transactional licensing services (each, a "Service").

1) **Definitions.** For purposes of these General Terms, the following definitions apply:

"License" is the licensed use the User obtains via the Marketplace platform in a particular licensing transaction, as set forth in the Order Confirmation.

"Order Confirmation" is the confirmation CCC provides to the User at the conclusion of each Marketplace transaction. "Order Confirmation Terms" are additional terms set forth on specific Order Confirmations not set forth in the General Terms that can include terms applicable to a particular CCC transactional licensing service and/or any Rightsholder-specific terms.

"Rightsholder(s)" are the holders of copyright rights in the Works for which a User obtains licenses via the Marketplace platform, which are displayed on specific Order Confirmations.

"Terms" means the terms and conditions set forth in these General Terms and any additional Order Confirmation Terms collectively.

"User" or "you" is the person or entity making the use granted under the relevant License. Where the person accepting the Terms on behalf of a User is a freelancer or other third party who the User authorized to accept the General Terms on the User's behalf, such person shall be deemed jointly a User for purposes of such Terms.

"Work(s)" are the copyright protected works described in relevant Order Confirmations.

2) **Description of Service.** CCC's Marketplace enables Users to obtain Licenses to use one or more Works in accordance with all relevant Terms. CCC grants Licenses as an agent on behalf of the copyright rightsholder identified in the relevant Order Confirmation.

3) **Applicability of Terms.** The Terms govern User's use of Works in connection with the relevant License. In the event of any conflict between General Terms and Order Confirmation Terms, the latter shall govern. User acknowledges that Rightsholders have complete discretion whether to grant any permission, and whether to place any limitations on any grant, and that CCC has no right to supersede or to modify any such discretionary act by a Rightsholder.

4) **Representations; Acceptance.** By using the Service, User represents and warrants that User has been duly authorized by the User to accept, and hereby does accept, all Terms.

5) **Scope of License; Limitations and Obligations.** All Works and all rights therein, including copyright rights, remain the sole and exclusive property of the Rightsholder. The License provides only those rights expressly set forth in the terms and conveys no other rights in any Works

6) **General Payment Terms.** User may pay at time of checkout by credit card or choose to be invoiced. If the User chooses to be invoiced, the User shall: (i) remit payments in the manner identified on specific invoices, (ii) unless otherwise specifically stated in an Order Confirmation or separate written agreement, Users shall remit payments upon receipt of the relevant invoice from CCC, either by delivery or notification of availability of the invoice via the Marketplace platform, and (iii) if the User does not pay the invoice within 30 days of receipt, the User may incur a service charge of 1.5% per month or the maximum rate allowed by applicable law, whichever is less. While User may exercise the rights in the License immediately upon receiving the Order Confirmation, the License is automatically revoked and is null and void, as if it had never been issued, if CCC does not receive complete payment on a timely basis.

7) **General Limits on Use.** Unless otherwise provided in the Order Confirmation, any grant of rights to User (i) involves only the rights set forth in the Terms and does not include subsequent or additional uses, (ii) is non-exclusive and non-transferable, and (iii) is subject to any and all limitations and restrictions (such as, but not limited to, limitations on duration of use or circulation) included in the Terms. Upon completion of the licensed use as set forth in the Order Confirmation, User shall either secure a new permission for further use of the Work(s) or immediately cease any new use of the Work(s) and shall render inaccessible (such as by deleting or by removing or severing links or other locators) any further copies of the Work. User may only make alterations to the Work if and as expressly set forth in the Order

Confirmation. No Work may be used in any way that is unlawful, including without limitation if such use would violate applicable sanctions laws or regulations, would be defamatory, violate the rights of third parties (including such third parties' rights of copyright, privacy, publicity, or other tangible or intangible property), or is otherwise illegal, sexually explicit, or obscene. In addition, User may not conjoin a Work with any other material that may result in damage to the reputation of the Rightsholder. Any unlawful use will render any licenses hereunder null and void. User agrees to inform CCC if it becomes aware of any infringement of any rights in a Work and to cooperate with any reasonable request of CCC or the Rightsholder in connection therewith.

8) **Third Party Materials.** In the event that the material for which a License is sought includes third party materials (such as photographs, illustrations, graphs, inserts and similar materials) that are identified in such material as having been used by permission (or a similar indicator), User is responsible for identifying, and seeking separate licenses (under this Service, if available, or otherwise) for any of such third party materials; without a separate license, User may not use such third party materials via the License.

9) **Copyright Notice.** Use of proper copyright notice for a Work is required as a condition of any License granted under the Service. Unless otherwise provided in the Order Confirmation, a proper copyright notice will read substantially as follows: "Used with permission of [Rightsholder's name], from [Work's title, author, volume, edition number and year of copyright]; permission conveyed through Copyright Clearance Center, Inc." Such notice must be provided in a reasonably legible font size and must be placed either on a cover page or in another location that any person, upon gaining access to the material which is the subject of a permission, shall see, or in the case of republication Licenses, immediately adjacent to the Work as used (for example, as part of a by-line or footnote) or in the place where substantially all other credits or notices for the new work containing the republished Work are located. Failure to include the required notice results in loss to the Rightsholder and CCC, and the User shall be liable to pay liquidated damages for each such failure equal to twice the use fee specified in the Order Confirmation, in addition to the use fee itself and any other fees and charges specified.

10) **Indemnity.** User hereby indemnifies and agrees to defend the Rightsholder and CCC, and their respective employees and directors, against all claims, liability, damages, costs, and expenses, including legal fees and expenses, arising out of any use of a Work beyond the scope of the rights granted herein and in the Order Confirmation, or any use of a Work which has been altered in any unauthorized way by User, including claims of defamation or infringement of rights of copyright, publicity, privacy, or other tangible or intangible property.

11) **Limitation of Liability.** UNDER NO CIRCUMSTANCES WILL CCC OR THE RIGHTSHOLDER BE LIABLE FOR ANY DIRECT, INDIRECT, CONSEQUENTIAL, OR INCIDENTAL DAMAGES (INCLUDING WITHOUT LIMITATION DAMAGES FOR LOSS OF BUSINESS PROFITS OR INFORMATION, OR FOR BUSINESS INTERRUPTION) ARISING OUT OF THE USE OR INABILITY TO USE A WORK, EVEN IF ONE OR BOTH OF THEM HAS BEEN ADVISED OF THE POSSIBILITY OF SUCH DAMAGES. In any event, the total liability of the Rightsholder and CCC (including their respective employees and directors) shall not exceed the total amount actually paid by User for the relevant License. User assumes full liability for the actions and omissions of its principals, employees, agents, affiliates, successors, and assigns.

12) **Limited Warranties.** THE WORK(S) AND RIGHT(S) ARE PROVIDED "AS IS." CCC HAS THE RIGHT TO GRANT TO USER THE RIGHTS GRANTED IN THE ORDER CONFIRMATION DOCUMENT. CCC AND THE RIGHTSHOLDER DISCLAIM ALL OTHER WARRANTIES RELATING TO THE WORK(S) AND RIGHT(S), EITHER EXPRESS OR IMPLIED, INCLUDING WITHOUT LIMITATION IMPLIED WARRANTIES OF MERCHANTABILITY OR FITNESS FOR A PARTICULAR PURPOSE. ADDITIONAL RIGHTS MAY BE REQUIRED TO USE ILLUSTRATIONS, GRAPHS, PHOTOGRAPHS, ABSTRACTS, INSERTS, OR OTHER PORTIONS OF THE WORK (AS OPPOSED TO THE ENTIRE WORK) IN A MANNER CONTEMPLATED BY USER; USER UNDERSTANDS AND AGREES THAT NEITHER CCC NOR THE RIGHTSHOLDER MAY HAVE SUCH ADDITIONAL RIGHTS TO GRANT.

13) **Effect of Breach.** Any failure by User to pay any amount when due, or any use by User of a Work beyond the scope of the License set forth in the Order Confirmation and/or the Terms, shall be a material breach of such License. Any breach not cured within 10 days of written notice thereof shall result in immediate termination of such License without further notice. Any unauthorized (but licensable) use of a Work that is terminated immediately upon notice thereof may be liquidated by payment of the Rightsholder's ordinary license price therefor; any unauthorized (and unlicensable) use that is not terminated immediately for any reason (including, for example, because materials containing the Work cannot reasonably be recalled) will be subject to all remedies available at law or in equity, but in no event to a payment of less than three times the Rightsholder's ordinary license price for the most closely analogous licensable use plus Rightsholder's and/or CCC's costs and expenses incurred in collecting such payment.

14) **Additional Terms for Specific Products and Services.** If a User is making one of the uses described in this Section 14, the additional terms and conditions apply:

a) ***Print Uses of Academic Course Content and Materials (photocopies for academic coursepacks or classroom handouts).*** For photocopies for academic coursepacks or classroom handouts the following additional terms apply:

i) The copies and anthologies created under this License may be made and assembled by faculty members individually or at their request by on-campus bookstores or copy centers, or by off-campus copy shops and other similar entities.

ii) No License granted shall in any way: (i) include any right by User to create a substantively non-identical copy of the Work or to edit or in any other way modify the Work (except by means of deleting material immediately preceding or following the entire portion of the Work copied) (ii) permit "publishing ventures" where any particular anthology would be systematically marketed at multiple institutions.

iii) Subject to any Publisher Terms (and notwithstanding any apparent contradiction in the Order Confirmation arising from data provided by User), any use authorized under the academic pay-per-use service is limited as follows:

A) any License granted shall apply to only one class (bearing a unique identifier as assigned by the institution, and thereby including all sections or other subparts of the class) at one institution;

B) use is limited to not more than 25% of the text of a book or of the items in a published collection of essays, poems or articles;

C) use is limited to no more than the greater of (a) 25% of the text of an issue of a journal or other periodical or (b) two articles from such an issue;

D) no User may sell or distribute any particular anthology, whether photocopied or electronic, at more than one institution of learning;

E) in the case of a photocopy permission, no materials may be entered into electronic memory by User except in order to produce an identical copy of a Work before or during the academic term (or analogous period) as to which any particular permission is granted. In the event that User shall choose to retain materials that are the subject of a photocopy permission in electronic memory for purposes of producing identical copies more than one day after such retention (but still within the scope of any permission granted), User must notify CCC of such fact in the applicable permission request and such retention shall constitute one copy actually sold for purposes of calculating permission fees due; and

F) any permission granted shall expire at the end of the class. No permission granted shall in any way include any right by User to create a substantively non-identical copy of the Work or to edit or in any other way modify the Work (except by means of deleting material immediately preceding or following the entire portion of the Work copied).

iv) Books and Records; Right to Audit. As to each permission granted under the academic pay-per-use Service, User shall maintain for at least four full calendar years books and records sufficient for CCC to determine the numbers of copies made by User under such permission. CCC and any representatives it may designate shall have the right to audit such books and records at any time during User's ordinary business hours, upon two days' prior notice. If any such audit shall determine that User shall have underpaid for, or underreported, any photocopies sold or by three percent (3%) or more, then User shall bear all the costs of any such audit; otherwise, CCC shall bear the costs of any such audit. Any amount determined by such audit to have been underpaid by User shall immediately be paid to CCC by User, together with interest thereon at the rate of 10% per annum from the date such amount was originally due. The provisions of this paragraph shall survive the termination of this License for any reason.

b) ***Digital Pay-Per-Uses of Academic Course Content and Materials (e-coursepacks, electronic reserves, learning management systems, academic institution intranets).*** For uses in e-coursepacks, posts in electronic reserves, posts in learning management systems, or posts on academic institution intranets, the following additional terms apply:

i) The pay-per-uses subject to this Section 14(b) include:

A) **Posting e-reserves, course management systems, e-coursepacks for text-based content,** which grants authorizations to import requested material in electronic format, and allows electronic access to this material to members of a designated college or university class, under the direction of an instructor designated by the college or university, accessible only under appropriate electronic controls (e.g., password);

B) **Posting e-reserves, course management systems, e-coursepacks for material consisting of photographs or other still images not embedded in text,** which grants not only the authorizations described in Section 14(b)(i)(A) above, but also the following authorization: to include the requested material in course materials for use consistent with Section 14(b)(i)(A) above, including any necessary resizing, reformatting or modification of the resolution of such requested material (provided that such modification does not alter the underlying editorial content or meaning of the requested material, and provided that the resulting modified content is used solely within the scope of, and in a manner consistent with, the particular authorization described in the Order Confirmation and the Terms), but not including any other form of manipulation, alteration or editing of the requested material;

C) **Posting e-reserves, course management systems, e-coursepacks or other academic distribution for audiovisual content,** which grants not only the authorizations described in Section 14(b)(i)(A) above, but also

the following authorizations: (i) to include the requested material in course materials for use consistent with Section 14(b)(i)(A) above; (ii) to display and perform the requested material to such members of such class in the physical classroom or remotely by means of streaming media or other video formats; and (iii) to "clip" or reformat the requested material for purposes of time or content management or ease of delivery, provided that such "clipping" or reformatting does not alter the underlying editorial content or meaning of the requested material and that the resulting material is used solely within the scope of, and in a manner consistent with, the particular authorization described in the Order Confirmation and the Terms. Unless expressly set forth in the relevant Order Conformation, the License does not authorize any other form of manipulation, alteration or editing of the requested material.

ii) Unless expressly set forth in the relevant Order Confirmation, no License granted shall in any way: (i) include any right by User to create a substantively non-identical copy of the Work or to edit or in any other way modify the Work (except by means of deleting material immediately preceding or following the entire portion of the Work copied or, in the case of Works subject to Sections 14(b)(1)(B) or (C) above, as described in such Sections) (ii) permit "publishing ventures" where any particular course materials would be systematically marketed at multiple institutions.

iii) Subject to any further limitations determined in the Rightsholder Terms (and notwithstanding any apparent contradiction in the Order Confirmation arising from data provided by User), any use authorized under the electronic course content pay-per-use service is limited as follows:

A) any License granted shall apply to only one class (bearing a unique identifier as assigned by the institution, and thereby including all sections or other subparts of the class) at one institution;

B) use is limited to not more than 25% of the text of a book or of the items in a published collection of essays, poems or articles;

C) use is limited to not more than the greater of (a) 25% of the text of an issue of a journal or other periodical or (b) two articles from such an issue;

D) no User may sell or distribute any particular materials, whether photocopied or electronic, at more than one institution of learning;

E) electronic access to material which is the subject of an electronic-use permission must be limited by means of electronic password, student identification or other control permitting access solely to students and instructors in the class;

F) User must ensure (through use of an electronic cover page or other appropriate means) that any person, upon gaining electronic access to the material, which is the subject of a permission, shall see:

- a proper copyright notice, identifying the Rightsholder in whose name CCC has granted permission,
- a statement to the effect that such copy was made pursuant to permission,
- a statement identifying the class to which the material applies and notifying the reader that the material has been made available electronically solely for use in the class, and
- a statement to the effect that the material may not be further distributed to any person outside the class, whether by copying or by transmission and whether electronically or in paper form, and User must also ensure that such cover page or other means will print out in the event that the person accessing the material chooses to print out the material or any part thereof.

G) any permission granted shall expire at the end of the class and, absent some other form of authorization, User is thereupon required to delete the applicable material from any electronic storage or to block electronic access to the applicable material.

iv) Uses of separate portions of a Work, even if they are to be included in the same course material or the same university or college class, require separate permissions under the electronic course content pay-per-use Service. Unless otherwise provided in the Order Confirmation, any grant of rights to User is limited to use completed no later than the end of the academic term (or analogous period) as to which any particular permission is granted.

v) Books and Records; Right to Audit. As to each permission granted under the electronic course content Service, User shall maintain for at least four full calendar years books and records sufficient for CCC to determine the numbers of copies made by User under such permission. CCC and any representatives it may designate shall have the right to audit such books and records at any time during User's ordinary business hours, upon two days' prior notice. If any such audit shall determine that User shall have underpaid for, or underreported, any electronic copies used by three percent (3%) or more, then User shall bear all the costs of any such audit; otherwise, CCC

shall bear the costs of any such audit. Any amount determined by such audit to have been underpaid by User shall immediately be paid to CCC by User, together with interest thereon at the rate of 10% per annum from the date such amount was originally due. The provisions of this paragraph shall survive the termination of this license for any reason.

c) ***Pay-Per-Use Permissions for Certain Reproductions (Academic photocopies for library reserves and interlibrary loan reporting) (Non-academic internal/external business uses and commercial document delivery).*** The License expressly excludes the uses listed in Section (c)(i)-(v) below (which must be subject to separate license from the applicable Rightsholder) for: academic photocopies for library reserves and interlibrary loan reporting; and non-academic internal/external business uses and commercial document delivery.

i) electronic storage of any reproduction (whether in plain-text, PDF, or any other format) other than on a transitory basis;

ii) the input of Works or reproductions thereof into any computerized database;

iii) reproduction of an entire Work (cover-to-cover copying) except where the Work is a single article;

iv) reproduction for resale to anyone other than a specific customer of User;

v) republication in any different form. Please obtain authorizations for these uses through other CCC services or directly from the rightsholder.

Any license granted is further limited as set forth in any restrictions included in the Order Confirmation and/or in these Terms.

d) ***Electronic Reproductions in Online Environments (Non-Academic-email, intranet, internet and extranet).*** For "electronic reproductions", which generally includes e-mail use (including instant messaging or other electronic transmission to a defined group of recipients) or posting on an intranet, extranet or Intranet site (including any display or performance incidental thereto), the following additional terms apply:

i) Unless otherwise set forth in the Order Confirmation, the License is limited to use completed within 30 days for any use on the Internet, 60 days for any use on an intranet or extranet and one year for any other use, all as measured from the "republication date" as identified in the Order Confirmation, if any, and otherwise from the date of the Order Confirmation.

ii) User may not make or permit any alterations to the Work, unless expressly set forth in the Order Confirmation (after request by User and approval by Rightsholder); provided, however, that a Work consisting of photographs or other still images not embedded in text may, if necessary, be resized, reformatted or have its resolution modified without additional express permission, and a Work consisting of audiovisual content may, if necessary, be "clipped" or reformatted for purposes of time or content management or ease of delivery (provided that any such resizing, reformatting, resolution modification or "clipping" does not alter the underlying editorial content or meaning of the Work used, and that the resulting material is used solely within the scope of, and in a manner consistent with, the particular License described in the Order Confirmation and the Terms.

15) **Miscellaneous.**

a) User acknowledges that CCC may, from time to time, make changes or additions to the Service or to the Terms, and that Rightsholder may make changes or additions to the Rightsholder Terms. Such updated Terms will replace the prior terms and conditions in the order workflow and shall be effective as to any subsequent Licenses but shall not apply to Licenses already granted and paid for under a prior set of terms.

b) Use of User-related information collected through the Service is governed by CCC's privacy policy, available online at www.copyright.com/about/privacy-policy/.

c) The License is personal to User. Therefore, User may not assign or transfer to any other person (whether a natural person or an organization of any kind) the License or any rights granted thereunder; provided, however, that, where applicable, User may assign such License in its entirety on written notice to CCC in the event of a transfer of all or substantially all of User's rights in any new material which includes the Work(s) licensed under this Service.

d) No amendment or waiver of any Terms is binding unless set forth in writing and signed by the appropriate parties, including, where applicable, the Rightsholder. The Rightsholder and CCC hereby object to any terms contained in any writing prepared by or on behalf of the User or its principals, employees, agents or affiliates and purporting to govern or otherwise relate to the License described in the Order Confirmation, which terms are in any way inconsistent with any Terms set forth in the Order Confirmation, and/or in CCC's standard operating procedures, whether such writing is prepared prior to, simultaneously with or subsequent to the Order Confirmation, and whether such writing appears on a copy of the Order Confirmation or in a separate instrument.

e) The License described in the Order Confirmation shall be governed by and construed under the law of the State of New York, USA, without regard to the principles thereof of conflicts of law. Any case, controversy, suit, action, or proceeding arising out of, in connection with, or related to such License shall be brought, at CCC's sole discretion, in any federal or state court located in the County of New York, State of New York, USA, or in any federal or state court whose geographical jurisdiction covers the location of the Rightsholder set forth in the Order Confirmation. The parties expressly submit to the personal jurisdiction and venue of each such federal or state court.

*Last updated October 2022*

## Request to reproduce an extract from a third party's published work

18/04/2024

Dear Dolphitech,

I am completing my PhD thesis at Imperial College London entitled ‘Data-driven Modelling for Guided Wave Structural Health Monitoring and Prognostic Health Management on Aeronautical Structures’.

I seek your permission to reprint, in my thesis an extract from: DolphiCam2 Transducer Module (TRM) Technology Note. The extract to be reproduced is: Figure in Page 1.

I would like to include the extract in my thesis which will be added to Spiral, Imperial's institutional repository http://spiral.imperial.ac.uk/ and made available to the public under a CC BY-NC 4.0 license.

If you are happy to grant me all the permissions requested, please return a signed copy of this letter. If you wish to grant only some of the permissions requested, please list these and then sign.

Yours sincerely,

Hongmin Zhu

**Permission granted for the use requested above:**

I confirm that I am the copyright holder of the extract above and hereby give permission to include it in your thesis which will be made available, via the internet, for non-commercial purposes under the terms of the user licence.

**[please edit the text above if you wish to grant more specific permission]**

Signed:

Name: Matthew Day

Organisation: Dolphitech Ltd.

Job title: UK & IE Sales Manager

# ELSEVIER LICENSE
# TERMS AND CONDITIONS

Apr 15, 2024

This Agreement between Mr. HONGMIN ZHU ("You") and Elsevier ("Elsevier") consists of your license details and the terms and conditions provided by Elsevier and Copyright Clearance Center.

| | |
|---|---|
| License Number | 5766131380167 |
| License date | Apr 11, 2024 |
| Licensed Content Publisher | Elsevier |
| Licensed Content Publication | Composite Structures |
| Licensed Content Title | An improved time reversal method for diagnostics of composite plates using Lamb waves |
| Licensed Content Author | Liping Huang,Liang Zeng,Jing Lin,Zhi Luo |
| Licensed Content Date | Apr 15, 2018 |
| Licensed Content Volume | 190 |
| Licensed Content Issue | n/a |
| Licensed Content Pages | 10 |
| Start Page | 10 |
| End Page | 19 |
| Type of Use | reuse in a thesis/dissertation |
| Portion | figures/tables/illustrations |
| Number of figures/tables/illustrations | 1 |
| Format | both print and electronic |
| Are you the author of this Elsevier article? | No |
| Will you be translating? | No |
| Title of new work | Data-driven Modelling for Guided Wave Structural Health Monitoring and Prognostic Health Management on Aeronautical Structures |
| Institution name | Imperial College London |
| Expected presentation date | Jul 2024 |
| Order reference number | abcd |
| Portions | Fig. 1. Schematic diagram of time reversal process in a composite plate. |
| Requestor Location | Mr. HONGMIN ZHU<br>Exhibition Road<br><br>London, other<br>United Kingdom<br>Attn: Mr. HONGMIN ZHU |
| Publisher Tax ID | GB 494 6272 12 |
| Total | **0.00 GBP** |
| Terms and Conditions | |

**INTRODUCTION**

1. The publisher for this copyrighted material is Elsevier. By clicking "accept" in connection with completing this licensing transaction, you agree that the following terms and conditions apply to this transaction (along with the Billing and Payment terms and conditions established by Copyright Clearance Center, Inc. ("CCC"), at the time that you opened your RightsLink account and that are available at any time at https://myaccount.copyright.com).

**GENERAL TERMS**

2. Elsevier hereby grants you permission to reproduce the aforementioned material subject to the terms and conditions indicated.

3. Acknowledgement: If any part of the material to be used (for example, figures) has appeared in our publication with credit or acknowledgement to another source, permission must also be sought from that source. If such permission is not obtained then that material may not be included in your publication/copies. Suitable acknowledgement to the source must be made, either as a footnote or in a reference list at the end of your publication, as follows:
"Reprinted from Publication title, Vol /edition number, Author(s), Title of article / title of chapter, Pages No., Copyright (Year), with permission from Elsevier [OR APPLICABLE SOCIETY COPYRIGHT OWNER]." Also Lancet special credit - "Reprinted from The Lancet, Vol. number, Author(s), Title of article, Pages No., Copyright (Year), with permission from Elsevier."
4. Reproduction of this material is confined to the purpose and/or media for which permission is hereby given. The material may not be reproduced or used in any other way, including use in combination with an artificial intelligence tool (including to train an algorithm, test, process, analyse, generate output and/or develop any form of artificial intelligence tool), or to create any derivative work and/or service (including resulting from the use of artificial intelligence tools).
5. Altering/Modifying Material: Not Permitted. However figures and illustrations may be altered/adapted minimally to serve your work. Any other abbreviations, additions, deletions and/or any other alterations shall be made only with prior written authorization of Elsevier Ltd. (Please contact Elsevier's permissions helpdesk here). No modifications can be made to any Lancet figures/tables and they must be reproduced in full.
6. If the permission fee for the requested use of our material is waived in this instance, please be advised that your future requests for Elsevier materials may attract a fee.
7. Reservation of Rights: Publisher reserves all rights not specifically granted in the combination of (i) the license details provided by you and accepted in the course of this licensing transaction, (ii) these terms and conditions and (iii) CCC's Billing and Payment terms and conditions.
8. License Contingent Upon Payment: While you may exercise the rights licensed immediately upon issuance of the license at the end of the licensing process for the transaction, provided that you have disclosed complete and accurate details of your proposed use, no license is finally effective unless and until full payment is received from you (either by publisher or by CCC) as provided in CCC's Billing and Payment terms and conditions. If full payment is not received on a timely basis, then any license preliminarily granted shall be deemed automatically revoked and shall be void as if never granted. Further, in the event that you breach any of these terms and conditions or any of CCC's Billing and Payment terms and conditions, the license is automatically revoked and shall be void as if never granted. Use of materials as described in a revoked license, as well as any use of the materials beyond the scope of an unrevoked license, may constitute copyright infringement and publisher reserves the right to take any and all action to protect its copyright in the materials.
9. Warranties: Publisher makes no representations or warranties with respect to the licensed material.
10. Indemnity: You hereby indemnify and agree to hold harmless publisher and CCC, and their respective officers, directors, employees and agents, from and against any and all claims arising out of your use of the licensed material other than as specifically authorized pursuant to this license.
11. No Transfer of License: This license is personal to you and may not be sublicensed, assigned, or transferred by you to any other person without publisher's written permission.
12. No Amendment Except in Writing: This license may not be amended except in a writing signed by both parties (or, in the case of publisher, by CCC on publisher's behalf).
13. Objection to Contrary Terms: Publisher hereby objects to any terms contained in any purchase order, acknowledgment, check endorsement or other writing prepared by you, which terms are inconsistent with these terms and conditions or CCC's Billing and Payment terms and conditions. These terms and conditions, together with CCC's Billing and Payment terms and conditions (which are incorporated herein), comprise the entire agreement between you and publisher (and CCC) concerning this licensing transaction. In the event of any conflict between your obligations established by these terms and conditions and those established by CCC's Billing and Payment terms and conditions, these terms and conditions shall control.
14. Revocation: Elsevier or Copyright Clearance Center may deny the permissions described in this License at their sole discretion, for any reason or no reason, with a full refund payable to you. Notice of such denial will be made using the contact information provided by you. Failure to receive such notice will not alter or invalidate the denial. In no event will Elsevier or Copyright Clearance Center be responsible or liable for any costs, expenses or damage incurred by you as a result of a denial of your permission request, other than a refund of the amount(s) paid by you to Elsevier and/or Copyright Clearance Center for denied permissions.

**LIMITED LICENSE**

The following terms and conditions apply only to specific license types:
15. **Translation**: This permission is granted for non-exclusive world **English** rights only unless your license was granted for translation rights. If you licensed translation rights you may only translate this content into the languages you requested. A professional translator must perform all translations and reproduce the content word for word preserving the integrity of the article.
16. **Posting licensed content on any Website**: The following terms and conditions apply as follows: Licensing material from an Elsevier journal: All content posted to the web site must maintain the copyright information line on the bottom of each image; A hyper-text must be included to the Homepage of the journal from which you are licensing at http://www.sciencedirect.com/science/journal/xxxxx or the Elsevier homepage for books at http://www.elsevier.com; Central Storage: This license does not include permission for a scanned version of the material to be stored in a central repository such as that provided by Heron/XanEdu.
Licensing material from an Elsevier book: A hyper-text link must be included to the Elsevier homepage at http://www.elsevier.com . All content posted to the web site must maintain the copyright information line on the bottom of each image.

**Posting licensed content on Electronic reserve**: In addition to the above the following clauses are applicable: The web site must be password-protected and made available only to bona fide students registered on a relevant course. This permission is granted for 1 year only. You may obtain a new license for future website posting.
17. **For journal authors:** the following clauses are applicable in addition to the above:
**Preprints:**
A preprint is an author's own write-up of research results and analysis, it has not been peer-reviewed, nor has it had any other value added to it by a publisher (such as formatting, copyright, technical enhancement etc.).
Authors can share their preprints anywhere at any time. Preprints should not be added to or enhanced in any way in order to appear more like, or to substitute for, the final versions of articles however authors can update their preprints on arXiv or RePEc with their Accepted Author Manuscript (see below).
If accepted for publication, we encourage authors to link from the preprint to their formal publication via its DOI. Millions of researchers have access to the formal publications on ScienceDirect, and so links will help users to find, access, cite and use the best available version. Please note that Cell Press, The Lancet and some society-owned have different preprint policies. Information on these policies is available on the journal homepage.
**Accepted Author Manuscripts:** An accepted author manuscript is the manuscript of an article that has been accepted for publication and which typically includes author-incorporated changes suggested during submission, peer review and editor-author communications.
Authors can share their accepted author manuscript:

- immediately
    - via their non-commercial person homepage or blog
    - by updating a preprint in arXiv or RePEc with the accepted manuscript
    - via their research institute or institutional repository for internal institutional uses or as part of an invitation-only research collaboration work-group
    - directly by providing copies to their students or to research collaborators for their personal use
    - for private scholarly sharing as part of an invitation-only work group on commercial sites with which Elsevier has an agreement
- After the embargo period
    - via non-commercial hosting platforms such as their institutional repository
    - via commercial sites with which Elsevier has an agreement

In all cases accepted manuscripts should:

- link to the formal publication via its DOI
- bear a CC-BY-NC-ND license - this is easy to do
- if aggregated with other manuscripts, for example in a repository or other site, be shared in alignment with our hosting policy not be added to or enhanced in any way to appear more like, or to substitute for, the published journal article.

**Published journal article (JPA):** A published journal article (PJA) is the definitive final record of published research that appears or will appear in the journal and embodies all value-adding publishing activities including peer review co-ordination, copy-editing, formatting, (if relevant) pagination and online enrichment.
Policies for sharing publishing journal articles differ for subscription and gold open access articles:
**Subscription Articles:** If you are an author, please share a link to your article rather than the full-text. Millions of researchers have access to the formal publications on ScienceDirect, and so links will help your users to find, access, cite, and use the best available version.
Theses and dissertations which contain embedded PJAs as part of the formal submission can be posted publicly by the awarding institution with DOI links back to the formal publications on ScienceDirect.
If you are affiliated with a library that subscribes to ScienceDirect you have additional private sharing rights for others' research accessed under that agreement. This includes use for classroom teaching and internal training at the institution (including use in course packs and courseware programs), and inclusion of the article for grant funding purposes.
**Gold Open Access Articles:** May be shared according to the author-selected end-user license and should contain a CrossMark logo, the end user license, and a DOI link to the formal publication on ScienceDirect.
Please refer to Elsevier's posting policy for further information.
18. **For book authors** the following clauses are applicable in addition to the above: Authors are permitted to place a brief summary of their work online only. You are not allowed to download and post the published electronic version of your chapter, nor may you scan the printed edition to create an electronic version. **Posting to a repository:** Authors are permitted to post a summary of their chapter only in their institution's repository.
19. **Thesis/Dissertation**: If your license is for use in a thesis/dissertation your thesis may be submitted to your institution in either print or electronic form. Should your thesis be published commercially, please reapply for permission. These requirements include permission for the Library and Archives of Canada to supply single copies, on demand, of the complete thesis and include permission for Proquest/UMI to supply single copies, on demand, of the complete thesis. Should your thesis be published commercially, please reapply for permission. Theses and dissertations which contain embedded PJAs as part of the formal submission can be posted publicly by the awarding institution with DOI links back to the formal publications on ScienceDirect.

**Elsevier Open Access Terms and Conditions**

You can publish open access with Elsevier in hundreds of open access journals or in nearly 2000 established subscription journals that support open access publishing. Permitted third party re-use of these open access articles is defined by the author's choice of Creative Commons user license. See our open access license policy for more information.

**Terms & Conditions applicable to all Open Access articles published with Elsevier:**

Any reuse of the article must not represent the author as endorsing the adaptation of the article nor should the article be modified in such a way as to damage the author's honour or reputation. If any changes have been made, such changes must be clearly indicated.

The author(s) must be appropriately credited and we ask that you include the end user license and a DOI link to the formal publication on ScienceDirect.

If any part of the material to be used (for example, figures) has appeared in our publication with credit or acknowledgement to another source it is the responsibility of the user to ensure their reuse complies with the terms and conditions determined by the rights holder.

**Additional Terms & Conditions applicable to each Creative Commons user license:**

**CC BY:** The CC-BY license allows users to copy, to create extracts, abstracts and new works from the Article, to alter and revise the Article and to make commercial use of the Article (including reuse and/or resale of the Article by commercial entities), provided the user gives appropriate credit (with a link to the formal publication through the relevant DOI), provides a link to the license, indicates if changes were made and the licensor is not represented as endorsing the use made of the work. The full details of the license are available at http://creativecommons.org/licenses/by/4.0.

**CC BY NC SA:** The CC BY-NC-SA license allows users to copy, to create extracts, abstracts and new works from the Article, to alter and revise the Article, provided this is not done for commercial purposes, and that the user gives appropriate credit (with a link to the formal publication through the relevant DOI), provides a link to the license, indicates if changes were made and the licensor is not represented as endorsing the use made of the work. Further, any new works must be made available on the same conditions. The full details of the license are available at http://creativecommons.org/licenses/by-nc-sa/4.0.

**CC BY NC ND:** The CC BY-NC-ND license allows users to copy and distribute the Article, provided this is not done for commercial purposes and further does not permit distribution of the Article if it is changed or edited in any way, and provided the user gives appropriate credit (with a link to the formal publication through the relevant DOI), provides a link to the license, and that the licensor is not represented as endorsing the use made of the work. The full details of the license are available at http://creativecommons.org/licenses/by-nc-nd/4.0. Any commercial reuse of Open Access articles published with a CC BY NC SA or CC BY NC ND license requires permission from Elsevier and will be subject to a fee.

Commercial reuse includes:

- Associating advertising with the full text of the Article
- Charging fees for document delivery or access
- Article aggregation
- Systematic distribution via e-mail lists or share buttons

Posting or linking by commercial companies for use by customers of those companies.

20. **Other Conditions**:

v1.10

**Questions? E-mail us at customercare@copyright.com.**

# Marketplace

This is a License Agreement between Hongmin Zhu (“User”) and Copyright Clearance Center, Inc. (“CCC”) on behalf of the Rightsholder identified in the order details below. The license consists of the order details, the Marketplace Permissions General Terms and Conditions below, and any Rightsholder Terms and Conditions which are included below.

All payments must be made in full to CCC in accordance with the Marketplace Permissions General Terms and Conditions below.

| | | | |
|---|---|---|---|
| **Order Date** | 11-Apr-2024 | **Type of Use** | Republish in a thesis/dissertation |
| **Order License ID** | 1472506-1 | | |
| **ISSN** | 0964-1726 | **Publisher** | IOP Publishing |
| | | **Portion** | Image/photo/illustration |

## LICENSED CONTENT

| | | | |
|---|---|---|---|
| **Publication Title** | Smart Materials and Structures | **Country** | United Kingdom of Great Britain and Northern Ireland |
| **Author/Editor** | Institute of Physics (Great Britain), Society of Photo-optical Instrumentation Engineers. | **Rightsholder** | IOP Publishing, Ltd |
| | | **Publication Type** | Journal |
| **Date** | 01/01/1992 | | |
| **Language** | English | | |

## REQUEST DETAILS

| | | | |
|---|---|---|---|
| **Portion Type** | Image/photo/illustration | **Distribution** | U.K. and Commonwealth (excluding Canada) |
| **Number of Images / Photos / Illustrations** | 2 | **Translation** | Original language of publication |
| **Format (select all that apply)** | Print, Electronic | **Copies for the Disabled?** | No |
| **Who Will Republish the Content?** | Academic institution | **Minor Editing Privileges?** | No |
| **Duration of Use** | Life of current edition | **Incidental Promotional Use?** | No |
| **Lifetime Unit Quantity** | Up to 4,999 | **Currency** | GBP |
| **Rights Requested** | Main product | | |

## NEW WORK DETAILS

| | | | |
|---|---|---|---|
| **Title** | Data-driven Modelling for Guided Wave Structural Health Monitoring and Prognostic Health Management on Aeronautical Structures | **Institution Name** | Imperial College London |
| | | **Expected Presentation Date** | 2024-07-01 |
| **Instructor Name** | Ferri Aliabadi | | |

## ADDITIONAL DETAILS

| | | | |
|---|---|---|---|
| **Order Reference Number** | N/A | **The Requesting Person / Organization to Appear on the License** | Hongmin Zhu |

## REQUESTED CONTENT DETAILS

| | | | |
|---|---|---|---|
| **Title, Description or Numeric Reference of the Portion(s)** | Figure 4, Figure 16 | **Title of the Article / Chapter the Portion Is From** | An enhanced Lamb wave virtual time reversal technique for damage detection with transducer transfer function compensation |
| **Editor of Portion(s)** | N/A | | |
| **Volume / Edition** | 28 | | |
| **Page or Page Range of Portion** | 7,14 | **Author of Portion(s)** | Institute of Physics (Great Britain); Society of Photo-optical Instrumentation Engineers. |
| | | **Issue, if Republishing an Article From a Serial** | N/A |
| | | **Publication Date of Portion** | 2019-07-01 |

## RIGHTSHOLDER TERMS AND CONDITIONS

These special terms and conditions are in addition to the standard terms and conditions for CCC's Republication Service and, together with those standard terms and conditions, govern the use of the Works. As the User you will make all reasonable efforts to contact the author(s) of the article which the Work is to be reused from, to seek consent for your intended use. Contacting one author who is acting expressly as authorised agent for their co-author(s) is acceptable. User will reproduce the following wording prominently alongside the Work: the source of the Work, including author, article title, title of journal, volume number, issue number (if relevant), page range (or first page if this is the only information available) and date of first publication; and a link back to the article (via DOI); and if practicable, and IN ALL CASES for new works published under any of the Creative Commons licences, the words "© IOP Publishing. Reproduced with permission. All rights reserved" Without the express permission of the author(s) and the Rightsholder of the article from which the Work is to be reused, User shall not use it in any way which, in the opinion of the Rightsholder, could: (i) distort or alter the author(s)' original intention(s) and meaning; (ii) be prejudicial to the honour or reputation of the author(s); and/or (iii) imply endorsement by the author(s) and/or the Rightsholder. This licence does not apply to any article which is credited to another source and which does not have the copyright line '© IOP Publishing Ltd'. User must check the copyright line of the article from which the Work is to be reused to check that IOP Publishing Ltd has all the necessary rights to be able to grant permission. User is solely responsible for identifying and obtaining separate licences and permissions from the copyright owner for reuse of any such third party material/figures which the Rightsholder is not the copyright owner of. The Rightsholder shall not reimburse any fees which User pays for a republication license for such third party content. This licence does not apply to any material/figure which is credited to another source in the Rightsholder's publication or has been obtained from a third party. User must check the Version of Record of the article from which the Work is to be reused, to check whether any of the material in the Work is third party material. Third party citations and/or copyright notices and/or permissions statements may not be included in any other version of the article from which the Work is to be reused and so cannot be relied upon by the User. User is solely responsible for identifying and obtaining separate licences and permissions from the copyright owner for reuse of any such third party material/figures where the Rightsholder is not the copyright owner. The Rightsholder shall not reimburse any fees which User pays for a republication license for such third party content. User and CCC acknowledge that the Rightsholder may, from time to time, make changes or additions to these special terms and conditions without express notification, provided that these shall not apply to permissions already secured and paid for by User prior to such change or addition. User acknowledges that the Rightsholder (which includes companies within its group and third parties for whom it publishes its titles) may make use of personal data collected through the service in the course of their business. If User is the author of the Work, User may automatically have the right to reuse it under the rights granted back when User transferred the copyright in the article to the Rightsholder. User should check the copyright form and the relevant author rights policy to check whether permission is required. If User is the author of the Work and does require permission for proposed reuse of the Work, User should select 'Author of requested content' as the Requestor Type. The Rightsholder shall not reimburse any fees which User pays for a republication license. If User is the author of the article which User wishes to reuse in User's thesis or dissertation, the republication licence covers the right to include the Version of Record of the article, provided it is not then shared or deposited online. User must include citation details. Where User wishes to share their thesis or dissertation online, they should remove the Version of Record before uploading it. User may include a Preprint or the Accepted Manuscript (after the embargo period) in the online version of the thesis or dissertation, provided they do so in accordance with the Rightsholder's policies on sharing Preprints or Accepted Manuscripts. User may need to obtain separate permission for any third party content included within the article. User must check this with the copyright owner of such third party content. Any online or commercial use of User's thesis or dissertation containing the article, including publication via ProQuest, would need to be expressly notified in writing to the Rightsholder at the time of request and would require separate written permission from the Rightsholder. As well as CCC, the Rightsholder shall have the right to bring any legal action that it deems necessary to enforce its rights should it consider that the Work infringes those rights in any way. For content reuse requests that qualify for permission under the STM Permissions Guidelines, which may be updated from time to time, the STM Permissions Guidelines supplement the terms and conditions contained in this license.

If you are producing a new book or article to be published by another STM Signatory publisher, please choose "Reuse in a book under STM Guidelines" or "Reuse in a journal under STM Guidelines." You can consult the STM Guidelines website to see whether your new publisher is a signatory to the STM Permissions Guidelines.

## Marketplace Permissions General Terms and Conditions

The following terms and conditions ("General Terms"), together with any applicable Publisher Terms and Conditions, govern User's use of Works pursuant to the Licenses granted by Copyright Clearance Center, Inc. ("CCC") on behalf of the applicable Rightsholders of such Works through CCC's applicable Marketplace transactional licensing services (each, a "Service").

1) **Definitions.** For purposes of these General Terms, the following definitions apply:

"License" is the licensed use the User obtains via the Marketplace platform in a particular licensing transaction, as set forth in the Order Confirmation.

"Order Confirmation" is the confirmation CCC provides to the User at the conclusion of each Marketplace transaction. "Order Confirmation Terms" are additional terms set forth on specific Order Confirmations not set forth in the General Terms that can include terms applicable to a particular CCC transactional licensing service and/or any Rightsholder-specific terms.

"Rightsholder(s)" are the holders of copyright rights in the Works for which a User obtains licenses via the Marketplace platform, which are displayed on specific Order Confirmations.

"Terms" means the terms and conditions set forth in these General Terms and any additional Order Confirmation Terms collectively.

"User" or "you" is the person or entity making the use granted under the relevant License. Where the person accepting the Terms on behalf of a User is a freelancer or other third party who the User authorized to accept the General Terms on the User's behalf, such person shall be deemed jointly a User for purposes of such Terms.

"Work(s)" are the copyright protected works described in relevant Order Confirmations.

2) **Description of Service.** CCC's Marketplace enables Users to obtain Licenses to use one or more Works in accordance with all relevant Terms. CCC grants Licenses as an agent on behalf of the copyright rightsholder identified in the relevant Order Confirmation.

3) **Applicability of Terms.** The Terms govern User's use of Works in connection with the relevant License. In the event of any conflict between General Terms and Order Confirmation Terms, the latter shall govern. User acknowledges that Rightsholders have complete discretion whether to grant any permission, and whether to place any limitations on any grant, and that CCC has no right to supersede or to modify any such discretionary act by a Rightsholder.

4) **Representations; Acceptance.** By using the Service, User represents and warrants that User has been duly authorized by the User to accept, and hereby does accept, all Terms.

5) **Scope of License; Limitations and Obligations.** All Works and all rights therein, including copyright rights, remain the sole and exclusive property of the Rightsholder. The License provides only those rights expressly set forth in the terms and conveys no other rights in any Works

6) **General Payment Terms.** User may pay at time of checkout by credit card or choose to be invoiced. If the User chooses to be invoiced, the User shall: (i) remit payments in the manner identified on specific invoices, (ii) unless otherwise specifically stated in an Order Confirmation or separate written agreement, Users shall remit payments upon receipt of the relevant invoice from CCC, either by delivery or notification of availability of the invoice via the Marketplace platform, and (iii) if the User does not pay the invoice within 30 days of receipt, the User may incur a service charge of 1.5% per month or the maximum rate allowed by applicable law, whichever is less. While User may exercise the rights in the License immediately upon receiving the Order Confirmation, the License is automatically revoked and is null and void, as if it had never been issued, if CCC does not receive complete payment on a timely basis.

7) **General Limits on Use.** Unless otherwise provided in the Order Confirmation, any grant of rights to User (i) involves only the rights set forth in the Terms and does not include subsequent or additional uses, (ii) is non-exclusive and non-transferable, and (iii) is subject to any and all limitations and restrictions (such as, but not limited to, limitations on duration of use or circulation) included in the Terms. Upon completion of the licensed use as set forth in the Order Confirmation, User shall either secure a new permission for further use of the Work(s) or immediately cease any new use of the Work(s) and shall render inaccessible (such as by deleting or by removing or severing links or other locators) any further copies of the Work. User may only make alterations to the Work if and as expressly set forth in the Order Confirmation. No Work may be used in any way that is unlawful, including without limitation if such use would violate applicable sanctions laws or regulations, would be defamatory, violate the rights of third parties (including such third

parties' rights of copyright, privacy, publicity, or other tangible or intangible property), or is otherwise illegal, sexually explicit, or obscene. In addition, User may not conjoin a Work with any other material that may result in damage to the reputation of the Rightsholder. Any unlawful use will render any licenses hereunder null and void. User agrees to inform CCC if it becomes aware of any infringement of any rights in a Work and to cooperate with any reasonable request of CCC or the Rightsholder in connection therewith.

8) **Third Party Materials.** In the event that the material for which a License is sought includes third party materials (such as photographs, illustrations, graphs, inserts and similar materials) that are identified in such material as having been used by permission (or a similar indicator), User is responsible for identifying, and seeking separate licenses (under this Service, if available, or otherwise) for any of such third party materials; without a separate license, User may not use such third party materials via the License.

9) **Copyright Notice.** Use of proper copyright notice for a Work is required as a condition of any License granted under the Service. Unless otherwise provided in the Order Confirmation, a proper copyright notice will read substantially as follows: "Used with permission of [Rightsholder's name], from [Work's title, author, volume, edition number and year of copyright]; permission conveyed through Copyright Clearance Center, Inc." Such notice must be provided in a reasonably legible font size and must be placed either on a cover page or in another location that any person, upon gaining access to the material which is the subject of a permission, shall see, or in the case of republication Licenses, immediately adjacent to the Work as used (for example, as part of a by-line or footnote) or in the place where substantially all other credits or notices for the new work containing the republished Work are located. Failure to include the required notice results in loss to the Rightsholder and CCC, and the User shall be liable to pay liquidated damages for each such failure equal to twice the use fee specified in the Order Confirmation, in addition to the use fee itself and any other fees and charges specified.

10) **Indemnity.** User hereby indemnifies and agrees to defend the Rightsholder and CCC, and their respective employees and directors, against all claims, liability, damages, costs, and expenses, including legal fees and expenses, arising out of any use of a Work beyond the scope of the rights granted herein and in the Order Confirmation, or any use of a Work which has been altered in any unauthorized way by User, including claims of defamation or infringement of rights of copyright, publicity, privacy, or other tangible or intangible property.

11) **Limitation of Liability.** UNDER NO CIRCUMSTANCES WILL CCC OR THE RIGHTSHOLDER BE LIABLE FOR ANY DIRECT, INDIRECT, CONSEQUENTIAL, OR INCIDENTAL DAMAGES (INCLUDING WITHOUT LIMITATION DAMAGES FOR LOSS OF BUSINESS PROFITS OR INFORMATION, OR FOR BUSINESS INTERRUPTION) ARISING OUT OF THE USE OR INABILITY TO USE A WORK, EVEN IF ONE OR BOTH OF THEM HAS BEEN ADVISED OF THE POSSIBILITY OF SUCH DAMAGES. In any event, the total liability of the Rightsholder and CCC (including their respective employees and directors) shall not exceed the total amount actually paid by User for the relevant License. User assumes full liability for the actions and omissions of its principals, employees, agents, affiliates, successors, and assigns.

12) **Limited Warranties.** THE WORK(S) AND RIGHT(S) ARE PROVIDED "AS IS." CCC HAS THE RIGHT TO GRANT TO USER THE RIGHTS GRANTED IN THE ORDER CONFIRMATION DOCUMENT. CCC AND THE RIGHTSHOLDER DISCLAIM ALL OTHER WARRANTIES RELATING TO THE WORK(S) AND RIGHT(S), EITHER EXPRESS OR IMPLIED, INCLUDING WITHOUT LIMITATION IMPLIED WARRANTIES OF MERCHANTABILITY OR FITNESS FOR A PARTICULAR PURPOSE. ADDITIONAL RIGHTS MAY BE REQUIRED TO USE ILLUSTRATIONS, GRAPHS, PHOTOGRAPHS, ABSTRACTS, INSERTS, OR OTHER PORTIONS OF THE WORK (AS OPPOSED TO THE ENTIRE WORK) IN A MANNER CONTEMPLATED BY USER; USER UNDERSTANDS AND AGREES THAT NEITHER CCC NOR THE RIGHTSHOLDER MAY HAVE SUCH ADDITIONAL RIGHTS TO GRANT.

13) **Effect of Breach.** Any failure by User to pay any amount when due, or any use by User of a Work beyond the scope of the License set forth in the Order Confirmation and/or the Terms, shall be a material breach of such License. Any breach not cured within 10 days of written notice thereof shall result in immediate termination of such License without further notice. Any unauthorized (but licensable) use of a Work that is terminated immediately upon notice thereof may be liquidated by payment of the Rightsholder's ordinary license price therefor; any unauthorized (and unlicensable) use that is not terminated immediately for any reason (including, for example, because materials containing the Work cannot reasonably be recalled) will be subject to all remedies available at law or in equity, but in no event to a payment of less than three times the Rightsholder's ordinary license price for the most closely analogous licensable use plus Rightsholder's and/or CCC's costs and expenses incurred in collecting such payment.

14) **Additional Terms for Specific Products and Services.** If a User is making one of the uses described in this Section 14, the additional terms and conditions apply:

a) ***Print Uses of Academic Course Content and Materials (photocopies for academic coursepacks or classroom handouts).*** For photocopies for academic coursepacks or classroom handouts the following additional terms apply:

i) The copies and anthologies created under this License may be made and assembled by faculty members individually or at their request by on-campus bookstores or copy centers, or by off-campus copy shops and other similar entities.

ii) No License granted shall in any way: (i) include any right by User to create a substantively non-identical copy of the Work or to edit or in any other way modify the Work (except by means of deleting material immediately preceding or following the entire portion of the Work copied) (ii) permit "publishing ventures" where any particular anthology would be systematically marketed at multiple institutions.

iii) Subject to any Publisher Terms (and notwithstanding any apparent contradiction in the Order Confirmation arising from data provided by User), any use authorized under the academic pay-per-use service is limited as follows:

A) any License granted shall apply to only one class (bearing a unique identifier as assigned by the institution, and thereby including all sections or other subparts of the class) at one institution;

B) use is limited to not more than 25% of the text of a book or of the items in a published collection of essays, poems or articles;

C) use is limited to no more than the greater of (a) 25% of the text of an issue of a journal or other periodical or (b) two articles from such an issue;

D) no User may sell or distribute any particular anthology, whether photocopied or electronic, at more than one institution of learning;

E) in the case of a photocopy permission, no materials may be entered into electronic memory by User except in order to produce an identical copy of a Work before or during the academic term (or analogous period) as to which any particular permission is granted. In the event that User shall choose to retain materials that are the subject of a photocopy permission in electronic memory for purposes of producing identical copies more than one day after such retention (but still within the scope of any permission granted), User must notify CCC of such fact in the applicable permission request and such retention shall constitute one copy actually sold for purposes of calculating permission fees due; and

F) any permission granted shall expire at the end of the class. No permission granted shall in any way include any right by User to create a substantively non-identical copy of the Work or to edit or in any other way modify the Work (except by means of deleting material immediately preceding or following the entire portion of the Work copied).

iv) Books and Records; Right to Audit. As to each permission granted under the academic pay-per-use Service, User shall maintain for at least four full calendar years books and records sufficient for CCC to determine the numbers of copies made by User under such permission. CCC and any representatives it may designate shall have the right to audit such books and records at any time during User's ordinary business hours, upon two days' prior notice. If any such audit shall determine that User shall have underpaid for, or underreported, any photocopies sold or by three percent (3%) or more, then User shall bear all the costs of any such audit; otherwise, CCC shall bear the costs of any such audit. Any amount determined by such audit to have been underpaid by User shall immediately be paid to CCC by User, together with interest thereon at the rate of 10% per annum from the date such amount was originally due. The provisions of this paragraph shall survive the termination of this License for any reason.

b) ***Digital Pay-Per-Uses of Academic Course Content and Materials (e-coursepacks, electronic reserves, learning management systems, academic institution intranets).*** For uses in e-coursepacks, posts in electronic reserves, posts in learning management systems, or posts on academic institution intranets, the following additional terms apply:

i) The pay-per-uses subject to this Section 14(b) include:

A) **Posting e-reserves, course management systems, e-coursepacks for text-based content,** which grants authorizations to import requested material in electronic format, and allows electronic access to this material to members of a designated college or university class, under the direction of an instructor designated by the college or university, accessible only under appropriate electronic controls (e.g., password);

B) **Posting e-reserves, course management systems, e-coursepacks for material consisting of photographs or other still images not embedded in text,** which grants not only the authorizations described in Section 14(b)(i)(A) above, but also the following authorization: to include the requested material in course materials for use consistent with Section 14(b)(i)(A) above, including any necessary resizing, reformatting or modification of the resolution of such requested material (provided that such modification does not alter the underlying editorial content or meaning of the requested material, and provided that the resulting modified content is used solely within the scope of, and in a manner consistent with, the particular authorization described in the Order Confirmation and the Terms), but not including any other form of manipulation, alteration or editing of the requested material;

C) **Posting e-reserves, course management systems, e-coursepacks or other academic distribution for audiovisual content,** which grants not only the authorizations described in Section 14(b)(i)(A) above, but also

the following authorizations: (i) to include the requested material in course materials for use consistent with Section 14(b)(i)(A) above; (ii) to display and perform the requested material to such members of such class in the physical classroom or remotely by means of streaming media or other video formats; and (iii) to "clip" or reformat the requested material for purposes of time or content management or ease of delivery, provided that such "clipping" or reformatting does not alter the underlying editorial content or meaning of the requested material and that the resulting material is used solely within the scope of, and in a manner consistent with, the particular authorization described in the Order Confirmation and the Terms. Unless expressly set forth in the relevant Order Conformation, the License does not authorize any other form of manipulation, alteration or editing of the requested material.

ii) Unless expressly set forth in the relevant Order Confirmation, no License granted shall in any way: (i) include any right by User to create a substantively non-identical copy of the Work or to edit or in any other way modify the Work (except by means of deleting material immediately preceding or following the entire portion of the Work copied or, in the case of Works subject to Sections 14(b)(1)(B) or (C) above, as described in such Sections) (ii) permit "publishing ventures" where any particular course materials would be systematically marketed at multiple institutions.

iii) Subject to any further limitations determined in the Rightsholder Terms (and notwithstanding any apparent contradiction in the Order Confirmation arising from data provided by User), any use authorized under the electronic course content pay-per-use service is limited as follows:

A) any License granted shall apply to only one class (bearing a unique identifier as assigned by the institution, and thereby including all sections or other subparts of the class) at one institution;

B) use is limited to not more than 25% of the text of a book or of the items in a published collection of essays, poems or articles;

C) use is limited to not more than the greater of (a) 25% of the text of an issue of a journal or other periodical or (b) two articles from such an issue;

D) no User may sell or distribute any particular materials, whether photocopied or electronic, at more than one institution of learning;

E) electronic access to material which is the subject of an electronic-use permission must be limited by means of electronic password, student identification or other control permitting access solely to students and instructors in the class;

F) User must ensure (through use of an electronic cover page or other appropriate means) that any person, upon gaining electronic access to the material, which is the subject of a permission, shall see:

- a proper copyright notice, identifying the Rightsholder in whose name CCC has granted permission,
- a statement to the effect that such copy was made pursuant to permission,
- a statement identifying the class to which the material applies and notifying the reader that the material has been made available electronically solely for use in the class, and
- a statement to the effect that the material may not be further distributed to any person outside the class, whether by copying or by transmission and whether electronically or in paper form, and User must also ensure that such cover page or other means will print out in the event that the person accessing the material chooses to print out the material or any part thereof.

G) any permission granted shall expire at the end of the class and, absent some other form of authorization, User is thereupon required to delete the applicable material from any electronic storage or to block electronic access to the applicable material.

iv) Uses of separate portions of a Work, even if they are to be included in the same course material or the same university or college class, require separate permissions under the electronic course content pay-per-use Service. Unless otherwise provided in the Order Confirmation, any grant of rights to User is limited to use completed no later than the end of the academic term (or analogous period) as to which any particular permission is granted.

v) Books and Records; Right to Audit. As to each permission granted under the electronic course content Service, User shall maintain for at least four full calendar years books and records sufficient for CCC to determine the numbers of copies made by User under such permission. CCC and any representatives it may designate shall have the right to audit such books and records at any time during User's ordinary business hours, upon two days' prior notice. If any such audit shall determine that User shall have underpaid for, or underreported, any electronic copies used by three percent (3%) or more, then User shall bear all the costs of any such audit; otherwise, CCC

shall bear the costs of any such audit. Any amount determined by such audit to have been underpaid by User shall immediately be paid to CCC by User, together with interest thereon at the rate of 10% per annum from the date such amount was originally due. The provisions of this paragraph shall survive the termination of this license for any reason.

c) ***Pay-Per-Use Permissions for Certain Reproductions (Academic photocopies for library reserves and interlibrary loan reporting) (Non-academic internal/external business uses and commercial document delivery).*** The License expressly excludes the uses listed in Section (c)(i)-(v) below (which must be subject to separate license from the applicable Rightsholder) for: academic photocopies for library reserves and interlibrary loan reporting; and non-academic internal/external business uses and commercial document delivery.

i) electronic storage of any reproduction (whether in plain-text, PDF, or any other format) other than on a transitory basis;

ii) the input of Works or reproductions thereof into any computerized database;

iii) reproduction of an entire Work (cover-to-cover copying) except where the Work is a single article;

iv) reproduction for resale to anyone other than a specific customer of User;

v) republication in any different form. Please obtain authorizations for these uses through other CCC services or directly from the rightsholder.

Any license granted is further limited as set forth in any restrictions included in the Order Confirmation and/or in these Terms.

d) ***Electronic Reproductions in Online Environments (Non-Academic-email, intranet, internet and extranet).*** For "electronic reproductions", which generally includes e-mail use (including instant messaging or other electronic transmission to a defined group of recipients) or posting on an intranet, extranet or Intranet site (including any display or performance incidental thereto), the following additional terms apply:

i) Unless otherwise set forth in the Order Confirmation, the License is limited to use completed within 30 days for any use on the Internet, 60 days for any use on an intranet or extranet and one year for any other use, all as measured from the "republication date" as identified in the Order Confirmation, if any, and otherwise from the date of the Order Confirmation.

ii) User may not make or permit any alterations to the Work, unless expressly set forth in the Order Confirmation (after request by User and approval by Rightsholder); provided, however, that a Work consisting of photographs or other still images not embedded in text may, if necessary, be resized, reformatted or have its resolution modified without additional express permission, and a Work consisting of audiovisual content may, if necessary, be "clipped" or reformatted for purposes of time or content management or ease of delivery (provided that any such resizing, reformatting, resolution modification or "clipping" does not alter the underlying editorial content or meaning of the Work used, and that the resulting material is used solely within the scope of, and in a manner consistent with, the particular License described in the Order Confirmation and the Terms.

15) **Miscellaneous.**

a) User acknowledges that CCC may, from time to time, make changes or additions to the Service or to the Terms, and that Rightsholder may make changes or additions to the Rightsholder Terms. Such updated Terms will replace the prior terms and conditions in the order workflow and shall be effective as to any subsequent Licenses but shall not apply to Licenses already granted and paid for under a prior set of terms.

b) Use of User-related information collected through the Service is governed by CCC's privacy policy, available online at www.copyright.com/about/privacy-policy/.

c) The License is personal to User. Therefore, User may not assign or transfer to any other person (whether a natural person or an organization of any kind) the License or any rights granted thereunder; provided, however, that, where applicable, User may assign such License in its entirety on written notice to CCC in the event of a transfer of all or substantially all of User's rights in any new material which includes the Work(s) licensed under this Service.

d) No amendment or waiver of any Terms is binding unless set forth in writing and signed by the appropriate parties, including, where applicable, the Rightsholder. The Rightsholder and CCC hereby object to any terms contained in any writing prepared by or on behalf of the User or its principals, employees, agents or affiliates and purporting to govern or otherwise relate to the License described in the Order Confirmation, which terms are in any way inconsistent with any Terms set forth in the Order Confirmation, and/or in CCC's standard operating procedures, whether such writing is prepared prior to, simultaneously with or subsequent to the Order Confirmation, and whether such writing appears on a copy of the Order Confirmation or in a separate instrument.

e) The License described in the Order Confirmation shall be governed by and construed under the law of the State of New York, USA, without regard to the principles thereof of conflicts of law. Any case, controversy, suit, action, or proceeding arising out of, in connection with, or related to such License shall be brought, at CCC's sole discretion, in any federal or state court located in the County of New York, State of New York, USA, or in any federal or state court whose geographical jurisdiction covers the location of the Rightsholder set forth in the Order Confirmation. The parties expressly submit to the personal jurisdiction and venue of each such federal or state court.

*Last updated October 2022*

# Marketplace

This is a License Agreement between Hongmin Zhu (“User”) and Copyright Clearance Center, Inc. (“CCC”) on behalf of the Rightsholder identified in the order details below. The license consists of the order details, the Marketplace Permissions General Terms and Conditions below, and any Rightsholder Terms and Conditions which are included below.

All payments must be made in full to CCC in accordance with the Marketplace Permissions General Terms and Conditions below.

| | | | |
|---|---|---|---|
| **Order Date** | 12-Apr-2024 | **Type of Use** | Republish in a thesis/dissertation |
| **Order License ID** | 1472518-1 | | |
| **ISSN** | 0964-1726 | **Publisher** | IOP Publishing |
| | | **Portion** | Image/photo/illustration |

## LICENSED CONTENT

| | | | |
|---|---|---|---|
| **Publication Title** | Smart Materials and Structures | **Country** | United Kingdom of Great Britain and Northern Ireland |
| **Author/Editor** | Institute of Physics (Great Britain), Society of Photo-optical Instrumentation Engineers. | **Rightsholder** | IOP Publishing, Ltd |
| | | **Publication Type** | Journal |
| **Date** | 01/01/1992 | | |
| **Language** | English | | |

## REQUEST DETAILS

| | | | |
|---|---|---|---|
| **Portion Type** | Image/photo/illustration | **Distribution** | U.K. and Commonwealth (excluding Canada) |
| **Number of Images / Photos / Illustrations** | 1 | **Translation** | Original language of publication |
| **Format (select all that apply)** | Print, Electronic | **Copies for the Disabled?** | No |
| **Who Will Republish the Content?** | Academic institution | **Minor Editing Privileges?** | No |
| **Duration of Use** | Life of current edition | **Incidental Promotional Use?** | No |
| **Lifetime Unit Quantity** | Up to 4,999 | **Currency** | GBP |
| **Rights Requested** | Main product | | |

## NEW WORK DETAILS

| | | | |
|---|---|---|---|
| **Title** | Data-driven Modelling for Guided Wave Structural Health Monitoring and Prognostic Health Management on Aeronautical Structures | **Institution Name** | Imperial College London |
| | | **Expected Presentation Date** | 2024-07-01 |
| **Instructor Name** | Ferri Aliabadi | | |

## ADDITIONAL DETAILS

| | | | |
|---|---|---|---|
| **Order Reference Number** | N/A | **The Requesting Person / Organization to Appear on the License** | Hongmin Zhu |

## REQUESTED CONTENT DETAILS

| | | | |
|---|---|---|---|
| **Title, Description or Numeric Reference of the Portion(s)** | Figure 11. Baseline-free damage imaging result of (a) the circular sensor array and (b) the helical sensor array under a 5-cycle, 50 kHz tone burst excitation. | **Title of the Article / Chapter the Portion Is From** | Baseline-free damage detection in composite plates based on the reciprocity principle |
| | | **Author of Portion(s)** | Institute of Physics (Great Britain); Society of Photo-optical Instrumentation Engineers. |
| **Editor of Portion(s)** | N/A | | |
| **Volume / Edition** | 27 | **Issue, if Republishing an Article From a Serial** | N/A |
| **Page or Page Range of Portion** | 8 | **Publication Date of Portion** | 2017-12-18 |

## RIGHTSHOLDER TERMS AND CONDITIONS

These special terms and conditions are in addition to the standard terms and conditions for CCC's Republication Service and, together with those standard terms and conditions, govern the use of the Works. As the User you will make all reasonable efforts to contact the author(s) of the article which the Work is to be reused from, to seek consent for your intended use. Contacting one author who is acting expressly as authorised agent for their co-author(s) is acceptable. User will reproduce the following wording prominently alongside the Work: the source of the Work, including author, article title, title of journal, volume number, issue number (if relevant), page range (or first page if this is the only information available) and date of first publication; and a link back to the article (via DOI); and if practicable, and IN ALL CASES for new works published under any of the Creative Commons licences, the words "© IOP Publishing. Reproduced with permission. All rights reserved" Without the express permission of the author(s) and the Rightsholder of the article from which the Work is to be reused, User shall not use it in any way which, in the opinion of the Rightsholder, could: (i) distort or alter the author(s)' original intention(s) and meaning; (ii) be prejudicial to the honour or reputation of the author(s); and/or (iii) imply endorsement by the author(s) and/or the Rightsholder. This licence does not apply to any article which is credited to another source and which does not have the copyright line '© IOP Publishing Ltd'. User must check the copyright line of the article from which the Work is to be reused to check that IOP Publishing Ltd has all the necessary rights to be able to grant permission. User is solely responsible for identifying and obtaining separate licences and permissions from the copyright owner for reuse of any such third party material/figures which the Rightsholder is not the copyright owner of. The Rightsholder shall not reimburse any fees which User pays for a republication license for such third party content. This licence does not apply to any material/figure which is credited to another source in the Rightsholder's publication or has been obtained from a third party. User must check the Version of Record of the article from which the Work is to be reused, to check whether any of the material in the Work is third party material. Third party citations and/or copyright notices and/or permissions statements may not be included in any other version of the article from which the Work is to be reused and so cannot be relied upon by the User. User is solely responsible for identifying and obtaining separate licences and permissions from the copyright owner for reuse of any such third party material/figures where the Rightsholder is not the copyright owner. The Rightsholder shall not reimburse any fees which User pays for a republication license for such third party content. User and CCC acknowledge that the Rightsholder may, from time to time, make changes or additions to these special terms and conditions without express notification, provided that these shall not apply to permissions already secured and paid for by User prior to such change or addition. User acknowledges that the Rightsholder (which includes companies within its group and third parties for whom it publishes its titles) may make use of personal data collected through the service in the course of their business. If User is the author of the Work, User may automatically have the right to reuse it under the rights granted back when User transferred the copyright in the article to the Rightsholder. User should check the copyright form and the relevant author rights policy to check whether permission is required. If User is the author of the Work and does require permission for proposed reuse of the Work, User should select 'Author of requested content' as the Requestor Type. The Rightsholder shall not reimburse any fees which User pays for a republication license. If User is the author of the article which User wishes to reuse in User's thesis or dissertation, the republication licence covers the right to include the Version of Record of the article, provided it is not then shared or deposited online. User must include citation details. Where User wishes to share their thesis or dissertation online, they should remove the Version of Record before uploading it. User may include a Preprint or the Accepted Manuscript (after the embargo period) in the online version of the thesis or dissertation, provided they do so in accordance with the Rightsholder's policies on sharing Preprints or Accepted Manuscripts. User may need to obtain separate permission for any third party content included within the article. User must check this with the copyright owner of such third party content. Any online or commercial use of User's thesis or dissertation containing the article, including publication via ProQuest, would need to be expressly notified in writing to the Rightsholder at the time of request and would require separate written permission from the Rightsholder. As well as CCC, the Rightsholder shall have the right to bring any legal action that it deems necessary to enforce its rights should it consider that the Work infringes those rights in any way. For content reuse requests that qualify for permission under the STM Permissions Guidelines, which may be updated from time to time, the STM Permissions Guidelines supplement the terms and conditions contained in this license.

If you are producing a new book or article to be published by another STM Signatory publisher, please choose "Reuse in a book under STM Guidelines" or "Reuse in a journal under STM Guidelines." You can consult the STM Guidelines website to

see whether your new publisher is a signatory to the STM Permissions Guidelines.

## Marketplace Permissions General Terms and Conditions

The following terms and conditions ("General Terms"), together with any applicable Publisher Terms and Conditions, govern User's use of Works pursuant to the Licenses granted by Copyright Clearance Center, Inc. ("CCC") on behalf of the applicable Rightsholders of such Works through CCC's applicable Marketplace transactional licensing services (each, a "Service").

1) **Definitions.** For purposes of these General Terms, the following definitions apply:

"License" is the licensed use the User obtains via the Marketplace platform in a particular licensing transaction, as set forth in the Order Confirmation.

"Order Confirmation" is the confirmation CCC provides to the User at the conclusion of each Marketplace transaction. "Order Confirmation Terms" are additional terms set forth on specific Order Confirmations not set forth in the General Terms that can include terms applicable to a particular CCC transactional licensing service and/or any Rightsholder-specific terms.

"Rightsholder(s)" are the holders of copyright rights in the Works for which a User obtains licenses via the Marketplace platform, which are displayed on specific Order Confirmations.

"Terms" means the terms and conditions set forth in these General Terms and any additional Order Confirmation Terms collectively.

"User" or "you" is the person or entity making the use granted under the relevant License. Where the person accepting the Terms on behalf of a User is a freelancer or other third party who the User authorized to accept the General Terms on the User's behalf, such person shall be deemed jointly a User for purposes of such Terms.

"Work(s)" are the copyright protected works described in relevant Order Confirmations.

2) **Description of Service.** CCC's Marketplace enables Users to obtain Licenses to use one or more Works in accordance with all relevant Terms. CCC grants Licenses as an agent on behalf of the copyright rightsholder identified in the relevant Order Confirmation.

3) **Applicability of Terms.** The Terms govern User's use of Works in connection with the relevant License. In the event of any conflict between General Terms and Order Confirmation Terms, the latter shall govern. User acknowledges that Rightsholders have complete discretion whether to grant any permission, and whether to place any limitations on any grant, and that CCC has no right to supersede or to modify any such discretionary act by a Rightsholder.

4) **Representations; Acceptance.** By using the Service, User represents and warrants that User has been duly authorized by the User to accept, and hereby does accept, all Terms.

5) **Scope of License; Limitations and Obligations.** All Works and all rights therein, including copyright rights, remain the sole and exclusive property of the Rightsholder. The License provides only those rights expressly set forth in the terms and conveys no other rights in any Works

6) **General Payment Terms.** User may pay at time of checkout by credit card or choose to be invoiced. If the User chooses to be invoiced, the User shall: (i) remit payments in the manner identified on specific invoices, (ii) unless otherwise specifically stated in an Order Confirmation or separate written agreement, Users shall remit payments upon receipt of the relevant invoice from CCC, either by delivery or notification of availability of the invoice via the Marketplace platform, and (iii) if the User does not pay the invoice within 30 days of receipt, the User may incur a service charge of 1.5% per month or the maximum rate allowed by applicable law, whichever is less. While User may exercise the rights in the License immediately upon receiving the Order Confirmation, the License is automatically revoked and is null and void, as if it had never been issued, if CCC does not receive complete payment on a timely basis.

7) **General Limits on Use.** Unless otherwise provided in the Order Confirmation, any grant of rights to User (i) involves only the rights set forth in the Terms and does not include subsequent or additional uses, (ii) is non-exclusive and non-transferable, and (iii) is subject to any and all limitations and restrictions (such as, but not limited to, limitations on duration of use or circulation) included in the Terms. Upon completion of the licensed use as set forth in the Order Confirmation, User shall either secure a new permission for further use of the Work(s) or immediately cease any new use of the Work(s) and shall render inaccessible (such as by deleting or by removing or severing links or other locators) any further copies of the Work. User may only make alterations to the Work if and as expressly set forth in the Order Confirmation. No Work may be used in any way that is unlawful, including without limitation if such use would violate applicable sanctions laws or regulations, would be defamatory, violate the rights of third parties (including such third parties' rights of copyright, privacy, publicity, or other tangible or intangible property), or is otherwise illegal, sexually explicit, or obscene. In addition, User may not conjoin a Work with any other material that may result in damage to the

reputation of the Rightsholder. Any unlawful use will render any licenses hereunder null and void. User agrees to inform CCC if it becomes aware of any infringement of any rights in a Work and to cooperate with any reasonable request of CCC or the Rightsholder in connection therewith.

8) **Third Party Materials.** In the event that the material for which a License is sought includes third party materials (such as photographs, illustrations, graphs, inserts and similar materials) that are identified in such material as having been used by permission (or a similar indicator), User is responsible for identifying, and seeking separate licenses (under this Service, if available, or otherwise) for any of such third party materials; without a separate license, User may not use such third party materials via the License.

9) **Copyright Notice.** Use of proper copyright notice for a Work is required as a condition of any License granted under the Service. Unless otherwise provided in the Order Confirmation, a proper copyright notice will read substantially as follows: "Used with permission of [Rightsholder's name], from [Work's title, author, volume, edition number and year of copyright]; permission conveyed through Copyright Clearance Center, Inc." Such notice must be provided in a reasonably legible font size and must be placed either on a cover page or in another location that any person, upon gaining access to the material which is the subject of a permission, shall see, or in the case of republication Licenses, immediately adjacent to the Work as used (for example, as part of a by-line or footnote) or in the place where substantially all other credits or notices for the new work containing the republished Work are located. Failure to include the required notice results in loss to the Rightsholder and CCC, and the User shall be liable to pay liquidated damages for each such failure equal to twice the use fee specified in the Order Confirmation, in addition to the use fee itself and any other fees and charges specified.

10) **Indemnity.** User hereby indemnifies and agrees to defend the Rightsholder and CCC, and their respective employees and directors, against all claims, liability, damages, costs, and expenses, including legal fees and expenses, arising out of any use of a Work beyond the scope of the rights granted herein and in the Order Confirmation, or any use of a Work which has been altered in any unauthorized way by User, including claims of defamation or infringement of rights of copyright, publicity, privacy, or other tangible or intangible property.

11) **Limitation of Liability.** UNDER NO CIRCUMSTANCES WILL CCC OR THE RIGHTSHOLDER BE LIABLE FOR ANY DIRECT, INDIRECT, CONSEQUENTIAL, OR INCIDENTAL DAMAGES (INCLUDING WITHOUT LIMITATION DAMAGES FOR LOSS OF BUSINESS PROFITS OR INFORMATION, OR FOR BUSINESS INTERRUPTION) ARISING OUT OF THE USE OR INABILITY TO USE A WORK, EVEN IF ONE OR BOTH OF THEM HAS BEEN ADVISED OF THE POSSIBILITY OF SUCH DAMAGES. In any event, the total liability of the Rightsholder and CCC (including their respective employees and directors) shall not exceed the total amount actually paid by User for the relevant License. User assumes full liability for the actions and omissions of its principals, employees, agents, affiliates, successors, and assigns.

12) **Limited Warranties.** THE WORK(S) AND RIGHT(S) ARE PROVIDED "AS IS." CCC HAS THE RIGHT TO GRANT TO USER THE RIGHTS GRANTED IN THE ORDER CONFIRMATION DOCUMENT. CCC AND THE RIGHTSHOLDER DISCLAIM ALL OTHER WARRANTIES RELATING TO THE WORK(S) AND RIGHT(S), EITHER EXPRESS OR IMPLIED, INCLUDING WITHOUT LIMITATION IMPLIED WARRANTIES OF MERCHANTABILITY OR FITNESS FOR A PARTICULAR PURPOSE. ADDITIONAL RIGHTS MAY BE REQUIRED TO USE ILLUSTRATIONS, GRAPHS, PHOTOGRAPHS, ABSTRACTS, INSERTS, OR OTHER PORTIONS OF THE WORK (AS OPPOSED TO THE ENTIRE WORK) IN A MANNER CONTEMPLATED BY USER; USER UNDERSTANDS AND AGREES THAT NEITHER CCC NOR THE RIGHTSHOLDER MAY HAVE SUCH ADDITIONAL RIGHTS TO GRANT.

13) **Effect of Breach.** Any failure by User to pay any amount when due, or any use by User of a Work beyond the scope of the License set forth in the Order Confirmation and/or the Terms, shall be a material breach of such License. Any breach not cured within 10 days of written notice thereof shall result in immediate termination of such License without further notice. Any unauthorized (but licensable) use of a Work that is terminated immediately upon notice thereof may be liquidated by payment of the Rightsholder's ordinary license price therefor; any unauthorized (and unlicensable) use that is not terminated immediately for any reason (including, for example, because materials containing the Work cannot reasonably be recalled) will be subject to all remedies available at law or in equity, but in no event to a payment of less than three times the Rightsholder's ordinary license price for the most closely analogous licensable use plus Rightsholder's and/or CCC's costs and expenses incurred in collecting such payment.

14) **Additional Terms for Specific Products and Services.** If a User is making one of the uses described in this Section 14, the additional terms and conditions apply:

a) ***Print Uses of Academic Course Content and Materials (photocopies for academic coursepacks or classroom handouts).*** For photocopies for academic coursepacks or classroom handouts the following additional terms apply:

i) The copies and anthologies created under this License may be made and assembled by faculty members individually or at their request by on-campus bookstores or copy centers, or by off-campus copy shops and other similar entities.

ii) No License granted shall in any way: (i) include any right by User to create a substantively non-identical copy of the Work or to edit or in any other way modify the Work (except by means of deleting material immediately

preceding or following the entire portion of the Work copied) (ii) permit "publishing ventures" where any particular anthology would be systematically marketed at multiple institutions.

iii) Subject to any Publisher Terms (and notwithstanding any apparent contradiction in the Order Confirmation arising from data provided by User), any use authorized under the academic pay-per-use service is limited as follows:

A) any License granted shall apply to only one class (bearing a unique identifier as assigned by the institution, and thereby including all sections or other subparts of the class) at one institution;

B) use is limited to not more than 25% of the text of a book or of the items in a published collection of essays, poems or articles;

C) use is limited to no more than the greater of (a) 25% of the text of an issue of a journal or other periodical or (b) two articles from such an issue;

D) no User may sell or distribute any particular anthology, whether photocopied or electronic, at more than one institution of learning;

E) in the case of a photocopy permission, no materials may be entered into electronic memory by User except in order to produce an identical copy of a Work before or during the academic term (or analogous period) as to which any particular permission is granted. In the event that User shall choose to retain materials that are the subject of a photocopy permission in electronic memory for purposes of producing identical copies more than one day after such retention (but still within the scope of any permission granted), User must notify CCC of such fact in the applicable permission request and such retention shall constitute one copy actually sold for purposes of calculating permission fees due; and

F) any permission granted shall expire at the end of the class. No permission granted shall in any way include any right by User to create a substantively non-identical copy of the Work or to edit or in any other way modify the Work (except by means of deleting material immediately preceding or following the entire portion of the Work copied).

iv) Books and Records; Right to Audit. As to each permission granted under the academic pay-per-use Service, User shall maintain for at least four full calendar years books and records sufficient for CCC to determine the numbers of copies made by User under such permission. CCC and any representatives it may designate shall have the right to audit such books and records at any time during User's ordinary business hours, upon two days' prior notice. If any such audit shall determine that User shall have underpaid for, or underreported, any photocopies sold or by three percent (3%) or more, then User shall bear all the costs of any such audit; otherwise, CCC shall bear the costs of any such audit. Any amount determined by such audit to have been underpaid by User shall immediately be paid to CCC by User, together with interest thereon at the rate of 10% per annum from the date such amount was originally due. The provisions of this paragraph shall survive the termination of this License for any reason.

b) ***Digital Pay-Per-Uses of Academic Course Content and Materials (e-coursepacks, electronic reserves, learning management systems, academic institution intranets).*** For uses in e-coursepacks, posts in electronic reserves, posts in learning management systems, or posts on academic institution intranets, the following additional terms apply:

i) The pay-per-uses subject to this Section 14(b) include:

A) **Posting e-reserves, course management systems, e-coursepacks for text-based content,** which grants authorizations to import requested material in electronic format, and allows electronic access to this material to members of a designated college or university class, under the direction of an instructor designated by the college or university, accessible only under appropriate electronic controls (e.g., password);

B) **Posting e-reserves, course management systems, e-coursepacks for material consisting of photographs or other still images not embedded in text,** which grants not only the authorizations described in Section 14(b)(i)(A) above, but also the following authorization: to include the requested material in course materials for use consistent with Section 14(b)(i)(A) above, including any necessary resizing, reformatting or modification of the resolution of such requested material (provided that such modification does not alter the underlying editorial content or meaning of the requested material, and provided that the resulting modified content is used solely within the scope of, and in a manner consistent with, the particular authorization described in the Order Confirmation and the Terms), but not including any other form of manipulation, alteration or editing of the requested material;

C) **Posting e-reserves, course management systems, e-coursepacks or other academic distribution for audiovisual content,** which grants not only the authorizations described in Section 14(b)(i)(A) above, but also the following authorizations: (i) to include the requested material in course materials for use consistent with Section 14(b)(i)(A) above; (ii) to display and perform the requested material to such members of such class in

the physical classroom or remotely by means of streaming media or other video formats; and (iii) to "clip" or reformat the requested material for purposes of time or content management or ease of delivery, provided that such "clipping" or reformatting does not alter the underlying editorial content or meaning of the requested material and that the resulting material is used solely within the scope of, and in a manner consistent with, the particular authorization described in the Order Confirmation and the Terms. Unless expressly set forth in the relevant Order Conformation, the License does not authorize any other form of manipulation, alteration or editing of the requested material.

ii) Unless expressly set forth in the relevant Order Confirmation, no License granted shall in any way: (i) include any right by User to create a substantively non-identical copy of the Work or to edit or in any other way modify the Work (except by means of deleting material immediately preceding or following the entire portion of the Work copied or, in the case of Works subject to Sections 14(b)(1)(B) or (C) above, as described in such Sections) (ii) permit "publishing ventures" where any particular course materials would be systematically marketed at multiple institutions.

iii) Subject to any further limitations determined in the Rightsholder Terms (and notwithstanding any apparent contradiction in the Order Confirmation arising from data provided by User), any use authorized under the electronic course content pay-per-use service is limited as follows:

A) any License granted shall apply to only one class (bearing a unique identifier as assigned by the institution, and thereby including all sections or other subparts of the class) at one institution;

B) use is limited to not more than 25% of the text of a book or of the items in a published collection of essays, poems or articles;

C) use is limited to not more than the greater of (a) 25% of the text of an issue of a journal or other periodical or (b) two articles from such an issue;

D) no User may sell or distribute any particular materials, whether photocopied or electronic, at more than one institution of learning;

E) electronic access to material which is the subject of an electronic-use permission must be limited by means of electronic password, student identification or other control permitting access solely to students and instructors in the class;

F) User must ensure (through use of an electronic cover page or other appropriate means) that any person, upon gaining electronic access to the material, which is the subject of a permission, shall see:

- a proper copyright notice, identifying the Rightsholder in whose name CCC has granted permission,
- a statement to the effect that such copy was made pursuant to permission,
- a statement identifying the class to which the material applies and notifying the reader that the material has been made available electronically solely for use in the class, and
- a statement to the effect that the material may not be further distributed to any person outside the class, whether by copying or by transmission and whether electronically or in paper form, and User must also ensure that such cover page or other means will print out in the event that the person accessing the material chooses to print out the material or any part thereof.

G) any permission granted shall expire at the end of the class and, absent some other form of authorization, User is thereupon required to delete the applicable material from any electronic storage or to block electronic access to the applicable material.

iv) Uses of separate portions of a Work, even if they are to be included in the same course material or the same university or college class, require separate permissions under the electronic course content pay-per-use Service. Unless otherwise provided in the Order Confirmation, any grant of rights to User is limited to use completed no later than the end of the academic term (or analogous period) as to which any particular permission is granted.

v) Books and Records; Right to Audit. As to each permission granted under the electronic course content Service, User shall maintain for at least four full calendar years books and records sufficient for CCC to determine the numbers of copies made by User under such permission. CCC and any representatives it may designate shall have the right to audit such books and records at any time during User's ordinary business hours, upon two days' prior notice. If any such audit shall determine that User shall have underpaid for, or underreported, any electronic copies used by three percent (3%) or more, then User shall bear all the costs of any such audit; otherwise, CCC shall bear the costs of any such audit. Any amount determined by such audit to have been underpaid by User shall immediately be paid to CCC by User, together with interest thereon at the rate of 10% per annum from the

date such amount was originally due. The provisions of this paragraph shall survive the termination of this license for any reason.

c) ***Pay-Per-Use Permissions for Certain Reproductions (Academic photocopies for library reserves and interlibrary loan reporting) (Non-academic internal/external business uses and commercial document delivery).*** The License expressly excludes the uses listed in Section (c)(i)-(v) below (which must be subject to separate license from the applicable Rightsholder) for: academic photocopies for library reserves and interlibrary loan reporting; and non-academic internal/external business uses and commercial document delivery.

i) electronic storage of any reproduction (whether in plain-text, PDF, or any other format) other than on a transitory basis;

ii) the input of Works or reproductions thereof into any computerized database;

iii) reproduction of an entire Work (cover-to-cover copying) except where the Work is a single article;

iv) reproduction for resale to anyone other than a specific customer of User;

v) republication in any different form. Please obtain authorizations for these uses through other CCC services or directly from the rightsholder.

Any license granted is further limited as set forth in any restrictions included in the Order Confirmation and/or in these Terms.

d) ***Electronic Reproductions in Online Environments (Non-Academic-email, intranet, internet and extranet).*** For "electronic reproductions", which generally includes e-mail use (including instant messaging or other electronic transmission to a defined group of recipients) or posting on an intranet, extranet or Intranet site (including any display or performance incidental thereto), the following additional terms apply:

i) Unless otherwise set forth in the Order Confirmation, the License is limited to use completed within 30 days for any use on the Internet, 60 days for any use on an intranet or extranet and one year for any other use, all as measured from the "republication date" as identified in the Order Confirmation, if any, and otherwise from the date of the Order Confirmation.

ii) User may not make or permit any alterations to the Work, unless expressly set forth in the Order Confirmation (after request by User and approval by Rightsholder); provided, however, that a Work consisting of photographs or other still images not embedded in text may, if necessary, be resized, reformatted or have its resolution modified without additional express permission, and a Work consisting of audiovisual content may, if necessary, be "clipped" or reformatted for purposes of time or content management or ease of delivery (provided that any such resizing, reformatting, resolution modification or "clipping" does not alter the underlying editorial content or meaning of the Work used, and that the resulting material is used solely within the scope of, and in a manner consistent with, the particular License described in the Order Confirmation and the Terms.

15) **Miscellaneous.**

a) User acknowledges that CCC may, from time to time, make changes or additions to the Service or to the Terms, and that Rightsholder may make changes or additions to the Rightsholder Terms. Such updated Terms will replace the prior terms and conditions in the order workflow and shall be effective as to any subsequent Licenses but shall not apply to Licenses already granted and paid for under a prior set of terms.

b) Use of User-related information collected through the Service is governed by CCC's privacy policy, available online at www.copyright.com/about/privacy-policy/.

c) The License is personal to User. Therefore, User may not assign or transfer to any other person (whether a natural person or an organization of any kind) the License or any rights granted thereunder; provided, however, that, where applicable, User may assign such License in its entirety on written notice to CCC in the event of a transfer of all or substantially all of User's rights in any new material which includes the Work(s) licensed under this Service.

d) No amendment or waiver of any Terms is binding unless set forth in writing and signed by the appropriate parties, including, where applicable, the Rightsholder. The Rightsholder and CCC hereby object to any terms contained in any writing prepared by or on behalf of the User or its principals, employees, agents or affiliates and purporting to govern or otherwise relate to the License described in the Order Confirmation, which terms are in any way inconsistent with any Terms set forth in the Order Confirmation, and/or in CCC's standard operating procedures, whether such writing is prepared prior to, simultaneously with or subsequent to the Order Confirmation, and whether such writing appears on a copy of the Order Confirmation or in a separate instrument.

e) The License described in the Order Confirmation shall be governed by and construed under the law of the State of New York, USA, without regard to the principles thereof of conflicts of law. Any case, controversy, suit, action, or

proceeding arising out of, in connection with, or related to such License shall be brought, at CCC's sole discretion, in any federal or state court located in the County of New York, State of New York, USA, or in any federal or state court whose geographical jurisdiction covers the location of the Rightsholder set forth in the Order Confirmation. The parties expressly submit to the personal jurisdiction and venue of each such federal or state court.

*Last updated October 2022*

# SAGE PUBLICATIONS LICENSE TERMS AND CONDITIONS

Apr 24, 2024

This Agreement between Mr. HONGMIN ZHU ("You") and SAGE Publications ("SAGE Publications") consists of your license details and the terms and conditions provided by SAGE Publications and Copyright Clearance Center.

**All payments must be made in full to CCC. For payment instructions, please see information listed at the bottom of this form.**

| | |
|---|---|
| License Number | 5775520440427 |
| License date | Apr 24, 2024 |
| Licensed Content Publisher | SAGE Publications |
| Licensed Content Publication | Structural Health Monitoring: An International Journal |
| Licensed Content Title | Time reversibility of Lamb waves in thin plates with surface-bonded piezoelectric transducers is temperature invariant at the best reconstruction frequency |
| Licensed Content Author | Bhabagrahi Natha Sharma, Santosh Kapuria, A Arockiarajan |
| Licensed Content Date | Sep 1, 2021 |
| Licensed Content Volume | 20 |
| Licensed Content Issue | 5 |
| Licensed Content Pages | 15 |
| Type of Use | Book |
| Requestor type | Non-commercial |
| Format | Electronic |
| Portion | Figure/table |
| Number of figures/tables | 1 |
| Will you be translating? | No, only English |
| Circulation | 1 |
| Title of new book | Data-driven Modelling for Guided Wave Structural Health Monitoring and Prognostic Health Management on Aeronautical Structures |
| Lead author | Hongmin Zhu |
| Publisher | Imperial College London |
| Expected publication date | Jul 2024 |
| Order reference number | 1234 |
| Portions | Figure 12. Effect of temperature on time reversibility of Lamb waves in a 3-mm aluminium plate, obtained from (a) experiment and (b) 2D FE simulation. |
| Requestor Location | Mr. HONGMIN ZHU<br>Exhibition Road<br><br>London, other<br>United Kingdom<br>Attn: Mr. HONGMIN ZHU |
| Publisher Tax ID | GB232600116 |
| Billing Type | Credit Card |
| Credit card info | Visa ending in 0176 |
| Credit card expiration | 04/2027 |
| Total | **33.71 GBP** |
| Terms and Conditions | |

**SAGE Terms and Conditions for Permissions Administered Through RightsLink**

You, the Requestor, are requesting to use the material specified in the permission request (the "Work"). Your agreement to the terms and conditions herein and completion of a permission request constitutes a Permission Request. You are in no way required to use the Work; however, should you decide not to use the Work after you complete this request, you agree to cancel your order through this website. Under the above conditions, and the following terms and conditions, permission to use Work ("Permission") is granted solely to you:

1. SAGE reserves the right to revoke any Permission, at SAGE's sole discretion, within two (2) business days of the request.
2. The number of copies ("Copies") for print use is defined as the total number of copies made for distribution or for repurposing, and the number of copies ("Copies") for electronic use is defined as the total number of viewers of the Work, recipients of copies of the Work, and individuals or entities who may have access to the Work. The Copies must not exceed the Copies as stated in the Permission Request.
3. Requests to post a full article on a website, internet, intranet, or any publicly accessible site must be submitted to the Publisher through the SAGE Permissions Portal (https://sage-cloud.atlassian.net/servicedesk/customer/portal/10).
4. Permission is granted only for the type of use specified in the Permission Request. If any information pertaining to your Permission Request changes, you must cancel this request and resubmit a new request with the correct and current permission request information. SAGE may exercise its right to revoke Permission, if SAGE finds, in SAGE's sole opinion, that the context in which you have used or repurposed the Work is considered libelous, in violation of any right of privacy, or otherwise unlawful; infringement or in violation of any copyright or other proprietary right of others; or can be construed to possibly cause harm or injury. You agree that use of Work will be professional, in the context of fact-based and generally acceptable professional practices.
5. Permission does not include the use within Custom Publishing Programs, and all use within such programs is explicitly prohibited.
6. Permission does not include use of the material within Massive Open Online Courses (MOOC's). For permission to include material in a MOOC, please contact SAGE directly through the SAGE Permissions Portal (https://sage-cloud.atlassian.net/servicedesk/customer/portal/10).
7. If your Permission Request includes the right to translate the Work, you agree that the translation of the material shall be made faithfully and accurately, and that abbreviations and/or alterations in the text and/or title of the Work shall be made only with SAGE's prior the written consent. Requestor shall not own or acquire any copyright or other proprietary rights in the Work or any other material furnished by SAGE, including without limitation translations or transcriptions thereof, all of which rights shall be owned by and/or are hereby assigned to SAGE. Requestor shall indemnify SAGE against any and all claims, including without limitation attorneys' fees and legal costs, that concern or relate to (a) inaccurate translation or transcription of the Work, (b) infringement claims arising out of the inclusion of material not furnished by SAGE or (c) infringement or other claims asserted by anyone retained by Requestor to translate the Work. Requestor agrees that the name of the Author (s), Copyright Holder, and Publisher shall appear in due prominence on the title page of every copy of the translation and in all advertisements for the translation, and that the translation shall include: (1) the Work's original copyright notice and original American title, both in English, and (2) notice in granted translated language in identifying the SAGE Publications as the original publisher and stating the translation is published by arrangement with SAGE. The rights licensed to Requestor are not transferrable. The translated article reprint must include the following disclaimer in English and in the language of the reprint: "While every effort has been made to ensure that the contents of this publication are factually correct, neither the authors nor the publisher accepts, and they hereby expressly exclude to the fullest extent permissible under applicable law, any and all liability arising from the contents published in this Article, including, without limitation, from any errors, omissions, inaccuracies in original or following translation, or for any consequences arising therefrom. Nothing in this notice shall exclude liability which may not be excluded by law. Approved product information should be reviewed before prescribing any subject medications."
8. Permission is granted for prospective use only, and does not apply to any use that has occurred prior to the date of the Permission Request.
9. Permission does not apply to any material (reprints, illustrations, figures, tables, etc.) not controlled by SAGE. Requests for permission to re-use third-party material should be submitted to the original copyright holder, as indicated in the credit line for the materials.
10. Full acknowledgment of your source must appear in every copy of your work as follows:

    - Author(s), Journal Title (Journal Volume Number and Issue Number)
    - pp. xx-xx, copyright © YEAR by (Copyright Holder)
    - Reprinted by Permission of SAGE Publications

11. Unless specified in the request or by prior arrangement with SAGE, payment is due from you within sixty (60) days after the completion of Permission.
12. It is assumed that the Requester is using the selection in question, and is subject to billing and collections procedures, unless otherwise noted.
13. Permission Requests for reuse of text excerpts shall not exceed 50% of the article's content.
14. No more than 20% of any one SAGE journal issue may be reused at one time.

**Other Terms and Conditions:**

v4.05

**Questions? E-mail us at customercare@copyright.com.**

# ELSEVIER LICENSE TERMS AND CONDITIONS

Apr 15, 2024

This Agreement between Mr. HONGMIN ZHU ("You") and Elsevier ("Elsevier") consists of your license details and the terms and conditions provided by Elsevier and Copyright Clearance Center.

| | |
|---|---|
| License Number | 5766141180447 |
| License date | Apr 11, 2024 |
| Licensed Content Publisher | Elsevier |
| Licensed Content Publication | Ultrasonics |
| Licensed Content Title | An efficient Lamb wave-based virtual refined time-reversal method for damage localization in plates using broadband measurements |
| Licensed Content Author | M. Kannusamy,Santosh Kapuria,Saptarshi Sasmal |
| Licensed Content Date | Aug 1, 2022 |
| Licensed Content Volume | 124 |
| Licensed Content Issue | n/a |
| Licensed Content Pages | 1 |
| Start Page | 106767 |
| End Page | |
| Type of Use | reuse in a thesis/dissertation |
| Portion | figures/tables/illustrations |
| Number of figures/tables/illustrations | 1 |
| Format | both print and electronic |
| Are you the author of this Elsevier article? | No |
| Will you be translating? | No |
| Title of new work | Data-driven Modelling for Guided Wave Structural Health Monitoring and Prognostic Health Management on Aeronautical Structures |
| Institution name | Imperial College London |
| Expected presentation date | Jul 2024 |
| Order reference number | abcd |
| Portions | Fig. 18. Damage probability contours for the dual-damage scenario, predicted by (a) VRTRM and (b) RTRM at the best reconstruction frequency (160 kHz). |
| Requestor Location | Mr. HONGMIN ZHU<br>Exhibition Road<br><br>London, other<br>United Kingdom<br>Attn: Mr. HONGMIN ZHU |
| Publisher Tax ID | GB 494 6272 12 |
| Billing Type | Invoice |
| Billing Address | Mr. HONGMIN ZHU<br>Exhibition Road<br><br>London, United Kingdom<br>Attn: Mr. HONGMIN ZHU |
| Total | **0.00 GBP** |

Terms and Conditions

## INTRODUCTION

1. The publisher for this copyrighted material is Elsevier. By clicking "accept" in connection with completing this licensing transaction, you agree that the following terms and conditions apply to this transaction (along with the Billing and Payment terms and conditions established by Copyright Clearance Center, Inc. ("CCC"), at the time that you opened your RightsLink account and that are available at any time at https://myaccount.copyright.com).

## GENERAL TERMS

2. Elsevier hereby grants you permission to reproduce the aforementioned material subject to the terms and conditions indicated.
3. Acknowledgement: If any part of the material to be used (for example, figures) has appeared in our publication with credit or acknowledgement to another source, permission must also be sought from that source. If such permission is not obtained then that material may not be included in your publication/copies. Suitable acknowledgement to the source must be made, either as a footnote or in a reference list at the end of your publication, as follows:
"Reprinted from Publication title, Vol /edition number, Author(s), Title of article / title of chapter, Pages No., Copyright (Year), with permission from Elsevier [OR APPLICABLE SOCIETY COPYRIGHT OWNER]." Also Lancet special credit - "Reprinted from The Lancet, Vol. number, Author(s), Title of article, Pages No., Copyright (Year), with permission from Elsevier."
4. Reproduction of this material is confined to the purpose and/or media for which permission is hereby given. The material may not be reproduced or used in any other way, including use in combination with an artificial intelligence tool (including to train an algorithm, test, process, analyse, generate output and/or develop any form of artificial intelligence tool), or to create any derivative work and/or service (including resulting from the use of artificial intelligence tools).
5. Altering/Modifying Material: Not Permitted. However figures and illustrations may be altered/adapted minimally to serve your work. Any other abbreviations, additions, deletions and/or any other alterations shall be made only with prior written authorization of Elsevier Ltd. (Please contact Elsevier's permissions helpdesk here). No modifications can be made to any Lancet figures/tables and they must be reproduced in full.
6. If the permission fee for the requested use of our material is waived in this instance, please be advised that your future requests for Elsevier materials may attract a fee.
7. Reservation of Rights: Publisher reserves all rights not specifically granted in the combination of (i) the license details provided by you and accepted in the course of this licensing transaction, (ii) these terms and conditions and (iii) CCC's Billing and Payment terms and conditions.
8. License Contingent Upon Payment: While you may exercise the rights licensed immediately upon issuance of the license at the end of the licensing process for the transaction, provided that you have disclosed complete and accurate details of your proposed use, no license is finally effective unless and until full payment is received from you (either by publisher or by CCC) as provided in CCC's Billing and Payment terms and conditions. If full payment is not received on a timely basis, then any license preliminarily granted shall be deemed automatically revoked and shall be void as if never granted. Further, in the event that you breach any of these terms and conditions or any of CCC's Billing and Payment terms and conditions, the license is automatically revoked and shall be void as if never granted. Use of materials as described in a revoked license, as well as any use of the materials beyond the scope of an unrevoked license, may constitute copyright infringement and publisher reserves the right to take any and all action to protect its copyright in the materials.
9. Warranties: Publisher makes no representations or warranties with respect to the licensed material.
10. Indemnity: You hereby indemnify and agree to hold harmless publisher and CCC, and their respective officers, directors, employees and agents, from and against any and all claims arising out of your use of the licensed material other than as specifically authorized pursuant to this license.
11. No Transfer of License: This license is personal to you and may not be sublicensed, assigned, or transferred by you to any other person without publisher's written permission.
12. No Amendment Except in Writing: This license may not be amended except in a writing signed by both parties (or, in the case of publisher, by CCC on publisher's behalf).
13. Objection to Contrary Terms: Publisher hereby objects to any terms contained in any purchase order, acknowledgment, check endorsement or other writing prepared by you, which terms are inconsistent with these terms and conditions or CCC's Billing and Payment terms and conditions. These terms and conditions, together with CCC's Billing and Payment terms and conditions (which are incorporated herein), comprise the entire agreement between you and publisher (and CCC) concerning this licensing transaction. In the event of any conflict between your obligations established by these terms and conditions and those established by CCC's Billing and Payment terms and conditions, these terms and conditions shall control.
14. Revocation: Elsevier or Copyright Clearance Center may deny the permissions described in this License at their sole discretion, for any reason or no reason, with a full refund payable to you. Notice of such denial will be made using the contact information provided by you. Failure to receive such notice will not alter or invalidate the denial. In no event will Elsevier or Copyright Clearance Center be responsible or liable for any costs, expenses or damage incurred by you as a result of a denial of your permission request, other than a refund of the amount(s) paid by you to Elsevier and/or Copyright Clearance Center for denied permissions.

## LIMITED LICENSE

The following terms and conditions apply only to specific license types:
15. **Translation**: This permission is granted for non-exclusive world **English** rights only unless your license was granted for translation rights. If you licensed translation rights you may only translate this content into the languages you requested. A professional translator must perform all translations and reproduce the content word for word preserving the integrity of the article.

16. **Posting licensed content on any Website**: The following terms and conditions apply as follows: Licensing material from an Elsevier journal: All content posted to the web site must maintain the copyright information line on the bottom of each image; A hyper-text must be included to the Homepage of the journal from which you are licensing at http://www.sciencedirect.com/science/journal/xxxxx or the Elsevier homepage for books at http://www.elsevier.com; Central Storage: This license does not include permission for a scanned version of the material to be stored in a central repository such as that provided by Heron/XanEdu.
Licensing material from an Elsevier book: A hyper-text link must be included to the Elsevier homepage at http://www.elsevier.com . All content posted to the web site must maintain the copyright information line on the bottom of each image.

**Posting licensed content on Electronic reserve**: In addition to the above the following clauses are applicable: The web site must be password-protected and made available only to bona fide students registered on a relevant course. This permission is granted for 1 year only. You may obtain a new license for future website posting.
17. **For journal authors:** the following clauses are applicable in addition to the above:
**Preprints:**
A preprint is an author's own write-up of research results and analysis, it has not been peer-reviewed, nor has it had any other value added to it by a publisher (such as formatting, copyright, technical enhancement etc.).
Authors can share their preprints anywhere at any time. Preprints should not be added to or enhanced in any way in order to appear more like, or to substitute for, the final versions of articles however authors can update their preprints on arXiv or RePEc with their Accepted Author Manuscript (see below).
If accepted for publication, we encourage authors to link from the preprint to their formal publication via its DOI. Millions of researchers have access to the formal publications on ScienceDirect, and so links will help users to find, access, cite and use the best available version. Please note that Cell Press, The Lancet and some society-owned have different preprint policies. Information on these policies is available on the journal homepage.
**Accepted Author Manuscripts:** An accepted author manuscript is the manuscript of an article that has been accepted for publication and which typically includes author-incorporated changes suggested during submission, peer review and editor-author communications.
Authors can share their accepted author manuscript:

- immediately
    - via their non-commercial person homepage or blog
    - by updating a preprint in arXiv or RePEc with the accepted manuscript
    - via their research institute or institutional repository for internal institutional uses or as part of an invitation-only research collaboration work-group
    - directly by providing copies to their students or to research collaborators for their personal use
    - for private scholarly sharing as part of an invitation-only work group on commercial sites with which Elsevier has an agreement
- After the embargo period
    - via non-commercial hosting platforms such as their institutional repository
    - via commercial sites with which Elsevier has an agreement

In all cases accepted manuscripts should:

- link to the formal publication via its DOI
- bear a CC-BY-NC-ND license - this is easy to do
- if aggregated with other manuscripts, for example in a repository or other site, be shared in alignment with our hosting policy not be added to or enhanced in any way to appear more like, or to substitute for, the published journal article.

**Published journal article (JPA):** A published journal article (PJA) is the definitive final record of published research that appears or will appear in the journal and embodies all value-adding publishing activities including peer review co-ordination, copy-editing, formatting, (if relevant) pagination and online enrichment.
Policies for sharing publishing journal articles differ for subscription and gold open access articles:
**Subscription Articles:** If you are an author, please share a link to your article rather than the full-text. Millions of researchers have access to the formal publications on ScienceDirect, and so links will help your users to find, access, cite, and use the best available version.
Theses and dissertations which contain embedded PJAs as part of the formal submission can be posted publicly by the awarding institution with DOI links back to the formal publications on ScienceDirect.
If you are affiliated with a library that subscribes to ScienceDirect you have additional private sharing rights for others' research accessed under that agreement. This includes use for classroom teaching and internal training at the institution (including use in course packs and courseware programs), and inclusion of the article for grant funding purposes.
**Gold Open Access Articles:** May be shared according to the author-selected end-user license and should contain a CrossMark logo, the end user license, and a DOI link to the formal publication on ScienceDirect.
Please refer to Elsevier's posting policy for further information.
18. **For book authors** the following clauses are applicable in addition to the above: Authors are permitted to place a brief summary of their work online only. You are not allowed to download and post the published electronic version of your chapter,

nor may you scan the printed edition to create an electronic version. **Posting to a repository:** Authors are permitted to post a summary of their chapter only in their institution's repository.
19. **Thesis/Dissertation**: If your license is for use in a thesis/dissertation your thesis may be submitted to your institution in either print or electronic form. Should your thesis be published commercially, please reapply for permission. These requirements include permission for the Library and Archives of Canada to supply single copies, on demand, of the complete thesis and include permission for Proquest/UMI to supply single copies, on demand, of the complete thesis. Should your thesis be published commercially, please reapply for permission. Theses and dissertations which contain embedded PJAs as part of the formal submission can be posted publicly by the awarding institution with DOI links back to the formal publications on ScienceDirect.

**Elsevier Open Access Terms and Conditions**
You can publish open access with Elsevier in hundreds of open access journals or in nearly 2000 established subscription journals that support open access publishing. Permitted third party re-use of these open access articles is defined by the author's choice of Creative Commons user license. See our open access license policy for more information.
**Terms & Conditions applicable to all Open Access articles published with Elsevier:**
Any reuse of the article must not represent the author as endorsing the adaptation of the article nor should the article be modified in such a way as to damage the author's honour or reputation. If any changes have been made, such changes must be clearly indicated.
The author(s) must be appropriately credited and we ask that you include the end user license and a DOI link to the formal publication on ScienceDirect.
If any part of the material to be used (for example, figures) has appeared in our publication with credit or acknowledgement to another source it is the responsibility of the user to ensure their reuse complies with the terms and conditions determined by the rights holder.
**Additional Terms & Conditions applicable to each Creative Commons user license:**
**CC BY:** The CC-BY license allows users to copy, to create extracts, abstracts and new works from the Article, to alter and revise the Article and to make commercial use of the Article (including reuse and/or resale of the Article by commercial entities), provided the user gives appropriate credit (with a link to the formal publication through the relevant DOI), provides a link to the license, indicates if changes were made and the licensor is not represented as endorsing the use made of the work. The full details of the license are available at http://creativecommons.org/licenses/by/4.0.
**CC BY NC SA:** The CC BY-NC-SA license allows users to copy, to create extracts, abstracts and new works from the Article, to alter and revise the Article, provided this is not done for commercial purposes, and that the user gives appropriate credit (with a link to the formal publication through the relevant DOI), provides a link to the license, indicates if changes were made and the licensor is not represented as endorsing the use made of the work. Further, any new works must be made available on the same conditions. The full details of the license are available at http://creativecommons.org/licenses/by-nc-sa/4.0.
**CC BY NC ND:** The CC BY-NC-ND license allows users to copy and distribute the Article, provided this is not done for commercial purposes and further does not permit distribution of the Article if it is changed or edited in any way, and provided the user gives appropriate credit (with a link to the formal publication through the relevant DOI), provides a link to the license, and that the licensor is not represented as endorsing the use made of the work. The full details of the license are available at http://creativecommons.org/licenses/by-nc-nd/4.0. Any commercial reuse of Open Access articles published with a CC BY NC SA or CC BY NC ND license requires permission from Elsevier and will be subject to a fee.
Commercial reuse includes:

- Associating advertising with the full text of the Article
- Charging fees for document delivery or access
- Article aggregation
- Systematic distribution via e-mail lists or share buttons

Posting or linking by commercial companies for use by customers of those companies.

20. **Other Conditions**:

v1.10

**Questions? E-mail us at customercare@copyright.com.**